DEVELOPMENT OF MOVING DEFORMABLE BARRIER REPRODUCING STRUCK CAR DEFORMATION IN REAL-WORLD CAR-TO-CAR SIDE IMPACT ACCIDENTS IN EUROPE AND JAPAN

Taisuke Fujiwara
Kenji Shigeta
Toyota Motor Corporation
Japan
Paper Number 09-0021

ABSTARCT

The test procedures described in current European and Japanese side impact regulations and assessments involve striking a moving deformable barrier (MDB) into a stationary test vehicle. However, since many car-to-car side impact accidents in the real world occur when the struck vehicle is also moving, the force direction into the struck vehicle in the configurations described by these regulations and assessments differs from that in those actual accidents.
Therefore, to simulate the force into a moving struck vehicle in the current test configuration, i.e., a perpendicular MDB side impact, it is necessary to integrate the stiffness characteristics of the front of the striking vehicle in a side impact accident where both vehicles are moving.
Consequently, a crabbed frontal impact test that simulates the force direction into the striking vehicle in a moving car to moving car side impact test was considered as an evaluation method for the frontal stiffness characteristics. This crabbed frontal impact test was confirmed to be capable of measuring the stiffness characteristics of the front of the striking vehicle occurring in a moving car to moving car side impact.
In addition, an MDB for simulating crabbed frontal impacts was developed based on the frontal stiffness characteristics obtained from the crabbed frontal impact test. It was confirmed that side impact tests using this MDB were capable of simulating the deformation and door moving velocity of the struck vehicle in a moving car to moving car side impact test.
As a result, vehicle safety enhancements based on a side impact test method using this MDB are expected to contribute to the development of appropriate body structures and restraint devices for real-world accidents.

INTRODUCTION

The test procedures described in current European and Japanese side impact regulations and assessments involve striking a moving deformable barrier (MDB) into a stationary test vehicle at right angles. However, in the real world, many car-to-car side impact accidents occur when both the struck and striking vehicles are moving.[1] As a result, the force direction into the struck vehicle in the regulations and assessments differ from that in those actual accidents.
One test method that simulates the force direction when both vehicles are moving is the crabbed side impact test. However, when force is applied at an oblique angle such as in a crabbed side impact, the compressive stress of the honeycomb decreases,[2] and concerns have also been raised about the stability of the stiffness characteristics of the honeycomb. In addition, although an oblique force is applied to the dummy in the struck vehicle, the response of the ES-2 dummy currently in widespread use in regulations and assessments differ depending on whether the impact is oblique or perpendicular.[3]
To resolve these concerns, this paper describes the development method and performance of an MDB capable of simulating force into a struck vehicle in a side impact while both vehicles are moving, while maintaining the configuration of the current perpendicular MDB side impact test.

1. CONSIDERATIONS FOR SIMULATING CAR-TO-CAR SIDE IMPACT ACCIDENTS

1-1 Study of Simulation Method

Many car-to-car side impact accidents in the real world occur as shown in Figure 1-a,[1] generating bending moment in the floor side members as shown in Figure 1-b. This moment causes horizontal bending in each floor side member, which originates in areas with a low modulus of section with respect to the H-axis in the H-W plane of the members.

Impact angle	Perpendicular
Struck vehicle condition	Not stationary
Rough impact velocity ratio	Striking × struck = 2 × 1

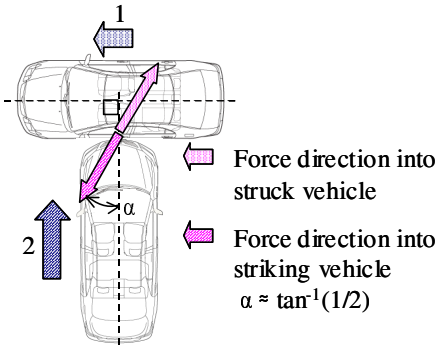

Figure 1-a. Typical form of car-to-car side impact accidents.

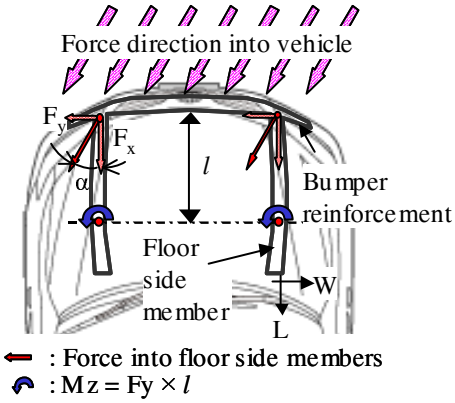

Figure 1-b. Force into floor side members and generated moment.

To simulate force into the struck vehicle in this configuration, force must be applied at crabbed angle α with respect to the front of the striking vehicle so that the stiffness characteristics of the front of the striking vehicle can be identified with the same bending moment generated in the floor side members.
For this purpose, a crabbed frontal impact test was developed using a rigid wall and a vehicle trolley as shown in Figure 2. This test generates bending moment in the floor side members of the vehicle to simulate the deformation modes of the striking vehicle in a car-to-car side impact shown in Figure 1-a.

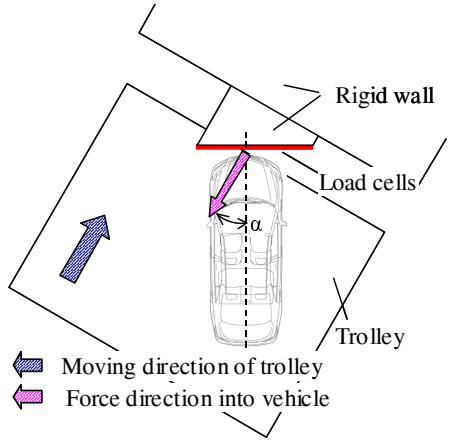

Figure 2. Outline of crabbed frontal impact test.

1-2 Validation of Simulation Method

The appropriateness of the crabbed frontal impact test was validated by comparing its results with those from the striking vehicle in a car-to-car side impact test conducted with both vehicles moving (i.e., a moving car to moving car side impact test). The results from a perpendicular frontal impact, which is the conventional method of examining frontal stiffness, are also shown for comparison in Figure 3.
Table 1 shows the conditions of the crabbed and perpendicular frontal impact tests, and Table 2 shows the conditions of the moving car to moving car side impact test.
Figure 3 shows the frontal deformation of the test vehicles.
Horizontal bending of the floor side members was identified respectively in the vehicle after the crabbed frontal impact and the striking vehicle after the moving car to moving car side impact. In contrast, vertical bending was found after the perpendicular frontal impact.

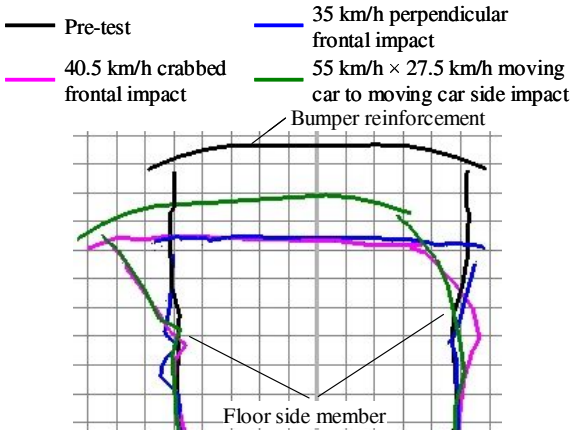

Figure 3. Test vehicle deformation (top view).

Figure 4 shows images of the front of the vehicles after the tests.
Horizontal bending of the left floor side member occurred in the same position of the vehicle after the

crabbed frontal impact and the striking vehicle after the moving car to moving car side impact.
In contrast, although clear horizontal and vertical bending positions in the right floor side member could be identified after the crabbed frontal impact, the position of the horizontal bending that occurred in the striking vehicle after the moving car to moving car side impact could not be clearly identified.
In addition, vertical bending was identified in both floor side members after the perpendicular frontal impact.

Figure 4-a. Left floor side member after crabbed frontal impact.

Figure 4-b. Left floor side member after moving car to moving car side impact.

Figure 4-c. Left floor side member after perpendicular frontal impact.

Figure 4-d. Right floor side member after crabbed frontal impact.

Figure 4-e. Right floor side member after moving car to moving car side impact.

Figure 4-f. Right floor side member after perpendicular frontal impact.

1-3 Discussions on Simulation Method

The results of the crabbed frontal impact and moving car to moving car side impact tests showed different deformation volumes.
This was probably caused by variations in deceleration and post-impact kinetic energy as a result of the different impact targets used in the tests (a rigid wall for the crabbed frontal impact test, and a moving vehicle for the moving car to moving car side impact test).
However, the deformation generated by the crabbed frontal impact was greater than that in the striking vehicle in the moving car to moving car side impact. This is thought to be because the frontal deformation in the moving car to moving car side impact represents only part of the deformation process measured in the crabbed frontal impact test. Consequently, if the volume of deformation were allowed to increase, the horizontal bending of the floor side member in Figure 4-e would approximate the deformation mode shown in Figure 4-d. Therefore, it should be possible to use the crabbed frontal impact test to measure the stiffness characteristics of the front of the striking vehicle in the moving car to moving car side impact more accurately than the conventional measurement method.

2. INVESTIGATION OF FRONTAL STIFFNESS CHARACTERISTICS

Perpendicular frontal impact and crabbed frontal impact tests were conducted on each vehicle to

compare the frontal stiffness characteristics.
The frontal stiffness characteristics of the Advanced European MDB (AE-MDB) V3.1 currently being developed in Europe and Japan are calculated based on the test results of perpendicular frontal impacts,[(4)(5)] and test methods are being studied where the AE-MDB is collided perpendicularly into the side of a stationary vehicle. Thus, by integrating the comparison results for the crabbed and perpendicular frontal impacts at areas corresponding to each block of the AE-MDB into the AE-MDB V3.1 specifications, it should be possible to simulate the force into the struck vehicle in a moving car to moving car side impact while maintaining the configuration of the perpendicular AE-MDB side impact test. Therefore, the frontal stiffness characteristics of the areas corresponding to each block of the AE-MDB were examined.

2-1 Test Conditions

Table 1 shows the test conditions.

Table 1.
Test conditions

	Perpendicular frontal impact	Crabbed frontal impact
Impact configuration	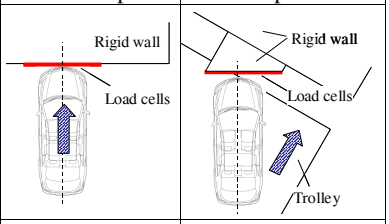	
Impact velocity	Vehicle 35.0 km/h*1	Trolley 40.5 km/h*2
Vehicle types	Compact car, hatchback, sedan, small SUV	
Vehicle mass	Vehicle mass specified in JNCAP*3 frontal impact tests	
Load cells	40 (size: 200 mm × 200 mm)*4 Plywood boards at impact surface (t: 20 mm)	

*1: Impact velocity in verification test for MDB dynamic characteristics specified by ECE Regulation No. 95[(6)]
*2: Velocity component in vehicle longitudinal direction coincided with perpendicular frontal impact test
*3: Japan New Car Assessment Program
*4: See Figure 5 for the layout of the load cells and AE-MDB.

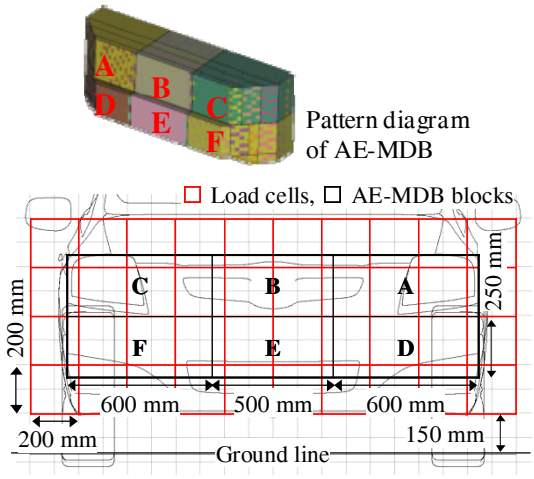

Figure 5. Layout of load cells and AE-MDB blocks.

2-2 Test Results

Figure 6 shows the frontal stiffness characteristics for each load cell block. The results shown below are for the hatchback, and those for the other vehicles are shown in the appendix. The force distribution for the crabbed and perpendicular frontal impacts differs since deformation in the crabbed frontal impact occurs as the vehicle slides to the right into the rigid wall.

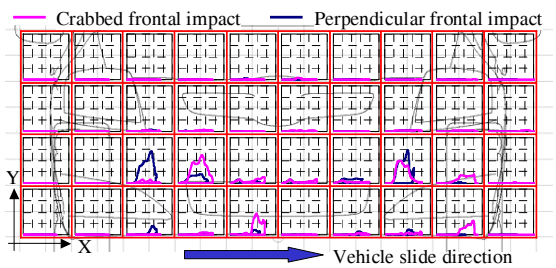

X-axis on each graph: maximum displacement = 500 mm,
Y-axis on each graph: maximum force = 200 kN

Figure 6. Vehicle frontal stiffness characteristics.

Figure 7 shows the stiffness characteristics of the whole AE-MDB and the characteristics of the areas corresponding to each block of the AE-MDB, as calculated from the force distribution above. The results for the other vehicles are shown in the appendix.
The force of the whole area generated in the crabbed frontal impact was less than in the perpendicular frontal impact since horizontal bending occurred in the floor side members after the crabbed frontal impact. In particular, force decreased significantly in block F due to the horizontal bending in the floor side members and the rightward shift in force distribution.
In contrast, force increased in block E with respect to the perpendicular frontal impact due to the shift in force distribution from block F.

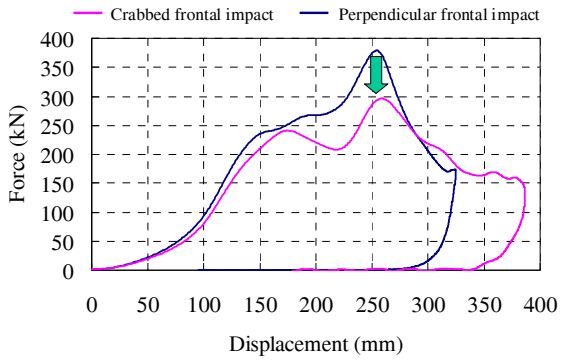

Figure 7-a. Stiffness characteristics of whole area of AE-MDB.

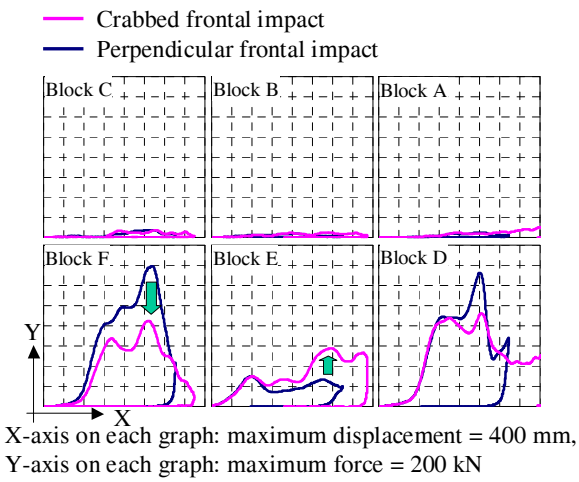

Figure 7-b. Stiffness characteristics for each block of AE-MDB.

The comparison method for frontal stiffness characteristics in the crabbed and perpendicular frontal impacts is defined as shown in Figure 8. Figure 9 shows the averaged force ratio of the four vehicle types. Compared with the perpendicular frontal impact, the frontal force in the crabbed frontal impact was roughly the same in block D, approximately 20% higher in block E, and approximately 20% lower in block F with a deformation volume close to 150 mm.

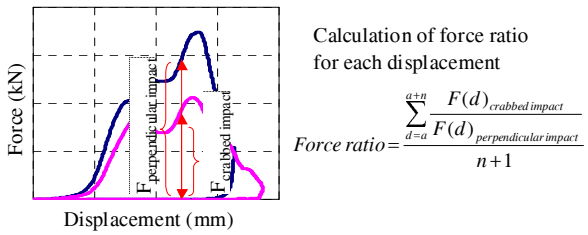

Figure 8. Calculation of averaged force ratio for crabbed and perpendicular frontal impacts.

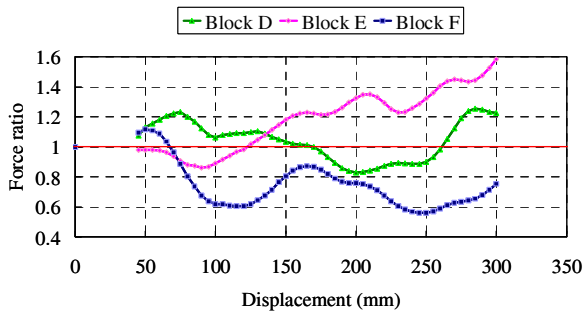

Figure 9. Averaged force ratio for each 5 mm displacement of blocks D, E, and F (averaged for all four vehicles).

3. DEVELOPMENT OF HONEYCOMB FOR CRABBED FRONTAL IMPACT SIMULATION AND VERIFICATION OF PERFORMANCE

3-1 Study of Crabbed Frontal Impact Simulation Corridors

The corridors for the honeycomb to simulate a crabbed frontal impact were created by multiplying the force ratio described above with the existing corridors for AE-MDB V3.1.[5]
Figure 10 shows the created corridors for blocks D, E, and F.
However, the same blocks were used for blocks A, B, and C as in AE-MDB V3.1. This was because this study featured only one vehicle type representing tall vehicles such as SUVs, thereby creating a lack of data for blocks A, B, and C. In addition, since the stiffness characteristics for blocks A, B, and C were set lower than for blocks D, E, and F, it was determined that there was little effect on the stiffness characteristics of the whole area even considering changes in force due to a crabbed frontal impact.

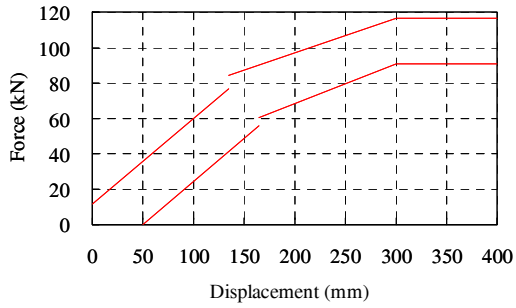

Figure 10-a. Corridor for block D.

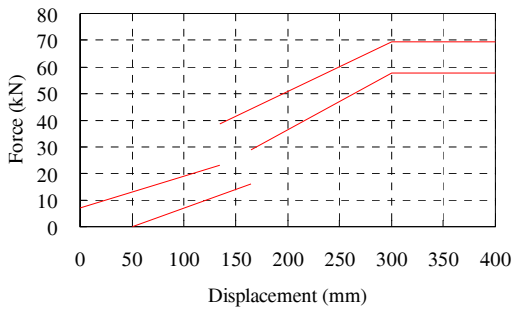

Figure 10-b. Corridor for block E.

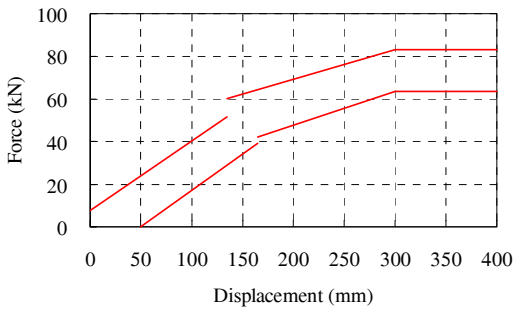

Figure 10-c. Corridor for block F.

3-2 Issues with Crabbed Frontal Impact Simulation Corridors

The following two issues were identified for the corridors shown in Figure 10.

1. Honeycomb asymmetry caused by differences between blocks D and F
2. Difficult honeycomb manufacturing due to the gap of approximately 150 mm created in displacement of block E

3-2-1 Blocks D and F - As an asymmetrical honeycomb is liable to cause usability issues, the left/right characteristics of the honeycomb were averaged to maintain the stiffness characteristics of the whole area (Figure 11).

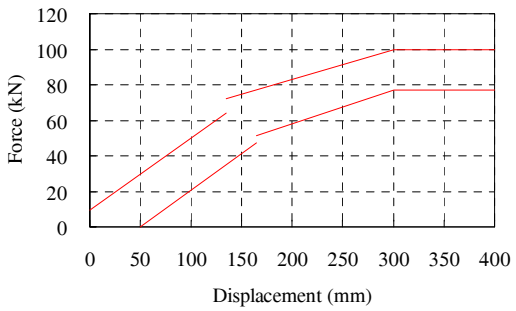

Figure 11. Averaged corridor for blocks D and F.

To verify the effect on the struck vehicle of averaging the characteristics of blocks D and F, perpendicular MDB side impact test simulations (impact point: SRP+250 mm, impact velocity: 55 km/h) were conducted using FEM analysis under two specifications: separate characteristics for blocks D and F, and averaged characteristics. Figure 12 shows the struck vehicle deformation and door moving velocity in these simulations.

Although slight variations in deformation volume occurred in the front and rear parts of the vehicles, no major differences in deformation mode or door moving velocity were identified. As a result, since these variations would not change the approach of vehicle safety enhancements or lead to large differences in dummy injury values, it was judged that averaging the characteristics of blocks D and F would only have a minimal effect.

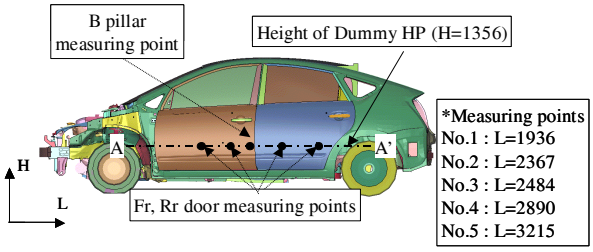

Figure 12-a. Measuring points.

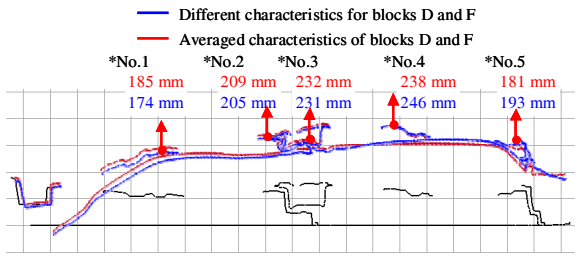

Figure 12-b. Vehicle deformation at section A-A' (time: 140 ms).

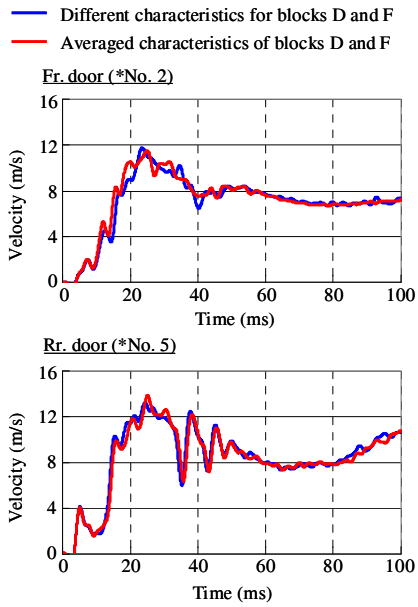

Figure 12-c. Moving velocity of front and rear doors.

3-2-2 Block E -Next, to eliminate the gap of approximately 150 mm in the corridor in block E, the corridor for block E in AE-MDB V3.9 was used,[7] which has almost the same maximum force (Figure 13).

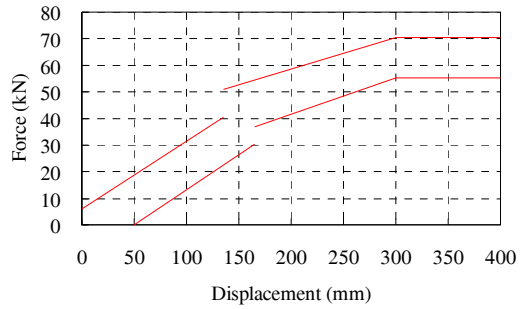

Figure 13. AE-MDB V3.9 block E corridor.

3-3 Development of Honeycomb for Crabbed Frontal Impact Simulation

A honeycomb (AE-MDB V3.10) for simulating crabbed frontal impacts was developed using the corridors shown in Figures 11 and 13. A dynamic test was then conducted to verify its stiffness characteristics. Excluding the mass of the trolley, these tests were implemented in accordance with the barrier certification method specified in ECE Regulation No. 95.[6] The trolley mass was set to 1,500 kg following the AE-MDB specifications. Figure 14 shows the results of the dynamic test. The results of the stiffness characteristics for each block and the whole area of the AE-MDB were confirmed to be within the tolerance range of the corridors.

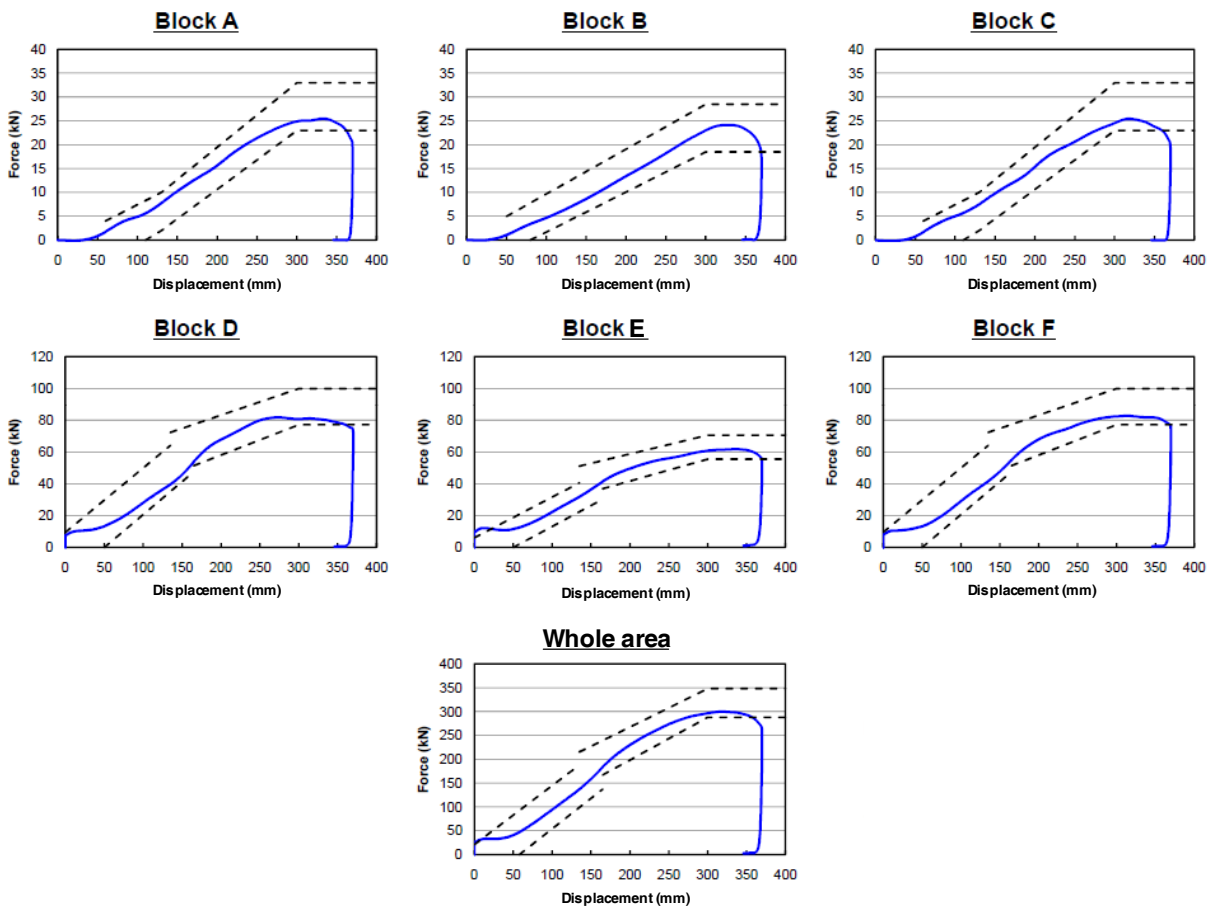

Figure 14. Results of dynamic test for AE-MDB V3.10.

3-4 Verification Test Using Real Vehicle with AE-MDB V3.10

Perpendicular side impact tests were conducted using AE-MDB V3.10 to confirm its performance in comparison to the moving car to moving car side impact test used to simulate real-world accidents.

3-4-1 Test Conditions - Table 2 shows the test conditions.

Table 2.
Test conditions

Impact configuration	Stationary 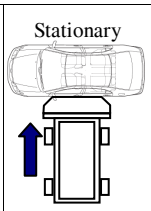	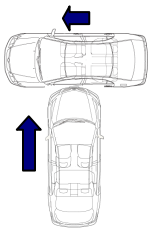
Impact point (mm)	SRP+250	SRP
Impact velocity (km/h)	55	Striking × struck = 55 × 27.5
Striking vehicle	AE-MDB V3.10 1,500 kg	Hatchback 1,500 kg
		Sedan 2,000 kg
		SUV 2,000 kg
Struck vehicle	1,500 kg	
Dummy	Fr: ES-2, Rr: ES-2	

3-4-2 Test Results - Deformation was measured before and after the tests at the door outer and pillar positions shown in Figure 15.

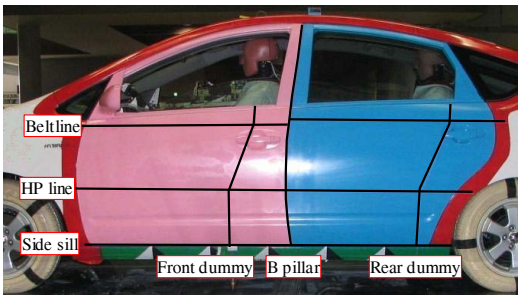

Figure 15. Deformation measuring points in struck vehicle.

Figure 16 shows the measurement results at each position.
At the front dummy and B pillar positions, the deformation volume with AE-MDB V3.10 was between that generated by the SUV and the hatchback. In the rear dummy position, the deformation was larger than with any of the vehicle types.

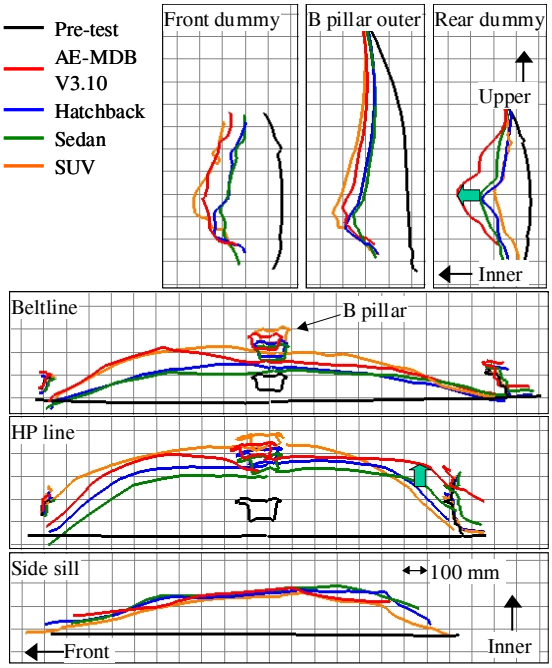

Figure 16. Struck vehicle deformation.

Figure 17 compares the moving velocities at the lateral positions of the front dummy in the beltline and HP line at the front door inner. The door moving velocities were calculated using accelerometers placed on door inner. The door moving velocities in the AE-MDB V3.10 and moving car to moving car side impacts were approximately the same.

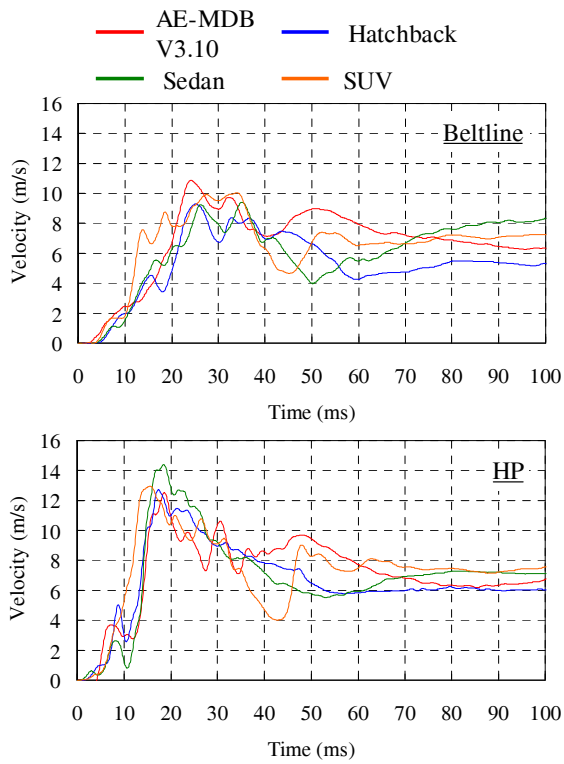

Figure 17. Front door moving velocity of struck vehicles.

3-4-3 Discussions - In the moving car to moving car side impact test, horizontal bending of the floor side members as shown in Figure 18-a prevented direct intrusion behind the rear door in the struck vehicle. However, in the AE-MDB side impact, the right side of the honeycomb intruded directly into behind the rear door (Figure 18-b). This is thought to be a factor in the differences in rear deformation.

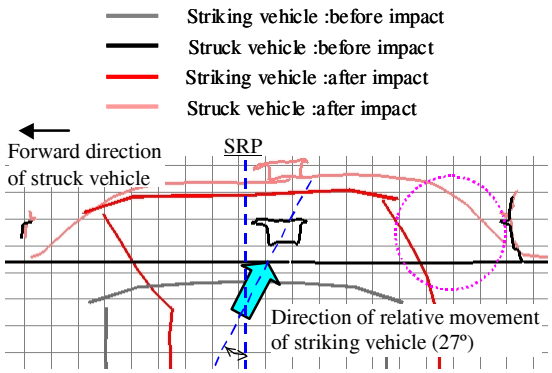

Figure 18-a. Position of striking vehicle in moving car to moving car side impact.

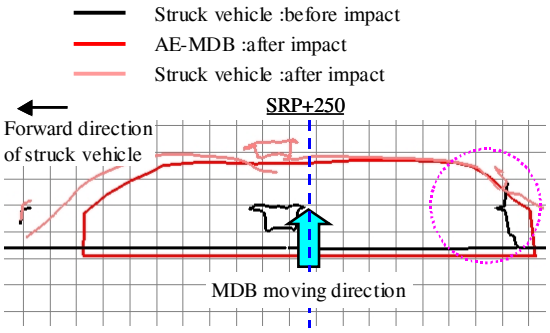

Figure 18-b. Position of honeycomb in AE-MDB V3.10 side impact.

The intrusion volume from the deformed B pillar was also considered. In a side impact test using the conventional AE-MDB V3.1, the deformation mode for door intrusions from the B pillar resembled an M shape. However, in the side impact test using AE-MDB V3.10, the intrusion of the B pillar was greater than that at the front and rear doors, and resulted in a C-shaped deformation mode. This was the same deformation mode as obtained in the moving car to moving car side impact tests (Figure 19).

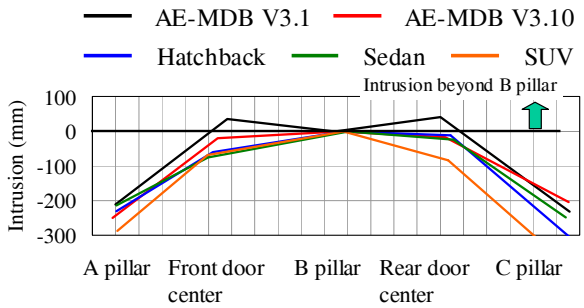

Figure 19. Intrusion volume from B pillar after deformation.

One purpose of the AE-MDB side impact test method is to evaluate the protection performance of the front and rear occupants of the struck vehicle at the same time. Therefore, the volume of rear door deformation in this test can be considered to be acceptable since the rear deformation volume was approximately the same as in the front, while the deformation mode matched that occurring in the moving car to moving car side impacts.
Based on the results and discussions on the struck vehicle as described above, a test using AE-MDB V3.10 is as stringent as the moving car to moving car side impact test based on deformation volume and moving velocity. In addition, in the deformation mode, the B pillar showed the largest intrusion, which approximates the struck vehicle deformation mode in the moving car to moving car side impact test.
This shows that a side impact test using AE-MDB V3.10 is capable of simulating actual moving car to moving car side impact accidents.
As a result, vehicle safety enhancements based on a side impact test method using AE-MDB V3.10 are expected to contribute to the development of appropriate body structures and restraint devices for real-world accidents.

CONCLUSIONS

The following results were achieved in this study.

1. The frontal stiffness characteristics of the striking vehicle were obtained in a side impact in which both vehicles are moving.
2. A honeycomb (AE-MDB V3.10) was developed simulating the frontal stiffness characteristics obtained in point 1 above.
3. An actual vehicle test using AE-MDB V3.10 simulated a car-to-car side impact test conducted with both vehicles moving.

ACKNOWLEDGEMENTS

The authors would like to express their gratitude to all those at the Japan Automobile Research Institute (JARI), the Japan Automobile Manufacturers Association (JAMA) Side Impact Working Group, the Japan Automobile Standards Internationalization

Center (JASIC), and Showa Aircraft Industry Co., Ltd. for their assistance and cooperation in this development.

REFERENCES

[1] Fujiwara, T., and Murayama, H. 2007. "Research into New Side Impact Test Based on Accidents in Europe and Japan." 20th ESV, Paper Number 07-0219

[2] Kojima, S., Yasuki, T., Mikutsu, S., and Takatsudo, T. 2006. "A Study on Yielding Function of Aluminum Honeycomb." Society of Automotive Engineers of Japan

[3] EEVC August 2001. "Development and Evaluation of the ES-2 Dummy." EEVC Working Group 12 report

[4] Yonezawa, H., Harigae, T., and Ezaka, Y. 2001. "Japanese Research Activity on Future Side Impact Test Procedures." 17th ESV, Paper Number 267

[5] Ueno, M., Hatano, K., Fukushima, N., and Tsuburai, Y. 2007. "Development of New Generation Mobile Deformable Barrier." 20th ESV, Paper Number 07-0299

[6] ECE No. 95. "Protection of the Occupants in the Event of a Lateral Collision."

[7] Versmissen, T., Van Schijndel, M., Edwards, M., and Langner, T. 2007. "Development and Evaluation of the Side Impact Test Procedure Proposed by IHRA." 20th ESV, Paper Number 07-0310

APPENDIX

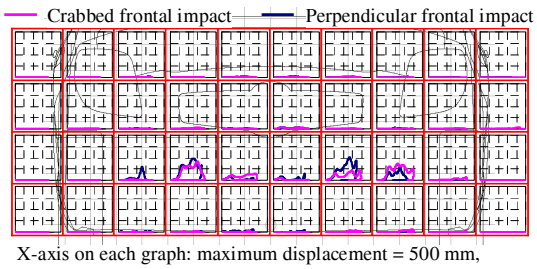

X-axis on each graph: maximum displacement = 500 mm,
Y-axis on each graph: maximum force = 200 kN

Figure 20-a. Frontal stiffness characteristics (compact car).

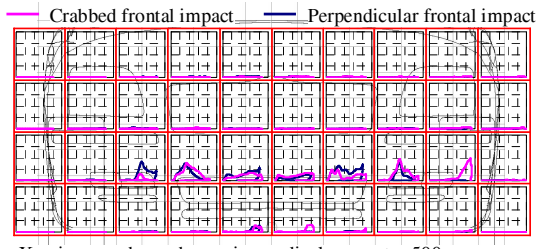

X-axis on each graph: maximum displacement = 500 mm,
Y-axis on each graph: maximum force = 200 kN

Figure 20-b. Frontal stiffness characteristics (sedan).

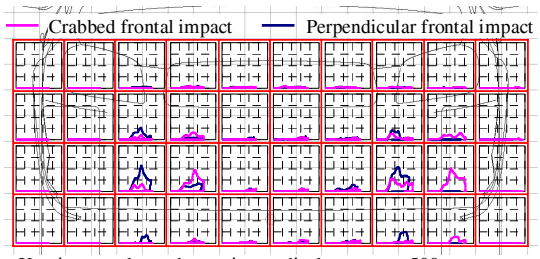

X-axis on each graph: maximum displacement = 500 mm,
Y-axis on each graph: maximum force = 200 kN

Figure 20-c. Frontal stiffness characteristics (small SUV).

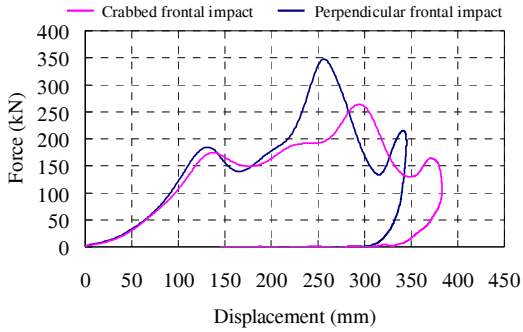

Figure 21-a. Stiffness characteristics of whole area of AE-MDB (compact car).

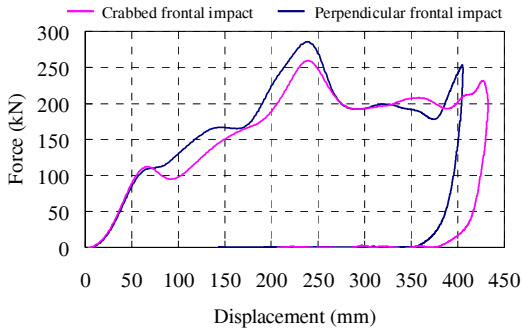

Figure 21-b. Stiffness characteristics of whole area of AE-MDB (sedan).

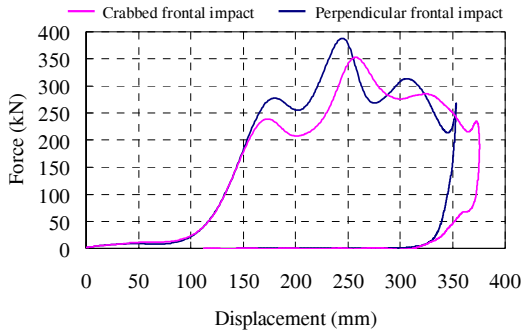

Figure 21-c. Stiffness characteristics of whole area of AE-MDB (small SUV).

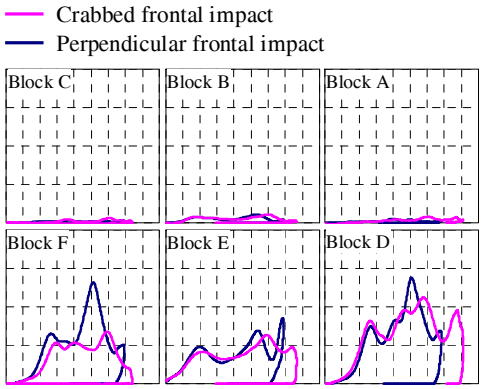

X-axis on each graph: maximum displacement = 450 mm,
Y-axis on each graph: maximum force = 200 kN

Figure 22-a. Stiffness characteristics for each block of AE-MDB (compact car).

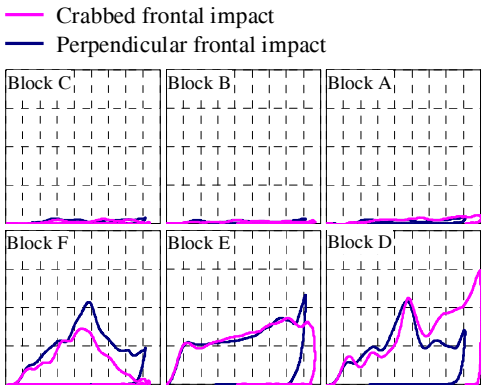

X-axis on each graph: maximum displacement = 450 mm,
Y-axis on each graph: maximum force = 200 kN

Figure 22-b. Stiffness characteristics for each block of AE-MDB (sedan).

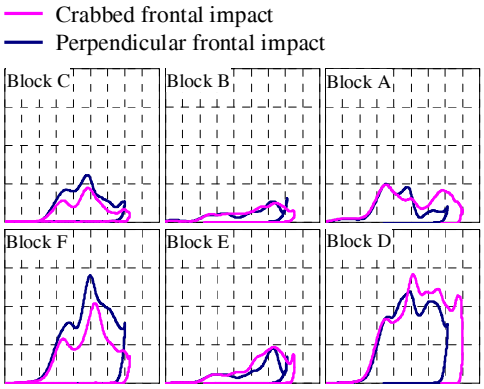

X-axis on each graph: maximum displacement = 450 mm,
Y-axis on each graph: maximum force = 200 kN

Figure 22-c. Stiffness characteristics for each block of AE-MDB (small SUV).

A HOLISTIC APPROACH TO PEDESTRIAN PROTECTION AND CRASH SENSING

Herbert Hofinger, Werner Bieck, Thierry Mousel
IEE S.A.
Luxembourg
Paper Number 09-0071

ABSTRACT

Recent legislation has increased the type approval requirements in the domain of pedestrian protection. A non design restrictive solution for the bonnet area is the implementation of pop-up bonnet systems. Obviously, such systems need a sensing element detecting and classifying the impact object in order to make a fire/no-fire decision for the bonnet lifting actuators.

The working principle of IEE's pedestrian protection sensor system not only allows the detection of pedestrian-type impacts, but also analyses crash event scenarios. Thus the same sensor is not only used for pedestrian protection, but can also contribute to passive safety by delivering information that can be used for enhanced occupant safety. In decision-making for the pop-up bonnet deployment, it is crucial to reliably distinguish between pedestrians and other objects like traffic signs, footballs or small animals, whereas in crash sensing, it is helpful to know as early as possible whether the collision object is a tree or a vehicle.

The pressure sensitive sensor is integrated into the vehicle front-end and detects parameters like T_0 (first contact), impact location, width of impacting object and impact dynamics. These data allow a more precise tuning of the restraint systems to specific crash events, the usage of less aggressive restraint systems due to the early T_0 signal, as well as the replacement of existing sensors (upfront, pole catchers, redundancy).

The sensors ability to deliver robust data in frontal crashes has been demonstrated in tests reflecting compliance, consumer and insurance testing requirements.

In order to provide even more information about crash situations and to offer optimised and cost-effective solutions for other applications, the goal is to develop a family of general impact sensors also covering the detection of rear-end collisions and side impacts.

INTRODUCTION

Regulations aiming at improved protection of pedestrians were first implemented in Europe and Japan in 2005. In November 2009, a UNECE GTR (Global Technical Regulation) with more stringent requirements was voted. The second phase of the European regulation, becoming effective in early 2013 [1], adopts this GTR.

The pedestrian protection regulation includes injury risk assessments for scenarios where a pedestrian head impacts onto the vehicle bonnet. Head impactors representing a child head and an adult head are propelled onto the vehicle bonnet with a speed of 35 km/h and the HIC (head injury criteria) values must comply with the regulation requirements. Compliance requires a certain amount of bonnet deflection, resulting in energy absorption and thus reducing the injury risk.

Vehicle types not having enough clearance between the bonnet and rigid engine bay components use so-called pop-up bonnet technology to guarantee regulation compliance. These vehicles have a sensor system in the front-end detecting an impact and discriminating between pedestrians and other collision objects. In case of a vehicle-pedestrian collision, the sensor signal triggers actuators lifting the bonnet by several centimetres and providing the necessary clearance.

IEE is currently investigating the potential of a PROTECTO™ pedestrian protection type sensor in the area of crash sensing.

FROM PEDESTRIAN PROTECTION TO OCCUPANCY SAFETY

Sensing Principle

The IEE bumper sensor is based on a flexible, foil-type pressure sensitive device which detects a frontal collision by providing four different impact related signals versus time: two switches react on specific force levels, and the impact width as well as the impact position is measured by means of a linear potentiometer. For that purpose a set of electrically conductive elements are printed on two flexible carrier foils which finally are laminated together by means of a double-sided adhesive film,

as schematically indicated in the cross-section view of Figure 1.

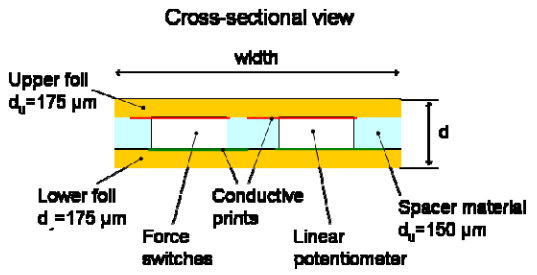

Figure 1. Schematics of a foil-type pressure sensor for pedestrian impact detection. Typical dimensions are: length l > 100 cm, width w = 2 cm, thickness d = 0.05 cm.

The adhesive layer contains a sequence of recess structures equally distributed over the complete length which allows establishing an electrical contact by deformation of both polymer foils in case of external pressure loads. The simultaneous parameter detection is accomplished by positioning the sensor somewhere between bumper skin and crossbeam (here: at the interface energy absorber – crossbeam, c.f. Figure 2). Hence, the integration can be handled quite flexibly. The major integration requirement is the presence of a mechanical support to build up the impact related reaction force which needs to be measured.

Sensor Integration

Figure 2 describes schematically a typical sensor integration concept based on detailed FE impact simulations which are performed in order to adjust sensor sensitivity and positioning within the bumper environment. In case of the presented example the contact sensor has been integrated in the energy absorber foam facing towards the crossbeam.

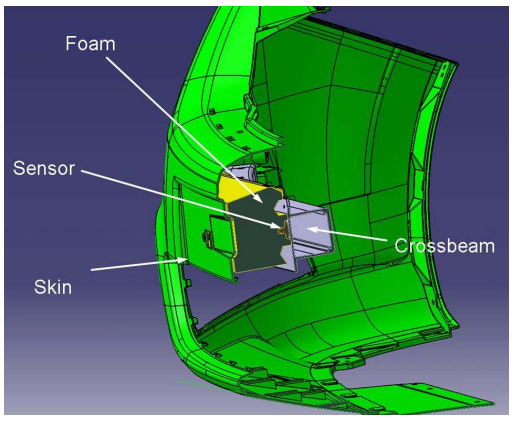

Figure 2. Sensor integration concept for a typical bumper configuration.

Simulation as Key Development Tool

Right from the start, the aim was to base the sensor development completely on simulation because of limited (and expensive) impact / crash test capabilities. Therefore, a virtual sensor development chain has been established which provides the following information:

- optimum sensor location in the bumper
- necessary bumper modifications to improve functionality / robustness
- impact data for calibrating the classification algorithm over the whole temperature range and the whole length of the bumper

Figure 3 describes the simulation based development concept to reduce lead time, test efforts and prototype needs.

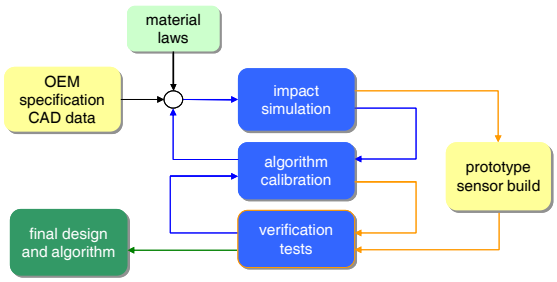

Figure 3. Flow chart describing the virtual development chain of the crash sensor.

Based on the OEM specification requirements and CAD data of the carline, the simulation model will be created by applying appropriate (validated) material laws developed for highly non-linear deformation processes. A set of crash impact simulations (partly defined by the OEM and based on legal requirements) allows identifying the optimum sensor integration and provides also preliminary data for algorithm calibration. After finalizing the virtual optimization loop, prototype sensors will be built to perform verification tests (pendulum tests, sled tests, OEM crash tests). The obtained data is used for fine-tuning the algorithm settings. The final design / algorithm will be integrated in the vehicle to pass the official crash test sequence defined in the car type approval process.

Pedestrian Impact Detection and Crash Sensing

In the event of an impact (pedestrian, pole, other vehicle), the sensor delivers signals to the ECU being attached to the sensor. The ECU acquires and analyses the sensor data in order to provide a trigger signal to fire pop-up bonnet actuators in case of low speed collision events involving humans, or to provide an additional input to the

airbag control unit. By using a certain set of input signals, a classification algorithm determines the impacting object or evaluates the crash severity. In a pedestrian protection scenario, the algorithm discriminates so-called misuse objects from a vulnerable road user to actuate only in the latter case the associated pedestrian protection system in a timely manner.

Pedestrian Detection - During a collision event, the IEE bumper sensor delivers four different signals versus time such as impact width, impact position and the activation of two threshold levels of the impact force cells (low and high force switch). Figure 4 shows the acquired impact width data for different collision scenarios. Human-like impacts are experimentally simulated by crash-test dummies which have been hit in a lateral position or dedicated human-like leg-impactors ("lower limit" impactors). At t = 20 ms the linear potentiometer indicates the impact event. This signal triggers the collision time measuring process, i.e. the timer is set to $t_{col} = 0$ ms.

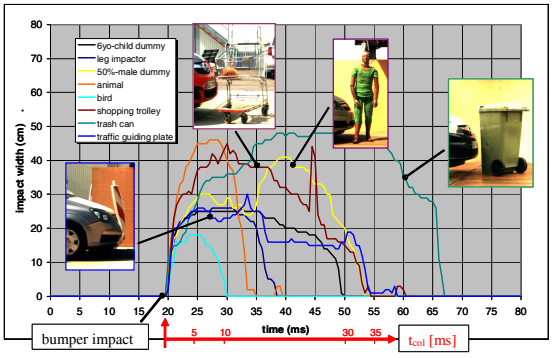

Figure 4. Example of the impact width signal evolution measured during the collision with different objects or dummies.

The impact width shows a typical increase in case of a human-like leg up to a level of w = 30 cm, which is reached about 6 ms after the impact detection. At $\Delta t_{col} = 15$ ms the second leg is also hit at a certain bumper distance offset with respect to the actual first impact location. About 25 ms after first contact detection, the collision process changes from the constitution into the restitution phase, therefore the impact width as well as the impact force started to decrease. Finally, the dummy looses the bumper contact about 35 ms after the first hit, which is monitored by the drop of the positioning signal of the linear potentiometer.

In parallel the impact location across the bumper is also measured (not shown) as well as the activation level of low force switch SWL and high force switch SWH which provide additional information about the strength of the impact. The plurality of data sets indicates an essential development problem, namely how to separate non-human impacts (misuse, e.g. animals, trash cans, traffic signs, etc.) from collision events with vulnerable road users for whom dedicated safety systems have to be activated. For a given object and a given bumper front-end the obtained data depend also on the impact location Y across the bumper, the impact speed and environmental conditions (basically temperature).

Crash Detection - As described above, IEE originally developed a sensor element dedicated for pedestrian collision detection in order to trigger active protection systems (e.g. lifting mechanisms of the bonnet, additional air-bags, etc.). That sensor element shows fast response time on any low-energy (i.e. low-speed and low-mass) collision event with vulnerable road users or other objects which can be found on the road. During the collision event it continuously provides information about the impact. The field of application can be extended from such low-energy impacts (causing reversible bumper deformation or minor damages of the outer bumper skin) towards destructive high-energy crash events (e.g. car-to-pole accidents) in order to detect and to classify crashes in such a way that active passenger protection measures can be triggered in a timely manner.
Crash tests showed that in comparison with standard crash sensing technology found in the vehicle front end, the new approach shows essential technical advantages:

- fast response time in case of impacts
- impact classification capabilities (strength, impact location / impact vector, type of collision object)
- ample mechanical robustness
- not affected by noise (i.e. vibrations due to rough road conditions)
- beneficial combination with pedestrian protection sensor thus reducing the number of needed sensor elements in the front-end

Indispensable is to categorize upper impact limits for human-like collision events in order to distinguish them from a crash.

Potential for Improved Occupant Safety
Automotive industry intends to establish more efficient passenger protection systems by means of improved active safety devices (e.g. multiple air-bag solutions, more sophisticated restraint systems, adapted system deployment strategies, etc.) due to more restrictive safety regulation requirements and general market development trends. In general, such techniques can benefit from having more lead time for their activation in order to provide their full protection capability, and / or they need additional data to be deployed in a more dedicated

way according to the crash situation. In case of a frontal collision event it is therefore essential to identify as early as possible strong impacts, i.e. in best case to have a collision object classification very shortly after T_0 which is the time of first contact with the car bumper. It can be crucial to know as soon as possible if the collision object is a tree or rather a vehicle. This information can then be provided to the airbag control unit, and the additional information can support an earlier or more appropriate airbag deployment. Standard g-sensor technology shows limitations in detection efficiency due to mechanically more soft material and design constraints of modern car front-ends which are needed in order to fulfil the passive pedestrian protection requirements (injury mitigation). As a consequence, strong impacts are detected with some delay during the collision process, hence, not providing enough time to establish more complex counter measures for improved passenger protection.

Outlook and Remaining Challenges

Besides frontal crashes also side crash events as well as rear crash detection in view of whiplash protection can be additional fields of application.

Because of comparatively short distances between passenger and impacting object, it is obvious that fast side crash detection is indispensable to protect the passenger's life. Timing is even more critical due to additional out-of position problems in case passenger's head is resting against the B-pillar.

Whiplash protection in case of rear crashes requires fast impact detection to provide sufficient lead time to activate systems like active head-rest positioning. About 80% of all passenger injuries caused by rear crash accidents are whiplash injuries covering in total about 75% of all insurance costs to be paid in case of any passenger injury [2]. Therefore, development and test activities focusing on automatic headrest positioning devices (for front and rear seats) are in the focus of interest. Fast crash detection capabilities can provide a valuable input for such systems.

Although the sensor in its current form already shows the ability to cover a wide range of impacts (small stones to crash), future development is aimed at enhancing the detection range in the high-mass impact area even further.

CONCLUSIONS

The IEE bumper sensor is based on a flexible, foil-type pressure sensitive device which detects a frontal collision by measuring T_0 (first contact), impact location, width profile of impacting object and impact dynamics. The pressure sensitive sensor is integrated into the vehicle front-end and its working principle allows combining two different fields of sensor applications:

1. Active Pedestrian Protection
Detecting accidents with vulnerable road users in order to trigger protective counter measures to save pedestrian's lives (e.g. deployment of the car bonnet, windscreen airbags, etc.).

2. Crash Detection
The identification and classification of crash events as early as possible in order to be able to trigger enhanced protective counter measures to save passenger's lives.

REFERENCES

[1] Official Journal of the European Union 04.02. 2009, Regulation EC No 78/2009

[2] Carhs "Safety Companion" 2009, p:58

STUDY ON IMPROVING OCCUPANT INJURY PERFORMANCE FOR FMVSS214 SIDE POLE IMPACT

Young Woong Kim
Byung Ryul Ham
In Ho Choi
Han Il Bae
Hyundai Motor Co. & KIA Motors Corp
Korea
Paper No. 09-0100

ABSTRACT

NHTSA(National Highway Traffic Safety Administration) has published an update to the FMVSS214 regulation which includes the Pole Impact test configuration using the ES-2re and SID-IIs dummy. This updated standard adds a new side pole test requirement in addition to modifying the test procedure used to perform dynamic side impact testing. This paper shows a new technique to improve the occupant injury performance during the Pole Impact test.

INTRODUCTION

NHTSA announced a final rule for FMVSS(Federal Motor Vehicle Safety Standard) No. 214, "Side impact protection" (72FR51908, No, NHTSA-29134)[1)] using ES-2re(50th Percentile Dummy) and SID-IIs(5th Percentile Dummy).
This final rule modified the test procedure and adopted technically advanced test dummies (ES-2re and SID-IIs) to enforce detailed requirements on the enhanced injury criteria which are the force, displacement and acceleration of the head, chest, pelvis and abdomen of occupant dummies. (Figure 1)

Final Rule Injury Criteria

	HIC_{36}	Chest deflection (mm)	Lower spine (g)	Abdominal force (N)	Pelvic force (N)
ES-2re	1,000	44 mm	N/A	2,500 N	6,000 N
SID- IIs	1,000	N/A	82 g	N/A	5,525 N

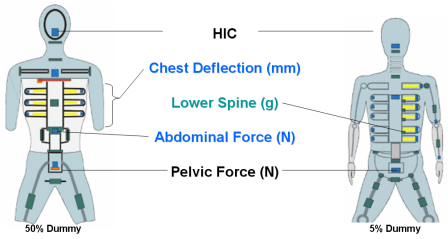

Figure 1. Dummy Injury Criteria

In addition to the MDB(Moving Deformable Barrier) dynamic FMVSS214 side impact test, new protocol requires a 75-degree oblique pole test in two different configurations so as to improve an occupant protection for the various side impact crashes. (Figure 2)

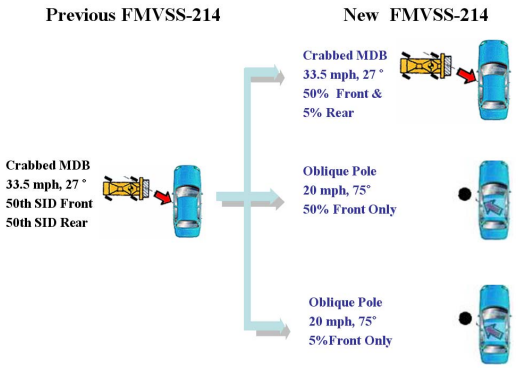

Figure 2. Updated FMVSS214 Side Impact Test Procedure

This paper focused on improving an occupant injury performance under the side pole impact test by optimizing a side-airbag performance. Following factors are considered in this study.
(1) Dummy structure mechanism of ES-2re and SID-IIs
(2) Packaging space for a side-airbag deployment
(3) Relation between side-airbag pressures and occupant injuries
This study shows that the deployment performance and airbag pressure are the two most important factors to improve occupant injuries in a pole impact test. Analyzing relation between airbag pressure and occupant injuries provided methodology to secure the optimal airbag deployment. This paper suggests guidelines to get a proper deployment space of the side-airbag to improve occupant injuries and discusses the relationship between occupant injuries and airbag pressures.

STRUCTURES OF A SIDE IMPACT DUMMY

ES-2re

The ES-2 dummy is a side impact test device designed to the specifications of the EURO NCAP. It represents a 50th percentile adult male without lower arms based on ES-1 dummy. The ES-2 has an improved rib module to fix the significant problem known as "Flat Top" which is one of the structural defects in ES-1. It means a higher possibility of RDC and VC measurement in ES-1[(2)]. 'Flat-Top', once it happens, is a period of a constant rib deflection maintained over 10~15ms time duration (Figure 3). It is rarely reported in 90 degree loading tests like EuroNCAP side impact, but in US oblique side impact test, 'Flat top' often occurs and it is also obserbed in oblique component test. [3)]

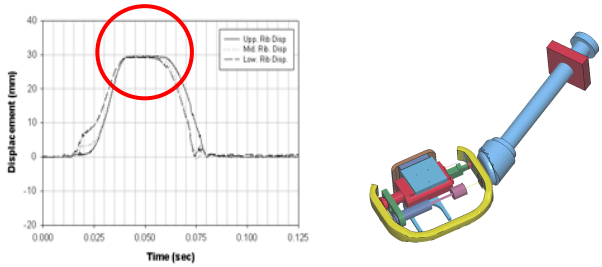

Figure 3. Flat Top Problem

ES-1 dummy's RDC can be diminished by inserting a bracket in a seat back frame for pushing the back plate of dummy, as shown in Figure 4. [4)]

Figure 4. Back Plate Problem

This kind of pushing mechanism is apt to cause a severe injury on human body in real-world accident. Therefore, Euro NCAP committee considered counter plan to regulate this unrealistic injury mechanism. ES-2 adopts a small-size back plate and a new load cell on it to solve this problem.

Despite of this effort, "Fat top" and "Back plate-effect" is still reported due to the unexpected loading conditions in side impact test. Recently, NHTSA announced a modified version of the ES-2, ES-2re has been mainly developed to minizie the interference between the back plate and seat structure that still may exist with the standard ES-2. (Figure 5)

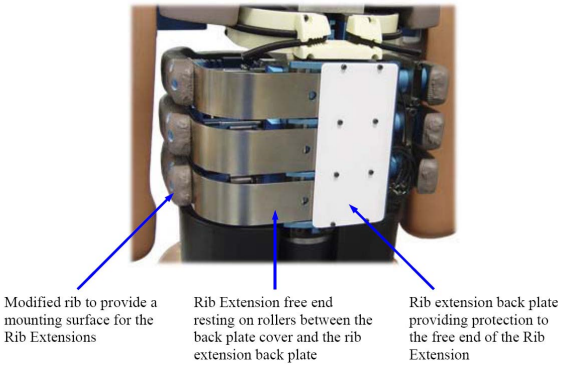

Figure 5. ES-2re

ES-2re shows an improved biofidelity by using the rib extension so that "Flat Top" problem is eliminated. [5)]

SID-IIs

NHTSA issued a final rule announcing the agency's regulation on anthropomorphic test devices to add specifications and qualification requirements for the 5th percentile adult female crash test dummy named SID-IIs. The SID-IIs is used for the oblique pole test and moving deformable barrier test on the FMVSS214 final rule. (Figure 6)

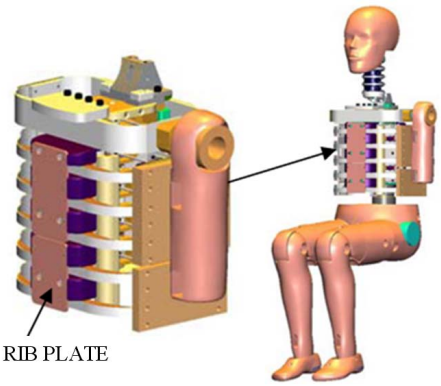

Figure 6. SID-IIs

RELATION BETWEEN SIDE-AIRBAG PRESSURES AND AN OCCUPANT INJURY

The oblique pole test in upgraded FMVSS214 was developed to provide protection for the head, chest, abdomen and pelvis during pole test. This pole test simulates a vehicle crashing sideways into narrow fixed object like a narrow pole or tree.

In the vehicle-to-pole crash, there are three main

energy absorbers, structure, trim and airbag. (Figure 7) Unlike usual MDB test, vehicle structure is not a main energy absorbing part due to less interaction between dummy and vehicle even if seat belt works. Hence, a side-airbag and door-trim should be optimized to improve an occupant injury.

In this paper, we analyzed a relationship between a side-airbag and occupant injuries and considered a new stratagy to improve occupant injuries.

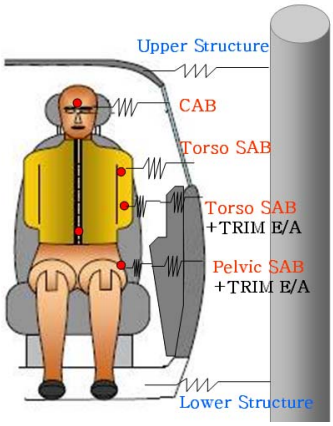

Figure 7. The oblique pole test

SAB (Side Impact Airbag) Analysis

The side impact airbag is a major safety device that functions to absorb side impact energy during the load of certain criteria to protect occupants. We developed it through the following sequence as shown in Figure 8.

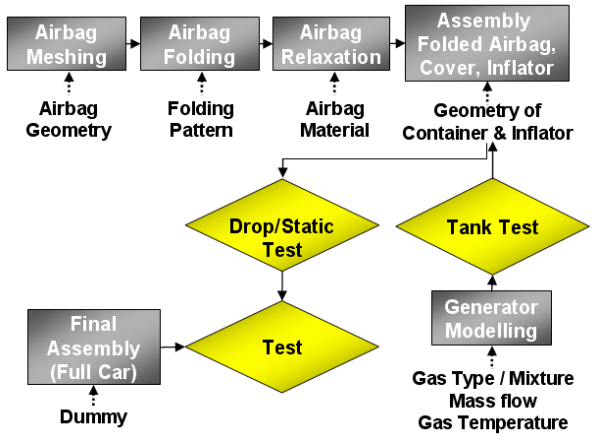

Figure 8. Side Impact Airbag Configuration

The side impact analysis airbag model needs a validation analysis including tank test, drop test and static deployment test. (Figure 9)

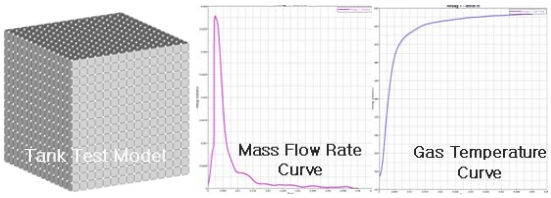

Tank Test

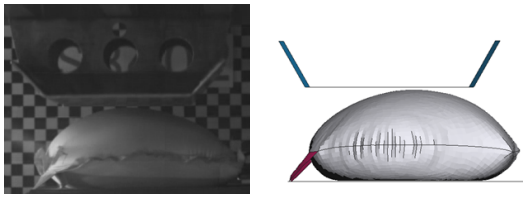

Drop Test

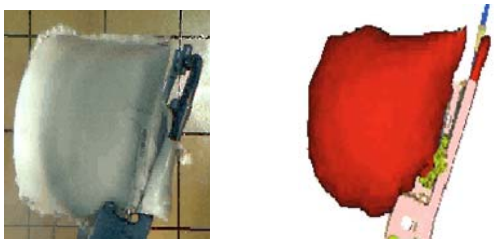

Static Test

Figure 9. Airbag Validation Analysis

5th & 50th Percentile Pole Impact

In this paper, we analyzed a relation between side-airbag pressure and occupant injuries in the mid-sized SUV during an oblique pole crash. The airbag pressure change was represented by mass flow rate (5%, -20% ~ +20%). Airbag on this analysis model is a 2-chambar type airbag which widely used to protect occupant in a side crash. (Figure 10)

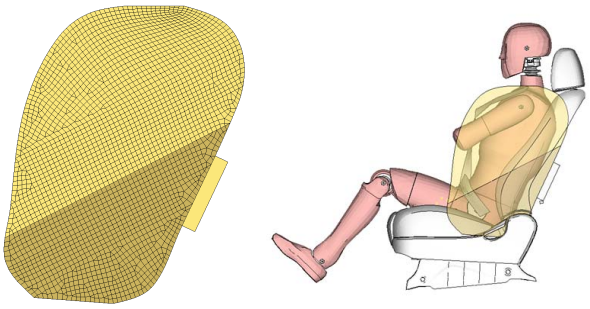

Figure 10. 2-Chambar Type Airbag

5th percentile oblique pole test evaluates head acceleration, lower spine acceleration and pelvic force. Analysis results are as follow. (Figure 11)

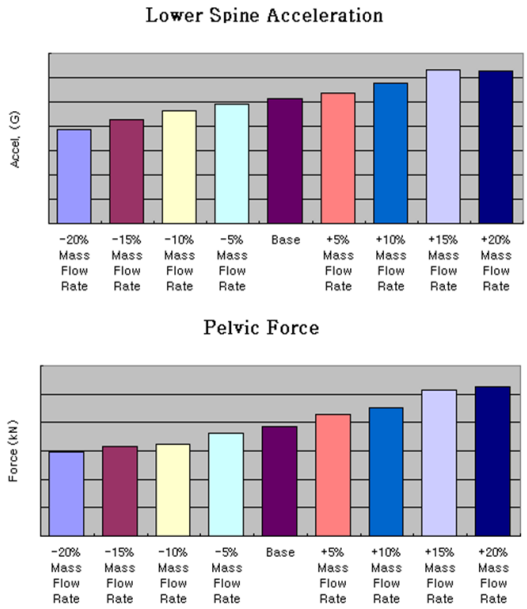

Figure 11. 5th Percentile Oblique Pole Analysis

According to these results, spine and pelvic injury were increased due to airbag pressure (mass flow rate) increase. 5th percentile adult female dummy, represent 44kg's smaller stature occupants, reacts to the airbag pressure more sensitively. Hence, occupant injuries increase in proportion to the side-airbag pressure until airbag bottoming-out condition. In the case of non bottoming-out condition, 5th percentile dummy's spine and pelvic injury will be improved as side-airbag pressure decrease.

50th percentile oblique pole test results, including head acceleration, rib deflection, abdominal force and pelvic force, are depicted in Figure 12.

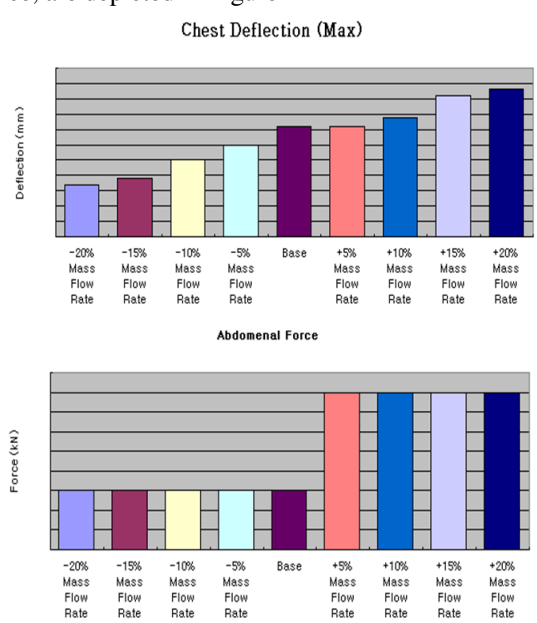

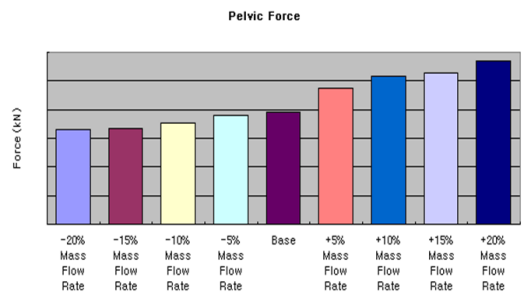

Figure 12. 50th Percentile Oblique Pole Analysis

In the case of 50th percentile oblique pole test, airbag pressure induces the rib deflection increasement. However, an abdominal injury response is not so sensitive compared to the rib response. It just slowly follows the airbag pressure response. The reason why an abdominal injury doesn't reflect airbag pressure change immediately is due to the existence of the fixed tether located on the abdomen. On the contrary, pelvic injury follows the airbag pressure response faithfully. It increases according to the airbag pressure increase.

One of the remarkable results is the chest injury tendency during an oblique pole test. In MDB test, it showed a decreased chest injury when airbag pressure in pelvic region increases. However, chest injury increased in pole test on the contrary. This result is originated from the fact that relative movement of dummy between rib and pelvis is small. This can be proved by measuring relative velocity of a dummy's rib and pelvis as Figure 13.

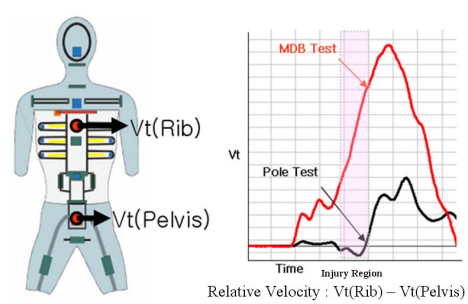

Figure 13. Relative Velocity between Rib and Pelvis

In conclusion, occupant injuries of 5th and 50th percentile oblique pole test get worse in proportion to the side-airbag pressure increase. Within non bottoming-out condition, we can improve occupant injuries by diminishing airbag pressure through an increased airbag-volume capacity and vent-hole.

PACKAGING SPACE FOR THE SAB (SIDE IMPACT AIRBAG) DEPLOYMENT

Occupant injuries are mainly affected by an airbag

performance especially the deployment condition during an oblique pole test. An airbag deployment performance can be improved by increasing an airbag deployable space or airbag pressure. In case of increasing airbag pressure, there is a limit because it causes higher abdominal and pelvic injury owing to airbag stiffness. Hence, it is the best way for improving occupant injuries to enlarge the airbag deployable space during crash event. Following is the analysis method for securing an airbag deployable space.

As shown in Figure 14, airbag deployment performance gets worse under a smaller airbag deployable region 'A'. 'A' will be getting smaller during the side impact crash.

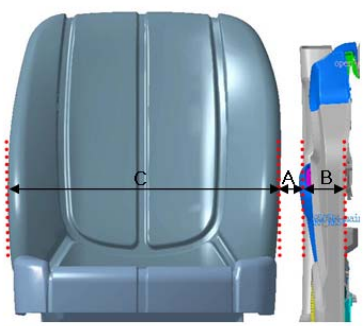

(A: Airbag Deployable Region, B: Door Trim Width, C: Seat Back Width)

Figure 14. Airbag Deployment Region

Therefore, a fully deployment of an airbag should precede the contact between a door trim and a seat. Contact time between a door trim and a seat can be measured by an acceleration sensor on the same position of a door inner panel, so that a door intrusion can be shown as below. (Equation 1) (Figure 15)

$$DoorIntrusion = \int_0^T (RHDoorVelocity - LHDoorVelocity) \quad (1).$$

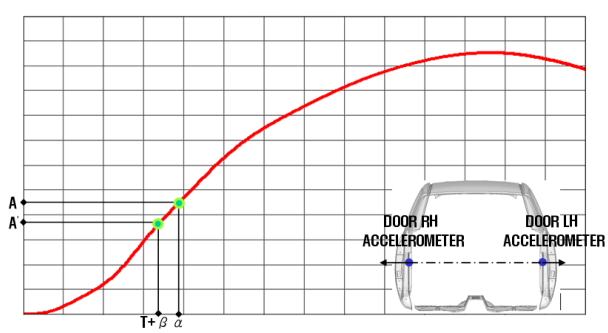

Figure 15. Door Intrusion

Contact time between a door trim and a seat, α, should be larger than summation of a TTF(Time to Fire) and an airbag deployment time (β). (Equation 2)

$$\alpha \geq (T + \beta) \quad (2).$$

As a result, reducing TTF or β for a deployment time of an airbag or delaying a contact time (α) results in the fully deployment condition of an airbag. It improves occupant injuries in side impact. Another way of improvement is to reduce armrest (B) and seat back foam size (C). It will cause to enlarge an airbag deployable region (A). (Equation 3)

$$A \geq A' \quad (3).$$

CONCLUSIONS

This paper suggests techniques of an improvement on an oblique pole crash and it can be summarized as follows.

(1) Airbag pressure affects occupant injuries especially an occupant's chest injury. Occupant injuries usually increase in proportion to airbag pressure under an oblique pole crash. Therefore, we should find an optimal pressure of a side-airbag to improve occupant injuries by controlling an airbag-volume capacity and vent-hole size.

(2) To improve a deployment performance of SAB, following three conditions should be satisfied; increasing deployment speed of an airbag, delaying contact time between a door trim and a seat and maintaing a gap between a door trim and a dummy.

REFERENCES

[1] NHTSA, "Federal Motor Vehicle Safety Standards", Docket No. NHTSA-29134, 2007.

[2] S. Sundararajan, K. Aekbote, C. Chou, "EuroSID-I Rib Module Performance and Evaluation", SAE, 1999.

[3] NHTSA, "Status of NHTSA Plan for Side Impact Regulation Harmonization and Upgrade", NHTSA, 1999.

[4] NHTSA, "Side Impact Protection in the United States", NHTSA, 2004.

[5] Matthew R. Maltese, "ES-2 Biofidelity and Injury Assessment Capability", NHTSA, 2001.

AN EVALUATION OF PDB TEST RESULTS FOR PARTNER PROTECTION AND SELF PROTECTION

Kaoru Tatsu
Akira Yamaguchi
Atsushi Hitotsumatsu
Tomosaburo Okabe
NISSAN MOTOR CO., LTD.
Japan
Paper Number 09-0109

ABSTRACT

The introduction of various vehicle safety standards and new car assessment programs in addition to automobile manufacturers' efforts to improve vehicle safety performance have led to significant improvements in vehicle safety performance over the past several years. Improving frontal impact compatibility is recognized as one approach to further enhancing vehicle safety performance. Various methods of improving frontal impact compatibility have been proposed and discussed.

In 1996, European Enhanced Vehicle-safety Committee Working Group 15 on Vehicle Compatibility was established to explore methods for assessing vehicle compatibility and to develop procedures for testing it. In their 2007 Final Report, EEVC WG15 proposed a Progressive Deformable Barrier (PDB) test as one candidate for testing vehicle compatibility. The PDB test was developed with the aim of assessing and improving partner protection while taking self protection into account as well.

This paper focuses on the PDB test. To assess its performance, several different category vehicles (small car, large car, midsize SUV, large SUV) were selected for study and PDB test results for them were compared with those obtained with the current ECE R94 offset deformable barrier (ODB) test and the vehicle-to-vehicle impact test. This study was simply an attempt to make an evaluation of the PDB test in comparison with other test procedures.

INTRODUCTION

Improving vehicle crash compatibility by reconciling self protection with partner protection has attracted greater attention in recent years as still another approach to further enhancing vehicle occupant safety. While various studies have been done on vehicle compatibility to date, more research is needed and this is still a much discussed subject [1]-[4]. In Europe, Working Group 15 (Car Crash Compatibility and Frontal Impact) was formed under the European Enhanced Vehicle-safety Committee (EEVC) in 1996 for the purpose of developing a test procedure and evaluation methods aimed at further improving vehicle compatibility in frontal impacts. In the final report of WG15's activities that was presented at the ESV Conference in 2007, the following three sets of combinations were proposed as possible candidates for a compatibility evaluation test procedure [5].

Set 1
- Full Width Deformable Barrier (FWDB) test
- Offset Deformable Barrier (ODB) test using an EEVC barrier

Set 2
- Full Width Rigid Barrier (FWRB) test
- Progressive Deformable Barrier (PDB) test

Set 3
- Combination of FWDB and PDB tests

The report also cited the following points as being essential aspects of any test procedure for evaluating compatibility:

1. It must be capable of evaluating structural interaction.
2. It must be capable of evaluating the frontal force level.
3. It must be capable of evaluating the passenger compartment stiffness.
4. There must not be any decline in the current level of self protection capability.

The PDB test was proposed by EEVC WG15 as one of the candidate evaluation procedures capable of assessing the four items above, though further discussion is deemed necessary concerning the evaluation criteria and parameters to be used with this test procedure.

Focusing on the PDB test, this study examined the issues currently under consideration and the suitability of the proposed evaluation parameters for assessing

self protection and partner protection. That was done by comparing PDB test results with vehicle-to-vehicle impact test results and the results obtained with the current ODB test procedure.

EVALUATION FOR PARTNER PROTECTION PARAMETERS OF PDB TEST

The Average Height of Deformation (AHOD) and the Average Depth of Deformation (ADOD) are the principal parameters of partner protection in the PDB test procedure. These parameters were examined using the test results obtained for five types of vehicles.

PDB Test Conditions

The PDB test conditions used in this study are shown in Table 1. The points that differed from the current ODB test conditions were the barrier construction, impact speed and overlap ratio.

Table 1. PDB impact conditions

Barrier	PDB+
Impact speed	60 km/h
Overlap ratio	50%
Dummies	DR: Hybrid-Ⅲ AM50
	PS: Hybrid-Ⅲ AM50

PDB Barrier Characteristics

The characteristics of the PDB barrier used in the tests are shown in Fig. 1. The barrier consisted of four blocks. The block at the front of the barrier had a constant level of reaction force. The next block to the rear consisted of upper and lower levels, with a gradually increasing reaction force characteristic. The reaction force of the lower level block was greater than that of the upper level one. The rearward-most block had a constant level of reaction force and was provided to prevent the bottoming out of the barrier with large vehicles [6].

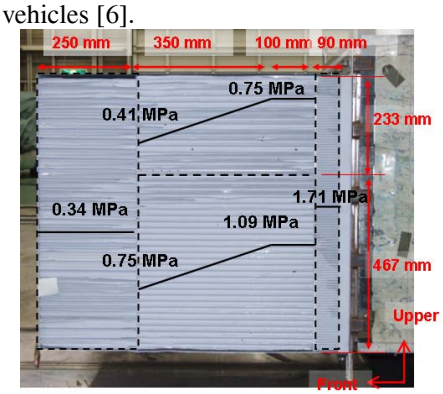

Figure 1. PDB+ Barrier Characteristics.

Calculation Method

The evaluation parameters used in the PDB test are calculated with a dedicated software program based on three-dimensional measurements of barrier deformation following the impact [7]. In this study, PDB Soft ver. 1.0 was used to calculate the parameters of AHOD, ADOD and barrier-absorbed energy. However, this software is for use with a barrier having a depth of 700 mm and is not compatible with the latest PDB+ barrier that is 790 mm deep. For that reason, the parameters were calculated by adding data for the extra 90 mm of depth. The equations used to calculate AHOD and ADOD are shown below as equations (1)-(4).

Average Height of Deformation (AHOD)

For a given rectangular investigation region, the "depth profile" is computed as a function of height.

$$\rho(z) = K \int_{y\,min}^{y\,max} X(y,z)dy \qquad (1)$$

Where K is a normalization constant ensuring that

$$\int \rho(z)dz = 1 \qquad (2)$$

The AHOD is then obtained as a mean value

$$AHOD = \int z\rho(z)dz \qquad (3)$$

The AHOD value indicates the average height of deformation over the barrier in the investigation area based on the deformed condition of the barrier. The aim of this parameter is to evaluate the position of the front-end structures of a vehicle.

Average Depth of Deformation (ADOD)

For a given investigation region with an area S

$$ADOD = \frac{1}{S}\int X(y,z)dydz \qquad (4)$$

The ADOD value indicates the average depth of deformation over the barrier in the investigation area based on the deformed condition of the barrier. The aim of this parameter is to evaluate the stiffness of a vehicle.

Investigation area

The investigation area used in this study in calculating these parameters is shown in Fig. 2. The dimensions of the investigation area were fixed in the vertical direction. For horizontal direction, the dimension from the centerline of a vehicle was fixed. However, the width of the investigation area was determined

separately for each test vehicle taking the vehicle width into account.

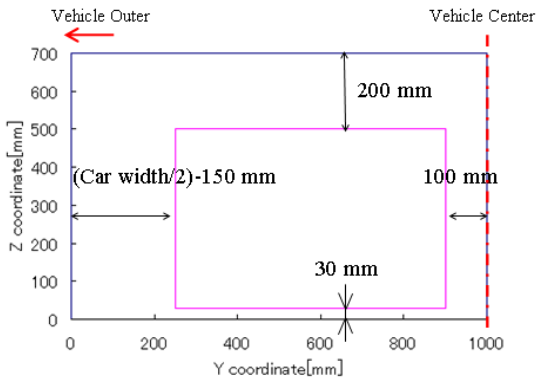

Figure 2. Investigation area.

Test Vehicles

Five types of test vehicles were used in this study and are denoted here as small car A, large car B, midsize SUV C, midsize SUV D and large SUV E. The midsize SUV D was the previous generation model of the midsize SUV C. The bumper beam on the latter vehicle was positioned higher than on the midsize SUV C. All of the test vehicles had a left-hand steering wheel. The specifications of each test vehicle and a simplified diagram of its front-end structure are shown in Figures 3-7, respectively.

Vehicle	Small Car A
Test Weight	1250 kg
Width	1660 mm
Drive	Front
Load Path	Single
Body	Unibody

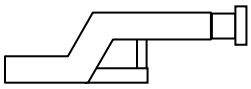

Figure 3. Small car A specifications.

Vehicle	Large Car B
Test Weight	1996 kg
Width	1800 mm
Drive	Rear
Load Path	Double
Body	Unibody

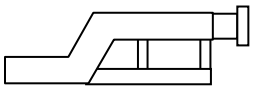

Figure 4. Large car B specifications.

Vehicle	Midsize SUV C
Test Weight	2063 kg
Width	1880 mm
Drive	AWD
Load Path	Double
Body	Unibody

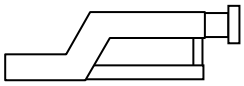

Figure 5. Midsize SUV C specifications.

Vehicle	Midsize SUV D
Test Weight	2087 kg
Width	1880 mm
Drive	AWD
Load Path	Double
Body	Unibody

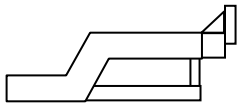

Figure 6. Midsize SUV D specifications.

Vehicle	Large SUV E
Test Weight	2754 kg
Width	2000 mm
Drive	AWD
Load Path	Single
Body	Body on frame

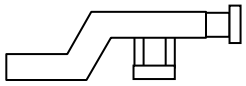

Figure 7. Large SUV E specifications.

PDB Test Results

The test results obtained for each vehicle in terms of the AHOD, ADOD and maximum barrier force are given in Table 2.

Table 2. PDB test results

Vehicle	S/Car A	L/Car B	M/SUV C	M/SUV D	L/SUV E
AHOD	414 mm	408 mm	436 mm	423 mm	453 mm
ADOD	236 mm	324 mm	366 mm	308 mm	397 mm
Fmax	347 kN	484 kN	461 kN	448 kN	597 kN

AHOD

Figure 8 shows the positional relationship between the AHOD and the top and bottom of the longitudinal members. The results indicate that the AHOD values were nearly the same for all five test vehicles, regardless of the position of their longitudinal members.

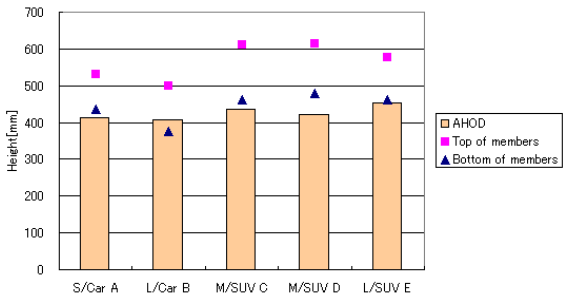

Figure 8. AHOD and the height of longitudinal members.

The relationship between the amount of barrier deformation caused by each test vehicle and the positions of the transmission, engine, tires and principal structural components are shown in Figures 9-13, respectively.

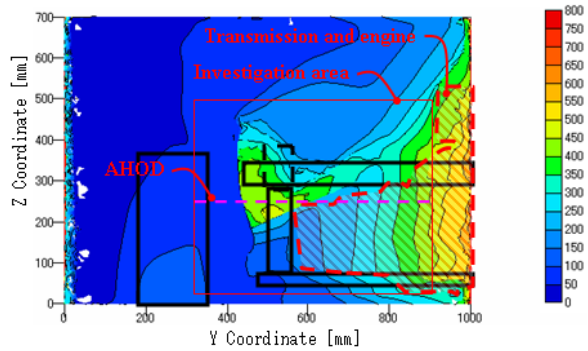

Figure 9. PDB barrier deformation with small car A.

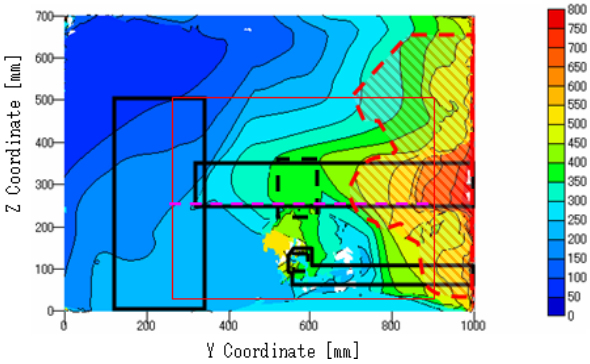

Figure 10. PDB barrier deformation with large car B.

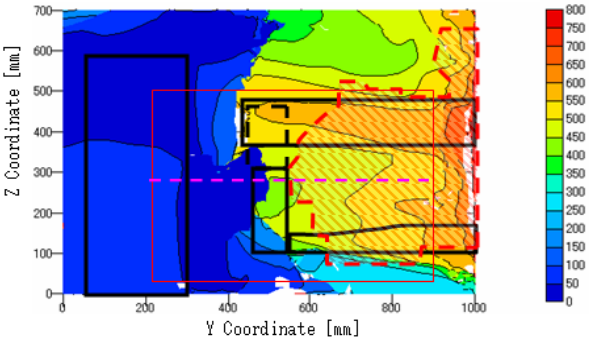

Figure 11. PDB barrier deformation with midsize SUV C.

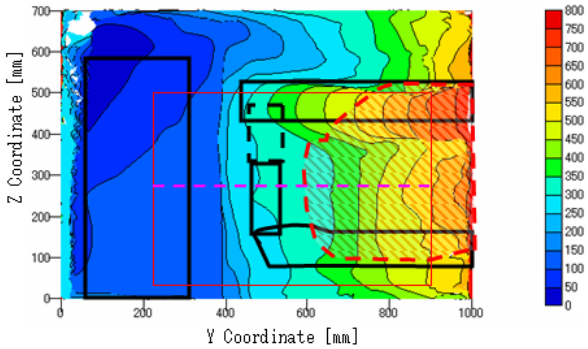

Figure12. PDB barrier deformation with midsize SUV D.

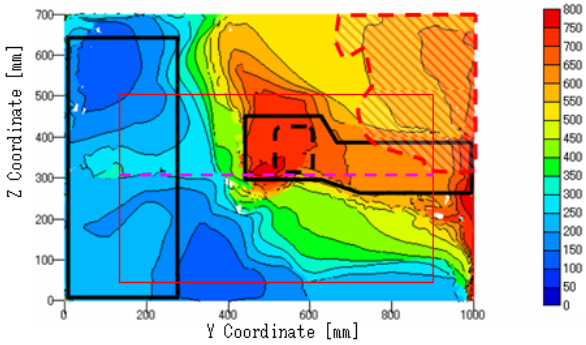

Figure13. PDB barrier deformation with large SUV E.

It is seen from the results in these figures that the transmission and the engine accounted for the greater part of the barrier deformation for many of the test vehicles. Because the AHOD parameter calculates the height of the average deformation in the investigation area, it is substantially influenced by the positions of the transmission and the engine. That is why all five test vehicles show similar AHOD values, regardless of the positions of their principal structural components. The presence of a lower load path is regarded as an important factor with respect to compatibility. However, no significant difference is seen in the

AHOD values between the vehicles with a lower load path (large car B, midsize SUV C and midsize SUV D) and those without one (small car A and large SUV E). These results indicate that it is difficult to detect the presence of a lower load path on the basis of the AHOD alone.

ADOD

The relationship between the ADOD and the test vehicle weight is shown in Fig. 14, and the relationship between the ADOD and the maximum PDB barrier force is shown in Fig. 15. The results indicate that the ADOD tended to increase with a heavier vehicle weight and a higher PDB barrier reaction force.

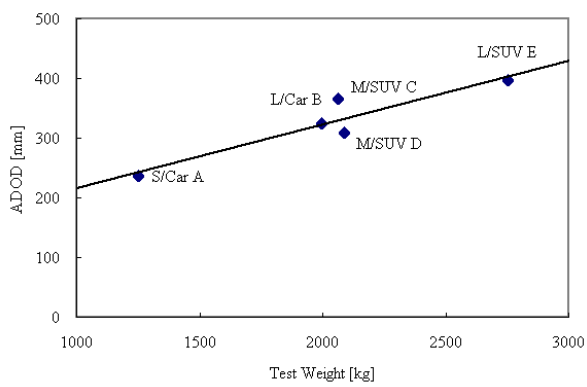

Figure 14. ADOD vs. test weight.

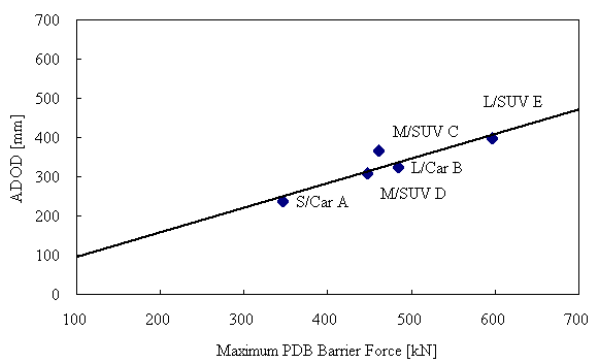

Figure 15. ADOD and maximum PDB barrier force.

An investigation was made of the general effect of changes in the vehicle weight and vehicle reaction force on the ADOD. The effect was considered in relation to the following patterns assumed for the characteristics of the PDB barrier reaction force and the vehicle reaction force.

Case 1: The ADOD increases to the extent of the increase in the vehicle reaction force.

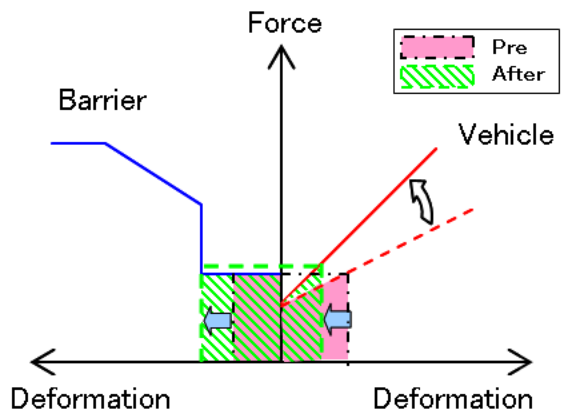

Figure 16. Deformation prediction for case 1.

Figure 16 illustrates the increase in the amount of barrier deformation (ADOD) corresponding to the increase in the vehicle reaction force. Since there is a proportional relationship between the vehicle reaction force and the ADOD, the latter value can be used in this case as a substitute for the former value.

Case 2: The ADOD increases only due to the influence of the increase in vehicle weight.

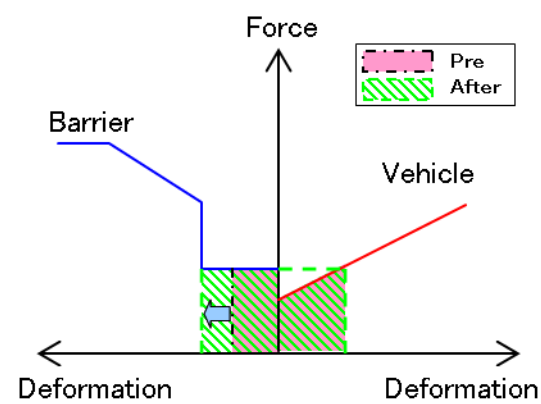

Figure 17. Deformation prediction for case 2.

Figure 17 shows a prediction of the barrier deformation in case 2 where the vehicle weight increases without any increase of the reaction force. In this case, the deformation of the barrier absorbs the increase in the kinetic energy due to the increased vehicle weight. In actuality, the vehicle also usually absorbs some of this kinetic energy, but this figure considers only the energy absorbed by the barrier to make the prediction easier to understand. The results for this case show that the ADOD increases when the

vehicle mass is simply increased without any change in the reaction force characteristic of the vehicle.

The factors defined for cases 1 and 2 are presumed to be the main reasons for the increase seen in the ADOD. In actuality, from the standpoint of self protection, the vehicle reaction force tends to increase with an increase of the vehicle mass. Accordingly, when these two factors occur simultaneously, the ADOD increases.

Case 3: There is little change in the ADOD despite an increase of the vehicle reaction force.

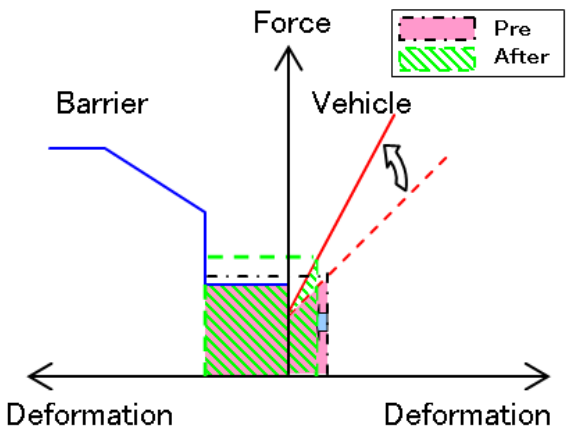

Figure 18. Deformation prediction for case 3.

Figure 18 shows the barrier deformation condition for case 3 in which the vehicle reaction force is increased further beyond the level in case 1. Even though the vehicle reaction force is increased in this case, the amount of barrier deformation does not increase appreciably and the ADOD shows little change in the range where the barrier strength increases rapidly.

In cases 2 and 3, the reaction force is not expressed correctly by the ADOD parameter. Similarly, the vehicle reaction force differs for the same ADOD between the case where the upper level of the second block is deformed and the case where the lower level is deformed. The reason for that is attributed to the difference in PDB characteristics between the upper and lower levels of the second block (Fig. 1). These factors presumably account for the cases where the ADOD values don't indicate the vehicle body stiffness accurately. Therefore, as a substitute for the vehicle reaction force, it is better to measure the barrier reaction force directly. Moreover, in order to take the kinetic energy into account, the vehicle weight should also be considered.

One point that is common to both the AHOD and ADOD parameters is that the necessary information cannot be obtained accurately on account of the averaging performed on the measured barrier deformation. The direct use of the maximum height of deformation or the maximum barrier force would provide more accurate information. In addition, the use of direct measurements would reduce the error due to the three-dimensional measurements of barrier deformation that are currently used in calculating these parameters.

EVALUATION OF PARTNER PROTECTION PARAMETERS USING VEHICLE-TO-VEHICLE TEST RESULTS

The parameters of partner protection were examined using the results of vehicle-to-vehicle frontal impact tests.

Vehicle-to-vehicle impact test conditions

The impact conditions used in the vehicle-to-vehicle tests are given in Table 2. Test 1 involved a frontal impact between the small car A and the large car B, and test 2 was between the small car A and the midsize SUV C. The overlap ratio was set at 50% of the small car A.

Table 3. Vehicle-to-vehicle impact conditions

Test	1		2	
Vehicle	Car A	Car B	Car A	SUV C
Test Weight	1203 kg	1996 kg	1202 kg	2058 kg
Impact Speed	50 km/h for each vehicle			
Overlap Ratio	50% of S/Car A			
Dummies	DR: Hybrid-Ⅲ AM50			
	PS: Hybrid-Ⅲ AM50			

Test Results

Structure deformation mode

The engine compartment deformation modes of the small car A and the large car B in the PDB test and the vehicle-to-vehicle impact test are shown in Figures 19 and 20, respectively.

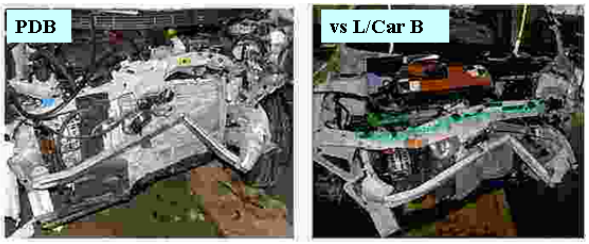

Figure 19. Small car A front deformation.

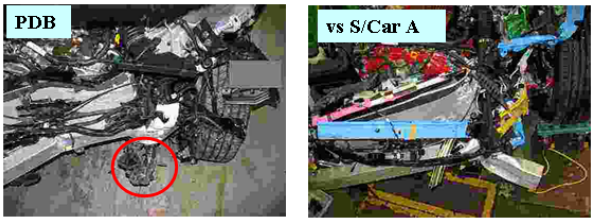

Figure 20. Large car B front deformation.

The results in Fig. 19 for the small car A show similar deformation modes for the longitudinal members in both tests in terms of their crush behavior.

On the other hand, the results in Fig. 20 for the large car B show that the lower members that served as the lower load path were partially crushed in the PDB test and fully crushed in the vehicle-to-vehicle test.

The engine compartment deformation modes of the small car A and the midsize SUV C in the PDB test and the vehicle-to-vehicle impact test are shown in Figures 21 and 22, respectively.

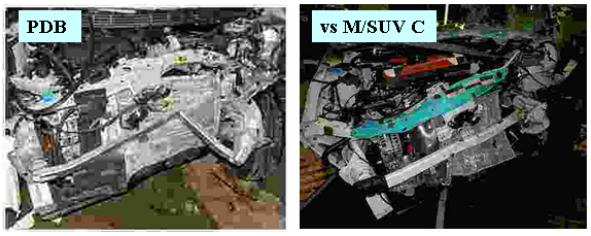

Figure 21. Small car A front deformation.

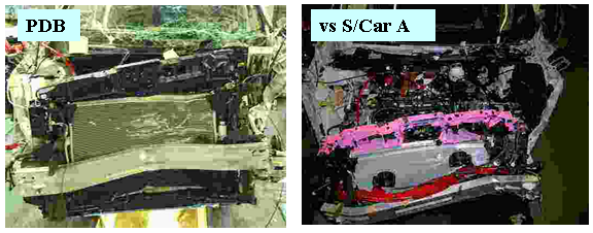

Figure 22. Midsize SUV C front deformation.

The results in Fig. 21 for the small car A indicate that the longitudinal members were more crushed in the vehicle-to-vehicle test, with the deformation mode differing from that of the PDB test. The reason for that is attributed to the good engagement of the structural components of the two vehicles during the impact in test 2 (small car A to midsize SUV C). The results in Fig. 22 for the midsize SUV C indicate that the deformation modes in the vehicle-to-vehicle and PDB tests were similar, which is attributed in part to the small amount of deformation that occurred in both tests. It is inferred from the overall results that the longitudinal members are more apt to display less deformation in a PDB test than in a vehicle-to-vehicle impact test.

Although the difference in the AHOD values of the vehicles was smaller in test 1 than in test 2, the structural members passed each other on the outside in the former test, while good structural engagement occurred in the latter test. Therefore, an assessment of structural engagement must take into account not only the vertical direction but also the horizontal direction.

Vehicle deformation

Figure 23 shows the relationship between the ADOD parameter, which indicates the vehicle stiffness, and the amount of deformation of the small car A in the vehicle-to-vehicle impact test.

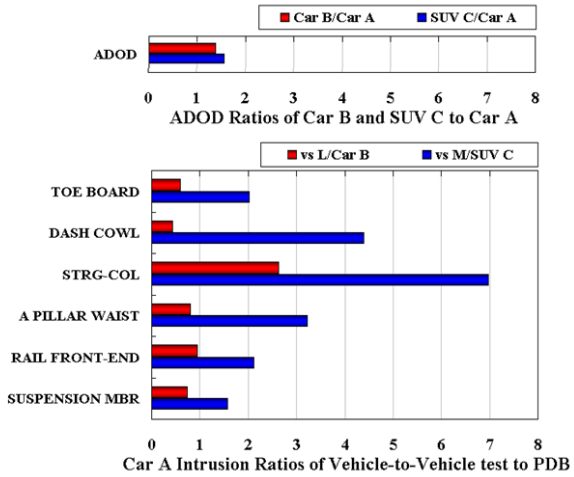

Figure 23. ADOD ratios and small car A intrusion ratios.

The upper graph in the figure shows the ratios of the ADOD values of the large car B and the midsize SUV C to that of the small car A. The lower graph shows the ratio of the body deformation of the small car A in the vehicle-to-vehicle impact test to that in the PDB test. The results in these graphs make it possible to compare the effect of the difference in the ADOD values on the amount of vehicle deformation in the vehicle-to-vehicle impact test. The comparison shows that as the ADOD ratio relative to the small car A increased, the

amount of deformation sustained by the small car A in the vehicle-to-vehicle impact test increased. However, the deformation ratios differed greatly. The reasons for that can be attributed to the differences in the following two points due to the variation in the engagement conditions during the impact:

(1) the reaction force generated in the vehicle and

(2) the crush stroke of the engine compartment in the impact.

As discussed here, because the amount of body deformation differs markedly depending on the engagement conditions, it is first necessary to make an assessment of the stable structural engagement between two colliding vehicles. In this case as well, the assessment should also take into account engagement in the horizontal direction.

EVALUATION OF PARAMETERS OF SELF PROTECTION

Comparison between The PDB Test and Current 64km/h Offset Barrier Test

The 60 km/h PDB test (60PDB) and the 64 km/h offset deformable barrier test (64ODB) currently conducted in many countries are compared here in terms of dummy injury measures, vehicle intrusion and energy absorbed by the barrier and the vehicle.

Dummy Injury Measures

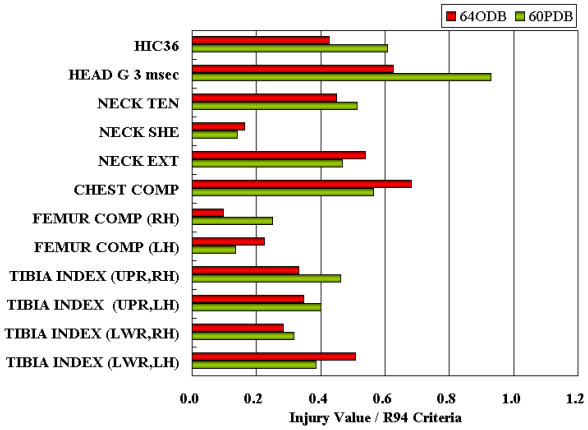

Figure 24. Small car A dummy injury measures.

The dummy injury measures shown in Fig. 24 for the small car A indicate that head injury values are higher in the 60PDB test than in the 64ODB test, but that the other values are nearly the same.

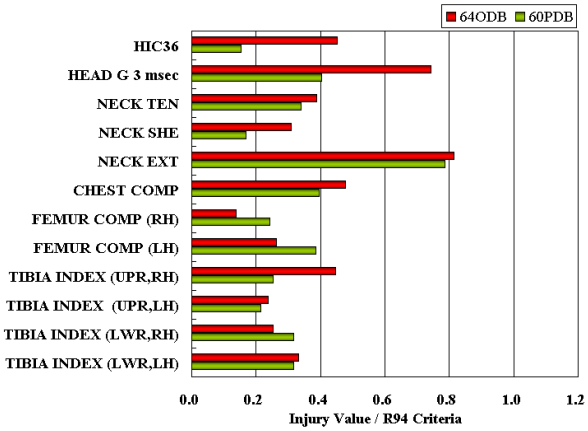

Figure 25. Large car B dummy injury measures.

For the large car B, head injury values are lower in the 60PDB test, while the other values are almost identical, as seen in Fig. 25. However, because the sitting position in the large car B in the 64ODB test differs somewhat from that in the 60PDB test, the injury values for the large car B are treated only as reference data.

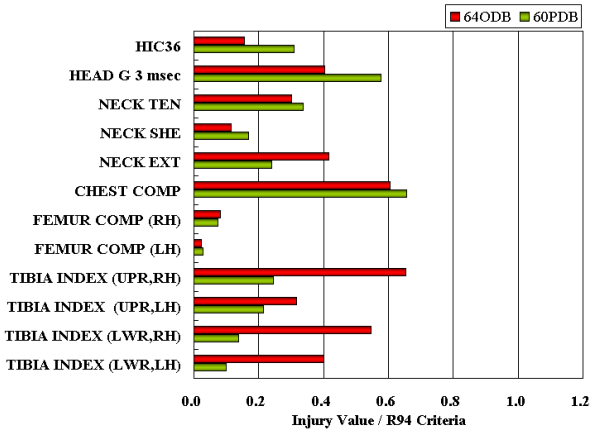

Figure 26. Midsize SUV C dummy injury measures.

The results in Fig. 26 for the midsize SUV C show that head injury values are slightly higher in the 60PDB test, but that all leg injury values are lower than in the 64ODB test.

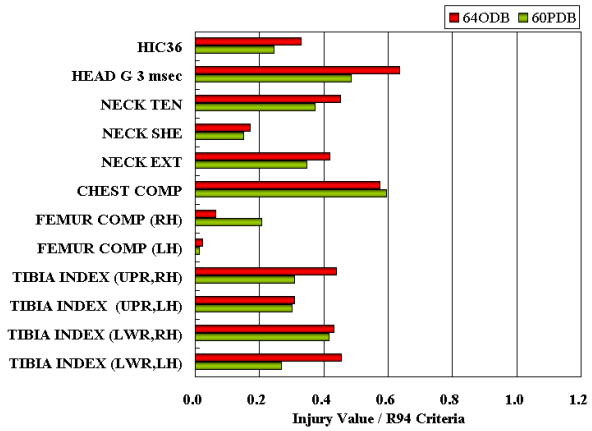

Figure 27. Midsize SUV D dummy injury measures.

As shown in Fig. 27 for the midsize SUV D, injury values tend to be lower overall in the 60PDB test, albeit only slightly.

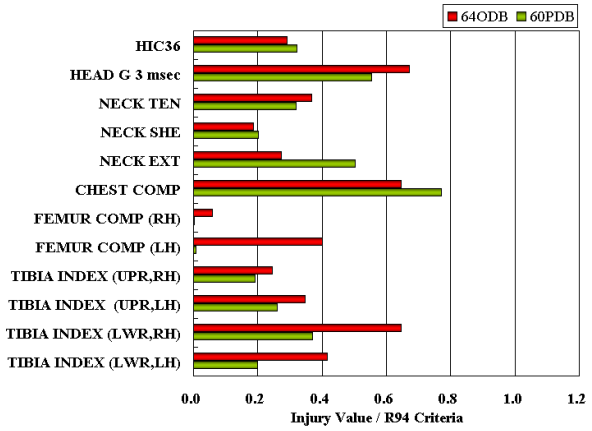

Figure 28. Large SUV E dummy injury measures.

The results for the large SUV E in Fig. 28 show that neck and chest injury values are somewhat higher in the 60PDB test, but that the injury values for the femur and tibia are generally lower than in the 64ODB test.

Because of the large variation in injury values, it is difficult to discern fine tendencies, but it is thought that the following observations can be made based on the results in these figures. For the small cars, both the 60PDB test and the 64ODB test tend to show almost the same injury values overall. As the vehicle size becomes larger, injury values mainly lower leg tend to be lower in the 60PDB test than in the 64ODB test.

Vehicle Intrusions

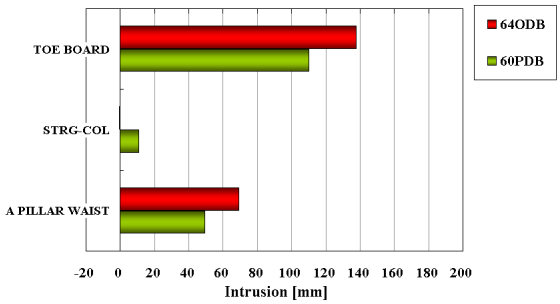

Figure 29. Small car A intrusions.

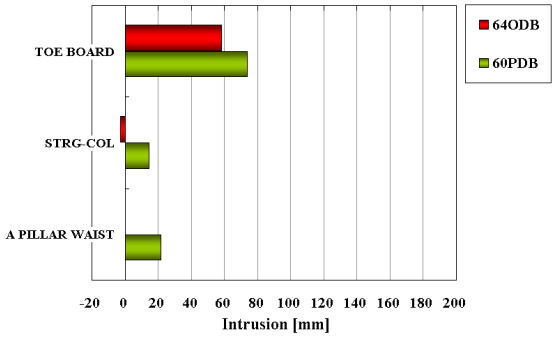

Figure 30. Large car B intrusions.

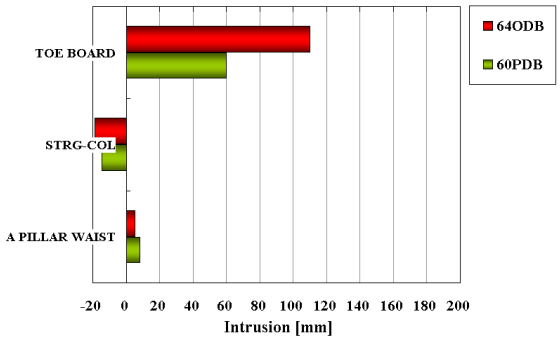

Figure 31. Midsize SUV C intrusions.

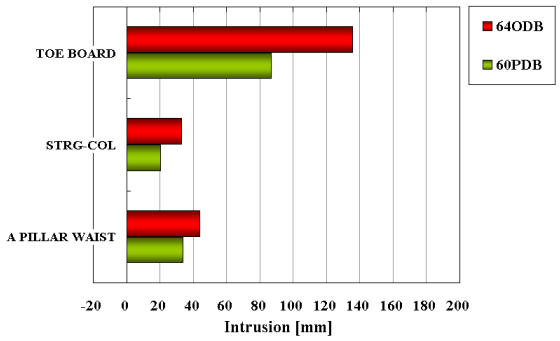

Figure 32. Midsize SUV D intrusions.

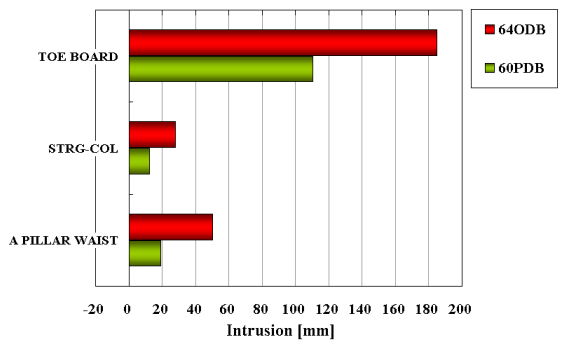

Figure 33. Large SUV E intrusions.

The intrusion data for each vehicle in the two tests are shown in Figures 29 to 33, respectively. No pronounced difference is seen in the intrusion data for the small car A and the large car B, but the intrusion values for the midsize SUV C, midsize SUV D and large SUV E are smaller in the 60PDB test than in the 64ODB test. The smaller amount of cabin intrusion that occurs with increasing vehicle size presumably accounts for the difference in injury values mentioned above, especially the difference in lower leg injury values.

Barrier Absorbed Energy

Figure 34 shows the amount of energy absorbed by the barrier in each test, as calculated from the amount of barrier deformation. A comparison of the values indicates that the barrier absorbed more energy in the 60PDB test than in the 64ODB test. This difference between the tests tended to increase as the size of the vehicle became larger. The reason why the amount of energy absorbed by the barrier did not increase with the larger vehicles in the 64ODB test is that the current barrier bottoms out with large vehicles. In contrast, because the barrier does not bottom out in the 60PDB test, the amount of energy absorbed by the barrier shows a pronounced increase for the larger vehicles.

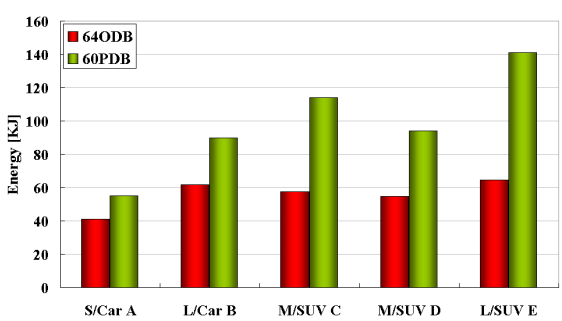

Figure 34. Barrier-absorbed energy.

Test Severity

Figure 35 shows the values of the Energy Equivalent Speed (EES) that were calculated based on the amount of energy absorbed by the vehicle in each test. The EES parameter expresses the amount of energy absorbed by a vehicle as the initial velocity at the time the vehicle crashes into a rigid barrier. It is given by Eq. (5) below.

$$EES(km/h) = 3.6 \times \sqrt{\frac{2 \times Eabs}{M}} \qquad (5)$$

Eabs = Energy absorbed by the vehicle [J]
= Kinetic energy – Energy in the barrier
M = mass of the vehicle [kg]

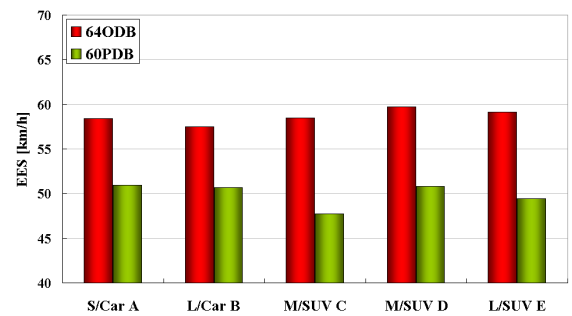

Figure 35. Energy Equivalent Speed.

The EES values for each vehicle were in a range of 57-60 km/h in the 64ODB test and 47-51 km/h in the 60PDB test. In order to examine the overall tendencies more closely, the number of vehicles (n) was increased by adding test data for other vehicle models. The relationship between the EES and test vehicle weight is shown in Fig. 36, which includes data obtained in 56 km/h offset deformable barrier (56ODB) tests using the current barrier.

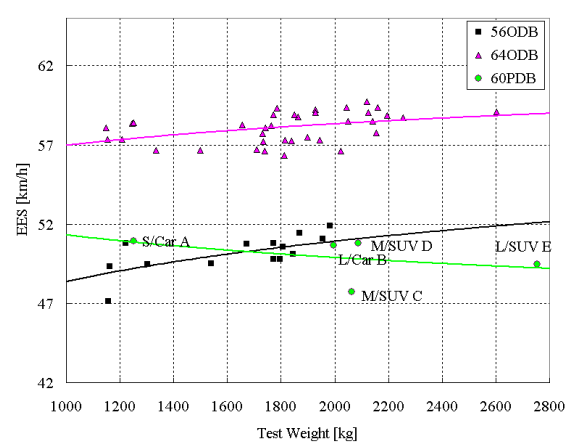

Figure 36. EES and test weight.

The data for the 64ODB test and 56ODB test show a gradual rise in the EES with increasing vehicle weight, whereas the 60PDB test data show a gradual decrease. As a result, the difference in the EES values between the 64ODB test and the 60PDB test becomes greater as the vehicle weight increases. This tendency explains the reason why the 64ODB and 60PDB tests showed a greater difference in the amount of vehicle deformation as the vehicle size increased. Between the 56ODB test that is the current regulatory test in Europe and the 60PDB test, the EES values become equal at around a test vehicle weight of 1,700 kg. For heavier vehicles above that level, the EES values are lower in the 60PDB test than in the 56ODB test. In connection with the introduction of the 60PDB test, it has been proposed this test replace the current regulatory 56ODB test at the initial stage. In that case, it is possible that the self protection performance of large vehicles would fall below the current assessment.

The United States, Japan and many other countries, excluding Europe, currently conduct Full Width Rigid Barrier (FWRB) tests and Offset Deformable Barrier (ODB) tests. In a FWRB test, because a wide area of the test vehicle's front end is crashed into the barrier, the amount of deformation is smaller and a higher deceleration pulse is generated in the vehicle. This test is designed to evaluate occupant protection performance, particularly that of the occupant restraint systems. In an ODB test, on the other hand, the input force is concentrated on one side of the test vehicle. This test is designed to evaluate occupant protection performance mainly in terms of the cabin strength.

The severity of the 60PDB test conditions was examined in relation to the FWRB and ODB test conditions. Figure 37 shows the forward displacement of the B-pillar as a function of the average G of the test vehicle in each test. The data used here for the FWRB test are for an impact velocity of 56 km/h (56FWRB) .

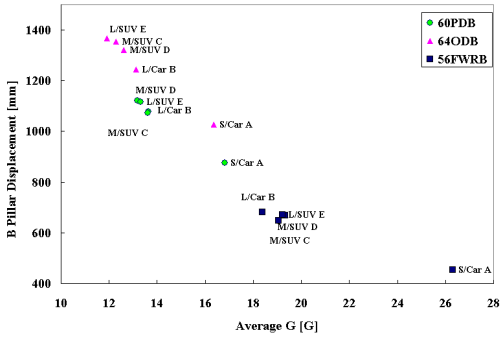

Figure 37. B pillar displacement and average G.

The data points for the PDB tests are generally located between the FWRB and ODB tests in Fig. 37. Conducting both the offset and full width barrier tests verifies the cabin strength and also confirms occupant protection performance based on the high deceleration pulse. Safety performance can thus be confirmed over a wider range of conditions compared with the verification of crashworthiness based on the PDB test alone.

CONCLUSIONS

Partner protection

•The Average Height of Deformation (AHOD) is strongly influenced by the engine and transmission and does not express the positions of the principal structural components such as the longitudinal members.

•The Average Depth of Deformation (ADOD) does not always indicate the vehicle body stiffness accurately.

•Because both the AHOD and ADOD parameters are found by averaging measured barrier deformation data, they do not accurately indicate the height or force of the structural components. Therefore, it is necessary to consider some other more direct methods of measurement such as directly measuring the barrier force.

•Evaluating the engagement of the structural components of two colliding vehicles is an important factor in assessing partner protection. Such engagement must be assessed in both the vertical and horizontal directions.

Self protection

•A comparison of the Energy Equivalent Speed (EES) values indicates that the current regulatory 56 km/h Offset Deformable Barrier (56ODB) test is more severe for heavier vehicles (a test vehicle weight of around 1,700 kg or more) than the Progressive Deformable Barrier (PDB) test. It is possible that the introduction of the PDB test to replace the current regulatory test might result in the self protection performance of heavier vehicles being evaluated at a lower level than at present.

•Conducting both the Full Width Rigid Barrier (FWRB) test and the ODB test makes it possible to verify the cabin strength and to confirm occupant protection performance based on the high deceleration pulse. This facilitates confirmation of crashworthiness over a wider range of conditions than what is possible on the basis of the PDB test alone.

Because the PDB test has many issues, it will be necessary to make further evaluations using a larger

number of vehicles. Moreover, it will be necessary to examine what effect the introduction of the PDB test might have on safety performance in real-world accidents.

REFERENCES

[1] Ablaßmeier, W., et al., "Opportunities for a Worldwide Compatibility Evaluation", 20th International Conference on the Enhanced Safety of Vehicles, Paper No. 07-0331, Lyon, France, 2007.

[2] Donat, C., et al., "Methodological Physical Analysis of FWDB and PDB Test Procedures Regarding Incompatible Physical Phenomena Observed in Real Car Accident", 20th International Conference on the Enhanced Safety of Vehicles, Paper No. 07-0244, Lyon, France, 2007.

[3] Delannoy, P., et al., "Comparative Evaluation of Frontal Offset Tests to Control Self and Partner Protection", 19th International Conference on the Enhanced Safety of Vehicles, Paper No. 05-0010, Washington, D.C., 2005.

[4] Mizuno, K., et al., "Japan Research on Compatibility Improvement and Test Procedures", 19th International Conference on the Enhanced Safety of Vehicles, Paper No. 05-0185, Washington, D.C., 2005.

[5] Faerber, E., et al., "EEVC Approach to Develop Test Procedure(s) for the Improvement of Crash Compatibility Between Passenger Cars", 20th International Conference on the Enhanced Safety of Vehicles, Paper No. 07-0331, Lyon, France, 2007.

[6] ECE/TRANS/WP.29/GRSP/2007/17

[7] PDB test protocol – EEVC WG15 website, www.eevc.org.

A PROPOSAL FOR AN IMPROVED METHOD OF EVALUATING VEHICLE COMPATIBILITY IN FULL-FRONTAL RIGID BARRIER TESTS

Akira Yamaguchi
Atsushi Hitotsumatsu
Tomosaburo Okabe
NISSAN MOTOR CO., LTD.
Japan
Paper Number 09-0110

ABSTRACT

In frontal collisions, injury risk can be reduced if the front body structure is able to absorb a greater amount of energy. In general, however, in front-to-front collisions between different-size vehicles, the smaller, lighter vehicle sustains greater damage than the larger, heavier one. To help improve vehicle compatibility in front-to-front collisions between such vehicles, what is required is better matching of the geometry and stiffness of the front structures of the colliding vehicles.

Several methods of measuring the geometry and stiffness of front structures have previously been reported. Among these are the AHOF400 and Kw400 metrics, which are measured in full-frontal rigid barrier tests using high-resolution barrier load cells. This paper proposes an improved method for evaluating compatibility in full-frontal rigid barrier tests based on a review of the purposes of and issues with the AHOF400 and Kw400 metrics.

The methods proposed in this paper are intended to help provide an improved compatibility assessment compared with the AHOF400 and Kw400 metrics by evaluating the forces on load cells in an area defined as the structural interaction zone. Like AHOF400 and Kw400, the aim of this research is to improve structural engagement and energy sharing in the event of a front-to-front collision.

INTRODUCTION

In front-to-front collisions involving vehicles of different sizes, the smaller vehicle tends to sustain greater damage because of the differences in mass and stiffness between the two vehicles. To help improve this situation, the front-end structures of both vehicles should deform appropriately to absorb more crash energy. In order to promote deformation of the front-end structures, they must be positioned so that they engage during collision and should be of similar stiffness. These aspects of compatibility are already widely known. Various organizations have reported methods for evaluating the height and stiffness of front-end structures for assessing compatibility.

One proposed approach to evaluating the height and stiffness of front-end structures is to use the AHOF400 and Kw400 metrics computed on the basis of barrier force data measured under the current US NCAP test conditions [1]-[2].

The AHOF400 metric is designed to evaluate the height (geometry) of front-end structures. To obtain force data for the calculation, load cells are positioned on the barrier so as to cover the entire front-end of the test vehicle. The Average Height of Force (AHOF) is calculated using the force measured with each load cell and the height of each load cell from the ground. The resultant AHOF value is a hypothetical average height of applied force and frequently does not indicate the actual height of the front-end structures.

The Kw400 metric, on the other hand, is designed to evaluate the stiffness of front-end structures. It indicates the force level calculated from the forces measured with all the load cells positioned so as to cover the entire front-end of the test vehicle, the same as for AHOF. The Kw400 value also includes forces other than those of the engaging front-end structures of the two vehicles involved in a car-to-car (CTC) frontal impact.

A limitation common to both AHOF400 and Kw400 is that one evaluation parameter is calculated from the force data of all the load cells. Consequently, the engaging structures of the two vehicles in a CTC frontal impact cannot be identified by the AHOF400 metric and the stiffness of the engaging structural components cannot be evaluated directly by the Kw400 metric.

We have researched an evaluation method that attempts to resolves these limitations. Our proposed

method defines a structural interaction zone in which the front body structures serve to manage the crash energy in a CTC frontal impact. Rather than calculating an evaluation parameter from the forces measured with all the load cells, our method evaluates the force loads within and outside the interaction zone separately. This approach makes it possible to estimate and compare the approximate force level that would be generated by each vehicle in a CTC frontal impact.

As for the test conditions for evaluating compatibility, this study focused on the current US NCAP test conditions that are used in calculating AHOF400 and Kw400. These conditions specify a full-frontal test using a rigid barrier instrumented with 125 mm x 125 mm load cells. The issues inherent in the method of evaluating AHOF400 and Kw400 under these test conditions were identified. An improved method for resolving these issues was then researched.

GEOMETRY EVALUATION: ISSUES WITH AHOF400

The AHOF400 metric for evaluating the height of front body structures is a parameter of the average height of force that is calculated using the individual force values measured with all of the load cells and the height of each load cell from the ground. The load cells are positioned on the barrier so as to cover the entire front-end of the test vehicle as shown in Fig. 1. One concern with this metric is that it is not known whether the front-end structures are actually at the height indicated by AHOF400. For example, light trucks or vans (LTVs) have a relatively high hood, so good engagement of the hood with the front-end structures of a passenger car cannot be expected. However the hood height influences the AHOF400 value. Moreover, although higher structures tend to have a lower probability of engagement with the other vehicle, as the height of the structure increases its proportional influence on AHOF400 also increases due to the calculation method.

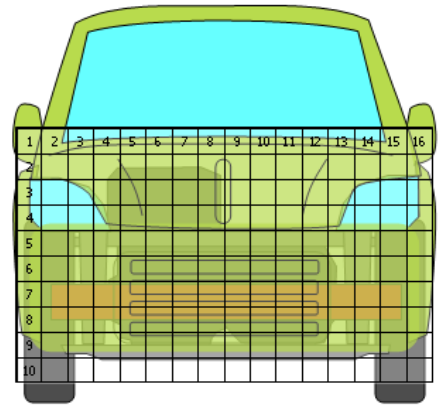

Fig. 1 Vehicle front-end and multi-load cell barrier

$$\mathbf{HOF}\,(x) = \sum_{i=1}^{n} f_i(x) \cdot H_i(x) \Big/ \sum_{i=1}^{n} f_i(x) \qquad (1)$$

where fi(x) is the force measured with a load cell and Hi is the height of each load cell.

$$\mathbf{AHOF400} = \sum_{x=25mm}^{400m} HOF(x) \cdot F(x) \Big/ \sum_{x=25m}^{400m} F(x) \qquad (2)$$

where F(x) is the vehicle force computed from the forces measured with all the load cells.

$$F(x) = \sum_{i=1}^{n} f_i(x)$$

Figure 2 shows the positional relationship between the main frame of the LTV used in the finite element analysis (FEA) conducted in this study and the barrier load cells, when the bottom of the barrier was at a height of 80 mm from the ground. The AHOF400 values are given in Table 1. The main frame of this LTV was positioned approximately in the center of the Part 581 zone, and the AHOF value calculated from the forces on all the load cells was 526 mm. That value was higher than the top of the Part 581 zone. An AHOF400 value of 503 mm was calculated for a hypothetical condition that excluded the forces on the top two rows of load cells corresponding to the hood height of this LTV. The latter AHOF value was located in the Part 518 zone. In other words, in order to position the AHOF400 value in the center of the Part 581 zone on this LTV, the height of the main frame would have to be lower than the center of the zone because of the influence of the hood height on

increasing the AHOF400 value. This same result has been reported in the literature [3].

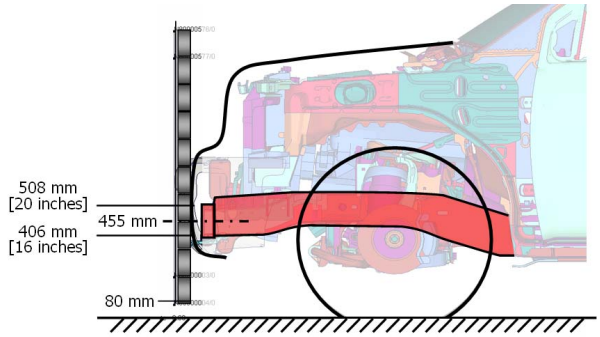

Fig. 2 Frame height on LTV used in FEA

Table 1 Calculated AHOF400 results

	AHOF
Forces on all load cells	526 mm
Forces on load cells excluding top 2 rows	503 mm

STIFFNESS EVALUATION: ISSUES WITH KW400

One issue with the Kw400 metric for evaluating the stiffness of front-end structures is that it is not as accurate as we could want in evaluating the actual stiffness levels of the engaging structures of the two vehicles in a CTC frontal impact. For example, the stiffness of the hood of the above-mentioned LTV would be included in the Kw400 value even though it would not likely be engaged with the front-end structures of a passenger car in an actual CTC frontal impact.

The equation for calculating Kw400 can be rewritten as shown below, which indicates that it is equivalent to evaluating the average force (Favr) in an evaluation range of 25 mm to 400 mm of vehicle displacement.

Kw400 is given as:

$$\mathbf{Kw400} = 2\int_{25mm}^{400mm} F(x)\,dx \Big/ [(400)^2-(25)^2] \qquad (3)$$

Favr is given as:

$$\mathbf{Favr} = \int_{25mm}^{400mm} F(x)\,dx \Big/ (400-25) \qquad (4)$$

Hence, Kw400 is proportional to Favr.

$$\mathbf{Kw400} = \frac{2 \cdot \mathbf{Favr}}{(400+25)} \propto \mathbf{Favr} \qquad (5)$$

Accordingly, the following issues can be envisioned.

(1) For example, depending on the size of the energy-absorbing bumper components within evaluation range installed for pedestrian protection, the Kw400 value will vary even at the same levels of vehicle stiffness as shown in Fig.3.

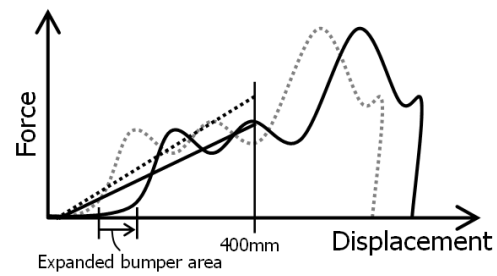

Fig. 3 Influence of bumper on Kw400

(2) The engine inertial force will be included in the Kw400 value in the case of small vehicles with a short front body, but it will not be included for large vehicles having a long front body. Accordingly, Kw400 values will not reflect the relationship of the actual vehicle body stiffness for those vehicles.

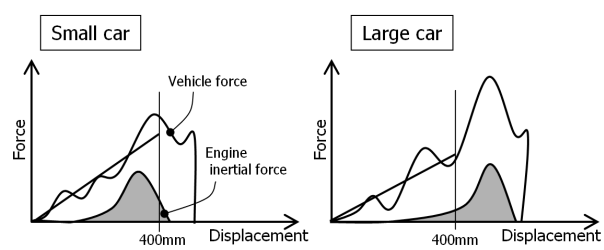

Fig. 4 Influence of engine inertial force on Kw400

Let us reconfirm here once again the issue of stiffness in vehicle compatibility. The rational requirements for compatibility can be summed up as follows. The front body of large cars having relatively high levels of stiffness must deform sufficiently, and small cars having relatively low levels of stiffness must have sufficient cabin stiffness to be able to deform the front body structures of large cars. In other words, an evaluation based on the peak force produced by the

engaging front-end structures of the two colliding vehicles is assumed to provide a better assessment of whether one vehicle body is crushed by the other vehicle than an evaluation of the average force of the vehicles in a certain given evaluation range, for example that of the Kw400 metric.

An evaluation range up to 400 mm of vehicle displacement may be suitable for evaluating the front body structures of large vehicles for which the high levels of force produced are generally the concern. However, for small vehicles for which the low levels of stiffness are the concern, evaluations should be made in a range up to the largest displacement under the NCAP conditions including consideration of the cabin stiffness. The new evaluation method proposed here is outlined in Fig. 5. The upper force limit is regarded as the peak force that occurs in an evaluation range up to 400 mm of vehicle displacement; the lower force limit is regarded as the peak force that occurs in an evaluation range up to the largest amount of vehicle displacement. The use of these rational force limits resolves the two concerns mentioned above.

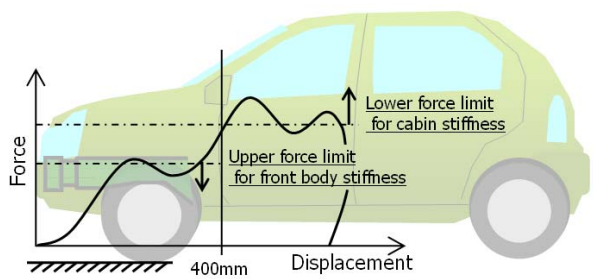

Fig. 5 Overview of new evaluation method

Let us also consider the issue of front end stiffness and self protection in the case of large vehicles. For good compatibility, the front body structures should be designed so that they deform easily while suppressing the peak force of each structure. On the other hand, to obtain the desired self protection performance, the front body structures must be capable of absorbing a certain level of impact energy. In other words, the vehicle force-displacement characteristic of large vehicles should have a rectangular curve exhibiting a low level of peak force and a high level of energy absorption. However, as shown in Fig. 6, the value of Kw400 increases as the force-displacement characteristic approaches a rectangular curve, even though the peak force generated is the same. That is because Kw400 is proportional to the average force and it causes misunderstanding as if it resulted in higher aggressivity.

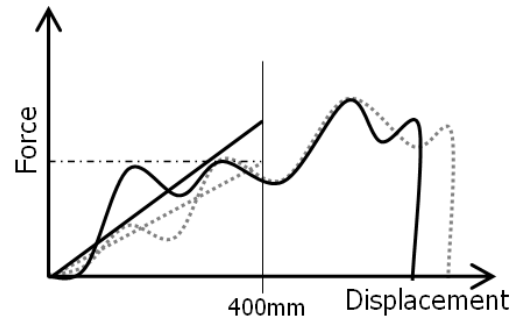

Fig. 6 Relationship between peak force in evaluation range and Kw400

BASIC CONCEPTS OF PROPOSED METHOD

The improved evaluation method researched in this study consists of the following three concepts.

(1) An interaction zone is defined in which energy management is performed by the front body structures that would be engaged in an actual CTC frontal impact.

(2) An evaluation is made of the combined force of the individual rows of barrier load cells corresponding to the interaction zone. This force is referred henceforth as the interaction force.

(3) An optional test is conducted to evaluate the interaction force in cases where it cannot be accurately detected in a full-frontal rigid barrier test. This optional test uses load cell rows 3 and 4 that are defined as the interaction zone extending from a rigid wall.

With regard to the third concept here, there is the concern that the load cells on a fully flat rigid barrier cannot accurately detect the stiffness of front body structures that are set more rearward among the many structural parts composing the front end of a vehicle. Consequently, the force in the interaction zone might not be detected accurately in cases where high levels of force are generated in areas outside the zone. This problem has been resolved by introducing the concept of the override barrier test proposed by the U.S. National Highway Traffic Safety Administration (NHTSA) [1]. The interaction force is then re-evaluated in a test conducted with the height of the contoured barrier set to match the interaction zone.

The three concepts of the proposed evaluation method are explained in detail in the following sections.

DIFINITION OF THE INTERACTION ZONE

Figure 7 shows the positional relationships of the 125 mm x 125 mm load cells, the Part 581 zone and the geometry requirements specified in the "Enhancing Vehicle-to-Vehicle Crash Compatibility" voluntary industry agreement in the U.S, when the bottom of the rigid barrier is set at 80 mm from the ground. Based on these two requirements that have already been introduced, the interaction zone can be appropriately defined as rows 3 and 4 of the load cells.

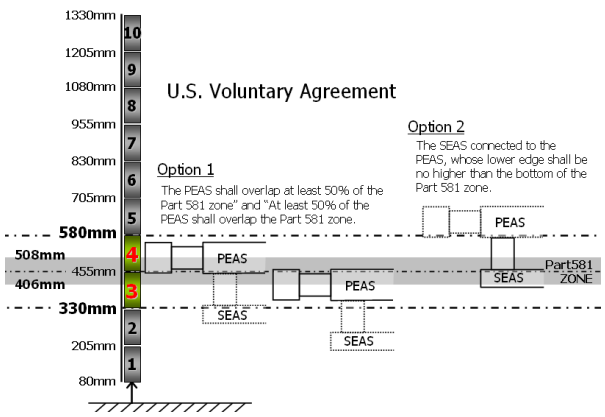

Fig. 7 Relationship between load cells, Part 581 zone and geometry requirements of U.S. voluntary agreement

EVALUATION OF INTERACTION FORCE

In order to determine a criterion for evaluating the interaction force, it is necessary to conduct accident analyses to examine the actual benefits under real-world conditions. An investigation was made of a force criterion that was deemed suitable with respect to the predicted real-world benefits reported in reference [2] concerning NHTSA's Kw400 metric.

In reference [2], Kw400 values above 1318 N/mm are defined as the High zone, values between 1004 and 1318 N/mm as the Medium zone and values below 1004 N/mm as the Low zone. A study was made of the effect on the injury rates sustained in large and small vehicles in CTC frontal impacts when categorized in terms of these zones. When the zones are divided on the basis of these criteria, it has been reported that injury rates are lower if the Kw400 values of the colliding vehicles are in the same zone than if their Kw400 values are in different zones.

In reference to these results, the relationship between the combined force on rows 3 and 4 of the load cells, which were defined here as the interaction zone, and Kw400 was plotted in a graph. An investigation was then made of the improvement effect that might be expected with the evaluation method researched in this study.

Figure 8 shows Kw400 as a function of the peak combined force generated on rows 3 and 4 of the load cells in a range of 25 to 400 mm of vehicle displacement, which is the same evaluation range used for the Kw400 metric. This relationship is shown in the figure for a total of 29 tests, 18 of which were conducted in-house at Nissan and 11 of which were NHTSA's research tests.

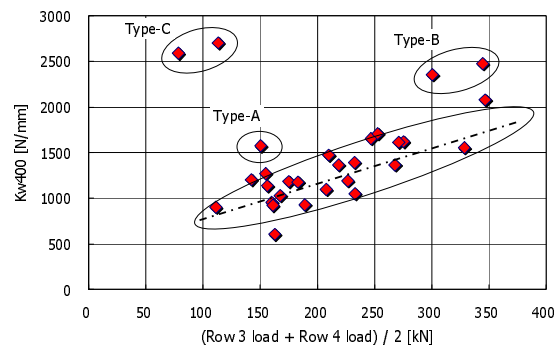

Fig. 8 Relationship between Kw400 and combined force on load cell rows 3 and 4

As noted above, Kw400 indicates the level of the average force in a vehicle displacement range of 25 to 400 mm. With the current vehicle body construction, the main frame usually generates the greater part of the vehicle force that occurs in the first half of an impact. When the main frame is located in the interaction zone, the vehicle force and the combined force on rows 3 and 4 show close values. Moreover, when the vehicle force and the combined force on rows 3 and 4 show linear curves, the value obtained by dividing the peak combined force by two is close to the average force. That is why a good correlation is seen in Fig. 8 between Kw400 and the value obtained by dividing the peak combined force on rows 3 and 4 by two.

It is known that the Type-A and Type-B vehicles that deviate from this correlation in Fig. 8 have the following characteristics:

Type-A: The vehicle's main frame is located outside the interaction zone.

Type-B: The vehicle's force characteristic is not a linear function that increases monotonically.

Type-C: A composite of Type-A and Type-B

The force-displacement curves of the vehicle group with a good correlation (normal type), Type-A vehicles and Type-B vehicles are shown in Figs. 9-11, respectively.

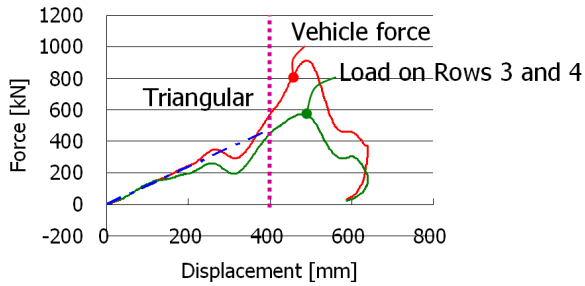

Fig. 9 Force-displacement curves for Normal-type vehicles

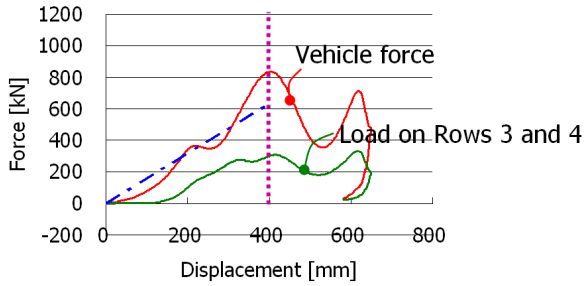

Fig. 10 Force-displacement curves for Type-A vehicles

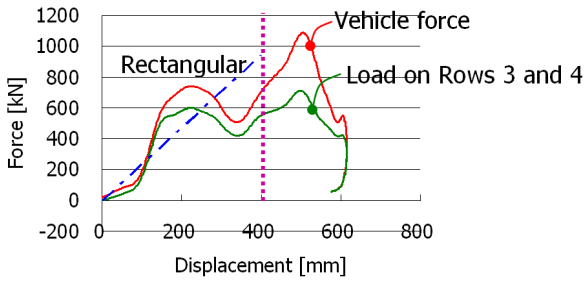

Fig. 11 Force-displacement curves for Type-B vehicles

For the vehicles classified as Type-A in Fig. 10, it is seen that a high level of force is generated outside the interaction zone. As a result, the combined force on rows 3 and 4 is smaller than the total force of all the load cells used in calculating Kw400. In this case, due to the poor engagement of the front-end structures, the force that occurs in an actual CTC frontal impact is assumed to be less than the total force of all the barrier load cells, i.e., the value of Kw400. It is possible that the combined force on rows 3 and 4 reflects the force actually produced in a CTC frontal impact better than Kw400. With the evaluation method researched in this study, the vehicles classified as Type-A would also be subjected to an override barrier test or some other optional evaluation to re-assess the combined force on rows 3 and 4 of the load cells.

As shown in Fig. 11, the vehicles classified as Type-B show a force characteristic curve that is almost rectangular, not linear. As was noted earlier, whether or not one vehicle unilaterally crushes the partner vehicle in a CTC frontal impact is presumably determined by the difference in stiffness between the two vehicles. Accordingly, it is probably determined by the peak force rather than by the average force such as that represented by Kw400.

As discussed here, there is a correlation between Kw400 and the peak combined force on rows 3 and 4 of the load cells. Even in cases which deviate from that correlation, it is possible that the combined force on rows 3 and 4 is a better representation of compatibility in an actual CTC frontal impact than the Kw400 value. Therefore, it can be estimated that the proposed evaluation method can probably obtain a real-world improvement effect equal to or greater than that reported in research studies concerning Kw400.

OPTIONAL TEST FOR DETECTION AND EVALUATION OF INTERACTION FORCE

As noted above, one concern with the proposed method is that the interaction force might not be detected accurately in a rigid barrier test. In order to resolve this concern, it is necessary to re-evaluate the force in the interaction zone by conducting an optional test such as the override barrier test proposed by the NHTSA. The necessity of conducting an optional evaluation is determined by whether forces outside the interaction zone are higher than the interaction force, regardless of whether the interaction force satisfies the specified force criterion or not.

Here we will consider a hypothetical case like that shown in the upper diagram in Fig. 12 where the position of the main frame corresponds only to row 4 of the load cells and does not overlap either row 3 or row 5. In this case, the combined force generated by the front-end structure on rows 3 and 4 divided by two is equal to the combined force on rows 4 and 5 divided by two. On the other hand, if the front-end structure overlaps row 5 even by a little (lower diagram in the figure), the combined force on rows 4 and 5 divided by two will be larger than the combined force on rows 3

and 4 divided by two. In other words, if the combined force on row n and row n+1 (n>4) divided by two is greater than that on rows 3 and 4 divided by two, the front-end structure is deemed to be positioned higher than row 4. In this case, the force in the interaction zone must be re-evaluated by conducting an override barrier test. This additional override barrier test results in a compound evaluation that includes not only a stiffness assessment but also a geometry assessment like that of the AHOF400 metric.

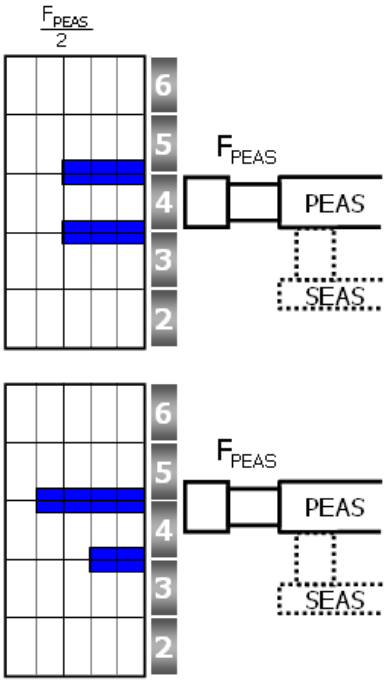

Fig. 12 Relationship between PEAS height and force generated on load cells

SUMMARY OF IMPROVED EVALUATION METHOD

The features of the improved evaluation method researched in this study are summarized below.

(1) Compatibility is evaluated using the interaction force, which is the value obtained by dividing the peak combined force on rows 3 and 4 of the load cells by two.

(2) An upper force limit is defined for the front body structure as the stiffness requirement. Because the objective is to evaluate the front body structure, the evaluation range is defined as the first half of the impact for vehicle displacement up to 400 mm, which is the same, for example, as that used for AHOF400 and Kw400.

(3) If force exceeding the interaction force is generated outside the interaction zone, which is defined as rows 3 and 4 of the load cells, an override barrier test is conducted to re-evaluate the interaction force. This test is conducted using a barrier that extends above the height of the interaction zone.

Based on the relationship between Kw400 and the interaction force, the medium zone of Kw400 reported in the literature serves as a reference for setting the evaluation criterion for the interaction force. However, the lower force limit must be examined anew because of the difference in the evaluation range. Similarly, the force criterion used in the override barrier test must take into account the differences in the test conditions.

EVALUATION RESULTS FOR UPPER FORCE LIMIT ONLY

It was shown above that there is a correlation between Kw400 and the interaction force, which is defined here as the combined force on rows 3 and 4 of the load cells. Accordingly, it was explained that the use of the interaction force can also be estimated to achieve a real-world improvement equal to or better than that assumed to be achievable with Kw400. To validate this hypothesis, the stiffness of the front body structure was evaluated using 300 kN as the upper limit of the interaction force in a vehicle displacement range up to 400 mm. This upper limit was set in reference to the average force (280.075 kN) obtained with Eq. (5) from the upper limit reported for the medium zone (1004-1318 N/mm) of Kw400. The results obtained are explained below.

Figure 13 shows the evaluation results obtained in tests conducted in-house at Nissan and in NHTSA's research tests. The types of vehicles evaluated and their test weights are also shown. Vehicles labeled with the letter "A" were ones for which the interaction force exceeded 300 kN. Vehicles labeled with the letter "B" were ones for which a re-evaluation of the interaction force in an override barrier test was deemed necessary because force higher than the interaction force occurred outside the interaction zone.

The results indicate that a re-evaluation in an override barrier test was necessary for the LTVs, which generally have a higher frame height. In addition, the results also identify several large LTVs for which a reduction in vehicle body stiffness would be necessary

according to the above criteria.

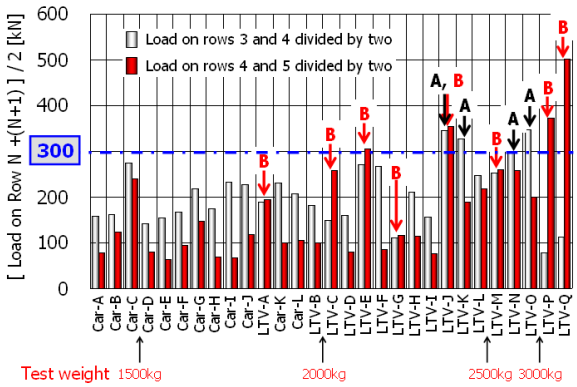

Fig. 13 Evaluation results of front body stiffness

CONCLUSION

This paper has described certain issues in evaluating vehicle compatibility with the AHOF400 and Kw400 metrics in full-frontal rigid barrier tests. A new compatibility evaluation method was presented that was researched in this study for the purpose of resolving these issues. The AHOF400 and Kw400 metrics represent separate parameters that are applied to evaluate geometry and stiffness, respectively. With the method proposed here, the impact forces inside and outside a defined structural interaction zone are evaluated separately. The proposed method was applied to evaluate a front body stiffness based on an upper force limit. The results showed that the proposed method can evaluate both geometry and stiffness simultaneously.

The real-world improvement effect that might be obtained with the proposed evaluation method was estimated only in an evaluation of the upper force limit of the front body structure in reference to research reports concerning Kw400. In future work, it will be necessary to conduct accident analyses that take into account the lower force limit in order to investigate a force criterion capable of yielding real-world benefits. In addition, it will be necessary to confirm whether the evaluation results are consistent with the compatibility shown in actual CTC frontal impacts by the vehicles sampled in this study. The accuracy of the proposed evaluation method must also be improved by increasing the number of vehicles considered.

REFERENCES

[1] Sanjay Patel., et al., "NHTSA's Recent Vehicle Crash Test Program on Compatibility in Front-to-Front Impacts", 20th International Conference on the Enhanced Safety of Vehicles, Paper No. 07-0231, Lyon, France 2007.

[2] John C. Brewer, et al., "Preliminary Evaluation Methodology in Front-Front Vehicle Compatibility", 2007 SAE, Paper No. 08B-401.

[3] Hayata Uwai, et al., "A Study on AHOF400 Which Is Possible Car to SUV Compatibility Evaluation Method", 20th International Conference on the Enhanced Safety of Vehicles, Paper No. 07-0391, Lyon, France, 2007.

NUMERICAL SIMULATION OF CRASH-TEST FOR A FORMULA SAE CAR

Simonetta Boria
Giuseppe Forasassi
University of Pisa
Pisa
Paper Number 09-0152

ABSTRACT

Crash-tests and numerical simulations are vital sources of information for designing car safety elements. The aim of this study is the design of a crash-box for a Formula SAE car and the investigation, through a numerical approach, of its dynamic behaviour in frontal impact conditions. The impact attenuator is obtained by the combination of honeycomb sandwich panels and aluminium sheets. Firstly experimental tests and numerical analysis on honeycomb structures were carried out in order to better understand their behaviour and model them properly. Afterwards a global 3D model was built and discretized with finite element method (FEM) in the Ansys code, while the simulation of the crash itself was done by means of the Ls-Dyna code. The crash-box has been optimized regarding several parameters so that the performances required by Formula SAE rules are achieved with minimal structural weight. The obtained results show that the impact attenuator by itself is able to absorb the total kinetic energy with dynamic buckling and plastic deformation of its structure with an average deceleration limited under a 20g value.

INTRODUCTION

The goal of an impact attenuator is to prevent the driver and the car from serious damages in case of impact with an obstacle. In order to meet the requirements of Formula SAE competition, the attenuator must guarantee specific performances in terms of average deceleration values and minimum acceptable dimensions during impact. Moreover the assembly of the crash-box is subjected to the following conditions:

- the impact attenuator must be installed in front of the bulkhead;
- it must be at least 200 mm long (along the main axis of the frame), 200 mm wide and 100 mm high;
- it must not penetrate the front bulkhead in case of impact;
- it must be attached to the front bulkhead by welding or, at least, 4 bolts (M8, grade 8,8);
- it must guarantee safety in case of off-axis and off-centre impact.

A crash-test should be demonstrated by the effectiveness of the energy absorbing structure. In the test the front part of the chassis, including the crash-box and the so called survival cell, is solidly attached to a trolley with a total weight of 300 kg. In this condition the crash-box and the front part of the survival cell hit a rigid barrier at a velocity of 7 m/s. During the test the average deceleration of the trolley must not exceed 20g and the final deformation must be limited to the crash-box only. An impact attenuator can be built with many different materials, like metal alloys and/or reinforced fiber composites. No matter the material, but how it absorbs the impact energy is the most important feature: the attenuator, in fact, must dissipate the total kinetic energy avoiding too high decelerations. An important aspect that can influence the crash-box design is the manufacturing cost. Because of the budget available to the Formula SAE Team, aluminium sandwich structure with hexagonal cells were used in the case discussed in this paper. The advantages of metallic laminas are:

- low cost;
- wide know-how on mechanical behaviour of metals;
- easy design and assembly;

while those of honeycomb core are:

- low weight;
- high energy absorption capability.

This last material is used mainly in aerospace and automotive competitions for obtaining high stiffness-to-weight and strength-to-weight ratios. Honeycomb is designed for being loaded in compression along the cell axis. The cells walls buckle under compression and generate several plastic hinges that absorb energy. Moreover, under bending , honeycomb core separates the skins so that the cross-section holds a high inertia moment. For the application under discussion the geometry and materials characteristics have been chosen and optimized by numerical simulation. Several FE models have been developed, using LS-DYNA code [1], to predict the material structural behaviour under dynamic loads. Actually, crash-tests that certify the quality of the attenuator were not available, but the carried out numerical

simulations are considered trustworthy in order to establish the performance of the crash-box in the preliminary design stage.

IMPACT ATTENUATOR: GENERAL SHAPE

Inspired by race competitions, for the attenuator general geometry a truncated pyramidal shape was chosen. With this shape the increasing cross-sectional area prevents from eulerian instability during the deformation. Moreover the angle between the load and the plane of the plates induce bending and the formation of local plastic hinges. With reference to Figure 1, the attenuator can be seen as a blunt hollow beam.

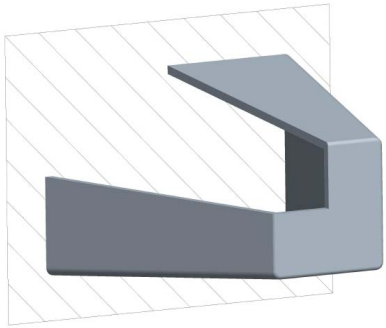

Figure 1. The attenuator as an hollow beam.

This structure is subjected to failure for plastic instability of the sandwich panels (considering the small thickness of the plate, in comparison with the overall dimensions of the body). The plate is substantially a cantilever beam loaded by a complex distribution of forces and moments along its surface. This distribution causes the yielding of a particular section and produces a plastic hinge. With the increase of plasticity deformation in the section, the overall load distribution changes, causing the onset of other plastic hinges.
Eventually the main energy absorption mechanism is due almost completely to yielding in the hinges. Along the skins (Figure 2) there is an alternation of hinges and straight zones. The straight pieces are practically not loaded as the hinges are plastically strained.

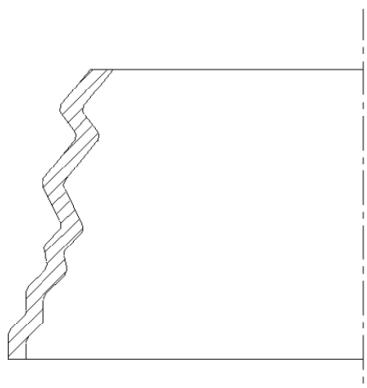

Figure 2. Hinges in plastic buckling.

During loading, the honeycomb skins come in contact one with each other. Now, the honeycomb in the straight piece of the plate is compressed, so it works at best. The hexagonal cells buckle under compression, causing a deep strain into the core; at this time the honeycomb structure stores energy effectively.
In the required performances, the energy to be absorbed is relatively low. Moreover, thanks to previous simulations of crash-boxes made of honeycomb, a well-designed attenuator built with only two sandwich panels seemed to be able to satisfy the quoted requirements..
Inducing the sandwiches fully work in the previously mentioned way, sheets of aluminium assembled between the sandwiches walls demonstrated to be useful to this aim. These membranes create higher stiffness areas and, consequently, trigger the instability and folding of the sandwiches. After the first impact, such aluminium sheets has no structural task; they work only as instability-starter.
A general shape of the attenuator is shown in Figure 3.

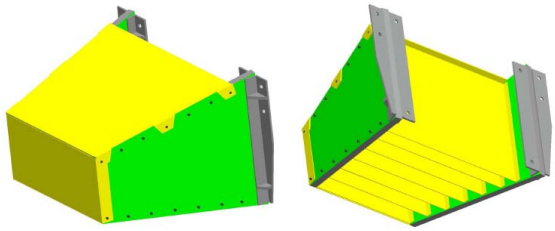

Figure 3. Attenuator's shape.

In the figure a sheet at the top of the attenuator is represented. It avoids that the structure, subjected to a non-frontal impact, behaves as a hinged parallelogram. It is attached directly to the sandwiches and transfers the impact load on both the panels in case of off-axis collision with an obstacle.
The plates are attached to the sandwich panels through rivets. The assembly plan should follow the following steps:

- folding two strips of each plate, for creating the surface to apply the rivets on;
- making holes in sheets and sandwiches for the rivets;
- applying rivets between sheets and panels;
- assembling the attenuator to the front bulkhead via bolts and two ribbed L-shaped joints.

MATERIALS USED

The sandwich panels were made of aluminium AA5052 (Table 1).

Table 1.
Skin alloy properties

	Yield stress (MPa)	Ultimate stress (MPa)	Elongation at break %
AA5052	130	210	9

The other sheets were built with aluminium AA5005 (Table 2).

Table 2.
Aluminium AA5005 properties

Density (kg/m^3)	2700
Elasticity modulus (GPa)	70
Poisson's modulus	0,3
Damping ratio	0,03
σ_y (MPa)	41
σ_u (MPa)	124
ε_{max}	0,07

Compressive tests have been performed on sandwich specimens with quasi-statically deformation. The specimen geometry is described in Table 3, with reference to Figures 4 and 5.
In Figure 6 force-to-specimen area ratio versus displacement-to-initial height ratio behaviours are shown. It is possible to see that an elastic response is followed by a plateau region. After a large displacement, the walls of the cells start touching each other and the core reaches a near total compaction condition. This situation causes a huge increase in stiffness and the core behaves nearly as solid aluminium block. The average stress in the plateau determines the main part of energy absorption capabilities of the honeycomb structure.

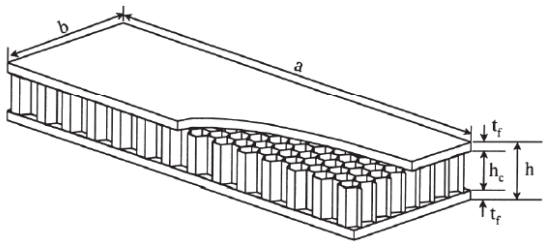

Figure 4. Sandwich panel's geometry.

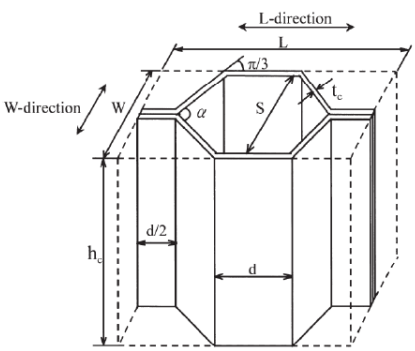

Figure 5. Honeycomb core's geometry.

Table 3.
Dimensions

a (mm)	70
b (mm)	70
h (mm)	13
h_c (mm)	12
t_f (mm)	0,5
S (mm)	6,35
α (°)	120
t_c (mm)	0,0381
d (mm)	3,67

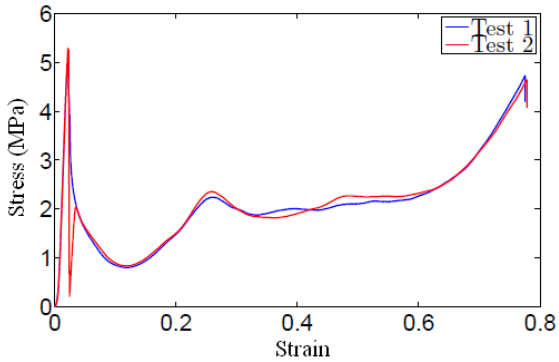

Figure 6. Stress vs strain under compression.

As shown by Enboa Wu and Wu-Shung Yiang [2] crush strength of aluminium AA5052 honeycomb increase linearly with initial impact velocity. There are three possible causes:

- strain rate effects of aluminium;
- compression and temperature increase of air hold into the cells;
- micro-inertial effects.

Aluminium alloys show strain rate effects only at extremely high strain rates (several hundreds per second). Actually, in the considered case, the impact velocity is 7 m/s, so it is hard to achieve high strain rates into a large portion of the sandwiches.
Air within the cells is also negligible, as shown by Hong et al. [3]. Actually air compression alone can not lead to the performance increase experimentally measured.
Inertial effects appear to be the most important factor [4], but their nature is not yet completely understood.
In this study this variation of crush strength is ignored.

MODEL ASSUMPTIONS

Assumptions on materials

The true stress-true strain curve for aluminium alloys can be approximately represented as a bilinear curve (Figure 7). The LS-DYNA code accepts only monotonously increasing material

characteristics curves (so that stress-strain relation is every-where unambiguously defined). Finally the assumed hardening law is isotropic, for computational purpose and the monotonous loading history.
A failure criteria on strains takes into account the final failure of sheets and skins. Failure means a lost of stiffness (e.g. load-carrying capabilities) of broken elements. Failure is detected if elongation at breakage point is reached, in any direction, by an element.
Bulk properties employed for aluminium alloys (kept from literature) are given in Table 2.

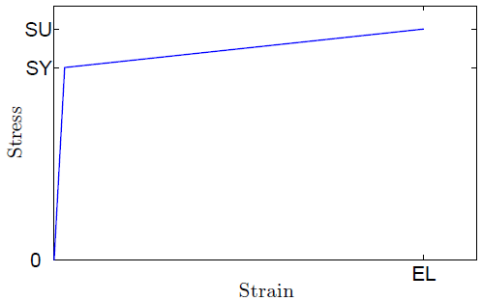

Figure 7. Bilinear curve.

Different approaches for modelling honeycomb structures by FEM exist. They differ in modelling, computational cost and accuracy of the results. Their adoption depends on the specific model size and loading case. A detailed representation of the hexagonal cells can predict the cell wall deformation reasonably well, but it is unsuitable for large-scale models. The model can be simplified by representing the cellular core as an homogenous orthotropic continuum using the honeycomb structure's effective material properties [5].
Three lines describe the true stress-true strain curve of honeycomb before completed compaction. The initial peak point has been neglected, because honeycomb in use was pre-crushed, so it does not show this phenomenon (Figure 8). After compaction honeycomb behaves as solid aluminium, so it shows a linear characteristic with a 70 GPa elasticity modulus. Coordinates of points A, B and C in Figure are shown in the Table 4 below.

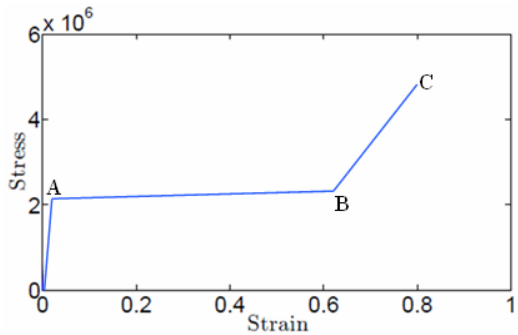

Figure 8. Honeycomb's behaviour

Table 4.
Coordinates

	A	B	C
Strain	0,02	0,62	0,833
Stress (MPa)	2,1	2,15	5

The largest mechanical properties are shown in compression along the cell axis. It means that in-plane properties are lower than out-of-plane ones. For obtaining the other orthotropic values some experimental tests were carried out, such as shear, bending and buckling under in-plane compression tests.
An accurate study of the behaviour of honeycomb model present into the software library shows a lack of stiffness in traction along the axis of the cells (Figure 9). Therefore for modelling tensile rigidity link elements have been used, as described in what follows.

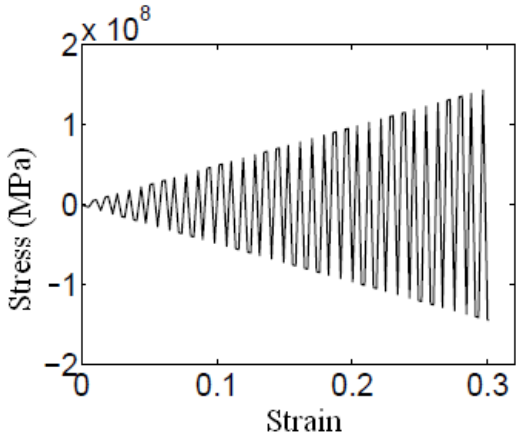

Figure 9. Honeycomb in traction.

Simplification on the model geometry

In order to reduce calculation times, symmetry with respect to two planes has been taken into account. So, only a quarter of the model has been represented (Figure 10). Moreover the upper sheet has been neglected. Actually the constraints imposed on this sheet do not allow the onset of many plastic hinges in bending. So this plate will not really affect energy absorption.
This model does not consider non-symmetric deformation shapes. Symmetry of geometry and load does not allow non-symmetric deformations. As a matter of fact, the manufacturing process will introduce many small shape-defects. However the aluminium sheets can be considered as "big defects" able to induce instability to a much larger extent than small manufacturing defects: this consideration drives to neglect non-symmetric deformations.

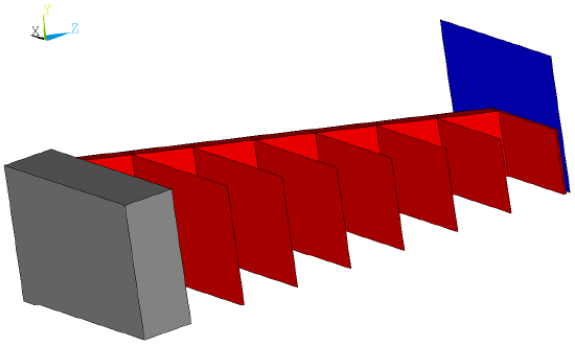

Figure 10. Quarter of model

Constraints have been applied on nodes belonging to the symmetry planes. In particular have been blocked the displacements along the orthogonal direction to the plane and the rotations around the directions in the plane.
Finally a mass of 75 kg represents the vehicle.

Assembly assumptions

The attenuator is hold to the front bulkhead by four ribbed L-shaped joints. Ribbons (Figure 11) and steel bolts attach the joints to the attenuator and to the bulkhead. So, stiffness and non-failure joints conditions during impact are plausible. Therefore the attenuator is considered fully constrained to the vehicle so that some nodes of the sandwich panels (placed near the vehicle) move together with it.

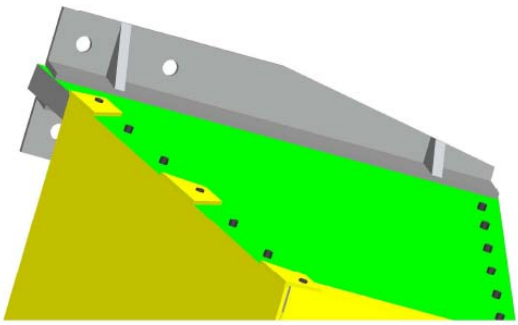

Figure 11. L-shaped joints.

Rivets are not represented in simulation, because of computational cost burden. Moreover failure will reach the aluminium sheets before reaching the rivets. Actually, the load that a sheet and its rivets has to carry is approximately the same and the rivets are much stronger than the sheets. So, sheets are considered attached directly to the corresponding nodes of the skin, without the folded strip mentioned above (Figure 12).

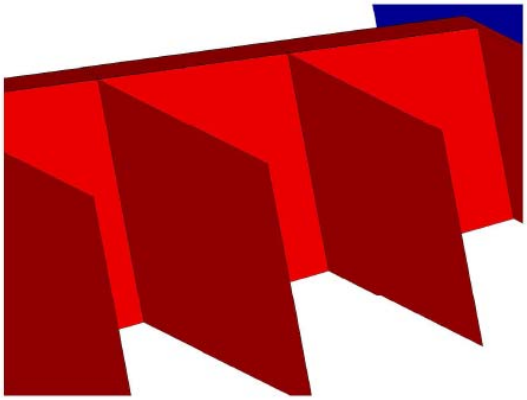

Figure 12. Neglected the folded strips.

Impact assumptions

The crash-box hits actually a rigid wall. The car body is considered rigid too. Assuming rigid wall and body is conservative, because this assumption cancels any time-delay during loading.
During the crash event there are two contacts: aluminium alloy-to-aluminium alloy contact and aluminium alloy-to-wall contact. In literature, friction coefficient between two aluminium surfaces is quoted between 1,1 and 1,7. The coefficient used in simulations is 0,9, because the explicit code does not accept coefficient greater than 1. The same coefficient is used for aluminium-to-wall contact. The heat developed by the hit certainly increases the friction between wall and the aluminium surface and the material of the wall is not a priori known, even if it might be steel.

Elements used

<u>Shell</u>
Aluminium sheets, the wall and the skins are meshed with the explicit dynamic element SHELL163. This is a 4-nodes element with both bending and membrane capabilities. It implements a fully-integrated Belytschko-Tsay element formulation, with 5 integration points in the thickness. The quadrature rule for integration is the Gauss one, faster than the trapezoidal rule and accurate enough for this study. Sheets are really thin (1 mm) and the use of a brick element is not justified.

<u>Brick</u>
The used explicit brick elements are SOLID164 and SOLID168. The first is an 8-node brick element, while the second is a 10-node tetrahedron one. SOLID168 is more accurate but computationally onerous. Actually, SOLID164 is sufficient for the aim of simulation and moreover has been used fully integrated to avoid the birth of hourglass phenomena.

<u>Link</u>
LINK167 is an explicit tension-only spare. It behaves like a cable, with no compressive nor

bending stiffness. This element gives honeycomb tensile rigidity linking the facing nodes of the skins. It is modelled as a spring, for computational saving. Moreover it is not useful to represent stretched honeycomb. The failure of glue between the inner honeycomb nucleus and the outer skins is reached before honeycomb yielding in traction. It is necessary that links reproduce the right tensile stiffness of the honeycomb core. For this aim, honeycomb is considered as a collection of aluminium hexagonal prisms. Each prism is considered as a beam whose area is the area of the transverse section of the cell. The elasticity modulus of aluminium of this beam is 70 GPa. In the model there are so many links as nodes on a skin. An equivalent area must be assigned to the link, so that the total stiffness of links equals the total stiffness of prisms.
The equivalent area is:

$$A_{eq} = \frac{A_{HEX} N_{HEX}}{N_N} \qquad (1).$$

where
- A_{eq} is the equivalent area to be assigned to the link (m^2);
- N_{HEX} is the number of hexagonal prisms filling the area of the skin;
- N_N is the number of nodes filling the area of the skin;
- A_{HEX} is the area of the transverse section of the prism (m^2).

In particular

$$A_{HEX} = \frac{4St_c}{\sqrt{3}} \qquad N_{HEX} \approx \frac{A_S}{(S^2\sqrt{3})/2} \qquad (2).$$

where
- A_S is the skin surface area (m^2).

Stiffness equivalency is obtained with good accuracy.
A failure criteria is given for the links too. Links break when the tensile stress reaches the ultimate stress of glue (in literature 15,5 MPa). So also the glue is simulated.

SUMMARY OF THE RESULTS

The length of the attenuator and the number of trigging sheets have been changed in each simulation. The number of sheets goes from 4 to 7 (no more than 7 sheets were assumed for technological reasons) and the lengths simulated are 300, 350 and 400 mm (no longer than 400 mm for weight saving). Under 300 mm the acceleration shows very high peaks. Actually, safety purposes induce to try to reduce the maximum acceleration values as much as possible.

The displacement during impact has to be checked because it is an index of the safety margin. A well carried out simulation shows the behaviour of the model, but the real attenuator is a bit different (for technological reasons) from the numerical model. This aspect is considered by the displacement-to-initial length ratio. This ratio must be far enough from 1, so that the attenuator can tolerate technological differences from the numerical model.
In Figures 13, 14 and 15 are shown the accelerations resulting from simulations of the attenuator. Accelerations are divided by 20g, for improving the readability of the plot.

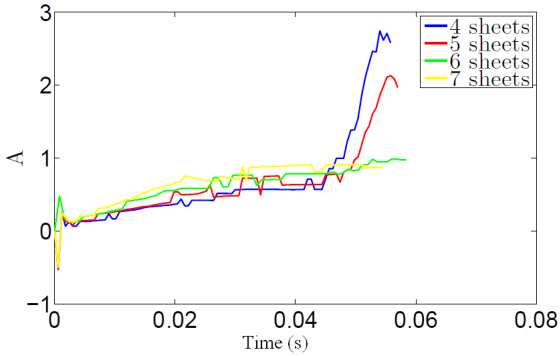

Figure 13. Acceleration vs time (300 mm long).

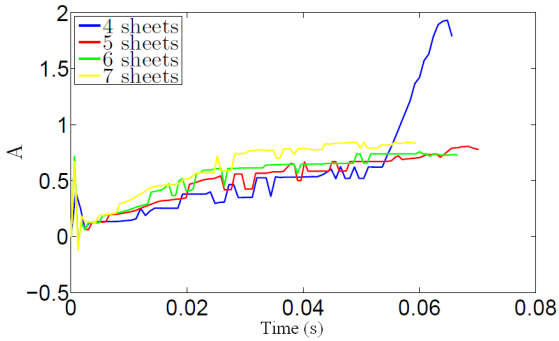

Figure 14. Acceleration vs time (350 mm long).

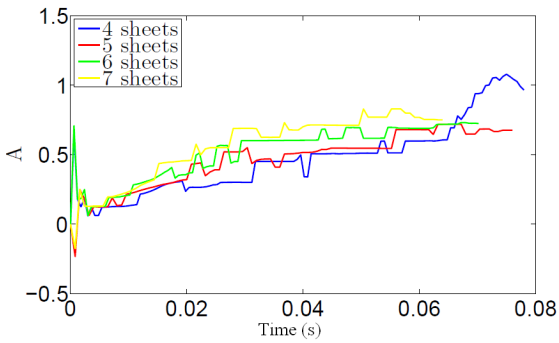

Figure 15. Acceleration vs time (400 mm long).

A 300 mm long attenuator with 4 or 5 transverse plates shows high peaks in the acceleration plot. The same phenomenon is shown by the 350 mm long attenuator with 4 sheets. This behaviour corresponds to a high final compression level

reached (more than 80% of initial length) by the attenuator, as shown in Figures 16, 17 and 18. This plots show the compression versus time of the attenuator divided by the initial length.

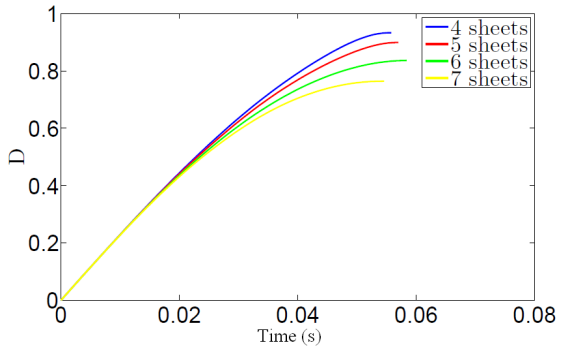

Figure 16. Deformation vs time (300 mm long).

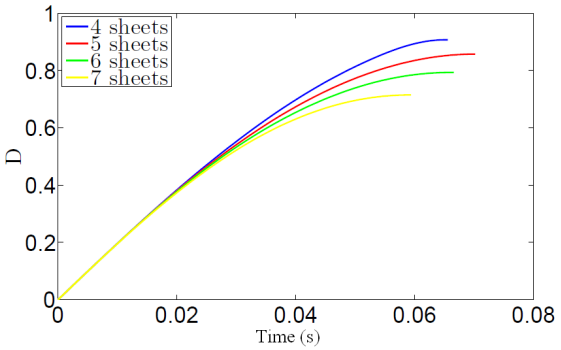

Figure 17. Deformation vs time (350 mm long).

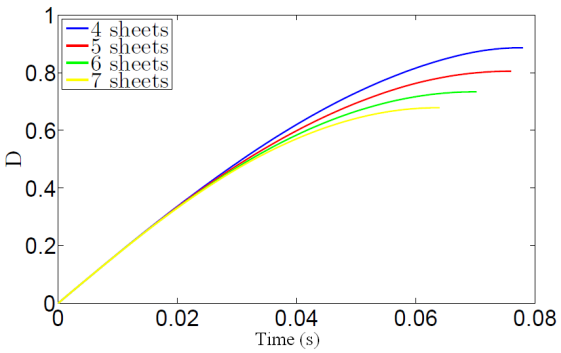

Figure 18. Deformation vs time (400 mm long).

A 300 mm long with 6 sheets attenuator (Figure 19, 20) appeared to be able to guarantee good performances with minimum weight, about 3 kg. In Figure 21 is represented the attenuator deformation sequence during the impact phenomenon.

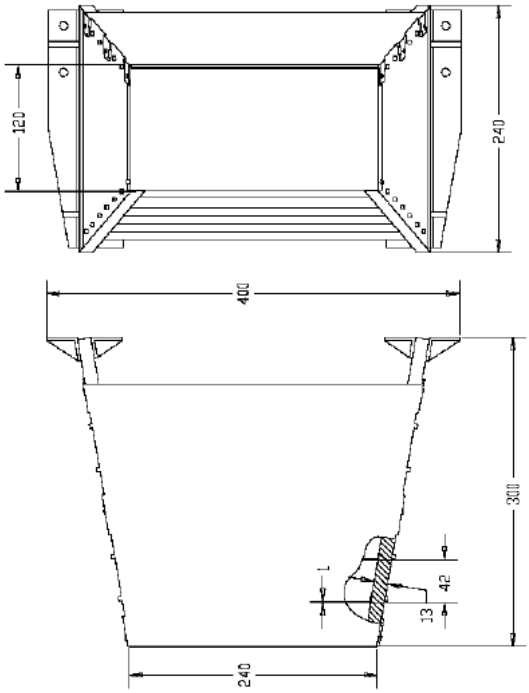

Figure 19. Draft of the attenuator.

Figure 20. Real crash-box.

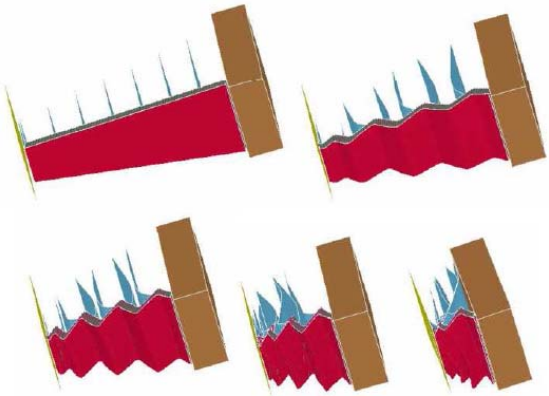

Figure 21. Frames of simulation.

CONCLUSIONS

The present paper describes a numerical investigation of an energy absorber for a Formula SAE race car. A finite element model has been

developed using LS-DYNA code doing a simplified optimization process in order to obtain the best configuration of crash-box in terms of average deceleration and stroke efficiency. On the test and numerical results the proposed procedure appeared to be adequate to design the attenuator from the practical application point of view of the considered sport car.

REFERENCES

[1] LS-DYNA, Keyword User's Manual, Version 971, LSTC, 2006;

[2] E.Wu, W.-S.Jiang, "Axial Crush of Metallic Honeycombs", International Journal of Impact Engineering, Vol. 19, 439-456, 1997;

[3] S.-T.Hong, J,Pan, T.Tyan, P.Prasad, "Dynamic crush behaviours of aluminium honeycomb under compression dominant inclined loads", International Journal of Plasticity, Vol.24, 89-117, 2008;

[4] H.Zhao, G.Gary, "Crushing behaviour of aluminium honeycomb under impact loading", International Journal of Impact Engineering, Vol.21,827-836,1998;

[5] L.Aktay, A.-F.Jhonson, M.Holzapfel, "Prediction of impact damage on sandwich composite panels", Computational Material Science, Vol.32, 252-260, 2005.

PERFORMANCE ANALYSIS METHODOLOGY BASED ON CRASH PULSE SEVERITY AND VEHICLE OCCUPANT PACKAGING FOR FULL FRONTAL CRASH EVENT.

Bo Pil Seo
Sung Jun Han
Won Chul Kim
Si Yeol Kim

Hyundai Motor Co. & KIA Motors Corp
Korea
Paper No. 09-0173

ABSTRACT

Under full frontal crash events, major factors affecting occupant injury are crash pulse severity, restraint system, and vehicle occupant packaging space. The crash pulse severity represents the total performance of collision energy absorbed by vehicle structure during the crash event. The pulse severity also has a close relationship with the energy absorbed by restraint system out of the occupant's total kinetic energy induced by crash event. The capacity of energy absorption by restraint system is affected by the vehicle occupant packaging space. Thus, it is important to perform both restraint system and packaging space optimization simultaneously to manage the energy transfer under given severity of crash pulse.

In this study, severity function is defined to represent the regression curve of resultant energy absorbed by occupant, based on G-D curve and occupant packaging space. To build the regression curve, US NCAP top rated vehicles were analyzed and the relation between crash pulse severity and severity function is derived for various vehicle grades. Based on the result, target requirements of crash pulse severity and severity function are determined to satisfy occupant safety performance goals. This methodology is very useful to evaluate the crashworthiness performance of vehicle body design concept efficiently at early development stage.

INTRODUCTION

Under the condition of full frontal crash events, major factors affecting occupant injury are crash pulse severity, restraint system, and vehicle occupant packaging space.

Since crash pulse that is shown as a type of deceleration represents crash performance of vehicle body, the vehicle crash pulse plays an important role to understand and analyze behavior of the vehicle structure during the crash event.

The vehicle crash pulse is usually measured at the rear sill, near the vehicle CG, or near occupant seat, and this pulse data is often used to assess the severity of crash event. Many technologies have developed to predict the severity in a view of occupant injury risk from the data itself.

In general, the vehicle crash pulse represents the total performance of collision energy absorbed by vehicle structure during the crash event. Those have foundation on the factors having close relation with the energy management absorbed by the structure.

So, several studies have been made on the characterization of vehicle crash pulse which affects occupant response. [1-5]

Recently, theoretical studies on the pulse severity which affects occupant response have been developed using SDOF (single-degree-of-freedom) mass-spring systems which characterizes restraint system as a simple linear elastic spring model which consists of acceleration versus displacement of dummy. [3]

In this study, we defined severity function as a type of mathematical equation through linear curve fitting about net energy absorbed by occupant. Developed severity function is based on G-D curve and vehicle occupant packaging space. To build the regression curve, this study analyzes top-rated vehicle in US

NCAP and derives the relation between vehicle crash pulse severity and severity function for various grades of vehicles. Using the result, we will find target requirements of severity for crash pulse to satisfy occupant safety performance goals.

SEVERITY FUNCTION

The kinetic energy of an occupant during a vehicle crash is transformed into work in deforming the restraint system and vehicle structure.

Even if restraint systems in the vehicle were same, different the vehicle crash pulse severity or occupant energy absorption space results in a different occupant injury.

In order to guarantee same occupant injury performance, much more restraint space is required for the vehicle which has higher crash pulse severity.

RTE(ResTraint Energy) is used to evaluate the crash pulse severity in this study. Also, we introduce the concept of Severity Function. Severity Function contains RTE and layout parameter of occupant packaging as its independent variable. Using this Severity Function, this study derives interrelation from these two independent variables. The relationship between RTE and occupant injury has been presented in previous research. [5]

Severity Function is an integral in regression curve of occupant chest acceleration-displacement.

SF(Severity Function) can be represented as like

$$SF(S,F_g,MCT)=F_g\times[(MCT-10)-\frac{1}{2}\times\frac{F_g}{S}] \qquad (1)$$

In Figure 1, MCT is a maximum chest travel, S is the slope during elastic restraining, and Fg is an average acceleration during plastic restraining stage.

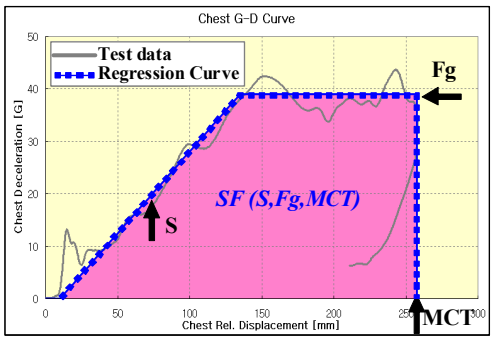

Figure 1. SF (Severity Function)

DERIVATION OF SEVERITY FUNCTION-RTE RELATIONSHIP

First of all, we analyze top-rated vehicles in US NCAP so as to find the relationship between RTE and SF. Table 1 shows linear regression relationship derived by analyzing test data for various grades of vehicles.

Table 1. The relationship of SF and RTE

Vehicle Class	Correlation Coefficient	Linear Regression	
		Equation	R-squared
Compact car	0.80	Y = 0.0048X + 18.790	0.65
Midsize car	0.82	Y = 0.0049X + 15.347	0.67
SUV	0.85	Y = 0.0059X + 18.597	0.57

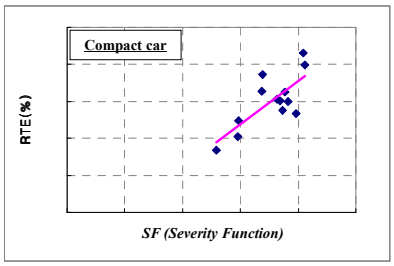

(a)

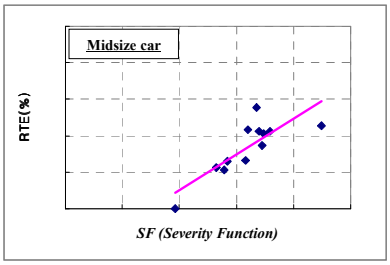

(b)

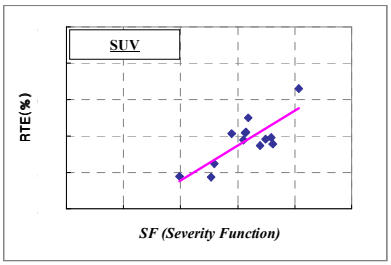

(c)

Figure 2. The relationship of SF and RTE for various vehicle grades. ((a) compact car, (b) midsize car, (c) SUV)

DERIVATION OF CS-RTE RELATIONSHIP

As for occupant package, CS is an horizontal distance between steering wheel center and occupant chest skin. It is affected by MCT. CS is defined in Equation 2.

A reference point and variable used to described the driver package as shown in Figure 3. All analysis was performed in two dimensions (side view). A is the horizontal distance between chest acceleration sensor and chest skin, B means the distance between chest acceleration sensor and steering wheel center when dummy reaches its maximum travel range with respect to the vehicle. C is a space obtained by column collapsing along a vehicle moving direction and C can be obtained by column setup angle and collapsed length along column axis.

$$CS = MCT + B - (A + C) \qquad (2)$$

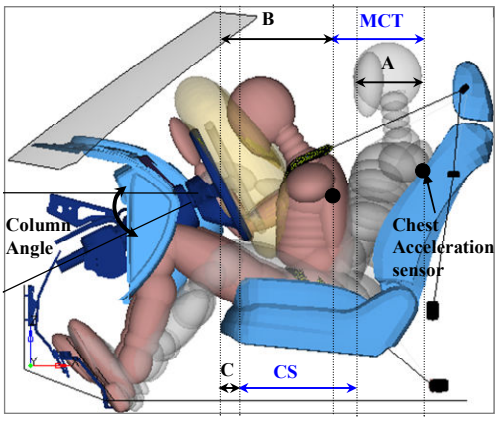

Figure 3. Dimensions in occupant package layout

Substituting Equation 2 for Table 1, we obtain interrelation between Severity Function and RTE as shown in Table 2. S and Fg are major variables in these interrelation and obtained by averaging test data.

Table 2. The relationship with CS and RTE

Vehicle Class	Average Value		CS-RTE Relationship
	S [G/mm]	Fg [G]	
Compact car	0.30	38.0	RTE=0.1824*CS-0.8540
Midsize car	0.27	37.0	RTE=0.1813*CS-3.4209
SUV	0.28	36.3	RTE=0.2142*CS+2.7818

Based on this result, target requirements of RTE and CS are determined so as to satisfy occupant safety performance goal as shown in Figure 4 and the following information can be drawn:

In order to improve performance in US NCAP

1) A Minimum requirement of CS when we know RTE about a specific vehicle.

2) A Maximum limit of RTE when CS is fixed. Here, CS and RTE concern an occupant package layout condition and an energy absorbing efficiency of vehicle respectively.

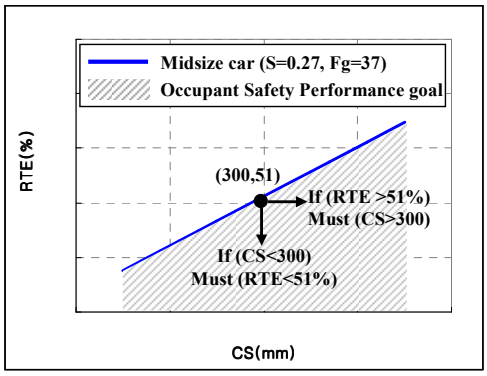

Figure 4. Requirement for occupant safety performance satisfaction (ex. Midsize car)

If CS is lower than its minimum requirement under given RTE, space to restrain occupant is insufficient. Excessive RTE results in increasing MCT and it can cause direct contact between chest and steering wheel. Moreover, to change a specification of the restraint system cannot solve these problems, since altering system specification has a possibility to increasing Fg in many case.

Figure 5 describes these phenomena.

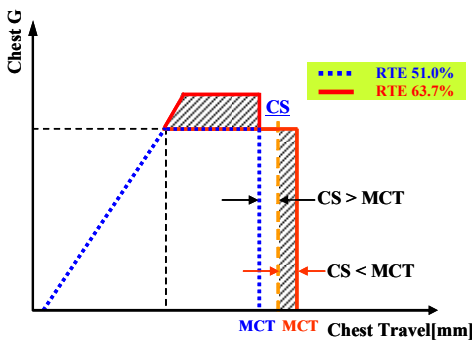

Figure 5. Effect of CS and RTE (S : 0.27)

DERIVATION OF BELT ANGLE(θ)-RTE RELATIONSHIP

One of many layout factors in occupant package, "belt angle(θ)" represents a horizontal distance from contact location between shoulder belt and upper torso to D-ring contact location as shown in Figure 6. This affects initial restraint efficiency of occupant.

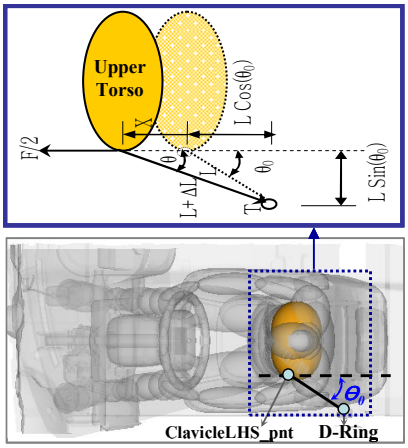

Figure 6. Dimensions in occupant package layout

In Figure 6, F is an inertial force of dummy upper torso and represented by dummy upper torso mass(m) and acceleration(a). T is tensile strength on shoulder belt, Shoulder belt length between D-ring and contact point on dummy upper increases from L to L+ΔL.

Standard Restraint Stiffness (K) is derived from Equation 3 and chest G-D Curve of test vehicles where belt setup location can be checked.

$$F = ma = \frac{2K\Delta L(LCos(\theta_0)) + X)}{(L+\Delta L)} \qquad (3)$$

$$\Delta L = \sqrt{(LSin(\theta_0))^2 + (LCos(\theta_0) + X)^2} - L$$

Interrelation between S and belt angle(θ) is obtained by Equation 3 and K. Finally, substituting this interrelation for Table 1, we obtain Table 3 as follows

Table 3. The Relationship of Belt angle(θ) and RTE

Vehicle Class	Average Value		Belt Angle(Θ)-RTE Relationship
	MCT [mm]	Fg [G]	
Compact car	245	38.0	RTE=-0.0034*Θ²+0.0457*Θ+52.884
Midsize car	252	37.0	RTE=-0.0033*Θ²+0.0449*Θ+50.931
SUV	286	36.3	RTE=-0.0039*Θ²+0.0526*Θ+68.319

Based on this result, target requirements of RTE and belt angle are determined so as to satisfy occupant safety performance goal as shown in Figure 7 and the following information can be drawn:

1) A Maximum limit of belt angle when we know RTE about a specific vehicle.

2) A Maximum limit of RTE when belt angle is fixed.

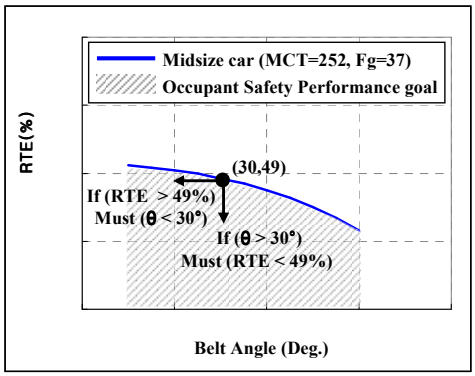

Figure 7. Requirement for occupant safety performance satisfaction (ex. midsize car)

If belt angle can not be guaranteed under given RTE, space to restrain occupant is insufficient by increasing. Excessive RTE results in increasing MCT and it can cause direct contact between chest and steering wheel because of MCT increasing. As mentioned, in many case we cannot solve this problems only by replacing or changing the specification of the restraint system.

Figure 8 describes these phenomena.

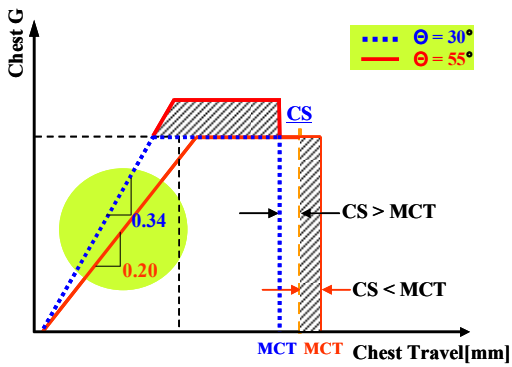

Figure 8. Effect of MCT and RTE (S : 0.27)

INITIAL CONCEPTUAL EVALUTION PROCESS

Up to now, we found the interrelation between SF and RTE and we proposed requirement conditions of each layout factor and RTE in order to satisfy occupant safety performance goal.

Based on this result, we set an initial conceptual evaluation process as shown in Figure 9. This process enables to evaluate crashworthiness performance for various grades of vehicles at early development stage.

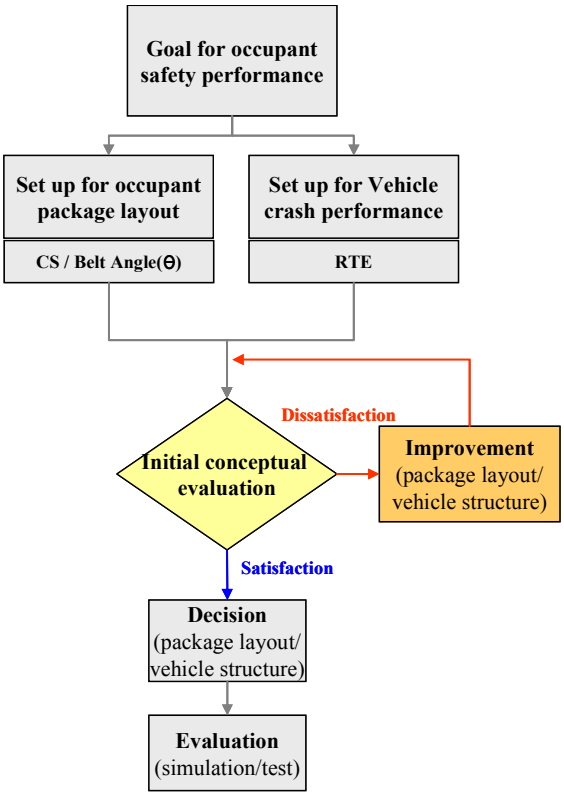

Figure 9. Initial conceptual evaluation process

When the occupant safety performance goal is set in the initial stage of vehicle development process, we can evaluate whether that is satisfied or not through given RTE, SF, and layout factors.

If given conditions be unable to satisfy performance target, vehicle developers improve layout and vehicle structure by analytical and practical method.

This study makes an initial conceptual evaluation sheet about each grade of vehicle in Figure 10. This sheet represents overall relationship among RTE, CS and belt angle and guides each requirement to satisfy performance target. This sheet helps vehicle developers to evaluate their vehicle.

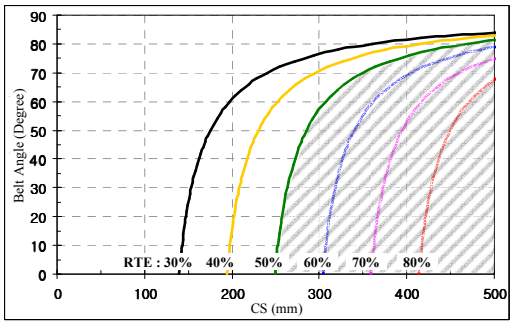

Figure 10. Initial conceptual evaluation sheet

CONCLUSIONS

In order to derive guideline about vehicle structure crash property and occupant package layout, this study analyzed top-rated vehicle in US NCAP.

Based on proposed severity function which depends on RTE and layout factors of occupant package, this study obtained results as follows

1) Through severity function, we find relationship among package space, belt angle, and RTE. Using these relationship, we suggest design guideline so as to achieve better safety performance in front NCAP

2) We propose the initial conceptual evaluation process in order to evaluate crashworthiness performance at early development stage.

We need to expand for additional layout parameter and have to construct data base about more vehicles. These data base can help vehicle designer to evaluate and obtain their required performance at early development stage.

In further study, we have a plan to analyze crash performance based on chest deformation for NEW NCAP.

REFERENCES

[1] M. Huang, G.P. Lawson, B.K. Powell, J.H. Walker, "Characterization of Vehicle Deceleration Time Histories in the Analysis of Impact Dynamics", SAE 770013, 1977

[2] M. Huang, "Vehicle Crash Mechanics", CRC PRESS, Chapter 1, 2002

[3] J. Wu, B. S. Bilkhu, G.S. Nusholtz, "An Impact Pulse-Restraint Energy Relationship and Its Applications", SAE World Congress, March 3-6, 2003

[4] W.D. Grimes, F.D. Lee, "The Effect of Crash Pulse Shape on Occupant Simulations", SAE Paper 2000-01-0460.

[5] S.Y. Kim, S.C. Choi, S.J. Han, " Characterization Methodology and Establishment on Analysis Method Based on Severity for Crash Deceleration", Hyundai-Kia Motors Conference, 2007CS0205,2007

[6] D.E. Martin, C.K. Kroell, "Vehicle Crush and Occupant Behavior", SAE Transaction, Vol. 76, 1968

[7] S.J. Song, S.Y. Kim, S. Bilkhu, "Front Impact Pulse Severity Assessment Methodology", SAE World Congress, April 11-14, 2005

DEVELOPMENT OF TEST METHODS FOR EVALUATEING CURTAIN AIRBAG DPLOYMENT FORCE

Eung-Seo Kim
Jae-Soon Cho
Dae-Young Kwak
Seung-Hoon Lee
HYUNDAI MOTOR COMPANY, Korea
Hyun-Yong Jeong
Sogang University, Korea
Chang-Soo Kim
Kwang-Soo Cho
HYUNDAI MOBIS, Korea
Paper Number 09-0174

ABSTRACT

It is well known that a CAB (Curtain Airbag) is one of the most effective restraint systems for protecting the occupant head from a side impact crash or preventing the occupant from ejection during a rollover accident. One of the most fundamental requirements for a CAB is to ensure a robust deployment. Specifically, a CAB should be deployed and positioned well in time without being trapped by any interior parts. Up to now, the deployment performance has been evaluated by measuring the fully-deployed time, which has limitation in that it is difficult to clearly discriminate performance differences resulting from design parameter changes.

The main purpose of this study is to develop a new methodology for evaluating the CAB deployment performance quantitatively and defining corresponding metrics representative of the deployment performance. For this, two test methods focusing on either the local or the global characteristics were developed in the present investigation. The first was designed to directly measure the deployment force exerted on the specific area by measuring the tension force acting on a webbing material using the load cell. The second was devised to show the overall profile of the deployment force and to measure the time history of total force by calculating the sum of inertial and elastic forces applied to a series of spring-bar impact systems. Afterward, several tests were carried out by each method in order to evaluate their repeatability and reproducibility. In addition, the tests were performed for several different CAB designs to evaluate discrimination capability of each test method. From this study, it was found out that the proposed test methods and corresponding metrics can be effectively used for evaluating the deployment performance of CAB's. It is also expected that the methodology can be applied to optimize design parameters of CAB's for the robust deployment performance.

INTRODUCTION

A CAB is the device that is generally equipped between the headliner and the side roof panel in a vehicle, and is to protect the occupant head from a side impact crash or to prevent the occupant from ejection during a rollover accident. As the importance of safety in side impact crashes and rollover accident is increasingly emphasized, NTHSA released the upgrade of FMVSS214 so as to encourage car makers to install CABs and SABs (Side Airbag) in their vehicles. Also, the cars with CABs as standard features are continuously increasing all over the world. Thus, it is most important to ensure the robust performance of a CAB.

The performance of a CAB can be generally evaluated by deployment performance and energy absorbing capability in case of an occupant head impact. The former one is a prior requirement which means the ability to be deployed and positioned well in time without being trapped by any interior parts.

Figure 1. The deployment of CAB and malfunction of a CAB hung on pillar trim.

However, in some cases the deployment time is delayed, the cushion moves unstable or it cannot fully deployed by the interference of neighboring interior parts such as pillar trims, headliner and so on. Figure 1 shows a typical problematic case where the CAB cushion is hung on the top of B-PLR Trim. The main factors to cause these abnormal behaviors are deformation of body panel from impact, low deployment force of cushion and structural inadequacy between the CAB and interior parts. Among these three factors, the deployment force can represent the characteristics of CAB itself and deployment performance.

Up to now, some researches have tried to calculate the deployment force by measuring the internal pressure or analyzed the stress distribution for checking the structural integrity of cushion using numerical simulations[1~3]. In addition, when the CAB is abnormally deployed in static deployment or barrier tests we solved these problems by just changing the structural factor of adjacent trim parts and then conducting the static deployment test for verification of the improved performance. However, this action is not sufficient to judge whether only such modification is enough or any other process should be applied like increasing the mass flow rate of the inflator for improvement. Also, it takes so long time and costs much to change the mold for interior parts by trial and error. Consequently, a method to evaluate the CAB deployment force quantitatively which may lead to a stable deployment is essentially required.

In this paper, two test methods measuring CAB deployment force focusing on either the local or the global characteristics are proposed. The first was verified by testing 20 different CAB designs and analyzing test data from the aspect of 3 design factors. Two distinctively different CAB designs are used to assess the second method finding out the deploying profile, force and energy. Finally, the merits of two methods are compared and summarized.

LOCAL EVALUATION METHOD OF CAB DEPLOYMENT FORCE

The Device and Test Method

The CAB deployment force mainly acts downward against resisting force from the headliner, the pillar trim and the body panel. The test device, shown in Figure 2, is designed to directly measure this force exerted on the webbing that a load cell is attached. It would be better to measure the deploying force in every location along a CAB. However, only the forces at the location around the B-PLR trim were measured.

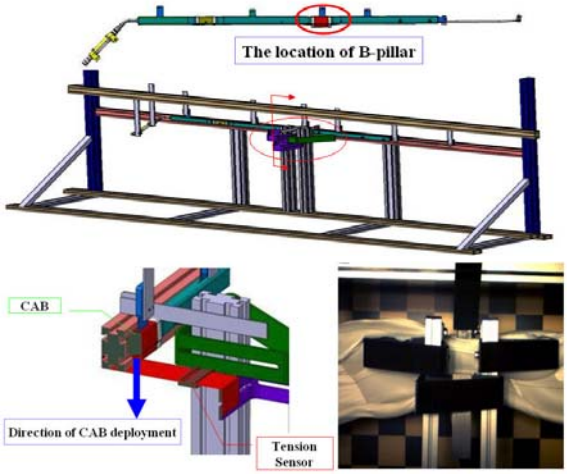

Figure 2. The schematic diagram of deployment force measuring device and the test.

The Metrics of a CAB Deployment Force

The maximum and average deployment forces, shown in Figure 3, are defined as metrics which can represent the deploying characteristics well and have good repeatability and reproducibility with the device's simplicity.

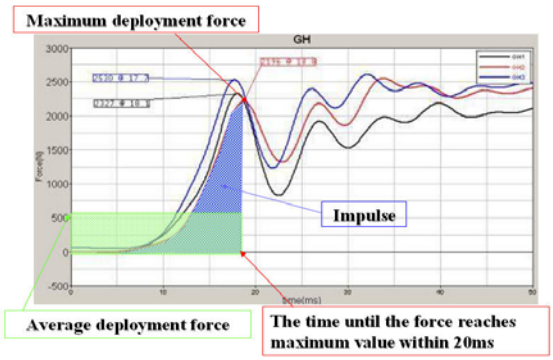

Figure 3. The standard of maximum and average deployment force.

The maximum deployment force is defined as the peak value within 20ms after a CAB is triggered, and the average deployment force is defined as the value which the impulse is divided by the corresponding time interval until the force reaches the maximum value. The definitions of maximum and average forces are expressed by the equations:

$$F_{\max} = Max\{F\} \qquad (0 \le t_{F_\max} \le 20ms) \qquad (1).$$

$$F_{avg} = \frac{1}{t_{F_\max}} \int_0^{t_{F_\max}} F dt \qquad (2).$$

where $t_{F_\max}$ is the time when F is at its peak value. Three tests were conducted for each CAB design, and the average was determined as the representative value.

Tests and the Results

The tests for measuring deployment forces for 20 kinds of CAB designs were carried out in order to evaluate their repeatability and reproducibility. The CAB modules were classified according to three factors, more specifically the location of inflator (gas injection nozzle), inflator type and vehicle segment. These factors can interact one another, but were chosen because they have major effect on CAB design concept and performance.

There are two kinds of center and rear module CABs according to the location of inflator shown in Figure 4. The former one has its gas injection nozzle in the middle of cushion and the latter one has it at the rear end. Their deployment test results are shown in Table 1, where the center module CAB is superior to rear module CAB by 64.5% in terms of average deployment forces. It is due to the close location of gas injection to the B-PLR Trim, and this shows that a center module CAB is more effective in its deploying capability by opening the headliner more quickly and forcefully.

The inflators used in CAB's are generally divided into two classes, the hybrid type using the compressed gas and pyrotechnic techniques, the stored gas type using only the compressed gas technique (usually He and/or Ar are filled).

Figure 4. Center and rear module CAB.

The latter one is also called Cold Gas Inflator because of low temperature of injected gas. It can be meaningless to compare one with the other without considering parameters such as capacity, size and geometry of nozzle, mass flow rate, and so on. Thus, two kinds of CAB's having a similar cushion volume are used for this test. In Table 2, it can be noticed that a CAB with the stored gas type inflator has a higher deployment force by 19.1% in average value, and this can be also figured out from tank test curve of inflator.

The relation between vehicle segments and their required force level for ensuring the stable deployment of CAB was investigated. Since the size of cushion and the capacity of inflator tend to be in proportion to that of vehicle's layout, CABs are classified into three groups, namely, vehicles under C segment, over D segment and SUV(including CUV). The average value of each group is shown in Table 3. The maximum and average forces of SUV

Table 4.
Comparison of deployment force according to inflator location

The location of inflator	Max. Deployment force(N)	Avg. Deployment force(N)
Center Module	2672.5(117.0%)	1251.9(164.5%)
Rear Module	2283.8(100%)	761.0(100%)

Table 5.
Comparison of deployment force according to inflator type

Inflator type	Max. Deployment force(N)	Avg. Deployment force(N)
HYBRID	2378.5 (100%)	855.7 (100%)
STORED GAS	2414.6(101.5%)	1019.4(119.1%)

Table 6.
Comparison of deployment force according to vehicle segment

Vehicle segment	Max. Deployment force(N)	Avg. Deployment force(N)
Under C	2140.5(100.0%)	776.1(101.8%)
Over D	2497.4(116.7%)	762.4(100.0%)
CUV, SUV	2561.3(119.7%)	1151.0(151.0%)

are greater than that of under C segment vehicle by 19.7% and 51.0% respectively. From these test results, it can be seen that the bigger the vehicle size is, the stronger the deployment force is required because the larger protection area of a CAB cushion needs the more powerful inflator.

GLOBAL EVALUATION METHOD OF CAB DEPLOYMENT FORCE

The Device and Test Method

It is not easy to directly measure the deployment force of a CAB during deployment because its cushion moves so fast and gets the reaction from the sensing equipment. A device that could measure the force indirectly by calculating the sum of inertia and elastic forces from the acceleration of a mass and deformation of a spring moved by the cushion was designed.

The deployment force measuring system shown in Figure 6 consists of 22 units of spring-bar impact device shown in Figure 5 along the longitudinal direction of a CAB. Each spring-bar impact device was equipped with two movable LM-GUIDEs (linear motion guides) standing vertically on the bottom plate, so that an impact bar could move up and down by the deploying force of the CAB cushion. A wire spring which passed over a pulley at the top of LM-GUIDEs was connected between the bar and the bottom plate to measure the elastic force. To calculate the acceleration of the bar from its displacement, a reference tape with the resolution of 1 inch was attached on the side of LM-GUIDE. The displacement was measured every 3ms from an analysis of film taken by using a high speed camera, and the acceleration was calculated by differentiating the displacement twice using the central difference method. Afterward, the displacement and acceleration obtained from this method were compared with those measured from a potentiometer and an accelerometer to ensure repeatability and reproducibility.

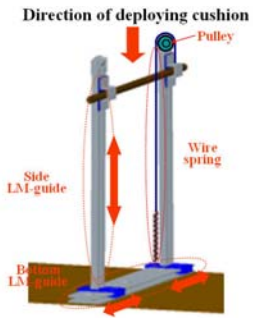

Figure 5. A unit of spring-bar impact device

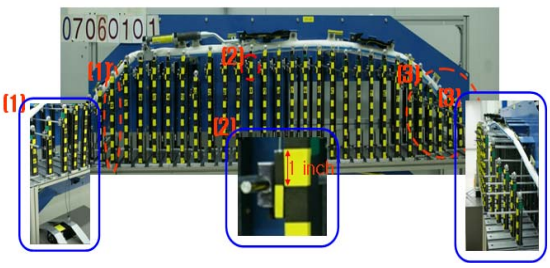

Figure 6. The global deployment force measuring system.

The Metrics of a CAB Deployment Force

The total deployment force of a CAB was calculated from the summation of the inertial and elastic forces applied to a series of spring-bar impact devices. This dynamic system is governed by the equation:

$$F = (m \times \ddot{x}) + (k \times x) \qquad (3).$$

where m : mass of moving part of a unit
k : spring constant of wire spring
x : deformation(displacement) of wire spring

The term of elastic force is the sum of spring forces of 22 spring-bar impact devices and is plotted in green color in Figure 7(b). The time history of every unit's displacement in Figure 7(a) shows the overall profile of a CAB, which can provide us with the deploying profile as well.

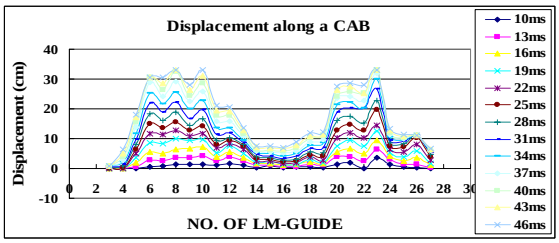

(a) The time history of displacement

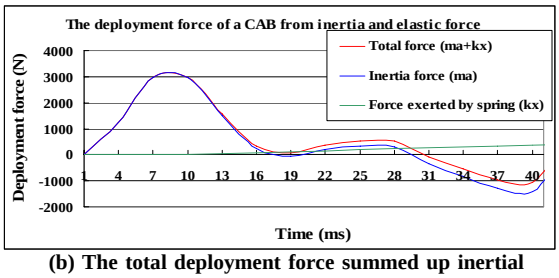

(b) The total deployment force summed up inertial and elastic forces

Figure 7. The deploying profile and force by global evaluation method.

The inertial force plotted in blue in Figure 7(b) was generated by the CAB deployment. From the test result in Figure 7, it can be noticed that the inertial force was the major component of the total deployment force.

Tests and the Analysis of Results

Two kinds of CABs were used in the tests with the interior parts equipped or not equipped. One was the CAB of D segment sedan of which the gas injector was located in the rear, and the other was that of CUV of which the injector was located in the middle. The test results were investigated in the aspect of deploying configuration (displacement), force and energy. The deployment force calculated in every position of LM-GUIDE along CAB was divided into 4 or 5 sections (Front, B-Pillar, Middle1-2 and Rear) shown in Figure 8, and each section was evaluated separately and compared with one another.

The Deploying Configuration of Center and Rear Module CABs – The displacement of each measuring point along the CAB was interpolated every 3ms in Figure 9. Figure 9(a) and 9(b) represent the results of the rear module CAB and center module CAB, respectively. Figure 9(a) shows that there was comparatively slow deployment in the region of (c) due to an inactive chamber of cushion behind the B-PLR Trim. The cushion of rear part (d) deployed faster than the other parts. This characteristic was related to the location of the gas injector and cushion shape, and could be discriminated clearly by comparing this with that of center module CAB in Figure 9(b). The fastest deployment velocity occurred in the region of (d) which was just in rear of the gas injector and had an active cushion chamber. The results also denote that the region (a) and (d) of the center module CAB where the occupant head's impact on uniformly reached their full displacement at 30ms, while that of the rear module CAB had the disparity of about 10~50%. This phenomenon could be also seen in a high speed film of deploying CAB just in empty space, but it did not show a distinct difference along a CAB.

The Regional Deployment Force along CAB – The deployment force in each region of CAB was analyzed. The result in Figure 10 clearly distinguishes the characteristic of two different CAB designs. The regional force deviation of the rear module CAB was much bigger than that of the center module. Especially the difference of maximum force between the region of (a)Front and (b)Rear in the rear module CAB is about 200N. There was also a time delay of 7ms in Front part (a) than in rear part (d) in terms of the time when the deployment force reached its peak value. But the center module CAB had comparatively similar maximum deployment force and peak force in every region.

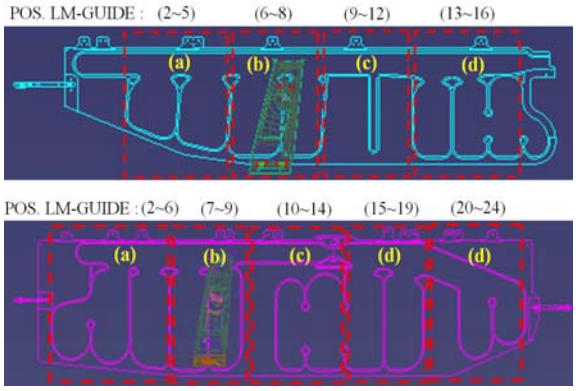

Figure 8. The regional classification of the rear and center module CAB and the location of LM-GUIDEs.

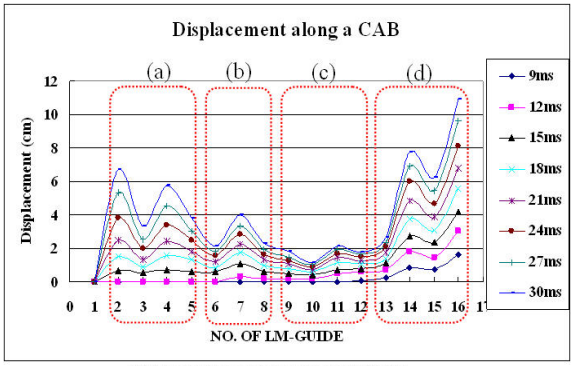

(a) The profile of rear module CAB

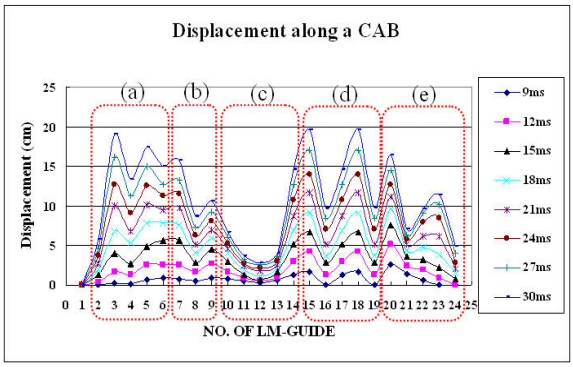

(b) The profile of center module CAB

Figure 9. The comparison of deploying profile according to the location of gas injector.

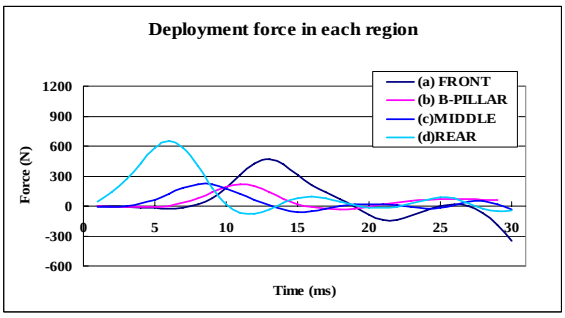

(a) The regional deployment force of rear module CAB

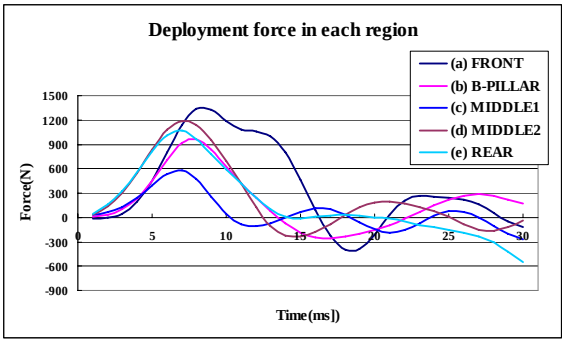

(b) The regional deployment force of center module CAB

Figure 10. The comparison of regional deployment force.

The Deploying Energy in Each Region of CAB

–The deployment test of the rear module CAB was carried out in a vehicle with interior parts equipped, and their results are shown in Figure 11. The deploying configuration in Figure 12(a) apparently shows two superior speeds near the region of (a) and (d) in comparison to Figure 9(a) although they were the test results of the same kind of CAB module. It seems that the interior parts had a deteriorating effect on the deployment of CAB, especially in front position of (a), rear position of (b) and (d) where the trim parts and headliner were coupled. The deploying energy of region (d) shown in Figure 12(b) rose fast, but finally that of region (a) reached twice the peak value of (d) within 30ms when the CAB was fully deployed. The energy level of each part along a CAB could easily estimated from this analysis.

CONCLUSION

In the present investigation, two different test methods were developed in order to evaluate the CAB deployment performance quantitatively. The first was designed to directly measure the deployment force on the specific area by measuring the tension force on a webbing material. From the

Figure 11. The deployment test in vehicle equipped with interior parts.

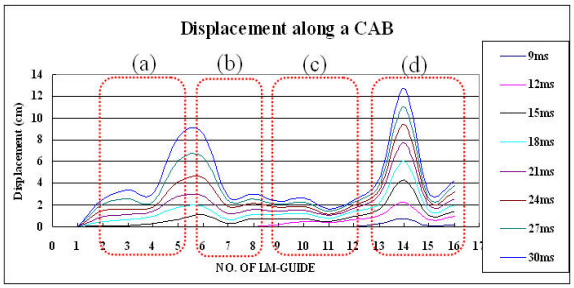

(a) The profile of rear module CAB

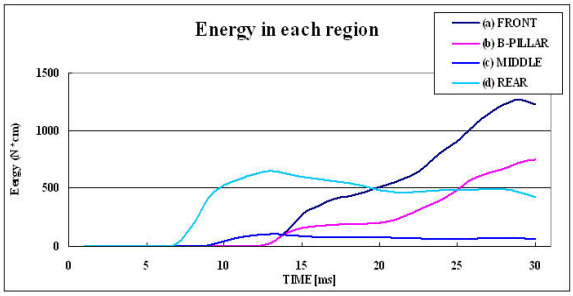

(b) The deploying energy in each region

Figure 12. The deploying energy in each region in vehicle with the interior parts equipped.

test results of 20 different CAB designs, it could be noticed that this test method showed good repeatability and reproducibility with appropriate discrimination capability for the CAB design factors. Also, a specification for CAB deployment force could be established by using this testing method for ensuring a robust deployment performance.

The second was designed to show the deploying profile along a CAB and to calculate overall deployment force and energy indirectly from the cushion's displacement. Also, this method helped compare the partial distribution of deployment force and energy along a CAB.

From the test results of two different CAB designs, it was found that the method could be effectively used to discriminate the deployment performance of CABs. In particular, it was shown that the deploying performance of a center module CAB was more stable than that of a rear module CAB.

REFERENCES

[1] Anders Ohlund, “The inflatable curtain (IC) – a new head protection system in side impacts”, SAE 98-S8-W-29

[2] Hyunsok Pang, Joseph Massa. “Curtain Airbag Gas Delivery System Development Using CFD Analysis” 20th International Technical Conference on the Enhanced Safety of Vehicles. Lyon, France, June 18-21, 2007.

[3] Honglu Zhang, Deren Ma, Srini V. Raman “CAE-Based Side Curtain Airbag Design”, SAE 01-0841, 2004

[4] David Shilliday, “Required airbag characteristics for occupant retention in rollover crashes”, NHTSA

[5] N. Claeson, S. Ryrberg, “The Door Monted Inflatable Curtain”, SAE 01-1437, 2006

[6] Koichi Kamiji , “Study of test procedure to evaluate airbag deployment force”, SAE 98-S5-O-12

[7] Takayuki Igarashi, “Development of side impact air bag system for head chest protection SAE 98-S8-O-05

[8] Gershon Yaniv, David Romeo, Klaus Kompass, Josef Mayer, “ITS, A New Restaint System for Side Impact Protection”, SAE 961018, 1996

[9] SAE Standard NO. J1630 “Driver or Passenger Airbag Module Deployment Test Procedure”

[10] Ton Versmissen et. Al. “Development and Evaluation of the Side Impact Test Procedure Proposed by IHRA”, 20th International Technical Conference on the Enhanced Safety of Vehicles. Lyon, France, June 18-21, 2007.

ENVIRONMENTAL PERCEIPTION FOR FUTURE INTEGRATED SAFETY SYSTEMS

Juergen Dickmann,
Fabian Diewald
Mirko Mählisch,
Jens Klappstein,
Sebastian Zuther,
Silvia Pietzsch,
Stefan Hahn,
DAIMLER AG,
Germany

Michael Munz,
University of Ulm,
Germnay
Paper Number 09-0175

ABSTRACT

World wide social developments towards Mega-Cities, define future tasks for automotive safety systems. Advanced driver Assistance systems in combination with new preventive safety systems offer great potential for mitigating accidents, reducing accident severity and increasing occupant protection. Traffic in Mega-Cities is characterised by a much higher degree in complexity and dramatically reduced observation time. Thus, automotive safety systems have to face much faster decision requirements compared to present day cruse control systems. Hence, the capability to assess and perceive the actual driving situation in complex traffic situations is the key enabler for future vehicle comfort- and safety systems. The symbiotic exploitation of the electromagnetic spectrum by means of Radar- and optical sensors like Scanner and Vision sensors allows the comprehensive and precise detection even at adverse conditions. The article describes possible approaches.

1. INTRODUCTION

With the introduction of the first brake assist function and it´s logical next step the emergency braking system (e.g. PRE-SAFE Brake® in the Mercedes-S-Class) it became obvious that environmental perception is the key technology to pave the ground for a new era of safety functions. A combination of near- and far range radars was fused to provide the required environmental information.
The next step towards integrated safety was introduced with enhancement of our Pre-Safe Brake function with Pre-Crash capability in the new E-Calls in 2009. Based on the environmental perception of two short range radars, the Pre-Safe occupant protection means are triggered in case of a critical object approach [1]. Up to now, assistance functions on the market concentrate on the use of one single sensor technology like ultra-sonic-, radar-fixed beam lidar-sensors and mono-vision. Sensor fusion enhances the information of one single sensor technology, as e.g. long range radar and near range radars for collision mitigation, to a level which enables the function tasks. This is sufficient for functions which operate in clear driving situations e.g. highways and/or have to perform moderate actions like distance control.
Future comfort- and especially safety functions will more and more address urban regions with dense traffic and therefore have to perform more complex tasks in more complex traffic environments. Thus, the near and mid range distance of the vehicles environment will become more important along with a wider lateral observation horizon in order to cover e.g. crossing scenarios or classical pre-crash situations ind driving direction as well as side-crash situations. This imposes challenging requirements for the environmental sensing, since it translates into dramatically shrinking time scales in terms of observation horizons and reaction times compared to classical ACC and collision mitigation functions of today.
Hence, a much faster up-date rate combined with more detailed and precise information about the traffic environment in terms of localisation and object type is mandatory to allow for a reliable situation assessment. This can be achieved over a two way strategy. First, enhance the sensing performance of each environmental sensor technology in terms of higher spatial resolution towards wide field of view image like properties.

One approach could be the introduction of imaging capabilities to Radars. Add classification knowledge as one perception aid to the sensor information. Second, synergetic exploitation of the electromagnetic spectrum by fusion of different physical sensor technologies, like Radar, Camera or Lidar.
More sophisticated optical sensors like scanning Lidar and Stereo-Vision sensors have made a great stride ahead to meet vehicle relevant maturity and packaging constraints, which will make employment in vehicle systems very likely in the near future.

2. SENSORS

Radar sensors have long been the leading edge in vehicular remote sensing. They determine highly precise distance information and provide instantaneously the corresponding target/object - velocity at nearly all environmental conditions. State of the art radars operate in multi mode covering long and short range distances in one sensor. One field for optimization of todays Radars is the limited field of view along with limited angular resolution, which limits the precision of the target/object localization.
Recent developments in short range radar technology overcome these limitations and are very promising candidates also for side crash scenarios as introduced in section 3. Up to now radars suffer from limited classification capability. On research level, imaging radar approaches are investigated, which definitely will close these present performance gaps to make radar an utmost device [2]. The potential is described in section 4.
Advances in scanning Lidar technology make it an interesting candidate for remote sensing, which offers excellent spatial information along with an extremely wide field of view starting from ±45° up to ±120° and cover ranges from 0 up to 200 m. Recent filter development on the supplier side has enabled velocity information to be provided nearly simultaneously to the spatial information. Since Lidar is an optical sensor, it suffers like vision systems from a limited all weather capability. However, the high end Lidar versions e.g. from Hella KGaA Hueck & Co, have considerably improved even in this area. The high information density allows much better object localisation including dimension and orientation information of the objects. As long as no classification information is required, they could operate as the ideal tandem arrangement to a radar. A very prominent example is described in section 5 for crossing scenarios where a very fast wide field of view and very precise object localisation is required to allow for pre-crash detection.

Vision systems add those information, which cannot easiliy or even never be provided by Radar or Lidar systems. Such as classification information lane-prediction, traffic sign recognition or classification of pedestrians, cylist, vehicle-type etc. . Thus, depending on the safety or comfort function to be realized, vision is the necessary supplement to both Lidar and Radar. Some approaches are described in section 6.

3. FUSION CONCEPT FOR SIDE CRASH SENSING

Viewing the last years, active and passive car safety systems have improved considerably. A lot of active driver assistance systems that support the driver are available on the market. These systems help to reduce the risk of accidents, but in some cases an accident is unavoidable. In these situations passive safety systems, like pre-crash systems [3;4], protect the passengers by activating restraint systems, e.g. reversible belt pretensioners [5].

Radar, LIDAR or camera sensors provide the basis for these applications. By now, most of these safety systems have a benefit in detecting front- and rear accidents. Figure 1 shows that front- and rear-accidents make up only 45% of all accidents causes. To protect the passengers in the 55% not covered by front- and rear sensors, another sensing scheme, possibly up to 360°, is necessary.

Figure 1. Accident impact angle statistics [8].

The importance for 360°-sensing shows up among others in EURO- and US-NCAP crash tests (see figure 2), which are based on crash statistics and cover the most usual accidents, including side crashes (car to side and pole impact). Although the severity of these accidents is reduced by passive safety structures, the passengers will benefit from electronic safety systems, which mitigate the consequences of the crash even more. Using a 360°-sensing method, not only the behaviour in crash tests, but the overall performance for real life safety [6] can be improved.

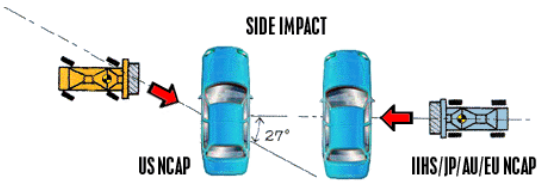

Figure 2. Example of European (EURO-NCAP) and United States (US-NCAP) side impact crash tests [9].

Sensor setup

To cover all accident causes, as shown in figure 1, a sensing method has to be incorporated to observe the car's entire environment. This can only be achieved by either a lot of sensors, or as pursued in this approach, a few sensors with a wide field of view. In addition to that, the sensors must work reliably in all weather conditions like rain, fog or snow. Weather conditions are still a problem for optical sensors like camera and LIDAR, whereas radar sensors can cope with bad weather conditions quite good. Until today, the field of view of automotive radar sensors is typically up to 80°, which is better than that of common cameras, but not sufficient for sensing more than just a small part of the car's surrounding. As radar technology advances and sensors get cheaper and better, radar sensors with a field of view of 150° and a range up to 60 m are becoming achievable. Suitable sensors, fulfilling the requirements for automotive side- or 360°-sensing are the multi-beam radar sensors provided by Valeo, which will be used here. To perceive the environment of the car, 4 of these multi-beam radar sensors are used. They are mounted on the corners of the car and placed invisibly behind the bumper. The surveillance region of the sensors is show in figure 3. With this sensor setup the environmental sensing of both car sides is possible by using only 4 sensors that cover mostly the entire car environment. Although not addressed here, other applications, e.g. front- and rear pre-crash, lane change support, and blind spot monitoring, are also addressable with this setup.

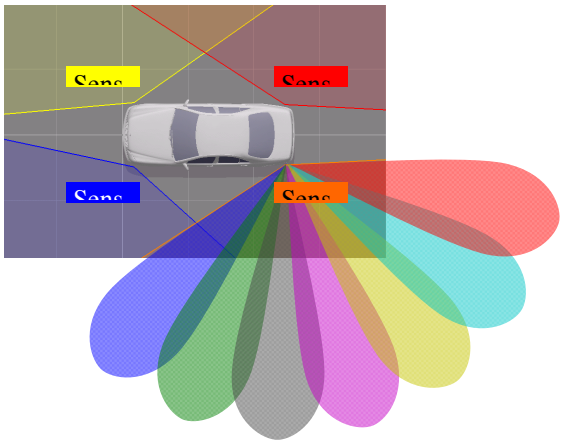

Figure FSZ3. Experimental setup of a test car using four multi-beam radar sensors.

Subsequently a suitable pre-processing technique, the multi-sensor fusion and the performance of this sensor setup will be shown.

Pre-Processing

The target detection list of each sensor is traversing a pre-processing algorithm before being incorporated in the main multi-sensor fusion.

Each sensor has seven beams where up to three beams have overlapping detection areas. Thus, such a multi-beam radar sensor may detect targets with larger radar cross sections in more than one beam. One way to cope with this, while still using a one-to-one data association algorithm, is to integrate the data sequentially (beam by beam) in the multi-sensor fusion. Another approach, which is taken here, is to pre-process the data to reduce the number of computations necessary in the fusion process. The pre-processing algorithm is shown in Figure 4.

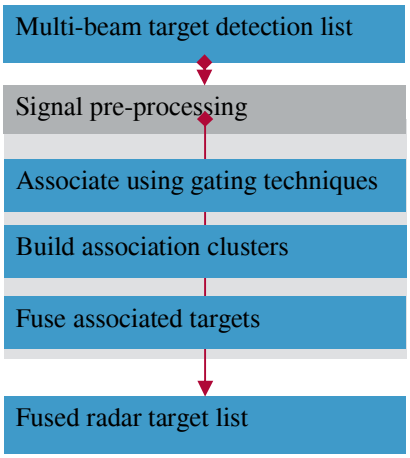

Figure 4. Multi-beam radar sensor signal pre-processing.

The first step in fusing the multi-beam target detection list is finding target-to-target associations with a nearest neighbour algorithm. The next step involves the building of association clusters [see JPDA clustering]. An association cluster contains all detections that have associations in common, e.g. Target 1+2, Target 2+3 → Cluster Target 1+2+3. With this information at hand the target list is then fused, hereby reducing the measurement errors of targets sharing multiple detections. Using this technique, the overall target count is reduced as well. An example of the outcome of the algorithm is shown in figure 5. Targets are pictured by rectangles, the measurement accuracy is shown by the 3□-ellipses, and detections of different beams can be distinguished by colours. The resulting target with smaller covariance is shown using a dotted line.

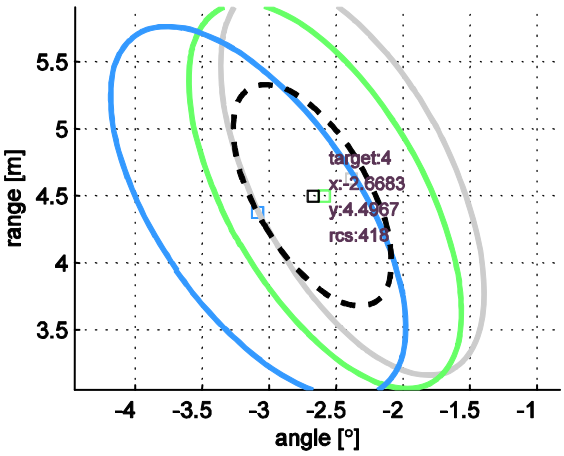

Figure 5. Example of a target which is detected by three beams. Beams are plotted using colours as seen in figure 3; the fused target is plotted using a dotted line.

The pre-processed data is then integrated into the multi-sensor fusion described in the next section.

Multi-sensor fusion

The multi-sensor fusion is realized using a multi-sensor multi-target tracking with the common technique of Kalman filtering. Figure 6 shows the sequence of the fusion process.

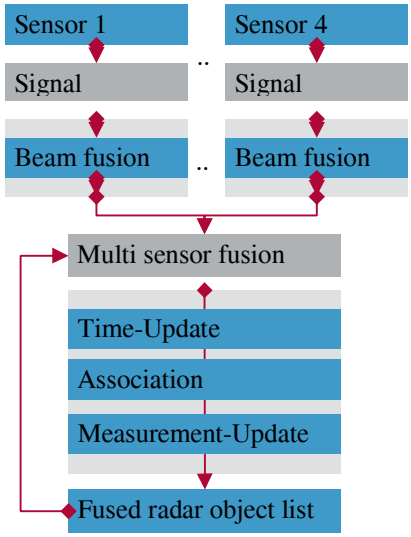

Figure 6. Multi-sensor fusion method for 360°-sensing.

The pre-processed target list data is integrated sequentially as follows. The track states of the system are predicted to the current measurement interval. Using the calibration data of the sensors, the new sensor measurements can be mapped to the car's coordinate system and vice versa. This way a measurement-to-track association is made and the measurement update of the Kalman filter is calculated. In this approach an extended Kalman filter is used for the estimation process, the measurement vector consists of the entries range, bearing and Doppler velocity. The Doppler information, the direct measuring of target speed which is a benefit of radar sensors, is used to initialize the state of the tracks [7]. This technique avoids wrong associations that result from the great velocity uncertainty if only position measurements where used. Filter settling times are also reduced, hereby improving the overall performance of the estimation process.

Triggering restraint systems

The demo vehicle, used to verify the algorithm's performance, has active seat belt pretensioners, but other actuators could be used as well. The actuators will be triggered just before an imminent crash is detected to reduce the severity of the accident. The position and velocity information of the estimated tracks is used to calculate a time to collision (TTC), and the point of impact (POI). In this approach a propagation of the covariance in time and space is performed, resulting in time (→TTC) and space (→POI) probabilities. The fused radar object list serves as input to this detection module, which is subsequently used to trigger restraint systems (see figure 7).

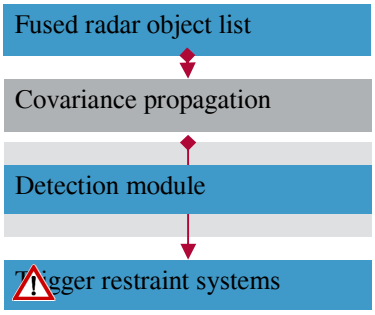

Figure 7. Decision algorithm for triggering restraint systems based on a fused radar object list.

Testing the algorithm with non-destructive tests is quite demanding, as own ship vehicle and target motion is highly dynamic. For testing the 360°-sensing capability of the presented system, a test facility on proving ground will be put into operation soon. By using this setup, predictable and repeatable test data will be gained and overall system performance in these challenging situations can be evaluated.
Side crash sensing is being deduced by the ever increasing safety functions in cars. New generation of radar sensors provide wider field of views, which are necessary for 360°-sensing, as well as further driver assistance systems. The packaging for automotive use is easy, because the sensors can be mounted invisibly behind the bumpers. The pre-processing of multi-beam radars reduces the demands on computation time and improves sensor accuracy. The multi-sensor fusion approach shown here is suitable for side-sensing, but is independent of the application.

Figure 8. Demo vehicle (Mercedes S-Class) with grill guard

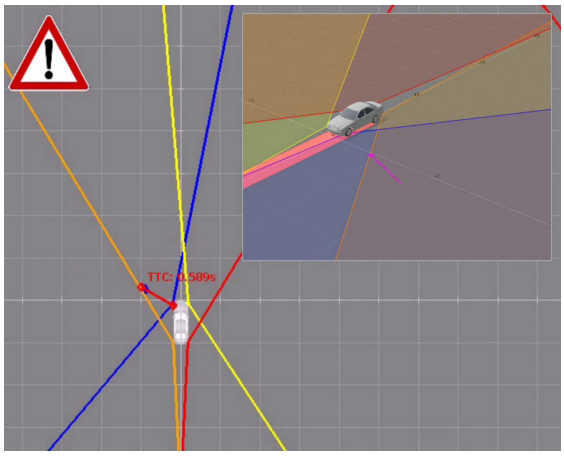

Figure 9. Example of an impact detection. The object is approaching the demo vehicle at an angle of approximately 60°.

It can be generalized to support front- and rear-precrash functionality and thus provides the basis for an automotive 360°-surveillance for a new generation of car safety functions.

4. Imaging Radar potential

Due to a variety of important advantages radar sensors have become common in driver assistance systems for about a decade. E. g., the robust performance even under poor weather conditions like fog or rain. Beyond these aspects, in contrast to lidar and camera sensors radar sensors can measure radial velocity towards the ego vehicle directly by the evaluation of the Doppler shift of the reflected electromagnetic wave. Another competitive edge of radar sensors is the measurement accuracy of the distance to other objects in a traffic scene. It can be

determined more accurately by radar than by stereo cameras, especially at mid to large distances and vehicle relevant stereo bases. These aspects are summarized in table 1.

Table 1.
Comparison of automotive sensor systems

	video	radar	radar (scanning)	lidar (scanning)
distance resolution	-	+	+	+
azimuth resolution	+	-	O	+
velocity measurement	-	+	+	-
weather robustness	-	+	+	-

Although radar sensors are commonly used in series vehicles for Adaptive Cruise Control (ACC), there is still demand for optimization. The determination of distance and velocity of other non-stationary vehicles is precise enough for the basic functionality of ACC.
However, former radar sensing technology had its limitations concerning ACC applications. A crucial point for the distinction of relevant stationary objects in the lane (e. g. at the end of a traffic jam) from irrelevant objects like traffic signs is the robust recognition of the oncoming lane course. Moreover, stationary objects have to be perceived separately from the road boundaries. This could not be achieved robustly by former radar sensors due to their comparatively low field of view and low resolution of the azimuth angle. Consequently present ACC systems only react on moving targets or stationary targets that have been seen in motion before.
On the other hand, there are radar-based driver assistance systems reacting on stationary targets as well. In the case of a possible collision with a stationary obstacle these systems warn the driver and e. g. activate the belt pretensioner. As soon as the collision becomes inevitable, the vehicle brakes autonomously and so mitigates the oncoming collision.
The inclusion of stationary obstacles in ACC functionality and the precise determination of the point after which a collision with a stationary obstacle gets inevitable are two examples for the importance of improvement of radar measurement accuracy. Autonomous breaking reactions as a severe intervention into the guidance of a vehicle may only be initialized when the driver does not have the chance to avoid the collision by steering any more

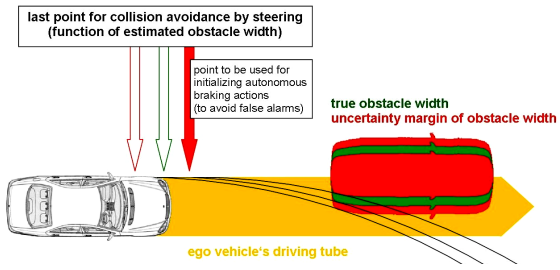

Figure 10. Relation between estimated obstacle width and the point to be used for initializing autonomous braking actions.

Figure 10 shows the relation between the lateral offset a vehicle has to build up for collision-avoidance with an obstacle and the last point at which the driver has the chance to avoid a collision by steering.
Not only the requirement of accurate measurements of single objects for collision mitigation systems leads to the need for enhanced sensor performance. The transfer of driver assistance systems' functionality from simple highway scenarios to highly complex urban scenarios in the typical Megacity of the 21st century requires the robust perception of highly complex traffic situations.
Robust means availability of service even under adverse weather conditions as well as highly precise localization of objects. For this reason, perception performance of radar sensors have to be further optimized. Radar may also benefit from vision systems and their better azimuth resolution. Object classification information, if required, can also be provided by camera systems. However, vision usually suffers from poor robustness under bad weather or backlighting conditions. Research activities investigate the fusion benefit (see section 5). Therefore, new radar approaches are the key. Whereas former radar systems only registered single points of reflections from the environment, imaging radar systems now provide a detailed image of the environment. Providing angular resolutions of about 1° they are already installed in series-production vehicles. Figure 11 shows an image from a mass-produced imaging radar sensor as the representation of a traffic scene. The new degree of detail leads to new chances and challenges in processing radar data. Research activities are trying to evaluate the performance of image processing algorithms used for the processing of radar images. In this connection, radar-specific characteristics have to be accounted for. E. g. the noisy raw data

from imaging radar

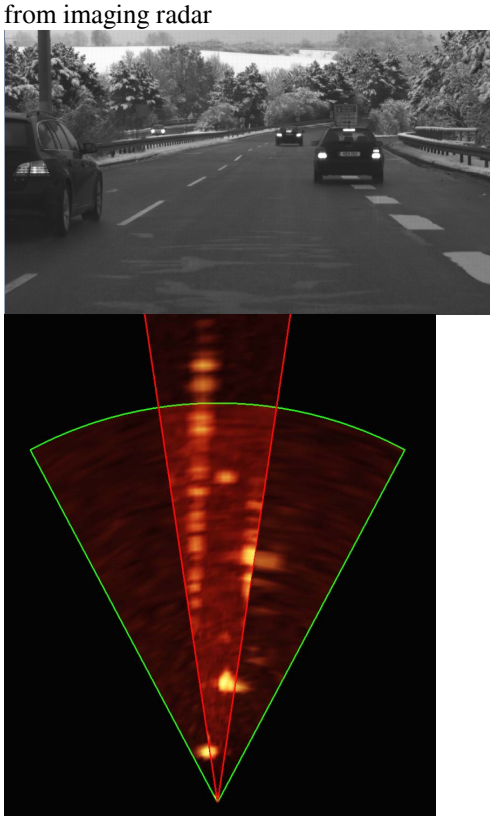

Figure 11. Image from an imaging radar sensor (red bordered area: long range radar, green bordered area: short range radar). The three vehicles and the lane boundaries (above) are clearly to be seen in the radar image (bottom). Integrating raw data over time or evaluating the Doppler shift of moving objects are only two possibilities to increase perception robustness.

sensors can be integrated over time, leading to an improved signal to noise ratio as sown in fig. 12. The radar image on the left (middle) shows the raw radar image of the scene (top) with a significant amount of noise. The radar image on the right (middle) is integrated over time. Here, the image from preceding measurements is weighted with 0.9 and the current measurement with 0.1, leading to significant noise reduction. As a consequence, this step can increase the robustness of following radar image processing steps. After a following Prewitt edge detection size and position of the two vehicles in front of the ego vehicle can be seen more clearly in the integrated image compared to the raw data image (bottom). The picture also shows radar sensors' capability to perceive vehicles hidden by others. Whereas the car in front of the nearest car can hardly be seen in the video picture (top),

Figure 12. Images from an imaging radar sensor without (left) and with (right) integrating raw data over time before (middle) and after (bottom) the application of a Prewitt edge detection algorithm.

it can clearly be seen in the radar image (middle/Bottom).

Another radar-typical benefit besides direct velocity measurement is the height determination of targets. The height of targets may be determined from the evaluation of the radar cross section (RCS) value over time (see fig. 13) [11]. There are also approaches trying to distinguish artificial from natural objects by evaluating polarisation differences of radar reflections [11].

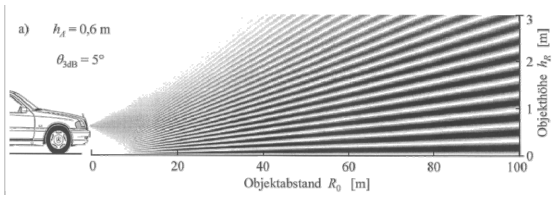

Figure 13. Waves emitted by continuous wave radar sensors lead to a typical, height-dependent interference pattern. The height-dependency may be used to distinguish relevant obstacles with low height from higher located irrelevant objects like traffic signs [11].

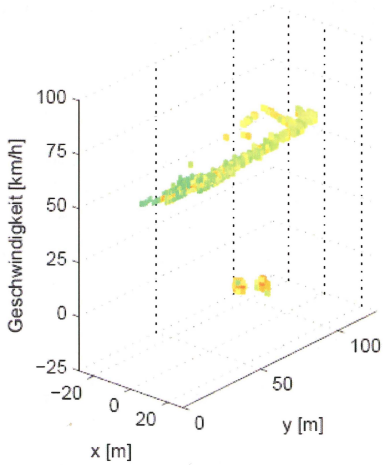

Figure 14. Three-dimensional statement of measurement data in lateral and longitudinal position and speed (here on the vertical axis) [10]. Including height information would provide a forth dimension for segmentation.

In a nutshell, treating data from imaging radar comes with its own challenges and chances. The most important challenge is the still comparatively bad angular resolution of 1°, usually. On the other hand, the directly measured radial velocity of targets (see fig. 14) and the determination of target height provide new dimensions for segmentation and object separation. Object classification strategies may be supported by evaluating polarisation differences of the reflections.
The increased necessity for computational power by new signal processing algorithms will be compensated by Moore's law – falling prices for computational power will help to achieve the aim of improved perceiving performance for future driver assistance systems.

5. Fusion of Laserscanner and Short Range Radars for Pre-Crash detection

Scanning laser devices emit laser pulses bound to fixed angle steps. Reflected by objects in the environment they generate distance measurement points using time-of-flight calculation. Because angle steps range from few degrees to a fractional amount of a degree, respectively, a multitude of reflections originates from a real world object, what leads to complex environmental scans showing the contours of real objects. Figure 15 shows an example. Large parts of the truck are simply not visible to the radar sensors (bigger circles), whereas the laser scanner perceives its dimensions (small dots). The ability to perceive object geometries together with a high measuring accuracy in position and a large field of view makes the laser scanner a profoundly appropriate device in a perception system utilized in complex environments like intersections and inner city areas.

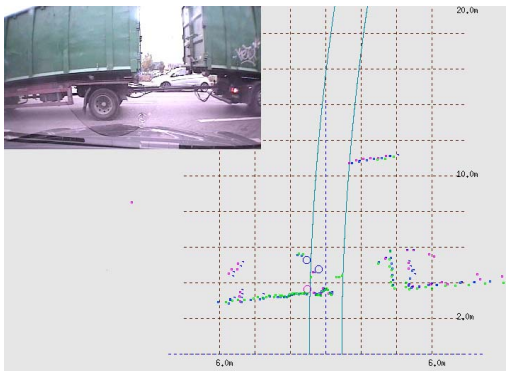

Figure 15. Environmental scan example. Single laser echos are shown as dots, the bigger circles represent radar targets.

Nevertheless, laser scanners as well as other optical sensors are sensitive to pollutions and bad weather conditions like heavy rain, snow or fog. A combination with radar sensors can provide support in order to make the complete system more robust. Another advantage of radar sensors is the capability to measure velocities directly whereas for laser scanner data the velocity information has to be derived from changes in position. With a skilful sensor data fusion the advantages of both sensor types can be combined to achieve a precise estimation of position and dynamics parameters of surrounding objects enhanced with dimension information with preferably short delay.
Depending on the used sensors and the requirements on the application, data fusion can be realized on different levels. Thereby, it is distinguished between signal level, target level (=midlevel) and object level fusion. In case of laser scanner in combination with radar sensors the different sensor principles exclude a fusion on raw data level due to missing correlations between single laser reflections and radar echos. Fusing on target level systematically

combines the advantages of each sensor that is, on the one hand, the precise position estimation provided by the laser scanner, and, on the other hand , the velocity estimation provided by the radar sensors.

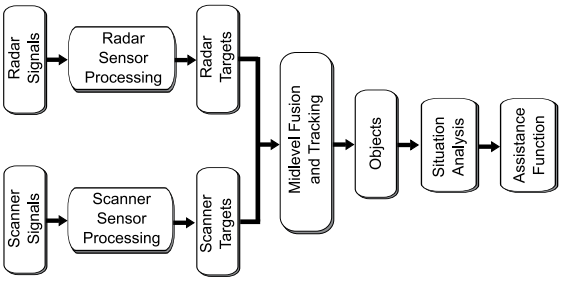

Figure 16. Target level fusion architecture

Figure 16 gives an overview of the system architecture. Data capturing is followed by a preprocessing step for each sensor separately. For the radar sensors preprocessing is the target formation from different echos. The preprocessing of raw laser scan data includes the segmentation of the point clouds followed by the feature extraction from the several segments.

Segmentation is performed using a grid-based approach. The design of the (radial) segmentation grid is based on the measurement principle of the scanner. Cell size increases with the distance to the scanner and the absolute value of the angle [12] [13]. In a first step, all scan points are projected onto the grid. In a second step adjacent occupied grid cells are melted together to form a segment.

A feature extraction step reduces the amount of data and generates object hypotheses that comprise information about position, orientation and dimension. The calculation of possible occlusions and the extraction of further segment describing features like convexity, compactness, aspect ratio, etc. are tackled in this processing stage as well.

Laser and radar targets are combined within a measurement vector fusion. For object tracking and object formation well-known Kalman-Filter techniques are used [14]. If measurements of both sensor types are within the gate of a predicted object a fused measurement updates the existing track. The property of the laser scanner to detect expanded objects necessitates investigation in special cases in the fusion step. If radar targets are located within a segment box, but far away from the reference point, the measurement vectors of both sensors are not fused in order to avoid high jitter in object tracking. Nevertheless, the information about the object being detected by the radar sensor at all, is not discarded, but can be used for object validation, afterwards.

Within the framework of APALACI (Advanced Pre-crash and LongitudinAl Collision mitigation), a subproject of the European Integrated Project PReVENT, an application that recognizes frontal collisions with stationary objects was developed based on the described architecture [12]. During the project a host vehicle was equipped with sensors, actuators and processing hardware to run the application in real-time (see Figure 17). The laser scanner has been mounted below the number plate covered by a black plastic faceplate that is transparent for the emission wavelength, thus it integrates into the car's design. In case an unavoidable collision is detected to happen within the next 200 ms the system triggers reversible belt pretensioner which bring the passenger into an upright position.

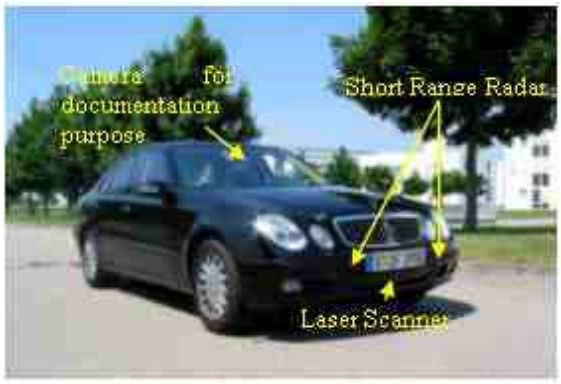

Figure 17. Experimental vehicle

The application has been validated in complex crash and non-crash scenarios conducted at a test site with foam cubes and cylinders as obstacles. The scenarios comprise factual and near missed collisions with stationary objects at different velocities, in curves, with deceleration, sudden lane changes and lane changes of a leading vehicle obstructing the sight to the obstacle. In total, the results were a false alarm rate of 1.1% (1 out of 95 test runs) and a missed alarm rate of 6.9% (7 out of 102 test runs). For a complete description of the test catalogue and a discussion of the results we refer to [13]. Furthermore, the application was tested in normal traffic on highways, rural roads and in urban areas. All in all, a distance of 1600 km was covered facing adverse weather conditions like rain, fog as well as different driving situations like rush hour, traffic jam and stop-and-go. No false alarms occurred during these tests.

Ongoing research investigates in refining and further improving the sensor data processing and fusion methods in order to provide advanced driver assistance functionality especially with regard to more complex and dynamic environments. Today's assistance and safety functions have to work in a very restrictive way in order not to risk severe false

alarms due to driver acceptability and product liability reasons [15]. Therefore, the development of algorithms for environmental perception aims at detecting impending threats both quickly and reliably. Providing further information about surrounding objects in excess of position and velocity like dimensions and possible occlusions helps to classify objects and facilitates situation analysis.

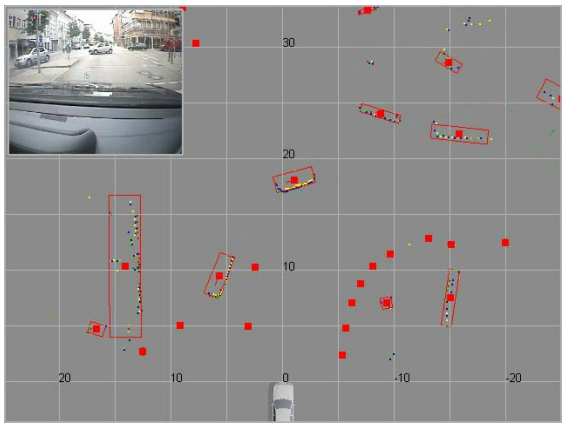

Figure 18. Sample data captured at an intersection and processing output. Red boxes represent confirmed tracked objects (stationary and moving)

Figure 18 shows results of object formation by means of a sample scene captured in city traffic. Object dimensions and orientations are calculated from laser segments and filtered over time. A small line at the object's middle point corresponds to the velocity vector, thus marking a moving object. The process of deriving good object state estimates from laser data can further be improved by a fusion with radar data. Laser objects form a region of interest where to look for radar targets. If radar targets are available, the (relative) velocity can be initialized directly with the Doppler information.

6. Sensor Fusion of Radar or Lidar with Mono-Vision for Pre-Crash detection

6.1 Sensor Setup, Alignment and Preprocessing

Future driver assistance functions will perform fully autonomous interventions like automatic emergency braking or the triggering of occupant restraint systems even before the crash happens. In comparison to today's assistance functions, an increased degree of certainty is required for the environment perception subsystem in the object state estimation domain and - even more important - in the object existence and classification domain. One way to achieve this reliability is the fusion of multiple sensor data. In this context, a fusion system overview with ranging sensors and a monocular video camera is presented. For the ranging sensor part, radar and lidar are exchangeable. A requirement for each sensor fusion setup is a spatial and temporal sensor alignment. A hardware synchronisation of both sensors was chosen, as it is the optimal choice with respect to inter-sensor data association and computation time aspects. However, all future serial sensors intended for sensor fusion systems must provide any mechanism for temporal alignment, whether it is an external measurement trigger signal input or the generation of timestamps in relation to an external master clock in free running mode. The spatial alignment is computed with novel calibration procedures published in [16].

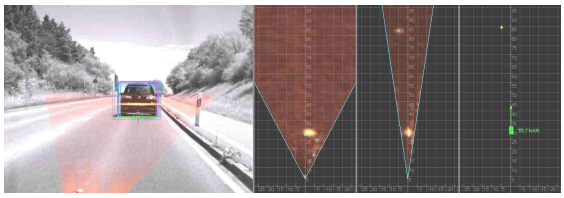

Figure 19 Sensorfusion with Radar and Video. The ranging data is associated with the image and measurements from both sensors are used for target tracking (right).

Using this alignment, the signal processing stage first projects the lidar or radar measurements into the image domain. The image regions containing an echo are further processed with a cascaded Boosting classifier based on Haar-like features [17]. This detection strategy combines the longitudinal position accuracy of the ranging sensors with the lateral position accuracy and the object classification performance of the video sensor. Beside these state refinements, a cross-validation of detections from both sensors increases the reliability of the environment model. In comparison to usual ranging sensor based systems, the presented sensor setup is not limited to moving objects.

Figure 20 Sensor mounting positions

6.2 Sensor Fusion Algorithm

The sensor independent fusion framework has a kernel-based design. The independent sensor modules deliver their measurements to the fusion system using their own measurement frequency. Each sensor module uses the same interface to the fusion module consisting of measurement vector **z**, corresponding uncertainties **P** and sensory existence measurements p_s. The fusion system uses the JIPDA method [18],[19],[20] for estimation of state and existence based on these measurements. Therefore, any optimization for the sensor setup is made in the sensor specific part of the models and the fusion kernel is completely sensor independent. The framework implementation comprises a complete existence probability based track management module, state and existence tracking. Furthermore, track splitting and merging can also be realized in the central track management module. Sensor modules need to provide measurements and have to implement a possibility to create and initialize new tracks according to the decisions of the fusion framework.

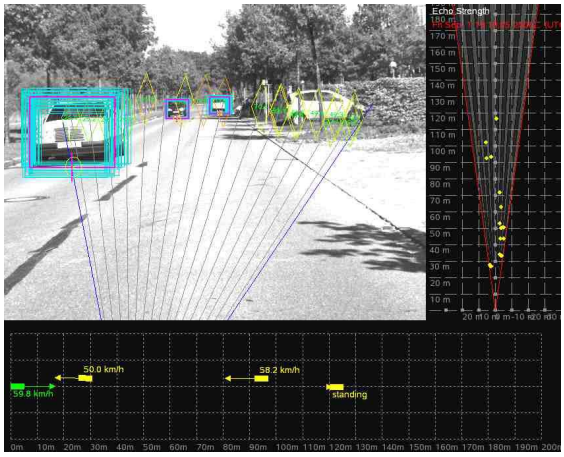

Figure 21 Lidar-Video sensor fusion: The Lidar echoes (top right) are projected into the image domain (top left). The image processing (cyan boxes) classifies objects as vehicles. Even non-moving vehicles can be tracked in distances up to 100 meters (bottom).

7. Conclusion

Introducing the PRE-SAFE Brake preventive protection system in the S-Class 2002, launched a system that for the first time employed the critical assessment of a vehicle´s driving dynamic state prior a propable impact for activating reversible safety counter measures. In 2009, the system has been enhanced in the new E-Class by the capability of the vehicle to monitor its near range environment to detect very likely collisions. This is the first step into real Pre-Crash situations and hence a great stride ahead towards urban area relevant safety functions. Further more effort is needed to fully exploit the potential of safety functions for dense traffic like f.e. Mega Cities. The paper has outlined that radar sensors will continue to be the key-technology and backbone of future safety functions. Especially Imaging Radar capabilities and intelligent fusion techniques will enhance the power of radar based safety systems. Assisted by optical sensor technologies, environmental sensing will be prepared to pave the ground for the safety needs in the future.

8. References

[1] R. Bachmann, U. Merz, R. Bogenrieder, Das PRE-SAFE-System neue Funktionen ergänzen den präventiven Insassenschutz, ATZextra I Januar 2009, pp.80-83

[2] Schneider R., Wenger J., “Advanced Microsystems for Automotive Applications 2003”, in VDI-Buch, Springer Berlin Heidelberg, ISBN-978-3-540-00597-1, 2003, pp. 97-111

[3] M. Skutek, M. Mekhaiel & G. Wanielik, “A precrash system based on radar for automotive applications”, Intelligent Vehicles Symposium, 2003, 37-41

[4] S. Mueller, H. Ritter, H. Rohling & M. M. Meinecke, “Signal processing strategies for a multi sensor pre-crash application”,VDI Gemeinschaftstagung, 2006

[5] C. Kurutas, K. Elsaber, D. Schramm, and M. Hiller, “Modeling and simulation of the effect of reversible belt pretensioners”, Mechatronics, pp. 119-124, 2006

[6] Daimler AG, “Real Life Safety”, Brochure 2008, Global Communications Mercedes-Benz Cars (COM/MBC)

[7] S. Yeom, T. Kirubarajan & Y. Bar-Shalom, “Track segment association, fine-step IMM and initialization with Doppler for improved track performance”, IEEE Transactions on Aerospace and Electronic Systems, 2004, 40, 293-309

[8] http://www.safecarguide.com/exp/usncap/usncap.htm, as of 2009, February 23

[9] http://www.safecarguide.com/exp/usncap/usncap.htm, as of 2009, February 23.

[10] Schmidt, T., „Verfahren zur Objekterkennung für ein bildgebendes Kfz-Radar“, Diplomarbeit Hochschule Ulm 2007

[11] Schneider R., „Bildgebendes Radar zur Erfassung von Verkehrsszenen“, Technischer Bericht DaimlerChrysler AG, 1998

[12] Skutek, M., “Ein PreCrash-System auf Basis multisensorieller Umgebungserfassung”, PhD-Thesis, TU Chemnitz, 2006

[13] Pietzsch, S., Vu, T. D., Burlet, J., Aycard, O., Hackbarth, T., Appenrodt, N., Dickmann, J., Radig, B., “Results of a Precrash Application based on Laser Scanner and Short Range Radars”, in Proc. of IEEE Intelligent Vehicles Symposium, 2008, pp. 367-372

[14] Kalman, R.E., “A New Approach to Linear Filtering and Prediction Problems”, in Transaction of the ASME – Journal of Basic Engineering, 1960, vol. 82, pp. 35-45

[15] Hillenbrand, J., Spieker, A. M., Kroschel, K., “A Multilevel Collision Mitigation Approach–Its Situation Assessment, Decision Making, and Performance Tradeoffs”, IEEE Transactions on. Intelligent Transportation Systems, vol. 7, nr. 4, 2006, pp. 528-540

[16] M.Maehlisch, R.Schweiger, W.Ritter, and K.C.J.Dietmayer, “Sensorfusion using spatio-temporal aligned video and lidar for improved vehicle detection,” in Proceedings of IEEE Intelligent Vehicles Symposium, Tokyo, Japan, 2006.

[17] P.Viola and M.Jones, “Robust real-time object detection,” in Second International Workshop on statistical and computational Theories of Vision-Modeling, Learning, Computing, and Sampling, Vancouver, Canada, July 13 2001.

[18] D. Musicki and R. Evans, “Joint integrated probabilistic data association: JIPDA”, IEEE Transactions on Aerospace and Electronic Systems, vol. 40, no. 3, July 2004.

[19] M. Maehlisch, M. Szczot, O. Loehlein, M. Munz and K. Dietmayer, Simultaneous Processing of Multitarget State Measurements and Object Individual Sensory Existence Evidence with the Joint Integrated Probabilistic Data Association Filter, 5th International Workshop on Intelligent Transportation, Hamburg, Germany, 2008

[20] Michael Munz, Mirko Mählisch, Klaus Dietmayer: “A Probabilistic Sensor - Independent Fusion Framework for Automotive Driver Assistance Systems”, 6th International Workshop on Intelligent Transportation, Hamburg, Germany, 2009

ANALYSIS OF INJURY TRENDS IN FRONTAL UNIVERSITY OF MICHIGAN CIREN CASES IN THE CONTEXT OF CRASH TESTS

Bridget O'Brien-Mitchell
Kacy Bailey
Daniel Faust
Jack Jensen
Julie Kleinert
Christine Wodzinski
Carla Kohoyda-Inglis
Stewart Wang
University of Michigan Program for Injury Research and Education
United States
Paper Number: 09-0188

ABSTRACT

Four-hundred forty two U-M CIREN (University of Michigan Crash Injury Research and Engineering Network) cases have previously been compared to crash tests used in the automotive industry. The comparison demonstrated that the majority of cases were similar in crash configuration and extent to industry crash tests, while smaller proportions either had a greater extent of crash deformation or had different crash configurations than those commonly produced in crash tests.

Of the 442 cases, 290 frontal cases were analyzed in greater detail to understand trends in injury causation while considering physical characteristics of occupants (gender, age, body mass index.) Those trends were then evaluated in the context of biomechanics of crash test tools such as Anthropomorphic Test Devices [ATDs] and injury risk curves. Several trends were identified and presented.

INTRODUCTION

Studies have demonstrated that fatality rates from motor vehicle crashes in the United States have been reduced over the last several decades. As an example the fatality rate per 100 million miles driven was 5.5 in 1966 and steadily declined to 1.41 in 2006. In addition, injuries have been reduced from 169 injuries per 100 million miles driven in 1988 to 85 in 2006. Despite the significant improvements in automotive safety, there continue to be about 38,500 annual fatalities due to motor vehicle crashes [1]. Therefore there is benefit to investigating the remaining fatalities and injuries due to motor vehicle crashes.

The goal of this project was to analyze the injuries sustained by occupants in frontal crash U-M CIREN cases and identify trends within crash configurations and Collision Deformation Classification (CDC) extent groups [2].

Of the 290 frontal case occupants, 73% were drivers and 19% were right front passengers. There were slightly more females, 51%, than males, 49%. The average age of the case occupants was 41 years old. 66% of the women and 50% of men were using 3-point seat belts. The average Body Mass Index (BMI) was 27.3 which is categorized as overweight [3].

BACKGROUND

Comparison of Frontal Crash U-M CIREN Cases to Existing Types of Crash Tests

Auto manufacturers routinely conduct crash tests to verify compliance to crash test regulations for any country in which a vehicle may be marketed, for evaluations of consumer metric tests, and for internal review of vehicle performance. Four-hundred forty two U-M CIREN (University of Michigan Crash Injury Research and Engineering Network) cases have previously been compared to crash tests used in the automotive industry. Table 1 lists the frontal crash test types that were developed for comparison to the U-M CIREN cases in the previous study [2].

Table 1.
Included Industry Crash Tests

0 Degree Frontal (FMVSS 208 or Frontal NCAP)
Left Angle or Offset (FMVSS 208 angle or IIHS offset)
Right Angle or Offset (FMVSS 208 angle)
Frontal Center Pole
Frontal Offset Pole
Bumper Underride

The cases were additionally divided by those with CDC extents above and below the extents assigned to these crash tests. Finally, the remaining frontal cases were grouped in new crash configuration categories as shown in Table 2.

Table 2.
Frontal Crash Types without a Corresponding Crash Test

Left small overlap
Right small overlap
Underride
High undercarriage
Sideswipe
Corner underride
Offset underride

It is important to acknowledge that this study is based solely on cases documented in the U-M CIREN database. As such, the uninjured population is not included for comparison. By the definition of the CIREN selection criteria, all of the case occupants are severely injured patients. Those crashes in which there are no injuries or only minor injuries are not included in the CIREN database or the U-M CIREN database, and are not referenced in this study. Thus it is not appropriate to use the CIREN database or the U-M CIREN database in isolation to estimate risk to the driving public.

The distribution of U-M CIREN frontal cases is shown in Figure 1. 53.8% of the 290 frontal cases studied matched an existing crash test configuration with an extent less than or equal to the test. 32.1% of the frontal cases matched an existing crash test configuration but with greater extent, and 14.1% did not match an existing crash test configuration.

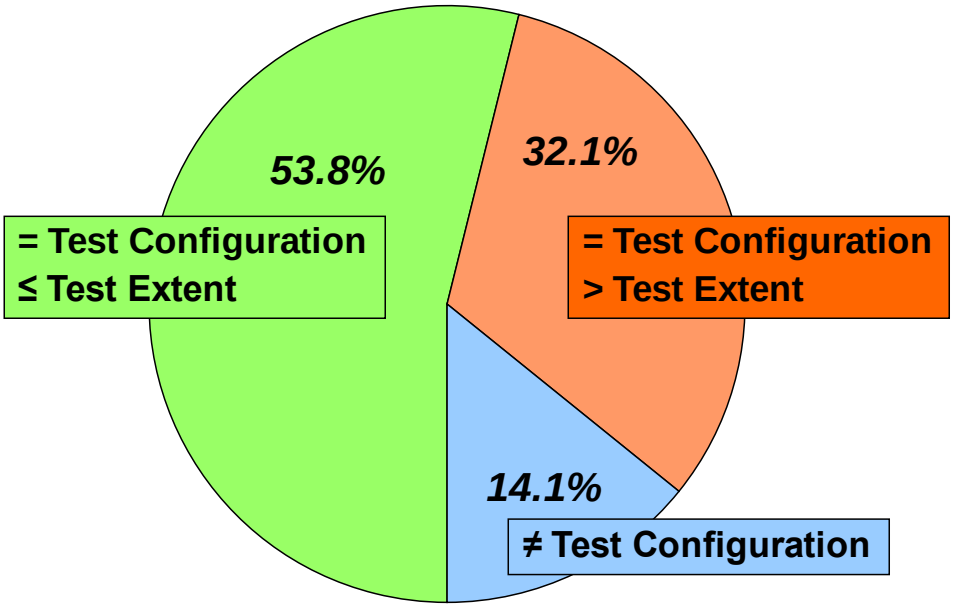

Figure 1. Distribution of U-M CIREN Frontal Cases.

Cases Matching Test Configuration and Extent

Figure 2 shows the distribution of the 53.8% of U-M CIREN crash cases that had configurations similar to and CDC extents less than or equal to current laboratory tests. For frontal crashes, the 0 degree frontal impact category was the most represented in U-M CIREN followed by the left angle or offset category.

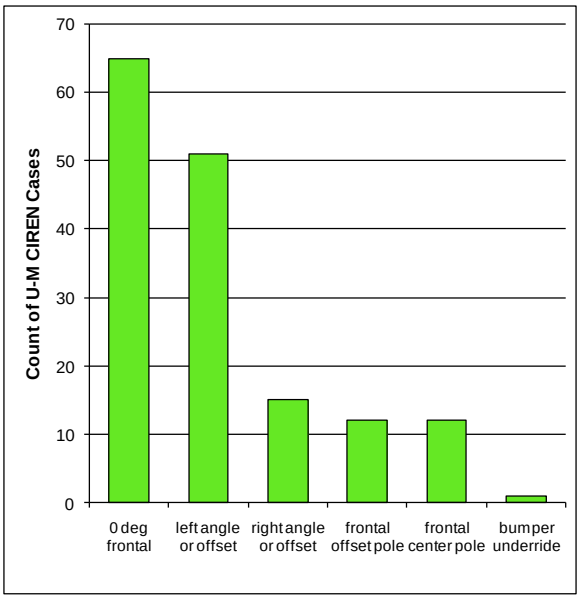

Figure 2. Distribution of U-M CIREN Cases for Crashes with Similar Configurations and CDC Extents Less Than or Equal to a Current Industry Crash Tests.

Cases Matching Test Configuration but with Greater Extent

Figure 3 shows the distribution of the 32.1% of U-M CIREN crash cases that had configurations similar to current laboratory tests with CDC extents greater than current crash tests. Similar to the cases with lesser extents, the 0 degree frontal was the most prevalent frontal impact, followed by the left angle or offset category. There were very few frontal pole crashes with extents greater than the industry crash tests.

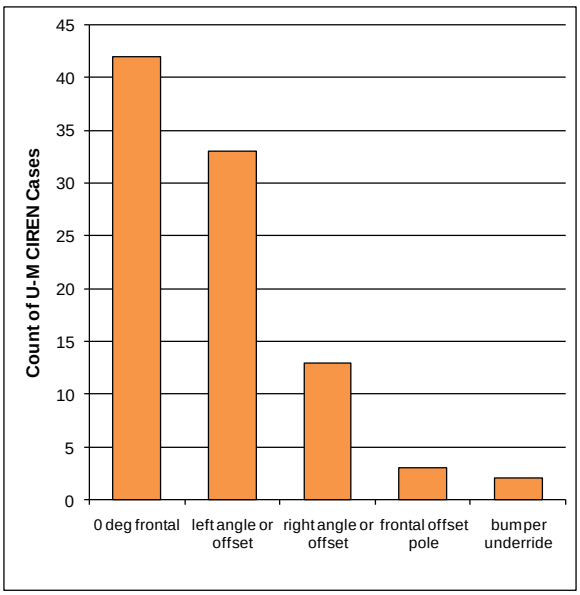

Figure 3 — Distribution of U-M CIREN Cases For Crashes with Similar Configurations and CDC Extents Greater than a Current Industry Crash Test

Cases Not Matching Test Configuration

Figure 4 shows the distribution of the 14.1% of U-M CIREN crash cases that did not match a current industry crash test configuration. The majority of these cases were left or right small overlap crashes. The small overlap crashes had deformations that were typically outside of the longitudinal rails.

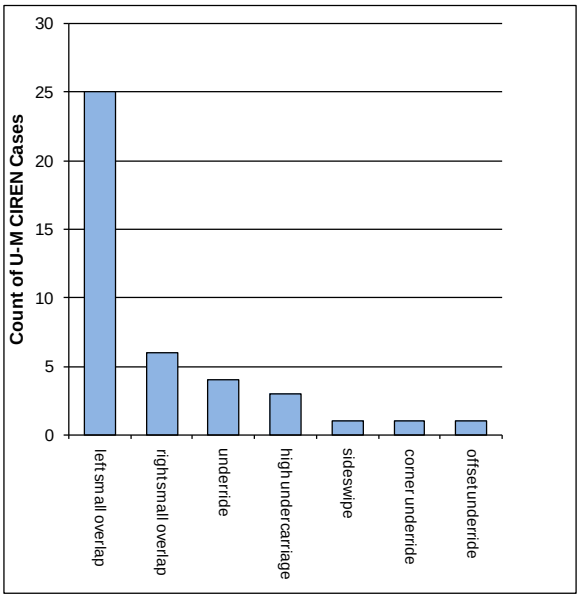

Figure 4. Distribution of U-M CIREN and CIREN Cases for Crashes That do Not Match a Current Industry Crash Test.

ANALYSIS

Injury Trends by Body Region

Figure 5 shows the distribution of AIS 3+ injuries by body region for each of the three frontal impact categories. The body regions with the highest number of injuries were the lower extremity, the thorax and the head.

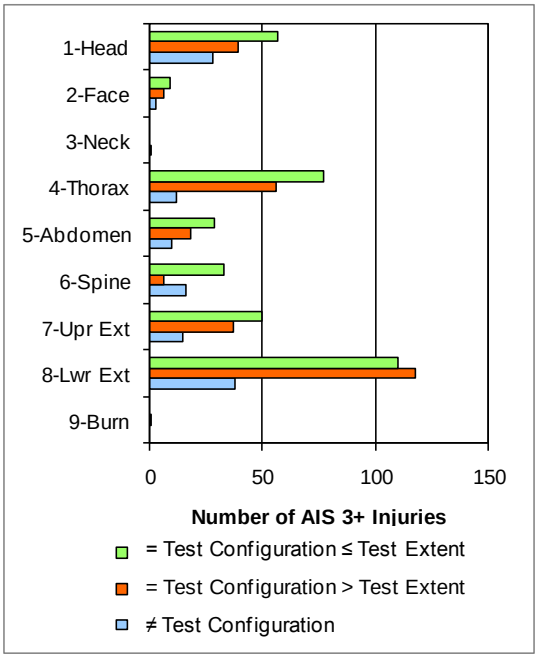

Figure 5. Frontal Impact Crashes – AIS 3+ Injuries by Body Region.

Injury Trends for Frontal Cases Matching Test Configurations and Extent

For frontal cases that had configurations similar to current laboratory tests and had extents less than or equal to current crash tests, the top ten contact locations were identified based on the number of AIS 3+ injuries assigned to that contact location. A contact location assigned to an injury in the CIREN database indicates that the injury was associated with direct contact with that location during the crash event. These contact locations are assigned during CIREN case reviews. The most common contact locations can be seen in Figure 6. 65% of injuries were due to contact with the instrument panel, seatbelt, steering wheel, and airbag while 11% of injuries were due to contact with the vehicle side structure and door. The vehicle side structure includes components such as the A-pillar, B-pillar, roof rail, and door glass.

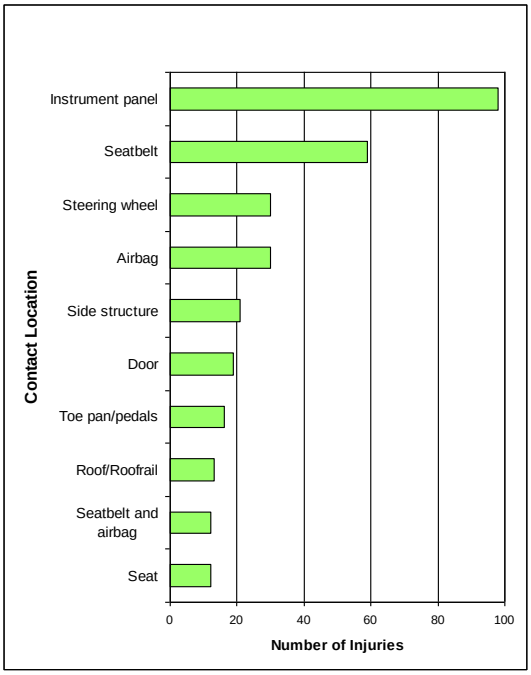

Figure 6. Frontal Impact Crashes - Top 10 Contact Locations - AIS 3+ Injuries.

<u>Injuries Assigned to the Instrument Panel</u> As seen in Figure 7, 72% of the AIS 3+ injuries attributed to the instrument panel were to the lower extremities including the femur, pelvis and tibia.

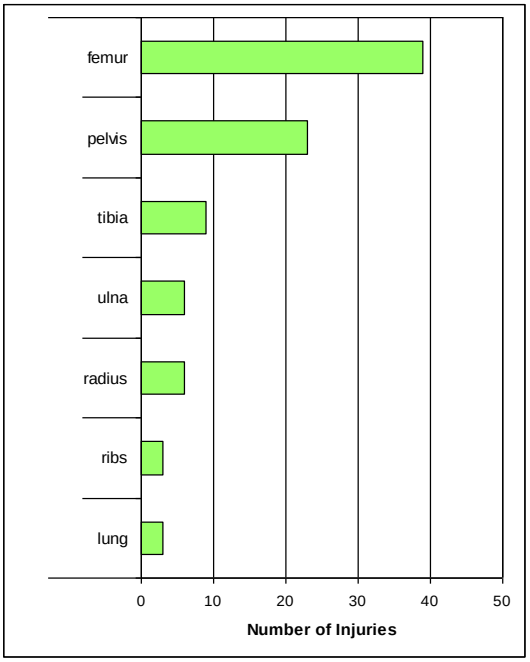

Figure 7. Frontal Impact Crashes - AIS 3+ Injuries Assigned to Instrument Panel (Body regions with ≤ 1 injury/region not shown).

While the majority of people in the frontal cases studied were belted, the majority of lower extremity AIS 3+ injuries occurred to unbelted occupants (Figure 8).

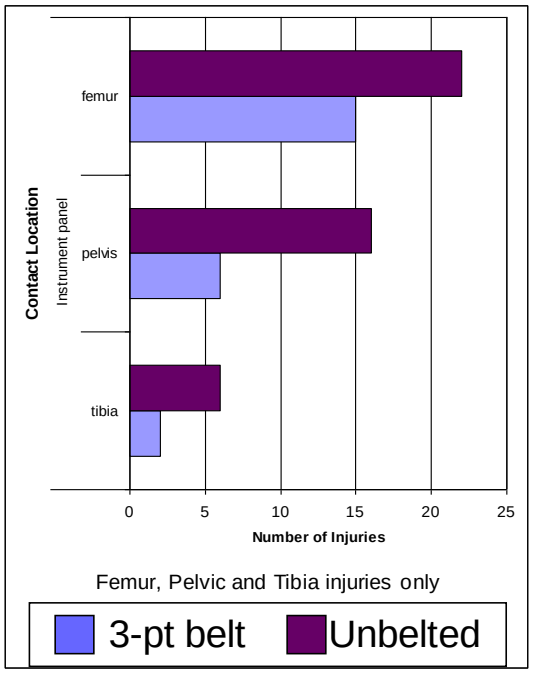

Figure 8. Frontal Impact Crashes - Lower Extremity AIS 3+ Injuries Assigned to Instrument Panel Contact.

Figure 9 shows that women had approximately half as many pelvic fractures as men. Pelvic fractures consist of fractures of any bone in the pelvis, including the acetabulum. In the U-M CIREN database, belt usage rates for men were 50%, while rates for women were 66%. This difference in seat belt usage rates alone did not completely account for the difference in pelvic fractures between men and women.

Wang reported that, men and women have differences in pelvic geometry and weight distribution [4].The male pelvic structure is taller and narrower than that of the female. In the male, the cup of the acetabulum or hip socket is oriented to face more laterally and the head of the femur is usually large in comparison to the relative size of the acetabulum. In contrast, female pelvic structures are wider and shorter. The cup of the acetabulum in the female pelvis faces more anteriorly and the female typically has a smaller femoral head as compared with the male. The laterally facing acetabulum of the male pelvis is more susceptible to fracture in a frontal collision because as the femur is loaded axially in a frontal crash, less surface area of the acetabulum is presented as a reaction surface to the femoral head. In addition the acetabular cup is generally thinner at the edges, and the edges are exposed to more crash forces with the lateral facing male acetabulum. The anteriorly facing acetabulum of the female is more resistant to fractures from the frontal crash forces. In women, the load is more adequately absorbed by the whole cup of the acetabulum rather than just the edge due the orientation of the cup [4].

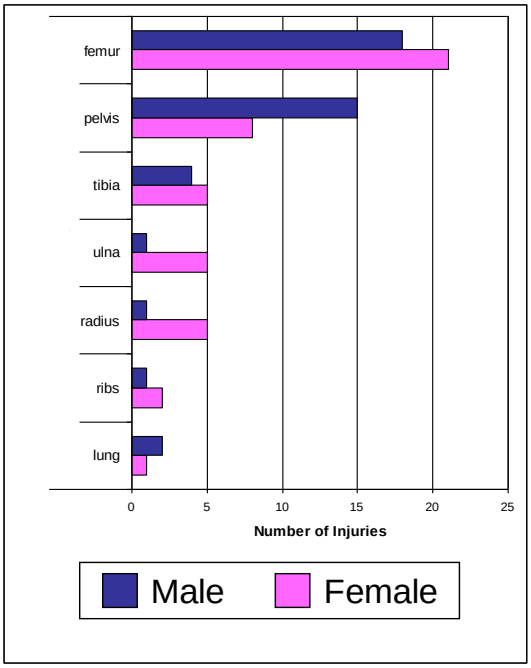

Figure 9. Frontal Impact Crashes - AIS 3+ Injuries Assigned to Instrument Panel (Body regions with ≤ 1 injury/region not shown).

Men and women also tend to carry their weight differently. Men tend to be more apple-shaped and carry their weight in their abdomen (android-type obesity) while women tend to be more pear-shaped and carry their weight in their hips and thighs (gynecoid-type obesity). In a frontal crash, when extra weight is carried more on the hips and thighs, the inertial load of the weight is primarily applied to the femur. When extra weight is carried in the abdomen, the inertial load of the weight is applied to the pelvic structure first and then to the femur. Because men tend to carry more weight in their abdomen, this could be a factor in why men sustained more pelvic fractures than women. Male pelvic structures are forced to carry more of their inertial load in a frontal crash.

Because the pelvis and femur share a load path in a frontal crash, when one of these structures break, the load on the other is relieved [10], [11].Therefore, if a

woman first experiences a femur fracture in an event, it is less likely that she will then also experience a pelvis fracture. This is supported by the data in Figure 9 which showed that women appeared to have slightly more femur and tibia fractures than men.

Femur loads are measured in the Hybrid III crash dummy and regulated in crash tests. Femur fractures, however, still occur in the field. . Potential for femur injury is evaluated by the Hybrid III crash dummy using axial loads cells in the femur (Figure 10). The Hybrid III pelvis does not have direct load measurement capability of the femoral head into the acetabulum. Currently, only femur loads and pelvic accelerations are measured.

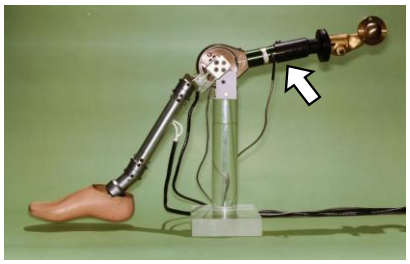

Figure 10. Location of Femur Load Cell.

Federal Motor Vehicle Safety Standard 208 (FMVSS 208) [5] limits for femur force represents a 35% risk of femur or patella fractures [6] (Figure 11). The regulated limit for the 50th percentile male is 10 kN while the limit for the 5th percentile female is 6.8 kN. Femur fractures are AIS 3 injuries and encompass most of the injuries in the case studies. Patella fractures are AIS 2 injuries and would not have been included in this study.

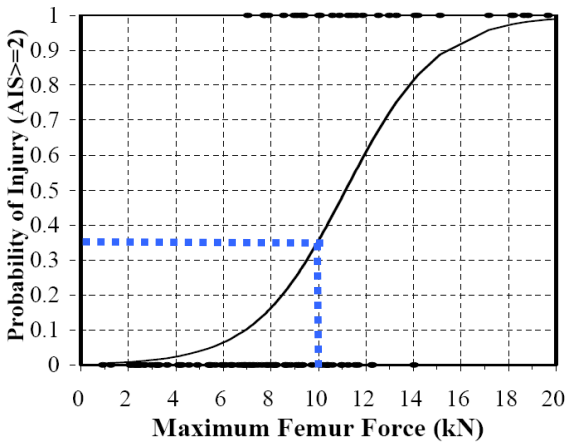

Figure 11. Femur Injury Risk Curve - 50th Percentile Male [7].

Figure 12 shows the occupant BMI distribution for lower extremity injuries and Figure 13 shows the BMI distribution for all frontal impact occupants in the U-M CIREN database.

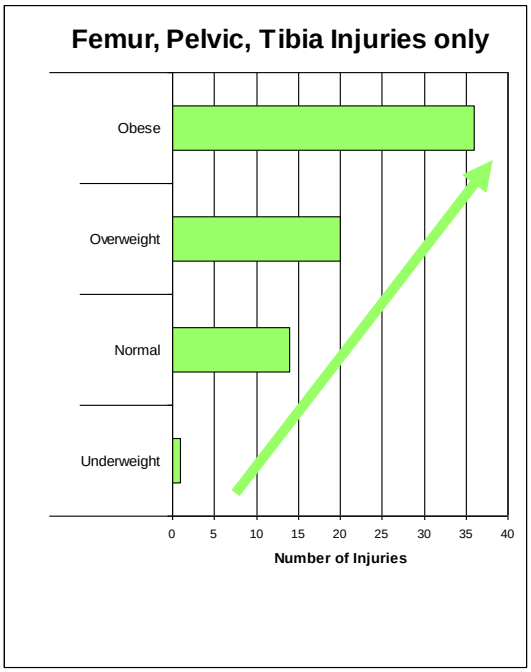

Figure 12. BMI Distribution for Lower Extremity AIS 3+ Injuries Assigned to Instrument Panel.

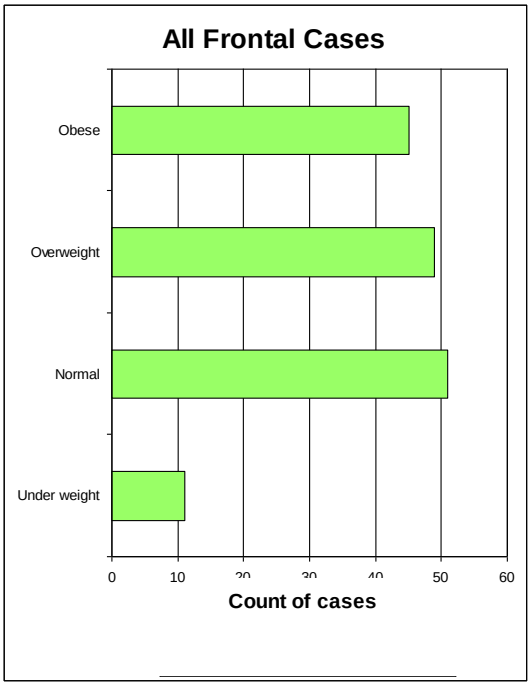

Figure 13. BMI Distribution for all Frontal Impact Occupants.

Obese occupants were over represented in the group with femur, pelvic and tibia injuries. As BMI

increased the number of lower extremity injuries also increased. An individual with a higher BMI has additional overall mass which increases the occupant energy without an equivalent increase in bone strength. This may contribute to the increased number of lower extremity injuries among the overweight and obese case study occupants.

Injuries Assigned to Seat Belts As can be seen in Figure 14, of the 58 AIS 3+ injuries assigned to seat belt contact in frontal impacts similar to current laboratory tests, the most frequent were rib fractures, hollow visceral injuries, and cervical spine injuries.

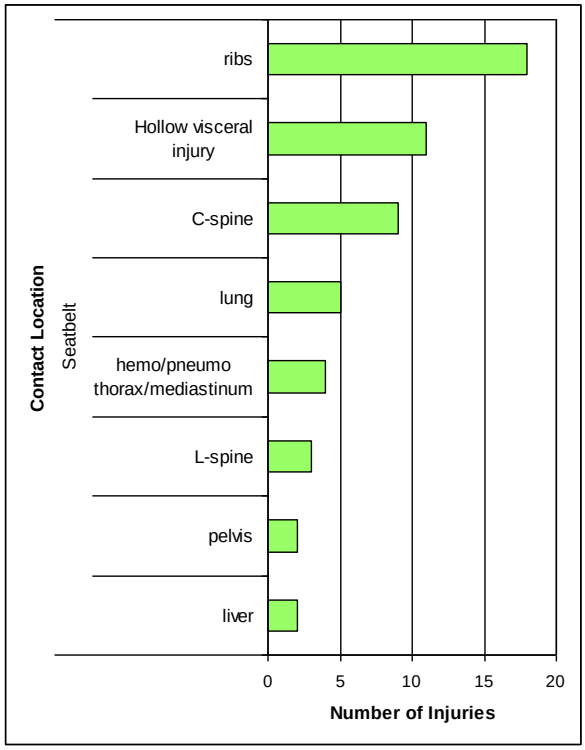

Figure 14. Frontal Impact Crashes - AIS 3+ Injuries Assigned to Seat Belt (Body regions with ≤ 1 injury/region not shown).

Reviewing the specific cases involving rib fracture indicated that older women were over represented in the group with AIS 3+ rib fractures. Of the 18 belted occupants in this group, 12 were women. Of those women, 8 of the 12 were over 50 years of age.

Figure 15 shows the distribution by occupant BMI of rib fractures assigned to seat belt contact.

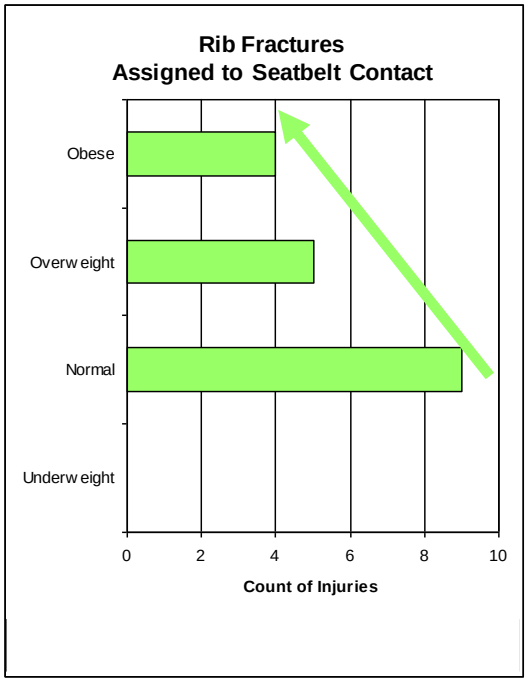

Figure 15. BMI Distribution for Rib Fractures Assigned to Seat Belt.

While the potential for femur, pelvic, and tibia fractures assigned to instrument panel contact appeared to increase with increased body mass index, the potential for seat belt related rib fractures appeared to decline with increased body mass index. Occupants with body mass indices categorized as overweight or obese were less represented in the group with AIS 3+ rib fractures assigned to seat belts, when compared to the population of all seriously injured occupants in frontal crashes in the U-M CIREN database. Body fat may have had an energy-absorbing and/or load-distributing effect that reduced the potential for rib fractures from belt loading.

The 8 occupants with AIS 3+ hollow visceral injuries were also reviewed. Five occupants were adults, and four of those adults had body mass indices in the over-weight category. The other three occupants with hollow visceral injuries occurred to lap-belt-only restrained children.

There were 7 occupants with cervical spine injury. Five of the cervical spine injury case occupants involved women 56 years of age or older. One occupant with a cervical spine injury involved a lap-shoulder belted 4 year-old female in a booster seat.

Figure 16 shows the distribution of AIS 3+ injuries assigned to seat belt contact by occupant age and gender and Figure 17 shows the age and gender

distribution for all frontal impact occupants in the U-M CIREN database.

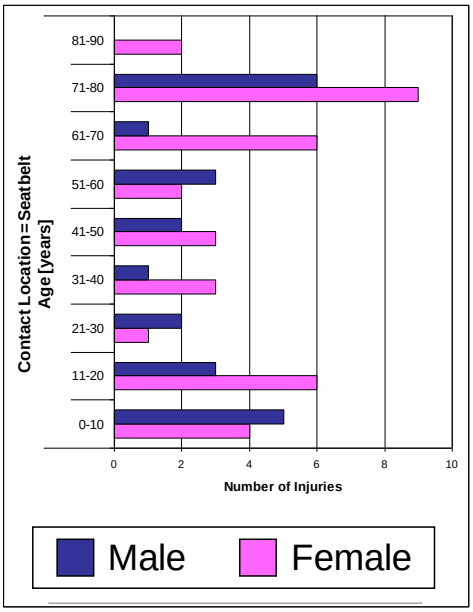

Figure 16. AIS 3+ Injuries Assigned to Seat Belt Contact by Age and Gender.

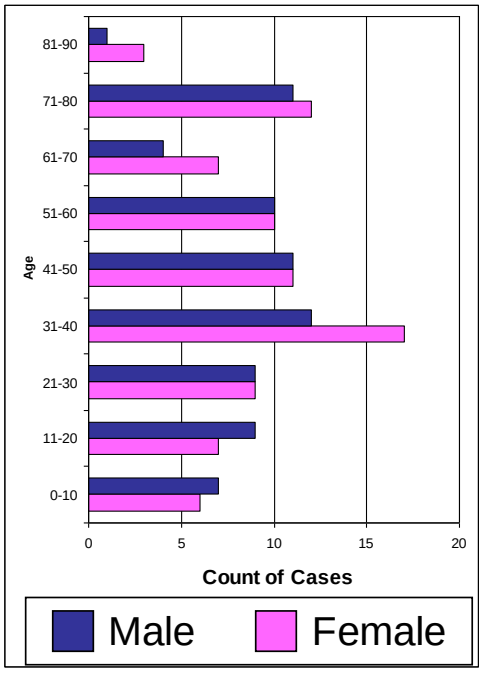

Figure 17. Age and Gender Distribution for All Frontal Impact Occupants.

Younger and older occupants were over represented in the group with injuries assigned to seat belt loading, compared to the population of all seriously injured occupants in frontal crashes in the U-M CIREN database. The greater frailty of older occupants, especially older women, was likely a contributing factor associated with increased potential for rib fracture and cervical spine injury. The relative head size to neck strength of children was likely a factor in the cervical spine injury observed in the one lap-shoulder belted 4 year-old female.

There are various possible explanations why AIS 3+ injuries assigned to seat belts have occurred in crashes even with configurations and damage extents similar to current laboratory tests. Substantial forces must be applied by seat belts to adequately manage the kinetic energy of vehicle occupants in moderate and severe frontal crashes, so it is foreseeable that some injury may result. Other factors include the test dummies, dummy instrumentation, and injury assessment reference values used to predict the potential for injury in current laboratory tests. Test dummies have been developed to represent average infants, 3 year-old children, 6 year-old children, 10 year-old children, small adult females, mid-size males, and large-size males. It is not practical to test, nor do dummies exist to represent all sizes and shapes of people. For example, no dummies exist that represent obese adults. While it is reasonable to assume that safety systems developed using existing test dummies will benefit the range of occupant sizes and shapes, it cannot be expected that injury will be eliminated. The dummies cannot collect data for assessing the potential for all types of injury. Furthermore, injury assessment reference values are set at levels to limit, not eliminate, the potential for certain types of injuries.

The family of Hybrid III ATDs used for frontal impact safety development is capable of measuring chest acceleration on the rigid portion of the spine where the ribs are attached. They are also capable of measuring chest compression on the sternum of the dummy (Figure 18).

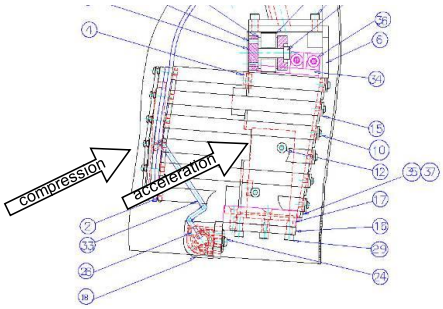

Figure 18. Location of Chest Compression and Acceleration Instrumentation in Hybrid III Dummy.

Chest compression and acceleration are measured in the Hybrid III crash dummy and regulated in crash tests. Rib fractures, however, still occur in the field. FMVSS 208 has regulated chest acceleration for over 30 years and has more recently regulated chest compression. Chest compression measurements have been required with the mid-size male Hybrid III since the 1998 model year but were previously allowed. Recently, the small female was added to the regulation, and the mid-size male chest compression requirements were made more stringent. FMVSS 208 chest compression limits for belt restrained Hybrid III ATDs (63 mm for the mid-size male and 52 mm for the small female)[5] represent an estimated 33 percent risk of AIS 3+ chest injury (Figure 19). Examples of AIS 3 injuries rib injuries are 1 rib fracture with a hemo- or pneumothorax or a flail chest without a lung contusion.

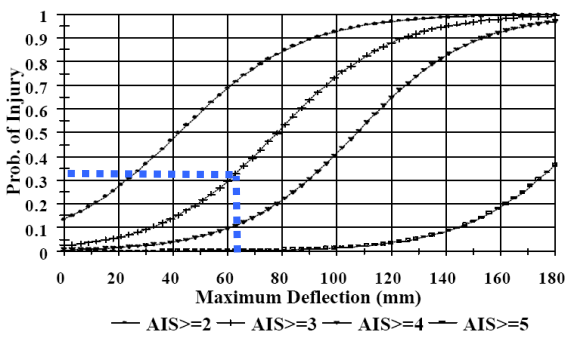

Figure 19. Chest Deflection Injury Risk Curve - Hybrid III 50th Percentile Dummy [8].

Injury Trends for Frontal Cases Matching Test Configuration but with Greater Extent

As is shown in Figure 20, the distribution of U-M CIREN frontal crash cases matching an existing crash test type with CDC extents above and below those generated in tests is similar. To make the comparison more clear, data above and below current test CDC extents were normalized by dividing the number of injuries by the number of cases (Figure 21).

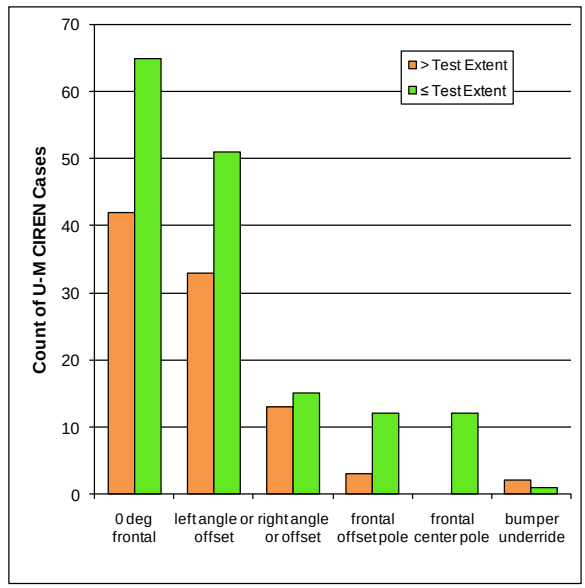

Figure 20. Frontal Cases with Configurations Similar to Current Test Types - CDC Extent Comparison.

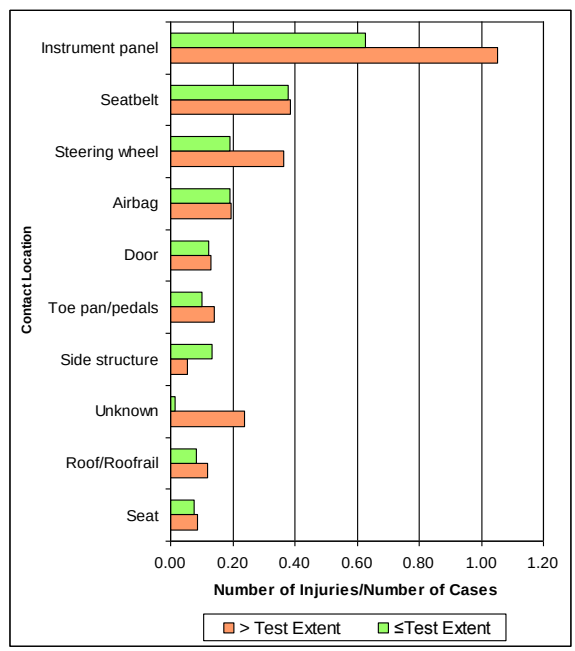

Figure 21. Frontal Impact Case Occupant Injuries by Assigned Contact Location and Extent

The top five vehicle contact locations associated with frontal injuries were instrument panel, seatbelt, steering wheel, airbag, and door. Injuries assigned to instrument panel and steering wheel contact increased with higher extents, however, those assigned to seatbelt and airbag did not increase. This was likely due to the fact that the air bag and seat belt have a finite restraint capacity and once the capacity has been exceeded the next point of contact is the steering wheel and the instrument panel structure behind it. Looking at the number of occupant injuries by assigned contact location and extent, the normalized trend was similar by contact location except for the instrument panel and steering wheel.

Figure 22 shows the distribution of frontal impact femur, pelvis and tibia injuries assigned to the instrument panel for cases with extent less than or equal to crash tests and Figure 23 shows these injuries for cases with extents greater than crash tests. Belts appeared to be more effective in reducing femur, pelvic, and tibia injuries in crashes with lower CDC extents than they were with crashes with higher CDC extents.

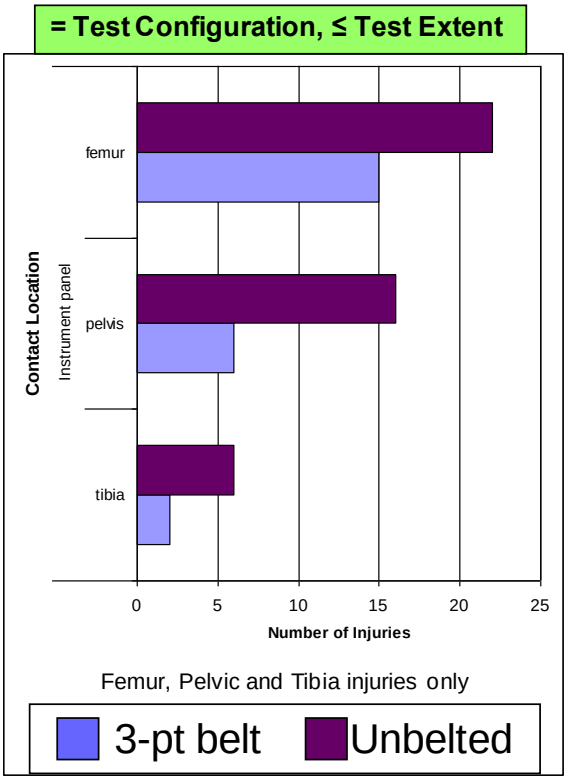

Figure 22. Distribution of Frontal Impact AIS 3+ Pelvic and Tibia Injuries - ≤ Test Extent.

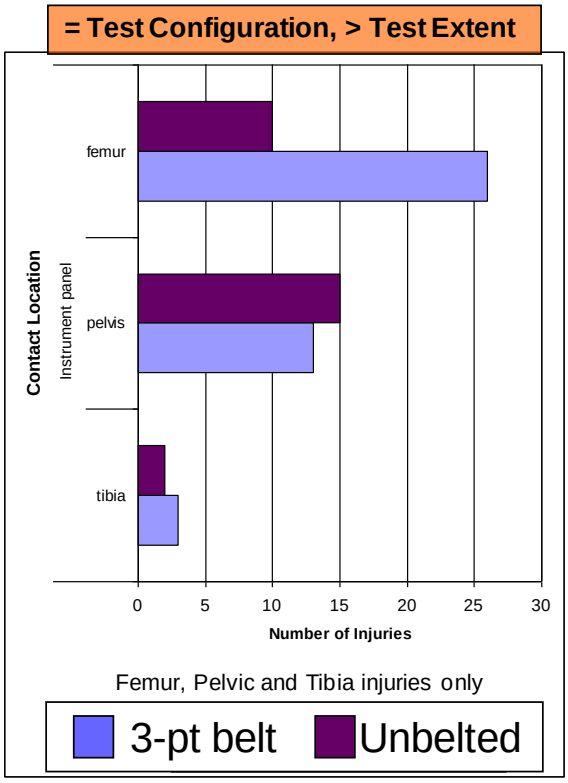

Figure 23. Distribution of Frontal Impact AIS 3+ Femur, Pelvic and Tibia Injuries - > Test Extent.

Overall, the distribution of cases that had an extent greater than the crash test extent was very similar to the distribution of cases that had an extent less than or equal to the crash test extent, however, greater extent cases were over-represented in the UMPIRE database. These cases were high crash severity events and as expected, the occupants were more likely to have injuries that permitted their inclusion in the database. For crashes with lesser extents, injuries were less likely therefore the total proportion of greater extent cases did not represent the actual proportion of these events in the field.

Injury Trends for Frontal Cases Not Matching Test Configurations

Of the 14.1% of frontal cases with configurations that were different from current crash test types, the majority were small overlap crashes. These crash configurations tend to involve localized, concentrated vehicle deformation. While the concentrated loads on the vehicle produced greater maximum crush than for a more distributed frontal crash type, the force generated would have been less, thereby producing lower accelerations of the occupant compartment.

Figure 24 shows the top 10 contact locations for AIS 3+ injuries in frontal crash cases with configurations different from current test types. As with the crash configurations that are similar to test types, injuries assigned to instrument panel contact were the most frequent. A significant difference between the crash cases that are not similar to crash test types and those that are is that injuries assigned to side structure and door contact were more frequent. The higher frequency of AIS 3+ injuries assigned to the side structure and door can be attributed to the greater occupant lateral motion, as well as greater lateral occupant compartment intrusion in small overlap frontal crashes as compared to other frontal crash types.

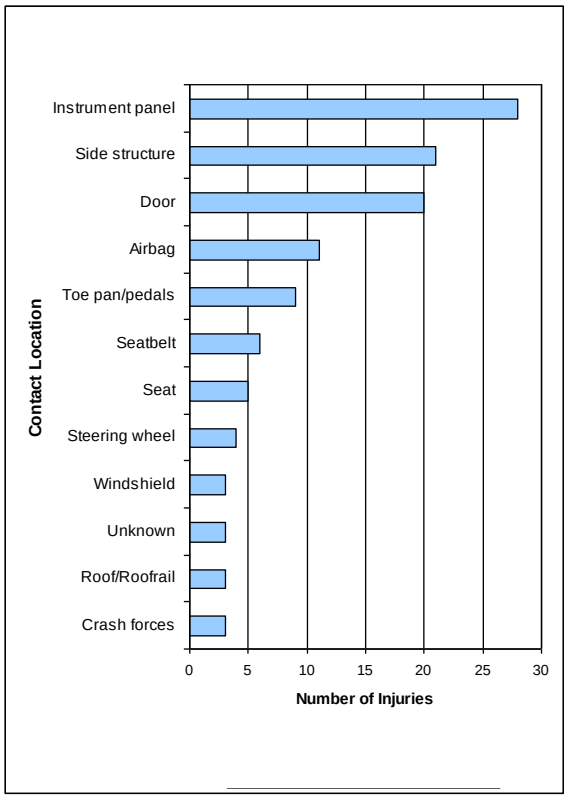

Figure 24. Cases with Frontal Crash Configurations Different from Current Test Types Top 10 Contact Locations (Body regions with ≤ 1 injury/region not shown).

All of the AIS 3+ injuries assigned to the side structure were head injuries attributed to head contact with the A-pillar in five small overlap crashes. These types of head/A-pillar contact injuries may result not only from the vehicle dynamics in small over lap frontal crashes which cause a larger lateral component directing the occupant towards the A-pillar but also due to greater crash induced A-pillar motion.

Figure 25 summarizes the nature of the A-pillar related AIS 3+ head injuries in these small overlap frontal crashes. These were most frequently coded as cerebrum injuries. Injuries to head vessels, basilar skull fractures, and facial fractures were also observed.

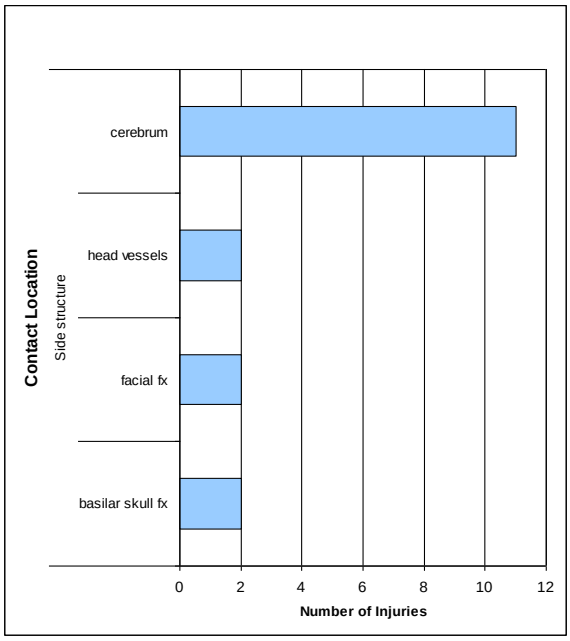

Figure 25. Side Structure Injuries in Cases with Frontal Crash Configurations Different from Current Test Types.

Crash test dummies and injury criteria exist to address these head injuries. The Hybrid III crash test dummy head is designed to measure longitudinal, lateral, and vertical acceleration. These measurements are used to calculate the resultant acceleration of the center of gravity of the head as shown in Figure 26 which in turn is used to calculate Head Injury Criteria (HIC).

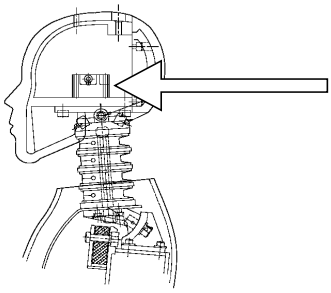

Figure 26. Location of Hybrid III Head Accelerometers.

FMVSS 208 currently limits 15ms HIC to 700. A HIC of 700 represents a 5 percent risk of AIS 4+

brain injury. Brainstem and diffuse axonal injuries are examples of AIS 4+ head injuries. Figure 27 contains the risk curve for AIS 4+ brain injury versus HIC.

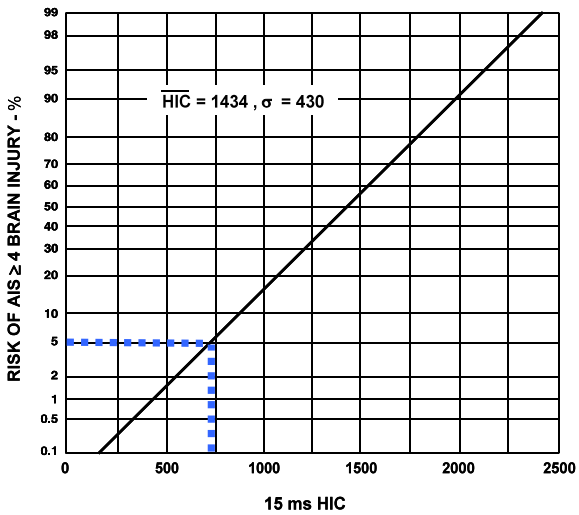

Figure 27. AIS 4+ Brain Injury Risk Curve Adults [9].

While FMVSS 208 and frontal impact air bags address head injuries in most frontal impact configurations, they may not prevent all head to A-pillar contact. FMVSS 201 (Occupant Protection in Interior Impact) currently regulates HIC produced from impacting many areas of the vehicle interior, including the A-pillars, with a head form at 24 km/h (15 mph). However, only a portion of the vehicles in the database met this requirement since it became effective for all new vehicles produced since September 1, 2002.

SUMMARY

Of the 290 UMPIRE frontal crash cases, over half had configurations and CDC extents similar to current crash tests. 65% of injuries in this category were assigned to contact with the instrument panel, seatbelt, steering wheel and airbag, while 11% of injuries were assigned to contact with the side structure of the vehicle and the door. 72% of injuries assigned to contact with the instrument panel were to the lower extremities, and these injuries tended to increase with increased BMI. 31% of injuries assigned to the seatbelt were rib fractures, but these injuries tended to decrease with greater BMI and were more frequent in the older population.

Approximately one third of the frontal cases had configurations that were similar to frontal crash tests but had greater CDC extents than the crash tests. In this category, again, the majority of injuries were assigned to contact with the instrument panel, seatbelt, steering wheel, and airbag. When this category was normalized and compared to the cases with extents less than or equal to those generated in laboratory crash tests, it was noted that injuries assigned to contact with the instrument panel and steering wheel increased with higher extent, whereas those assigned to seatbelt and airbag did not. This difference may be attributed to restraint system characteristics as well as load sharing between the components of the restraint system.

The remaining frontal cases had configurations that were different than current laboratory crash tests, with the majority of these cases categorized as small overlap crashes. As in the other two categories, injuries assigned to contact with the instrument panel were the majority, however, injuries assigned to contact with the side structure of the vehicle and the door were more frequent than in the other categories. All of the injuries assigned to contact with the side structure of the vehicle were head injuries assigned to A-pillar contact. The injuries assigned to the side structure and door may be attributed to the combination of lateral occupant motion relative to the vehicle and A-pillar and door displacement in the small overlap crashes.

RECOMMENDATIONS

Specific recommendations fall within three major observations.

First, the majority of injuries occurred in crashes similar to current tests that are conducted by the industry. Injury trends identified in these cases that match crash tests suggest that further study in some areas may be appropriate. Specifically differences observed in male and female acetabulum fractures suggest that further development of test measurement devices could be considered. As an example, the possible inclusion of direct acetabulum measuring load cell in frontal impact crash dummies could be investigated. In addition trends were identified relative to the effect of BMI on injury risk – some injuries increased with increased BMI while others decreased. An investigation of testing or modeling techniques to evaluate injuries to overweight occupants should also be considered.

Second, rib fractures still occurred despite chest acceleration and chest compression being measured and regulated for model years of essentially all vehicles in the database. The current FMVSS 208 chest compression limit represents an estimated 33

percent risk of AIS 3+ chest injury. The July 2008 revision to NHTSA's frontal NCAP program requires a lower chest compression limit for a vehicle to achieve a 5-star rating. Further investigation into the effects of this change in NCAP may indicate a reduction in rib fractures. In addition, it may be beneficial to research the possibility of new technologies capable of identifying occupants in terms of age, gender, BMI etc. to essentially "individualize" a restraint system to mitigate certain injuries.

Lastly, small overlap crashes comprised the majority of the cases with frontal crash configurations that were different from current crash test types. These crash configurations tend to involve localized vehicle deformation and lateral occupant motion. Current IIHS and FMVSS 208 offset deformable barrier tests have resulted in improvements to the vehicle's front structure and occupant compartment structural integrity. The case vehicles in which the cerebrum injuries occurred were older model years and may not have had the current offset deformable barrier tests or the current FMVSS 201 head impact tests as specific design objectives when they were developed. In addition, new technologies that provide for curtain air bag deployment in frontal impacts and curtain air bag designs which include A-pillar coverage may show a reduction of these injuries. The effect of new performance objectives and new technologies in more recently designed vehicles on injury trends in small overlap frontal crashes should be studied.

ACKNOWLEDGMENT

This work was supported by grants #DTNH22-00-H-07444 and #DTNH22-05-H-31001 from the US Department of Transportation – National Highway Traffic Safety Administration as well as educational grants from General Motors. The views expressed are those of the authors and not necessarily those of the sponsor.

REFERENCES

[1] "Traffic Safety Facts 2006", US Department of Transportation, National Highway Traffic Safety Administration, Publication No. DOT HS 810 818.

[2] "Comparison of University of Michigan CIREN Cases to Existing Types of Crash Tests," O'Brien-Mitchell B, Bailey K, Faust D, Jensen J, Kleinert J, Wodzinski C, & Wang S. ESV 09-0185.

[3] "Defining Overweight and Obesity". Department of Health and Human Services, Centers for Disease Control. June 20, 2008. http://www.cdc.gov/ nccdphp/dnpa/obesity/defining.htm

[4] "Gender Differences in Hip Anatomy: Possible Implications for Injury Tolerance in Frontal Collisions," Wang SC, Brede C, Lange D, Poster CS, Lange AW, Kohoyda-Inglis C, Sochor MR, Ipaktchi K, Rowe SA, Patel S, Garton HJ. Annual Proceedings of the Association for the Advancement of Automotive Medicine. 48:287-301, 2004.

[5] National Highway Traffic Safety Administration Standard No. 208; Occupant Crash Protection 49 CFR 571.208

[6] Supplement: Development of Improved Injury Criteria for the Assessment of Advanced Automotive Restraint Systems – II, Eppinger R, Sun E, Kuppa S, Saul R, 2000

[7] Development of Improved Injury Criteria for the Assessment of Advanced Automotive Restraint Systems, Kleinberger M, Sun E, Eppinger R, Kuppa S, Saul R, 1998

[8] Development of Improved Injury Criteria for the Assessment of Advanced Automotive Restraint Systems – II, Eppinger R, Sun E, Bandak F, Haffner M, Khaewpong N, Maltese M, Kuppa S, Nguyen T, Takhounts R, Tannous R, Zhang A, Saul R, 1999

[9] Biomechanical Scaling Bases for Frontal and Side Impact Injury Assessment Reference Values, Mertz H, Irwin A, Prasad P, Stapp Car Crash Journal, October 2003

[10] The tolerance of the human hip to dynamic knee loading, Rupp, J.D., Reed M.P., Van Ee, C.A., Kuppa, S., Wang, S.C., Goulet, J.A., and Schneider L.W, Stapp Car Crash Journal 46: 211-228, 2002.

[11] Tolerance and response of the knee-femur-pelvis complex to axial impact-Sled tests, Melvin and Nusholtz, Report UM-HSRI-80-27. The University of Michigan, Highway Safety Research Institute, Ann Arbor, MI, 1980

FIREWORTHINESS: A FINAL REPORT ON THE TECHNOLOGY BASE

Kennerly H. Digges
R Rhoads Stephenson
Motor Vehicle Fire Research Institute
USA
Paper Number 09-0211

ABSTRACT

The findings provide a technology base for fireworthiness including the following: fire statistics on crash modes; the behavior of plastic gasoline tanks when subjected to fire and impact tests; finite element analysis of fuel tanks subjected to crash conditions; assessments of automotive fuel components that relate to fire safety; underhood temperatures under driving conditions; flammability of underhood liners; ignition and flammability properties of plastics and underhood fluids; an analysis and synthesis of 22 vehicle burns; fire suppression needs and a laboratory design and test; and examination of fire safety aspects of future vehicle technologies such as 42-volt electrical systems and hydrogen fueled vehicles.

These research results in conjunction with the GM/DoT Fire Research Project have been analyzed and recommendations for fire safety improvements have been proposed. The recommendations include vehicle level fire tests to increases survivability time for crashed vehicles subjected to exterior fires, particularly those that originate under the hood.

INTRODUCTION

On March 7, 1995, the U.S. Department of Transportation (DOT) and General Motors Corporation (GM) entered into an administrative agreement, which settled an investigation that was being conducted by the National Highway Traffic Safety Administration (NHTSA) regarding an alleged defect related to fires in GM C/K pickup trucks [NHTSA, 1994; NHTSA, 2001].

Under the GM/DOT Settlement Agreement, GM agreed to provide support to NHTSA's effort to enhance the current Federal Motor Vehicle Safety Standard (FMVSS) 301, regarding fuel system integrity, through a public rulemaking process. GM also agreed to expend $51.355 million over a five-year period to support projects and activities that would further vehicle and highway safety. Approximately ten million dollars of the funding was devoted to fire safety research [NHTSA, 2001].

Subsequent to the GM/DOT Settlement, GM agreed to fund an additional $4.1 million in research related to impact induced fires. This latter research project was included under the terms of a judicial settlement. The fire safety project objectives are defined by the White, Monson and Cashiola vs. General Motors Agreement dated June 27, 1996 [White, 1996]. All research under the project has been made public for use by the safety community.

The Motor Vehicle Research Institute (MVFRI) was formed to administer and conduct this research. The work started in late 2001 and will be completed in early 2009. The purpose of this paper is to document our major results and provide recommendations whereby the fire safety of motor vehicles can be improved. There is a unique opportunity now to take advantage of the results of some $14 M worth of fire safety research to advance the cause of improved automobile fire safety.

Research projects that have been completed by MVFRI include the following:

1. A statistical analysis of field data to determine the frequency of fuel leaks and fires by model year and by other crash attributes (See Bahouth, 2006 and 2007, Digges, SAE 2005b, 2006 and 2007b, Fell, 2004 and 2007, Friedman, 2003 and 2005, and Kildare, 2006).
2. A case-by-case study of fuel leaks and fires in NHTSA's crashworthiness database (NASS/CDS) and an assessment of opportunities for reduction of vulnerability (See Bahouth, 2005, Digges, SAE 2007c; 2008 and 2009).
3. The assessment of the state-of-the-art technology to reduce the frequency of fires in motor vehicles and/or to delay the time for fires to propagate to the fuel or the interior of the occupant compartment (See Fournier, Dec 2004, April 2005). Additional work was done on leak prevention during rollover from severed lines connected to fuel tanks. (See Fournier, July 2004 and September, 2006)
4. The evaluation of gasoline fuel tanks of various shapes when subjected to fire and impact testing required by European (ECE) or other government standards (See J. Griffith, 2005).

5. The development of test procedures for the prevention of fires in vehicles equipped with 42-volt electrical systems; including high intensity arc testing, and carbon tracking properties of plastics (See Wagner 2003; Stimitz, 2004; Stephenson, 2005). Abuse tests were also conducted on 14 and 42 volt lead-acid batteries. (See Weyandt, May 2005)
6. The evaluation of the toxicity of the combustion products of motor vehicle components used in engine compartment and under-hood applications (See L. Griffith, 2005).
7. The evaluation of rescue times for first responders as it pertains to fire propagation into the passenger compartment (See Shields 2004, Digges, ESV 2005).
8. A comprehensive analysis of data from studies sponsored by GM, Motor Vehicle Fire Research Institute (MVFRI), and NHTSA (See Tewarson, April 2005; October 2005; 3 volumes and Digges et al, 2007d).
9. The development of an underhood foam fire suppression system (See Gunderson 2004, 2005).
10. The development of FEM models of fuel filled tanks subjected to crash forces (See Bedewi, 2004 and 2007).
11. Measurement of fire resistance of underhood insulation materials and of the electrical conductivity of underhood fluids. (See Fournier, Aug. 2005, Dey, 2004).
12. The measurement of underhood temperatures of four vehicles (See Fournier Sept. 2004 and Sept. 2006).
13. A bonfire test of an automotive type 4 compressed hydrogen fuel tank (See Zalosh, 2005 and Weyandt, 2005).
14. A full-scale SUV vehicle burn with a Type 3 compressed hydrogen tank. (See Weyandt, 2006).
15. Hydrogen and underhood leak experiments (See Weyandt, Dec. 2006).
16. A fatal compressed Natural Gas tank explosion was investigated for possible lessons learned to be applied to hydrogen tanks. (See Stephenson, 2008)
17. Research to support a special fire investigation methods appropriate for Hybrid and Hydrogen Vehicles for possible inclusion in NFPA 921. (See Stephenson, 2006)
18. A computer-based fire investigation training course was developed. (See Shields 0547, 2007 and Shields 0548, 2007)
19. The results of all the above research projects were summarized and placed on the MVFRI website. All final reports and summaries are located at mvfri.org.

BACKGROUND

Automobiles fires are the single largest cause of death among all consumer goods sold in the United States [Ahrens, 2003 and 2005]. Of the nearly two million fires each year in the U.S., one out of five (300,000) are vehicle fires [USFA, 2002 and FEMA, 2003]. This is comparable to the number of fires in houses and apartments but vehicle fires claim more lives than either [Ahrens, 2005, USFA, 2002 and FEMA, 2003]. Three quarters of vehicle fires are caused by mechanical or electrical failures during normal operation, but these are not particularly deadly because the occupants are usually able to escape. Less than 10% of vehicle fires are caused by collisions but escape is more difficult in these situations, and collisions account for the overwhelming majority (60-75%) of vehicle fire fatalities [Bennett, 1990; USFA, 2002]. Vehicle fires cause some 3000 injuries and claim about 500 lives per year in the U.S., [Ahrens, 2005]. The rapid progression of fire and incapacitation of passengers were contributing factors in two thirds of vehicle fire deaths [USFA, 2002]. It has been suggested that the number of fatalities attributed to motor vehicle fires is an underestimate because of ambiguous reporting methods [Ahrens, 2005, Fell, 2004], but there is no doubt that motor vehicles are a major component of the national fire death problem.

The fire safety of motor vehicles is regulated by Federal Motor Vehicle Safety Standard (FMVSS) 301 for fuel system integrity, which was first issued by the NHTSA in 1967 and FMVSS 302 for flammability of interior materials in passenger cars, multipurpose passenger vehicles, trucks, and buses, which became effective on September 1, 1972. The requirements of FMVSS 301 are intended to strengthen and protect the vehicle's fuel system, so that in a crash event, the chances of fuel leakage, and consequently the chances of fire and occupant injury, will be reduced. For fatal crashes in which fire is coded as the most harmful event, over half are due to front impact. Rollovers account for about 25%, and the rest are about evenly divided between side and rear impacts [Digges, 2008]. Over the past decade, fires in frontal and rollovers crashes have increased in frequency. NASS data shows that for the major crash related fires that enter the occupant compartment over 60% originate underhood. For frontal crashes, 85% originate underhood. For rollovers, the underhood origin accounts for 50% [Digges, ESV 2007a]. These statistical studies show the need to focus fire safety improvements on underhood fires resulting from frontal crashes and rollovers

Since it went into effect, FMVSS 301 has reduced fires due to fuel tank rupture, but the number of fire deaths has remained relatively constant over the past few decades because of an increasing number of vehicle crashes and a ten fold increase in the amount of combustible materials used inside and outside the vehicle.

The intent of the FMVSS 302 standard for flammability of materials was to reduce deaths and injuries to motor vehicle occupants caused by vehicle fires, especially those originating in the interior of the vehicle from sources such as matches or cigarettes. At the time that FMVSS 302 was under development, a study estimated that 30% to 40% of vehicle fires originated in the interior (passenger compartment and trunk) [Goldsmith, 1969]. Over the past decade, less than 5% of the post-crash fires originate in the vehicle interior [Digges, 2007b]. As collisions have become more impact-survivable and fuel tanks better protected, the amount of combustible plastic has increased. In most of today's vehicles there is more combustible material outside the fuel tank than inside it [Digges, 2009].

RECENT RESULTS

The results from a series of vehicle burn tests conducted by General Motors were analyzed to determine the effect of vehicle construction materials on passenger survivability in a post-crash vehicle fire [Tewarson, 2005 Vol. 1-3]. The authors concluded that when the fire originates in the engine compartment, flames penetrate the vehicle interior within 10-20 minutes. Once flames penetrate the passenger compartment they spread several times faster than allowed by FMVSS 302 [Tewarson, 2005 Vol. 1], resulting in occupant death in 1 to3.5 minutes. For the rear end collisions characterized in the test program by a gasoline pool fire, flames penetrated the vehicle interior through body openings within 2 minutes, after which flame spread by interior materials was 10 times faster than allowed by FMVSS 302 [Tewarson, 2005 Vol. 1]. Consequently, once flames penetrate the passenger cabin from either the front or rear, death of all occupants will occur within about two minutes due to simultaneous effects of heat, burns, and toxic gases [Tewarson, 2005 SAE]. The rapid flame spread observed in vehicle fire tests is the dominant factor in fatal vehicle fires and the major cause of vehicle fire deaths [USFA, 2002]. Tewarson reported that the orientation of the combustible material, the radiant heating by the fire, and the burning of molten plastic that drips away from the fire, all induced more severe burn conditions than created in the FMVSS 302 regulatory test.

Southwest Research Institute summarized eleven series of automobile fire tests conducted in the United States, Europe and Japan [Janssens, 2008]. The data generally confirmed the high intensity of fires that burn the materials in the occupant compartment. Figures 1 and 2 show typical test results from a series of vehicle fire tests conducted in 2002 by the Building Research Institute (BRI) in Japan. Figure 1 shows the progression of an engine compartment fire 20 minutes after ignition. Figure 2 shows the same fire at 30 minutes when the occupant compartment is totally engulfed in flames.

Figure 1. Tests by BRI of engine compartment fire -20 minutes after fire initiation.

Figure 2. Tests by BRI of engine compartment fire -30 minutes after fire initiation.

Rescue data from FARS showed that in rural crashes, the 75 percentile rescue time was 24 minutes [Digges, 2005 ESV]. For urban crashes the equivalent time was 12 minutes. The survivability time measured in the GM vehicle burn tests was often less that that needed for first responders to reach a typical rural accident scene and begin rescue operations for trapped or incapacitated passengers.

DISCUSSION

The changing design of motor vehicles is such that collisions are more impact-survivable, most fuel tanks are better protected in rear collisions and plastics have surpassed gasoline as the main fire load. These changing conditions present new safety challenges and opportunities. The following observations were based on recent test data or observed changes in the vehicle fleet:

1. Automobile fires account for 95% of motor vehicle fires and 92% of vehicle fire fatalities. The vast majority of fatal automobile fires result from sources outside the passenger compartment rather than from ignition of interior materials by a cigarette or small flame as envisioned when FMVSS 302 was issued.

2. Plastics that are exterior to the passenger cabin (i.e., in the engine compartment and body panels) represent a comparable fire load and fire hazard to the interior materials but are not required to pass FMVSS 302 or any other fire safety standard.

3. The flame spread rate of combustible materials inside the occupant compartment increases significantly when in proximity to a vehicle fire, but this factor was neglected in the FMVSS 302 test. Fire tests of vehicles indicate a tenability time of less than four minutes once an external fire penetrates the occupant compartment [Tewearson, 2005].

4. Tests of aircraft materials fireworthiness indicate that it is not possible to use a material-level flame test, e.g., FMVSS 302, to predict the fire behavior of a vehicle without validating the material-level performance at full-scale [Hill, 1979, 1985].

5. Tests of fire safety features in current vehicles indicate that many vehicles incorporate features to improve fire safety, but the features are not uniformly applied [Digges, 2009; ESV 2007a]. There was no relationship between the cost of the vehicle and the presence or absence of some of the fire safety features.

In view of the increased frequency of crash induced fires in frontal crashes and rollovers, regulations that would encourage technology to delay the penetration of fire into the highly flammable occupant compartment appear to be warranted.

For hydrogen fueled vehicles, an occupant compartment fire poses a threat to the high pressure hydrogen tank(s). Safety standards need to insure that the safety systems will protect people and structures in the vicinity of a vehicle fire from the explosive pressures that would occur in the event of a hydrogen fuel tank rupture. The safety standards should include fire tests of vehicles that have been exposed to representative crash scenarios.

RECOMMENDED RULEMAKING CHANGES

1. FMVSS 301 – Fuel System Integrity

a. Add a door opening requirement to the FMVSS 301 crash tests. FMVSS 301 currently does not require that the doors on a crashed vehicle be able to be opened. Such a requirement was considered by NHTSA during the last revision of FMVSS 301 but it was not included due to the lack of a door opening test procedure. A recommended procedure is contained in Appendix A.

b. Consider a lower fluid leakage limit for flammable fluids. The original requirement was for a maximum of one ounce per minute of leakage. This was later changed to 28 grams per minute. The selection of the present leak rate was not based on fire science considering the probability of ignition or flame propagation to other parts of the vehicle. It was chosen as the smallest amount that could be conveniently measured in a cup to collect any leaks. It was also similar to the volume of a carburetor float chamber (carburetors are rarely used anymore since fuel injection has become nearly universal). One could consider a lower leak limit based on real ignition and fire propagation tests.

c. Consider conducting all crash tests (including NCAP) with all electrical systems charged and connected, with all underhood fluids present, and with the engine running and hot. If a post-crash fire breaks out, the vehicle would have failed the test. (See Digges, ESV 2009, Santrock, 2007)

2.FMVSS 302 - Flammability of Materials

a. Most of the fire experts who conducted research on our projects consider FMVSS 302 to be outdated. It was developed 40 years ago when a lighted cigarette was the most frequent threat to originate an occupant compartment fire. In response to the fire threat from an underhood fire, the tenability time of materials that comply with 302 is less than 5 minutes [Digges ESV, 2005a]. Extensive

research on alternative test methods has been conducted under NHTSA, GM/DoT, and the MVFRI projects. A better test method is required with more stringent acceptance criteria that will result in less flammable interior materials. See [Digges et al, 2007d] and [SwRI, 2003] for more discussion.

b. Regulate the flammability of underhood solid materials. .Most auto fires start in the engine compartment. There are many solid materials under the hood that are flammable and can spread the fire into the passenger compartment. In fact in modern cars, plastic materials have surpassed motor fuel as the main underhood fire load. This regulation on underhood materials could either be an extension of FMVSS 302 or a new fire safety standard. See [SwRI, 2003]. Special attention should be paid to underhood liners. Measurements show that the heat release rate of underhood liners varies by a factor of 100 between different vehicles [Fournier, Aug 2005]. Since these are attached to the underside of the hood, they are at the top of the compartment and are readily exposed to flames which can then spread horizontally. Using the best of currently used liner materials could reduce the rate of fire propagation and growth. As a minimum, the underhood liner should not add fuel to the engine compartment fire.

3.FMVSS 303 – Natural Gas Fuel System Integrity

a. Upgrade the rear impact speed and barrier to match that of FMVSS 301.

4. FMVSS 304 – Natural Gas Tanks

a. Replace the tank-level bonfire test with a vehicle level-test. (See Appendix B for a proposed compressed gas vehicle burn test). Appendix B is written in a way that it can be applied to both compressed H2 and CNG vehicles.

b. If NHTSA decides to keep a bare tank bonfire test similar to FMVSS 304 (for Natural Gas and/or Hydrogen), then perform an additional tank bonfire test without a PRD to establish the baseline tank burst time. This gives information about the tank. This information will allow NHTSA to establish a time margin between the beginning of fire exposure and the time of tank burst. (See Appendix C for more details)

c. If NHTSA doesn't do the vehicle-level burn test, consider adding a localized fire tank test which will simulate a tank exposed to a localized fire away from the location of the pressure relief device (PRD).

d. Require a thermal shield between the passenger compartment and the tank(s).

e. Prohibit "vent boxes" which shield the PRD from hot gases or flames (vent boxes are designed to collect and vent small CNG leaks).

f. The bonfire test fire should be standardized. We should agree on the fuel (propane or natural gas) and the heat release rate (We suggest using a flow rate that will provide 200 to 300 kW of fire power) [Zalosh, 2005; Tamura, 2006]. Standardizing these parameters will make the test more repeatable from test-to-test and from test facility to test facility. Steps should also be implemented to shield the tank test area from wind. These improvements should reduce the standard deviation of the exposure heat input.

5. FMVSS 305 – Battery Safety

a. Upgrade the rear impact speed and barrier to match that of FMVSS 301. (A current NPRM proposes to do this.)

b. Add a requirement that there be "no fire" after the vehicle crash tests. This will address the possibility of a fire starting in or around the high-energy traction battery.

6. Future Hydrogen Fueled Vehicle Standards

a. See Section 4 (a) above. We propose that NHTSA consider a full vehicle burn test for compressed gas vehicles. See Appendix B.

b. A hydrogen (H2) blue diamond sticker should be required on the back of the vehicle. This is for the benefit of emergency responders.

7. A New Fireworthiness Standard

NHTSA should adopt a strategy for improving vehicle fire safety that is consistent with its philosophy of using system (vehicle) level tests to develop minimum performance requirements based on objective measures of human tolerance. In particular, NHTSA should address the magnitude and changing character of the motor vehicle fire problem by developing fire performance (fireworthiness) requirements for motor vehicles that will guarantee sufficient time for escape or rescue from a post-crash

fire. Supporting standards should be developed based on human tolerance to the effects of fire and toxic gases (especially carbon monoxide), which are well defined [Tewarson, 2005 Vol. 1] and easily measured [Tewarson, 2005 Vol. 1; Hill, 1979 and 1985]. To have a meaningful effect on post crash survivability, fireworthiness standards will guarantee passengers survivable conditions until rescue crews can arrive in the event of restricted egress or incapacitation. Based on the analysis of emergency rescue operations 10-24 minutes are needed for emergency personnel to arrive at the scene after an incident occurs [Digges, ESV 2005a]. An additional 5-10 minutes are probably required to perform the rescue operations (e.g., jaws of life), so that a realistic survival time is of the order of 15-30 minutes after impact. Based on the analysis of full-scale vehicle fire test data [Tewarson ,2005 Vol. 1; Hill, 1979 and 1985], there are a variety of technologies for improving fireworthiness.

There are a number of technologies that will act to delay the fire penetration from the engine compartment to the passenger compartment [Digges, ESV 2007a]. These include: preventing the leakage of all flammable fluids, reducing the flammability of plastics used under the hood, fire-hardening bulkheads, openings, and conduits between the engine and passenger compartments, using fire resistant materials or intumescent seals around penetrations, and using less-flammable underhood liners, or other active or passive fire suppression systems.

ACKNOWLEDGMENT

The authors would like to recognize that funding for this research was provided by General Motors in accordance with the White, Monson and Cashiola vs. General Motors Settlement Agreement.

REFERENCES

Ahrens, M.,"The U.S. Fire Problem Overview: Leading Causes and Other Patterns and Trends," National Fire Protection Association, Quincy, MA, June 2003.

Ahrens, M., "U.S. Vehicle Fire Trends and Patterns," National Fire Protection Association, Quincy, MA, August 2005.

Bahouth, J., and Kusnestov, A., "Automotive and Fire Safety Research", The George Washington University, January 2005. www.mvfri.org

Bahouth , G., "Analysis of Fire Related Crash Fatalities and Crashed Vehicle Rescue Times", Report prepared for MVFRI, March 30, 2007. www.mvfri.org

Bahouth, G., "Post Crash Exterior Crush Patterns and Motor Vehicle Fire Occurrence" SAE Paper 2006-01-0789, April, 2006.

Bedewi, N., and Tarek, O., "Modeling of Automotive Fuel Tanks Using Smoothed Particle Hydrodynamics", SAE paper 2007-01-0682, April 2007.

Bedewi, N., "Evaluation of Fuel Tank Drop Tests and ASTM Tensile Tests conducted by Southwest Research Institute", Prepared for MVFRI, Final Report December 13, 2004. www.mvfri.org

Bennett, R., "Fire Safety Needs to Protect Road Transport Passengers," Fire Engineers Journal, 26 (1990)

Dey, W., "Conductivity Measurements for New Engine Compartment Fluids," Chilworth Technology, Inc., Report to MVFRI, May 2004. www.mvfri.org

Digges, K and Stephenson, R, "The Basis for a Fluid Integrity NCAP Rating, ESV Paper Number 09-0215, June 2009.

Digges, K., "Fire Occurrence in Frontal Crashes Based on NASS/CDS", SAE 2008-01-0256, SAE Publication SP-2166, Fire Safety, 2008, pp. 9-16, April 2008.

Digges, K., "Technologies to Improve Impact Related Fire Safety", Paper, 07-0480, 20th *ESV Conference*, June 2007a

Digges, K., Stephenson, R, "Recent MVFRI Research in Crash-Induced Vehicle Fire Safety", SAE paper 2007-01-0880, April 2007b.

Digges, K., and Kildare, S., "Fire Occurrence in Rollover Crashes Based on NASS/CDS", SAE paper 2007-01-0875, April 2007c.

Digges, K., Gann, R., Grayson, S., Hirschler, M., Lyon, R., Purser, D., Quintiere, J., Stephenson , R., and Tewarson, A.,"Improving Survivability in Motor Vehicle Fires," *Fire and Materials Conference*, January 2007d.

Digges, K., Stephenson, R, "Summary of Research in Crash-Induced Vehicle Fire Safety", SAE paper 2006-01-0551, April 2006.

Digges, K., and Stephenson, R. "A Research Program to Study Impact Related Fire Safety," *19th International Technical Conference on the Enhanced Safety of Vehicles*, May, 2005a.

Digges, K., Stephenson, R., and Bedewi, P., "Research Programs in Crash-Induced Fire Safety," SAE paper 2005-01-1425, April 2005b

Digges, K., Stephenson, R., and Bedewi, P., "A Research Program in Crash-Induced Fire Safety," SAE paper 2004-01-0475, March 2004.

Digges, K., Stephenson, R., and Bedewi, P., "Fire Safety Performance of Motor Vehicles in Crashes," *18th International Technical Conference on the Enhanced Safety of Vehicles*,, May 2003.

Fell, J., Tippets, S., and Bahouth, J., "An Analysis of Vehicle Fire Rates in Fatal Crashes: Is There an Indication of Underreporting?" SAE paper 2007-01-0876, April, 2007.

Fell, J., Pacific Institute for Research and Evaluation, Interim Report to MVFRI on FARS Missing Data, November 2004. www.mvfri.org

F.E.MA., "Motor Vehicle Fires: What You Need to Know," Federal Emergency Management Agency, U.S. Fire Administration, FA-243, April 2003.

Fournier, E. and Bayne, T, "Assessment of Thermocouple Attachment Techniques for Measuring Exhaust Manifold Temperature," Biokinetics and Associates, Ltd., Report R06-23, Sept. 2006. Available at www.mvfri.org

Fournier, E. and Bayne, T., "Anti-siphoning and Leak Prevention Technology Review,' Biokinetics and Associates, LTD, Report R06-20, Sept. 2006. Available at www.mvfri.org

Fournier, E. and Bain, T., "Cone Calorimeter Testing of Underhood Insulation", Biokinetics Report R05-13b, August 2005. www.mvfri.org

Fournier, E., Kot, J., and Sullivan, D.,"Assessment of Fuel System Technology Use in 2003 Model Year Vehicles, SAE paper 2005-01-1423, April 2005

Fournier, E. and Kot, J.,"Comparison of Internal Tank Components – 20 Fuel Systems," Biokinetics and Associates, Ltd. July 2004. Available at www.mvfri.org

Fournier, E., and Keown, M. "Survey of the State-Of-The-Art in Fuel System Fire Safety – Phase 4," Prepared for Motor Vehicle Fire Research Institute by Biokinetics and Associates, Ltd. December 2004. www.mvfri.org

Fournier, E. and Bain, T., "Underhood Temperature Measurements of Four Vehicles", Biokinetics Report R04-13, September 2004. www.mvfri.org

Friedman, K., Holloway, E., and Kenny, T., "Final Report, Impact Induced Fires & Fuel Leakage: Statistical Analysis of FARS and State Data Files (1978-2001)", prepared for MVFRI by Friedman Research Corporation, July 2003. www.mvfri.org

Friedman, K., Holloway, E., and Kenny, T., "Impact Induced Fires: Statistical Analysis of FARS and State Data Files (1978-2001)", SAE paper 2005-01-1421, April 2005.

Goldsmith, A., "Flammability Characteristics of Vehicle Interior Materials," Final Technical Report, J6152, Illinois Institute of Technology Research Institute, Chicago , 1969.

Griffith, A. Leigh, Janssens, Marc L., and Wilson, Keith R., "Evaluation of Smoke Toxicity of Automotive Materials According to Standard Small-Scale Test Procedures", SAE paper 2005-01-1558, April 2005.

Griffith, J., Machado, C., Bendele, B, "Comparative Evaluation of Automotive Fuel Tanks in General Accordance with ECE R34.01, Annex 5 Section 5.0 "Resistance to Fire," SAE paper 2005-01-1561, April 2005.

Gunderson, J., and di Marzo, M., "Feasibility Study for a Vehicle Underhood Nitrogen Foam Fire Suppression System," SAE paper 2005-01-1789, April 2005.

Gunderson, J. and di Marzo, M, "Nitrogen Fire Suppression System for Automobile Under-Hood Post-Collision Fire Protection," Report to MVFRI, University of Maryland, November 2004. www.mvfri.org

Hill, R., Eklund, T., Sarkos, P., "Aircraft Interior Panel Test Criteria Derived from Full-Scale Fire Tests," DOT/FAA/CT-85/23, September 1985.

Hill, R., Johnson, G., and Sarkos, C., "Postcrash Fuel Fire Hazard Measurements in a Wide-Body Aircraft Cabin," FAA-NA-79-42, December 1979.

Janssens, M., "Development of a Database of Full-Scale Calorimeter Tests of Motor Vehicle Burns", Report prepared for MVFRI by SwRI; 01.096939.01.003, March 11, 2008. www.mvfri.org

Kildare, S, and Digges, K., "Analysis of Fire Occurrence in Automotive Crashes Using NASS CDS Data (1994-2004)", GWU Report, Prepared for MVFRI, November 2006. www.mvfri.org

Lyon, R., and Walters, R., "Flammability of Automotive Plastics", Report prepared for MVFRI, August 2005. www.mvfri.org

National Highway Traffic Safety Administration, "U.S. DOT/General Motors Settlement Agreement Status Report, Year 4", NHTSA 2001.

National Highway Traffic Safety Administration, Office of Defects Investigation, "Engineering Analysis Report and Initial Decision that the Subject Vehicles Contain A Safety Related Defect", National Highway Traffic Safety Administration, Engineering Analysis EA92-041, October 17, 1994.

Santrock, J. and Hodges, S., "Evaluation of Automatic Fire Suppression Systems in Full Scale Vehicle Fire Tests and Static Vehicle Fire Tests", SAE paper 2005-01-1788, April, 2005.

Shields, L. and Scheibe, R., "Computer-Based Training in Vehicle Fire Investigation Part 1: Ignition Sources," SAE paper 2006-01-0547, April 2006.

Shields, L. and Scheibe, R., "Computer-Based Training in Vehicle Fire Investigation Part 2: Fuel Sources and Burn Patterns," SAE paper 2006-01-0548, April 2006.

Shields, L., "Emergency Response Time in Motor Vehicle Crashes: Literature and Resource Search," Leland E. Shields, Inc., Seattle, WA, Report prepared for MVFRI, January 2004. www.mvfri.org

Stimitz, J., Wagner, R., "Two Test Methodologies for Evaluating the Resistance to Electrical Arcing Properties of Polymeric Materials for use in Automotive 42 V Applications," SAE paper 2004-01-1722, March 2004.

Stephenson, R., "CNG Vehicle Tank Burst During Filling," SAE paper 2008-01-0557, April 2008.

Stephenson, R., "Fire Investigation for Hybrid and Hydrogen-fueled Vehicles," International Symposium on Fire Investigation, 2006.

Stephenson, R., "Physics of DC Carbon Tracking of Plastic Materials," *Fire and Materials Conference*, Jan. 2005. www.mvfri.org

SwRI, "Comparison of Fire Properties of Automotive Materials and Evaluation of Performance Levels," Battipaglie, et al; SwRI Report 01-05804, October, 2003. See www.mvfri.org

Tewarson , A., Quintiere , J., and Purser, D., "Fire Behavior of Materials in Vehicle Crash Fires and Survivability of the Passengers", SAE paper 2005-01-1555, April 2005.

Tewarson , A., "Thermophysical and Fire Properties of Engine Compartment Fluids", SAE paper 2005-01-1560, April 2005.

Tewarson, A., Quintiere, J., and Purser, J., "Post Collision Motor Vehicle Fires." FM Global Technical Report #0003018009, Volume I, October 2005. www.mvfri.org

Tewarson, A., Quintiere, J., and Purser, J., "Theory and Testing for the Fire Behavior of Materials for the Transportation Industry" FM Global Technical Report #0003018009, Volume II, October 2005. www.mvfri.org

Tewarson, A., Quintiere, J., and Purser, J., "Thermophysical and Fire Properties of Automobile Plastic Parts and Engine Compartment Fluids" FM Global Technical Report #0003018009, Volume III, October 2005. www.mvfri.org

Tamura, Y., Suzuki, J., and Watanabe, S, "Improvement of Flame Exposure Test for High Pressure Hydrogen Cylinders to Achieve High Reliability and Accuracy," SAE paper 2006-01-0128, 2006.

U.S.F.A., "Highway Vehicle Fires," Topical Fire Research Series, Vol. 2, No. 4, U.S. Fire Administration, March 2002.

Wagner, R. and Stimitz, J, "Properties of Plastic Materials for Use in Automotive Applications: Study of Arc Track Properties of Plastic Materials when subjected to DC Voltages Ranging from 12 V DC – 150 V DC," Underwriters Laboratory, December 15 2003. www.mvfri.org

Weyandt, N., "Ignited Hydrogen Release from a Simulated Automotive Fuel Line Leak," Report prepared for MVFRI, SwRI, December, 2006. www.mvfri.org

Weyandt, N., "Catastrophic Failure of a 5,000-psig Hydrogen Cylinder Installed on a Typical SUV," Report prepared for MVFRI, SwRI report 01.06939.01.005, November 2006. www.mvfri.org

Weyandt, N., "Comparative Abuse Testing of 36V and 12V Battery Designs in General Accordance with SAE 2464, SWRI final report 01.06939.01.002, May 2005. www.mvfri.org

Weyandt, N., "Analysis of Induced Catastrophic Failure of a 5000 psig Type IV Hydrogen Cylinder," SwRI, February 2005. www.mvfri.org

White, Monson and Cashiola vs. General Motors", Judicial District Court "Agreement of Settlement Number 42,865, DIV."D", 18th Judicial District Court, Parish of Iberville, Louisiana, June 27, 1996.

Zalosh, R., Weyandt, N., "Hydrogen Fuel Tank Fire Exposure Burst Test," SAE paper 2005-01-1886, April 2005

APPENDICES

APPENDIX A: DOOR OPENING TEST PROCEDURE

BACKGROUND:

The first part of this paper is the proposed test procedure, and it is recommended that this be added to FMVSS 301. The second part of this paper describes a simple R & D project to determine a reasonable value for the maximum door opening force.

PROPOSED DOOR OPENING TEST PROCEDURE FOR FMVSS 301:

1. The vehicle should be subjected to the three crash tests as specified in the upgraded FMVSS 301. A given car only needs to be crashed once.

2. At least one door per seating row which has a door that must be able to be opened after the crash. This should apply to both hinge and sliding doors.

3. The door latch should be able to be unlatched with a force (or torque) no more than twice that which is needed for an un-crashed vehicle.

4. After the crash, the door should be able to be opened by applying a force of no more than X pounds. This force can be applied from either the inside or the outside of the door. For the inside, the force should be applied at the normal shoulder position with the seat far forward. For the outside pull, the force should be applied at the door handle.

R & D TEST TO DETERMINE THE MAXIMUM DOOR OPENING FORCE:

It is suggested that the maximum allowable door-opening force, X, be determined by doing a simple experiment on a few un-crashed cars.

The latch should be removed entirely. Then attach a load cell to the door. Have several volunteers push or pull on the door as hard as they can. The subjects should include an elderly woman, a 5% adult female, and a 50% male. They should both push from inside the car, and also try to open the door from the outside (as if they are trying to rescue someone). The load cell will hold the door in fixed position. The door does not need to actually open in this force test.

Once the data is in hand, NHTSA can set the force maximum by deciding what percentile of the population you want to protect. Maybe the 5% female will be enough and not design for the frail elderly. You might assume that the rescuer (from outside) will on average be stronger than the occupant inside.

The tests should be cheap because the vehicles will NOT be damaged. This does not require any crash tests.

APPENDIX B: COMPRESSED GAS VEHICLE BURN TEST

Scope: This is a proposed comprehensive vehicle-level test for compressed hydrogen or compressed natural gas vehicles. It can be used to replace or supplement the current fully-engulfed, bare-tank bonfire test (FMVSS 304 or a future hydrogen version of it).

Rationale: There are about 290,000 vehicle fires per year and about 520 fire fatalities per year [Ahrens,

2008]. Many of these fires are non-crash fires which initiate in the engine compartment but can spread to the passenger compartment. Over 60% of the crash fires start under the front hood (for conventionally fueled vehicles with IC engines) and can also propagate into the passenger compartment [Digges 2005a, 2005b and 2007a]. These crash-induced fires are particularly harmful when the occupants are injured or entrapped. As vehicles become more energy efficient, increasing amounts of plastics and other flammable materials are being employed. Consequently, the amount of fuel available to feed an underhood fire is expected to increase.

Many of the 290,000 vehicle fires do not spread. About half of the crash induced fires spread to the occupant compartment. Some fires, especially those that engulf the occupant compartment will burn at high intensity and can attack the compressed gas fuel storage tank(s). If a compressed gas tank explodes, there can be additional harm to emergency responders and by-standers, or to surrounding buildings.

Compressed gas tanks are protected from burst by one or more thermally-activated Pressure Relief Devices (PRD). The PRD is sensitive to the increased temperature caused by a fire and is supposed to open and vent the contents of the tank(s) to the atmosphere before the tank wall structure becomes weakened and bursts.

Bursts of a high pressure tank are very damaging because of the large amount of mechanical potential energy stored in the tank – independent of the chemical energy contained in the fuel. Recent real world incidents and tests have shown the catastrophic results of high pressure tank bursts [Zalosh, 2005; Weyandt, 2007; Hansen, 2007; Perrette, 2007 and Stephenson, 2008].

In an MVFRI research project [Zalosh, 2005] a typical Type 4 composite 5000 psi compressed hydrogen tank was exposed to a bonfire to evaluate the consequence of fire induced tank rupture. The tank was tested without a PRD. The composite tank material supported combustion after about 45 seconds of exposure to the bonfire and ruptured after about 6.5 minutes. In this test, blast pressures of 6 psi were measured 21 ft away from the tank, and debris weighing 30 lbs. was propelled more than 250 ft. At the time of tank rupture, the pressure inside the 5,000 psig tank had only increased by 180 psi and the temperature at the cylinder ends had risen only to 103 ^{o}F.

In another MVFRI research project [Weyand, 2007], a typical Type 3 (aluminum liner) 5000 psi compressed hydrogen tank was mounted under an SUV and exposed to a bonfire test. The tank was tested without a PRD. Tank pieces and various vehicle components were ejected up to 300 feet from the vehicle. An exclusion zone if 150 feet was required to avoid overpressure greater than 0.3 psi (a lower limit to avoid ear drum damage to humans). However, higher overpressure could occur beyond the 150 feet radius if reflected waves from surrounding buildings came into play [Weyandt, 2007].

In two recent incidents the fire started in the passenger compartment and attacked the tank(s) through holes in the back of the rear seats [Hansen, 2007, NHTSA, ODI]. These two incidents occurred in vehicles made by OEM vehicle manufacturers – so these problems are not limited to aftermarket vehicle converters. The tank bursts are thought to have occurred because the fire attacked the tank away from the PRD and the PRD did not get hot enough to activate before the tank burst.

Every vehicle model design will have a unique tank(s) placement, vehicle geometry, and different pathways for the fire to approach the tank(s). Some will have physical (metal) or thermal barriers surrounding the tank compartment. The best way to demonstrate the correct operation of the PRD(s) is to conduct a real vehicle burn test.

Proposed Test Procedure: Four vehicles should be tested:

(1). An undamaged vehicle

(2). A vehicle after conducting the FMVSS 301 rear impact test*

(3) A vehicle after conducting the FMVSS 301 side impact test

(4) A vehicle after conducting the FMVSS 301/303 frontal impact test

The Following Procedures Apply to Tests of Vehicles 1 through 3:

The vehicles should be fully fueled and all the electrical systems charged and connected.

The ignition source for the fire should be a rag soaked in alcohol. It should be large enough to

ensure ignition of the passenger compartment materials. It should be placed under the dashboard or on the floor under the dashboard. Two windows should be partially opened to provide adequate ventilation for the fire to spread.

It is suggested that the fire be started in the front passenger compartment because:

(1) There may be many fewer underhood fires in H2/fuel cell vehicles.

(2) Even if the fire starts under the front hood, the fire doesn't become dangerous until it spreads into the passenger compartment.

(3) In many H2 vehicle configurations, the H2 tanks are toward the rear of the vehicle

* FMVSS 301 is specified for the rear impact since it has a higher rear impact speed (80 km/h) than FMVSS 303 and uses the deformable barrier.

The Following Procedures Apply to Test of Vehicle 4:

After being subjected to the FMVSS 301 frontal crash, the vehicle would be tested for fire safety in the event of a major underhood fire. The test vehicle should be fully fueled and all the electrical systems charged and connected. The ignition source should be located near the front of the engine compartment The fire test procedure should be similar to that recommended by Hamins and incorporated in a research projected funded by MVFRI [Gunderson 2005]. This test procedure involved initiating a fire of a sufficient intensity to ignite conventional engine compartment solid materials and fluids. Two passenger compartment windows should be open as in the tests of vehicles 1 thru 3.

It is proposed that the fire be started in the engine compartment because:

(1) Most fires in frontal crashes originate there [Digges, 2005a]

(2) About 2/3 of the crash fires with fatalities originate there [Digges, 2005b]

(3) Most underhood fires are fueled primarily by underhood fluids and solid materials other than the motor fuel [Digges, 2008].

Instrumentation: The pressure in each compressed gas tank shall be measured in a way which will survive the fire. A recommended way is to run high-pressure tubing from the tank(s) to several feet from the vehicle and attach the pressure transducers to the end of the tube(s) away from the fire. The pressure instrumentation will confirm that the tanks have vented down to at most 20 bar without burst.

Test Criteria: A successful test is one in which the compressed gas tanks vent to less than 20 bar (ca 300 psi) before any of the tanks burst.

If the fire goes out, or does not spread in the direction of the tank(s), the test should be repeated with a larger ignition source fire. It is necessary to provide adequate ventilation to ensure that the fire spreads and grows.

Safety Caution: If a tank has been exposed to fire and is still pressurized, it can still burst – even after some delay. Personnel should stay safely away from the vehicle until the tank is de-pressurized. This can be accomplished by a remotely activated valve (not in the fire zone) or by puncturing the wall of the tank with a rifle bullet.

Discussion: A full-scale vehicle burn test was conducted by SwRI [Weyandt, 2007]. In this case the ignition source was a propane burner under the vehicle simulating a pool fire.

GM conducted a large series of well-instrumented vehicle burn tests under its agreement with DOT [Project B.3]. These were for conventionally-fueled vehicles.

It is believed that several OEMs have performed vehicle burn tests for CNG vehicles – in some cases to validate the fix for the tank bursts [Hansen 2007, NHTSA]

Another report containing over 20 vehicle burn tests with heat release rate versus time curves is available [Janssens, 2008]. So clearly performing such vehicle burn tests is feasible.

It should also be noted that the government and industry have been conducting full scale crash tests for occupant crash protection for many decades. It is obvious that testing a complete vehicle is preferable to testing the various components that are involved in a vehicle crash. A similar rationale shows that a complete vehicle burn is the best way to demonstrate vehicle fire safety. The best way to test a complex system is to test it as a complete vehicle system.

Advantages of performing this vehicle burn test include:

1. The combustible materials are those of the real vehicle.

2. The flame spread paths are the same as for the actual vehicle. Thus the direction that the fire attacks the tank(s) is representative of the real world

3. The tank(s) and PRD(s) are in the intended positions relative to other parts of the vehicle.

4. All physical and thermal barriers are in place as designed.

5. The PRD(s) will then experience real temperatures which should demonstrate that it can protect the tank(s). Demonstrating this during the design qualification phase will prevent accidents and possible recalls after the vehicles are on the road.

6. Test vehicles 2, 3 and 4 would have real world crash deformations and are performed in standardized tests used by the government and industry for many years.

Disadvantages of performing these tests:

1. There are personnel safety issues that must be carefully considered (there are similar issues with the current bonfire test.)

2. One additional vehicle (the undamaged one) will need to be tested. (Note: the front, rear, and side impact vehicles already need to be crashed for FMVSS 301/303).

3. Cost of performing the four tests.

REFERENCES

Ahrens, M., "U. S. Vehicle Fire Trends and Patterns," NFPA, July 2008.

Digges, K., and Stephenson, R., "A Research Program to Study Impact Related Fires", ESV Paper 05-0448, 2005a. www.mvfri.org

Digges, K., and Stephenson, R., "Research Programs in Crash-Induced Fire Safety", SAE Paper 2005-01-1425, 2005b . www.sae.org

Digges, K. , "Fire Occurrence in Frontal Crashes Based on NASS/CDS", SAE Paper 2008-01-0256, 2008. www.sae.org

Gunderson, J., and di Marzo, M., "Nitrogen Fire Suppression System for Automobile Underhood Post-Collision Fire Protection," Report prepared for MVFRI by Univ. of Maryland, Nov. 2004. www.mvfri.org

Hansen, R., "Fire Fighter Near Miss: Auto Fire with Compressed Natural Gas (CNG) Fuel Tank Explosion," (Report on Seattle Honda CNG Vehicle Incident, March 2007). Available at:http://www.mvfri.org/index/presentations

Janssens, M., "Development of a database of full-scale Calorimeter Tests of Motor Vehicle Burns," Report prepared for MVFRI by SwRI, March 2008. www.mvfri.org

NHTSA Office of Defects Investigation, "Ford Crown Victoria Police Cruiser 1996 - 2003 Recall," Campaign Number 03V472000.

Perrette, L., and Wiedermann, H., "Safe Storage of Natural Gas on Urban Buses: Case Early Investigation and Learnings," SAE Paper 2007-01-0430, 2007.

Project B 3, "Eleven GM Vehicle Fire Initiation and Propagation Tests". available at www.mvfri.org; (click on "Complete Listing and Download of GM/DOT Fire Safety Reports")

Weyandt, N., "Intentional Failure of a 5000 psig Hydrogen Cylinder Installed in a SUV without Standard Required Safety Devices," SAE paper 2007-01-0431, 2007. www.sae.org

Zalosh, R., & Weyandt, N., "Hydrogen Fuel Tank Fire Exposure Burst Test," SAE Paper 2005-01-1886, 2005. www.sae.org

APPENDIX C: BONFIRE TEST BURST TIME MARGIN

Scope: This test procedure applies to any high-pressure Compressed Hydrogen or Compressed Natural Gas vehicular storage tanks.

Rationale: A vehicle-level burn test (See Appendix D) is preferable to a bare-tank bonfire test. But if it is

decided to keep the tank-level (or high pressure containment system) bonfire test, then it should be improved to provide a burst time margin.

The current fire exposure test (bonfire test) for compressed gas storage tanks and their protective thermally-activated Pressure Relief Devices is a pass/fail test on a single tank. There is no information on whether the tank "passes" (fails to burst) by 5 seconds or 5 minutes.

Tank burst is a very violent event [Hansen, 2007; Perrette, 2007; Weyandt, 2007; and Zalosh, 2005]. These referenced tests and real-world tank explosions caused by fire show that sizable tank and/or vehicle fragments can be thrown up to 350 feet. These fragments can do damage to people or property and thus the probability of occurrence of a tank burst must be kept very low.

Other common tank-level tests which are designed to avoid burst have explicitly known margins.

-Tank burst – >1.8 times nominal working pressure

-Sample size in design qualification = 3 (SAE J2579 Section 5.2.2.3.3)

-Fatigue life – 3 times expected number of cycles.

- Sample size in design qualification = "at least one" (SAE J2579)

Proposed Test Procedure: The bonfire should be set up as specified in FMVSS 304 (CNG) or SAE J2579 (H2). One tank should be bonfire tested without a PRD to establish a baseline tank burst time. A second tank with the PRD and other specified hardware in the high pressure containment system should be tested as specified in FMVSS 304 or SAE J2579. Subsequent to the bonfire test, the tank should be pressurized until burst (without the PRD) to determine its strength margin.

Instrumentation: The pressure in the compressed gas tank should be measured in a way which will survive the fire. A recommended way is to run high-pressure tubing several feet from the tank and attach the pressure transducer to the end of the tube away from the bonfire.

This pressure measurement will document the PRD activation time and the tank vent-down, and confirm that the tank does not burst until it reaches 20 bar (ca 300 psig) or below. The 20 bar vent-down pressure is thought to be low enough that even if the tank would burst, that the damage would be minimal. Also, in most systems, the venting will occur more rapidly than the tank wall will weaken – so once the PRD starts venting it is unlikely that the tank will subsequently burst.

Test Criteria: A successful test is one in which the second compressed gas tank vents to less than 20 bar (ca 300 psi) at 60% or less of the baseline tank burst time. The resulting 40% time margin should be adequate to cover tank-to-tank and test-to-test variations.

It is suggested that the post-test burst pressure be greater than 1.5 times the nominal working pressure.

Safety Caution: If a tank has been exposed to fire and is still pressurized, it can still burst – even after some delay. Personnel should stay safely away from the tank until the tank is de-pressurized. This can be accomplished by a remotely activated valve (not in the fire zone) or by puncturing the wall of the tank with a rifle bullet.

Discussion: The purpose of the pressure burst test is to demonstrate a fire exposure time margin and a burst strength margin for the surviving tank of test two.

Advantages of performing this extra bonfire test include:

1. It will establish a known time margin between the exposure to fire and the tank burst.

2. We will know the residual strength of the tank after successful venting of its contents

3. It is consistent with the demand and capability probability distribution (SAE J2579, Figure C1).

For the bonfire test the level of stress represents time. The "demand distribution" is the severity of the fire exposure (either in the bonfire test itself or in real world vehicle fires). The "response distribution" represents the probability of a tank burst if the PRD does not successfully open and vent the tank. The time margin (shown by the vertical arrow) provides a separation of these two distributions.

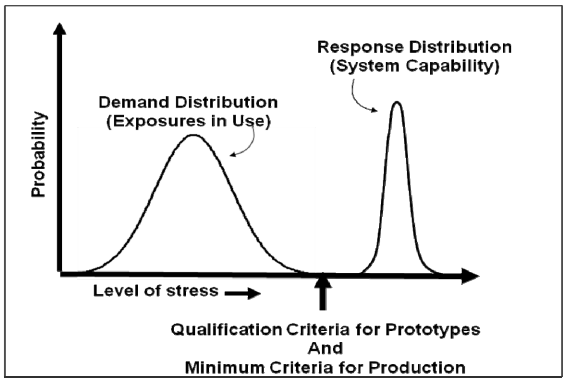

Figure C1. Basis of Criteria for Bonfire Test

Disadvantages of performing this extra test:

1. Requires one extra tank and tank test.

2. The extra cost to perform the first test.

REFERENCES

Hansen, 2007. "Fire Fighter Near Miss: Auto Fire with Compressed Natural Gas (CNG) Fuel Tank Explosion," (Report on Seattle Honda CNG Vehicle Incident, March 2007), Hansen. Available at:: www.mvfri.org

Perrette, 2007. "Safe Storage of Natural Gas on Urban Buses: Case Early Investigation and Learnings," Perrette & Wiedermann, SAE paper 2007-01-0430, April 2007. www.sae.org

Weyandt, N., "Intentional Failure of a 5000 psig Type IV Hydrogen Cylinder, Installed in an SUV Without Standard Required Safety Devices," SAE paper 2007-01-0431, April 2007. www.sae.org

Zalosh, 2005. "Hydrogen Fuel Tank Fire Exposure Burst Test," Zalosh & Weyandt, SAE paper 2005-01-1886. www.sae.org

IN-DEPTH FIELD INVESTIGATIONS OF BELT-RESTRAINED CHILDREN IN FARSIDE CRASHES

Matthew R. Maltese[1]
Caitlin M. Locey[1]
Jessica S. Jermakian[1]
Kristy B. Arbogast[1,2]
[1]The Children's Hospital of Philadelphia
[2]The University of Pennsylvania School of Medicine
United States
Paper Number 09-0218

ABSTRACT

Recent attention has focused on adults in farside crashes but little attention has been given to children in farside crashes. Thus, we sought to elucidate Injury Causation Scenarios (ICS's) in children in center and farside seat positions. Crash investigation cases were drawn from the Partners for Child Passenger Safety Crash Investigation database, and the Crash Injury Research and Engineering Network database. Included in the study were children aged 4 to 15 years, involved in a side impact crash, seated on the center or farside in the rear rows, restrained by a seat belt alone (no booster seats or side airbags) and who received an AIS 2+ injury. Excluded cases were those where the only documented AIS 2+ injury was an altered state of consciousness (concussion, amnesia, or brief loss of consciousness). Seventeen cases met the inclusion criteria for this study. The three most frequently injured body regions to receive an AIS 2+ injury were: head, abdomen, and thorax, with thoracic injuries being quite rare. Intracranial injuries included cerebral contusions, subarachnoid hematoma/hemorrhage, edema, and extradural/epidural hematoma. Skull and facial injuries consisted of vault, orbit and maxillary fractures. Eight occupants had torso injuries: lung contusion, clavicle fracture, spleen laceration or rupture, liver laceration or contusion, and laceration or contusion to the digestive tract organs of the lower abdomen. Our results indicate that injury patterns and mechanisms are unique to children, and thus require a mitigation approach different than the adult. Of note, thoracic injuries, which are common in adult farside crashes, are relatively rare in pediatric farside crashes. Farside abdominal injury patterns suggest a lap belt submarining mechanism in children, injuring primarily the intestinal viscera. These findings further support that children require a different approach to injury mitigation than the adult, and have abdominal injuries in farside crashes that may be addressed by injury mitigation solutions for frontal impact.

INTRODUCTION

Successful development of side impact safety systems for the rear rows of passenger cars requires an understanding of factors that contribute to injury causation and mitigation. When considering the rear row, of particular interest to the vehicle safety system designer should be injury to children, who are frequent occupants there. Development of pediatric vehicle safety systems is justified and should be guided by real world crash data. To set priorities for protecting specific age and restraint groups, safety system designers should use epidemiological data on the incidence and frequency of car crashes involving children. To set design specifications for safety systems requires an understanding of specific Injury Causation Scenarios (ICS's), including a complete description of injuries received, the components within the vehicle that contribute to injury, and the biomechanics of the injury. Using such ICS studies, biomechanical experiments with post-mortem human subjects, animal surrogates and/or human volunteers can be conceived which are reflective of real world impact conditions and injury outcome, but conducted within a controlled laboratory environment with appropriate instrumentation. Such tests then form the basis for biofidelic anthropomorphic test devices and associated injury criteria and, coupled with an appropriate safety system test procedure, can potentially lead to enhanced safety systems.

Seeking information on ICS's, the safety system designer can turn to detailed in depth case reviews of convenience samples of real world crashes. For example, Howard et al. (2004) studied 19 children aged 0 to 12 years involved in side impacts in all types of restraint conditions and seating positions, who were admitted to one of two children's hospitals in Canada. The authors found injuries occurred both with and without direct intrusion into the occupant compartment, suggesting that injuries may occur in center and farside seat positions, which are distant from struck side structures. As the Howard study attempted to describe injury causation across a wide range of restraint conditions, seating positions, and

occupant ages, the applicability of the results may be limited for restraint designers. Focusing on children 0 to 5 years old in child restraints, Sherwood et al. (2003) examined 92 reports of FARS crashes of all crash directions. Studying detailed crashes involving children by particular restraint type groupings is a useful approach to determine ICS's, as occupants are all exposed to similar restraint loading mechanisms. In a sample of 32 side impact crashes, for example, Arbogast et al. (2005a) studied CRS-restrained occupants, and noted the important role of intrusion, the forward component of the crash forces, and the rotation of the CRS toward the side of the crash, as common contributing factors to injury. Focusing on older children (4 to 15 years) not in CRS (belt-restraint only) in struck side crashes, Maltese et al. (2007) found the majority of head and face interior contact points were horizontally within the rear half of the window, and vertically from the window sill to the center of the window. In that same study, the most common cause of torso and abdominal injury was contact with the side interior structure.

Recent attention has focused on adults in farside crashes or side impact crashes where the occupant is seated opposite the struck side of the vehicle (Frampton et al. 1998; Stolinski et al. 1998; Gabler et al. 2005). For adults, the injury patterns in farside crashes differ from struck side crashes in meaningful ways. For example, Yoganandan et al. (2000) noted increases in liver and intestinal injuries, and decreases in splenic injuries, in belted and unbelted farside adult occupants, as compared to the struckside. To our knowledge, no farside studies have yet focused on children. Thus, the purpose of this research was to elucidate injury causation scenarios for children in farside crashes. These data are useful for guiding the development of vehicle injury mitigation concepts for children, and ensuring ATD biofidelity and injury criteria studies address injuries and injury mechanisms observed in the real world.

METHODS

The research presented herein was conducted in accordance with a protocol that has been approved by the Institutional Review Board of The Children's Hospital of Philadelphia.

Crash investigation cases were drawn from two databases: 1) the Partners for Child Passenger Safety (PCPS) Crash Investigation database, and 2) NHTSA's Crash Injury Research and Engineering Network (CIREN) database. The PCPS Crash Investigation database consists of crashes involving injured child passengers reported to an automobile insurance company in the United States, and selected for detailed crash investigation. The CIREN database obtains its data from patients admitted to a network of level-one trauma centers in the United States, who are subsequently selected for a detailed crash investigation. Inclusion criteria were as follows:

1. Occupants restrained by a 2-pt or 3-pt seatbelt, regardless of misuse,
2. 4 to 15 years of age,
3. Seated in one of the rear rows and in the center or farside (away from the side of the vehicle damaged during the crash) position during a side impact crash, and
4. Received a maximum Abbreviated Injury Scale (MAIS) injury of 2 or more (AAAM 2001).

A "side impact" was defined as one in which the case occupant's vehicle sustained damage to its side plane with a principle direction of force that is 45 to 135° or 225 to 315°. Excluded cases were those where the only documented AIS 2+ injury was an altered state of consciousness (concussion, amnesia, or brief loss of consciousness), as such a diagnosis does not provide sufficient physical evidence to support determination of an ICS.

Crash investigators examined the interior and exterior of the vehicles involved, looking for evidence of occupant contact, including scuff marks and tissue, hair, bodily fluid and clothing fabric transfer, and associated such evidence with injuries to specific body regions. Occupant contact points on the interior side structure are thus identified by photograph and included in the detailed crash report. Cases meeting the inclusion criteria were subject to a preliminary quality control review including checks for sufficient information on occupant injuries, vehicle dynamics and damage, and interior contact points. To determine ICS's, a multi-disciplinary Case Review Team (CRT) was established consisting of trauma surgeons, emergency medicine physicians, bioengineers, crash investigation specialists, and database analysts. The case review process included review of crash conditions, restraint and occupant characteristics, occupant injuries, and occupant contact points within the vehicle.

Following review of the case, AIS 2+ injuries were coded using the CIREN BioTAB method developed by Schneider (2005). The BioTAB approach to analyzing occupant injuries in a crash allows the researcher to attribute one or more injury causation

scenarios (ICS) to each injury, where each ICS includes the set of all factors that the researcher believes are essential for the injury to have occurred. Each ICS includes "involved physical components" (things external to the occupant) that are thought to have played an essential role in the injury. Because it is not always possible to know for sure what caused an injury, the researcher must also assign confidence levels of "Certain", "Probable", and "Possible" to each ICS and to each involved physical component within each ICS.

Data was stored in a relational database for analysis. Data analysis, summary and presentation are divided into two stages. First, the crash environment and overall injury patterns are summarized. Second, the injury descriptions, and ICS's are presented.

RESULTS

Seventeen cases met the inclusion criteria for this study; nine from the CIREN database and eight from the PCPS database (Table 1). Before discussing the nature of the injuries, it is necessary to describe the circumstances of the crashes. The vehicles in which the case occupants were riding were most often passenger cars (82%), followed by Minivans (12%) and Sport Utility Vehicles (6%). The bullet vehicle type was most often a Sports Utility Vehicle (41%), followed by passenger cars (35%), and an equal number of minivans, pickup trucks, and large trucks (6% each). Contact with a narrow object (i.e. utility pole) made up 6% of impacting objects. The average Delta V was 23.2 km/h with a standard deviation of 9.1 km/h. 88% of impacts had a principle direction of force (PDOF) between pure lateral and 30 degrees forward of pure lateral. All cases had a non-zero frontal component in the PDOF of the crash. Side impacts to the case vehicles occurred most often on the right side due to the case vehicle turning left across oncoming traffic. The primary area of damage in case vehicles encompassed the passenger compartment and rear lateral side (47%). In 35% of cases, the damage was only to the passenger compartment, and in 18% it included the passenger compartment and the front lateral side of the vehicle. Case vehicle model year distribution was as follows: 29% of vehicles were manufactured between 1990 and 1994, 59% between the years of 1995 and 1999, and 12% of vehicles were manufactured in the year 2000 or later.

Table 1.
Vehicle and Crash Characteristics for Sample of Belt-Restrained Children in Farside Crashes

ID	Occupant's Vehicle Type	Bullet Vehicle Type	Impact Side	PDOF* (degrees)	CDC	Delta V (km/h)
1	4-dr Passenger	4-dr Passenger	L	40	10LYEW5	38
2	4-dr Passenger	SUV	L	30	10LZAW3	21
3	Minivan	Pickup	R	30	2 RZEW2	7
4	4-dr Passenger	4-dr Passenger	L	30	10LPEW2	18
5	4-dr Passenger	SUV	R	15	4 RZAW4	29
6	4-dr Passenger	4-dr Passenger	R	30	02RPEW3	n/a
7	4-dr Passenger	SUV	R	10	3 RPAW3	27
8	SUV	SUV	L	60	11LYEW4	33
9	Minivan	Pole	R	10	00RPAW3	20
10	4-dr Passenger	4-dr Passenger	R	10	03RPEW2	18
11	4-dr Passenger	Minivan	L	10	09LZEW1	n/a
12	4-dr Passenger	2-dr Passenger	R	30	02RZEW1	11
13	4-dr Passenger	SUV	R	20	02RZAW3	23
14	4-dr Passenger	4-dr Passenger	R	20	02RPAW3	19
15	2-dr Passenger	SUV	R	10	03RZAW3	38
16	4-dr Passenger	Large Truck	R	10	03RYAW3	n/a
17	4-dr Passenger	SUV	R	20	02RZAW4	23

*PDOF defined here as the angle with respect to pure lateral; positive value indicates an angle forward of pure lateral.

The average age of the case occupants was 8 years old, with a standard deviation of 2 years, and a range of 5 to 13 years (Table 2). 65% of the case occupants were male. Because our study examines the occupant's interaction with the seat belt and the vehicle interior – factors influenced by occupant size rather than age - we concluded that the occupants would be better grouped by height than by age. Using the Center for Disease Control (CDC) growth charts, we established height ranges according to 50th percentile 4 to 8 year olds, 9 to 12 year olds, and 13 to 15 year olds, then reclassified each occupant according to the equivalent 50th percentile for his or her height. The heights of two occupants were unknown; in these cases the actual age was used. 59% of case occupants fell in the 4-8 year equivalent height range (104 to 131 cm), 29% were in the 9-12 equivalent height range (132 to 152 cm), and the remaining 12% had a height equivalent in the 13-15 year range (153 to 172 cm).

59% of the case occupants were seated in the farside position, which is the position furthest away from the impact. In the farside position, all case vehicles had a

Table 2
Occupant Characteristics for Sample of Belt-Restrained Children in Farside Crashes

ID	Height (cm)	Body Mass (kg)	Actual Age (yrs)	Height-Adjusted Age Range** (yrs)	Sex	Seat Position*	Restraint	MAIS
1	122	27	7	4-8	M	23	Lap/shoulder belt	3
2	115	20	7	4-8	F	23	Lap/shoulder belt	4
3	122	27	7	4-8	M	32	Lap belt improperly worn	3
4	114	16	6	4-8	M	23	Lap/shoulder belt	3
5	n/a	30	7	4-8	F	22	Lap belt	4
6	165	n/a	12	13-15	F	21	Lap/shoulder belt	5
7	122	25	7	4-8	F	21	Lap/shoulder belt with shoulder under arm	3
8	123	19	6	4-8	M	23	Lap/shoulder belt with shoulder behind back	3
9	152	40	11	9-12	M	31	Lap/shoulder belt	3
10	152	32	7	9-12	M	22	Lap belt	2
11	168	66	13	13-15	M	23	Lap/shoulder belt	3
12	122	n/a	6	4-8	F	22	Lap belt	3
13	132	24	8	9-12	M	22	Lap/shoulder belt with shoulder behind back	2
14	140	25	7	9-12	M	22	Lap belt	2
15	109	25	5	4-8	M	21	Lap/shoulder belt	3
16	n/a	n/a	5	4-8	F	22	Lap belt improperly worn	2
17	132	34	9	9-12	M	21	Lap/shoulder belt	2

* For seat position, the first digit indicates the row (2 = 2nd row, and 3 = 3rd row), and the second digit indicates the position on the row (1 = left, 2 = center, 3 = right).
** For height adjusted age range, we established height ranges according to 50th percentile 4 to 8 year olds, 9 to 12 year olds, and 13 to 15 year olds, and then reclassified each occupant according to the equivalent 50th percentile for his or her height.

lap and shoulder belt available; however 20% of the occupants misused the restraint, placing the shoulder portion of the belt behind their back or under their arm, so that they were effectively lap belt restrained only. 41% of case occupants were seated in the center position, where a lap belt was the only restraint available in 86% of these cases. However, all center-seated occupants were effectively lap belt restrained only due to misuse. Overall, for both the center and far-side seating positions, 53% of occupants were effectively lap belt restrained only. In addition, 12% of center-seated occupants misused the lap belt by wearing it very loosely.

It is important to note that over 70% of the children in our study were aged 4 to 7 years and are thus considered improperly restrained without a booster seat, according to recommended practice (AAP 2007). All case occupants had injuries of AIS 2 or greater, as it was an inclusion criterion. 71% of occupants had injuries of AIS 3 or greater and 18% had injuries that met or exceeded AIS 4. The three most prevalent injured body regions to receive an AIS 2+ injury were: head (71%), abdomen (36%), and thorax (12%). Specific injuries are described

Table 3
Head and Face Injury Characteristics for Sample of Belt-Restrained Children in Farside Crashes

ID	Body Region	IPC to Body Region Contacted	IPC Confidence	Specific Injury Description	AIS Code
2	Head	Other occupant to head	Certain	Cerebrum hematoma/hemorrhage epidural or extradural small	140632.4
				Vault skull fracture comminuted	150404.3
				Cerebrum subarachnoid hemorrhage	140684.3
3	Head	Window to head	Probable	Small right cerebrum contusion	140606.3
		C-pillar to head	Probable	LOC <1 hour with neurological deficit	160204.3
4	Head	Seatback to head	Probable	Left vault skull fracture comminuted	150404.3
		Other occupant to head	Possible	Left cerebellum subarachnoid hemorrhage	140466.3
5	Head	Window sill to head	Probable	Unconscious 1-6 hours (GCS <9)	160810.3
		Other occupant to head	Possible		
9	Head	Unknown to head	Unknown	Concussion (NFS)	161000.2
10	Head	Right interior surface hardware to head	Certain	Non-displaced frontal skull fracture	150402.2
11	Head	Unknown to head	Possible	Right anterior cerebrum contusion	140602.3
12	Head	Other occupant to head	Certain	Closed head injury with brief LOC (convulsions/combative)	160202.2
				Fractured right occipital bone	150200.3
13	Face	Door interior to face	Certain	Right orbit fracture	251200.2
				Right maxillary fracture	250800.2
14	Head	RF seatback to head	Possible	Concussion (NFS)	161000.2
		RF headrest to head	Probable		
15	Head	Other occupant to head	Possible	Brain "swelling" (induced coma)	140660.3
		Seatback to head	Possible		
16	Head	Unknown to head	Unknown	Severe head laceration (NFS)	190604.2
17	Head	Other occupant to head	Probable	Concussion (NFS)	161000.2

below, grouped by regions of the body that have similar contact points within the vehicle: a) head and face injuries, b) thorax, abdomen, upper extremity, and pelvis injuries. No AIS 2+ injuries were suffered to the spine or lower extremities.

Head and Face Injuries

13 occupants received an AIS 2 or greater head or face injury (Table 3). 12 of the occupants had head injuries without accompanying facial injury, and the remaining case had facial injuries without accompanying head injury. Intracranial injuries included cerebral contusions (2 cases), subarachnoid hematoma/hemorrhage (2 cases), edema (1 case), and extradural/epidural hematoma (1 case). Extracranial injuries consisted of vault skull fractures (4 cases), and one case each of orbit and maxillary fracture. A severe scalp laceration was also an injury for one case. Loss of consciousness was coded for 6 of the cases, being the sole head/face injury for four cases. For three of these cases, the loss of consciousness was considered severe (AIS 3) due to an extended period of unconsciousness, convulsions/combative behavior, or resulting neurological deficit. For the remaining three cases, the diagnosis of concussion was not supported with additional medical evidence, and thus was given the outcome "not further specified."

The BioTAB method allows multiple ICS to be associated with a single injury in a single case, which occurs when the CRT concludes that there are multiple ways in which the injury occurred. For example, the head injury in case 15 may have been caused by contact with another occupant, or contact to the right front seatback.

Head and face injury was attributed most often to contact with another passenger seated between the case occupant and the impact (33%). This additional occupant was present in only 54% of cases with a head/face injury, but of this number, 86% of cases listed the other occupant as a source of injury. The second most common source of head and face injury was the interior structure on the struck-side door (28%), with one occurrence each of window, c-pillar, window sill, interior hardware, and door interior contact. For 22% of head/face injuries, contact was attributed to the seatback or headrest of the seat that was both in front of the occupant and closest to the side of impact. For the remaining 17% of head and face injury causation scenarios, the source of injury was unknown.

Thorax, Abdomen, Upper Extremity, and Pelvis Injuries

Eight occupants had injuries to the "trunk" of the body, consisting of the thorax, abdomen, upper extremity and pelvis (Table 4). Injuries included lung contusions (2 cases), spleen lacerations or ruptures (2 cases), liver lacerations and contusions (2 cases), jejunum-ileum lacerations (2 cases), colon lacerations and contusions (2 cases), and one case each of clavicle fracture, myocardium heart contusions, retroperitoneum hemorrhage, mesentery contusion, small intestine laceration, and displaced iliac wing fracture.

Overall, 88% of individual torso injuries were caused by contact with the belt, including the lap, shoulder, or some combination of the two. For the upper torso, encompassing the upper extremities, thorax, and superior abdominal organs (specifically the liver and spleen), the shoulder belt was the most common injury source (accounting for 75% of individual injuries and 66% of unique causation scenarios). In one of these cases, the shoulder belt was worn incorrectly under the occupant's arm, however for all others the shoulder belt was worn properly with the lap belt. Contact with another occupant or with a child restraint seat each account for an equal part of the remainder of upper torso injures. All injuries to the lower torso, consisting of the inferior abdominal organs (small intestine, mesentery and colon) and pelvis were attributed to contact with the lap belt. For 88% of injures and 80% of unique injury causation scenarios, the case occupants were effectively lap belt restrained only due to both belt availability and misuse. The remaining occupants with lower torso injuries were restrained by both lap and shoulder belt.

DISCUSSION

Our work presented herein is the first that investigates ICS's in belt-only restrained children in farside crashes, and complements other population-based injury risk and in-depth crash investigation studies of the same restraint and age group (Maltese et al. 2005a; Maltese et al. 2005b; Maltese et al. 2007), as well as studies of children in forward facing child restraints in side impacts (Arbogast et al. 2004a; Arbogast et al. 2005a), and children in booster seats in side impacts (Arbogast et al. 2005b). These data provide guidance for increasing protection of children in these distinct restraint conditions.

Table 4
Thorax, Abdomen and Pelvis Injury Characteristics for Sample of Belt-Restrained Children in Farside Crashes

ID	Body Region	IPC to Body Region Contacted	IPC Confidence	Specific Injury Description	AIS Code
1	Abdomen	Lap belt to abdomen	Certain	Inferior/lower jejunum-ileum laceration/perforation (OIS Grade III)	541121.3
5	Thorax	Other occupant to torso	Certain	Bilateral inferior lower lung contusion	441410.4
	Upper Extremity	CRS to shoulder	Certain	Left clavicle fracture (OIS Grade I or II)	752200.2
6	Thorax	Shoulder belt to chest	Certain	Bilateral lung contusion	441410.4
				Minor central myocardium heart contusions	441004.3
	Abdomen	Shoulder belt to abdomen	Certain	Right complex liver laceration	541828.5
				Right minor liver contusion	541812.2
7	Abdomen	Incorrectly worn shoulder belt to abdomen	Certain	Moderate spleen laceration (OIS Grade III)	544224.3
8	Abdomen	Lap belt to abdomen	Certain	Retroperitoneum hemorrhage	543800.3
				Jejunum-ilium laceration	541422.2
				Mesentary contusion	542010.2
				Colon contusion	540810.2
9	Pelvis	Lap belt to pelvis	Certain	Right comminuted superior anterior displaced iliac wing fracture	852604.3
11	Abdomen	Lap/shoulder belt to abdomen	Certain	Lacerated/ruptured spleen	544220.2
				Lacerated small intestine	541020.3
16	Abdomen	Loosely worn lap belt to abdomen	Certain	Torn colon with internal bleeding	540822.2

Over the past several years, our research Center has studied children in side impact crashes who are restrained by seat belts and who are seated on the rear rows. As rear rows of many vehicles accommodate three seat positions (struck-side, center, and farside), our studies compare injury rates and patterns for all three positions across each rear row. This research line has yielded several important findings that help elucidate the injury problem in side impact. For example, the farside injury risk for belt-restrained children is nearly half that of struck side children (OR:0.55, 95% Confidence Interval: 0.33-0.93), however, the center seat position has injury risk comparable to the struck side (OR; 1.15, 95% CI: 0.50, 2.66) (Maltese et al. 2005b). Our population-based studies provide context for studies such as those presented herein. That is, the present study is a convenience sample, with no formal consideration for sample representativeness to the population. Thus, where possible it is important to compare variables common to both population and convenience studies to validate the latter. Toward this end, the most frequently injured body region for belt restrained farside child occupants in population-representative studies (Maltese et al. 2005a) is the head (56% of occupants have head injuries) followed by the face (24 %), abdomen (11 %) and then the chest (8%). The data presented herein also reflect this injury pattern, as 13 of 17 cases had head and face injuries, 6 of 17 cases had abdominal injuries, and 2 of 17

cases had chest injuries. The head injuries in our cases consisted of common adult intracranial injuries including hemorrhage/hematoma (subarachnoid, epidural, or extradural, but no subdural), contusion, concussion, and loss of consciousness. Extracranial injuries included vault fractures and facial bone fractures. All brain injuries were attributed to contact with a vehicle interior or exterior structure. No brain injuries were associated with "non-contact" events, where the occupant receives a brain injury but does not strike their head on any surface or structure.

Our finding of infrequent chest injury among farside child occupants herein and in our population-based study (Maltese et al. 2005a), stands in stark contrast to farside adult occupants analyses, where the chest is highlighted as the most frequently injured body region (34% of all injuries), followed by the head (27%), extremities (25%) and abdomen (7%) (Gabler et al. 2005). This suggests that children present a farside injury mitigation problem that is different than the adult's.

The question then arises as to the reason for the fewer thoracic injuries in children compared to the adult – is it biomechanical, environmental, or a combination thereof? One could argue that there are environmental differences between Gabler's farside population, who are largely front seated, and the data presented herein which are exclusively seated in the rear rows. Gabler notes that the primary injury source in the farside crashes with adults is the struck side front seatback, whereas herein the injury sources in the two cases with thoracic injuries were the belt and the adjacent occupant.

From a biomechanical standpoint, inspection of the torso maturation process reveals substantial differences in the structure and material composition between the adult and child chest. The sternum consists of 6 main bones – the manubrium superiorly, followed by sternebrae 1 through 4 and the xiphoid process. The 4th sternebra appears at age 12 months, while the xiphoid process appears at 3 to 6 years. Fusing between sternebrae begins at age 4 years and continues through age 20 years. The sternum as a whole descends with respect to the spine from birth up until age 2 to 3 years, causing the ribs to angle downward when viewed laterally, and the shaft of the rib to show signs of axial twist deformation (Scheuer and Black 2000). The costal cartilage also calcifies with age, likely influencing its flexibility. As discussed by Kent et al. (2005), aging bone shows a decrease in elastic modulus beyond adult middle age, and ribs alone in bending demonstrate decreased breaking strength with increased age. These material and morphological changes during the maturation and aging phases of human life likely influence the injury response of the chest. For example, no rib fractures were found in a recent series of blunt impacts into the thoraces of nine post-mortem human subjects ages 2 to 12 years (Ouyang et al. 2006), yet the same type of test performed on adults produced rib fractures in 18 of 22 subjects (Kroell et al. 1974). These maturation-related changes of the chest highlight the uniqueness of the pediatric restraint problem from the perspective of ATD design, injury criteria selection and tolerance, and design of restraints such as seat belts.

Behind the head, the abdomen was the second most frequently injured body region (6 of 17 cases), the same injured body region rank as population-representative studies (Maltese et al. 2005a). Elucidation of the mechanism of these injuries can be found by first comparing struck-side abdominal injuries vs. center and farside abdominal injuries. Our previous study of struck side injuries revealed primarily spleen or liver injuries, with the injury (liver vs. spleen) depending on which organ was on the struck side of the crash. However of the 11 AIS coded abdominal injuries presented herein, only 4 injuries were those similar to struck side child victims (spleen and liver); the remaining 7 were injuries to the viscera of the abdomen (jejunum-ileum, retroperitoneum, mesentery, colon, small intestine). These highlight a decidedly different injury mechanism for the farside / center occupants that bears resemblance to abdominal injuries in frontal crashes. That is, in a population-representative study of abdominal injuries in children, stomach and intestinal injuries were represented in 77% of those children with AIS2+ abdominal injuries involved in frontal crashes, and injuries to the liver, spleen and kidney were each less than 10% (Arbogast et al. 2004b). The high incidence of stomach and intestine injuries in the frontal impacts was attributed to lap belt submarining, where the boney pelvis slides under the lap portion of the belt and the abdominal viscera are exposed to compression by the belt (Arbogast et al. 2007). Despite the fact that the cases presented herein were side impacts, the injury patterns observed are similar to lap belt submarining injuries observed in frontal crashes.

CONCLUSIONS

Injury causation scenarios for belt restrained children in farside crashes have been delineated. Combined with data from the literature, our results indicate that thoracic injuries are the predominant injury in adult

farside crashes, but are rare in pediatric farside crashes. Further, farside abdominal injury patterns suggest a lap belt submarining mechanism in children, injuring primarily the intestinal viscera. These findings further support that children require a different approach to injury mitigation than the adult, and have abdominal injuries in farside crashes that may be addressed by injury mitigation solutions for frontal impact.

ACKNOWLEDGEMENTS

Funding for this analysis has been provided by the Center for Child Injury Prevention Studies and its member companies: Britax Child Safety, Inc., Nissan Technical Center North America, TK Holdings Inc., Toyota Motor, Inc. NA, State Farm Insurance Companies, Dorel Juvenile Products and Volkswagen of America. This work would not have been possible without the cooperation of State Farm and their commitment and financial support of the creation and ongoing maintenance of the Partners for Child Passenger Safety (PCPS) program. The PCPS and CIREN serve as the sources of data for the analysis conducted herein. The views expressed are those of the authors and do not represent the views of State Farm, the Center for Child Injury Prevention Studies or its member companies.

REFERENCES

AAAM (2001). Abbreviated Injury Scale (AIS) 1990 - Update 1998. AAAM, Association for the Advancement of Automotive Medicine.

AAP (2007). Car Safety Seats: A Guide for Families 2007. A. A. o. Pediatrics, American Academy of Pediatrics (AAP) http://www.aap.org/healthtopics/carseatsafety.cfm. Accessed June 21, 2007.

Arbogast, K., Y. Ghati, et al. (2005a). "Field investigation of child restraints in side impact crashes." Traffic Injury Prevention 6(4): 351-60.

Arbogast, K. B., I. Chen, et al. (2004a). Injury Risks for Children in Child Restraint Systems in Side Impact Crashes. International Research Council on the Biomechanics of Impact Conference.

Arbogast, K. B., I. Chen, et al. (2004b). Predictors of Pediatric Abdominal Injury Risk. Stapp Car Crash Journal. Nashville, Tennessee, USA. 48: 113-126.

Arbogast, K. B., M. J. Kallan, et al. (2005b). Effectiveness of high back and backless belt-positioning booster seats in side impact crashes. 49th AAAM Conference, Association for the Advancement of Automotive Medicine, Barrington, IL.

Arbogast, K. B., R. W. Kent, et al. (2007). "Mechanisms of abdominal organ injury in seat belt-restrained children." Journal of Trauma-Injury Infection & Critical Care 62(6): 1473-80.

Frampton, R. J., R. Brown, et al. (1998). The importance of non-struck-side occupants in side collisions. 42nd Annual Proceedings of the Association for the Advancement of Automotive Medicine.

Gabler, H., K. Digges, et al. (2005). Side Impact Injury Risk for Belted Far Side Passenger Vehicle Occupants. SAE World Congress Society of Automotive Engineers, Warrendale, PA.

Howard, A., L. Rothman, et al. (2004). "Children in side-impact motor vehicle crashes: seating positions and injury mechanisms." Journal of Trauma Injury Infection & Critical Care 56(6): 1276-85.

Kent, R., S.-H. Lee, et al. (2005). "Structural and material changes in the aging thorax and their role in crash protection for older occupants." Stapp Car Crash Journal 49(October): 231-249.

Kroell, C., D. Schneider, et al. (1974). Impact tolerance and response of the human thorax II. 18th Stapp Car Crash Conference, Society of Automotive Engineers, Warrendale, PA.

Maltese, M., I. Chen, et al. (2005a). Effect of increased rear row occupancy on injury to seat belt restrained children in side impact crashes. 49th AAAM Conference, Boston, Association for the Advancement of Automotive Medicine, Barrington, IL.

Maltese, M., I. Chen, et al. (2005b). The effect of rear row seating position on the risk of injury to belted children in side impacts in passenger cars. 19th International Technical Conference on the Enhanced Safety of Vehicles. Washington, DC, United States Department of Transportation, National Highway Traffic Safety Administration, Washington, DC.

Maltese, M. R., C. M. Locey, et al. (2007). "Injury Causation Scenarios in Belt-Restrained Nearside Child Occupants." The Stapp Car Crash Journal 51(October 2007).

Ouyang, J., W. Zhao, et al. (2006). "Thoracic impact testing of pediatric cadaveric subjects." Journal of Trauma: 1492-500, 2006 Dec.

Scheuer, L. and S. Black (2000). Developmental Juvenile Osteology. London, Academic Press Limited.

Schneider, L. (2005). Personal Communication. University of Michigan Transportation Research Institute.

Sherwood, C. P., S. A. Ferguson, et al. (2003). Factors leading to crash fatalities to children in child restraints. Association for the Advancement of Automotive Medicine.

Stolinski, R., R. Grzebieta, et al. (1998). Vehicle far-side impact crashes. 16th International Technical Conference on the Enhanced Safety of Vehicles.

Yoganandan, N., F. A. Pintar, et al. (2000). "Patterns of abdominal injuries in frontal and side impacts." 44th Annual Proceedings, Association for the Advancement of Automotive Medicine: 17-36.

IMPROVEMENT OF AIRBAG PERFORMANCE THROUGH PRE-TRIGGERING

Gregor Gstrein
Wolfgang Sinz
Vehicle Safety Institute – Graz University of Technology
Austria

Walter Eberle
Julien Richert
Wilfried Bullinger
Daimler AG
Germany
Paper Number 09-0229

ABSTRACT

In the near future road cars will be able to detect probable collisions before they happen. Then it will be possible to avoid some accidents by specific actions of driver assistance systems. If a crash is unpreventable, the passenger can be prepared for the collision during the residual time.
This project determines the potential for a reduction of the injury-risk for car-occupants through an airbag deployment considerably before t_0. The goal is to demonstrate possible improvements in order to stimulate the further development of pre-crash-sensors. Through the pre-crash deployment of the airbag various advantages for the occupant can be obtained: If the airbag is fired before t_0 it can be designed in a significantly bigger way in comparison to conventional trigger times because the passenger hasn't moved forward. Thereby a very early coupling of the passenger and resulting low loads are achieved. Another advantage is that the airbag can be inflated more slowly due to much more time available. So the deployment of the airbag can be performed in a gentle way which leads to a less aggressive system that promises improvements especially in out-of-position (OOP) situations.
There is still no future perspective for a hundred percent detection rate of pre-crash-sensors, so the airbag-system will additionally be designed for conventional trigger times. It is mandatory that in case of a failure of the pre-crash-sensors the occupant is protected at least as well as in today's series-production vehicles.
This analysis investigating the potential of pre-crash activated airbags is based on multibody-simulations with different dummies and crash-scenarios. The results of the simulations are going to be verified by principle tests and full-scale sled tests.

Keywords: Airbag, PreCrash, OOP

INTRODUCTION

Since the implementation of restraint systems in road cars, the risk of being killed in an accident has decreased significantly. Nowadays, with a properly designed restraint system, it is possible to survive even severe crashes without life-threatening injuries. The main components of a typical restraint system for frontal collisions in modern road-cars are a 3-point safety belt with one or more pretensioners, a beltforce-limitation and an airbag-system with one ore more inflator stages. These components are triggered by accelerometers in combination with sophisticated control logics. Subject to collision-type the trigger-times vary from 10ms to 30ms after the first impact.
Within this hardware-environment the possibilities of a reduction of the injury risk for occupants are more or less exploited.
Nevertheless, in order to keep improving the occupant protection, it is necessary to apply some more sophisticated technology in future restraint systems. The focus of recent development is the adaptivity of the restraints to different occupant classes and crash severities (e.g.: [1], [2]).
Further studies discuss the activation of restraint systems significantly before t_0 (e.g.: [3]).
In order to be able to set a trigger signal before the impact, specific sensor information is required. For this purpose, for instance the existing sensors of comfort and assistance systems could be used. These systems are becoming more and more popular in new cars, which leads to an increasing amount of sensors in the cars that can detect the driving environment. It is conceivable, that a collision detection can be realized as a by-product of driver assistance systems.
In this regard, sensors that are already in use or in development are Radar, Lidar and stereo cameras or combinations thereof. Each system has its advantages and shortcomings (see [4]).

The existing sensor information can be used to foresee possible collisions and set actions in order to prevent the accident and "prepare" the occupants for the impact. There are, for example, already cars on the road, in which reversible restraint systems (e.g.: reversible belt-pretensioner, [5]) are activated.
This study discusses the activation of an irreversible restraint system (frontal passenger airbag). The goal is to work out the potential for reducing the injury risk as well as to discuss the shortcomings of such systems.
Which beneficial characteristics can be expected of an airbag-system that can be activated significantly before t_0?
Firstly, the passenger hasn't moved forward prior to the impact, which makes it possible to design a bigger cushion in comparison to conventional trigger times. The bigger airbag leads to an earlier coupling of the passenger to the chassis-movement. This results in lower mean loads.
Secondly, the loads on the dummy coming from the airbag affect a bigger surface and therefore are preferable to the more local loads of the safety belt. The share of the airbag on the total restraint-forces can be higher in a pre-crash-activated airbag-system.
Thirdly, due to the very early triggering, the cushion can be inflated much more slowly and in that way more gently in comparison to conventional trigger methods. This circumstance promises a considerable reduction of the injury risk for the car occupant in the so-called OOP-situations.
Before these advantages and potential benefits for the passenger-safety in frontal collisions can be exploited in a series-vehicle, some nowadays still insuperable problems have to be resolved.
Whereas a faulty activation of a reversible restraint system (e.g.: reversible belt-pretensioner) is not quite problematical, it can be very dangerous if, for instance, an airbag deploys due to a malfunction of a sensor system. The problem is that there is an endless number of possible crash-constellations in road traffic and the sensor systems are not yet, and won't be able in the foreseeable future, to interpret every constellation correctly. So a compromise between detection-rate and detection-certainty has to be found. Keeping in mind the risk that implicates a faulty activation, it is reasonable not to deploy the airbag in case the sensors cannot definitely interpret the traffic situation.
That leads to another problematic issue. The less accident-constellations can be detected correctly and as a consequence the airbag can be triggered before the impact, the more important remains a backup-strategy. If the sensor-system was able to recognize 95 percent of all possible accident-scenarios only the residual 5 percent would need a backup-strategy in terms of an alternative activation of the restraint systems. The problem is that the importance of the backup is more or less opposing the potential of the pre-crash-activation of the restraint systems since it directly affects the possible airbag-size.

Methodology

The idea was, to elaborate a completely new pre-crash airbag system for an existing road car for the frontal passenger. Comparing the results with the performance of the existing series airbag system the potential for injury-reduction should be illustrated.
Therefore some boundary conditions for the development of this new pre-crash airbag were set up:
- The earliest possible trigger-time is 80ms prior to the first contact.
- A "backup" has to be considered. In the case of a non-detection of the pre-crash-sensors, the system has to work with conventional trigger-times as well. In this case, the injury risk for the passenger must not be higher than it is with the conventional airbag-system.
- The airbag system must not be designed for just one single loading condition, in order to allow an impartial comparison to the series production status which is a compromise for many load cases. Therefore the new airbag system has to be designed for different dummy-sizes and accident-types. More precisely, it has to fulfill partly opposing requirements of the 5th percentile female, 50th percentile and 95th percentile male dummies in the Euro NCAP, US-NCAP crash test-scenario. Furthermore the unbelted FMVSS208 crash test has to be taken into account.
- As this study is not only theoretical but also consists of an experimental validation of the simulation results, the hardware package must be "realizable".

Within these limitations viable parameter configurations for the different dummy/loadcase-combinations were developed, using the multibody-simulation-tool MADYMO. The results are going to be validated exemplarily by sled tests during autumn 2009. The performance in terms of OOP has already been demonstrated and the results are discussed later on.

Definitions

With respect to the timeline, two scenarios have to be distinguished: On the one hand, we have the pre-collision activation of the restraint systems at the earliest of 80ms before the impact. As mentioned before also a "backup"-strategy is necessary in case of a malfunction of the pre-crash-sensors. So the second scenario consists of the activation of the same hardware components with conventional trigger-systems. This leads to a big

difference in time available for the deployment of the airbag which makes an adaptivity of the inflation inevitable.
As a first step different hardware packages were evaluated with respect to their anticipatory compliance to the set requirements. The discussed hardware components were the inflator, the airbag-shape and the vent-holes.
As mentioned before, one boundary condition was the feasibility of the hardware package. Keeping this in mind, the most promising variant is made up of an inflator with three stages and two airbag-shapes that can be transformed into each other for example by releasing tethers. Furthermore the airbag features an active vent and a vent hole that opens as soon as the airbag pressure exceeds a certain limit.
Each one of the two airbag-shapes is designed to fit a specific dummy type. The smaller cushion (~90l) is deployed for the 5th percentile female dummy, while the bigger airbag-shape (~120l) fits for the two other dummies (50th- and 95th-percentile male). Obviously you can gain more potential for lower injury risk when bigger airbags are used, but then you'll have to face the following problems in the backup-scenario. Firstly you have to inflate a bigger volume within a very short time which leads to a more aggressive inflator-characteristic. And secondly you run a higher risk, that the deploying airbag hits the passenger.
The two airbag-shapes have to be filled by the three stages of the inflator. Stage I and stage III are designed to blow up the 90l-airbag to operating pressure, stage I in a time of 120ms and stage III in 40ms. Subject to the trigger-scenario the required stage is fired. If the 120l-airbag has to be deployed, stage II is activated additionally in order to fill up the bigger volume to operating pressure. The pressure dependent standard vent hole is necessary in order to avoid massive gas-loss during the long lasting deployment of the airbag in case of a pre-collision activation.
The selected hardware components allow a high number of possible combinations for the different load cases and dummies. In the following, the most promising processing strategies are presented qualitatively:

PreCrash-Scenario:
PreCrash-sensors foresee an upcoming collision and 80ms before the impact the airbag is triggered.
For the 50th- and the 95th-percentile male dummy inflator-stage I slowly deploys the big cushion (BagShape 1; ~120l). After a specific time, that depends on the load-case and whether it is a 50th- or 95th-percentile dummy, inflator-stage II is activated in order to fill up the airbag to operating pressure. After a certain time the active vent is triggered to allow more dummy-movement making thereby best use of the space available. The trigger-times for inflator-stage II and the active vent vary subject to dummy and load case, as can be seen in the following figure (diagonally hatched → deploying airbag; cross hatch → airbag is positioned and ready to restraint):

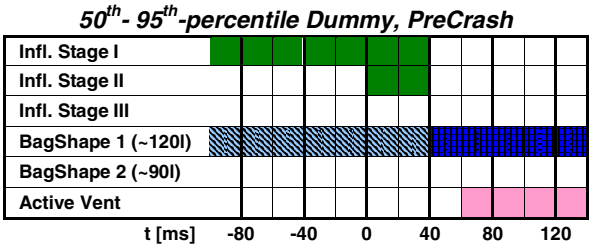

Figure 1: Deployment logics for the 50th- and 95th-percentile male dummy - PreCrash

It seems to be reasonable to work out adapted strategies in terms of trigger-timing and vent opening for both the 50th- and the 95th-percentile male dummy, in order to reduce the injury risk as much as possible.
Also for the 5th-percentile female, the airbag is activated by pre-crash-sensors 80ms prior to the collision. For approximately 120ms the small cushion (BagShape 2; ~90l) deploys gently and gets in position around 40ms after the impact, the time when the occupant begins his/her forward movement. Since the airbag-shape for the 5th-percentile female dummy has less volume, stage I fills the cushions sufficiently. In order to keep the restraint-loads below the biomechanical limits of small, lightweight persons it is necessary to activate the active vent early. The timing for vent-opening depends on the load-case. Figure 2 illustrates the setup of the airbag system for the 5th-percentile woman in one specific loading condition:

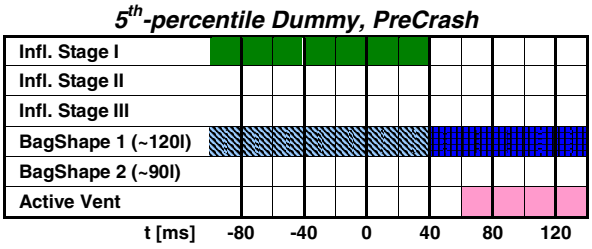

Figure 2: Deployment logics for the 5th-percentile female dummy - PreCrash

Backup-Scenario:
For any reason the pre-crash-sensors were not able to detect the collision and the conventional trigger-system has to set the trigger-time for the restraint systems. In this case it is essential to deploy the airbag as fast as possible in order not to lose deceleration-space.

So for the 50th- and 95th-percentile male dummy inflator stages II and III are fired at the same time. Around 40ms after the impact the airbag cushion is positioned and able to take restraint loads. Subject to crash-scenario and dummy-weight the active vent is opened at a specific time after the impact.

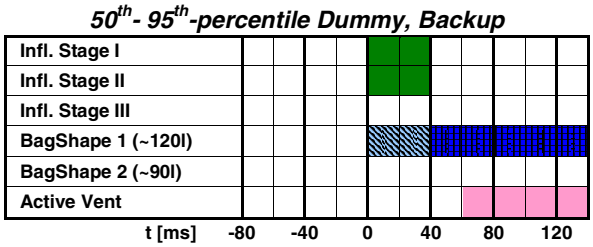

Figure 3: Deployment logics for the 50th- and 95th-percentile male dummy - Backup

Equivalent considerations need to be done also for the 5th-percentile female dummy. In this case only stage II of the airbag inflator is activated at conventional trigger-times. Within a very short time the cushion is positioned and able to restrain the passenger. Subject to the crash-scenario, the active vent has to be opened early in order to avoid too high loads on the occupant.

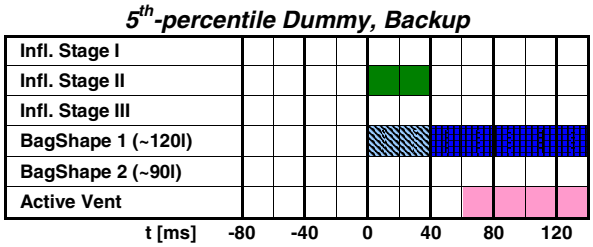

Figure 4: Deployment logics for the 5th-percentile female dummy - Backup

The earlier specified deployment strategies have a direct impact onto the geometry of the airbag-cushion. The development of the two required airbag-shapes is discussed in the following:

Airbag Geometry

The highest potential for reducing the injury risk by a pre-crash-activation of an airbag-system results in an optimized shape. If the airbag is fired considerably before the impact the passenger doesn't move forward during the deployment. So the shape can be designed with more extension in the longitudinal direction of the car, closer towards the occupant.

If the person is decelerated within a longer distance, the mean loads decrease proportionally. So an earlier coupling of the dummy to the chassis-movement can reduce the injury risk significantly.

In order to make best benefit of this circumstance it is necessary to provide an airbag shape that spreads the restraint loads evenly to a surface as big as possible. Also large gaps between the dummy-head and the cushion should be avoided, to ensure the early coupling and evade load peaks.

In order to achieve, that the airbag can apply restraint loads onto the passenger from the very first forward movement, some design criteria have to be fulfilled. The cushion has to contact the occupant evenly on the thorax and the thighs. Furthermore it is necessary that the cushion supports itself on the instrument panel (IP) and the windscreen. If there is some space between the deployed airbag and the IP, the person will push the airbag forwards until it contacts the dashboard. The distance lost here leads to increasing loads on the dummy.

Figure 5 highlights the areas, where the airbag needs to brace in order to be able to build up effective restraint forces.

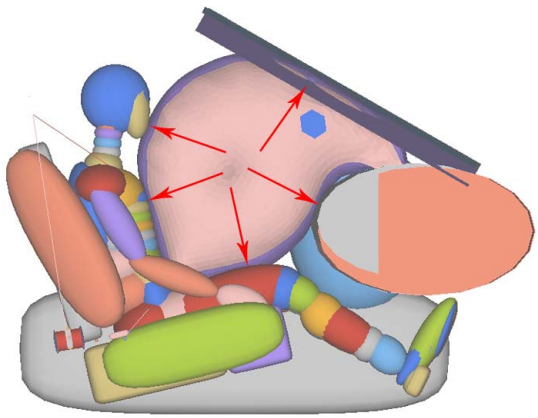

Figure 5: Design criteria for a well working precrash-airbag

As mentioned above, for this study it was necessary to design a dual-stage airbag-system. The chosen deployment-strategy made it inevitable to put quite some emphasis on the backup-scenario. Therefore the airbag-volumes are comparable to a conventionally triggered series-vehicle airbag which in shape and volume represents an optimized compromise for many loading conditions. Another point that has to be taken into account is, that the bigger the airbag volume is, the higher the inflation mass flow has to be in order to fill the cushion sufficiently in the backup-scenario. That leads to a more aggressive deployment of the airbag and possible problems in OOP-situations.

Due to these reasons the goal of airbag-design was to achieve more extension of the cushion in the longitudinal direction of the car, without a dramatic increase of the volume. As the airbag always tries to assume a more or less spherical form, the longer you design it, the wider it gets, and the volume basically increases with the power of three. For that reason it appeared to be necessary to provide an internal transversal tether for the airbag-shape for

the 50th- and 95th-percentile dummy. In the left image of Figure 6, the transversal tether can be seen.

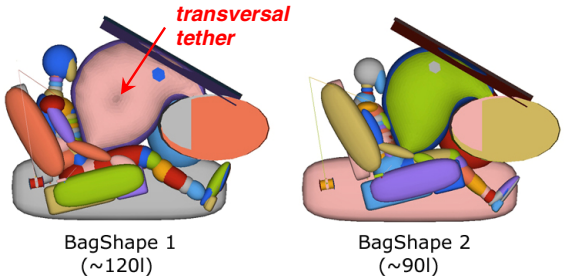

Figure 6: Airbag-shapes for different dummies

Furthermore additional tethers are necessary to realize two airbag-shapes out of one cushion. Initially the tethers are constrained in any case and the small airbag-shape for the 5th-percentile female dummy is deployed. A system, that is able to classify the passenger (e.g.: by weight or by seating position) gives the signal that the bigger shape is necessary and the tethers are released by an actuator.

Inflator-Requirements

At the beginning of this study it was not clear, with which hardware the slow deployment of the airbag could be realized. It turned out to be quite difficult to find available inflators which were able to provide a gas flow-characteristic that would fill up the cushion in approximately 120ms.
So for a first step, generic mass flow-curves were assumed. In a further simulation-loop before the validation tests these characteristics are going to be substituted by measured properties of the inflators that are going to be applied in the tests. In Figure 7 the generic mass flow curves of the different inflator-stages are illustrated.
The principal idea was to use an inflator with three stages, where each stage has a specific "function". One stage (Stage I) is necessary for the slow, gentle deployment of the cushion in a case of a pre-collision activation. This stage is capable of filling the bag-shape of the 5th-percentile female dummy up to operating pressure.

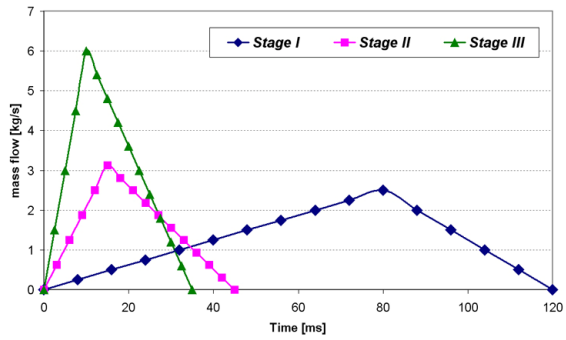

Figure 7: generic mass flow-characteristics of the three gas-generator stages

If the airbag-shape for the 50th- and 95th-percentile male dummies is deployed, the bigger volume cannot be filled sufficiently with stage I. So it is necessary to trigger an additional inflator-stage (Stage II) that delivers enough gas to reach the operating pressure. The timing for the deployment of stage II depends on the load-case and the dummy-size. The goal is that the airbag is fully inflated, positioned and ready to take restraint loads as soon as the forward movement of the passenger begins.
If the pre-crash sensors don't work correctly, the trigger-signal for the airbag is set by conventional sensor systems. In this case it is crucial that the airbag is deployed as fast as possible since valuable time has already been lost for the detection of the impact. Therefore stage III of the inflator is capable of filling the small cushion for the 5th-percentile female dummy rapidly, within around 35 milliseconds. This performance corresponds roughly to typical today's inflators. Analogously to the pre-crash activation, if the bigger airbag-shape for the 50th- and 95th-percentile male dummy is deployed, it is necessary to fire inflator stage II additionally.
One further aspect has to be taken into account: Stage I should be used for the OOP-tests of the US-regulatory requirements because the slow inflation promises significant improvements. Therefore it is necessary that the onset of the inflator is designed moderately.

In-Crash-Potential

As discussed before, the earlier coupling of the passenger to the chassis-movement due to an optimized airbag shape promises the biggest reduction of injury risk. A further advantage of quenching the passenger with the airbag instead of the seatbelt is that a big surface of the person is affected. The risk for fractures of the clavicle or abdominal injuries that can result from the high local loads of the seatbelt is reduced.
These two potential benefits of a pre-collision activated restraint system should be realized as well

as possible, when the scenarios mentioned beforehand were elaborated.
The job to adjust the hardware components properly for the three frontal load cases (US-NCAP, Euro NCAP and FMVSS208, unbelted) and the three dummy-sizes (5th-percentile female, 50th- and 95th-percentile male) at two completely different trigger-scenarios turned out to be very challenging. The parameters to be varied were:

1. diameter base vent
2. diameter active vent
3. timing active vent
4. performance of inflator stage I
5. performance of inflator stage II
6. performance of inflator stage III
7. timing inflator stage I
8. timing inflator stage II
9. timing inflator stage III

The high number of possible combinations made it necessary to apply a systematic variation of the influencing parameters. In this regard, the program modeFrontier was a useful tool for the preparation of the DOE-tables and for the illustration of the effect of the single influencing factors.
With the found set of parameters it cannot be claimed that the very best solution has been worked out. Therefore it would have been necessary to run many iteration loops, which have not been performed in this study. In this phase of the analysis, the goal was to elaborate a good working configuration as a basis for demonstrating the principal potential for a reduction of the injury risk.
In the following, the specific problems of the two trigger-scenarios and the results of the simulations are going to be discussed:

Simulation results: Backup-Scenario
Since the requirement has been set, that the injury risk in the backup-strategy must not be higher than it is in the series-vehicle, this scenario was the starting point for the development of the airbag system. The performances of the single stages of the inflator were the first hardware parameters, which were freezed. As mentioned earlier, stage III is designed to fill up the smaller airbag size (BagShape 2, ~90l) to operating pressure. Stage II provides the additionally required gas mass to fill up the bigger airbag size (BagShape 1, ~120l) sufficiently. Once the inflator was set, suitable vent-diameters were elaborated. The diameter of the base-vent is mainly driven by the heavy 95th-percentile male dummy in the unbelted FMVSS208 load case. Comparable restraint performance could also be achieved with bigger vents and corresponding increased inflator performance, but the goal was to get along with the lowest possible inflator power.

The diameter of the active vent is primarily set by the forward movement of the 5th-percentile female dummy in the US-NCAP-loading condition. All the other dummy-loading-combinations must be covered with an adapted timing of the single stages and the active vent.
The simulation results of the backup-scenario are presented on behalf of the 50th-percentile male dummy, beginning with the Euro NCAP loading condition:

The charts in Figure 8 give an overview of selected injury criteria comparing the conventional airbag deployment of the series vehicle and the results of the backup-scenario. It stands out, that especially the loads on the head are reduced significantly whereas the loads on chest and pelvis remain roughly unchanged.

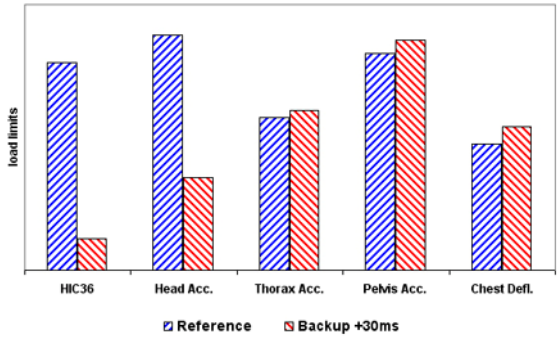

Figure 8: simulation results: 50th-percentile male dummy, Euro NCAP

In Figure 9 the timeline of the head-acceleration illustrates the tremendous reduction of the peak value to less than half of the reference. Due to the adapted airbag-shape, the head contacts the cushion earlier. Furthermore the resulting inflation-power of the two concurrently fired inflator stages II and III is significantly higher than the series-vehicle inflator. As a result, the cushion deploys faster, and imposes restraint loads onto the dummy earlier. Finally the properly adjusted trigger timing of the active vent allows the torso more forward movement, whereby the available space for deceleration can be exploited optimally. All these circumstances lead to the almost ideal rectangular form of the head acceleration.

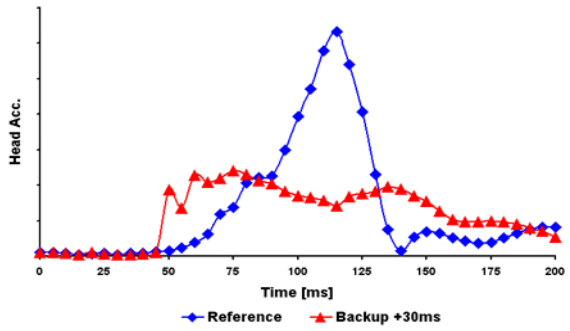

Figure 9: time line of the head acceleration of the 50th-percentile male dummy, Euro NCAP

In Figure 10 the time dependent characteristic of the thorax acceleration is shown. The slight peak at about 50 ms after t_0 results in the fast deploying airbag that contacts the dummy with a high relative velocity. This is a consequence of the compromise in the airbag geometry. It is designed closer towards the passenger in order to arise potential for reduced injury risk in a pre-crash activation. The peak value of the thorax acceleration and the time point, when it occurs is more or less equivalent to the series vehicle.

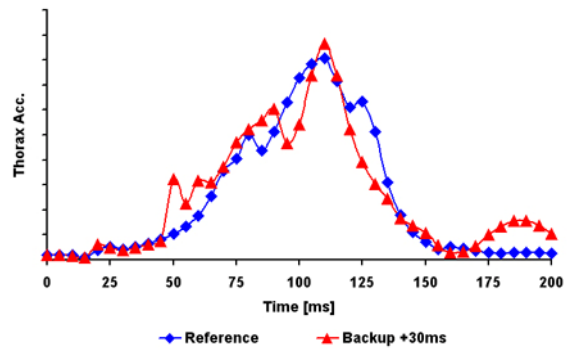

Figure 10: time line of the thorax acceleration of the 50th-percentile male dummy, Euro NCAP

The pelvis acceleration shows similar characteristics as shown in Figure 11. The review of the animation-files of the simulation pointed out, that the peak in the acceleration curves of thorax and pelvis at around 100ms after t_0 has two origins. Firstly at this time the torso penetrates the seat cushion at most which indicates high loads in the pelvis-z-direction. Secondly, the knees contact the dashboard, which leads to a high load in the pelvis-x-direction. As these two effects are mainly influenced by the lap belt, which has not been changed in comparison to the series vehicle, changes resulting from the new airbag system cannot be seen clearly.

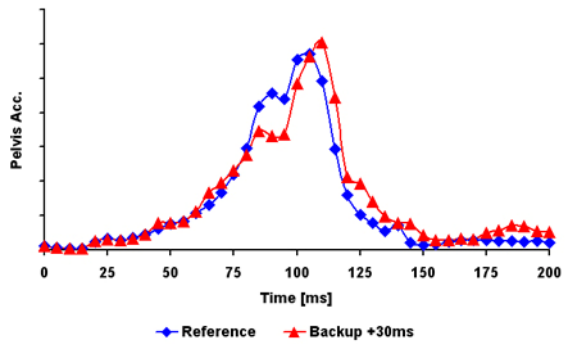

Figure 11: time line of the pelvis acceleration of the 50th-percentile male dummy, Euro NCAP

In Figure 12 the effect of the faster deploying airbag in the backup scenario on the chest deflection can be detected. Until about 50 ms after t_0, the pretensioned seatbelt in combination with the dummy inertia leads to a slightly increasing chest deflection. Due to the earlier contact with the harder airbag cushion, the chest deflection increases considerably with respect to the reference, whereby the peak value is about four millimeters higher.

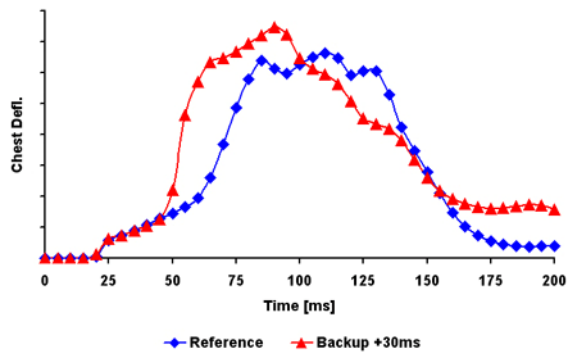

Figure 12: time line of the chest deflection of the 50th-percentile male dummy, Euro NCAP

The second scrutinized loading condition was the US-NCAP-rating crash test. Due to the configuration with the 100 percent overlap and the rigid barrier, this test is characterized by a significantly shorter duration and higher peak loads. Figure 13 illustrates the performance of the developed airbag system in the backup scenario. It can be seen, that the tendency is comparable to the Euro NCAP loading discussed beforehand. The risk for head injuries is reduced considerably whereas the loads onto thorax and pelvis remain more or less the same as in the series vehicle.

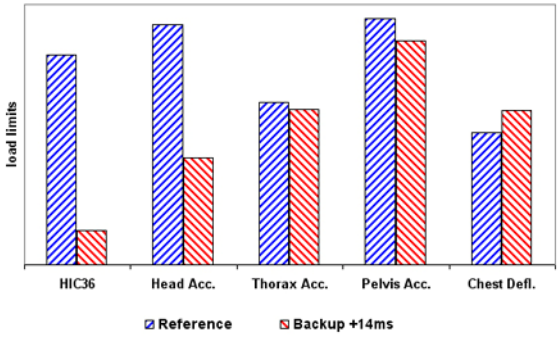

Figure 13: simulation results: 50th-percentile male dummy, US-NCAP

Finally the US regulatory test FMVSS208 was analyzed. Since in the United States today the use of seatbelts is still not obligatory in all states, the regulations prescribe a crash test without seatbelt. This test-configuration sets very specific demands onto the setup of the airbag-system.
Although the test-speed is remarkably slower than it was in the two previous discussed crash tests, the risk that the dummy punches through to the dashboard is very high. The missing seat belt facilitates a rotation of the dummy since the pelvis is not braced into the seat by the lap belt. As a result of this rotation the head of the dummy can approach the windscreen and the dashboard very closely. Due to this, especially the heavy 95th-percentile male dummy requires high inflator performance and small vents. Figure 14 gives an overview of simulation results of selected injury criteria:

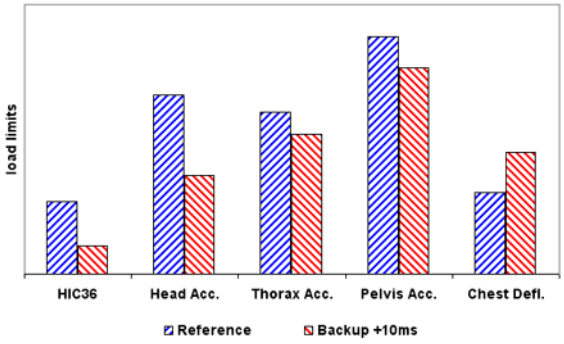

Figure 14: simulation results: 50th-percentile male dummy, FMVSS208 (unbelted)

Also in this case, the tendency is roughly the same whereas the chest deflection has increased considerably. The distance of the dummy head to the dashboard and the windscreen can be compared between the series vehicle and the developed backup-strategy.

Simulation results: PreCrash -Scenario

Most of the variables of the hardware package (performance of inflator stage II and III; vent diameters) have already been set in the backup-scenario. Only the performance of stage I can be adjusted to get an optimum in the pre-crash-scenario. In this context a specific problem of the slowly deploying airbag has to be taken into account. If the base-vent is open during the complete inflation time, a lot of gas is lost into the passenger compartment. This problem could be compensated by an increased capacity of the inflator, which has drawbacks referring to the size and weight of the airbag-module and the aggressiveness of the inflator. So it is reasonable to apply a vent that remains closed during the inflation and opens as soon as the airbag pressure increases due to the dummy contact. In order to provide sufficient restraint capacity for each combination of dummy and crash test-configuration, a proper set of trigger time points has to be found.
The simulation results of the precrash-scenario are going to be presented by means of the 5th-percentile female dummy. The tendencies of the results for the two male dummies are comparable, but due to its growing relevance in future regulations, the female dummy was selected. The first loading condition to analyze is the US-NCAP-Rating:
Figure 15 gives an overview of selected injury-criteria. It demonstrates that especially the load on the head is considerably reduced. Furthermore the chest-acceleration has decreased slightly whereas the peaks of chest-deflection and pelvis-acceleration have roughly remained unchanged.

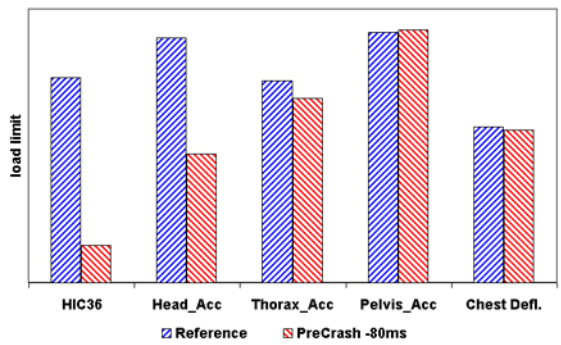

Figure 15: simulation results: 5th-percentile female dummy, US-NCAP

The time-dependent behavior of the head acceleration is shown in Figure 16. It can be seen, that the head contacts the cushion about 20 ms earlier than in the series vehicle. This leads to a rough bisection of the peak load on the head and to a tremendous reduction of the HIC-value.

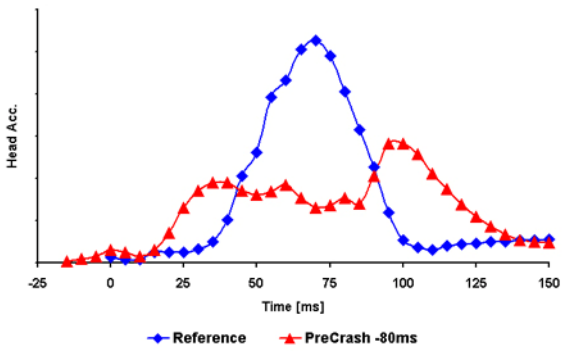

Figure 16: time line of the head acceleration of the 5th-percentile female dummy, US-NCAP

Figure 17 and Figure 18 display the loads on the thorax of the dummy. It has to be kept in mind, that the thorax is not only affected by the restraint loads of the airbag but also by those of the seatbelt.
The time line of the thorax acceleration shows, that in comparison to the head accelerations an earlier coupling of the chest to the airbag-cushion leads to reduced peak loads although the improvement is considerably smaller.

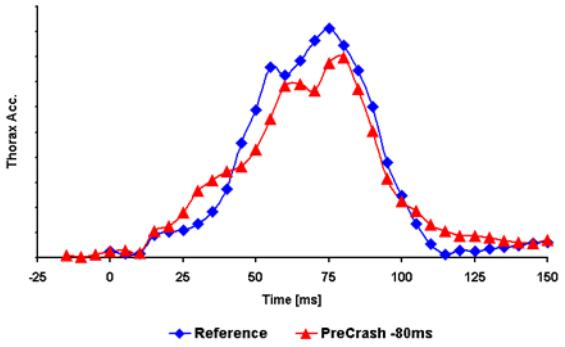

Figure 17: time line of the thorax acceleration of the 5th-percentile female dummy, US-NCAP

This effect unfortunately doesn't apply to the chest deflection. Although the cushion imposes loads onto the dummy at an early stage, the peak load equals to the conventional system.

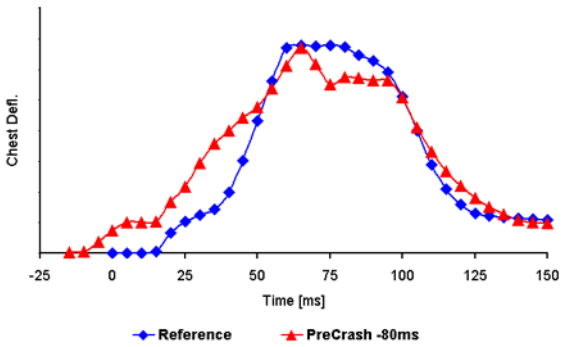

Figure 18: time line of the chest deflection of the 5th-percentile female dummy, US-NCAP

Unlike the head and the thorax, the pelvis is not braced by the airbag and so an earlier coupling cannot be seen. This effect could already be noticed in the backup-scenario.

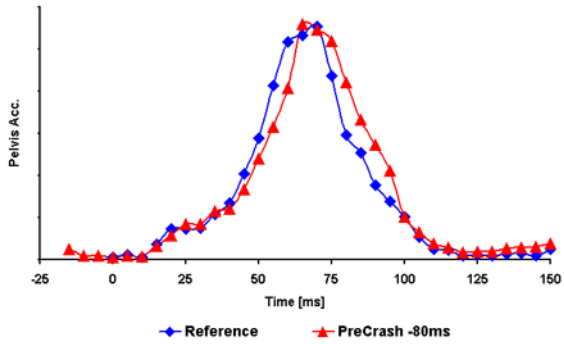

Figure 19: time line of the pelvis acceleration of the 5th-percentile female dummy, US-NCAP

In Figure 19 it can be detected, that an airbag that is activated 80 milliseconds before t_0 doesn't have influence on the pelvis loads. In order to reduce the loads on the pelvis, changes at the belt system have to be considered.

The second analyzed scenario is the Euro NCAP-frontal crash test: In comparison to the US-NCAP-rating, the Euro NCAP is performed with a deformable barrier and only 40 percent overlap. This leads to an about 50 percent longer impact-duration within which the occupant has to be restrained properly. This circumstance entails some problems in the timing adjustment. In order to evade, that the dummy punches through the airbag and contacts the dashboard, the active vent has to be opened very late. The drawback of this solution is that it leads to a more "triangular" shape of the acceleration curves, which is undesirable. Alternatively to the late opening of the active vent, the inflator can be triggered later. This variant has the effect, that the inflator still delivers gas, when the occupant is already moving forward and so the cushion is "harder" at an early stage of the impact. For the Euro NCAP loading condition it turned out to be advantageous to fire inflator stage I about 60 milliseconds before t_0. The simulation results for this configuration are illustrated in Figure 20:
It can be seen, that the tendency is similar to the above mentioned US-NCAP-loading. The risk for head injuries is reduced significantly, whereas the other injury criteria remain roughly unchanged.

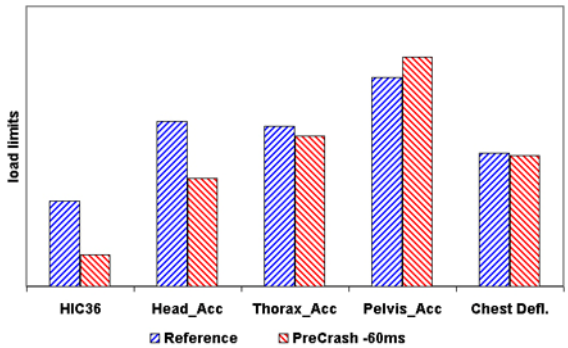

Figure 20: simulation results: 5th-percentile female dummy, Euro NCAP

The third investigated loading condition was the unbelted US legal test FMVSS208 with its specific requirements. Figure 21 shows the simulation results of the 5th-percentile female dummy.
It can be observed, that in comparison to the two belted load cases, the reduction of the thorax-acceleration is remarkably better. Since there is no seatbelt, this load case shows only the impact of the two different airbag-systems onto the thorax load. The other injury criteria show the same behavior as before.

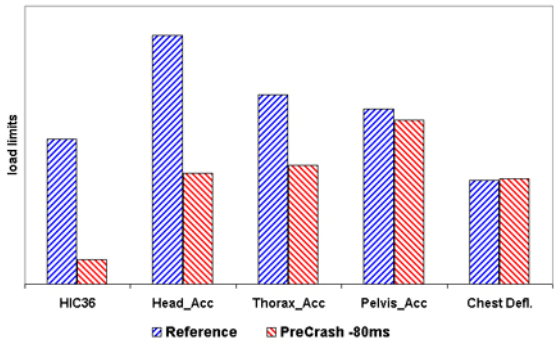

Figure 21: simulation results: 5th-percentile female dummy, FMVSS208 (unbelted)

During autumn 2009 the presented simulation results are going to be validated exemplarily by means of sled tests. Afterwards, another simulation loop is planned in order to improve the simulation model and increase its predictive capacity. After a further optimization loop, more impartial conclusions about the potential of pre-crash activated restraint systems can be drawn.

Test result: OOP-Potential

Since 2003 the US-regulation FMVSS208 has required the consideration of different OOP-situations in the development of the airbag system. It is up to the OEM whether the airbag is activated or not when a child is seated on the passenger seat, or in case it stands out of position. Another possibility is the so-called low risk deployment of the airbag whereby the inflator is fired with reduced power. Since the sensors for the detection of the position of the car occupant are still in development (e.g.: [6]), the low risk deployment is commonly applied nowadays. To reduce the loads on the dummy in these OOP-tests special cushion folding methods (e.g.: [7]) were developed and inflators were tuned to provide a gentle onset.
As mentioned earlier, another potential improvement of an airbag-system that is deployed significantly before t_0 is, to inflate the cushion more slowly and in this way with reduced aggressiveness. The problem is that this effect cannot be foreseen certainly, because the influence of the airbag-door in the dashboard on the deployment of the airbag is not clear. In the worst case, the slowly deploying cushion doesn't have the necessary initial "punch" to open the door. Then the airbag would possibly deploy within the dashboard. Another scenario is that the airbag-door doesn't open due to the initial "punch". It opens later as a result of the rapidly increasing bag-pressure and the airbag deploys with even more power. This circumstance can possibly lead to worse OOP-results. In order to clarify this issue, it needed to be analyzed.
The used simulation-model of the airbag is not suitable to predict characteristics of the deploying cushion (uniform pressure method). Furthermore the door in the dashboard is not represented in the model. So it was necessary to prove this effect by physical tests.
The US-Regulation FMVSS208 prescribes five different out-of-position tests for the passenger-side, using three different crash-test dummies. It contains tests with the 12-month-old CRABI child dummy seated in a child safety seat, the three and six year old Hybrid III dummies in two different positions.
For the evaluation of the reduced injury-risk due to a slowly deploying airbag, the three-year-old dummy was chosen, as it is the most critical case, which was known from former test results. For this dummy both prescribed positions were examined.
Position two (head on instrument panel) causes higher loads on the dummy, therefore this out-of-position test was the main focus of the series.

Figure 22: OOP position two, Head on IP

In order to demonstrate the potential for a reduced injury risk in OOP-situations the following testing-environment was chosen: The reference was the conventional airbag system of an existing road car. For the "slow" deployment, the inflator of the series-vehicle was substituted by a prototype inflator system with inflation times of 80 and 100 milliseconds. This inflator roughly matches the necessary characteristics of stage I of the earlier presented deployment strategy. The airbag-cushion itself remained the same for all tests.
Firstly two tests were performed with the conventional system to get a comparable reference. Afterwards for each configuration, two tests with an inflator capable for a precrash activation were carried out.
In Figure 23 the test-results of the legal injury criteria are displayed. It can be seen, that especially the neck-forces are reduced significantly. Looking at the 100ms inflation both the tension and the compression are halved in comparison to the conventional system. Although already on a very low level in the series vehicle, also the Head Injury Criterion (HIC15) and the cumulative 3ms acceleration of the thorax are reduced noticeably.

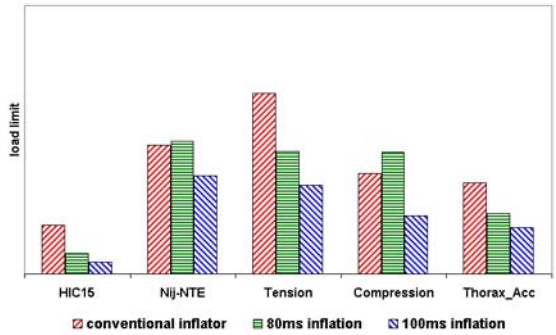

Figure 23: test results OOP Pos 2, Head on IP

The 80ms inflation was analyzed in order to get an insight into the tendency of the values, when the inflation duration is changed. The total exhausted gas mass of the inflator remains unchanged. The cushion is just filled up to the same extent within a shorter time. As expected the results are more or less between the conventional inflation and the very slow deployment during 100ms. It is conspicuous, that the neck compression force has its highest value at the 80ms inflation. After inspecting the high-speed-videos it turned out, that the prototype inflator has a higher onset than the conventional inflator. So, after opening the airbag-door the cushion hits the dummy head with a higher velocity, and as a consequence this results in a higher compression force. This compression force has its origins in the airbag deployment direction. The cushion opens the door, contacts the windscreen and then hits the dummy-head from above.
In order to get a proof-grounded conclusion about this topic, also tests with position one (chest on instrument panel) were performed. In this configuration, only reference-tests and tests with 100ms inflation-time were carried out.

Figure 24: OOP position one, Chest on IP

The results are comparable to position two. Figure 25 illustrates the test-results of the injury-criteria. As it turned out in position two, especially the highest values are reduced remarkably

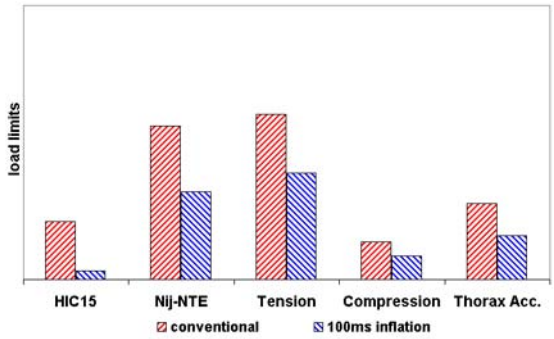

Figure 25: test results OOP Pos 1, Chest on IP

To sum up, even though the tested prototype inflator has not been "tuned" for OOP and it is

fitted into an existing airbag-module without further adaptations, the gentle deployment of the airbag-cushion results in a significant reduction of the dummy-loads.

DISCUSSION

When reflecting the simulation results it stands out, that the reduction of the risk for head injuries is comparable in both, the pre-crash activated and the conventionally triggered backup scenario.
The reason for this effect is that the improvements of the backup-scenario are a result of the considerably faster deploying airbag in comparison to the reference. This configuration is a lot more aggressive than the conventional inflator and would possibly fail to pass OOP-tests. So in the developed restraint system the described strategy can only be realized, because in low speed crashes (and consequently in the OOP-test-configuration) the gently deploying inflator stage I is fired.

The above described restraint system has been worked out, because it promised considerable improvements of the injury risk for all the passenger classes (weight and size). In the initial brainstorming, also other strategies with more anticipatory pre-crash-potential for the 50th- and 95th-percentile male dummy came up. But these variants were discarded, since the importance of these two dummy-sizes will diminish in the future. It can be observed in recent regulatory and rating tests that the 5th-percentile female dummy achieves higher weight. Since small and lightweight persons have a higher injury risk than big and heavy ones, it seems to be reasonable to determine further restraint-strategies with special focus onto this passenger class.

During the simulation it pointed out that the developed airbag-shape for the 50th- and 95th-percentile male dummy might have a drawback in terms of stability. The internal transversal tether leads to a relatively narrow cushion that might not work very well if the impact direction is not exactly frontal. In the worst case, in a slightly slant crash the passenger might push the cushion aside and punch through to the A-pillar.

Furthermore the simulation results have shown that the development of an airbag system is not possible without a close examination of the seatbelt. The loads on the thorax are a combination of the restraint forces of the airbag and the seatbelt. These two components need to be adapted properly to each other in order to achieve low injury risk. So in a following study also the seatbelt will be analyzed for potential in terms of activation prior to the impact. Then especially the pre-tensioning of the seatbelt will be subject to explore.

CONCLUSION

The activation of irreversible restraint systems significantly before the collision arises remarkable potential for the reduction of the injury risk of the frontal car occupant.
The extent of this potential depends strongly on the relevance of the backup since the setup of the airbag system is a compromise between the two different scenarios on the timeline. The lower the detection-rate and -certainty is, the more important remains the backup and as a consequence the more the compromise shifts to the conventional deployment.
This study presents the potential of a system where the backup still plays a very important role. The seatbelt was taken out of the series vehicle without any further adaptations. Nevertheless the simulation- and test-result demonstrated enormous improvements especially concerning the risk for head injuries and also significant reductions regarding the dummy loading in OOP-situations.
It has to be kept in mind that even more effect can be gained if the detection certainty rises because then the single hardware components can be optimized for the pre-activation in a larger scale. So there should be a big stimulation for further development of the sensor technology.

REFERENCES

[1] Thomas Scott, Hawthorn Laura, DUAL DEPTH PASSENGER AIRBAG, Paper No. 2005-01-1226, SAE World Congress 2005, Detroit, USA

[2] Paulitz Timothy J., Blackketter Donald M. Rink Karl K., FULLY-ADAPTIVE SEATBELTS FOR FRONTAL COLLISIONS, Paper No. 05-0127, ESV-Conference 2005, Washington DC, USA

[3] Wohlebe Thomas, Gonter Mark, Meinecke Marc-Michael, POTENTIAL OF PRE-CRASH RESTRAINTS IN FRONTAL COLLISIONS, Airbag2006 Conference, Karlsruhe, Germany

[4] Eichberger Arno, INTEGRIERTE FAHRZEUGSICHERHEIT, Script of lecture no. 333.052, summer term 2008, TU Graz

[5] Schoeneburg Rodolfo, Breitling Thomas, ENHANCEMENT OF ACTIVE & PASSIVE SAFETY BY FUTURE PRE-SAFE® SYSTEMS, Paper No. 05-0080, ESV-Conference 2005, Washington D.C., USA

[6] Freienstein Heiko, Engelberg Thomas, Bothe Hans Dieter, 3-D VIDEO SENSOR FOR DYNAMIC OUT-OF-POSITION SENSING, OCCUPANT CLASSIFICATION AND ADDITIONAL SENSOR FUNCTIONS, Paper No. 2005-01-1232, SAE World Congress 2005, Detroit, USA

[7] Mao Yiqin, Appel Hermann, INFLUENCE OF AIR BAG FOLDING PATTERN ON OOP-INJURY POTENTIAL, Paper No. 2001-01-0164, SAE World Congress 2001, Detroit, USA

[8] Schönekäs André, FRONTALAUFPRALL, Grazer Safety Update 2008 Conference, Graz, Austria

[9] v.a., SAFETY COMPANION 2009, carhs.training gmbh, Alzenau, Germany

CRASH TYPE DISTINCTION USING STRUCTURE-BORNE SOUND SENSING

Sebastian Brust
Dr. Mario Nagelstraßer
Willibald Watzka
BMW Group
Germany
Paper Number 09-0230

ABSTRACT

Current crash sensing systems are normally based on acceleration sensing. Therefore, the deceleration pulses affecting the car's body are used to apply the firing thresholds of the restraint systems. A new kind of crash sensing consists of measuring high frequent chassis vibration regarding frequencies up to 20 kHz: crash sensing based on structure-borne sound (SBS). The main benefit of this technology will be to support the common deceleration-based crash detection in crash type distinction during the early crash phase. To be able to use the acquired data in a physically reasonable way, the events causing SBS during crash important to know.

In the proceeding of the study, the events occurring during a crash are interpreted as shock excitations of different impulse lengths that can be divided into hard and soft events. Valuable results from a multitude of component crash tests on a drop tower test stand are transferred to vehicle crashes in serial development. The applicability of crash separation criteria is examined. The crash type distinction of hard/soft crashes based on structural vibration sensing is the main idea to support the differentiation of hard no fire tests and soft must fire tests. The study shows that shock excitation of the vehicle structure is the most important cause of high frequent vibration signals acquired during vehicle crashes.

The article deals with the usage of high frequent structural vibration in the range up to 20 kHz for crash detection. The understanding of the vehicle being a structure under linear elastic shock excitation leads to a physically plausible usage of the signals for crash type distinction.

INTRODUCTION

Today, architectures of current crash detection systems, used to activate passive safety restraint systems, are based on processing data of a multitude of sensors distributed in the vehicle. This is needed to fulfil the high and complex requirements of legislation, consumer and insurance organisations. For frontal collision detection, mainly acceleration sensors are used to process the deceleration of the vehicle's structure and its velocity reduction during the crash. Figure 1 shows a symbolic representation of a current sensor architecture consisting of acceleration sensors mounted at the vehicle's central position and at four satellite positions (one at each B-pillar and two at the front of the vehicle).

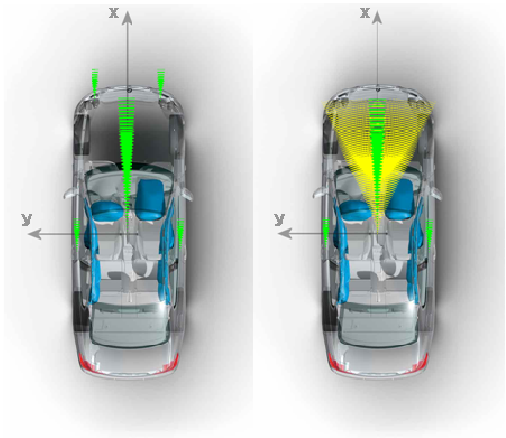

Figure 1. Sensor architectures for frontal collision detection showing symbolic representations with current (left) and reduced number of satellite sensors including an additional structure-borne sound sensor (right).

The performance of the frontal satellites strongly depends on their mounting position, which leads to a high effort during development [1]. Replacing them by a more innovative technology like SBS sensing at the central sensor position using a special sound sensor is preferable. On the right side of Figure 1, a possible sensor architecture is represented that only provides two satellite positions at the B-pillars and a single central position including both, current acceleration sensor and SBS sensor.

Separation of Hard and Soft Crash Types

Basically, the main task in crash detection is the distinction of must fire and no fire cases. While in must fire cases at least one restraint system (e.g. seat belt retractor or air bag) has to be activated, no restraint system must be activated during the whole crash for no fire cases. A particular challenge is the distinction of so called hard or soft crash types. The crash type is defined by the over all crash stiffness not only depending on the front end stiffness of the own vehicle, but also on the stiffness, position and

orientation of the barrier or the crash partner. The higher the crash stiffness, the harder the crash. Examples for hard crash tests are:

- AZT (**A**llianz **Z**entrum für **T**echnik) crash repair test: frontal offset crash with 40 % overlap against a rigid barrier, vehicle speed 15-16 kph, no fire [2]
- USNCAP (**US N**ew **C**ar **A**ssessment **P**rogram): frontal crash 100 % overlap against a rigid barrier, vehicle speed 56 kph, must fire [3]

Important examples for soft crash types are the ODB tests (**O**ffset **D**eformable **B**arrier):

- Euro NCAP (**Euro**pean **N**ew **C**ar **A**ssessment): frontal offset crash with 40 % overlap against a deformable barrier, vehicle speed 64 kph, must fire [4]
- FMVSS 208 (**F**ederal **M**otor **V**ehicle **S**afety **S**tandard): see Euro NCAP, but: vehicle speed 40 kph [5]

In the following, the ODB 40 kph will be treated as the typical representative of the soft crash type. As described below, the distinction between the ODB 40 kph and the AZT is very challenging.

During a hard impact, the velocity reduction begins early and proceeds relatively quickly. During a soft impact, even at high vehicle speed, the velocity reduction occurs much more delayed. In the TTF (TTF: **T**ime **T**o **F**ire < 30-40 ms) zone, the velocity reduction level for slow hard crash tests corresponds to the velocity reduction of much faster soft crash types. Based on this single criteria, the distinction of soft must fire tests (ODB) and hard no fire tests is not possible.
Figure 2 shows that a clear distinction based on the detected velocity reduction is not possible before 80th millisecond.
The additional information of SBS that can be measured in the central position allows a better recognition of the actual impact characteristics. Knowing the impact characteristic can be used to support the classical acceleration-based fire logic by using a hard-soft-classification. In addition to the vehicle's deceleration in x- and y-direction and dependent on the chosen algorithm concept, the crash type is an important factor for activating the restraint systems in the required time range. The following paragraph describes the data processing of SBS signals as it is implemented by sensor manufacturer to allow the usage of SBS in a crash detection algorithm.

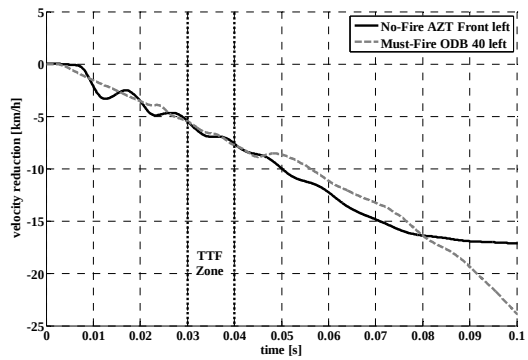

Figure 2. Velocity reduction for AZT and ODB, trigger: $t = 0 = t_0$.

STRUCTURE-BORNE SOUND – MEASUREMENT AND DATA ANALYSIS

SBS is defined as elastic waves in a frequency range between 16 Hz and 20 kHz, propagation in solid structures [6]. SBS signals are commonly measured using high frequency acceleration sensors. To avoid aliasing effects in the relevant frequency range up to 20 kHz, the sampling frequency must be chosen to have at least twice the highest interesting frequency [7]. Such a highly resolved raw signal, however, is not applicable for serial utilization because of the required bus loads and computational demands. Instead, a data reduction is processed so that the signals can be transferred using a standard sampling rate. Therefore, a band pass filter extracts the signal of the interesting frequency range. Based on this high frequent signal, the envelope is created by rectification followed by a final low pass filter procedure. The resulting signal can be sampled at a lower rate depending on the chosen low pass frequency while the content of the relevant information is preserved. The integrative characteristic of the envelope processed on a frequency band is similar to the generation of a windowed RMS (**R**oot **M**ean **S**quare) value. Although the envelope basically can be realized using analogue electric components, digital signal processing of high resolution reference sensors is highly recommended using sampling frequencies of at least 40 kHz. The transferability between the reference signals and the occurring signals of a series production sensor in a central position must be guaranteed. Here, a detailed knowledge of the properties of serial and reference sensors is very important. In addition, the transfer path between these both sensors must not change, especially not during a crash. In this regard, SBS sensing is very sensitive to variation. In the field of low frequency acceleration sensing, individual transfer functions are determined to map both, the reference signals and the series production sensor signals for the application of the crash detection algorithms. The algorithm development can therefore be realized

using only reference signals. Signals of sensors for serial production are only considered in the final development of the vehicle to confirm the system's performance. This demand also applies on SBS sensing. The satisfiability of this demand, however, highly depends on the position, integration and sensor type of the reference sensors. An important aspect for being capable to use SBS signals in a reasonable way is to understand the effects that cause SBS emission. The processes that lead to a SBS emission during a vehicle crash are described in the following.

Structure-Borne Sound Excitation in Case of a Vehicle Crash

Earlier works on material research describe sound emission during plastic deformation of metallic structures. The sound emission is caused by various effects like dislocation movement within the crystal lattice and is usually observed in the ultrasonic frequency range (>20 kHz) [1], [8]. Beside the continuous sound emission in case of plastic deformation of metal, the impact characteristic of a crash has been identified as important factor in the frequency range up to 20 kHz. The impact characteristic is mainly defined by the shock excitation of the vehicle structure. The excited spectral distribution depends on the shock duration and the pulse shape. A long soft impact produces a spectral response in a lower frequency range. Short hard impacts additionally generate a higher amount of high frequency content [7], [9].
Figure 3 schematically shows two impact forces of different stiffness. The impulse area *A* is equivalent to the integrated impact force and is identical for both shocks. Only the duration of the impulse τ separates both shocks in hard with $\tau = \tau_1$ and soft with $\tau = \tau_2$.

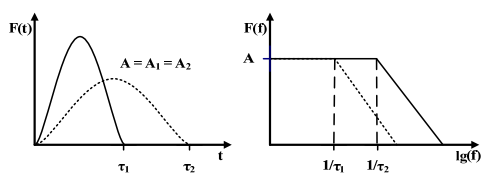

Figure 3. Shock impulses over time (left) and corresponding spectral distribution (right) according to [9].

This corresponds to an experiment in which, for example, a ball drops from a constant height on two surfaces of different hardness. The measured signal is the force applied from the ball onto the surface. Each of both impulses of equivalent area generates a force spectrum that can be estimated by the method described in [9]. There, it is explained that amplitudes are constant for low frequency domains when varying the impulse duration, but for high frequencies, they decrease in the majority of practical cases with -40 dB/frequency decade beginning at a critical frequency defined by:

$$f_{s,i} = 1/\tau_i \qquad (1).$$

This characteristic spectral distribution does not vary in case of identical stiffness conditions but different impulse height since the impulse duration is not influenced. Here, only the spectral amplitude rises. The shock impulse excites all resonance frequencies of the structure inside the spectrum. The general relation between time and frequency domain is described by the Fourier integral:

$$F(t) = \frac{1}{2\pi}\int_{-\infty}^{\infty} \check{F}(\omega) e^{j\omega t} d\omega ;$$

$$\check{F}(\omega) = \int_{-\infty}^{\infty} F(t) e^{-j\omega t} dt \qquad (2).$$

In case of a vehicle crash the characteristic of the shock impulse is indeed very complex. The example mentioned above describes the ideal case of an elastic shock. During a crash, instead, plastic deformation usually occurs which principally has a spreading influence on the impulse shape. But it can be shown that there still remain shock excitations exciting the structure of the vehicle.
To analyze these excitation processes under a high amount of reproducibility, the SBS generation is observed in component crash tests on a drop tower test stand. The crash proceedings can be isolated and observed in detail thanks to a strongly reduced complexity of the used structure. Only crash-relevant body components that are important for the impact excitation in the early crash phase are used: the bumper cross member with its deformation elements (crash boxes) and the frontal part of the longitudinal beam (Figure 4).

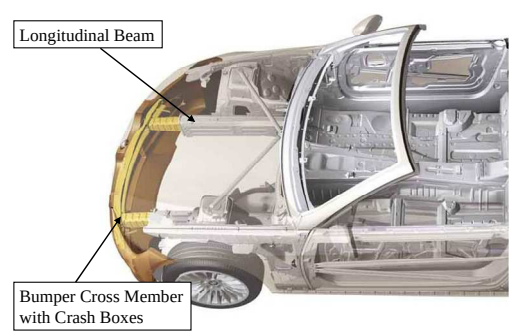

Figure 4. Frontal structure of a BMW 3 Series Convertible.

The tests are realized in AZT configuration with the structural components mounted vertically on the floor. The impact is generated by a rigid metallic barrier falling onto the structure with a partial overlap of 40 %. Two barrier types are considered for these tests: the older barrier with an angle of 0° as well as the newer testing configuration [2] using a barrier with an angle of 10°.

The impact velocity is varied to evaluate the velocity influence, too. The following representation of the test results consists of the analysis of two different serial bumper systems. They mainly differ in the junction between the different parts of the bumper cross member as well as the junction to the longitudinal beam (Figure 5).

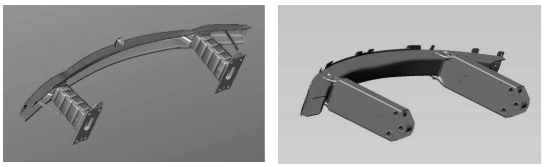

Figure 5. Different bumper systems with a welded cross member and longitudinal screw connection (left) and lateral screw connections within the cross member and longitudinal beam (right).

The left structure is characterized by the solid welded connection between the cross member and the crash boxes and the screw connection between the crash box and the longitudinal beam. These two solid and force-transferring connections lead to a high degree of reproducibility which is especially needed for SBS generation analysis.
In case of the right structure instead, the lateral screw connections cause influences in the SBS excitation due to a clearance passage within the screw joint. Such clearance passages induce glitches that have a strong influence on the variance of the measured signals. The clearance cannot be eliminated completely in the vehicle mounting. Therefore, the influence of a clearance passage is examined as well at the drop tower test bench.

Results

An acceleration sensor mounted on the dropping mass delivers data of the deceleration that is applied on the mass during the crash. The measured deceleration is proportional to the force integrated over the contact area of both structures. A small sampling rate does not allow the exact spectral analysis according to equation (2). but a qualitative analysis of the deceleration progress gives valuable insights on the deformation processes of the early crash phase. Two main deformation phases can be identified using the test configuration with 0° barrier angle. Both deformation phases, as described later, are each linked to an initial shock event. The first contact of the barrier causes a bending of the cross member which already dissipates a certain amount of energy. The force applied on the section of the crash box still is small. The duration of this phase is only a few milliseconds. The following compression of the crash box leads to a significant rise of the deceleration.
Because of its inclination, the 10° barrier touches down to the crash box much more directly which leads to a lack of the initial bending of the cross member. The deceleration of the mass increases more quickly.
Figure 6 shows the deceleration of the drop tower barrier for AZT configurations with barrier angles of 0° and 10°. The representation of the three measurements performed allows a statement about the variance of the test. All curves are very close to each other and only in the later proceeding of the test they differ lightly. The reproducibility of both, the test and the deformation process of the welded structure, is very high. All following explanations are referring to the black mean signal.
At the beginning, the abrupt rise of the mass deceleration is obvious for the 10° barrier. The decrease towards local minima represents the folding process, the deformation of the crash box. In the bottom figure the two deformation phases of the 0° barrier test can be identified. A shock precedes both deformation processes and leads to a short impulse excitation of the structure. Although the deceleration signals of the drop tower mass are strongly low pass filtered these impulses can be recognized in the measurement as short deviations of the curve's shape. These passages are mainly responsible for the SBS excitation and are marked with arrows in the figure below.

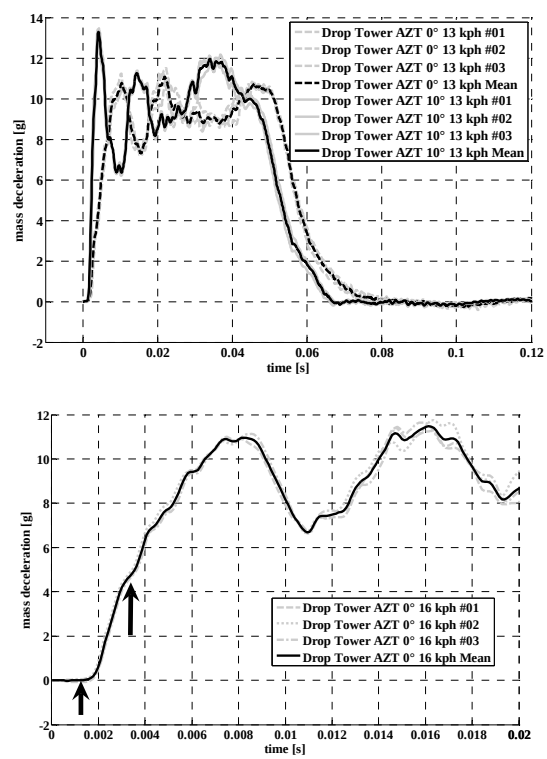

Figure 6. Measured deceleration of the barrier for 0° and 10° AZT drop tower test at 13 kph (above), 0° AZT drop tower test at 16 kph zoom 0-20 ms (below).

Because of their broad-band spectral characteristics, these shocks act as emission source for high

frequency SBS in the domain up to 20 kHz. Figure 7 shows the corresponding SBS envelope together with the view of the deformation of the bumper structure of three 16 kph 0° barrier tests. The variance of the measurements is shown by the illustration of three tests of the same configuration with their mean signal. The existing time offset of 1-2 ms compared to the mass deceleration is due to minimal asynchronies in trigger time stamps of both measurements. The SBS signal was measured on the longitudinal beam in a distance of 100 mm away from the flange. In comparison with the deceleration signal, the importance of shock excitation to the generation of SBS signals becomes obvious. At the 2nd millisecond, the initial contact between the barrier and the cross member has generated the first SBS peak. The following bending of the cross member does not affect the generation of additional SBS. The envelope amplitude slightly decreases. When the crash box is hit by the barrier (about 5th millisecond) the major part of SBS is measured (see central view in Figure 7).

The beginning folding process is generally accompanied by decreasing SBS amplitudes even though the force deviation causes further SBS excitation. The shift between longitudinal pressure load and the buckling of the crash box generates new impulses. But the isolated analysis of these secondary processes is hardly feasible. In the proceeding of the deformation, different excitation processes superpose, single events are difficult to separate.

A detailed analysis of the processes generating SBS requires a high degree of reproducibility. This is the case for the examples just mentioned before. Unlike, connection joints presenting a possible clearance passage have a much higher influence on the SBS generation than the shock excitation during the deformation of the crash box mentioned before. Clearance passages represent very short shocks that generate a high amount of high frequent SBS. The reproducibility of the SBS measurements is massively decreased compared to clearance-free structure parts. Lateral connections, like the screw connection in Figure 5 on the right are defined as connections having their axis orientated perpendicularly to the longitudinal axis of the vehicle. Here, the friction force affected within the connection is overcome very quickly, even at very low collision speeds. The parts slip through the connection which is followed by a very strong shock that is affected directly to the vehicle's body via the longitudinal beam. The procedure can generate a multitude of SBS signal produced by the deformation of clearance-free parts (Figure 8).

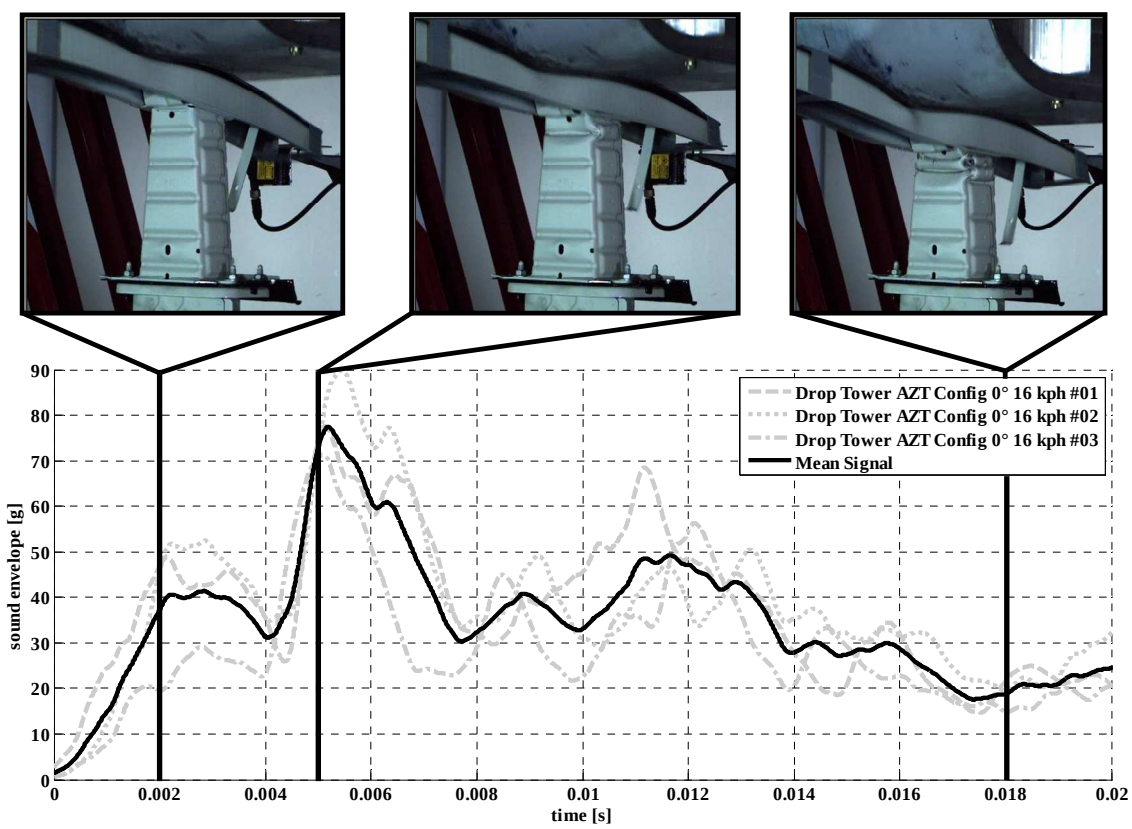

Figure 7. View of the deformation with measured SBS signal for three equal tests (black solid line corresponds to the mean signal).

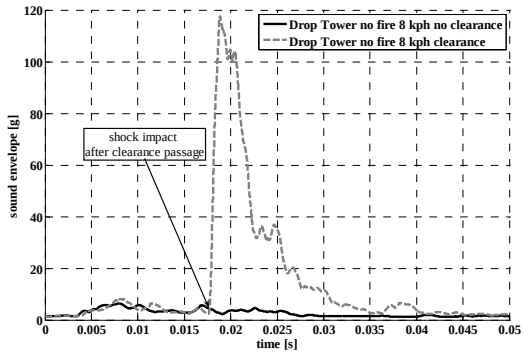

Figure 8. SBS signal measured at the longitudinal beam in a low speed drop tower test with (dotted line) and without clearance passage (solid line).

Such deviations in signal amplitude reaching an order of magnitude of much more than 500 % cannot be processed reasonably in a crash detection algorithm. Tests with clearance-free connections of the structural parts have shown that SBS envelope amplitudes in peaks can vary about ±50 % of the mean signal. Clearance-free connections like welding and longitudinal screw connections are recommended in order to avoid too high signal deviations. The resultant consequences of clearance passing for crash detection systems cannot be fixed at this point. But most algorithm concepts will not be able to handle such signal deviations.
In the following paragraph, it is described how the physical principle behind the SBS generation by shock excitation can be used in a crash detection system and what the restrictions are to be aware of.

Resulting Consequences on the Crash Detection Algorithm

For the classical acceleration-based crash detection, the influence of clearance passages is not proven yet. It was shown that clearance passage, dependent on the constructive realization of the bumper systems, will lead to a highly increased signal variation. Crash detection criteria purely based on amplitude processing of high frequent SBS signals cannot necessarily be used to discriminate must fire and no fire crash cases. The AZT, defined as hard no fire, produces high SBS amplitudes and then, can reach magnitudes of must fire crash tests. High ODB signals with coexistent low AZT signals could not be observed. In Figure 9, the measurements of three typical frontal crash tests are shown for a small vehicle having welded connections between the cross member and the crash boxes as well as clearance-free longitudinal screw connections between the crash boxes and the longitudinal beam.

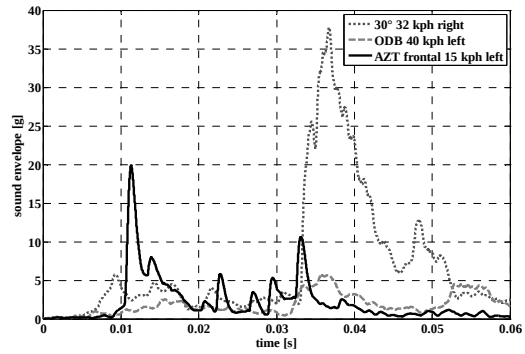

Figure 9. SBS signal examples of typical crash tests, measured in the central position.

The chosen examples are very important for the crash type separation:

- AZT representing the hard no fire test
- ODB 40 kph and an angular test (30°, 32 kph) representing the soft must fire tests in the early crash phase ($t < 30$ ms)

The crash stiffness of the ODB is mainly characterized by the energy dissipation of the deformable barrier. The barrier prevents the occurrence of shock impulses by its own deformation. The generation of great magnitudes of SBS signal is not possible.
In the case of the 30° angular crash, the resulting crash stiffness is reduced in the early crash phase due to the inclined force input. On the other hand, body parts, e.g. mud guard wings, soften the impulse by their deformation. Further more, a much more important fact is that the force input is not orientated directly in direction of the longitudinal beam. The resulting bending of the structural components in the first 30 ms generates relatively low SBS signals even if the barrier is not deformable. The high SBS amplitudes of the AZT are very interesting since they are remarkably higher than the must fire signals in the relevant time range of 30 ms.
This fact can be used to separate AZT from ODB by a hard/soft distinction criterion. This offers the possibility to separate soft must fire crashes and hard no fire tests at an early point. In combination with the classical acceleration-based crash detection, the hard/soft distinction can help to fulfil current and future requirements on passive restraint systems. A first algorithm concept can be described as a simple regulation of the fire threshold $f_{\Delta v}$ giving the *fire* decision. This threshold still is processed on the velocity reduction Δv measured by the classical acceleration-based crash sensors. On the one hand, $f_{\Delta v}$ is increased when hard impacts are registered. This means that hard impacts require an increased velocity reduction in the same time period. On the other hand, $f_{\Delta v}$ is decreased for soft

impacts to become more sensitive for soft must fire decisions. The following expression describes the relations in a simple generic and abstracted way:

$$fire = \begin{cases} 1 \text{ if } \Delta v \geq f_{\Delta v} \cdot h \\ 0 \text{ else} \end{cases}$$

with:

$$h = \begin{cases} = 1 \text{ if no information} \\ > 1 \text{ if hard positive} \\ < 1 \text{ if soft positive} \end{cases} \qquad (3).$$

CONCLUSION

Structure-Borne Sound (SBS) sensing in the field of crash detection mainly applies on a crash type distinction of hard and soft crash scenarios. Therefore, the shock waves that are generated during the crash and travelling through the vehicle structure are very important. The vehicle's resonant frequencies are excited by short impulses that depend on the stiffness of the crash. To be capable to use the SBS signals the relations that lead to SBS excitation are essential to know. In addition to sound emission in the ultrasonic range due to plastic deformation of metallic structures, highly dynamic impact shocks produce a great amount of SBS in the frequency domain up to 20 kHz.
Hard impulses (e.g. AZT) generate high frequencies while soft impacts (e.g. ODB) usually don't in the early crash phase.
Clearance passage and the following disturbing impulse increase the signal variance significantly and must be avoided for not provoking false decisions in the crash detection logic.

REFERENCES

[1] Brandmeier, T., Lauerer, C., Spannaus, P., Feser M.: Crasherkennung durch Körperschallmessung. In: *Sensoren im Automobil* (2006). S. 187-203

[2] http://www.rcar.org/papers/rcar_test-_protocol_angled_barrier.pdf, 13.03.2009.

[3] http://www.safecarguide.com/exp/-usncap/idx.htm, 13.03.2009

[4] http://www.euroncap.com/tests/-frontimpact.aspx, 13.03.2009.

[5] http://www.iihs.org/ratings/frontal-_test_info.html, 13.03.2009

[6] Cremer, L., Heckel, M.: *Körperschall – Physikalische Grundlagen und technische Anwendungen*. Berlin, Heidelberg, New York: Springer, 1982.

[7] Natke, Hans, G.: *Einführung in Theorie und Praxis der Zeitreihen- und Modalanalyse: Identifikation schwingungsfähiger elastomechanischer Systeme*. 3., rev. edition – Braunschweig; Wiesbaden: Vieweg, 1992.

[8] Teßmar, H.: Untersuchung der kontinuierlichen Schallemission bei der plastischen Deformation von ausgesuchten Stählen. Dissertation Otto von Guericke University Magdeburg. 1984

[9] Storm, Rainer; Kompendium Maschinenakustik : Studienskript. University of Darmstadt; 2007

ASSESSMENT OF INJURY SEVERITY OF NEARSIDE OCCUPANTS IN POLE IMPACTS TO SIDE OF PASSENGER CARS IN EUROPEAN TRAFFIC ACCIDENTS – ANALYSIS OF GERMAN AND UK IN-DEPTH DATA

Dietmar Otte
Medical University Hanover
Germany
Raimondo Sferco
Roland Schäfer
Volker Eis
Ford Motor Company
Germany
Pete Thomas
Ruth Welsh
Loughborough University
United Kingdom
Paper Number 09-0243

ABSTRACT

The national accident statistics demonstrate that the situation of passenger car side impacts is dominated by car to car accidents. Car side to pole impacts are relatively infrequent events. However the importance of car side to pole impacts is significantly increasing with fatal and seriously injured occupants.
For the present study the German in-depth database GIDAS (German In-Depth-Accident Study) and the UK database CCIS (Co-operative Crash Injury Study) were used. Two approaches were undertaken to better understand the scenario of car to pole impacts. The first part is a statistical analysis of passenger car side to pole impacts to describe the characteristics and their importance relevant to other types of impact and to get further knowledge about the main factors influencing the accident outcome. The second part contains a case by case review on passenger cars first registered 1998 onwards to further investigate this type of impact including regression analysis to assess the relationship between injury severity and pole impact relevant factors.

1. DATABASES

National accident statistics are not detailed enough to get information on the characteristics of impact types therefore two in-depth databases were used, the German In-Depth Accident Study (GIDAS, Germany) and the Co-operative Crash Injury Study (CCIS, UK).

GIDAS

GIDAS (German In-Depth Accident Study) is a joint project of the Federal Highway Research Institute (BASt) Germany and the German Association for Research in Automobile Technology (FAT). It started in 1999 in the two research areas Dresden and Hanover based on the established research activities of the Medical University Hannover (Otte, 1990). About 2,000 accidents involving all kinds of traffic participants are recorded each year in a statistical random procedure resulting in a representative sample of the national German accident statistic (Pfeiffer, 2006). The teams consisting of technical and medical students investigate the data at the accident scene and the hospitals. Each case is encoded in the database with about 3,000 variables. The database contains detailed information about: environment (meteorological influences, street condition, traffic control), vehicle (deformations, technical characteristics, safety measures), person (first aid measures, therapy, rehabilitation) and injury (severity, description, causation). On the basis of full-scaled sketches of the accident scene and the vehicle deformations every accident is reconstructed.

CCIS

The objective of CCIS (Co-operative Crash Injury Study) is to investigate and correlate car crash data, with a view to increase the understanding of human injury mechanisms, and the effectiveness of car secondary safety systems. The study provides the mechanism to monitor in-depth crash performance of car structures, occupant protection systems and the benefits of countermeasures now becoming available. CCIS is a collaborative project. The UK Department for Transport, several motor vehicle manufacturers and a vehicle component supplier jointly fund the programme of research. Currently, information on approximately 1300 vehicles is gathered each year for inclusion into the database. It is possible to weight the CCIS data in order to address the sampling bias towards serious injury; however this study uses unweighted data. Data col-

lection consist of sampling criteria, i.e. passenger cars 7 years old or younger at the time of accident, injury occurred to an occupant in the car and the vehicle was towed from the accident scene.
In detail the following basic query criteria/parameter were examined for the present study:

Basic inquiries applied to GIDAS 07/2007 and CCIS 2007 (combined phase 6y, 7o and 8c)
Passenger cars
o Impacts to vulnerable road users were excluded from GIDAS (not necessary in CCIS dataset) o All vehicles 1998 onwards which had only one impact to the side (single side impacts) o Cars with rollover before or after the side impact where excluded.
Pole impacts
o Cars with single impact to pole (tree, lamp post, traffic light post…) o Resulting injury severity and individual injuries for belted occupants only

2. INTRODUCTION

The national accident statistics demonstrate that the situation of passenger car side impacts is dominated by car to car accidents. Car side to pole impacts are relatively infrequent events. However the importance of car side to pole impacts is significantly increasing with fatal and seriously injured occupants.
Pole impacts, especially lateral, comprise one of the most aggressive impact environments for automobile structures. Due to the close proximity of occupants to the side structure, these pole impacts represent a more severe crash exposure than comparable impacts to other structures for instance to the front of a car (Varat et al 1999). Especially if the pole impact is directly to the compartment area the risk to receive severe injuries is high. A study of Zaouk et al (2001) postulated by using NASS and FARS data for 1988 to 1997 with respect to side impacts, that direct impacts of narrow objects with the occupant compartment have a high portion of MAIS3+injuries.
A considerable step in the improvement of side impact protection for passenger cars has already been done. With additional and improved structures in the doors and/or pillars of a vehicle and with the industry wide introduction of various types of side airbags, occupant protection has reached a high level.
The regulatory frameworks for these developments are the FMVSS 214 (Kahane, 1999) on the US side and the ECE 95 (Economic Commission for Europe) in Europe. In addition consumer testing by US-NCAP and EU-NCAP established also side impact testing protocols not only for the car-to-car side impact but also for pole impacts. The latter are the focus for the current study, which was part of the work of the European Enhanced Vehicle Safety (EEVC) working group 21 (Accident Studies) for the EEVC WG13 (Side Impact) to develop recommendations for future regulatory side impact test procedures. The working group 21 was founded for compiling experiences and scientific results from existing in-depth-investigations of European research teams supporting the different activities of EEVC.

Two approaches were undertaken within this study to better understand the characteristics of car to pole impacts. The first part is a statistical analysis of pole impacts to describe the characteristics and their importance relevant to other types of impact and to get further knowledge about the main factors influencing the accident outcome. The second part contains a case by case review on cars registered 1998 onwards only, to further investigate car side to pole impacts focussing on factors that influence the injury severity and finding injury mechanisms of struck side occupants.

3. STATISTICAL ANALYSIS OF SIDE TO POLE IMPACTS

3.1. Relevance of Side to pole impacts

Beside the frontal impact the side impact is the most common impact type. In GIDAS 16% of the passenger cars have single side impacts in CCIS 18.4% (fig. 1). The passenger car side impacts are dominated by car-to-car impacts. Car side to pole impacts are relatively infrequent events with a share of less than 2% in both databases.

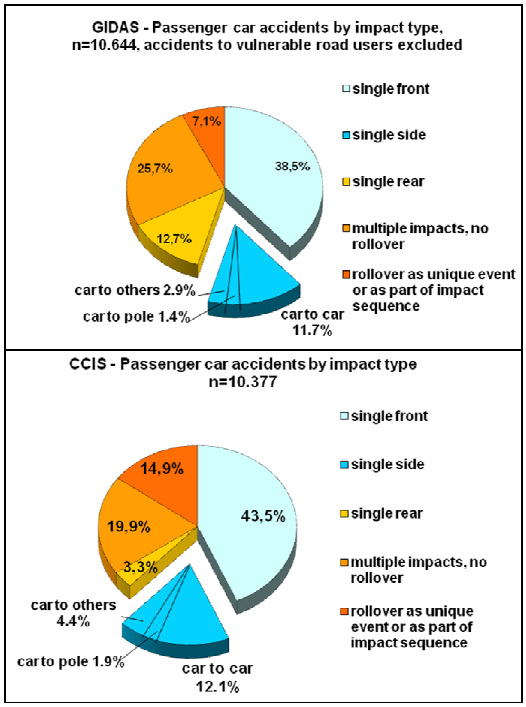

Figure 1: Passenger Car Accidents by Impact Type

However the importance of car side to pole impacts is significantly increasing with fatal and seriously injured occupants. Single side to pole impacts have the highest proportion of MAIS3+ injured occupants compared to the other accident types (fig. 2). The obvious difference in the injury severity distribution between GIDAS and CCIS with a higher share of MAIS3+ injured occupants is caused by the difference in sample criteria of the studies.

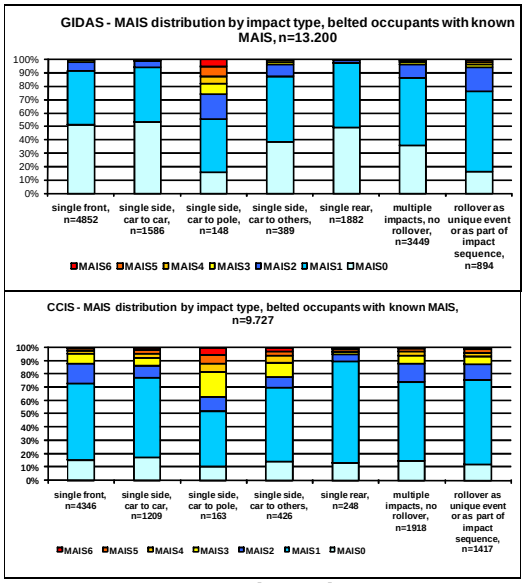

Figure 2: MAIS Distribution by Impact Type, Belted Occupants only

3.2 Effect of ESC on the Occurrence of Car Side to Pole Impacts

To further demonstrate the effectiveness of ESC in reducing car to pole impacts GIDAS data were analysed.
1.5%/2.8% of the cars (in GIDAS) without ESC have single side/front to pole impacts, for cars with ESC these shares are with 0.6%/1.5% less than half. The share of accidents with rollover is halved as well from 7.5% to 3.8%.

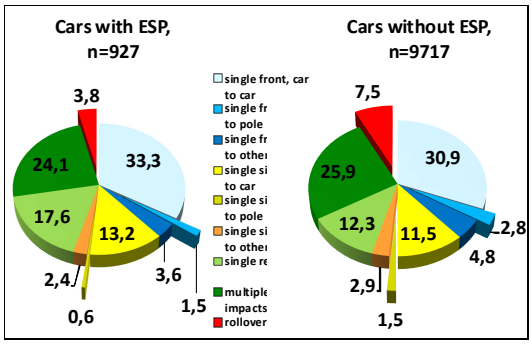

Figure 3: Passenger Car Accidents by Impact Type with and without ESC; accidents to vulnerable road users are excluded (GIDAS)

Especially the share of accidents with rollover and pole impacts is definitely lower for cars equipped with ESC compared to cars without ESC. This would indicate for an effectiveness rate of 40 to 54% for ESC equipped cars against pole impact risk.

3.3 Characteristics of the Impact

Delta v and Impact Speed

To differentiate the impact severity relative to the injury severity the delta v was analysed on the occupant level. In GIDAS 50% of the occupants in single side to pole impacts receive a delta v less than 35 km/h, in CCIS this 50% rate is reached at 29 km/h (fig. 4). This difference is even more remarkable because in contrast the share of MAIS3+ injured occupants in single side to pole impacts is in CCIS with 37.5% clearly higher than in GIDAS 26.4%.

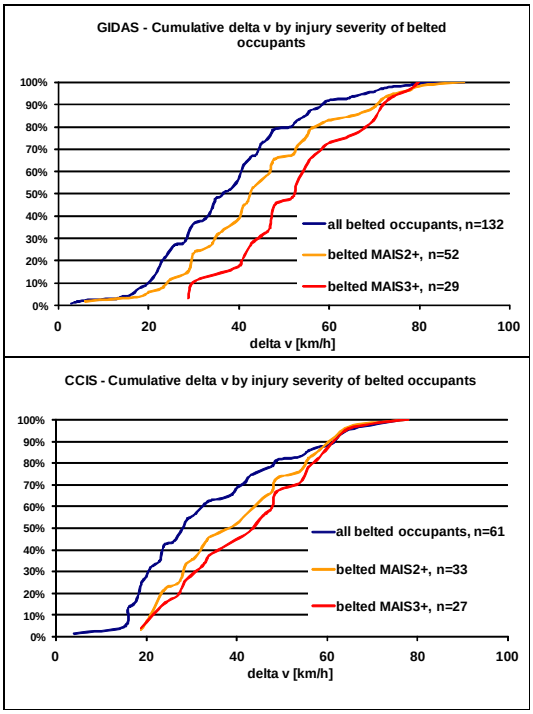

Figure 4: Cumulative Delta v Distribution for Different MAIS Classes in Pole Impacts, Belted Occupants only

The GIDAS database provides also the possibility to analyse the impact speed of the passenger car, due to the full reconstruction of the accident. 50% of all occupants had a side to pole impact with an impact speed below 46 km/h (fig. 5).

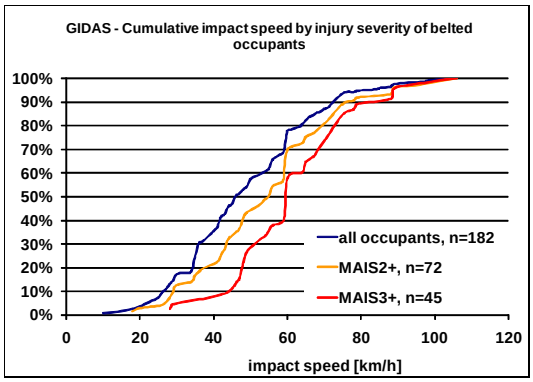

Figure 5: Cumulative impact speed distribution by MAIS classes in single side to pole impacts, belted occupants only

Impact Force Angle

The CDC direction of principle force with its clock-face differentiation of directions was used to analyse the impact force angle. The most frequent direction of impact force with 40% is perpendicular or 90° ± 15° (3 and 9 o'clock) in both databases (fig. 6), with the majority of impacts to the drivers side (left in GIDAS and right in CCIS).

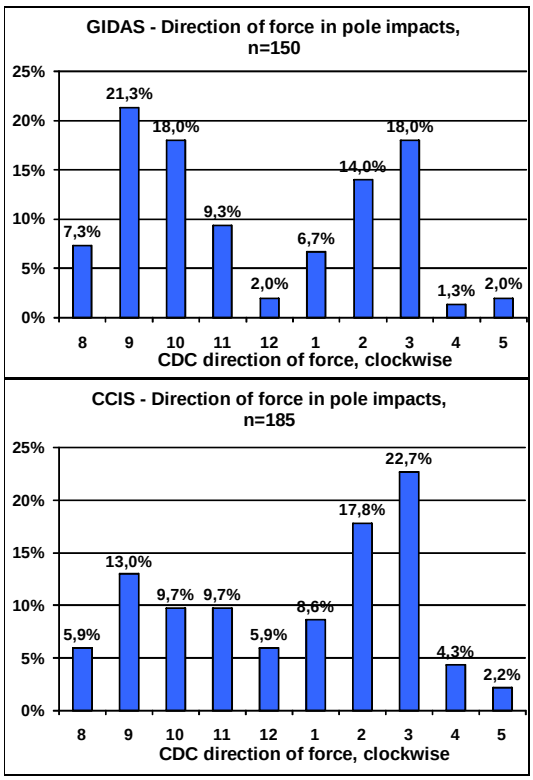

Figure 6: CDC Direction of Force in Single Side to Pole Impacts

The majority of the MAIS3+ injured occupants have also been found in perpendicular ± 15° impacts biased to the driver's side (fig. 7).

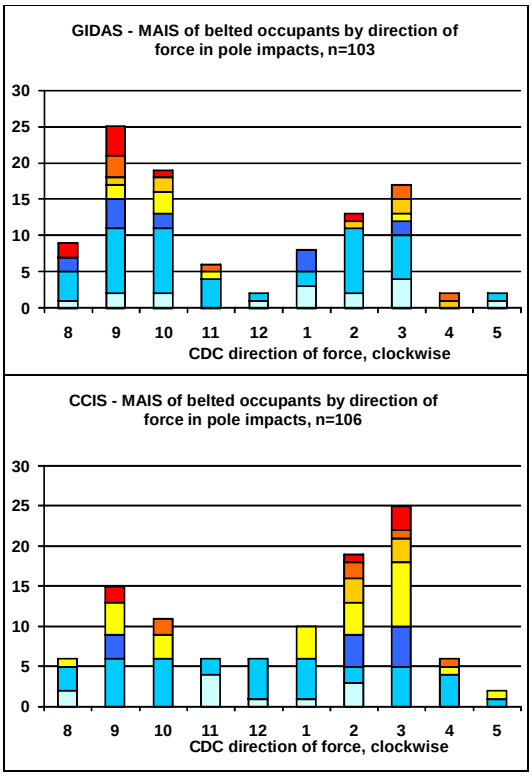

Figure 7 MAIS Distribution by Direction of Force, Belted Occupants only

Damage Area

The by far highest proportion (50%) of all pole impacted passenger cars show damage exclusively in the passenger compartment (fig. 8). Pole impacts affecting the area in front of the A-pillar occur second most (around 20%), impacts behind the C-pillar occur rarely (around 3%).
Severe and especially fatal injuries only occur when the passenger compartment is affected (fig. 9).

GIDAS
CCIS

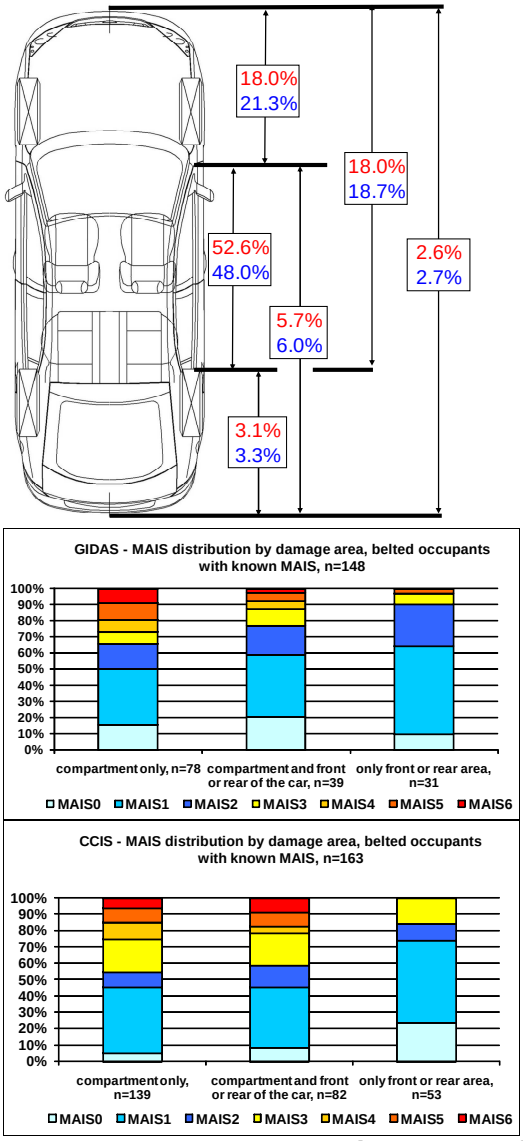

Figure 8 Damage Area in Pole Impacts and MAIS distribution by damage area

Crash weight of the car

In the GIDAS data there seems to be a correlation between MAIS and crash weight of the car, but the numbers of cars in the individual weight groups are very small. In CCIS there is no correlation visible. Finally it can be stated that in side impacts to pole the crash weight of the car has no, or only minor influence on the injury severity (fig. 9).

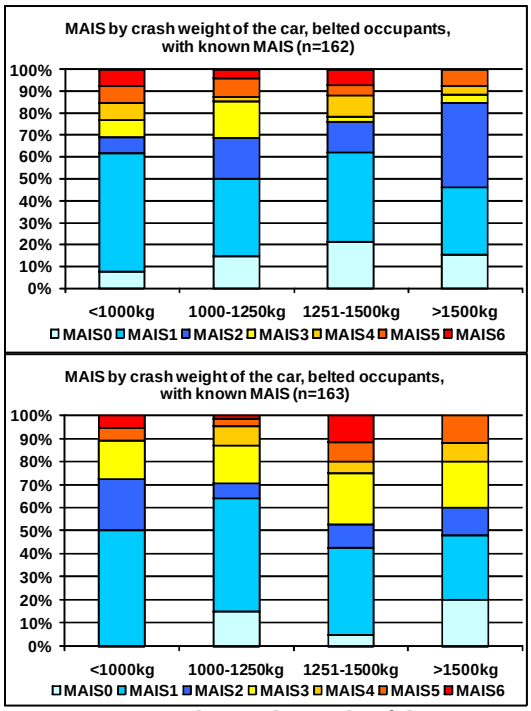

Figure 9 MAIS by Crash Weight of the Car

Pole Diameter

In the GIDAS database 60% of the impacted poles have a diameter less than 40 cm. In CCIS nearly one half of the single side to pole impacts happen to poles of this size.
GIDAS provides also more detailed information on the distribution of pole diameters. Biggest group with more than 25% are the poles with diameter between 21 and 30 cm.

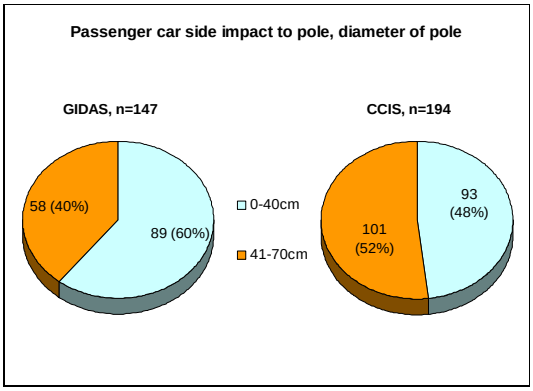

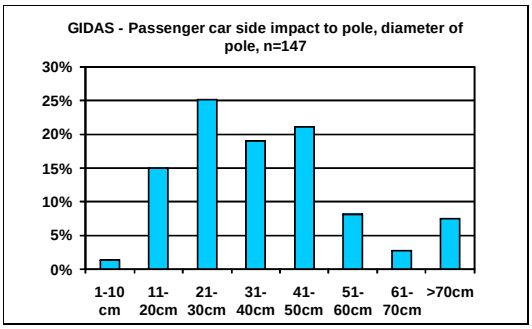

Figure 9 Diameter of Pole in Car to Pole Impacts

3.4 Occupant Parameters

Age

The share of young drivers is significantly higher in car to pole impacts compared to all other side impacts. Clearly more than 40% of all drivers in pole impacts are younger than 26 years. In other side impact configurations this share is around 25% (fig. 10). Side to pole impacts are generally single vehicle accidents. Other studies show that especially in this type of accident young drivers are overrepresented [STBA 2006].

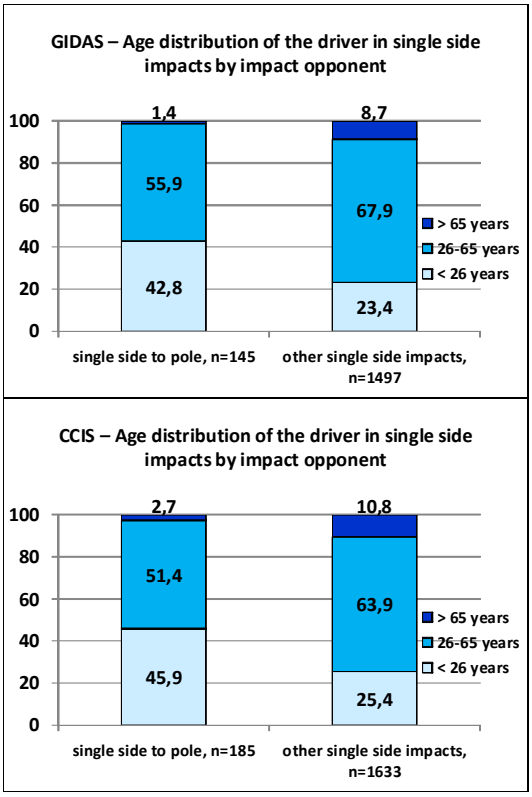

Figure 10 Driver Age Distribution in Side Impacts and Pole Impacts of Cars

Injuries per Body Region in Pole Impacts

Looking at all injuries, occupants received in car side to pole impacts the head, the thorax and the extremities account for more than 80% of the injuries (fig. 14). Slight injuries are dominated by the head and the extremities. The combined share is about 75%. For AIS3+ injuries the share of injuries to the thorax rises to 32% in GIDAS and 38% in CCIS.
The share of abdominal injuries is 4% in GIDAS for slight and severe injuries. In CCIS abdominal injuries have a share of 11% for AIS1&2 and 5% for AIS3+ injuries.

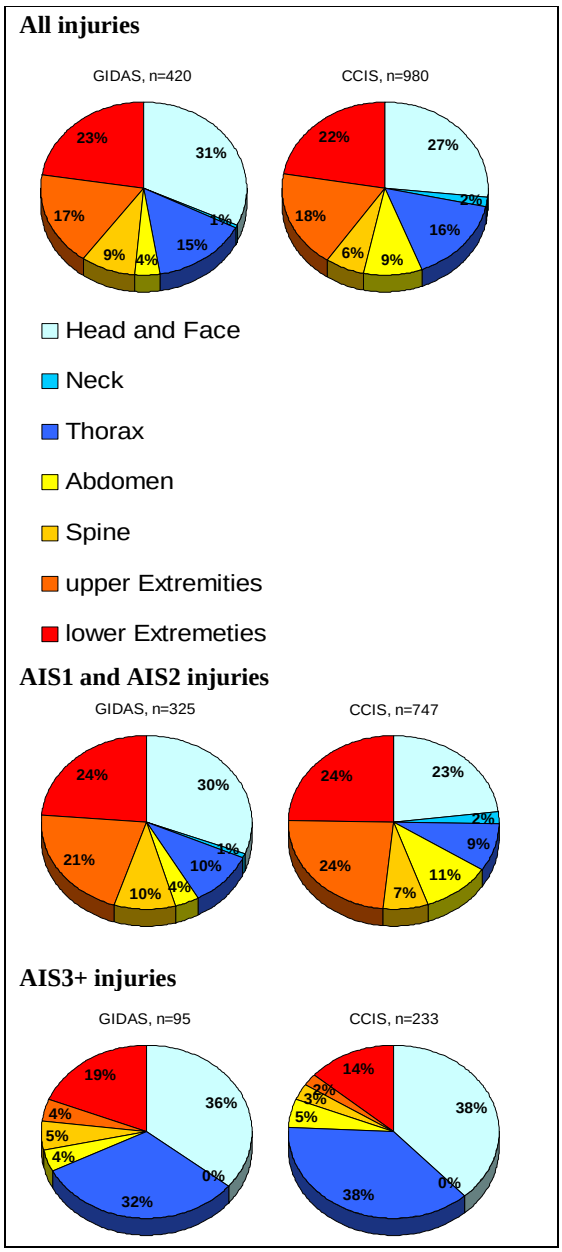

Figure 12 Injury Distribution per Body Region in Pole Impacts

4. CASE BY CASE ANALYSIS

Complementary to the statistical analysis on all car side to pole impacts a case-by-case analysis was carried out. It is focussed on a detailed in-depth-investigation by using the original accident files, the accident images, injuries and its causation factors and the vehicle deformation pattern.

Data sample for case by case analysis

The data set on side to pole impacted cars is based on the data that was used for statistical analysis. In addition the case by case analysis is focussed on struck side occupants in cars registered 1998 onwards resulting in a sub sample with **n=26 cases out of the GIDAS data base and n=97 cases out of CCIS**.

Methodology of case by case analysis

For the analysis the car exterior is classified into a matrix system A, B, C, and D (fig. 13). The area A describes the area in front of the A-pillar, B describes the area between A- and B-pillar, C the area between B- and C-pillar and D the area in the rear of the car. The principle direction of force (fig. 13) was classified into rectangular (R) and oblique from the front (F) and oblique from the rear (B).

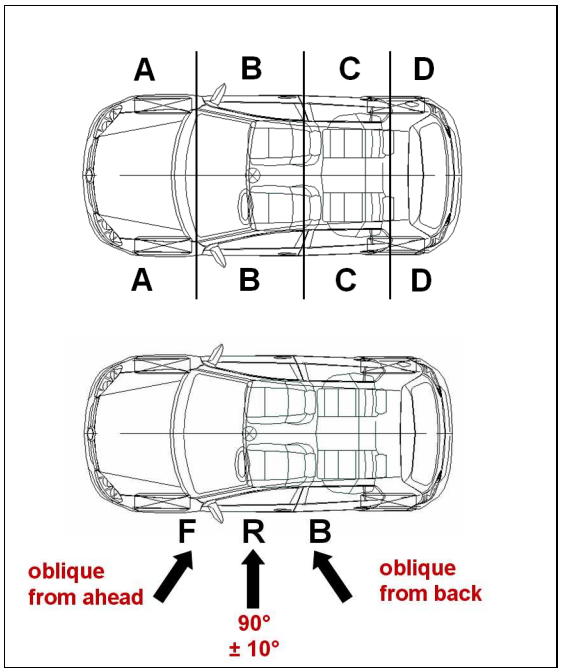

Figure 13: Definition of the 4 impact areas and principle direction of force

The frequency for these different classifications in side to pole impacts is given in the figures below (fig. 14). The most frequent impact area is the B-area with 44.5%. The most frequent impact direction is in oblique direction from the front in nearly the half of all cases (48.2%). A rectangular impact ±10 degree can be seen in 40.9%. Impacts from the rear direction occur rarely (10.9%).

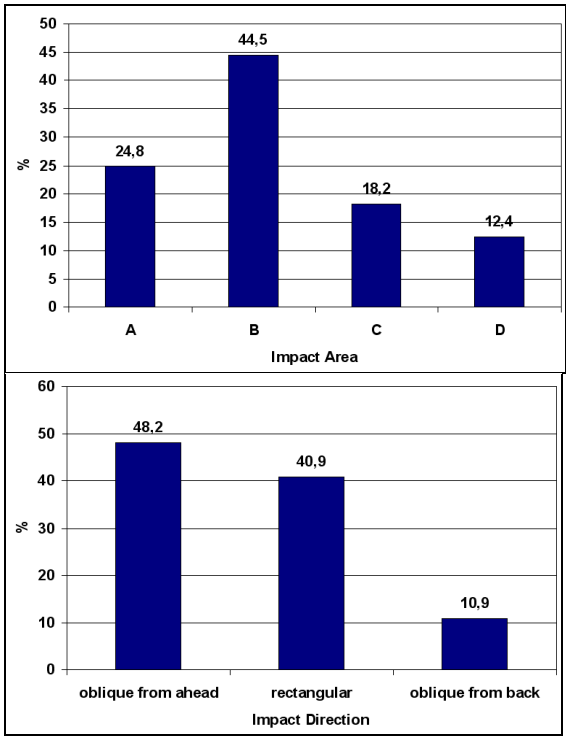

Figure 14: Frequencies of impact area and impact direction

The most frequent combinations of impact areas and directions are AF, BF, BR and CR (fig. 19), together they cover 68% of all situations. Around 19% of all impacts occur in the area between A- and B-pillar with force direction from front respectively perpendicular direction. Focussing on seriously injured struck side occupants (MAIS3+) more than the half had an impact from the frontal or perpendicular direction to the B area. Impacts to the front or the rear of the car occur rarely.

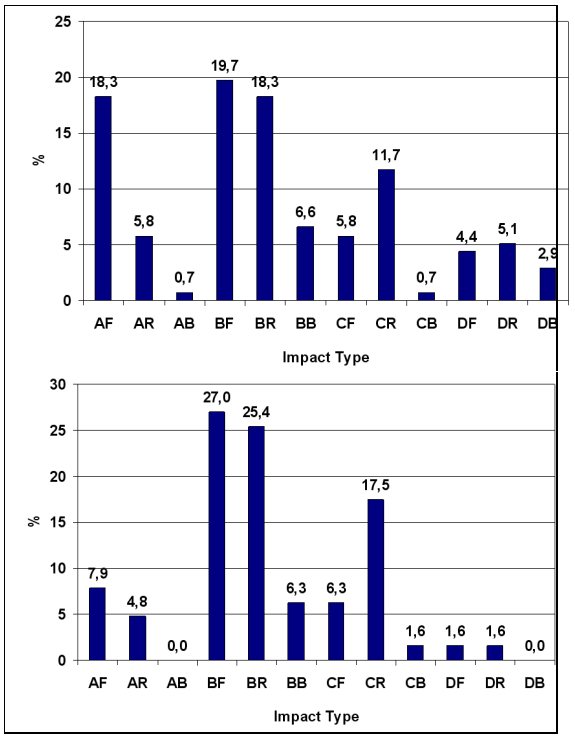

Figure 19: All struck side occupants (upper chart) and MAIS 3+ struck side occupants (lower chart), Combinations of impact area and direction

Statistical Analysis of Car-Side-Pole-Impacts within the Case by Case Analysis

Ordinal logistic regression

To identify the relevant factors for the MAIS of the struck side occupants an ordinal logistic regression was carried out. As potential factors/variables the delta v, year of first registration, impulse angle, depth of deformation, country, diameter of pole and damage location were used.

In Table 1 the p-values for the Chi square test are given for the correlation of the variables and MAIS, respectively MAIS in individual body regions. According to this delta v has significant influence on the overall MAIS, on the injury severity in head and abdomen. The depth of deformation has significant influence on the injury outcome of the extremities, and the damage area on MAIS and the injury severity in thorax and lower extremities. The impulse angle has only significant influence on MAIS, the pole diameter only to the head injury severity and country only to the injury severity of the lower extremities. Having only cars registered 1998 onwards presented in this sample; this variable has no significant influence on the injury severity levels.

Variable	Degree of Freedom	MAIS	Head AIS	Thorax AIS	Abdomen AIS	Upper Ex-tremities AIS	Lower Ex-tremities AIS
Delta-v	1	0.0002	0.2836	0.0011	0.0022	0.0590	0.0547
Year of first Registra-tion	1	0.2024	0.5139	0.3297	0.2341	0.5039	0.1382
Impulse Angle	1	0.0242	0.5742	0.2418	0.8825	0.0858	0.6958
Depth of Deforma-tion	1	0.2716	0.5308	0.1071	0.5839	0.0462	0.0213
Country	2	0.3494	0.6573	0.8830	0.3151	0.1845	0.0122
Pole Diameter	1	0.9178	0.0286	0.6395	0.4471	0.6758	0.6684
Damage Area	4	0.0221	-	0.0341	0.1619	0.2379	0.0010

Table 1: p-values for the ordinal logistic regression analysis, correlation of given variables and injury severity of struck side occupants.

CART-analysis

To get more information on the influence of delta-v on the injury outcome a Tree- or CART-Analysis was carried out. It gives more information on the thresholds of a variable (delta v) where changes in the target parameter (MAIS) are visible. The CART method is an empirical, statistical method based on recursive partitioning analysis (Breiman *et al*, 1984); the aim is to form prediction rules by constructing binary trees.

First there is an upper change of significance at a statistically evaluated delta-v of 61.5 km/h describing an over proportional significance to high injury severity grades. Above this delta-v value the injury severity is increasing rapidly, explained by the highly deformation of the cars similar to catastrophic pattern. Next level of remarkable change can be found for a statistically evaluated delta-v of 27.5 km/h. This value of delta-v 27.5 km/h is approximately the discussed test speed of 29 km/h.

The CART-analysis gives the indication that real world side to pole impacts have a significant level of accident severity at 27.5 km/h, where the injury severity is expected to increase over proportional (Figure 20).

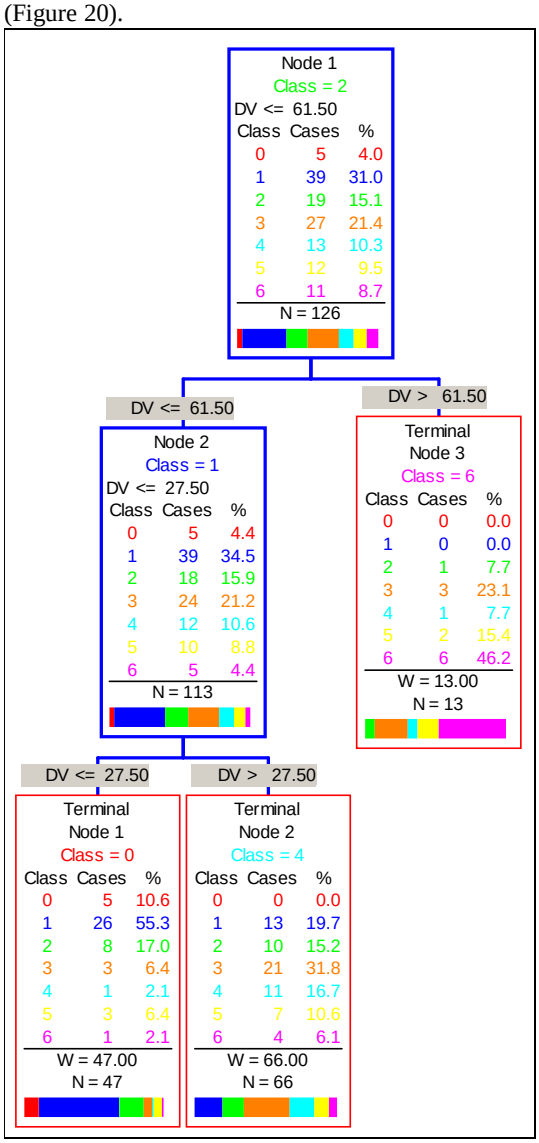

Figure 20: CART-analysis of car side impacts with poles

It can be seen in the analysis, that delta-v has a significant influence, first there is an upper change of significance at a statistically evaluated delta-v value of 61.5 km/h describing an over proportional significance to high injury severity grades. Above this level of accident severity the injury severity is increasing rapidly, explained by the highly deformation of the cars similar to catastrophic pattern. Another level of remarkable changes can be found for a statistically evaluated delta-v value of 27.5 km/h. This value of delta-v 27.5 km/h is nearly the discussed test speed of 29 km/h and is shown that current real accidents are having here an important level of accident severity where the injury severity are increasing over proportional.

A 3-dimensional graphic (fig. 21) is shown for all impacts on the compartment area the overall correlation of significant influence on pole impacts on the lateral part of the vehicle BF + BR:

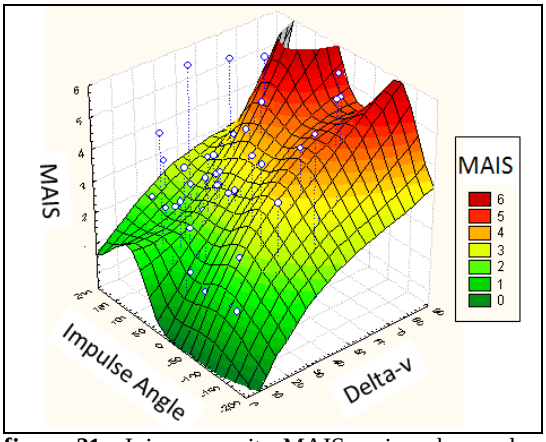

figure 21 : Injury severity MAIS vs impulse angle vs delta-v

There are major impact conditions leading in relatively high injury severity, i.e. angle of force momentum = 90 degree, delta-v 40 km/h onwards, especially very severe are impact conditions from rectangular combined with high delta-v.

CONCLUSION

From this study the following conclusion can be drawn:

- Pole impacts are relatively rare events compared to other impact types. But the importance of side to pole impacts increases by focussing on seriously injured occupants (MAIS3+).
- Cars equipped with ESC show a by far lower share of car side to pole impacts and in consequence have reduced numbers of injured car occupants. Currently 10% of the vehicles in the GIDAS dataset were equipped with ESC. In the future the higher market penetration of ESC will further reduce the number of car side to pole impacts.
- In GIDAS 50% of the occupants in single side to pole impacts receive a delta v less than 35 km/h, in CCIS this 50% rate is reached at 29 km/h. This is in contrast to the injury severity distribution in both studies. The share of MAIS3+ injured occupants in single side to pole impacts is in CCIS with 37.5% clearly higher than in GIDAS 26.4%.
- The most frequent direction of impact in car side to pole impacts is oblique from the front. Perpendicular impacts are the sec-

ond frequent one. Damaged passenger compartments causing the vast majority of severe and fatal injuries.

- The injury outcome does not correlate with the vehicle mass.
- The highest proportion with approximately 50% of all car side to pole impacts happen to poles with a diameter of less than 40 cm (CCIS 48% and GIDAS 60%).
- Head and thorax injuries of the occupants are of highest importance when looking at severe and fatal injuries. Their share is above 70% of all MAIS 3+ injuries.
- Delta-v can be identified as most significant influence factor for MAIS.
- At a delta-v value of 27.5 km/h the injury severity is expected to increase over proportional.

Most critical point in the discussion of future side impact testing criteria is the test speed. However a comparison between individual cases and a categorisation of the cases into cases of comparable severity within the individual in-depth study is possible.

Several studies have already demonstrated the potential of ESC in terms of traffic safety. The list below (table 2) provides a brief overview of what has been investigated so far.

Reference	**Estimated traffic safety effect**	**Source of data**
Sferco et al. (2001)	34% reduction of fatal accidents 18% reduction of injury accidents	EACS
Aga and Okado (2003)	35% reduction of single car accidents	ITARDA
Grömping et al. (2004)	44% reduction of loss of control accidents	GIDAS
Lie et al. (2004)	22.1% (± 21) reduction of accidents more efficient on slippery road conditions	Insurance data (Folksam)
Lie et al. (2006)	16.7% (± 9.3) reduction of all injury crash types 21.6% (± 12.8) reduction of fatal and serious crashes more efficient on slippery road conditions	Insurance data (Folksam)
Page and Cuny (2006)	44% reduction of relative risk of ESP pertinent accidents	French national accident census
Farmer (2004)	41% (27-52) reduction of single vehicle crashes involving personal injury	State data System maintained by NHTSA
Langwieder et al. (2003)	25-30% reduction of all car crashes involving personal injury	Several data bases

Table 2: Estimated Traffic Safety Effect of ESC [1]

For the presented study based on GIDAS especially the share of accidents with rollover and pole impacts is definitely lower for cars equipped with ESC compared to cars without ESC.

ACKNOWLEGEMENTS

This paper uses accident data from the United Kingdom Co-operative Crash Injury Study (CCIS) collected from 1996 to 2006. CCIS is managed by TRL Limited on behalf of the UK Department for Transport (DfT) Transport Technology and Standards Division who fund the project along with Autoliv, Ford Motor Company, Nissan Motor Company and Toyota Motor Europe. Daimler-Chrysler, LAB, Rover Group Ltd, Visteon, Volvo Car Corporation, Daewoo Motor Company Ltd and Honda R&D Europe(UK) Ltd have also funded CCIS. The data were collected by teams from the Birmingham Automotive Safety Centre of the University of Birmingham, the Vehicle Safety Research Centre at Loughborough University, TRL Limited and the Vehicle & Operator Services Agency of the DfT. Further information can be found at <http://www.ukccis.org>.

For the present study accident data from GIDAS (German In-Depth Accident Study) was used. GIDAS is the largest in-depth accident study in Germany. The data collected in the GIDAS project is very extensive, and serves as a basis of knowledge for different groups of interest. Due to a well defined sampling plan, representativeness with respect to the federal statistics is also guaranteed. Since mid 1999, the GIDAS project has collected on-scene accident cases in the areas of Hannover and Dresden. GIDAS collects data from accidents of all kinds and, due to the on-scene investigation and the full reconstruction of each accident, gives a comprehensive view on the individual accident sequences and its causation. The project is funded by the Federal Highway Research Institute (BASt) and the German Research Association for Automotive Technology (FAT), a department of the VDA

(German Association of the Automotive Industry). Use of the data is restricted to the participants of the project. However, to allow interested parties the direct use of the GIDAS data, several models of participation exist.
Further information on GIDAS can be found at http://www.gidas.org

REFERENCES

Breiman L, Friedman JH, Olshen RA, Stone CJ. (1984) Classification and Regression Trees. Chapman & Hall (Wadsworth, Inc): New York, USA

ECE 95 (2005) UNIFORM PROVISIONS CONCERNING THE APPROVAL OF VEHICLES WITH REGARD TO THE PROTECTION OF THE OCCUPANTS IN THE EVENT OF A LATERAL COLLISION, Economic Commission for Europe

Kahane, C. (1999) Evaluation of FMVSS 214 - Side Impact Protection: Dynamic Performance Requirement, NHTSA Report Number DOT HS 809 004

Otte, D. (1990) Comparison and Realism of Crash Simulation Tests and Real Accident Situations for the Biomechanical Movements in Car Collisions. Proc. 34th STAPP Car Crash Conference, Orlando, USA

Otte, D., Krettek, C., Brunner, H., Zwipp, H. (2003) Scientific Approach and Methodology of a New In-Depth-Investigation Study in Germany so called GIDAS. ESV Conference, Japan, 2003

Otte, D. (2005) 3-D Laser systems for scaled accident sketches and documentation of the traces after traffic accidents as basis of biomechanical analysis. IRCOBI Conference, 435-438

Pfeiffer, M., Schmidt, J. (2006) Statistical and Methodological Foundations of the GIDAS Accident Survey System, 2nd ESAR Conference, Hannover, 2006

stats19 (2005) Road Casualties Great Britain: 2005. Department for Transport (DfT - UK)

STBA (2006) Statistical data of traffic accidents in Germany 2005, Stat. Bundesamt Wiesbaden, Fachserie P, Reihe 7, Verlag Metzler-Poeschel, Stuttgart 2006

Varat, M., Husher, S. (1999) Vehicle Crash Severity Assessment in Lateral Pole Impacts. SAE Technical Paper, 1999-01-0100

Zaouk, A., Eigen, A., Digges, K. (2001) Occupant Injury Patterns in Side Crashes. SAE Technical Paper , 2001-01-0723

Coupled Human Body Side Impact Model to Predict Thoracic Injury

Brett Campbell
Duane Cronin
University of Waterloo
Canada
Yih-Charng Deng
General Motors Corporation
United States
Paper number 09-0255

ABSTRACT

The goal of this study was to evaluate side impact crash conditions using a detailed human body model and side impact crash model to provide an improved understanding of side impact injury and the primary contributing factors. This study builds on an advanced numerical human body model, including a detailed thorax, which has been validated using available PMHS test data for pendulum and side sled impact tests. Crash conditions were investigated through use of a coupled side impact model, used to reproduce full scale crash tests. The model accounts for several important factors that contribute to occupant response as noted in the literature: the relative velocities between the seat and door, the occupant to door distance, the door shape and compliance. The coupled side impact model was validated using FMVSS 214 and IIHS side impact test data, comparing the thoracic response predicted by the model to that of the ES-2 dummy used in the crash tests. Importantly, the door and seat models were developed based on experimental data in the literature.

The side impact model was used to investigate the effects of door to occupant spacing, door velocity profile, restraint system, and seat foam properties. The current study was limited to the use of velocity profiles in the direction of impact and did not consider rotational effects or motion perpendicular to the impact direction. It was found that injury as predicted using the detailed human body model and the Viscous Criterion (VC) was controlled by the second velocity peak typically found in door velocity profiles.

INTRODUCTION

Although there have been tremendous improvements in crash safety there has been an increasing trend in side impact fatalities, rising from 30% to 37% of total fatalities from 1975 to 2004 [1]. Between 1979 and 2004, 63% of AIS≥4 injuries in side impact resulted from thoracic trauma [1]. Lateral impact fatalities, although decreasing in absolute numbers, now comprise a larger percentage of total fatalities. Safety features are typically more effective in frontal collisions compared to side impact due to the reduced distance between the occupant and intruding vehicle in side impact collisions.

Automotive research is a challenging field due to the complexity and cost associated with full-scale vehicle testing. Recent efforts have focused on the development of advanced finite element models of vehicles and occupants capable of reproducing the response present in crash scenarios.

Forbes [2,3] developed a detailed numerical human thorax model with simplified models of the remaining body regions. The human body model developed by Forbes [2,3] was validated by correlating the response of pendulum and sled simulations to tests performed on PMHS. This study has integrated the human body model in crash scenarios representing FMVSS 214 side impact testing. This research is intended to provide a detailed understanding of thoracic response due to side impact using the numerical human body model previously developed [2-5]. The first goal of this study was to develop and validate a side impact model capable of reproducing the conditions present in full scale crash testing. The second goal of this study was to perform a parametric study varying conditions in the side impact model to provide an understanding of loading and its effect on thoracic trauma in side impact collisions.

SIDE IMPACT MODEL DEVELOPMENT AND VALIDATION

The side impact model (Figure 1) was developed to reproduce the important conditions present in side impact crash scenarios. The model accounts for several factors that contribute to occupant response based on the literature [5-11] including: the relative velocities between the seat and door, the occupant to door distance, door shape, and door compliance.

Although some components were simplified in terms of geometry, they were based on geometries found in typical vehicles and material characteristics determined by experiment or found in the literature.

The side impact model consisted of several components modeled as rigid materials, including the seatbelt anchors, sled base, and outer door. The seat, seatbelts, and door were based on representative geometries and material properties determined by experimental testing and data from the literature [7,12-17].

The simplified door was based on a cross section of a Ford Taurus model door [18] for consistency with the side impact test data used in this study. The door was sectioned through the area that had the greatest armrest depth in order to produce a conservative door model geometry. The mechanical response of the simplified door model was set to produce the same force-deflection characteristics as found in the literature [13].

The seat pan, sled base, and door were given prescribed velocity profiles based on full-scale crash tests from the NHTSA database, applied for the duration of the simulation. The sled was constrained vertically and in the direction perpendicular to impact to prevent rotations. Although rotational velocities do exist in full scale crash testing, any significant rotation tends to occur long after the maximum thoracic response is observed and was not considered for this study.

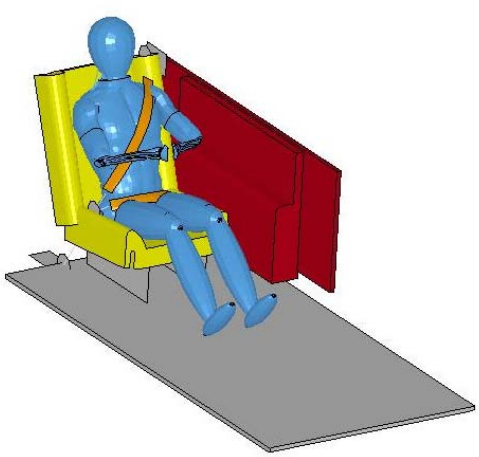

Figure 1 Side Impact Model.

The validation of the side impact model was done by comparing the thoracic response of the human body model to experimental results from an ES-2 for two side impact crash scenarios reported here. Velocity inputs from two specific cases were selected and the side impact model was modified to represent a FMVSS 214 test of a Ford Taurus and an IIHS test of a Nissan Maxima. For brevity, only the Ford Taurus data is presented in this paper. These two test cases were selected for several reasons. First, accurate velocity profiles for the vehicle CG, seat, and door were required to provide input conditions for the side impact model. However, door accelerometers are not regularly included in side impact test procedures, therefore narrowing the test cases to those tests that do include door accelerometers. Second, current and past research using the human body model has focused on VC response to predict injury. However, typical side impact test procedures use a Side Impact Dummy (SID) with TTI injury criteria based on accelerations. This further narrowed the available side impact tests to those that use the ES-2 since VC is used as the injury criteria. Finally, two test types (FMVSS 214 and IIHS) with different test procedures were selected to validate the side impact model under differing test conditions.

Side Impact Model Input Profiles

Based on information for similar sled tests in the literature [10,19,20], input velocities for the sled, seat, and door were determined by the integration of accelerations recorded by uniaxial accelerometers positioned at the vehicle CG, driver seat track, and inner door panel respectively. Full-scale crash data was obtained from a FMVSS 214 and an IIHS test [21,22]. These tests used a modified 50th percentile ES-2 dummy so comparison of the simulated occupant response to the ES-2 response was based on rib deformation compression, velocity, and the Viscous Criterion. Input pulses for the FMVSS 214 test are shown in Figure 2 and application to the side impact model in Figure 3.

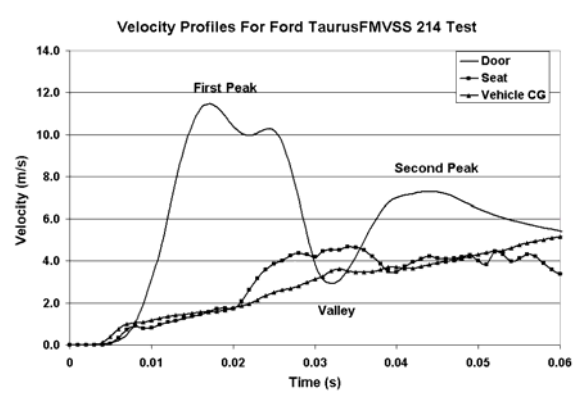

Figure 2 Input Velocity Profiles [22].

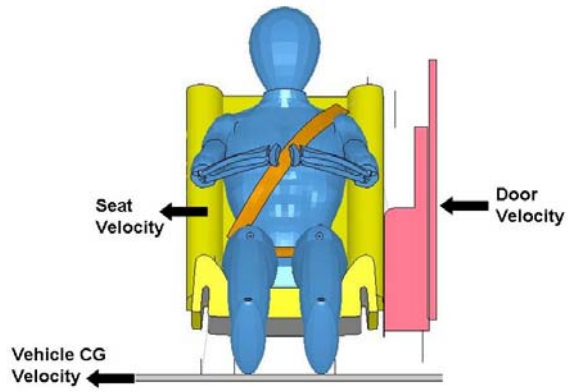

Figure 3 Side Impact Model with Input Velocities

It should be noted that vehicles were equipped with several accelerometers; however, the exact location often varies from vehicle to vehicle. Also, because the door was directly impacted by the intruding moving deformable barrier (MDB), sensors may rotate during the collision. This can result in inaccurate results, as acceleration will not be measured with respect to the expected coordinate system. However, for the purposes of this study, it was assumed that the accelerometer data was accurate and rotation occurred after injury was predicted, approximately 50 msec after the initial impact.

Measuring Thoracic Response

The ES-2 records numerous acceleration, displacement, and force responses throughout the duration of a crash event. However, for this study, only the lower, middle, and upper rib responses were evaluated for comparison with the human body model. For purposes of comparison, three levels have been selected on the human body model, representing anatomically equivalent areas to the lower, middle, and upper ribs of the ES-2 (Figure 4).

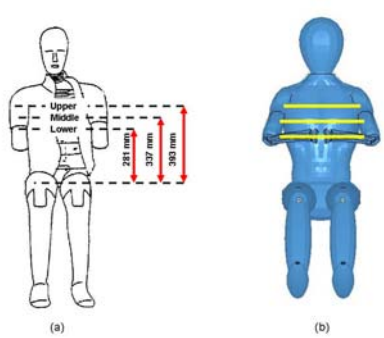

Figure 4 Response Locations (a) ES-2 Rib Location (b) Model Chest Levels.

The ES-2 measures deflection based on the half thorax dimension, by measuring the deflection of the ribs on the struck side. To ensure comparable results, the response of the human body model was also predicted using the half thoracic deflection as defined by Samaha et al. [23].

The degree of injury was measured using the Viscous Criterion developed by Lau & Viano [24]. Lau & Viano defined the viscous response (VC) as the product of deformation velocity, V(t), and the instantaneous normalized compression, C(t).

$$VC(t) = V(t) x C(t) \qquad (1).$$

Where $C(t) = \dfrac{D(t)}{D_o}$ and $V(t) = \dfrac{d[D(t)]}{dt}$

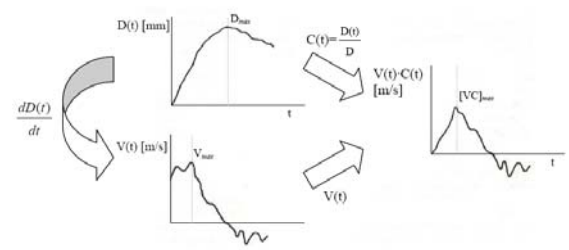

Figure 5 The Viscous Criterion [24].

Validation with FMVSS 214 Crash Test

The human body side impact simulation response during an impact with velocity profiles (Figure 2) and Arm to Door (AD) distance as determined by the FMVSS 214 side impact testing of a Ford Taurus is shown in Figure 6.

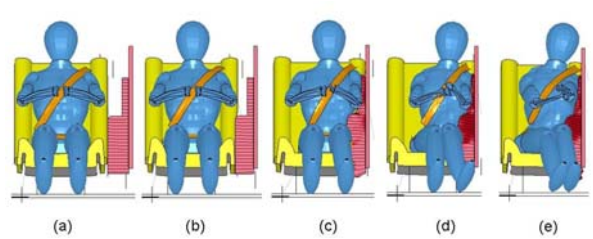

Figure 6 Impact Sequence of Ford Taurus Side Impact Simulation (a) t=0 ms (b) t=15ms (c) t=30ms (d) t=45ms (e) t=60ms.

The simulated compression, velocity, and VC response for the upper chest band described in Figure 4 is compared to the ES-2 response obtained from a full-scale FMVSS 214 crash test in the figures below (Figure 7, 8 and 9). Additional data and comparisons can be found in Campbell [12].

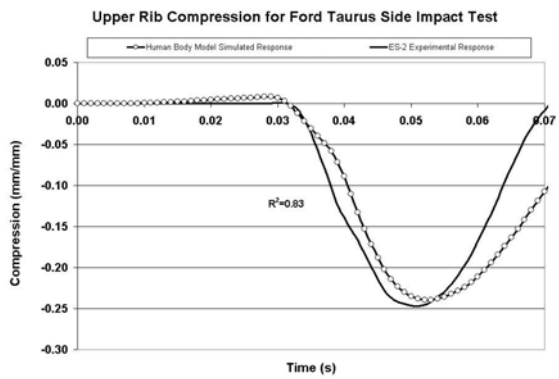

Figure 7 Upper Rib Compression Response for the Side Impact Model with Ford Taurus Inputs.

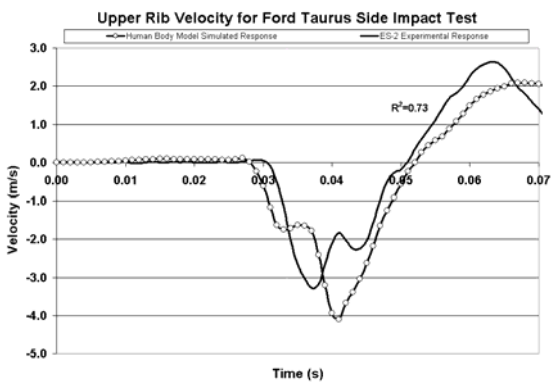

Figure 8 Upper Rib Velocity Response for the Side Impact Model with Ford Taurus Inputs.

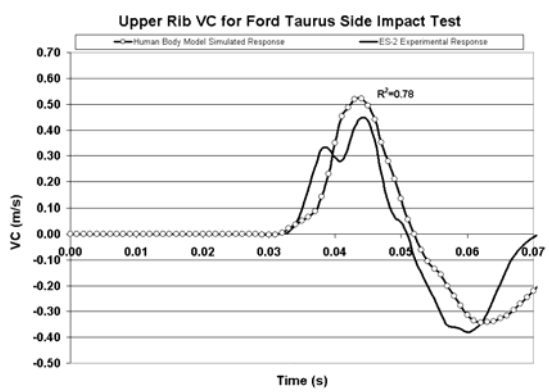

Figure 9 Upper Rib VC Response for the Side Impact Model with Ford Taurus Inputs.

Model assessment was undertaken following the methods used by Forbes. The predicted thoracic response was compared to ES-2 based on data for loading, peak, unloading, and overall r-squared for the curves. The following qualitative measures as applied in previous validation of the human body model [2,3] have been used to compare the simulated response to the experimental response (Table 1):

- Good — Falling close to the experimental response at the discretion of the author
- Reasonable — Falling reasonably close to the experimental response at the discretion of the author
- Poor — Falling significantly far from the experimental response at the discretion of the author

Table 1 Side Impact Simulation vs Ford Taurus v3522 Injury Response Correlation

CHEST BAND	IMPACT PHASE	CORRELATION		
		Compression (mm/mm)	Velocity (m/s)	VC (m/s)
Upper Rib	Loading	Good	Reasonable	Good
	Peak	Good	Reasonable	Reasonable
	Unloading	Reasonable	Good	Good
	R^2	0.83	0.73	0.78
Middle Rib	Loading	Good	Good	Good
	Peak	Good	Good	Good
	Unloading	Reasonable	Reasonable	Reasonable
	R^2	0.67	0.56	0.58
Bottom Rib	Loading	Reasonable	Reasonable	Poor
	Peak	Reasonable	Poor	Poor
	Unloading	Reasonable	Reasonable	Reasonable
	R^2	0.53	0.51	0.40

The information presented in Table 1 shows that the side impact model closely reproduced the timing and injury response as measured in the FMVSS 214 test, producing *good* to *reasonable* response overall. Discrepancies are attributed to minor differences in occupant positioning, door positioning and compliance, and geometric differences between the ES-2 and human body model at the specified chest band locations.

SIDE IMPACT SIMULATION - PARAMETRIC STUDY RESULTS

The side impact and human body models were used to undertake a parametric study to evaluate the different factors that contribute to injury response.

For this aspect of the study, injury was evaluated based on full thorax deformation (as opposed to half thorax for the ES-2 comparison) using the same chest band locations implemented by Forbes [2,3] to ensure consistency with prior human body model usage and PMHS testing in the literature [2,3,25].

Thoracic response was measured using upper, middle, and lower chest bands located at the lateral level of the 4th rib, level of the xiphoid process, and the level of the 10th rib respectively (Figure 11). Also, it was found that the half thoracic deflection was lower than the full thoracic deflection, in agreement with the literature [26]. This indicates that a considerable amount of deformation occurs on the non-struck side, which is unaccounted for when using the half thoracic response. Maltese et al. [26] clearly show that the half thoracic deflection is often approximately 60% of the full thoracic deflection. Similar differences between full and half thoracic deflection were found for the human body model as seen in Figure 10.

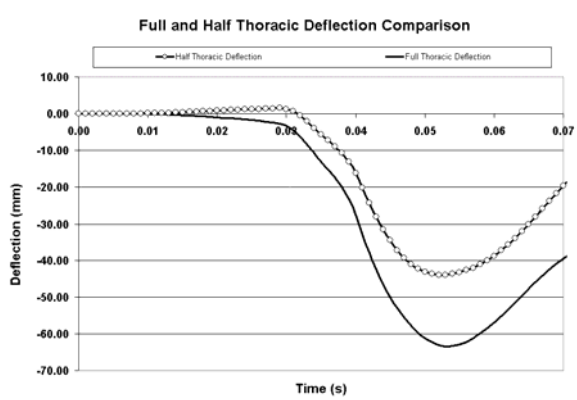

Figure 10 Human Body Model Full and Half Thoracic Deflection Comparison.

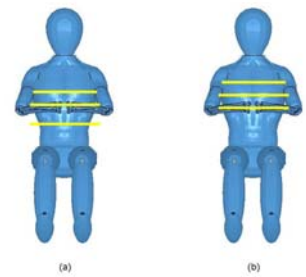

Figure 11 Chest band location: (a) Parametric Study Location (b) Validation Case Location.

Side Impact Model Baseline Conditions

The velocity profiles, door compliance, and occupant position for the validation case above were used as the baseline for the parametric study (Figure 2).

Full-scale side impact tests typically produce door intrusion velocity profiles that consist of three common characteristics; first peak, valley, and second peak [10]. The first peak occurs immediately after the barrier contacts the door causing the door velocity to rapidly increase to its initial peak. The door velocity then decreases to its valley as the vehicle side structure transfers load to the main structure of the vehicle [11]. The second peak in door velocity is caused by stiffening of the barrier prior to slowing to its final velocity. It has been found that the overall kinematics of the door is essentially unaltered by the interaction with the occupant [27].

The Effect of Varying Door to Occupant Distance

This study investigates the effect of the door to occupant distance by using two door types; a rigid plate and a representative door with armrest (Figure 12). The AD spacing used in this study was selected to cover a range as determined by the maximum and minimum values found in FMVSS 214 test reports [28].

One would expect that increasing the spacing between the occupant and the intruding door would reduce occupant injury. The amount of space between the occupant and the door has a direct effect on the contact velocity as well as the contact timing with respect to the velocity profile [10]. The effect of the occupant to door spacing was investigated by varying the spacing of an intruding rigid door and

armrest in the side impact model. As discussed in the previous section, the velocity profiles applied to the side impact model were controlled by the crushing of the vehicle structure and were independent of occupant positioning. Therefore, the velocity profiles for the baseline case were applied for each AD distance in this study.

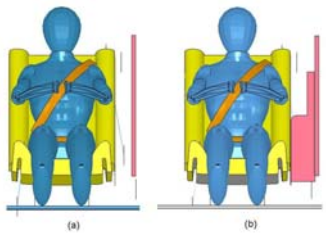

Figure 12 Door Type (a) Rigid Door (b) Armrest.

Two cases were used to investigate the effects of door to occupant spacing. First, a rigid door as seen in Figure 12 was used to investigate the effect of varied AD distance excluding effects caused by armrest geometry and compliance. Second, the same AD study was performed to investigate differences in thoracic response caused by the presence of an armrest in comparison to a flat rigid door.

Rigid Door Simulation - The upper band VC response for varying door to occupant distances for an intruding rigid door is shown in Figure 13.

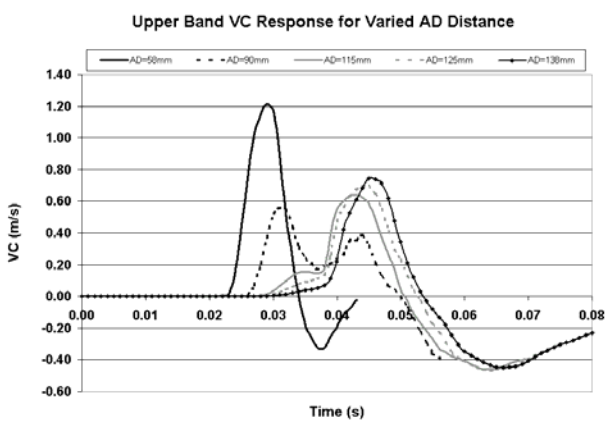

Figure 13 Upper Band VC Response for Varied AD Distance of an Intruding Rigid Door.

Investigating the VC response shown in Figure 13 can provide some insight into the timing of injury and the role of the occupant to door distance. Two curves (58mm & 90mm) had their peak injury response occurring just after the first peak in the door intrusion velocity profile (Figure 14). The remaining three scenarios (115mm, 125mm, and 138mm) had their maximum injury response closely coinciding in time with the second peak of the door velocity profile. Further insight may be provided by examining the contact timings of the door to chest as determined by the upper band velocity response shown in Figure 14.

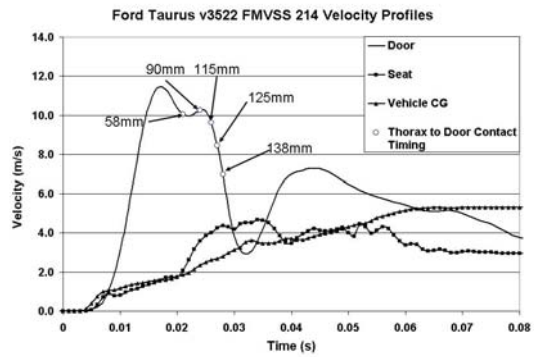

Figure 14 Contact Timing for Varying Door to Occupant Spacing.

The contact timings for the five AD spacings discussed occur within 7 ms of each other, but have a significant influence on occupant injury despite the minor differences in contact timing. The variance in injury responses may be explained by examining the occupant motion relative to the sled base by tracking the velocity of the center of the occupant chest relative to the sled floor (Figure 15).

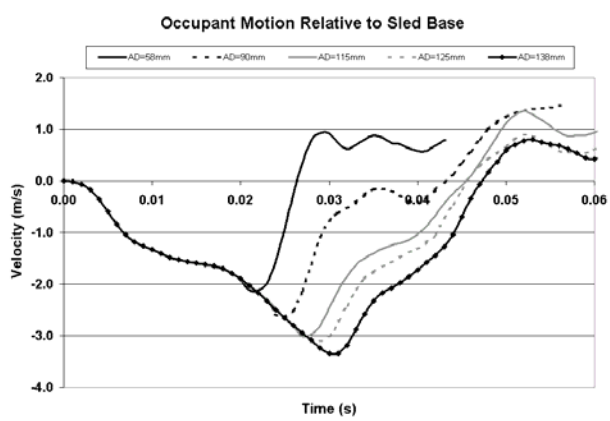

Figure 15 Occupant Motion Relative to Sled Base for Varied Door to Occupant Spacing.

The occupant response relative to the sled base in Figure 15 essentially consists of a decrease in occupant velocity relative to the sled floor prior to

door contact followed by an increase in occupant velocity after contact. Therefore, the decreasing relative velocity actually represents the sled floor moving while the occupant remains relatively stationary due to its inertia. When contact with the door occurs the occupant velocity begins to catch-up to and surpass the velocity of the sled.

One would expect that thoracic response would inversely correlate to AD distance, such that an increase in AD distance would cause a decrease in injury. This inverse correlation does occur to some extent in the scenario presented and would likely occur for all AD distances if not for the second peak in the door velocity profile.

For a door to occupant distance of 58mm, the VC response is controlled by the first peak and VCmax occurs just before the door velocity profile valley. The thoracic compression present at the onset of the second peak in door velocity was 20.9% and was the maximum compression observed in the study [12]. The velocity of chest compression at the onset of the second peak is near zero, confirming that the chest has in fact reached the maximum compression at this point. The occupant motion relative to the sled base prior to the second peak suggests that the occupant has surpassed the velocity of the sled floor due to the aggressive impact with the intruding door.

The 90mm door to occupant scenario can be described in much the same way as the 58mm case. However, the 115mm case differs as it was controlled by the second peak in the door velocity profile. The first peak did produce minor thoracic response as observed in the VC response shown in Figure 13, but was superseded by the injury produced by the second peak. This response can be largely explained by the time of contact and occupant response prior to the second peak. As seen in Figure 14, the contact timing for an AD of 115mm occurs as the door was decelerating to its valley, which decreased the time for the door to compress the chest and accelerate the occupant. In this case, the chest compression is only 5% prior to the second peak [12]. Also, the occupant velocity relative to the sled base suggests that the occupant was beginning to accelerate due to contact with the intruding door, but was still moving considerably slower than the sled floor. These factors significantly increase the effect of the second peak because the occupant was not accelerated enough to minimize the impact of the second peak.

The same reasoning can be applied to the final two cases (125mm and 138mm). Injury in both cases was highly influenced by the second peak due to the time of contact with the intruding door. As intuition would suggest, the first peak response continually decreases as AD distance increases, but this decrease in first peak response causes an increase in the effects of the second peak, thus creating the observed VC response. The later contact time reduces the ability of the first peak to accelerate the occupant, thereby causing the second peak to be far more injurious than observed in scenarios with smaller AD distances.

Padded Armrest Simulation - The VCmax of an occupant for varied AD spacing of a simplified door including an armrest is compared to that of a rigid flat door in the following bar chart (Figure 16). Trend lines are included to track VCmax for varying AD spacings.

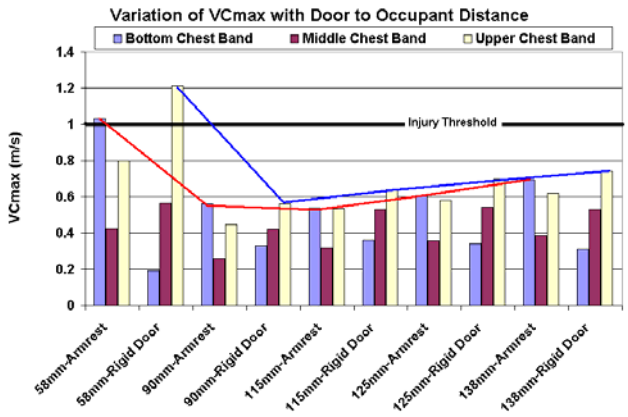

Figure 16 Variation of VCmax with Door to Occupant Distance.

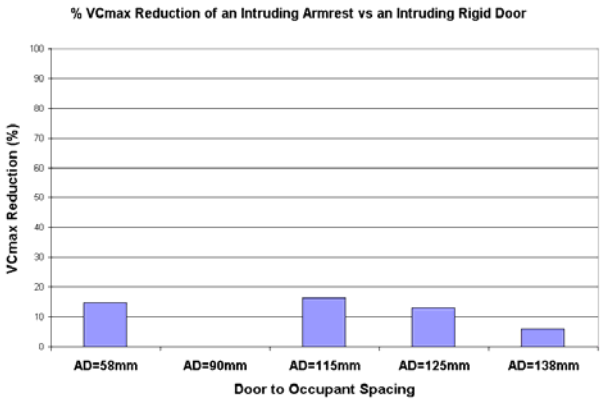

Figure 17 VCmax Reduction of an Intruding Deformable Door vs an Intruding Rigid Door.

As one would expect, the presence of an armrest tends to increase the injury response at the level of the lower chest band in comparison to the rigid door. This response can be attributed to an earlier time of contact with the thorax due to the geometry of the armrest effectively reducing the door to occupant spacing. Also, the armrest caused the localized deformation of the thorax, therefore resulting in higher levels of compression and VC response. Although the peak VC response observed does not change drastically, the maximum injury was found at the level of the lower chest band when an armrest was present. However, the presence of an armrest tended to reduce the VCmax observed by a maximum of 16% compared to the VC response caused by an intruding rigid door (Figure 17). This shows that door compliance and shape plays a significant role in thoracic response. The VC response of the upper chest band is presented in Figure 18.

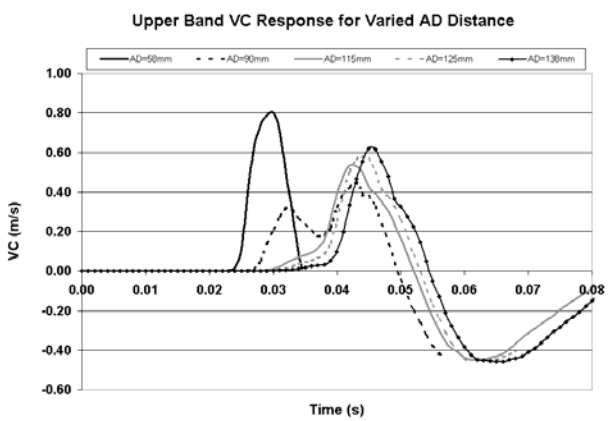

Figure 18 Upper Band VC Response for Varied AD Distance, Deformable Door.

The effect of door to occupant spacing on the thoracic response of an occupant due to an intruding armrest can be explained in a similar fashion to the case of a rigid intruding door previously discussed.

The Effect of Varying Door Intrusion Velocity

Based on information from the literature and the arm to door distance investigation, it is clear that the door interaction with the occupant is an important factor in occupant injury. The occupant to door distance study above showed that the distance was an important factor in determining thoracic response, but the relationship between VCmax and AD distance was not linear. This is largely due to the effects of the velocity profile and variation in contact timing. The following study examines the effect of the velocity profile by varying the first and second peak of the velocity profile by +/- 15% as shown in Figure 19. This velocity profile study was based on the research performed by Morris et al. [10]. As in the previous case study, it was assumed that the velocity profiles applied to the side impact model were independent of occupant positioning.

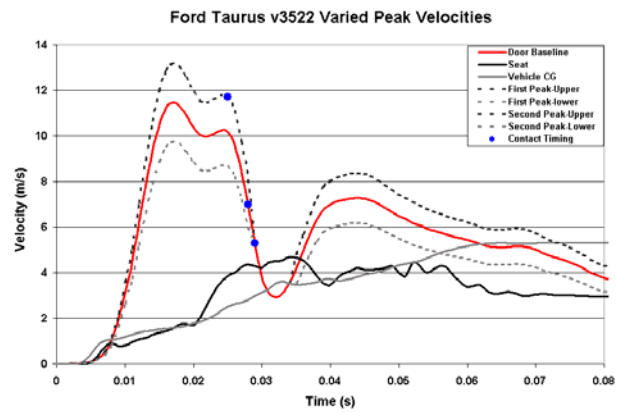

Figure 19 Varied Door Intrusion Velocity Profile & Contact Times.

Figure 20 shows the relationship between injury and velocity profile for variations in first and second peak velocity.

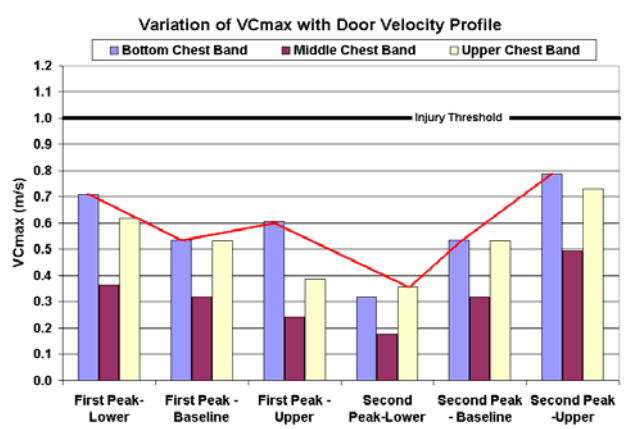

Figure 20 Variation of VCmax with Door Velocity Profile.

The VC responses for the upper chest band are shown below. As expected, the variation in velocity profile has a significant effect on occupant response.

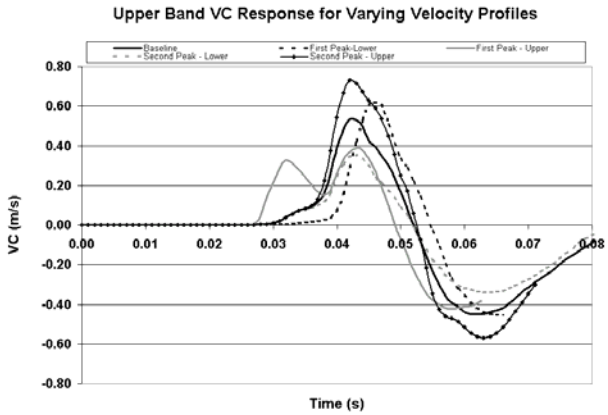

Figure 21 Upper Band VC Response for Varying Velocity Profiles.

Figure 21 shows that the peak VC response in each scenario corresponds in time with the second peak of the door velocity profile. However, varying the first peak had a significant impact on the magnitude of VC response produced by the second peak. This can be explained by investigating the occupant motion relative to the sled base (Figure 22). As it has been shown that VC response was largely dependant on the second peak in velocity profile, increasing the velocity of the second peak would clearly increase thoracic response and a decrease in peak velocity would result in a decreased VC response.

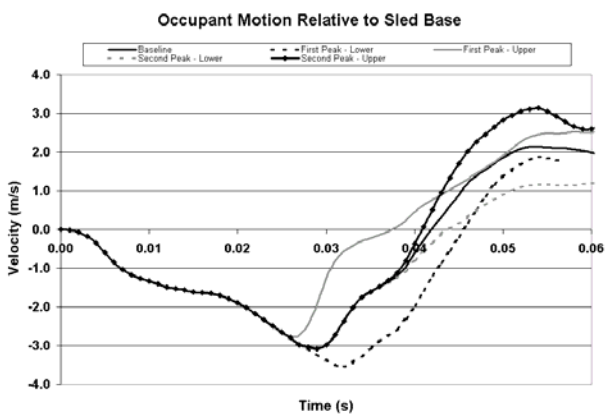

Figure 22 Occupant Motion Relative to Sled Base for Varied Door Intrusion Velocity Profile.

Similar to the previous study on varied AD distance, variation in velocity profile had a somewhat counter-intuitive effect on occupant injury. Although VC response in the current scenario corresponds in time with the second velocity peak for all cases, the first peak directly contributes to the degree at which the second peak influenced VC.

For the baseline case and therefore the cases varying the second peak velocity, the effect of the first peak was the same in terms of chest compression, velocity of compression, VC, and occupant motion relative to the sled base. Since the conditions prior to the second peak were known and constant for the baseline, upper second peak, and lower second peak it was possible to understand the effect of the second peak velocity irrespective of the effects of the first peak. It is clear that the second peak of the door intrusion velocity profile follows conventional expectations, such that an increase in velocity would cause an increase in injury and a decrease in velocity would cause a subsequent decrease in injury.

However, the first peak acts as a means to accelerate the occupant following contact with the door, thereby increasing the occupant velocity and minimizing the impact of the second peak. An increase in first peak velocity would reduce the effect of the second peak, while a decrease in the first peak would increase the influence of the second peak. This effect can be observed by comparing the occupant motion relative to the sled base (Figure 22) and VC response (Figure 21) for the baseline, upper first peak, and lower first peak.

Figure 23 shows that increasing the first peak velocity by 15% can reduce the Upper Band VCmax by 27% and decreasing the first peak velocity by 15% can increase the Upper Band VCmax by 16%. However, increasing the second peak velocity by 15% increases the Upper Band VCmax by 37% and decreasing the second peak velocity by 15% caused a 33% reduction of the Upper Band VCmax.

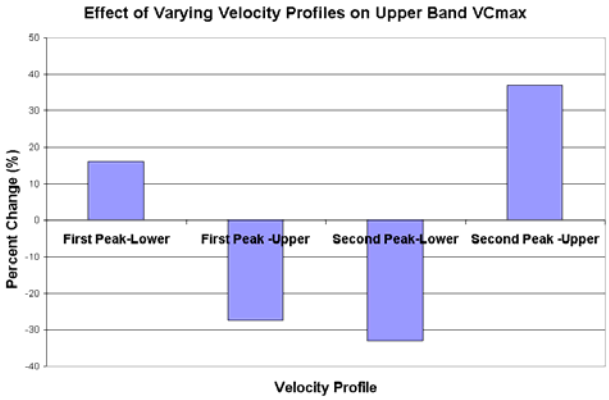

Figure 23 The Effect of Varying Velocity Profiles on Upper Band VCmax.

The middle chest band follows the same tendencies as the upper band in response to varied velocity profiles. However, the response of the lower chest band did not follow the same trend as the middle and upper band for the case of an increase in first peak velocity (Figure 20). This discrepancy was due to the high contact velocity at the lower chest band caused by the reduced door to occupant distance due to the armrest geometry.

As shown in Figure 24, the Lower Band VCmax occurred at the first peak in the response. Although the first peak did not control injury for the middle and upper chest bands in this study, a greater increase in first peak velocity would result in injury being dominated by the first peak, similar to the response of the lower chest band.

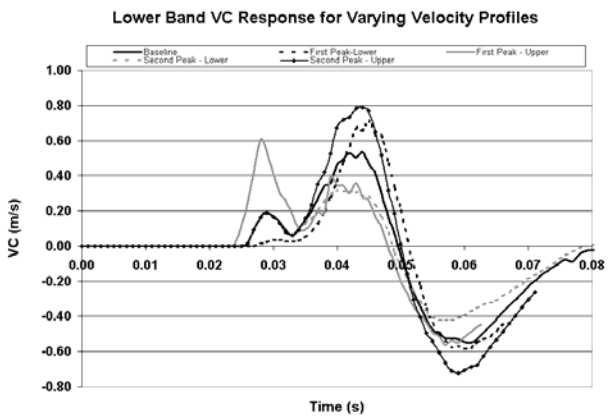

Figure 24 Lower Band VC Response for Varying Velocity Profiles.

The Effect of Varying Seat Foam on Thoracic Trauma

The seat acts as a primary point of interaction between the occupant and the vehicle, although seat foam is predominately used as a means of improving occupant comfort. While the mechanical properties of common seat foams fall within a relatively small range, their impact on occupant injury can be significant despite being largely developed for comfort rather than safety. This study presents the relevance of seat foam in side impact by comparing the occupant response in a seat modeled using a high stiffness (Foam 2) and a low stiffness (Foam 4) foam characterized for varying rates of strain [7,12]. The results are summarized in the bar chart presented in Figure 25.

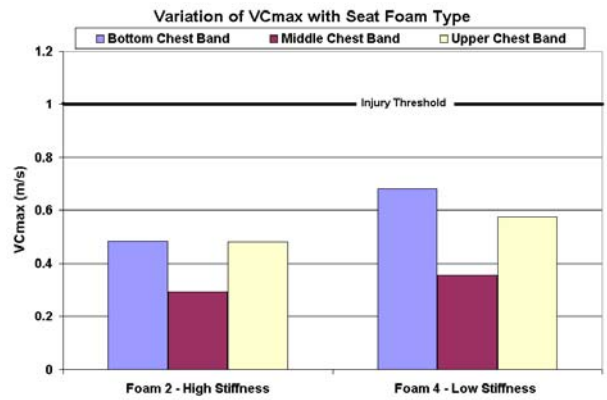

Figure 25 Variation of VCmax with Seat Foam Type.

Despite modest differences in mechanical properties, seat foam clearly plays a significant role in side impact occupant safety. Figure 26 shows that using the low stiffness foam instead of the high stiffness foam caused a 41% increase in the observed VCmax value.

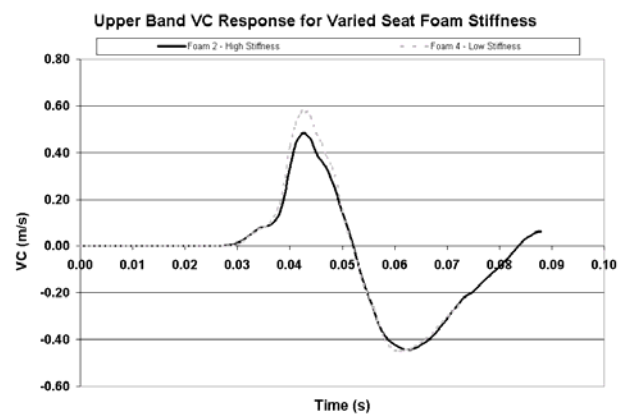

Figure 26 Upper Band VC Response for Varied Seat Foam Stiffness.

The response of the three chest bands were comparable in terms of their shape and timing, however the peak response observed when using Foam 4 was elevated for the compression, velocity, and VC [12]. This variation in response may be explained by comparing the occupant motion relative to the sled for each foam (Figure 27).

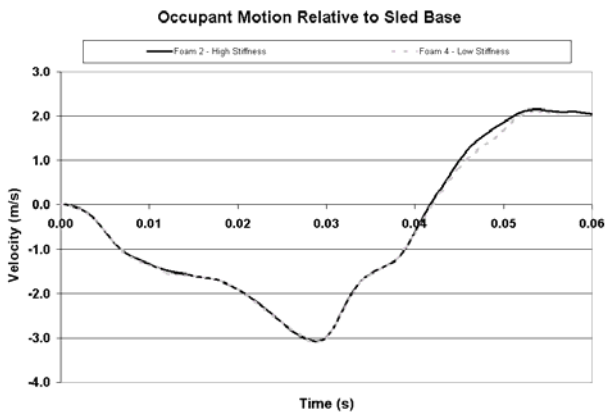

Figure 27 Occupant Motion Relative to Sled Base for Varied Foam Stiffness.

It can be seen that seat foam had minimal effect on occupant motion relative to the sled; however, the minor differences observed translated to considerable differences in thoracic response. A stiffer foam, such as Foam 2 in this case, was more capable of applying a load to the occupant, thus increasing the occupant velocity and reducing the effect of the intruding door.

Although the differences in mechanical properties between the seat foams compared in this study were relatively small the effect on thoracic trauma was noteworthy. Stiffer seat foams and more encompassing side bolsters may have the potential to significantly reduce injury.

The Effect of Restraint Systems on Thoracic Trauma

The effect of restraints on the reduction of occupant trauma in frontal collisions is well-known. However, the effect of restraints in side impact is not as clear. According to a study performed by NHTSA [1], the reduction of fatalities in near-side impacts as a result of restraint systems was a mere 5 percent. In comparison, the fatality reduction as a result of seat belt usage was 39 percent in farside impacts, 50 percent in frontals, and 74 percent in rollovers.

However, because of large variation in crash scenarios it is difficult to quantify the effect of restraints in side impact. The study performed in this section compares the thoracic response of a belted and un-belted occupant under identical crash conditions to determine the effect of restraints. A summary of the results is presented in the bar chart in Figure 28.

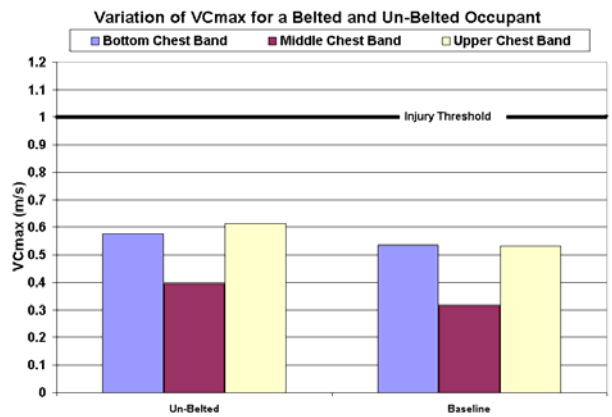

Figure 28 Variation of VCmax for a Belted and Un-Belted Occupant.

The small spacing between the occupant and the intruding door makes energy dissipation difficult and contact inevitable. However, it is clear that the presence of restraints reduces the thoracic response at each chest band level and can reduce VCmax by up to 13% compared to an un-belted occupant.

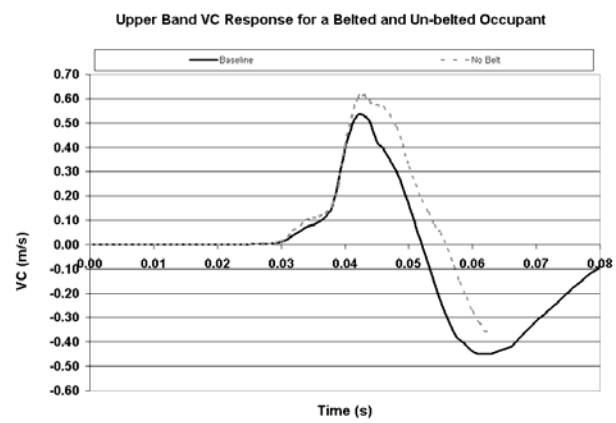

Figure 29 Upper Band VC Response for a Belted and Un-Belted Occupant.

As seen in Figure 28 and Figure 29 the VC response for the un-belted occupant was slightly elevated in comparison to the belted occupant. The modest difference in thoracic response may be explained by investigating the occupant motion relative to the sled base (Figure 30).

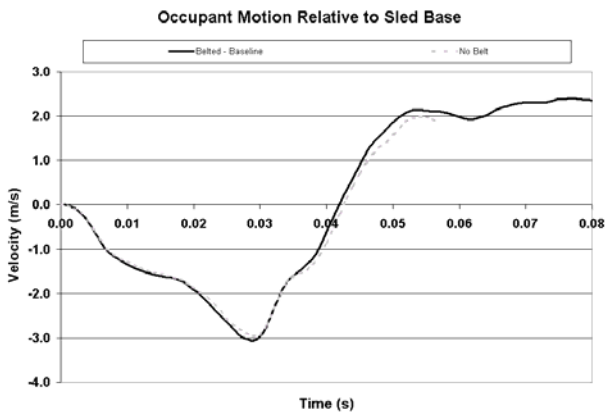

Figure 30 Occupant Motion Relative to Sled Base for a Belted and Un-Belted Occupant.

The presence of a seatbelt accelerates the occupant slightly more than in the case of the un-belted occupant, thereby moderately reducing the impact of the intruding door. It is likely that the increase in occupant velocity relative to the sled base was due to an increased interaction with the seat, facilitated by the restraint system. This displays the modest improvements to thoracic response in side impact collisions as a result of restraint systems.

CONCLUSIONS AND RECOMMENDATIONS

A numerical side impact model has been developed to investigate factors and crash conditions present in full scale crash tests. The model was developed to account for several important factors that contribute to occupant response including the relative velocities between the seat and door, the occupant to door distance, as well as door shape and compliance.

Validation of the side sled model was undertaken by reproducing the crash conditions present in FMVSS 214 and IIHS side impact tests and comparing the thoracic response determined by the model to the response of the ES-2 dummy used in the crash tests. The side impact model was shown to produce *good* to *reasonable* injury response with respect to the full-scale FMVSS 214 side impact test of a Ford Taurus, as well as the IIHS side impact test of a Nissan Maxima.

The side impact model was then used to investigate the effects of door to occupant spacing, door velocity profile, seat foam stiffness, and the use of a restraint system. It was found that injury as predicted by the Viscous Criterion was controlled by both the first and second peaks typically found in door velocity profiles, but the influence of each varied depending on the situation.

The parametric study presented in this paper has provided valuable insight into the factors influencing thoracic trauma in side impact collisions. Clearly, occupant protection in side impact scenarios is a difficult task due to the limited door to occupant spacing associated with lateral collisions. The study performed has shown that thoracic injury was largely dependant on relatively small changes in a number of factors such as AD distance, door intrusion velocity, and seat foam properties.

It has been shown that the presence of a deformable door compared to a rigid door can reduce VCmax by up to 16%, showing that door geometry and compliance plays a roll in safety. Also, it was shown that the shape of the door intrusion velocity profile highly influences thoracic response. Therefore, altering the structural properties of the vehicle to minimize door intrusion or idealize the door intrusion velocity profile may significantly reduce VCmax.

The seat foam study performed has shown that using the low stiffness foam instead of the high stiffness foam can cause a 41% increase in the observed VCmax value. This was based on the investigation of seat foams falling in a relatively limited range of material properties. Clearly, seat foam plays an important role in crash safety and improving side bolsters and increasing foam stiffness may contribute to better side impact safety.

Although the effect of pre-tensioning restraint systems are limited in side impact crash, this study has shown that this can reduce VCmax by improving the contact between the occupant and the seat. The improved occupant to seat contact minimizes the impact of the intruding door by accelerating the occupant with the seat, thereby reducing the relative velocity between the occupant and intruding door. Thus causing a 13% decrease in VCmax in this study.

It should be noted that the current study was limited to velocity profiles obtained from a specific FMVSS 214 test and therefore results and observations are restricted to the confines of the input conditions used. Also, although based on vehicle geometries, the side impact model has been developed using simplified geometries for the seat, armrest, and restraints and may not fully encompass all vehicle designs. However, the side impact model developed is a useful tool for evaluating factors influencing side

impact and can be used to determine occupant response in any side impact crash scenario when the appropriate input conditions are provided.

ACKNOWLEDGMENTS

The authors would like to express their appreciation to General Motors of Canada Limited and the Premier's Research Excellence Award for funding this work.

REFERENCES

[1] NHTSA Side Impact Evaluation, 2004

[2] Forbes, P. A., 2005, Development of a Human Body Model for the Analysis of Side Impact Automotive Thoracic Trauma, MASc Thesis, University of Waterloo, Waterloo, Ontario, Canada

[3] Forbes, P.A, Cronin, D.S., Deng, Y.C., 2005, Multi Scale Human Body Model to Predict Side Impact Thoracic Trauma, IJCrash 2006 Vol 11 No. 3 pp. 203-216

[4] Chang, F., 2001, The Development of a Finite Element Human Thorax Model for Impact Injury Studies, Proceedings of the 2001 ASME International Mechanical Engineering Congress and Exposition, AMD Vol. 251, 2001, pp. 103-111

[5] Aekbote K., Sundararajan S., Chou C.C., Lim G.G., Prater J.A.., 1999, A New Component Test Methodology Concept for Side Impact Simulation, SAE 1999-01-0427

[6] Aekbote K., Sobick J., Zhao L., Abamcyk J.E., Maltarich M., Stiyer M., Bailey T., 2007, A Dynamic Sled-to-Sled Test Methodology for Simulating Dummy Responses in Side Impact, SAE 2007-01-0710

[7] Campbell, B.M., Cronin, D.S., Salisbury, C.P, 2007, High Rate Characterization of Automotive Seat Foams, Society of Experimental Mechanics Conference, Springfield, MA

[8] Deng, Y.C., Kong, W., Ho, H., 1999, Development of a Finite Element Human Thorax Model for Impact Injury Studies, SAE International Congress and Exposition, Detroit, MI, SAE Paper 1999-01-0715

[9] Deng, Y.C., 1989, The Importance of the Test Method in Determining the Effects of Door Padding in Side Impact, Proceedings of the 33rd Stapp Car Crash Conference, 892429

[10] Morris R.A, Crandall J.R, Pilkey W.D., 1998, Multibody Modelling of a Side Impact Test Apparatus, IJCrash 1999 Vol 4 No. 1 pp. 17-30

[11] Payne, A.R., Mohacsi, R., Allan-Stubbs, B., 1997, The Effects of Variability in Vehicle Structure and Occupant Position on Side Impact Dummy Response Using the MIRA M-SIS Side Impact Technique., Society of Automotive Engineers, 970571

[12] Campbell, B.M., 2009, A Numerical Side Impact Model to Investigate Thoracic Injury in Lateral Impact Scenarios, MASc Thesis, University of Waterloo, Waterloo, Ontario, Canada

[13] Deng Y.C., P Ng, 1993, Simulation of Vehicle Structure and Occupant Response in Side Impact, SAE 933125

[14] Du Bois, P.A., 2003, A Simplified Approach to the Simulation of Rubber-Like Materials Under Dynamic Loading, 4th European LS_DYNA Users Conference, Material I

[15] Du Bois, P.A., 2004, Crashworthiness Engineering Course Notes, Livermore Software Technology Corporation

[16] Du Bois, P.A., Generation of Foam Material Input Data for LS-DYNA law 83

[17] Serifi, E., Hirth, A., Matthaei, S., Mullerschon, H., 2003, Modeling of Foams using Mat83-Preparation and Evaluation of Experimental Data, 4th European LS-DYNA Users Conference

[18] NHTSA Website, 2007, http://www-nrd.nhtsa.dot.gov/departments/nrd-11/FEA_models.html

[19] Teng, Tso-Liang, Chang, Kuan-Chun and Wu, Chien-Hsun, 2007, Development and validation of side-impact crash and sled testing finite-element models,Vehicle System Dynamics,45:10,925 — 937

[20] Deng Y.C., Tzeng B., 1996, Side Impact Countermeasure Study Using a Hybrid Modeling Technique, SAE 962413

[21] MGA Research Corporation, Nissan Maxima v3668, 2001, NHTSA

[22] MGA Research Corporation, Ford Taurus v3522, 2000, NHTSA

[23] Samaha R., Maltese M., Bolte J., 2001, Evaluation of the ES-2 Dummy in Representative Side Impacts, Seventeenth International Technical Conference on the Enhanced Safety of Vehicles, Paper No. 486, NHTSA

[24] Lau, I.V., Viano, D.C., 1986, The Viscous Criterion - Bases and Applications of an Injury Severity Index for Soft Tissues, Proceedings of the 30th Stapp Car Crash Conference, 861882

[25] Pintar, F.A., Yoganandan, N., Hines, M.H., Maltese, M.R., et al., 1997, Chestband Analysis of Human Tolerance to Side Impact, Proceedings of the 41st Annual Stapp Car Crash Conference, 973320

[26] Maltese M., Eppinger R., Rhule H., Donnelly B., Pintar F., Yoganandan N., 2002, Response Corridors of Human Surrogates in Lateral Impacts, Proc. Fourty-sixth Stapp Car Crash Conference, pp. 321 351, SAE, Warrendale, PA.

[27] Chung J., Cavanaugh J.M., Mason, M., King, A.I., 1997, Development of a Sled-to-Sled Subsystem Side Impact Test Methodology, Society of Automotive Engineers, 970569

[28] NHTSA Database, 2008

IMPACT AND INJURY PATTERNS IN FRONTAL CRASHES OF VEHICLES WITH GOOD RATINGS FOR FRONTAL CRASH PROTECTION

Matthew L. Brumbelow
David S. Zuby
Insurance Institute for Highway Safety
United States
Paper No. 09-0257

ABSTRACT

Modern vehicle designs tested as part of US consumer information programs achieve high ratings for frontal crash protection. Research is needed to determine how these tests can be upgraded to further improve occupant protection in real-world frontal crashes. The present study is a detailed analysis of real-world cases with serious injuries resulting from frontal crashes of vehicles rated good for frontal crash protection.

Queries of 2000-06 data from the National Automotive Sampling System-Crashworthiness Data System produced 116 occupants meeting selection criteria. These were drivers and right front passengers who sustained serious injuries in frontal crashes despite being coded as belted. Patterns of vehicle impact and occupant injury were categorized and discussed in the context of potential upgrades to current crash tests.

Asymmetric or concentrated loading across the vehicle front often resulted in occupant compartment intrusion and associated injury. However, just as many occupants were in crashes without substantial intrusion and were injured by restraint system forces or impacts with the vehicle interior not prevented by restraints. Crashes producing injury without intrusion involved multiple impacts more than twice as often.

Future test programs promoting structural designs that absorb energy across a wider range of impacts, such as small overlap, could reduce serious injuries in frontal crashes. Further restraint system improvements may require technologies that adapt to occupant and crash circumstances. It is unclear what types of full-scale crash testing would encourage these improvements.

INTRODUCTION

There are two consumer evaluation programs of vehicle frontal crashworthiness in the United States. The National Highway Traffic Safety Administration (NHTSA) assigns occupant protection ratings of 1 to 5 stars for drivers and right front passengers based on vehicle performance in a full-width test into a rigid wall at 35 mi/h (56 km/h). The Insurance Institute for Highway Safety (IIHS) assigns vehicle ratings of good, acceptable, marginal, or poor based on performance in a 40 mi/h (64 km/h) test in which 40% of the vehicle front impacts a deformable barrier. Since these programs were introduced, structural and restraint system designs have improved substantially, and high test performance now is treated as a *de facto* standard. Among vehicles rated in the IIHS frontal offset test between January 2005 and May 2008, 85% received good ratings, with the rest receiving the second highest rating of acceptable. Under NHTSA's frontal New Car Assessment Program (NCAP), 95% of 2008 model year vehicles achieved a 4- or 5-star rating for both the driver and right front passenger [1].

Consumer evaluation programs are most useful when they provide comparative information to those purchasing new vehicles. The consistent good performance under the current test configurations has prompted both NHTSA and IIHS to consider changes to their frontal crashworthiness programs. After researching various alternatives, NHTSA announced plans to keep the full width configuration but use different anthropomorphic test devices (ATDs) and include additional injury metrics [2]. IIHS has conducted pole impact research tests to determine whether this crash configuration poses problems that offset testing does not address. It is important that any test program be driven by the types of crashes occurring in the field so that the design changes the program encourages have benefits in real-world crashes. Studies have found that higher ratings in both NHTSA and IIHS test programs correlate to reduced injury risk [3][4]. To ensure this correlation continues, a better understanding of real-world crashes is needed to support informed decision making for future frontal test programs.

Progress made in improving the vehicle fleet's frontal crashworthiness and the promise of emerging active safety technologies such as electronic stability control [5] have resulted in less focus being placed on further passive safety improvements. Some new passive safety advancements are being developed, such as new

structural designs [6] and restraint systems [7], but the primary focus has shifted toward implementing active safety technologies while maintaining the current level of crashworthiness. However, no combination of active technologies is expected to completely prevent all crashes. A large number of fatal and serious injuries will continue to occur in frontal crashes, and further improvements in crashworthiness will be needed to address them.

The present study provides a new perspective on the frontal crash picture in the United States. Frontal crashes in the National Automotive Sampling System-Crashworthiness Data System (NASS-CDS) that produced fatal or serious injuries to belted front-seat occupants were analyzed with the goal of categorizing them according to potential crash test configurations. For each case, vehicle structure performance and restraint system performance were assessed and compared with injury outcomes. Study findings allowed a more detailed understanding of the types of frontal crashes still producing injuries to occupants protected by modern safety technology and identified some remaining steps that can be taken to improve frontal crashworthiness.

METHODS

The NASS-CDS crash data collection program is conducted and maintained by NHTSA. Twenty-seven teams stationed around the United States investigate a sample of police-reported towaway crashes in their geographic regions. The annual number of total crashes investigated each year ranged from around 4,000 to 5,600 during 2000-06, the years used in the present study. Each case is assigned a sample weight based on its likelihood of being investigated. These weights are intended to allow nationwide estimates from the crash data.

Vehicles selected for analysis received good ratings in the IIHS frontal offset test because this is a design criterion for virtually every new vehicle model and the study objective was to identify crashworthiness issues not addressed by the test. A minimum level of performance in the frontal NCAP test was not required, but all the vehicles in the final sample had 4- or 5-star ratings for both occupants except one, which had a 3-star rating for the driver. Only vehicles of model year 2000 or later were included to capture restraint system changes such as depowered airbags, load-limiting seat belts, and belt crash tensioners. Frontal crashes were defined as those that were coded with primary general area of deformation values (GAD1) of "F" by the NASS-CDS investigators. All such cases were included when a belted outboard front-seat occupant sustained an injury with a severity of 3 or greater on the abbreviated injury scale (AIS $\geq$ 3), unless the only such injury was to the upper or lower extremities. All fatally injured occupants were included regardless of the coded maximum AIS.

Although extremity injuries are not inconsequential, the study objective was to identify the crash configurations that still are producing fatal or potentially fatal injuries. Injuries were categorized by the AIS body regions of head, chest, abdomen, spine, or pelvis.

Detailed reviews were conducted of each case meeting the inclusion criteria in 2000-06 NASS-CDS. Relevant coded variables were included, and crash descriptions, scene photographs, vehicle photographs, and injury diagrams were analyzed. Vehicles and occupants were grouped according to the various criteria outlined below.

Crash Configurations

Study vehicles were assigned a crash configuration based on photographs of damaged vehicle components and the struck object. Beyond the initial "F" code, the collision deformation classification (CDC) assigned by the NASS investigator was not used to designate any of these crash configurations. Instead, the configurations were defined in reference to the longitudinal structures typically designed to manage the crash energy involved in frontal crashes. Differences between CDC and the crash configurations used in this study, as defined below, are discussed later.

Center impact – major load path was between the two main longitudinals; all case vehicles in this configuration struck a pole, post, or tree, but this was not a specific requirement.

Small overlap – major load path was outboard of all major longitudinal structure; deformation of this structure may have occurred but was judged not a major source of energy absorption.

Moderate overlap – major load path was along one longitudinal member and associated structures; offside member may have been loaded, but this either was less substantial, was induced by cross beams connecting the two members, or occurred separate from the initial engagement with the struck object or partner vehicle.

Full width – major load paths were along both longitudinal structural members.

Underride – major load paths were along components vertically above the bumper bar and longitudinals.

Override – major load paths were along components vertically below the bumper bar and longitudinals.

Low severity – minor loading to all structural components; insignificant longitudinal crush, if any.

Nonfrontal/unreproducible – miscoded primary deformation location or extreme crash scenario with limited relevance to general crashworthiness.

The first four crash configurations, illustrated in Figure 1, describe lateral locations of vehicle structures loaded during the crash. In some instances, one of these configurations seemed applicable in addition to either underride or override, so a judgment was made about which configuration was most significant to crash outcome. However, in two cases, a vehicle was assigned the underride configuration in addition to one of the lateral configurations because both appeared to be major factors in producing occupant injury.

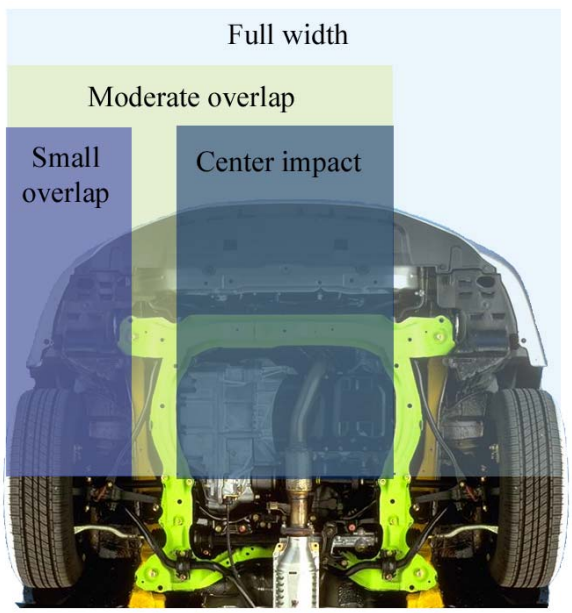

Figure 1. Locations of crash loading for various configurations

Cases categorized as nonfrontals or unreproducible were not analyzed further, as they were not meaningful for evaluating the types of frontal crashes with the potential to be addressed by crash test programs.

Injury categories

Although the crash configurations describe the types of impacts for case vehicles, on their own they do not explain how occupants were injured. The first requirement of a crashworthy vehicle design is a structure that is able to control deformation in such a way that the occupant compartment remains intact. Given sufficient survival space, the second requirement is a restraint system that controls occupant loading to minimize injury risk. In some cases, both of these criteria are met but injury still occurs due to some other factor such as safety belt misuse or loading from an unrestrained rear-seat occupant. To summarize the major factors producing injuries in the crashes being studied, each occupant was assigned to one of four injury categories, as described below:

Intrusion – injuries attributed mainly to compromise of occupant survival space.

Restraint factor – injuries attributed to inability of restraint system to sufficiently control occupant motion or loading; occupant compartment integrity was maintained, but occupant sustained injury either from loading by restraint system itself or from impact with interior component not prevented by restraints.

Occupant factor – occupant behavior or characteristic (e.g., misuse of restraint, loading by another occupant, extreme obesity with use of seat belt extender) likely contributed to injury more than any intrusion or restraint factor; age alone was not considered an occupant factor, but some fatally injured occupants were assigned to this category because they developed postcrash complications that may have been age related, or they had pre-existing health conditions.

Unknown: occupant/restraint – occupant behavior or other characteristic may have contributed to injury, but evidence was unclear; structural integrity was good, but injury still occurred due to restraint factor, occupant factor, or some combination of factors.

RESULTS

There were 116 occupants that met the initial inclusion criteria. In 8 cases, the driver and right front passenger in the same vehicle met the criteria. In one case, occupants of two different vehicles were included.

Twenty occupants were in crash configurations defined as nonfrontal or unreproducible. These cases were removed (see Appendix A), leaving 96 occupants for further analysis. Weighting factors for the remaining cases ranged from 1 to 1,722, with a total weighted count of 6,709. NASS-CDS weighting factors are more difficult to interpret when analyzing smaller case samples. For example, 3 of the 96 occupants studied represented 45% of the total weighted occupant count. To reduce the possibility that any single case could substantially affect the conclusions, only unweighted counts were analyzed.

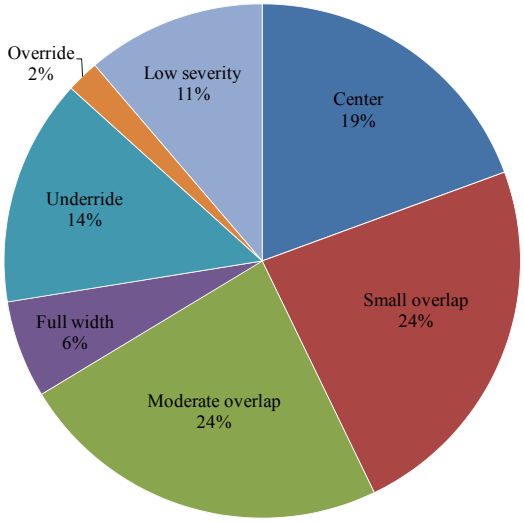

Figure 2. Distribution of crash configurations

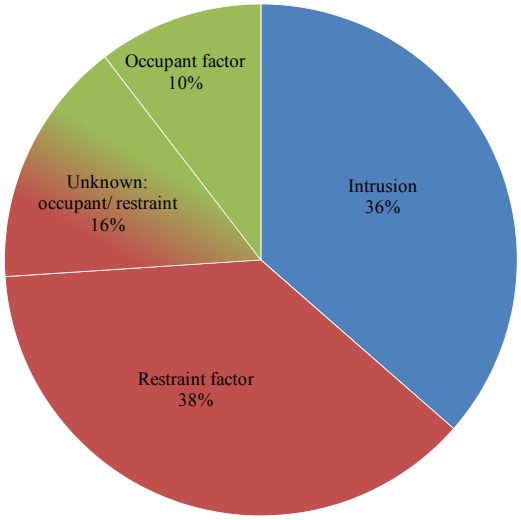

Figure 3. Distribution of injury categories

Figure 2 shows crash configurations for cases involving the 96 occupants. Center impact, small overlap, and moderate overlap configurations represented similar numbers of crashes and together comprised two-thirds of the cases. Underride and low-severity configurations were the next largest categories, together making up one-quarter of the total. Full-width and override configurations comprised the remaining 8% of crashes.

Figure 3 shows the distribution of injury categories. Intrusion and restraint factors each comprised more than one-third of the cases. Occupant factors made up 10% of the cases. For the remaining 16% of cases, it was not possible to determine whether occupant or restraint factors were predominant in causing injury.

Figure 4 shows the different contributions of injury factors for each crash configuration. Intrusion was most commonly related to injury in small overlap and underride crashes. For center, full-width, override, and low-severity crashes, restraint and occupant factors were predominant. Moderate overlap crashes had the most even mix among the various injury factors.

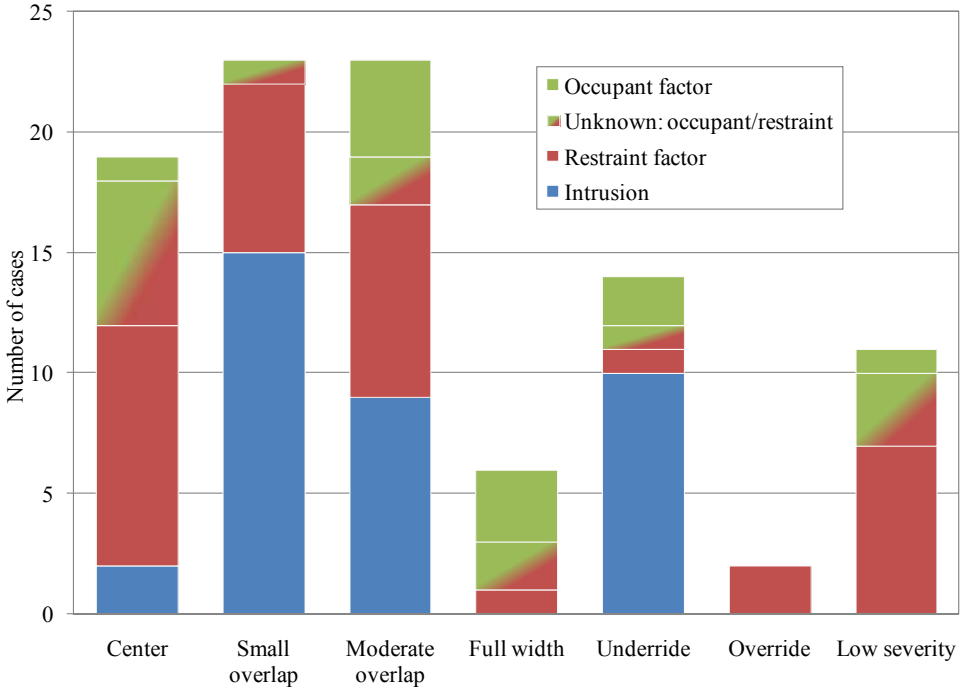

Figure 4. Distribution of injury categories by crash configuration

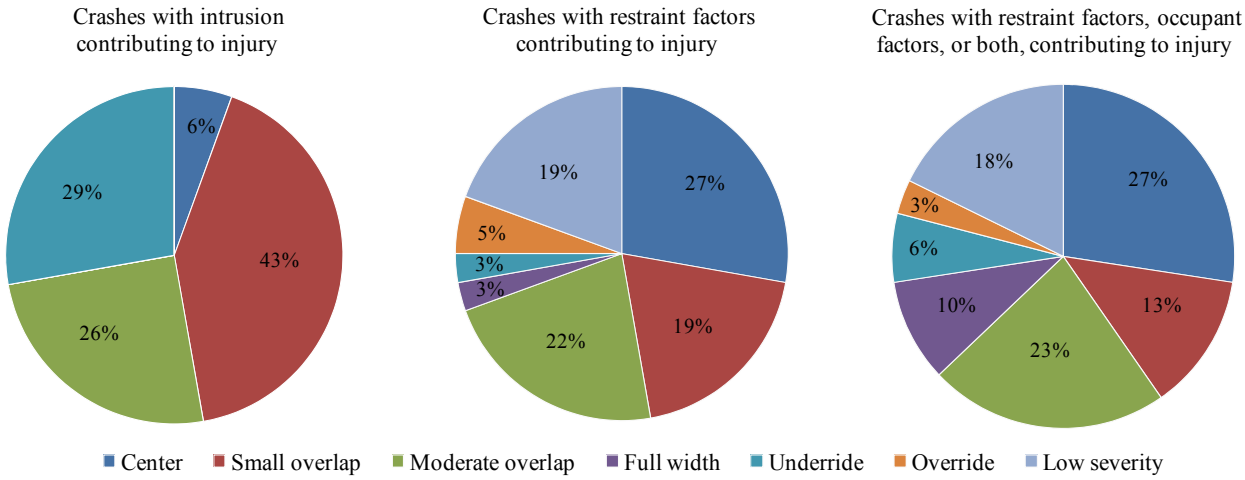

Figure 5. Distribution of crash configurations for various injury groups

Figure 5 shows the distribution of crash configurations for three injury category groups: crashes where intrusion contributed to injury, crashes where restraint factors contributed to injury, and all crashes where vehicle structure performed adequately but injury occurred from any restraint factor, occupant factor, or combination.

Injuries

Of the 96 occupants involved in crashes relevant to frontal crashworthiness analyses, 89 had detailed injury data available. Injury comparisons in this section are based on these occupants. The median injury severity scores (ISS) for occupants in each crash configuration and injury category are shown in Figure 6, with the number of occupants in parentheses. Occupants in underride and override crashes had the highest median ISS, although the override value is based on only two observations. Occupants in low-severity and moderate overlap crashes had the lowest median ISS. For injury categories, median ISS was higher for occupants with injuries attributed to intrusion than for other occupants.

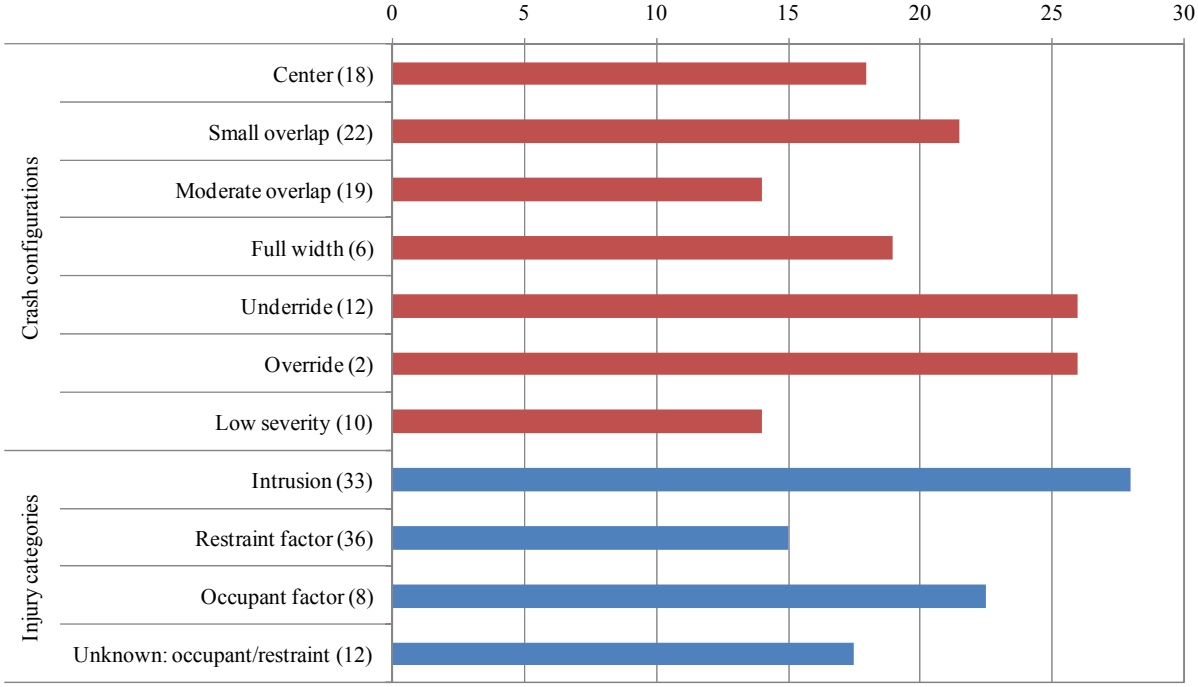

Figure 6. Median injury severity scores for occupants in each crash configuration and injury category, with number of occupants in parentheses

Figure 7 shows the percentage of occupants who sustained at least one AIS ≥ 3 injury to each body region. The chest was the most commonly injured body region at the AIS ≥ 3 level. This was true for the entire sample as well as for the subsamples of occupants in center, small overlap, moderate overlap, and full-width crashes. When injuries were attributed to intrusion or restraint factors, more occupants had serious chest injuries than any other injury type. After chest injuries, a higher percentage of occupants sustained serious injuries to the head than to other body regions. Head injuries were the most common type of AIS ≥ 3 injury for occupants in underride crashes and the second most common in center, small overlap, and moderate overlap crashes, as well as in crashes where injury was attributed to intrusion or restraint factors. Overall, a similar percentage of occupants sustained serious injuries to the abdomen, spine, or pelvis, but there was substantial variation across specific categories.

Many additional observations can be made about this sample of cases. Some of those most relevant to the present study are displayed in Figure 8 and Figure 9. The column names are descriptions of a certain number of cases in each category, not groupings that sum to 100%. For example, 11% of occupants in center impacts were fatally injured, whereas 50% of occupants in underride crashes were killed. The number of cases in each category is given in parentheses. Because there were only two override cases, they were not included in Figure 8.

DISCUSSION

Difference between Crash Configuration Groupings and CDC Values

Methods used in this study provide a more complete picture of factors contributing to crash severities and resulting injuries than can be obtained by grouping crashes according to CDC codes. NASS-CDS investigators assign CDC codes based on evidence of direct damage to any part of the vehicle exterior. This can result in an overestimate of the extent to which structural members were significantly loaded during the crash. Figure 10 shows the distribution of CDC codes for the specific lateral area of damage (SHL1) by crash configuration for the study sample.

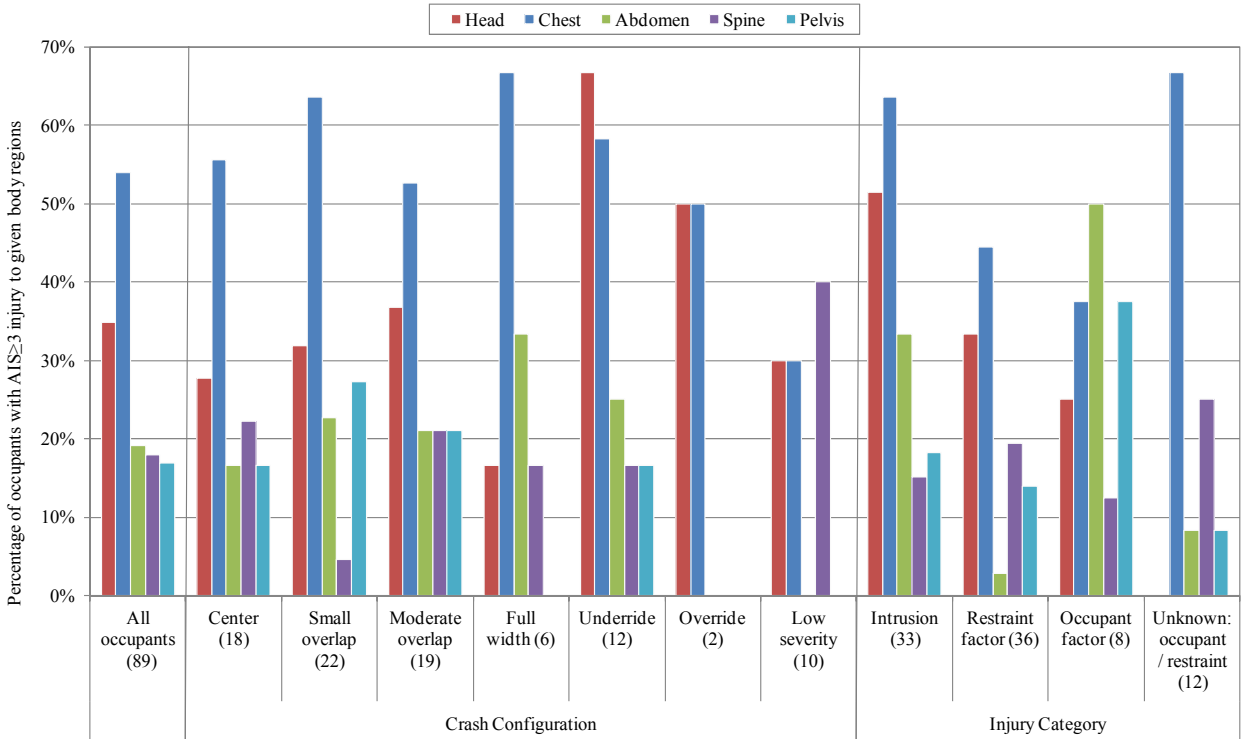

Figure 7. Percentage of occupants with AIS ≥ 3 injuries to given body regions, with number of occupants in parentheses

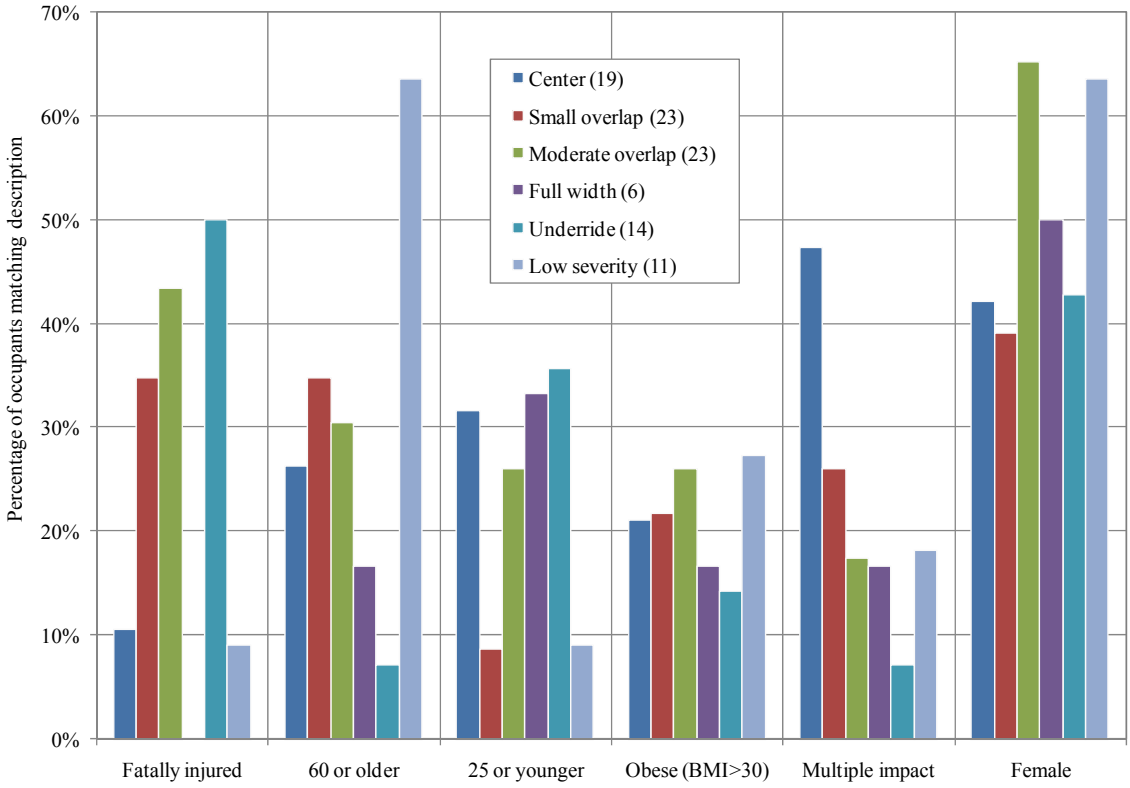

Figure 8. Relevant characteristics for each crash configuration

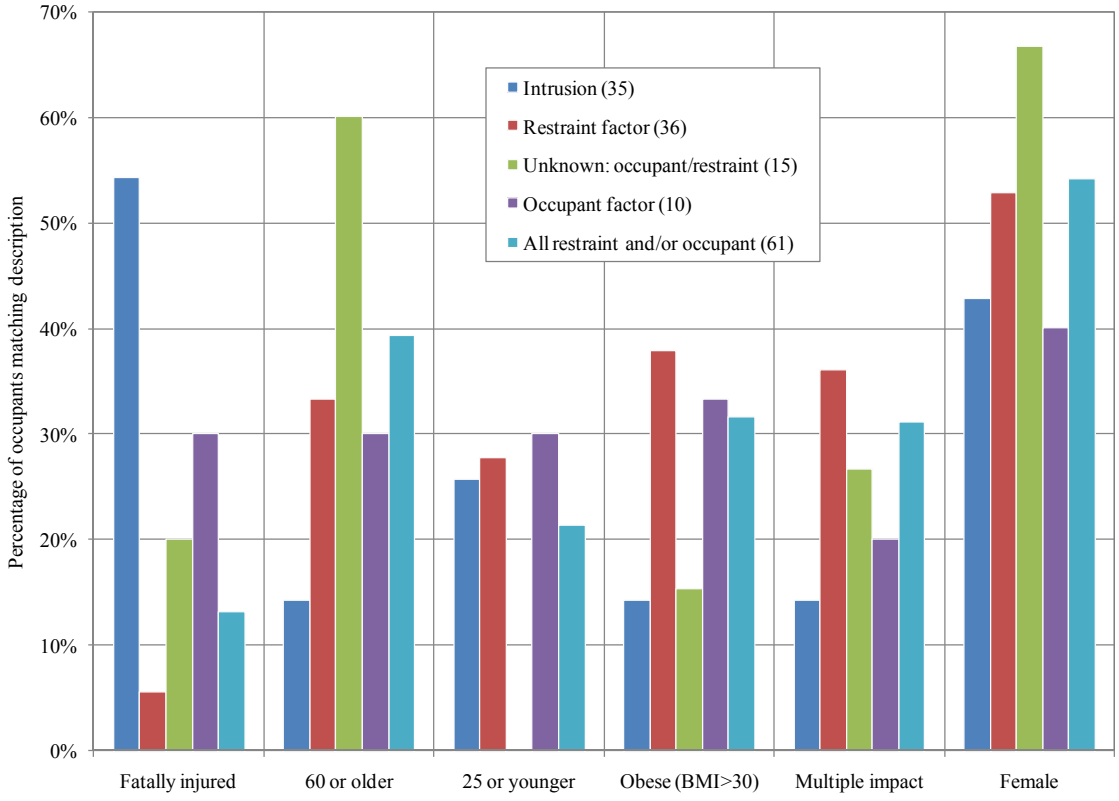

Figure 9. Relevant characteristics for each injury category

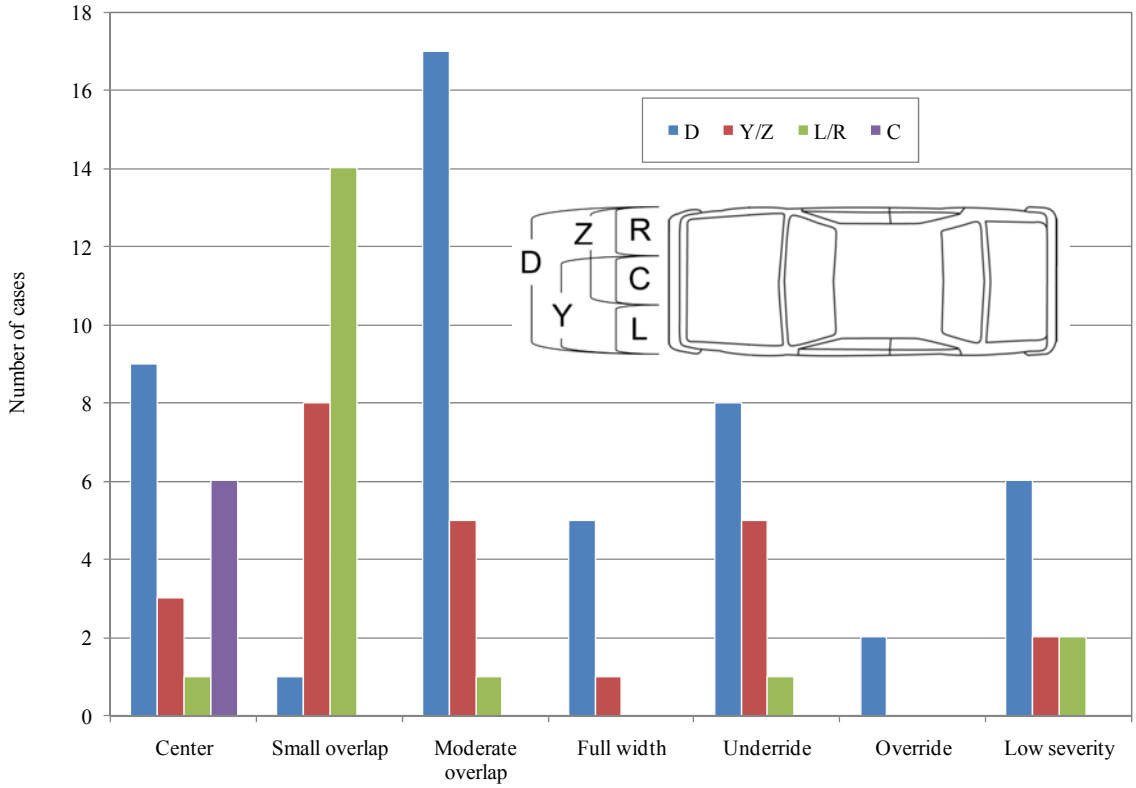

Figure 10. Distribution of CDC SHL1 codes for study crash configurations

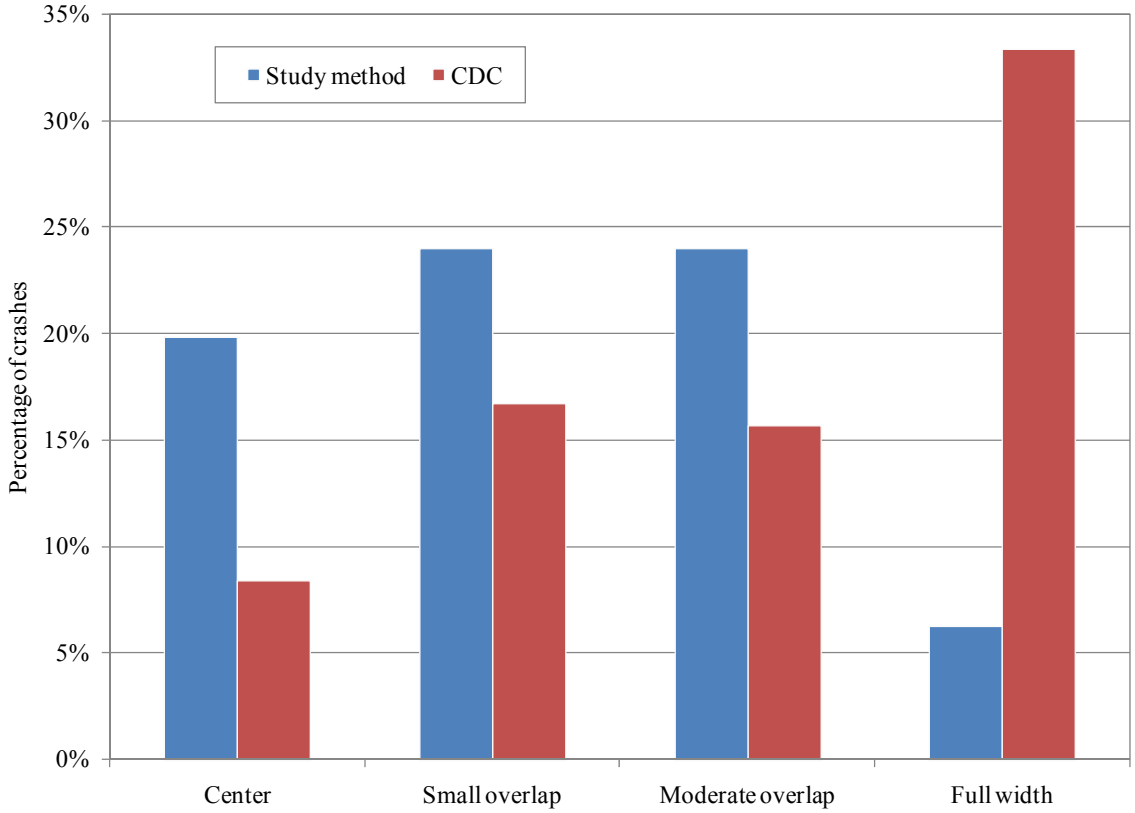

Figure 11. Distribution of crashes for study crash configurations and CDC codes

Figure 11 shows how the crashes in the sample might be categorized according to CDC compared with the configurations using the study methods. Underride, override, and low-severity crashes were removed because CDC codes for vertical area of damage and longitudinal extent of damage had very little correlation with these categories. Center impacts were defined with SHL1 values of C or, if damage distribution was coded as narrow, Y/Z. The remaining Y/Z codes were considered moderate overlap, L/R codes small overlap, and D codes full width. Figure 10 and Figure 11 show that the larger areas of direct damage in CDC can obscure patterns in the structural loading of underlying vehicle components. This is similar to findings by Lindquist et al. [8] who used a different method to study a sample of fatal crashes in Sweden.

Current Crashworthiness Evaluation Programs

Analyzing CDC codes alone could lead to an overestimate of the number of real-world crashes represented by the full-width NCAP test [9][10]. Only 6% of occupants in this sample were in full-width crashes. No occupants were killed, and all vehicles had very little intrusion or none at all. Based on this sample of cases, relatively few restrained occupants seriously injured in frontal crashes are in impacts that resemble the NCAP test configuration.

Moderate overlap is the other crash configuration currently used to evaluate the frontal crashworthiness of the fleet. This configuration was one of the two largest categories of crashes in the sample, even though good performance in the IIHS offset test was an inclusion requirement. However, as shown in Figure 12, one-third of the occupants in these crashes were seated on the opposite side of the impact (i.e., drivers injured in front-right overlap crashes, or passengers injured in front-left overlap crashes). Among occupants seated on the same side as the impact, about half (8 of 15) were in crashes where substantial intrusion occurred, likely contributing to injury. Calculated delta-Vs for these 8 crashes ranged from 70 to 94 km/h. This compares with an average delta-V of 44 km/h for the IIHS test when calculated with the SMASH algorithm used by NASS investigators [11]. The moderate overlap crashes with substantial intrusion in this study all likely were higher speed crashes than the IIHS frontal offset test.

Of the 23 occupants in moderate overlap crashes, 14 were injured due to factors other than intrusion; there appeared to be adequate postcrash survival space for the restraint system to operate. Because the selection criteria for the present study included the requirement that an occupant sustain an AIS ≥ 3 injury, it is unknown how many occupants survived serious moderate overlap crashes without such injury. Nevertheless, the sample suggests that many injuries sustained by restrained occupants in moderate overlap and other frontal crashes can be attributed to the interaction between the occupant and restraint system in the absence of substantial structural collapse.

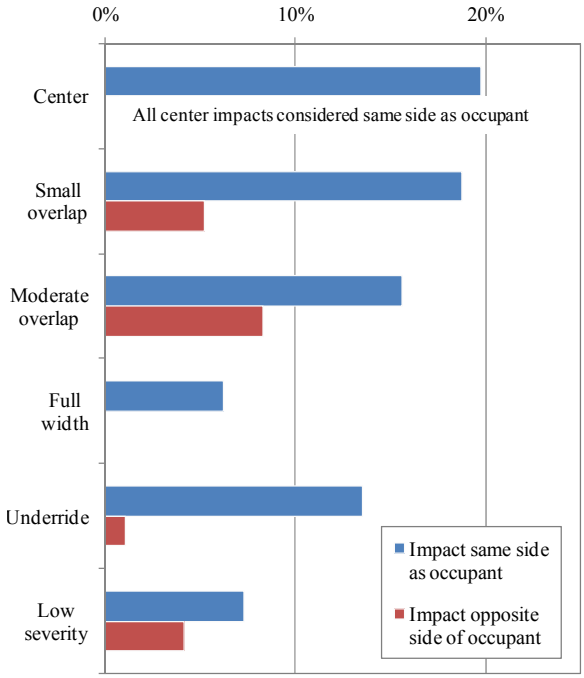

Figure 12. Crash configurations relative to injured occupant's seat position

Potential Future Test Configurations

The test configurations used in the current NCAP and IIHS frontal evaluations represent 22% of the crashes in the study sample (full-width and moderate overlap crashes on the same side as the injured occupant). The remaining crashes warrant further discussion with respect to potential future test programs.

Crashworthiness evaluations must encourage design changes that are beneficial in real-world crashes. It is not obvious from this sample of cases that injuries related to restraint and occupant factors require countermeasures that can be evaluated adequately with current full-scale crash testing. These are cases where the structural design prevented intrusion into the occupant compartment but serious injury still occurred. Figure 9 shows that occupants who were injured due to factors other than intrusion were more than twice as likely to be 60 or older or to be obese (defined as having a body mass index exceeding 30), compared with those injured in crashes with intrusion.

The ATDs currently available have only limited ability to address the unique risks of the populations of older or overweight occupants [12][13]. The most commonly used ATDs represent the 50th percentile male, but more than half of the case occupants injured in crashes without occupant compartment intrusion were female.

An additional consideration is that occupants who sustained injury from factors other than intrusion were more than twice as likely to have been in multiple-impact crashes. These were crashes in which some initial event (e.g., striking a curb, running over a small tree, being sideswiped) preceded the primary impact. Initial events could lead to occupants being out of position for the subsequent crash event, or to airbag deployment in some cases. In many of the multiple-impact cases, overall injury risk may be related less to the specific configuration of the most severe crash event than to the occupant not being in an ideal position for the event.

The center impacts in the sample highlight some of the complications involved in designing future crash test programs. Center impacts were the most common configuration when accounting for the side of the vehicle being impacted (Figure 12). Vehicle structure prevented substantial intrusion in all but 2 of the 19 cases. Because all center impacts were to trees, poles, or posts, they all were off-road crashes, and almost half involved initial impacts preceding the primary crash event. Due to these factors, it is unclear what design changes are necessary to reduce injury risk in center impacts, and whether these changes could be driven by a single standardized laboratory test condition.

Fewer occupants were injured in crashes with substantial intrusion than without (Figure 3). However, when intrusion was a factor in producing injury, the median ISS was higher (Figure 6) and occupants more often were killed (Figure 9). Figure 5 shows that more than 70% of these crashes were either small overlap or underride, with most of the remainder being moderate overlap crashes at higher speeds than the IIHS test speed, as discussed above.

Half of the 14 underride crashes produced fatalities. In 8 cases, underride occurred when the case vehicle struck a medium- or heavy-duty truck or trailer (4 front and 4 rear), suggesting a need for improved underride protection on large commercial vehicles. Federal Motor Vehicle Safety Standards 223 and 224 establish requirements for rear-impact guards on heavy-duty trailers in the United States. However, crash tests showing that underride still can occur with these guards prompted Canadian regulators to develop stricter standards [14]. One case in the present study included on-scene photographs showing that the trailer's guard deformed during the crash and failed to prevent underride. There are no front underride prevention requirements for large trucks in the United States. Research in Europe [15][16] has investigated front underride guards, and United Nations Economic Commission for Europe Regulation 93 contains requirements for such guards [17].

The remaining 6 underride cases in the sample involved impacts with light truck vehicles (LTVs). Three of these were front-to-front crashes. This configuration is being addressed to some extent by manufacturers' voluntary commitment to lower the front-end structures of their LTVs [18]. One of the partner vehicles in the underride cases was an SUV that met the criteria of the voluntary agreement, and occupant compartment intrusion was limited. However, the SUV structure did not actually engage the main longitudinals of the case vehicle, and a higher severity crash may not have been survivable. Vehicles underrode the rear of an LTV in two cases and the side in another case. High-speed compatibility is not being addressed in either of these configurations.

A crash test designed to represent a real-world underride configuration could produce vehicle structures that are compatible with a larger range of partner vehicles, or that reduce the severity of intrusion when there is incompatibility. However, such a test may have only limited effect in the field until there is some improvement in the design and implementation of underride prevention for the fronts, sides, and rears of large trucks, trailers, and LTVs.

The small overlap configuration was the most common among crashes where intrusion contributed to injury (Figure 5) and the second most common in the entire sample when accounting for the side of the vehicle being loaded (Figure 12). Of the 22 small overlap crashes, 19 were impacts with the front or side of another vehicle and 3 were impacts with a pole, post, or tree. When included, delta-V estimates for these crashes likely were inaccurate because they were based on crush measurements taken at the bumper bar, which was loaded very little or not at all.

Currently there are no regulatory or consumer test programs evaluating protection in small overlap crashes. Such a program could result in vehicle design changes that expand the structural protection across the full width of the vehicle. Some occupants in moderate overlap and full-width crashes also would likely benefit from this increased load sharing, as well as occupants in some crashes with CDC codes indi-

cating left or right side impacts where oblique loading leads to some front structure involvement.

Restraint Factor Injuries

Many cases evaluated had little intrusion in the areas of the injured occupants. In 37 of these cases, restraint factors appeared to contribute to injury. It was not always clear exactly how these injuries occurred. In some cases, there appeared to be an injury pattern consistent with belt-induced loading. In other cases, steering wheel deformation or other evidence suggested restraint forces from the airbag and seat belt were insufficient to prevent hard contacts with the vehicle interior. Of 32 drivers with injuries attributed to restraint factors, 10 had evidence of steering wheel loading. However, in most cases it was unclear whether the coded injuries were caused by excessive or insufficient restraint loads. This especially was true for chest injuries, the body region most commonly injured at the AIS ≥ 3 level (Figure 7).

Among occupants injured due to restraint factors, the specific body regions sustaining AIS ≥ 3 injuries varied by occupant age (Figure 13). The biggest disparity was in the distribution of chest and head injuries. Occupants 60 or older more often received at least one serious chest injury than a serious head injury. The opposite was true for occupants younger than 30. Other research has found that belt force thresholds related to chest injury risk vary widely with occupant age [19]. Although not conclusive, the cases analyzed

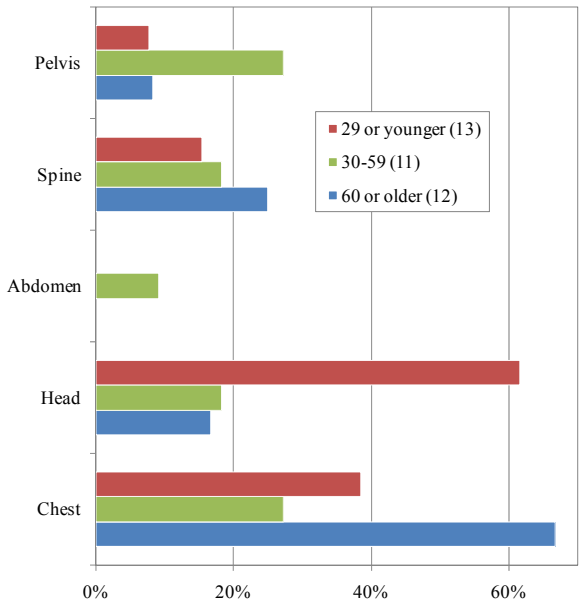

Figure 13. Occupants with AIS ≥ 3 injuries to certain body regions by age for restraint factor crashes

in this study suggest that increasing excursion to reduce belt forces also may have an age-related effect with respect to the occurrence of head injuries.

NASS-CDS contains codes for the sources attributed to each injury by the case investigator. However, there was inconsistency in these codes, and some seemed highly improbable given the loading direction. Often the "source confidence" codes were questionable as well. Many investigators listed the same confidence level for every injury to an occupant, even when more than 20 injuries occurred with a wide range of severities. In some cases, the source confidence was listed as "certain" even though no details of the injury were known. For these reasons, and to limit influence of the differences in the investigators' techniques, the "injury source" and "source confidence" variables were not analyzed for this study.

The crash sample suggests current restraint systems can be improved. Occupants with injuries attributed to restraint factors in the absence of intrusion were involved in multiple impact crashes nearly 40% of the time (Figure 9). If airbags deploy or load-limiting seat belts spool out during initial impacts, occupants may be more vulnerable during subsequent impacts. Even if the initial impact is the most severe, it is possible that a less severe subsequent impact could cause serious injury if the airbag and seat belt no longer offer sufficient protection. Additionally, many occupants in real-world crashes may be loading restraint systems more obliquely than the loading in crash tests. Of the 8 moderate overlap crashes with injuries attributed to restraint factors, 5 were impacts to the opposite side of the front from the injured occupant, and the other 3 were crashes against vehicles moving perpendicularly to the case vehicle.

Study Limitations

A clear limitation of the present study is the sample size. Patterns of crashes and injuries that exist in the sample may vary from the larger population of frontal crashes producing injury in the United States. Additionally, the sample only includes occupants with serious injuries, so there is no way to know the injury risk for the different crash types that have been described. For example, it might be assumed that underride and small overlap crashes have a higher rate of serious injury per involvement than moderate overlap or full-width crashes, but there is no way to determine this with the current dataset.

CONCLUSIONS

The present study analyzes the types of frontal crashes causing serious injuries and fatalities to belted

front-seat occupants in vehicles achieving good performance in current crashworthiness evaluation programs. Potential future test programs are considered by describing the real-world crash configurations in relation to the major longitudinal structures designed to absorb energy in most modern vehicles. Based on this sample, it is apparent that a large number of serious injuries occur in frontal crashes despite good structural integrity. A variety of factors may contribute to injury risk in these cases, such as occupants being out of position due to preceding impacts, loading from other occupants, or restraint misuse. In addition, restraint systems may be unable to adequately balance the need for varying restraint forces based on occupant age, size, and crash severity.

These restraint and occupant factors merit continued research to develop improved countermeasures that adapt to the occupant and crash circumstances and to determine which test conditions would allow meaningful evaluation of the countermeasures. Until this research is complete, it appears more promising for crashworthiness evaluation programs to address the substantial number of frontal crashes that are producing collapse of the occupant compartment and resulting injuries. Small overlap, underride, and high-velocity moderate overlap crashes are the most common configurations producing substantial amounts of intrusion in frontal crashes. Full-scale crash testing may have the greatest potential to improve fleet crashworthiness in small overlap crashes.

ACKNOWLEDGMENT

This work was supported by the Insurance Institute for Highway Safety.

REFERENCES

[1] National Highway Traffic Safety Administration. 2007. Buying a safer car, 2008. Report no. DOT HS-810-872. Washington, DC: US Department of Transportation.

[2] Office of the Federal Register. 2008. *Federal Register*, vol. 73, no. 134, pp. 40016-40049. National Highway Traffic Safety Administration – Final decision notice. Docket no. NHTSA-2006-26555; Consumer Information; New Car Assessment Program. Washington, DC: National Archives and Records Administration.

[3] Farmer, C.M. 2005. Relationships of frontal offset crash test results to real-world driver fatality rates. *Traffic Injury Prevention* 6:31-37.

[4] Kahane, C.J.; Hackney, J.R.; and Berkowitz, A.M. 1994. Correlation of vehicle performance in the New Car Assessment Program with fatality risk in actual head-on collisions. Paper no. 94-S8-O-11. *Proceedings of the 14th International Technical Conference on the Enhanced Safety of Vehicles*, 1388-1404. Washington, DC: National Highway Traffic Safety Administration.

[5] Farmer, C.M. 2006. Effects of electronic stability control: an update. *Traffic Injury Prevention* 7:319-24.

[6] Honda Motor Company Ltd. 2003. Honda introduces new crash compatibility body frame structure that both enhances self protection and reduces aggressivity. Press release. Tokyo, Japan.

[7] Rouhana, S.W.; Bedewi, P.G.; Kankanala S.V.; Prasad, P.; Zwolinski, J.J.; Meduvsky, A.G.; Rupp, J.D.; Jeffreys, T.A.; and Schneider, L.W. 2003. Biomechanics of 4-point seat belt systems in frontal impacts. SAE Technical Paper Series 2003-22-0017. Warrendale, PA: Society of Automotive Engineers.

[8] Lindquist, M.; Hall, A.; and Bjornstig, U. 2004. Car structural characteristics of fatal frontal crashes in Sweden. *International Journal of Crashworthiness* 9:587-97.

[9] Park, B.T.; Partyka, S.C.; Morgan, R.M.; Hackney, J.R.; Lee, J.; Summers, L.; Lowrie, J.C.; and Beuse, N.M. 2000. Comparison of vehicle structural integrity and occupant injury potential in full-frontal and offset-frontal crash tests. SAE Technical Paper Series 2000-01-0879. Warrendale, PA: Society of Automotive Engineers.

[10] Stucki, S.L.; Hollowell, W.T.; and Fessahaie, O. 1998. Determination of frontal offset test conditions based on crash data. Paper no. 98-S1-O-02. *Proceedings of the 16th International Technical Conference on the Enhanced Safety of Vehicles*, 164-84. Washington, DC: National Highway Traffic Safety Administration.

[11] Aylor, D.A.; Nolan, J.M.; Zuby, D.S.; and Baker, B.C. 2006. How the 64.4 km/h (40 mi/h) frontal offset deformable crash test relates to real-world crash severity. *Proceedings of the Second International Expert Symposium on Accident Research* (CD-ROM). Hannover, Germany: Hannover Medical School.

[12] Li, G.; Braver E.R.; and Chen, L-H. 2003. Fragility versus excessive crash involvement as determinants of high death rates per vehicle-mile of travel

among older drivers. *Accident Analysis and Prevention* 35:227-35.

[13] Mock, C.N.; Grossman, D.C.; Kaufman, R.P.; Mack, C.D.; and Rivara, F.P. 2002. The relationship between body weight and risk of death and serious injury in motor vehicle crashes. *Accident Analysis and Prevention* 34:221-28.

[14] Boucher, D. and Davis, B.T. 2000. Trailer underride protection – a Canadian perspective. SAE Technical Paper Series 2000-01-3522. Warrendale, PA: Society of Automotive Engineers.

[15] Riley, B.S.; Penoyre, S.; and Bates, H.J. 1985. Protecting car occupants, pedestrians, and cyclists in accidents involving heavy goods vehicles by using front underrun bumpers and sideguards. *Proceedings of the 10th International Technical Conference on Experimental Safety Vehicles*, 883-96. Washington, DC: National Highway Traffic Safety Administration.

[16] Goudswaard, A.P.; Nieboer, J.J.; and Janssen, E.G. 1991. Truck front underrun protection. *Proceedings of the 1991 International IRCOBI Conference on the Biomechanics of Impacts*, 185- 203. Bron, France: International Research Council on the Biomechanics of Impacts

[17] United Nations Economic Commission for Europe. 1994. UNECE Vehicle Regulations – 1958 Agreement (E/ECE/324, E/ECE/TRANS/505, Rev.1/Add.92); Addendum 92 (Feb 1994) – Regulation no. 93: Uniform Provisions Concerning the Approval of: I. Front Underrun Protective Devices. Geneva, Switzerland. Available: http://www.unece.org/trans/main/wp29/wp29regs81-100.html.

[18] Baker, B.C.; Nolan, J.M.; O'Neill, B.; and Genetos, A.P. 2008. Crash compatibility between cars and light trucks: benefits of lowering front-end energy-absorbing structure in SUVs and pickups. *Accident Analysis and Prevention* 40:116-25.

[19] Foret-Bruno, J.Y.; Trosseille, X.; Le Coz, J-Y.; Bendjellal, F.; Steyer, C.; Phalempin, T.; Villeforceix, D.; Dandres, P.; and Got, C. 1998. Thoracic injury risk in frontal car crashes with occupant restrained with belt load limiter. SAE Technical Paper Series 983166. Warrendale, PA: Society of Automotive Engineers.

APPENDIX A

Cases excluded from injury analysis due to their irrelevance to frontal crashworthiness evaluation programs.

Year	PSU	Case	Details
2002	45	39	Vehicle traveled down slope, pitched downward at impact with trees.
2003	11	18	Oncoming snowmobile became airborne, crashed through windshield.
2004	43	343	(2 occupants) Postcrash fire destroyed vehicle, may have contributed to injury.
2004	45	118	Rollover was most severe event.
2004	72	40	After pole impact, electrical utility box fell from pole through windshield.
2005	9	64	Vehicle struck trees while airborne and pitched forward, involving roof.
2005	49	137	Unreproducible kinematics resulting from three impact events with vehicles, two with poles and an unrestrained rear occupant.
2005	82	18	Vehicle traveled off end of open drawbridge, fell 40 feet to ground.
2006	9	131	Subsequent rollover likely contributed to injury.
2006	11	106	(2 occupants) Vehicle traveled up steep slope to contact underside of overpass.
2006	13	213	Rollover was most severe event.
2006	41	132	Rear impact was most severe event.
2006	43	89	Vehicle traveled down slope, pitched downward at tree impact, involving roof.
2006	50	120	Rollover was most severe event.
2006	75	37	Injury caused by side mirror being knocked through window into driver's face.
2006	76	72	Rollover was most severe event.
2006	81	39	(2 occupants) Subsequent rollover likely contributed to injury.

EVALUTION OF A FINITE ELEMENT MODEL OF THE THOR-NT DUMMY IN FRONTAL CRASH ENVIRONMENT

Costin Untaroiu
Jae Yong Lim
Jaeho Shin
Jeff Crandall
Center of Applied Biomechanics, University of Virginia,
United States

Daniel P. Malone
Rabih E. Tannous
AASA Inc.
United States

Paper Number 09-0272

ABSTRACT

The THOR-NT dummy has been developed and continuously improved by NHTSA to provide manufactures an advanced tool that can be used to asses injury risk in crash tests. With the recent improvements of finite element (FE) technology and the increase of computational power, a validated FE model of the THOR-NT provides an efficient tool for design optimization of vehicles and their restraint systems. The main goal of this study is to assess the current version of THOR-NT FE dummy model in the frontal crash environment. A three-dimensional (3D) FE model of the dummy was developed in LS-Dyna based on the drawings of the THOR-NT dummy. The material properties of the deformable parts and the properties of joints connecting rigid components were derived from the impact test data. To provide validation data for the assembled dummy model, two 40 km/h sled tests were conducted with the dummy restrained by a standard belt system and positioned in a rigid seat with the legs constrained at the knees. The upper body kinematics of the dummy was recorded by means of a 3D motion capture system that tracked the movement of retro-reflective markers attached to the dummy and to the buck. The dummy model fidelity was quantitatively assessed by comparing the displacement time histories of upper body and the reaction forces from the crash simulation with the corresponding data from the sled test. While the relatively low score of the model (0.55 -on a scale from 0 to 1) suggests the need of additional model improvements and validations under different test conditions (e.g., different shapes of deceleration pulses, and initial velocities), its reasonable performance in the direction of sled deceleration during 40 km/h frontal crash event would recommend it for use in impact simulations intended to improve the design of new vehicles and their restraint systems.

INTRODUCTION

Anthropometric test devices (dummies) are frequently used in crash testing to evaluate injury risk for vehicle occupants. The THOR (Test device for Human Occupant Restraint) dummy has been developed and continuously improved by the NHTSA (National Highway Traffic Safety Administration), and has shown improved biofidelity in impact tests relative to the Hybrid III, the dummy used in the current regulations (Shaw et al. 2002). While experiment testing is the current basis of crashworthiness evaluation for new car models, rapid advances in both computational power and crash simulation technology enables the use of a complementary computational component during the manufacturer's design process, especially in the optimization of vehicle components or restraint systems (Untaroiu et al. 2007). In order to provide maximal utility of the dummy model, its kinematical and dynamical predictions must be extensively verified under various crash scenarios before use in the vehicle design process.

The main goal of this study was to evaluate a FE model of THOR-NT Dummy in a frontal impact environment. A crash simulation with the deceleration pulse of a sled test was performed with the THOR-NT FE dummy model and the three-point restraint system positioned in a test setup model developed in LS-Dyna software (vers. 971, Livermore, CA, US). The displacement time histories of several characteristic nodes on the dummy surface (corresponding to the markers used in

testing), and dummy interaction loads with the belt and the sled obtained from the simulation, were compared with test data using objective rating criteria developed in previous studies (Jacob et al. 2000, Hovenga et al. 2004 and 2005). It is believed that the rating methodology and the associated 'objective' values can help identify priorities for further improvements in the THOR-NT dummy model.

METHODOLOGY

The Finite Element Model of the THOR-NT

A three-dimensional finite element model was developed to represent the THOR-NT dummy using the LS-Dyna software package (vers. 971). CAD drawings of the THOR-NT physical dummy were used to construct the geometry of the model. Most head-neck elements (Figure 1) were modeled as rigid bodies except the elastomers (neck pucks and neck bumpers, OC joint stops), the non-linear springs (front and rear spring subassemblies), the foam material (face padding and head skin), and the steel neck cables. The rigid bodies that articulated relative to each other were connected with joint elements. The head-neck FE model was constructed to output equivalent measurements as those recorded in the physical THOR-NT Head-Neck: an upper and lower neck load cell; force in the front and rear spring assemblies; face load cells, and rotation of the OC joint. The completed FE model was correlated with the physical THOR-NT Head-Neck by simulating a head drop test and a frontal flexion test (Malone et al. 2007a).

In the thorax FE model (Figure 2), deformable materials have been used in the following components: elastomer (shoulder and neck bumpers, flex joints, jacket and bib), foam material (upper abdomen and mid-sternum), and the steel (ribs). Joint elements were defined between the articulating rigid bodies and a variety of contact definitions were used to define the interaction between rigid bodies and deformable materials. The thorax FE model outputs the same measurements as the THOR-X CRUX (Compact Rotary Unit), that is deflection units in four locations and one accelerometer located on the Mid-Sternum. The thorax FE model was correlated with the physical THOR-X by simulating two Kroell impact tests, one at 4.3 m/sec and the other at 6.7 m/sec, and comparing to the experimental results. The force deflection curves for impactor force vs. chest deflection derived from the simulation were well correlated with those obtained from experimental data. It was concluded that the FE model can be used to accurately predict the results of physical tests performed with the THOR-X (Malone et al. 2007b).

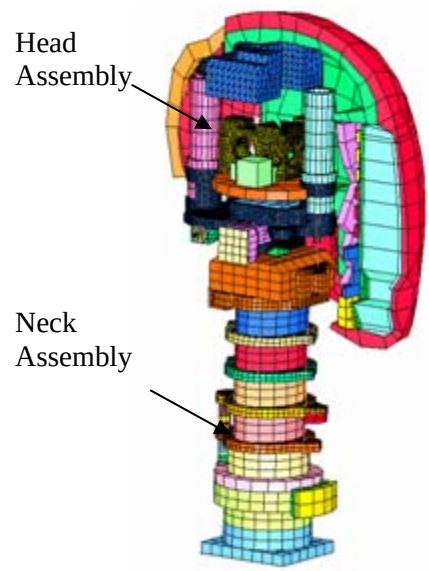

Figure 1. The Thor-NT Head-Neck Assembly

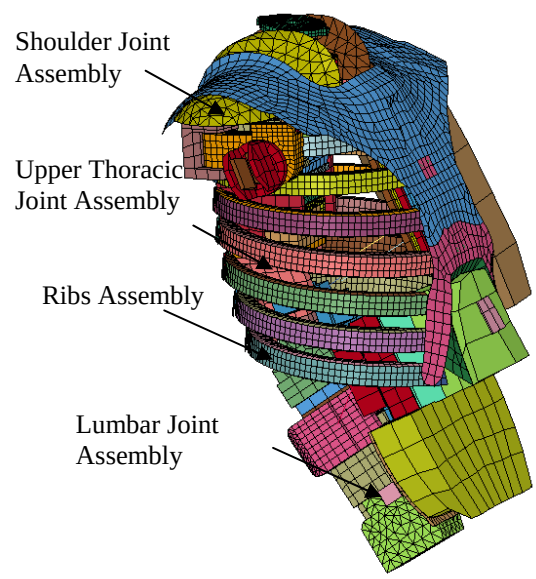

Figure 2. The Thor-NT Thorax FEM

In the lower extremity FE model (Figure 3), the parts defined as deformable were the following: the tibia skin, foot skin, tibia compliance spring, the heel padding/shoe, and the Achilles'cable. To account for the movement of the leg and ankle, one translational joint was created for compression of the tibia and three revolute joints were created to allow movement of the ankle. Stiffness and damping properties were assigned to each of the joints to represent the mechanical properties in the physical THOR-LX. The finite element model outputs the same measurements as the THOR-LX dummy: two

six-axis load cells, two accelerometers, and rotation angles of the ankle. The completed finite element model was correlated with the physical THOR-LX by simulating ten physical experiments and comparing the results (Varellis et al. 2004). Three impacts to the forefoot were conducted to evaluate the dorsi joint performance. Two heel impacts were performed to evaluate the tibia compliance. Three Achilles' tests were conducted to assess the Achilles' cable forces. Two skin tests were performed to determine the effect of the skin on the tibia forces. The time histories of impactor deceleration, load cell forces, joint angles and moments calculated for these tests all compared well to the experimental data. Therefore, it is concluded that the finite element model can be used to accurately predict the results of physical tests performed with the THOR-LX

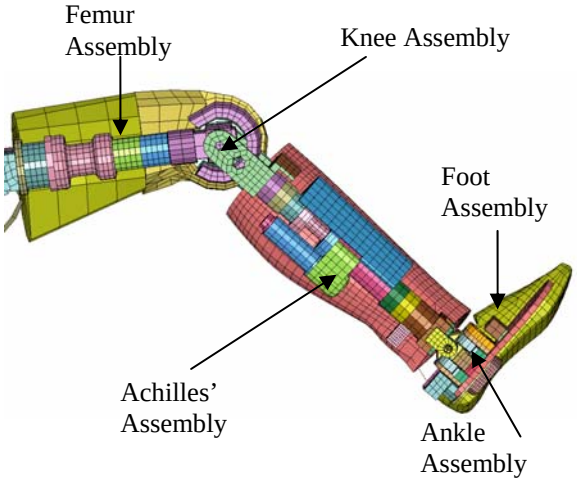

Figure 3. The Thor-NT lower extremity FEM

The THOR-NT FE model (Figure 4) has 329 parts (components) and almost 340,000 elements, majority of them (93%) defined as rigid. The material models and joint definitions used in the FE model can be find in the THOR-NT manuals (Malone et al. 2007a, 2007b, Varellis et al. 2004).

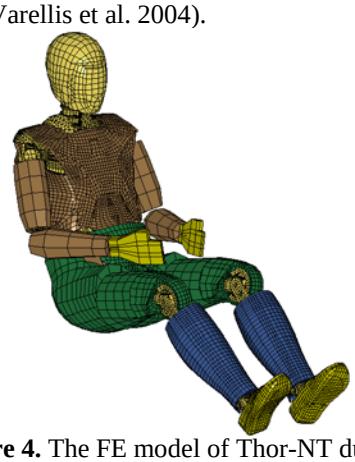

Figure 4. The FE model of Thor-NT dummy

The THOR-NT dummy in frontal crash environment

The THOR-NT dummy was subjected to two 40 km/h frontal sled tests in order to provide test data for the validation of THOR-NT FE model. The dummy was positioned on a rigid planar seat and its torso was restrained by a standard 3-point shoulder and lap belt system (without pre-tensioner an/or load limiter systems). Since the primary goal of this test was the response evaluation of the dummy upper body regions (thorax, neck, and head), additional restraints for the lower regions of the dummy were applied (Untaroiu et al. 2009). A rigid knee bolster was used to restrain the motion of the pelvis and lower extremities, and ankle straps were applied to constrain the feet on a footrest. The dummy was positioned on the seat in a specified posture that approximated the posture of a front seat passenger (Figure 5a). The linear and angular dimensions, that characterize the dummy and belt initial position (e.g. H-point position, lower extremity angles, belt angles) with respect to the sled system, were recorded prior to testing (Table 1). Dummy kinematics were recorded by means of a 3D motion capture system that consisted of 16 cameras (Vicon MX13) arrayed to track the movement of retro-reflective markers attached to the dummy and to the sled buck during the impact event (Figure 5). In addition, load cells were used to record the interaction forces between the dummy and the sled or belt system.

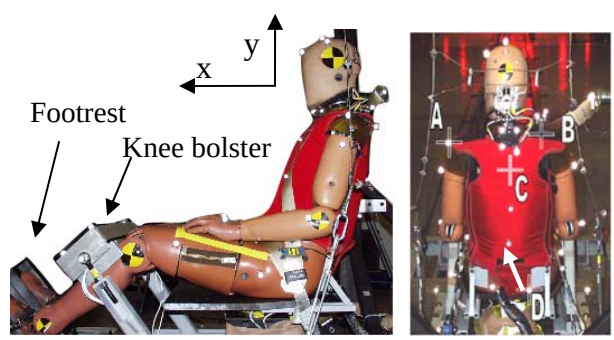

Figure 5. The Thor-NT dummy test setup. The Vicon marker positions A) Left shoulder, B) Right shoulder, C) Upper spine, and D) Lower spine.

Table 1. Initial posture setup

Measurement	Test	FE
Belt angle (deg)	24.9-25.2	25.7
Sternal angle (deg)	66.2-67.6	68.9
Femur angle (deg)	6.4 -7.1	6.6
Tibia angle (deg)	34.7	40.6

The frontal crash test was simulated in the LS-Dyna software (ver. 917, Livermore, CA, USA) using THOR-NT dummy FE model and the FE model of the test setup developed using the sled CAD design (Figure 5b). The dummy and the finite element (FE) belts were positioned based on the corresponding data recorded prior to the test. FE belts were modeled with quadrilateral elements which have been assigned a material model with tensile force-deflection characteristics determined from testing (6-8% elongation, 6000 lbf minimum tensile strength). A set of the nodes corresponding to locations of Vicon markers used in testing was defined, and their trajectories were calculated during the crash simulation. Since the dummy feet were tied to the footrest using straps during the tests, a tied contact was defined between the nodes corresponding to the FE models of shoes and the foot rest in the FE simulation. Surface-to-surface contacts were defined between each leg and the knee bolsters, and between the seat belts and thorax. The time histories corresponding to these contacts were calculated during the impact simulation.

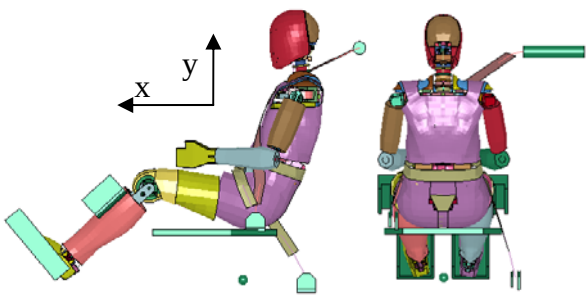

Figure 6. The Thor-NT FE model in pre-impact position

The crash was simulated by applying the time history of linear buck acceleration recorded in Test 1 to the sled model along the x-direction (Figure 7) and constraining the sled motion in all other directions.

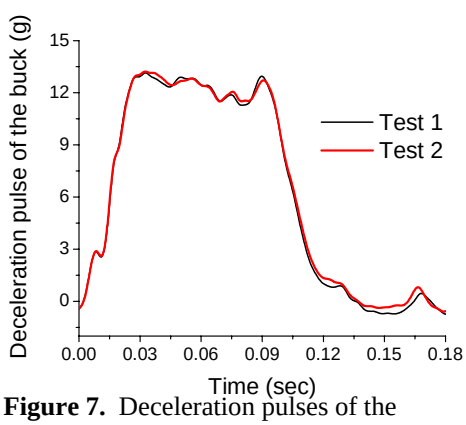

Figure 7. Deceleration pulses of the sled tests

The evaluation of THOR-NT FE model response in frontal crash environment using objective rating methods (ORM)

Continuous development of crash simulation technology considerably increases the utility of virtual testing for the development of restraint systems. However, a dummy model must be evaluated relative to test data before using in crash applications.

Traditionally, model evaluations have been performed by comparing the peak values of the test and simulation data, by evaluating the overall curve shapes qualitatively, or by satisfying several certification guidelines. Recently, there have been several efforts (Jacob et al. 2000, Hovenga et al. 2004, and 2005) focused on developing systematic methodologies for model evaluations, especially in a crash event where a large number of channels must be compared. Based on the characteristics of the data channel to be evaluated, Jacob et al 2000 developed four different methods: the Global Evaluation Method (GEM)- for "normal" channels, the Threshold Evaluation Method (TEM) – for "poor interest" channels, the Criterion Evaluation Method (CEM) – for "criterion" channels. and Limit Evaluation Method(LEM) – for corridor data. In each of these methods, specific criteria were defined based on the local and global characteristics of the test curves. Hovenga et al. 2004 suggested three criteria for evaluating the similarity of the two curves: the peak criterion, the peak-timing criterion, and the Weighted Integrated Factor (WIFac). The first two are the methods in which scalar values, simply the peak values or the times to the peak values from both the simulation and test, are compared. The similarity of overall shapes from two curves is compared by WIFac, defined as:

$$C_{WIFAC} = 1 - \sqrt{\frac{\int \max\left(\left|f(t)\right|, \left|f^*(t)\right|\right)\left[1 - \frac{\max\left(0, f(t) f^*(t)\right)}{\max\left(f^2(t) f^{*2}(t)\right)}\right]^2 dt}{\int \max\left(\left|f(t)\right|, \left|f^*(t)\right|\right) dt}} \quad (1)$$

where $f(t)$ and $f^*(t)$ are the time histories of the experimental signal and the simulation signal, respectively.

In our study, the load signals and the displacement signals that recorded peaks values exceeding 40 mm (in absolute value) in testing were considered as "high interest" channels and were calculated as a linear combination of the peak criterion C_p, the peak to time criterion C_{p_time}, and the WIFac.

$$C_{channel}^{high} = w_p C_p + w_{pt} C_{p_time} + w_{wh} C_{WIFAC} \quad (2)$$

where the peak criterion C_p and the peak to time criterion C_{p_time} were defined as in Jacob et al. 2000.

$$C_p = 1 - \frac{\left| f_p - f_p^* \right|}{f_p} \quad (3)$$

$$C_{p_time} = 1 - \frac{\left| t_p - t_p^* \right|}{\Delta t_{ref}} \quad (4)$$

where $\Delta t_{ref} = 0.4 \cdot \Delta t_{eval}$ (Jacob et al.2000)

The peak criteria was considered the most important followed by the peak time criteria and WIFac and have been assigned the following weighting factors: $w_p = 0.5;\ w_{pt} = 0.3;\ w_{wh} = 0.2;$

The TEM ((Jacob et al. 2000) was used for the displacement signals that recorded low peak displacements in testing (under 40 mm in absolute value). The channels included in this category were the following: z-displacement of upper spine marker, and y and z displacements of pelvis and lower spine. This method just evaluates how much the signal of the model stays within a prescribed corridor defined based on its maximum values (Figure 8). First criteria of this method was defined based on maximum value of the signal with respect to the threshold

$$C_{v_th} = 1 - \frac{\max\left(\left|\Delta V_j\right|\right)}{\max\left(\left|Threshold\right|\right)} \quad (5)$$

where $Threshold = 1.5V_m$ ((Jacob et al. 2000)

The second criterion used by this method is defined based on the time the signal remains in the corridor as:

$$C_{t_th} = 1 - \frac{\sum \Delta T_i}{\Delta t_{ref}} \quad (6)$$

where $\Delta t_{ref} = 0.4 \Delta t_{eval}$ (Jacob et al. 2000)

The total score of the "low interest" channels was calculated as a linear combination of both criteria

$$C_{channel}^{low} = w_{v_th} C_{v_th} + w_{t_th} C_{t_th} \quad (7)$$

The total score of the displacement of each marker was computed as a weighted average of all cartesian displacements as:

$$C_{ch} = w_x C_{ch_x} + w_y C_{ch_y} + w_z C_{ch_z} \quad (8)$$

The score in the direction of deceleration was considered the most important with a weighting factor $w_x = 0.7;$ the weighting factors of other two cartesian scores were defined as $w_y = w_z = 0.15;$. The kinematic and load scores of the model were defined as the average of markers scores and the load scores, respectively.

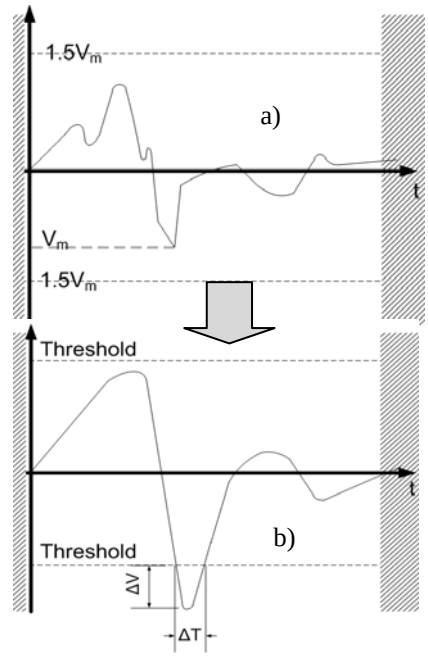

Figure 8. Schematic diagram of TEM criterion a) threshold line setting from the test results and b) procedure of TEM scoring

RESULTS

Since a good repeatability was observed between tests in term of the time histories of buck pulse deceleration (Figure 7) and the dummy kinematics (Figure 9), the simulation results were compared with data from only one test (Test 1). A qualitative comparison between the relative motion of the dummy with respect to the buck and corresponding data predicted using the THOR-NT FE model was performed at different time steps (Figure 10). The time histories of marker displacements along each coordinate axis obtained from the analysis of the Vicon data were compared to the similar data obtained from tracking a set of dummy nodes located at the positions of photo-target markers (Figure 11).

Two significant time intervals can be observed in the dummy motion during the frontal crash test. First, the dummy has an almost translational motion under the inertia forces generated by the deceleration pulse until about 60 ms. In this phase, the thorax rotates slightly in the sagittal plane and the dummy spine becomes almost vertical at the end of 60 ms. In the second phase, the dummy thorax begins to rotate in the transverse plane toward

the right side in addition to continued anterior motion (along to the deceleration direction). The neck-head and upper extremities assemblies begin to move forward relative to the thorax (restrained by the shoulder and lap belts) to almost horizontal positions at the end of the simulation (120 ms).

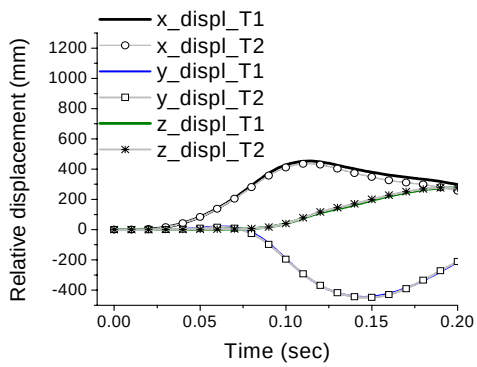

Figure 9. Comparison between the dummy head displacements relative to the buck recorded in testing

In the frontal crash FE simulation, two specific time intervals can be delimitated in the motion of THOR-NT FE relative to the buck as well. As in testing, the model demonstrates a translational motion until 60 ms. The time histories of displacements along the direction of deceleration (x-axis) predicted by the THOR-NT FE model were almost identical to the corresponding data recorded in testing (Figure 11 a-b). However, several differences start to occur in the time histories of the right shoulder and the pelvis x-axis displacements (Figure 11 c, f) which are lower and respectively higher than the corresponding test data due to the sagittal rotation observed in testing, but not in the FE simulation. Time histories of contact forces at the knee bolster and footrest predicted by the FE model are in good agreement with test data, except a region around 40 ms when high force spikes occur in the knee bolster force and a drop in footrest force (Figure 12 d-f). In the second part of the crash (after 60 ms), all time histories of the x-displacement predicted by the model show similar trends to the test data, but differences occur in the peak levels of this data, due to the inability of the THOR-NT model to replicate the sagittal rotation of the dummy spine observed in testing. The Thorax model exhibits mostly translational motion, as observed in the low levels of maxima (20 mm) of time histories of y and z displacements of thorax and pelvis markers, except for the right shoulder where the attached marker showed displacements similar to the test data along the z-direction, but generated much lower values in the y-direction (Figure 11 c).

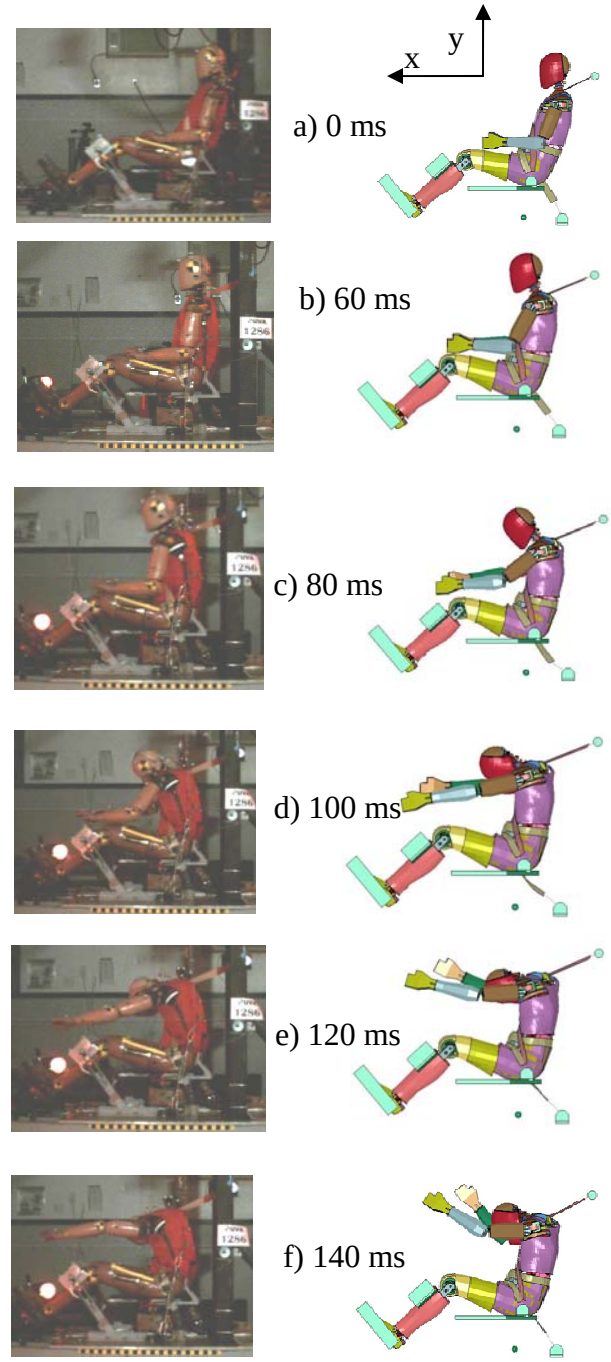

Figure 10. The overall dummy kinematics in frontal sled test. Comparison between test and FE simulation

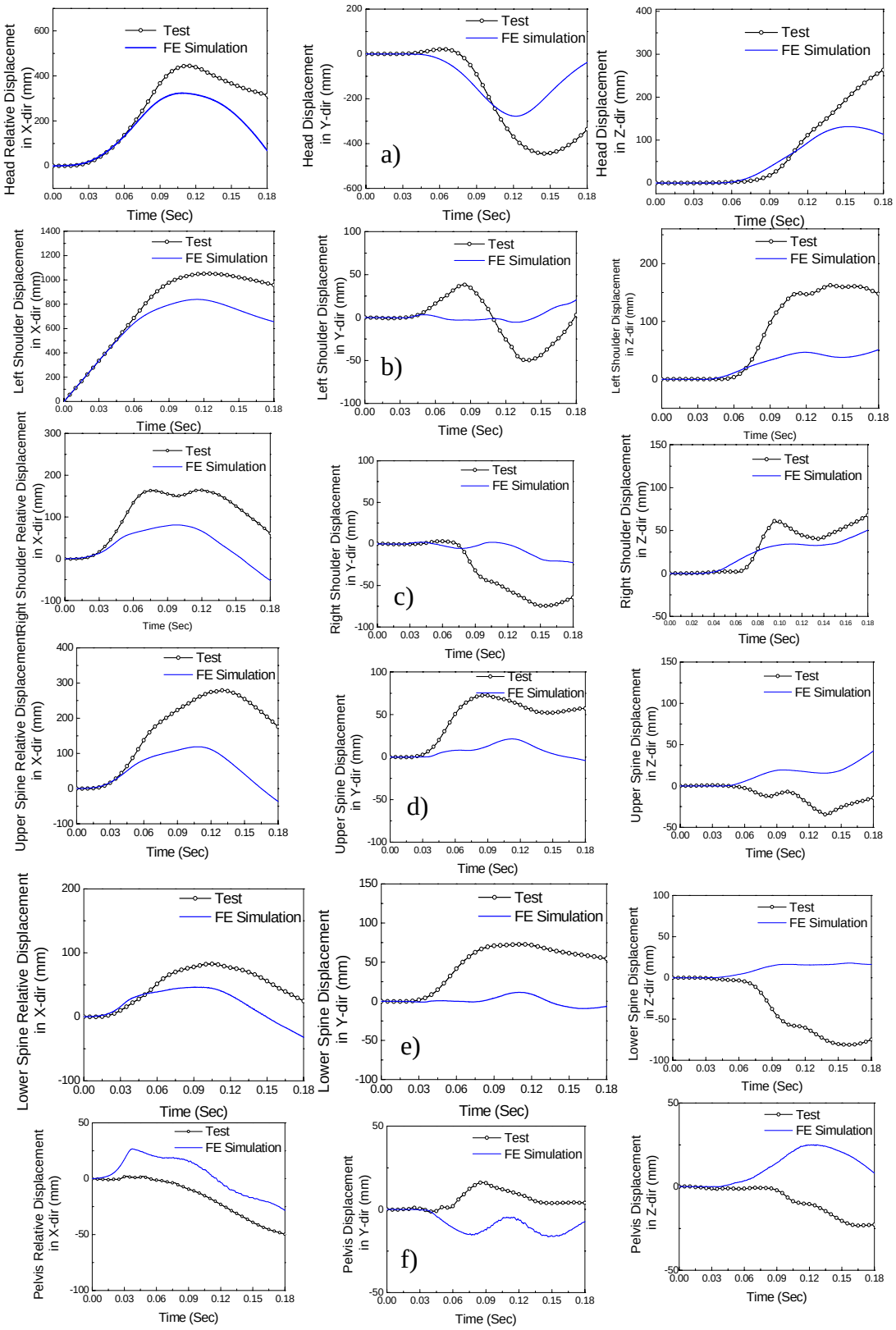

Figure 11. The time histories of marker displacements a) head, b) left shoulder c) right shoulder d) upper spine e) lower spine and f) pelvis

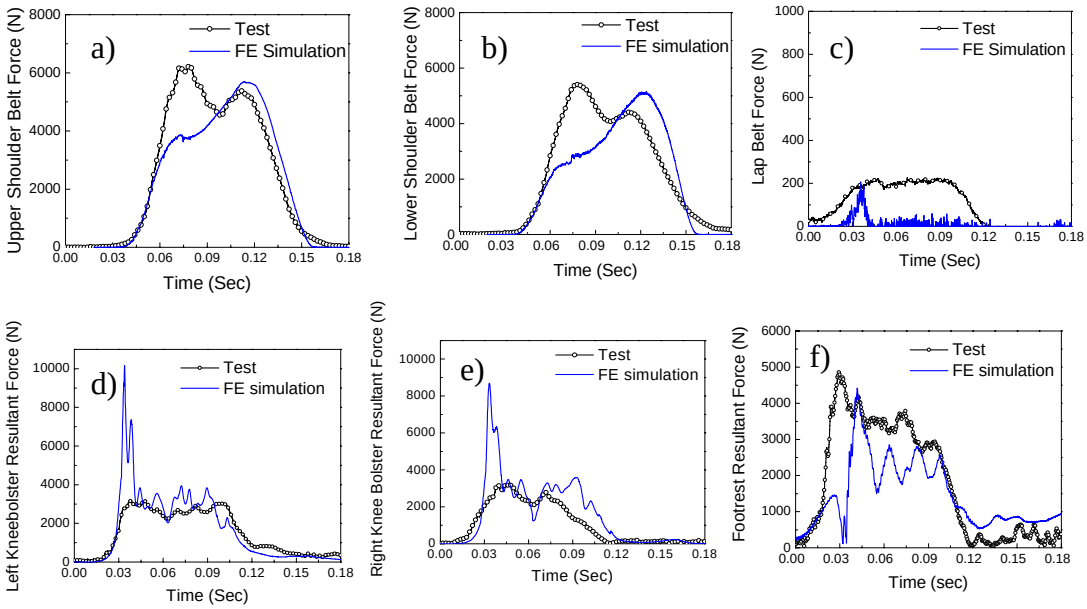

Figure 12. The time histories of resultant force in a)upper shoulder belt, b) lower shoulder belt c) lap belt d) left knee bolster e) right knee bolster f) footrest

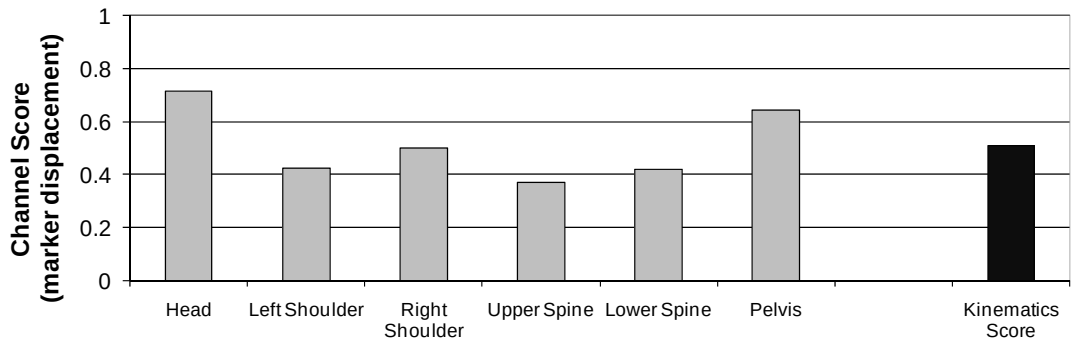

Figure 13. The channel scores of the time histories of marker displacements

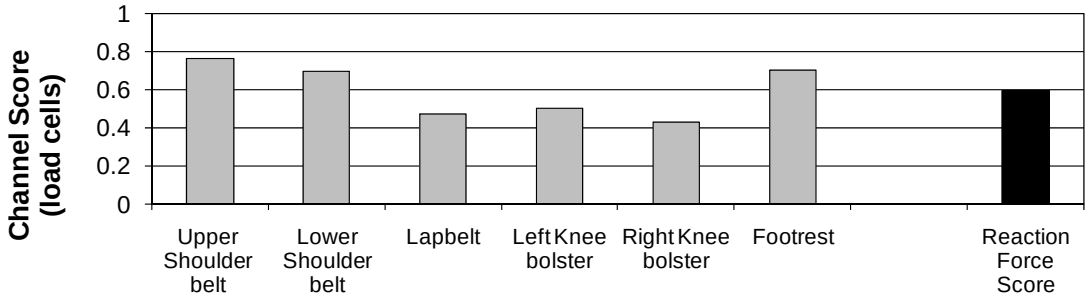

Figure 14. The channel scores of the time histories of reaction forces

The time histories of the shoulder belt loads recorded during testing showed a bi-modal trend with maximum values around 6.2 kN and 5.6 kN at the upper location and lower location, respectively. A diminished bi-modal trend was observed in the shoulder belt forces predicted by the model, and the maximum values were recorded on the second peaks instead of the first ones as in testing (Figure 12 a-b). While an almost constant load (0.2 kN) was recorded in the lapbelt in testing, the load belt was almost negligible in the simulation after a 0.2 kN peak at about 35 ms. (Figure 12 c). Reasonable correlation between test and simulation was observed in the time histories of resultant force in the dummy contacts with knee bolsters and the footrest during the second part of the crash simulation (Figure 12 d-f).

The rating scores of each marker displacement (Figure 13) and loadcell channels (Figure 14) were calculated using the procedure explained in the previous section. The displacement of head marker recorded the highest kinematic score (0.71) and the upper spine the lowest (0.37). The highest loadcell score was calculated in upper shoulder belt (0.76) and the lowest in right knee bolster (0.43). The average kinematics and loadcell scores were 0.51 and 0.59, respectively.

DISCUSSION

This study presents a multifaceted assessment of a FE model of THOR-NT dummy in a frontal crash environment. In addition, to visual comparison of dummy kinematics used mainly in all previous validation studies (e.g. Dsouza and Bertocci 2009), a new quantitative kinematics comparison was introduced. This new approach employed the displacement time histories of retro-reflective markers attached to specific dummy body regions, which were recorded during a frontal crash event by an array of 16 Vicon cameras. These tri-dimensional measurements recorded with a high measurement precision (under 1 mm) help to better understand the complex interaction of the dummy with the restraint systems and test setup and allow a quantitative comparison with similar data calculated easily by computer models. In addition, to the kinematics component, load time histories in belts (shoulder and lapbelt) and in the lower limb contacts with the test setup were measured and compared with the FE model predictions.

Although the numerical simulation showed a reasonable qualitative correlation with testing in terms of overall motion of the dummy relative to the test setup, some discrepancies were observed in the time histories of marker displacements and the external loads (belts and test setup). In addition to the forward translation along the direction of deceleration pulse, the thorax of THOR-NT dummy recorded two significant rotations in sagittal and transverse planes. The FE simulation predicts well the forward motion of the dummy, but not the levels of thorax rotations. While the causes of these un-correlations are still unknown, it is obvious that these causes are internal, due to the THOR-NT dummy FE model, or external, due to a poor replication of the dummy-test setup interaction.

The dummy Thorax FE model was developed according to CAD drawings of the THOR-NT physical dummy and its components were assumed either deformable or rigid. While deformable parts require to be assigned material properties, the rigid parts are connected by defined joints which required structural properties (e.g. moment vs. angle). Both material and structural properties are generally strain rate dependent. The deformable parts (e.g. foam and rubber) were usually defined based on force vs. deflection curves recorded in tension and compression at discrete strain rates (using Mat 181 in Ls-Dyna). More material characterization tests, in different loading conditions (e.g. shear tests, more strain rates) and then material parameter identifications using optimization techniques (Untaroiu et al. 2007) would improve the accuracy material properties of deformable parts. In addition, validations of the upper thoracic and lumbar joints, and then of the whole thorax against tests more appropriate to the frontal crash test than the Kroell tests (e.g. dynamic belt tests – Kent et al. 2004) would certainly increase the capability of Thorax FEM to replicate the dummy response.

The external causes of test-simulation un-correlations include the pre-impact position of the dummy relative to the test setup and the inaccurate characterization of dummy-test setup interfaces. The dummy was positioned in the test setup according to angular (e.g. sternal angle, belt angle, femur angle, tibia angle etc.) and linear (e.g. neck to medial belt edge etc) positioning data recorded prior the impact test. Although this test data was generally matched well in the model, some inherent differences occurred in a few parameters (e,g. tibia angle). While the influence of these positioning parameters on the overall behavior of the model is unknown, a sensitivity study based on FE simulations is recommended. It is believed that the results of this study would help both future tests and simulations in giving a greater importance to the measurement or matching to test data of the most sensitive positioning geometrical parameters. Although the level of lapbelt force (max. 0.2 kN) was much lower than the level of shoulder belt (max. around 6 kN), a special attention should be allowed in future tests and simulations of pre-impact positioning of this belt. The definition of dummy-buck contacts may have also a significant influence on the dummy kinematics, especially through the friction force between seat and dummy. Therefore, in the future tests it would be recommended the measurement of the time histories of seat–to-dummy contact forces, and verification of this data in FE simulations.

A model of the dummy is considered to be good if it can replicate accurately the dummy kinematics and reaction forces with the test setup recorded in testing. A quantitative comparison between physical dummy and its model is difficult to obtain, especially when the number of channels is high, as in the current test. The objective rating methods, recently developed and used in other

previous study, can be a promising tool for model assessment. The THOR-NT dummy FE model obtained relatively closed scores in the kinematic and kinetics assessment (0.51 and 0.59, respectively). If the average of these scores is calculated, the total score of the model will be 0.55 which place it in a poor quality range according to Jacob et al 2000's classification (1 is the best score, and 0 is the worst). However, it should be mentioned that the quality values used in these rating methods are heavily dependent on the criteria and weighting factors applied. Therefore, these methods are especially useful for comparing models that use the same rating conditions.

Although it is obvious that the THOR-NT FE dummy model requires additional improvements and validations under additional test conditions (e.g., pulses of different shapes, and directions), its relatively reasonable performance in 40 km/h sled tests would recommend it for use in impact simulations intended to improve the design of new vehicles and their restraint systems.

CONCLUSIONS

This study presents a multifaceted assessment of a finite element model of THOR-NT dummy in a frontal crash environment. First, the three-dimensional kinematics of certain points on the dummy and the interaction forces between the dummy and the test setup were accurately recorded in a 40 km/h sled test with an advanced optical system and load cells. The FE of the dummy, developed and validated at the component level in previous studies, was positioned with respect to a FE model of the test setup according to the test configuration recorded prior to the test. The load and displacement signals (especially along the deceleration direction) show a similar trend with the test data, but some discrepancies were observed: their peak values and in sagittal and transversal motion of the dummy. While the main causes of the low capability of the model to predict the torso rotations observed in testing are unknown, several ideas for model improvement were suggested for the future development and validation of the model. Objective rating techniques, which quantify the similarity of peak level, peak time, and overall shape of two curves, were employed to compare the results of simulations with the test data. Although, the rating values calculated are greatly dependent on the criteria and the weighing factors used in their definition, it is believed that the rating approach would be useful for comparing different versions of the dummy model which will use the same rating condition. In addition to further refinements of current THOR-NT model, the numerical approach presented in this study, which try to determine an overall score from comparison of numerous time histories curves, can be applied in the process of verification/validation of other dummy or human models used in crash simulations.

ACKNOWLEDGMENTS

The authors are grateful for the financial support received from US Department of Transportation, NHTSA. The views and opinions expressed in this paper are those of the authors and not NHTSA

REFERENCES

[1]. Dsouza R., Bertocci G. (2009) "Development and validation of a computer crash simulation model of an occupied adult manual wheelchair subjected to a frontal impact" Medical Engineering & Physics (in press)

[2]. Hovenga P.E., Spit H.H., Uijldert M., Dalenoort A.M. (2005) "Improved Prediction of Hybrid-III Injury Values Using Advanced Multibody Techniques and Objective Rating" , Paper 2005-01-1307, SAE Congress 2005.

[3]. Hovenga P.E., Spit H.H., Uijldert M (2004) "Rated facet Hybrid-III 50th model with improved user-friendliness introduced", 10th International MADYMO Users Meeting.

[4]. Jacob C., Charras F., Trosseille X., Hamon J., Pajon M., Lecoz J.Y. (2000) "Mathematical models integral rating", Int. J. of Crashworthiness, vol. 5(4):417-432.

[5]. Kent R, Lessley D, Sherwood C. (2004) "Thoracic response to dynamic, non-impact loading from a hub, distributed belt, diagonal belt, and double diagonal belts" Stapp Car Crash J. 2004 Nov;48:495-519

[6]. Malone D.P., Tannous R.E., Takhounts E., Eppinger R. (2007a) "Development and Validation of a Finite Element Model of the Thor-NT Thorax " NHTSA Report, January 2007

[7]. Malone D.P., Tannous R.E., Takhounts E., Ridella S. (2007b) "Development and Validation of a Finite Element Model of the Thor-NT Head and Neck Assembly " NHTSA Report, August 2007

[8]. Shaw G., Crandall J., Butcher J. (2002) ”Comparative evaluation of the THOR advanced frontal crash test dummy”, International Journal of Crashworthiness, 7(3), 239-254.

[9]. Untaroiu C., Shin J., Crandall J.(2007) “A Design Optimization Approach of Vehicle Hood for Pedestrian Protection”. International Journal of Crashworthiness, 12(6):581-589.

[10]. Untaroiu C., Meissner M., Crandall J., Takahashi Y., Okamoto M., Ito, O. (2009) “Crash Reconstruction of Pedestrian Accidents using Optimization Techniques”. International Journal of Impact Engineering, 36:210-219.

[11]. Untaroiu C., Lim J., Shin J., (2009). "Evaluation of a Thor dummy rigid-body model in frontal crash environment using objective rating techniques" Biomedical Sciences Instrumentation, 45 (in press).

[12]. Varellis J., Quinn Campbell J., Tannous R. (2004) “Development and Validation of a Finite Element Model of the Thor Lower Extremity “ NHTSA Report, February 2004

EVALATION OF THE PERFORMANCE OF COMPETITIVE HEADFORMS AS TEST TOOLS FOR INTERIOR HEADFORM TESTING

Tobias Langner
Oliver Zander
Federal Highway Research Institute (BASt)
Germany
Felix Hänel
University of Applied Science Aachen
Germany

on behalf of APROSYS SP1
Paper No. 0279

ABSTRACT

The European Research Project APROSYS has evaluated the interior headform test procedure developed by EEVC WG 13, representing the head contact in the car during a lateral impact. One important aspect within this test procedure was the selection of an appropriate impactor. The WG13 procedure currently uses the Free Motion Headform as used within the FMVSS 201. The ACEA 3.5 kg headform used in Phase 1 of the European Directive and the future European Regulation on Pedestrian Protection is still discussed as a possible alternative.

This paper reports work performed by the Federal Highway Research Institute (BASt) as a part of the APROSYS Task 1.1.3. The study compares the two headform impactors according to FMVSS and ACEA, in a series of basic tests in order to evaluate their sensitivity towards different impact angles, impact accuracy, the effect of differences to impactors of the same type and the effects of the repeatability and reproducibility of the test results. The test surface consisted of a steel tube covered with PU foam and PVC, representing the car interior to be tested.
Despite of the higher mass of the FMH the HIC values of this impactor were generally lower than those of the ACEA headform. The FMH showed a higher repeatability of test results but a high sensitivity on the angle of roll, the spherical ACEA impactor performsed better with regards to the reproducibility. In case of the ACEA impactor-, the angle of roll had no influence.

INTRODUCTION

The terms of reference of WG 13 indicate a critical review of the competing headforms:

> ...
> 5) Interior Surface Test.
> Review the proposed EEVC interior surface test procedure, including any validation testing that has been completed and, if necessary, refine the procedure such that it is fit for regulatory application.
> *Deliverables*
> *a. A report of the outcome of validation testing and a critical review of the competing headforms*
> *b. Development of a refined test procedure that is suitable for regulatory application.*
> *EEVC Steering Committee March 2006*
> ...

To identify differences and advantages from one headform to the other an elementary test programme was necessary. Tests on simplified structures representing surfaces like, A-, B-, C-pillars and side roof rails were of interest.

The following investigations assess the quality of test results by checking how sensitive the headforms are at small variations of the

- impact angle
- target accuracy
- head orientation
- use of different headforms of the same type.

CHOICE OF HEADFORMS AND USE IN REGULATIONS

The EEVC WG13 test procedure currently uses the FMH (Free Motion Headform) impactor to assess the interior car structure concerning head injury risk in lateral impacts. Due to difficulties in head alignment and in finding the appropriate impact target

on the calibrated impact zone of the FMH impactor, the question was raised to review suitable headforms. To simplify testing, a headform that is all-over calibrated and not sensitive on impact direction would be beneficial. A spherical headform like those used in pedestrian testing fulfils these requirements. Therefore the ACEA (European Automobile Manufacturer Association) headform impactor used for headform to bonnet rating in EC-Directive 2003/102/EC was chosen.

Both headforms, the FMH and ACEA, are used in regulations to assess the severity of a head contact during a crash. The FMH is used in the American FMVSS201 for interior headform testing, the ACEA headform is used in the European EC-directive 2003/102/EC and the Japanese Regulation TRIAS 63 for pedestrian headform testing.

The first obvious difference of the two competing headforms is the shape. While the FMH is only symmetrical to its z-x plane, the ACEA headform is symmetrical to its z-x and z-y plane with the exception of the backplate.

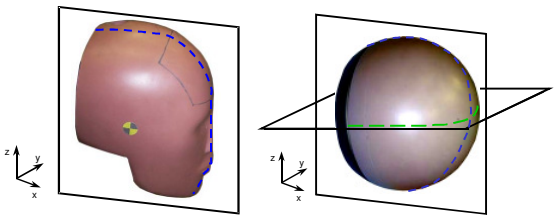

Figure 1. Side view of competing headforms.

Further information about the differences of the impactors are available in Annex A.

BASIC TEST SPECIFICATION

The validation and comparison of two different types of impactors requires a simple and robust experimental set-up. Each impactor gets tested on the structure several times. Therefore it is very important that the structure offers the same basic conditions at each test run to achieve reliable and comparable results. To minimise the influence of the tested structure, a very repeatable and homogeneous structure was necessary.
A structure was chosen, that fulfils the following requirements:

Test structure:

- Rotation-symmetric assembly (tube)
- Similarity to typical car structures (e.g. B-pillar)
- Mix of typical car-body materials
- Dimensioning of sample structure on realistic HIC values
- No plastic deformation after test

Also fixed boundary conditions are necessary to avoid any interference, simplify testing and reduce tests costs.

Boundary conditions

- High stiffness of restraints
- Stress-free deformation of the tube
- Vibration-free bearing of the test tube
- Rotational free supports
- Easy replacement of the test sample
- Removable and simple assembly
- Low cost

This resulted in the following test structure:

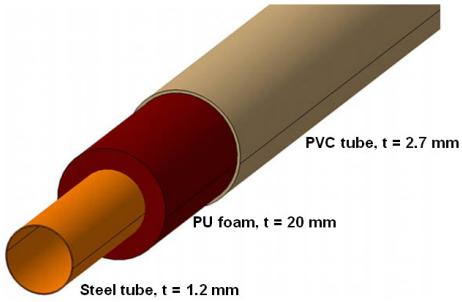

Figure 2. Rig testing tube assembly.

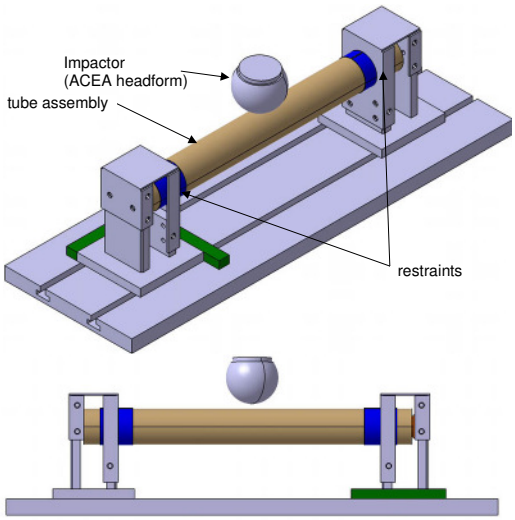

Figure 3. ISO and side-view of the complete rig testing set-up.

For more detailed test specification please see Annex B.

Test set-up and parameters

The test runs are carried out on the test bench of BASt.

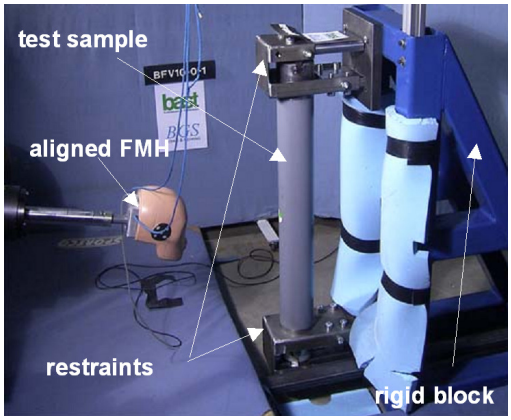

Figure 4. Test-set-up showing aligned FMH impactor.

Sensitivity on impact angles variation

Finding the correct perpendicular vector to the selected target is often complicated at curved structures. The configurations shown in the figures below should lead to information about the influence of the angle deviation in headform testing.

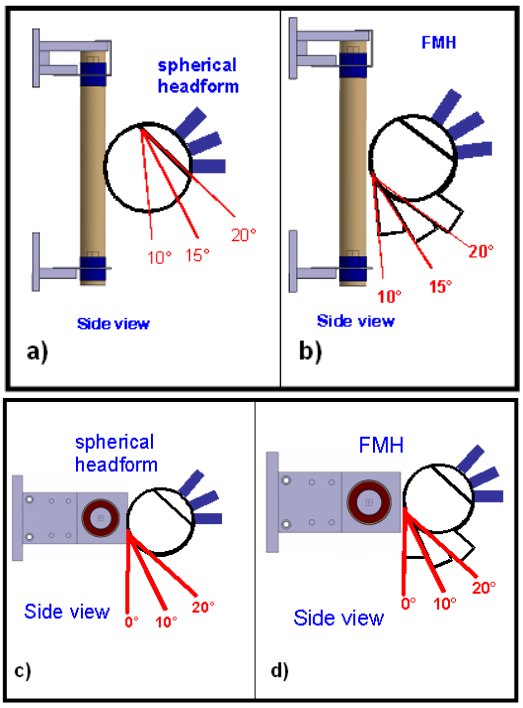

Figure 5.
Top: Angle variation on vertical tube (a, b).
Bottom: Angle variation on horizontal tube (c, d).

Sensitivity on target accuracy

It was observed, that the contact on the impactor during a test varied from one test laboratory to another. On the one hand this was due to a missing definition of contact location in the calibrated field. Therefore a consistent procedure was developed. On the other hand variations in contact location in the calibrated can still occur. The test procedure allows a 10mm radius accuracy of the target point. This means possible target locations can be 20mm apart. It is of interest how both headforms react on deviations from the initial position.

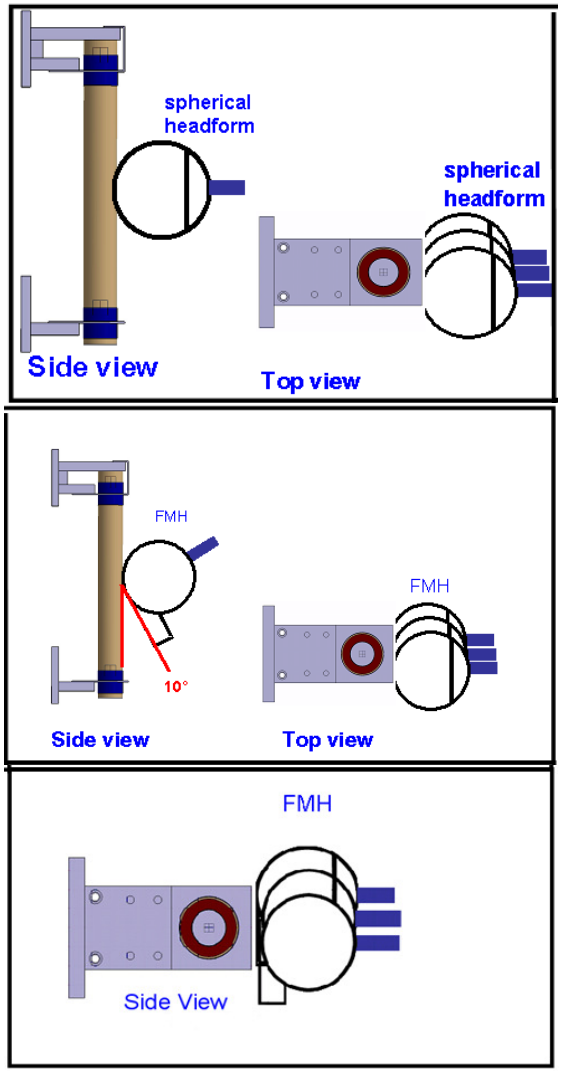

Figure 6. Top: ACEA headform - target deviation on vertical tube (same set-up on horizontal tube).
Mid: FMH headform on target deviation vertical tube.
Bottom: FMH headform on target deviation horizontal tube.

Influence by using different headforms / reproducibility

Variations in test results may not only occur because of differences in the test set-up. It may also occur because of differences in the test device / headform. Therefore comparisons of different impactors of the same type can provide information about the reproducibility of test results.

The following figures show the used headforms. Already visible are differences of the FMH impactors.

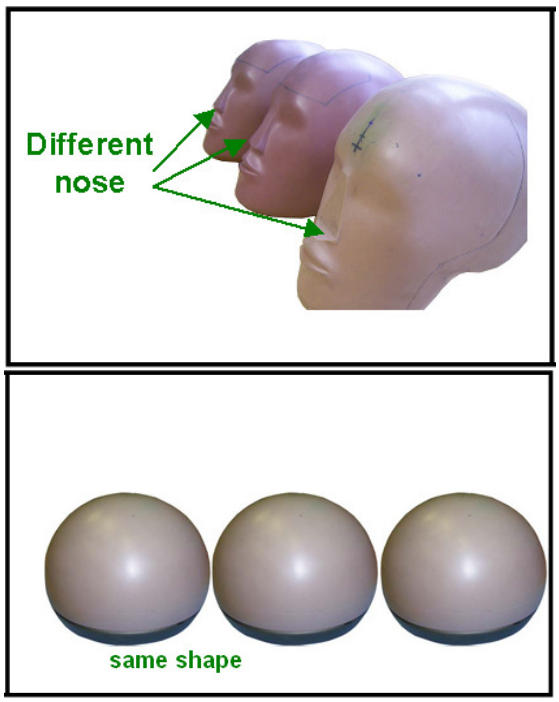

Figure 7. Different FMH and ACEA headforms.

Assessment parameters

Both impactor types will be compared by the HIC value and not the HIC_d value. The HIC_d is calculated from the measured HIC of the FMH taking into account the connection of the dummy head to the rest of the body ($HIC_d = 0.75446 * HIC_{FMH} + 166.4$)
This formula cannot be used for the ACEA headform as the dummy related HIC_d value is only related from the FMH impactor to the dummy headform.

For both impactor types the absolute HIC deviation and the deviation in percentage, within test repetitions, are determined to evaluate reproducibility. The deviation of HIC in dependency of an increasing impact angle and a displacement of impact vector will be shown and analysed regarding the impactors' sensitivities.

To achieve reliable results and to obtain additional information about repeatability, tests were performed three times. Additionally information could be gained about repeatability. After one test the tube was turned by 180° and after the second test the tube was replaced by a new tube.
Altogether 73 tests were performed (see test matrix in the Annex C)

RESULTS: INVESTIGATION ON IMPACT ANGLE SENSITIVITY

Sensitivity on impact angle (vertical tube)

In the case of vertical tube orientation, the initial alignment of both impactors is pitched by 10°. This action is required by the clean-contact requirement of the FMH. Plotting the average HIC values for FMH and ACEA headform, in dependency of an increasing impact angle, shows a nearly similar and linear allocation for both impactor types (see figure 8 and 9). The absolute HIC values of the ACEA headform are always higher in average than those of the FMH. This can be explained by less headform rotation, caused by the mid-central position of the spherical headform's CoG. Increasing the impact angle by additional 5° causes a HIC value decrease of about 11 % for both impactor types. A further increase up to a total impact angle deviation of 10° from the initial position shows a HIC decrease of 18.5 % for the FMH and 15.8 % for the ACEA headform.

The variation of the HIC values, within test repetitions, is quite different between the impactors. Testing under vertical tube orientation, the FMH results do vary 0.6 % between minimum and maximum value in the initial position of 10° head pitch, the ACEA headform varies about 10 times higher. With a variation of about 10 % at 15° head pitch, the ACEA varies twice as high as the FMH. Under these test conditions the FMH shows a better test repeatability.

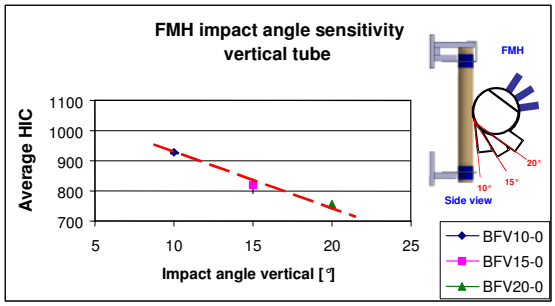

Figure 8. Variation of impact angle, FMH vertical tube.

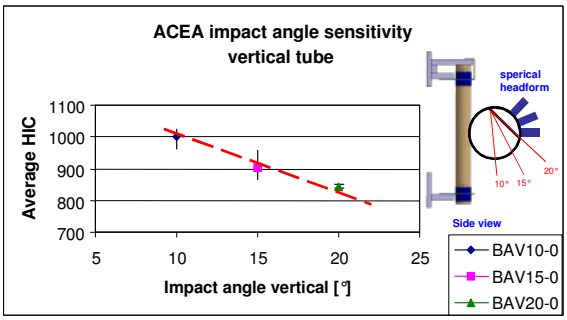

Figure 9. Variation of impact angle, ACEA headform vertical tube.

Sensitivity on impact angle (horizontal tube)

The horizontal tube orientation defines the initial position of both impactors at 0° head pitch and 0 mm lateral offset relative to the test tube.

The measured values show a nearly similar dependency between impact angle and HIC-value decrease for the ACEA and FMH impactor. Under horizontal tube orientation the load level between FMH and ACEA differs considerably to that seen in the vertical tube position. This is caused by the fact that the external diameter of the tube is smaller than the size of the FMH and therefore the FMH impactor freely rotates without having a secondary impact with its chin on the structure.
While the HIC results between FMH and ACEA headform differ in average about 10 % in case of vertical tube orientation, the difference at horizontal tube testing was an average of 21 %.

The following figures show the variation of the HIC values under horizontal tube alignment. Up to 10° impact angle, the deviation is nearly identical for both impactor types. While the variation of the FMH impactor decreases below 5 % when increasing the impact angle up to 20°, the HIC values of the ACEA headform was very sensitive to further angle deviation, with a variation of about 20 %. It should be noticed that the number of repeated tests is too low to draw a precise conclusion.

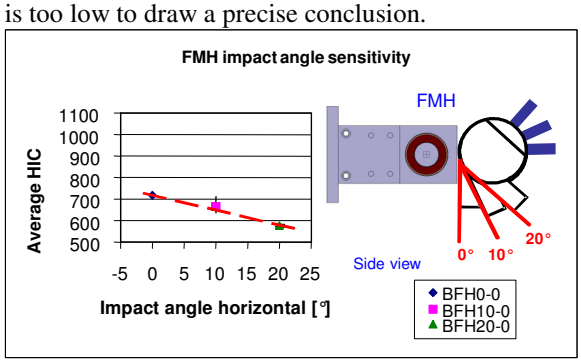

Figure 10. Variation of impact angle, FMH horizontal tube.

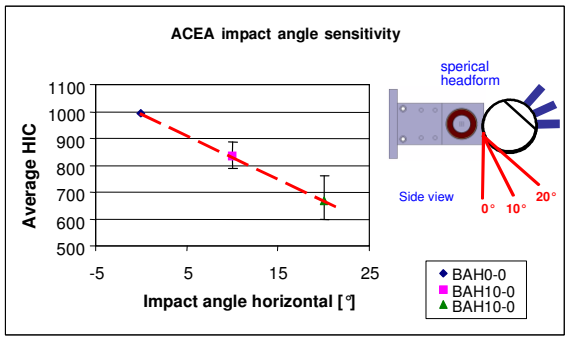

Figure 11. Variation of impact angle, ACEA headform horizontal tube.

Table 1 gives an overview of the HIC results for the FMH and ACEA impactors. In addition to the absolute HIC values the relative deviation for each test setup is shown.

tube orient.	FMH			ACEA		
	impact angle [°]	average HIC	HIC decrease [%]	impact angle [°]	average HIC	HIC decrease [%]
Vertical	10	926		10	1002	
	15	821	11.4	15	900	10.2
	20	755	18.5	20	844	15.8
Horizontal	0	719		0	992	
	10	666	7.4	10	834	15.9
	20	577	19.8	20	668	32.6

Table 1. Results of physical rig tests (impact angle)

The following figures show the data quality in accordance to the impact angle. The values of repeated tests of the FMH impactor are closer together than the values of the ACEA impactor.

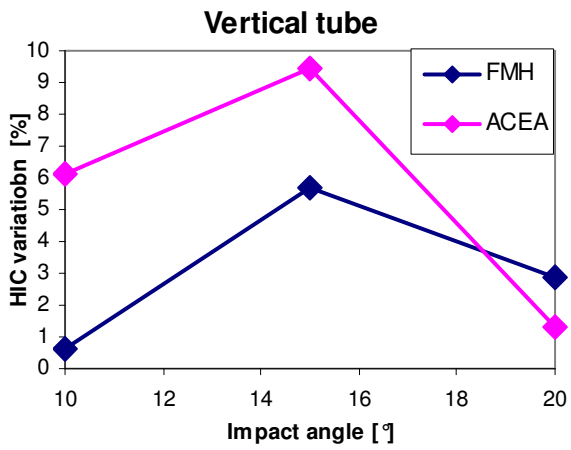

Figure 12. Comparison of test variation for impact angle deviations (vertical).

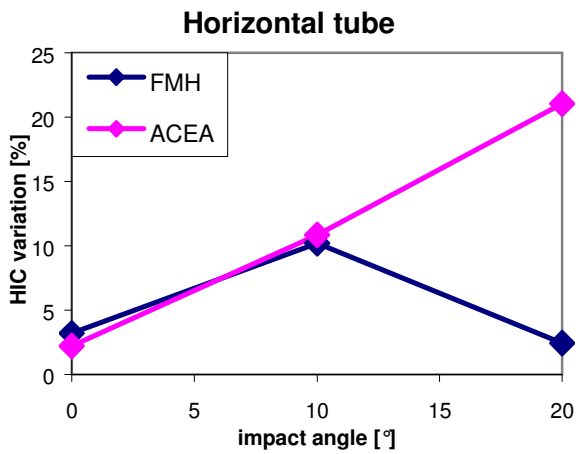

Figure 13. Comparison of test variation for impact angle deviations (horizontal).

INVESTIGATION ON IMPACT VECTOR DISPLACEMENT SENSITIVITY

Sensitivity on impact vector displacement (vertical tube)

The initial position of the FMH is defined as 10° head pitch and 0 mm offset to the vertical tube axis; the ACEA headform will be aligned under 0° head pitch and 0 mm offset. The impactors get aligned with a lateral vector offset to the headform's horizontal axis in increments of 10mm.

The ACEA impactor shows a linear decrease of HIC values due to an offset of the impact vector (see figure 14). At a displacement of 10 mm from the initial position, the HIC-value decreases about 2.5 %, at 20 mm 5.4 %. For the FMH the HIC values decrease about 1.6 % for 10 mm axis offset and 7.4 % at 20 mm offset.

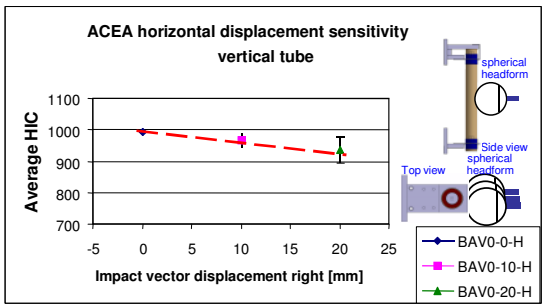

Figure 14. Sensitivity on impact vector displacement, ACEA headform (vertical tube).

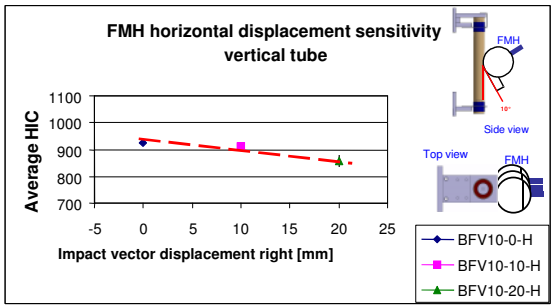

Figure 15. Sensitivity on impact vector displacement, FMH (vertical tube).

Sensitivity on impact vector displacement (horizontal tube)

Under horizontal tube orientation the impactors get aligned with an increasing impact vector offset moving down on the head's local z-axis. The performance characteristic of both headforms is nearly linear as on vertical tube alignment. The FMH's lower face parts do "under-run" the test structure. Because of the zx-symmetry of the ACEA headform, testing under a lateral vector offset needs only to be performed in the vertical tube position. The influence of gravity during the short free flight distance can be neglected.

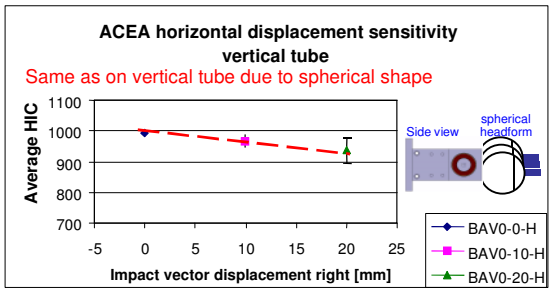

Figure 16. Sensitivity on impact vector displacement, ACEA headform (horizontal tube).

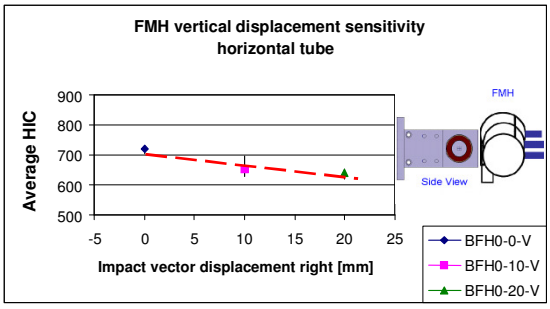

Figure 17. Sensitivity on impact vector displacement, FMH (horizontal tube).

Table 2 gives an overview of the HIC results for the two different impactor types FMH and ACEA.

tube orient.	FMH			ACEA		
	offset [mm]	average HIC	HIC decrease [%]	offset [mm]	average HIC	HIC decrease [%]
vertical	0	926		0	992	
	10	912	1.6	10	967	2.5
	20	858	7.4	20	938	5.4
horizontal	0	719		-	-	-
	10	652	9.4	-	-	-
	20	639	11.2	-	-	-

Table 2. Results of physical rig tests (impact vector offset)

The variation of results within the test repetitions is shown in figure 18 and 19. For both impactor types the reliability of the results is decreasing due to an increase of impact vector offset under vertical tube orientation. Up to 10 mm deviation the variation is in an acceptable range, minor to 5 %. At 20 mm offset the ACEA impactor shows a nearly 50 % higher variation in the HIC-values than the FMH.

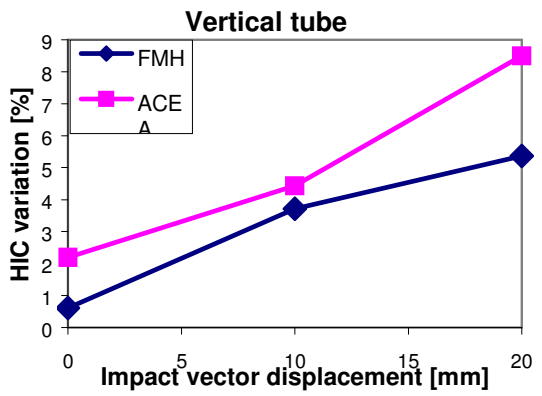

Figure 18. Comparison of test variation for impact displacement deviations (vertical).

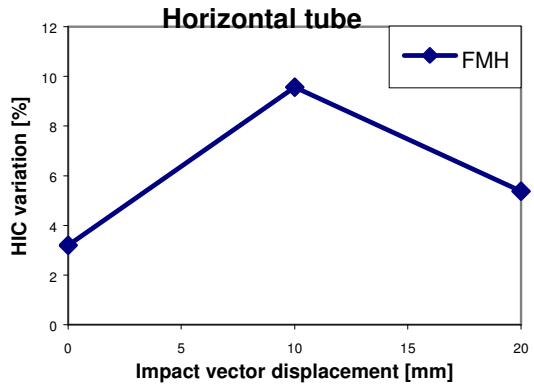

Figure 19. Comparison of test variation for impact displacement deviations (horizontal).

COMPARISON OF IMPACTORS OF SIMILAR DESIGN

Additional tests were performed to check the reproducibility depending on the differences in design between impactors. Therefore two ACEA and FMH impactors have been borrowed from TÜV to be compared with the BASt impactors. In addition to this the skins have been exchanged between the BASt and TÜV impactors. Some of the previous mentioned test conditions were used for the impactor comparison.

An optical comparison between the three FMH, regarding outer geometry and surface condition, shows significant geometrical differences (see figure 20). While the nose of the BASt FMH is completely removed and the lips stick out, the FMH models from the TÜV are designed with a visible nasal-bone reaching down to the lips. The differences in the FMH skins probably are the result of different manufacturers (Denton and FTSS). A definition of the nose shape is quite dificult. The ACEA spherical headform is easier to define. Because of the head rotation over its face, those differences in nose design could cause deviations in the kinematic behaviour of the FMH headform impactor.

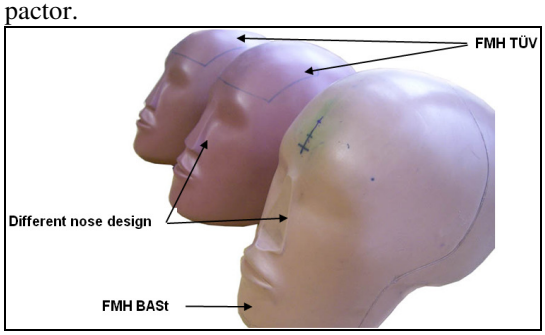

Figure 20. Different designs of FMH impactors.

The analysis of the high-speed videos show "fluttering" of the TÜV FMH skin on the aluminium body and a marginal relative displacement of the skin in the direct contact area on the forehead. The skin of the FMH impactor from BASt is tightly fixed to the inner skull and does not slide under impact. All three FMH impactors do have the same mass of 4.5 kg.

Figure 21 shows clear differences in HIC results between the compared FMH impactors. The BASt FMH achieves about 14 % higher HIC-values in average than the TÜV FMH impactors. The exchange of the skins demonstrates that the BASt skin causes higher HIC-values. The inner aluminium skulls of all three impactors are identical in mass and geometry. Both TÜV impactors achieve nearly identical results. The results support the assumption that the different skin design has an influence on the results. But also the inner skulls do vary as they are not completely identical. On the inside balance weights are attached to compensate the differences of the moment of inertia Using the BASt skin with the TÜV 1 skull also reduced the HIC. As a result, skins and skulls cause variations in HIC results for the FMH. Calibrations have been performed after changing the skin.
The variation within the respective test repetitions does not exceed 5 %.

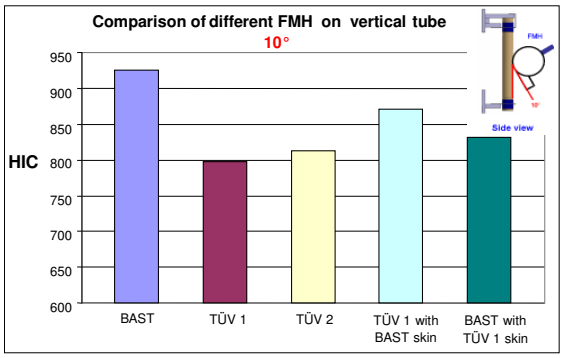

Figure 21. Comparison of different FMH impactors.

The same tendency could be observed by horizontal displacement of the both FMH types (with and without nose) at 10mm and 20mm displacement.

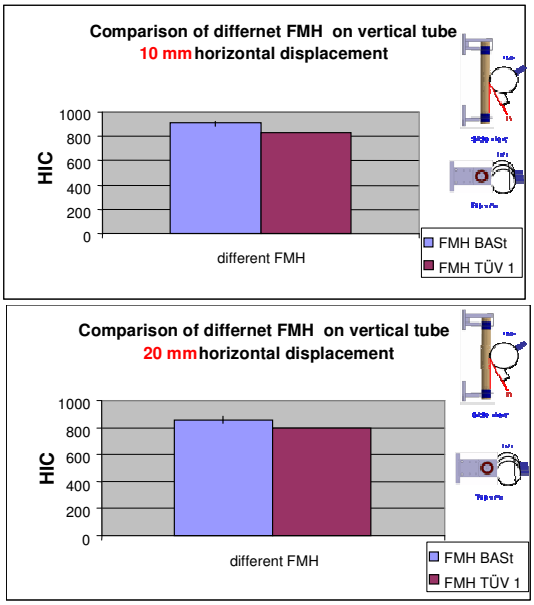

Figure 22. Comparison of different FMH impactors with impact displacement.

The comparison of the ACEA headforms (see figure 23) indicates lower differences between the impactors. The average deviation between BASt and TÜV HIC is below 3 %; the variation within the respective test repetitions is about 4%, that means higher than the deviation between the headforms itself. Furthermore the ACEA impactors do not show any differences in geometry, surface design or mass.

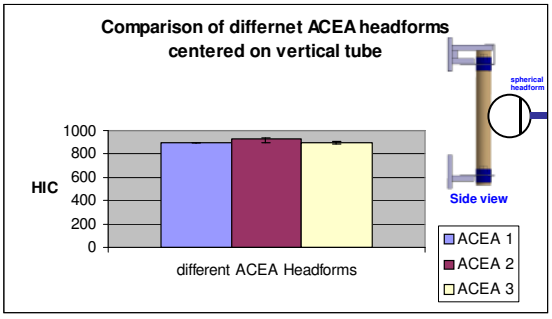

Figure 23. Comparison of different ACEA impactors.

SENSITIVITY ON HEADFORM ORIENTATION

The current WG13 interior headform test procedure includes a 90° roll of the FMH, in case the gap between chin and structure is less than 10°. It was of interest to investigate differences in HIC result, when testing identical targets with the same impactor with this two possible head orientations. A rotation up to 90°, leads to a HIC-value decrease of

about 30% for the FMH. The analysis of the high-speed videos shows higher head rotation than in vertical tube position, caused by the missing secondary contact of the chin. Beside the 90° roll of the impactor, this would also mean a 30% difference, testing identical target structures on a vertical pillar or horizontal side roof rail.
Because of the over-all symmetry of the ACEA headform, testing 90° rolled has no influence on the HIC.

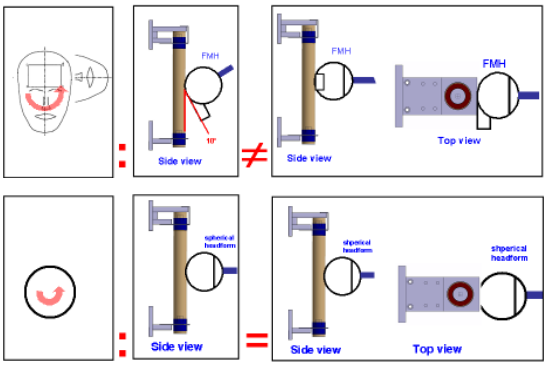

Figure 24. Influence of head roll.

CONCLUSION

In this study two different headform impactors have been compared, regarding their sensitivities to deviations of defined test parameters. A test rig and a specific test sample, representing a typical car structure (e.g. B-pillar), were developed and produced. Extensive test runs were performed at the test facility of BASt.
A simplified summary of the sensitivities of the different headform impactors towards a variation of impact parameters are shown in Table 3.

	FMH	ACEA Headform
repeatability	+	o
head orientation (90°roll)	--	++
sensitivity in impact angle	+	+
sensitivity on target accuracy	o	o
use of different headforms of the same type	o	+

++ very good, + good, o acceptable. – insufficient, -- very insufficient

Table 3. Comparison of impactor sensitivities

At vertical tube orientation the FMH and the ACEA headform impactor show similar results. An exact impactor alignment regarding the head pitch is very important. Both headforms are more sensitive to deviations of the head impact angle than to lateral offset of the impact vector from the mid-axis. The variation of the ACEA impactor rig test results is higher than the variation of the FMH.
At horizontal tube orientation the FMH impactor shows lower variation and sensitivities to the test parameters than the ACEA headform. The rig test results of the ACEA headform impactor show a high variation and sensitivity to impact angle deviations.

The FMH impactor is sensitive to the orientation of the tube structure. In the initial alignment position, the HIC results differ about 30 % between vertically and horizontally orientated tubes. This is unacceptable. In contrast, the spherical ACEA headform impactor shows no sensitivity to this parameter and offers an easier handling during rig tests.

To achieve reproducible and comparable results for tests on real car structures precise first-contact point alignment has to be clearly defined.

The comparison of FMH impactors of same design shows differences in geometry and surface design. A different nose design of the FMH impactors influences the kinematic behaviour and the HIC results. The FMH impactors from the TÜV achieve 13 % lower HIC-values than the FMH impactor from BASt.

The ACEA headform impactors from TÜV achieve less than 3 % lower HIC-values than the ACEA impactor from BASt. This is less than the deviation using the same impactor. The geometry, surface design and mass of the compared ACEA headforms are identical.

REFERENCES

[1] Free Motion Headform Impactor for RADIOSS, IMPERIA GmbH, Aachen

[2]: Code of federal regulations, Title 49-Transport, §571.201, Occupant protection in interior impact

[3] ACEA Headform Impactor for RADIOSS, IMPERIA GmbH, Aachen

[4] Directive 2003/102/EC of the European Parliament and of the Council of 17.11.2003, relating to the protection of pedestrians and other vulnerable road users before and in the event of a collision with a motor vehicle and amending Council Directive 70/156/EEC

ANNEX A

DESCRIPTION OF THE IMAPCTORS

Characteristics of the FMH impactor - FMVSS201

The FMVSS 201 was introduced by the NHTSA (National Highway Traffic Safety Administration) in the US to enhance the safety standards for the protection of passengers regarding head impacts on interior structures. Since the year 2002 this regulation is applied to all vehicles up to 4.5 tons total mass.

The impactor is the head of the Hybrid 3 Dummy with its nose removed. This Free-Motion-Headform (FMH) impactor of 4.5 kg mass gets impacted on selected target points on the car interior surface, with a minimum free-flight distance of 25 millimetres and a speed of 24.1 km/h, the latter being the average velocity for the onset of severe injuries in a car accident. Typical target areas in the passenger compartment are the A- and B-pillars, the steering wheel, the dashboard and exposed parts like the belt fixing and handholds.

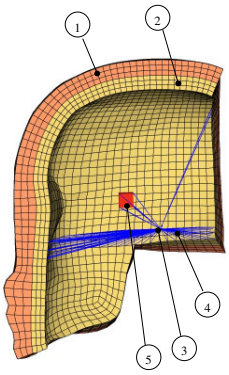

pos.	description
1	Part 1: Skin PVC-Rubber
2	Part 2: Aluminium Skull
3	Part 3: Rigid Body
4	Part 4: Added Balancing Mass
5	Part 5: Accelerometer

Figure 25. Characteristics of the FMH impactor [1].

The test procedure mandates that the calibrated forehead region of the FMH hits the target point first without contacting any other part outside of the specified impact zone.

The severity of head impacts is assessed by the HIC_d

$$HIC_d = 0.75446 \times HIC + 166.4$$

Figure 26. HIC_d formula, calculation for comparison with dummy values.

The HIC_d is a dummy-related value which diminishes high HIC values and considers the fact that the headform is detached from the neck of the Hybrid 3 dummy. The acceptance criterion is $HIC_d < 1000$.

Calibration Procedure FMH impactor

According to FMVSS 201 the free-motion headform impactor must be calibrated and verified. Therefore a free-fall drop test is described (see figure 27). The headform gets dropped from a height of 376mm +/- 1mm on a flat rigid steel plate. To avoid secondary contact of the chin a rotation of the impactor of 28° +/- 0.5° about the horizontal axis is required. The measured resulting acceleration must not exceed a value of 250g +/- 25g.

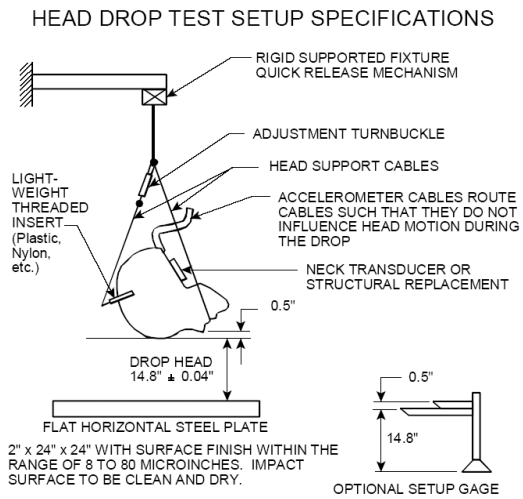

Figure 27. FMH head drop test setup specifications [2].

Characteristics of the ACEA impactor - EC-Directive 2003/102/EC

Since 2005 the new pedestrian safety legislation is effective as EC-Directive 2003/102/EC phase 1. Besides leg and hip impact tests, two types of free motion head impactors are impacted on the front end of passenger cars. These headforms are of spherical shape with 165 mm in diameter and correspond to the ACEA design. The child / small adult headform of 3.5 kg and the adult headform of 4.8 kg mass get impacted on selected target points within defined areas on the bonnet and windshield. An internal tri-axial acceleration sensor measures the corresponding acceleration-time function from which the Head Performance Criterion HPC (equal to HIC described under FMVSS 201) is computed.

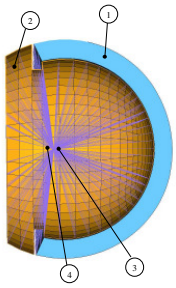

pos.	description
1	Part 1: Skin PVC-Rubber
2	Part 2: Aluminium Skull
3	Part 3: Rigid Body
4	Part 4: Accelerometer

Figure 28. Characteristics of the ACEA head-form impactor [3].

Calibration Procedure ACEA impactor

The calibration of the ACEA spherical headform impactors is different to the FMH drop-test procedure. While the FMH impactor is calibrated only in a limited area on the forehead, the ACEA headform is calibrated in a wide area of the sphere surface.

As shown in the figure below, the headform is suspended on a wire with the rear face at an angle between 25° and 90° with the horizontal. A linear guided certification impactor of 1 kg mass is propelled horizontally at a velocity of 7 m/s into the stationary headform. The certification impactor must be positioned so that the centre of gravity of the headform impactor is located on the centre line of the certification impactor with a tolerance of five millimetres. The tests have to be performed on three different impact locations on the headform impactor. Previously used and/or damaged skins shall be tested in those specific areas.

The peak resultant acceleration measured by one tri-axial accelerometer in the headform shall not be less than 290 g and not more than 350 g. The resultant acceleration time curve shall be uni-modal.

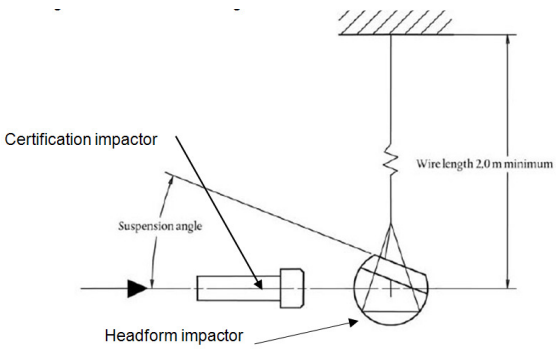

Figure 29. Calibration test setup for ACEA spherical headform [4].

ANNEX B

DEFINITION OF TEST SET UP

The adequate design of the test sample support has an important influence on the informational value of the results. On the one hand a fixed clamping on both sides of the tube represents a nearly realistic connection of a vehicle pillar at the roof rail and rocker-rail. On the other hand stress-free deformation is not warranted. So the complete restraints and its fixing to the test rig could deform. Resulting vibrations can influence the quality of measurement.
Figure 30 shows a mechanical replacement system including a simply supported bearing of the test-tube according to a three point bending test. The tube can bend freely in the direction of impact.

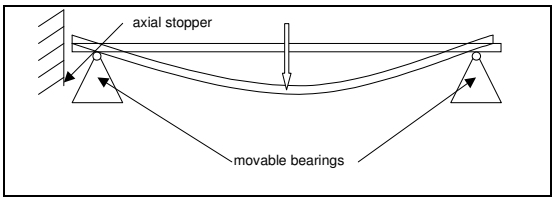

Figure 30. Substitute mechanical system for rig testing set-up.

Construction of test object and test rig
The headform impactors get impacted on a tube-assembly of 1000 mm length. The external overall diameter is 110 mm, the inner diameter measures 62.6 mm. The structure as shown in figure 2 consists of a thin walled steel tube with a gauge of 1.2 mm, an energy absorbing PUR-foam of 20 mm thickness and a PVC tube of 2.7 mm thickness.
This assembly should represent a typical car body structure, like a B-pillar which consists of an inner steel sheet, damping material and interior covering. The rotation-symmetric setup determines a specific mounting position in the test rig. To avoid rotation of the different material layers amongst each other, a light press fit is applied.

Figure 31 shows the assembled test rig with aligned ACEA headform. To avoid deformation and vibrations in the test rig the tube assembly gets supported according to a three point bending test.

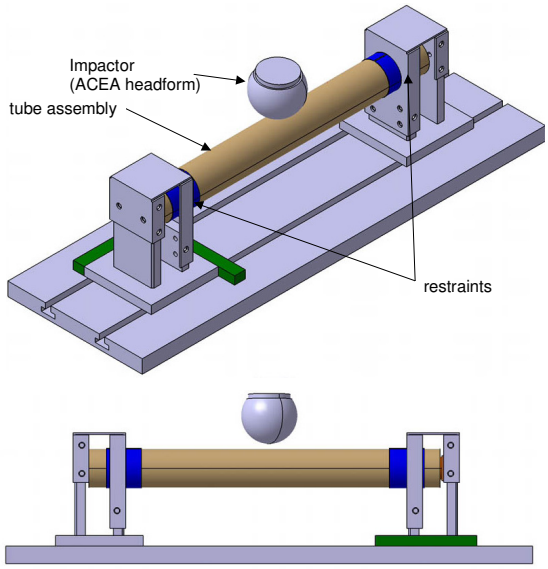

Figure 31. ISO and side-view of the complete rig testing set-up.

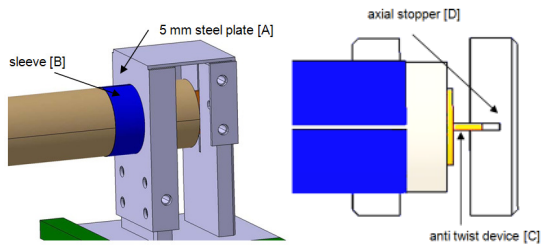

Figure 32. Tube clamping and anti-twist device.

On both sides of the restraints the tube assembly bears on a steel plate [A] of 5 mm thickness. The small overlap between sleeve [B] and steel plate in relation to the total tube length of one meter ensures a nearly freely jointed bearing.

Test configurations with an impact vector vertical to the tube axis could cause twisting of the tube assembly. Therefore a so called anti twist device [C] is welded on one side of the steel tube as shown in figure 32, right side. This device fits in a groove which is milled in the axial stopper [D] of the restraint. The tube can still bend freely but rotation around its longitudinal axis is suppressed. The foam and outer PVC tubes are joined with a press fit.

To avoid stress concentration and carving of the steel plate in the outer PVC tube, two slotted, thin-walled steel sleeves are mounted on each side of the restraints.

ANNEX C

Test Matrix Basic Tests at BASt

Comparison BASt FMH vs. BASt ACEA headform

No.	Test	Headform	tube orientation	Impact angle [°]	Impact vector displ. [mm]	Impact vector displ. orientation	V [m/s]	Acceleration [g] max	HPC	HPCd	average HPC	maximum deviation HPC	difference per step HPC			HPC from one setup to the other [%]	Scattering [%] refered to max. value	Difference ACEA to FMH	Difference ACEA to FMH average
1	BFV10-0-1	FMH	vertical	10	0	-	6,57	250,6	922,5	862,4	926,3			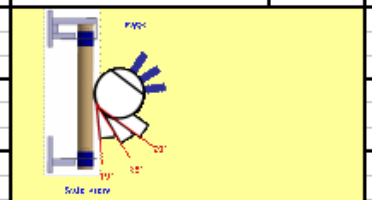				8,2	
2	BFV10-0-2	FMH	vertical	10	0	-	6,65	143,6	928,1	866,6	1,9	5,7					0,6		
3	BFV10-0-3	FMH	vertical	10	0	-	6,70	147,7	928,2	866,7	3,8		-105,1						
4	BFV15-0-1	FMH	vertical	15	0	-	6,60	132,1	791,9	763,9	821,1					11,4		9,6	9,9
5	BFV15-0-2	FMH	vertical	15	0	-	6,69	136,8	831,7	793,9	18,7	47,9					5,7		
6	BFV15-0-3	FMH	vertical	15	0	-	6,63	139,2	839,8	800,0	29,2		-66,0						
7	BFV20-0-1	FMH	vertical	20	0	-	6,63	129,7	760,2	739,9	755,1					18,5		11,7	
8	BFV20-0-2	FMH	vertical	20	0	-	6,72	129,0	763,6	742,5	8,5	22,1					2,9		
9	BFV20-0-3	FMH	vertical	20	0	-	6,73	130,7	741,5	725,8	13,6								
10	BAV10-0-1	ACEA	vertical	10	0	-	6,71	167,6	1023,7	938,7	1002,3			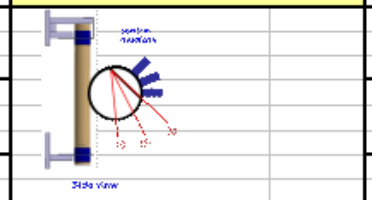					
11	BAV10-0-2	ACEA	vertical	10	0	-	6,69	158,6	961,1	891,5	21,4	62,6					6,1		
12	BAV10-0-3	ACEA	vertical	10	0	-	6,73	165,3	1022,0	937,5	41,2		-102,0						
13	BAV15-0-1	ACEA	vertical	15	0	-	6,72	152,6	866,8	820,4	900,3					10,2			
14	BAV15-0-2	ACEA	vertical	15	0	-	6,68	151,1	877,1	828,1	56,7	90,2					9,4		
15	BAV15-0-3	ACEA	vertical	15	0	-	6,73	156,8	957,0	888,4	33,5		-56,7						
16	BAV20-0-1	ACEA	vertical	20	0	-	6,71	151,5	841,2	801,1	843,6					15,8			
17	BAV20-0-2	ACEA	vertical	20	0	-	6,74	145,6	850,4	808,0	6,8	11,2					1,3		
18	BAV20-0-3	ACEA	vertical	20	0	-	6,75	155,1	839,2	799,5	4,4								
19	**BFV10-0-H-1**	FMH	vertical	10	0	right	6,57	250,6	922,5	862,4	926,3			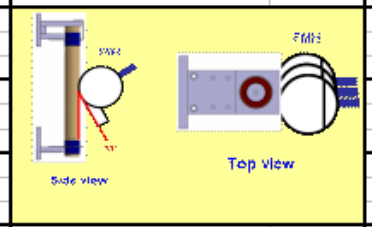				7,0	
20	**BFV10-0-H-2**	FMH	vertical	10	0	right	6,65	143,6	928,1	866,6	1,9	5,7					0,6		
21	**BFV10-0-H-3**	FMH	vertical	10	0	right	6,70	147,7	928,2	866,7	3,8		-14,8						
22	BFV10-10-H-1	FMH	vertical	10	10	right	6,72	134,0	917,6	858,7	911,5					1,6		6,1	7,5
23	BFV10-10-H-2	FMH	vertical	10	10	right	6,71	135,2	925,6	864,7	14,1	34,4					3,7		
24	BFV10-10-H-3	FMH	vertical	10	10	right	6,73	135,2	891,2	838,8	20,3		-53,5						
25	BFV10-20-H-1	FMH	vertical	10	20	right	6,72	134,6	833,7	795,4	858,0					7,4		9,3	
26	BFV10-20-H-2	FMH	vertical	10	20	right	6,73	138,2	859,3	814,7	22,9	47,2					5,4		
27	BFV10-20-H-3	FMH	vertical	10	20	right	6,77	137,8	880,9	831,0	24,3		133,6						
28	BAV0-0-H-1	ACEA	vertical	0	0	right	6,67	173,1	1003,8	923,7	991,6								
29	BAV0-0-H-2	ACEA	vertical	0	0	right	6,71	167,7	989,1	912,6	12,2	22,0					2,2		
30	BAV0-0-H-4	ACEA	vertical	0	0	right	6,73	165,0	981,8	907,1	9,8		-24,8						
31	BAV0-10-H-1	ACEA	vertical	0	10	right	6,69	163,6	945,6	879,8	966,7					2,5			
32	BAV0-10-H-2	ACEA	vertical	0	10	right	6,72	163,2	965,2	894,6	22,7	43,8					4,4		
33	BAV0-10-H-3	ACEA	vertical	0	10	right	6,73	164,2	989,4	912,9	21,1		-29,2						
34	BAV0-20-H-1	ACEA	vertical	0	20	right	6,72	165,2	976,9	903,4	937,6					5,4			
35	BAV0-20-H-2	ACEA	vertical	0	20	right	6,73	158,2	893,9	840,8	39,3	83,0					8,5		
36	BAV0-20-H-4	ACEA	vertical	0	20	right	6,70	160,4	941,9	877,0	43,7								

Comparison BASt FMH vs. BASt ACEA headform

No.	Test	Headform	tube orientation	Impact angle [°]	Impact vector displ. [mm]	Impact vector displ. orientation	V [m/s]	Acceleration [g] max	HPC	HPCd	average HPC	maximum deviation HPC	difference per step HPC		HPC from one setup to the other [%]	Scattering [%] refered to max. value	Difference ACEA to FMH	Difference ACEA to FMH average
37	BFH0-0-1	FMH	horizontal	0	0	-	6,76	143,5	723,1	712,0	719,1			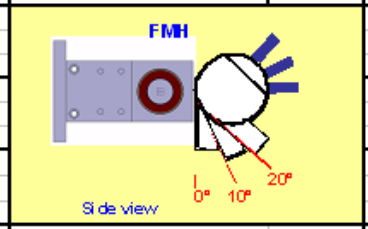				
38	BFH0-0-2	FMH	horizontal	0	0	-	6,69	143,2	728,8	716,3	9,7	23,3						
39	BFH0-0-3	FMH	horizontal	0	0	-	6,67	140,3	705,5	698,7	13,6		53,2					
37	BFH10-0-1	FMH	horizontal	10	0	-	6,73	137,4	649,3	656,3	666,0						25,2	20,5
38	BFH10-0-2	FMH	horizontal	10	0	-	6,72	132,5	638,1	647,8	44,5	72,4				10,2		
39	BFH10-0-3	FMH	horizontal	10	0	-	6,73	142,4	710,5	702,4	27,9		-89,0					
40	BFH20-0-1	FMH	horizontal	20	0	-	6,74	121,8	568,5	595,3	577,0				13,4		15,8	
41	BFH20-0-2	FMH	horizontal	20	0	-	6,69	120,1	579,9	603,9	5,6	14,1				2,4		
42	BFH20-0-3	FMH	horizontal	20	0	-	6,71	129,2	582,6	605,9	8,5							
43	**BAV0-0-H-1**	ACEA	vertical	0	0	-	6,67	173,1	1003,8	923,7	991,6			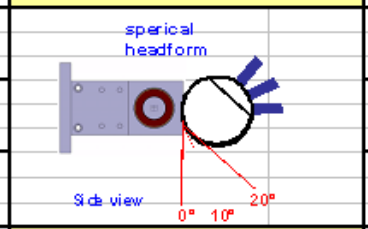				
44	**BAV0-0-H-2**	ACEA	vertical	0	0	-	6,71	167,7	989,1	912,6	12,2	22,0						
45	**BAV0-0-H-4**	ACEA	vertical	0	0	-	6,73	165,0	981,8	907,1	9,8		-157,5					
43	BAH10-0-1	ACEA	horizontal	10	0	-	6,69	147,9	790,3	762,6	834,0							
44	BAH10-0-2	ACEA	horizontal	10	0	-	6,67	152,3	825,5	789,2	52,3	96,0				10,8		
45	BAH10-0-3	ACEA	horizontal	10	0	-	6,67	151,6	886,3	835,1	43,7		166,1					
46	BAH20-0-1	ACEA	horizontal	20	0	-	6,66	122,2	598,7	618,1	667,9				19,9			
47	BAH20-0-2	ACEA	horizontal	20	0	-	6,76	131,0	646,8	654,4	90,3	159,5				21,0		
48	BAH20-0-3	ACEA	horizontal	20	0	-	6,77	142,9	758,2	738,4	69,2							
49	BFH0-0-V-1	FMH	horizontal	0	0	down	6,76	143,5	723,1	712,0	719,1						37,9	
50	BFH0-0-V-2	FMH	horizontal	0	0	down	6,69	143,2	728,8	716,3	9,7	23,3				3,2		
51	BFH0-0-V-3	FMH	horizontal	0	0	down	6,67	140,3	705,5	698,7	13,6		67,6					
52	BFH0-10-V-1	FMH	horizontal	0	10	down	6,65	135,9	628,3	640,4	651,6				9,4		48,4	44,4
53	BFH0-10-V-2	FMH	horizontal	0	10	down	6,72	142,7	694,7	690,5	43,1	66,4				9,6		
54	BFH0-10-V-3	FMH	horizontal	0	10	down	6,68	133,8	631,7	643,0	23,3		12,9					
55	BFH0-20-V-1	FMH	horizontal	0	20	down	6,72	131,4	643,4	651,8	638,6				11,2		46,8	
56	BFH0-20-V-2	FMH	horizontal	0	20	down	6,68	134,9	653,8	659,7	15,2	35,1				5,4		
57	BFH0-20-V-3	FMH	horizontal	0	20	down	6,70	138,7	618,7	633,2	19,9							
58	BAV0-0-H-1	ACEA	vertical	0	0	right	6,67	173,1	1003,8	923,7	991,6							
59	BAV0-0-H-2	ACEA	vertical	0	0	right	6,71	167,7	989,1	912,6	12,2	22,0				2,2		
60	BAV0-0-H-4	ACEA	vertical	0	0	right	6,73	165,0	981,8	907,1	9,8		-24,8					
61	BAV0-10-H-1	ACEA	vertical	0	10	right	6,69	163,6	945,6	879,8	966,7				2,5			
62	BAV0-10-H-2	ACEA	vertical	0	10	right	6,72	163,2	965,2	894,6	22,7	43,8				4,4		
63	BAV0-10-H-3	ACEA	vertical	0	10	right	6,73	164,2	989,4	912,9	21,1		-29,2					
64	BAV0-20-H-1	ACEA	vertical	0	20	right	6,72	165,2	976,9	903,4	937,6				5,4			
65	BAV0-20-H-2	ACEA	vertical	0	20	right	6,73	158,2	893,9	840,8	39,3	83,0				8,5		
66	BAV0-20-H-4	ACEA	vertical	0	20	right	6,70	160,4	941,9	877,0	43,7							

Comparison vs. 3 different FMHs and vs. 3 different ACEA headforms

No.	Test	Headform	tube orientation	Impact angle [°]	Impact vector displ. [mm]	Impact vector displ. orientation	V [m/s]	Acceleration [g] max	HPC	HPCd	average HPC	maximum deviation HPC	difference between different impactors		HPC from one impactor to the other [%]	Scattering [%] refered to max. value
58	BFV10-0-1	FMH	vertical	10	0	-	6,57	250,6	922,5	862,4	926,3			BASt		
59	BFV10-0-2	FMH	vertical	10	0	-	6,65	143,6	928,1	866,6	1,9	5,7		BASt		0,6
60	BFV10-0-3	FMH	vertical	10	0	-	6,70	147,7	928,2	866,7	3,8			BASt		
61	BFV10-0-4	FMH	vertical	10	0	-	6,70	130,8	781,5	756,0	797,1		129,2	F1074 (TÜV)	13,9	
62	BFV10-0-5	FMH	vertical	10	0	-	6,70	129,9	808,4	776,3	11,3	26,9		F1074 (TÜV)		3,3
63	BFV10-0-6	FMH	vertical	10	0	-	6,69	123,7	801,4	771,0	15,6			F1074 (TÜV)		
64	BFV10-0-7	FMH	vertical	10	0	-	6,70	109,1	827,0	790,3	813,1		-16,0	F1076 (TÜV)	12,2	
65	BFV10-0-8	FMH	vertical	10	0	-	6,69	127,8	788,3	761,1	13,9	38,7		F1076 (TÜV)		4,7
66	BFV10-0-9	FMH	vertical	10	0	-	6,72	134,0	824,0	788,1	24,8			F1076 (TÜV)		
67	BFV10-0-10	FMH	vertical	10	0	-	6,74	128,6	870,2	822,9			-57,1	F1074 (TÜV) mit BF1 (Bast) Haut (02270066)	6,1	
68	BFV10-0-11	FMH	vertical	10	0	-	6,69	137,4	831,3	793,6			38,9	BF1 (Bast) mit F1074 (TÜV) Haut (1046)	10,3	
69	BFV10-10-H-1	FMH	vertical	10	10	right	6,72	134,0	917,6	858,7	911,5					
70	BFV10-10-H-2	FMH	vertical	10	10	right	6,71	135,2	925,6	864,7	14,1	34,4		BASt		3,7
71	BFV10-10-H-3	FMH	vertical	10	10	right	6,73	135,2	891,2	838,8	20,3		-53,5			
75	BFV10-10-H-4	FMH	vertical	10	10	-	6,74	127,3	831,7	793,9				F1074 (TÜV)	8,8	
72	BFV10-20-H-1	FMH	vertical	10	20	right	6,72	134,6	833,7	795,4	858,0					
73	BFV10-20-H-2	FMH	vertical	10	20	right	6,73	138,2	859,3	814,7	22,9	47,2		BASt		5,4
74	BFV10-20-H-3	FMH	vertical	10	20	right	6,77	137,8	880,9	831,0	24,3		-63,9			
76	BFV10-20-H-4	FMH	vertical	10	20	-	6,67	128,4	794,1	765,5				F1074 (TÜV)	7,4	
77	BFV20-0-1	FMH	vertical	20	0	-	6,63	129,7	760,2	739,9	755,1			BASt		
78	BFV20-0-2	FMH	vertical	20	0	-	6,72	129,0	763,6	742,5	8,5	22,1		BASt		2,9
79	BFV20-0-3	FMH	vertical	20	0	-	6,73	130,7	741,5	725,8	13,6		-755,1	BASt		
80	BFV20-0-4	FMH	vertical	20	0	-	6,66	123,7	637,8	647,6				F1074 (TÜV)	15,5	
81	BAV0-0-H-5	ACEA	vertical	0	0	-	6,65	156,2	932,9	870,2	922,9			F1093 (TÜV)		
82	BAV0-0-H-6	ACEA	vertical	0	0	-	6,70	151,4	898,4	844,2	14,4	38,9		F1093 (TÜV)		4,2
83	BAV0-0-H-7	ACEA	vertical	0	0	-	6,66	149,5	937,3	873,6	24,5			F1093 (TÜV)		
84	BAV0-0-H-8	ACEA	vertical	0	0	-	6,73	156,6	907,7	851,2	898,7			F1094 (TÜV)	2,6	
85	BAV0-0-H-9	ACEA	vertical	0	0	-	6,66	152,0	888,2	836,5	9,0	19,5		F1094 (TÜV)		2,1
86	BAV0-0-H-10	ACEA	vertical	0	0	-	6,65	151,2	900,2	845,6	10,5			F1094 (TÜV)		
87	BAV0-0-H-11	ACEA	vertical	0	0	-	6,66	152,5	900,4	845,7				BASt	-0,2	

DEVELOPMENT OF NEW AIRBAG SYSTEM FOR REAR-SEAT OCCUPANTS

Seiji Aduma
Kouichi Oota
Hiroshige Nagumo
Tomosaburo Okabe
Nissan Motor Co., Ltd.
Japan
Paper Number 09-0288

ABSTRACT

In addition to seatbelts, most vehicles today are fitted with airbags in the front seats as restraint devices for protecting occupants in frontal collisions. However, various constraints in the rear seats have prevented progress in adopting the same type of airbag system as that used in the front seats. Therefore, a new airbag system has been developed as a crash energy absorbing device to improve protection of the head and neck of rear-seat occupants. This new airbag system can be installed under the traditional constraints present in the rear seats.

INTRODUCTION

Research on rear-seat occupant restraint systems is under way in many countries around the world today accompanying the rising concern in recent years about protection for rear-seat occupants in frontal collisions. In Japan, the Road Traffic Law was amended on June 1, 2008 to make the use of seatbelts mandatory in the rear seats as well, in addition to mandated use for the driver and front passenger. Beginning from April 1, 2009, a test procedure for evaluating rear-seat occupant protection is scheduled to be included in the New Car Assessment Program in Japan. As a result, information about rear-seat occupant safety performance will be made available to the general public.

At present, passenger vehicles are generally fitted with seatbelts and airbags in the front seats and seatbelts in the rear seats as restraint devices for protecting occupants in frontal collisions. It has been reported that the use of seatbelts by rear-seat occupants could have the effect of reducing their present levels of fatal and serious injuries by approximately one-half and their fatality rate by approximately two-thirds[1]. These figures are indicative of the effect that using seatbelts could have on improving rear-seat occupant protection.

A breakdown of the locations of fatal and serious injuries incurred by belted rear-seat occupants in frontal collisions shows that the most frequent region of the body in descending order are the chest, arms, head, legs and neck (Figure 1). For fatal injuries, in a similar way are the chest, abdomen, head and neck (Figure 2)[2].

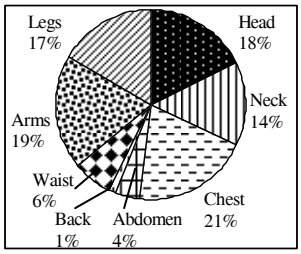

Figure 1. Location of fatal and serious injuries.

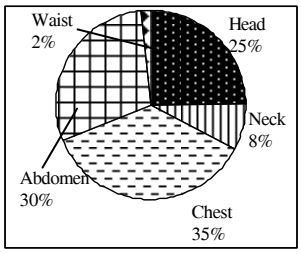

Figure 2. Location of fatal injuries.

It has been reported that, among these injury locations, seatbelt systems work to improve chest protection for rear-seat occupants[3]. However, little research has been done so far on protection for the head and neck, which account for approximately 30% of both fatal/serious injuries and fatal injuries.

The purpose of this research is to improve protection

performance for the head and neck of rear-seat occupants. A new rear-seat airbag system has been developed that does not require any airbag mounting part or any reaction force support structures in front of the occupants. This makes it possible to install the system even under the traditional constraints present in the rear seats. This paper presents an outline of the new airbag system, an analysis of bag deployment behavior and the results of sled tests conducted to confirm the effect of the system on reducing occupant injury levels.

OVERVIEW OF NEW AIRBAG SYSTEM

Structure

In order for an airbag to absorb an occupant's kinetic energy, the bag must be supported so that it can generate reaction force toward the occupant when it receives force from the occupant. In the front seats, the steering wheel, steering column and instrument panel are among the forward parts that can serve to support the airbags, enabling them to absorb the occupants' kinetic energy.

In contrast to that situation, the rear-seat airbag system described here generates reaction force by deploying two airbags in the area between an occupant's head and thighs when the occupant's upper body tilts forward in a frontal collision. This mechanism serves to absorb the occupant's kinetic energy.

The shoulder belt cover and lap belt cover of a three-point seatbelt system each house one airbag. In the event of a frontal collision, the bags split the covers in the process of deploying in front of an occupant (Figure 3).

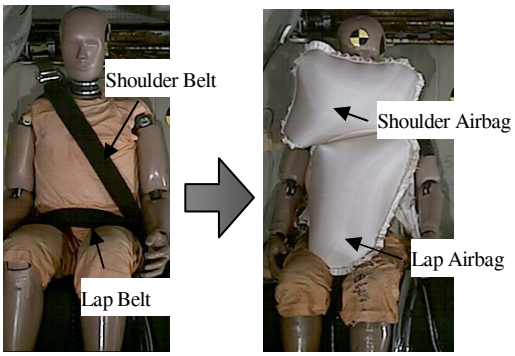

Figure 3. The bags deploy and split the covers in front of an occupant.

Gas is supplied from an inflator incorporated in the buckle to the shoulder belt airbag through a pipe built into the tongue. For the lap belt airbag, gas is supplied directly to the bag from an inflator positioned at the side of the seatbelt anchor (Figures 4, 5).

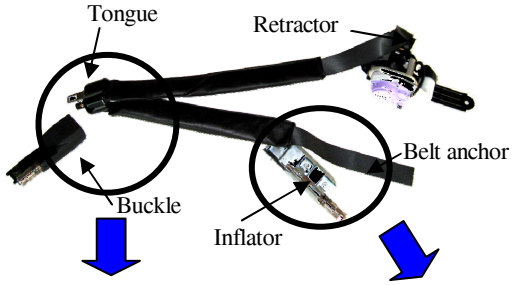

Figure 4. System overview.

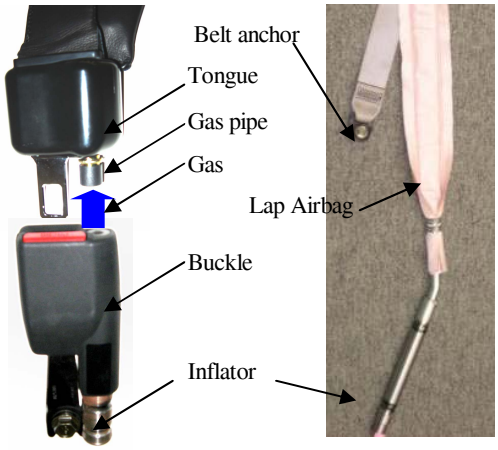

Figure 5. Buckle, tongue and belt anchor.

Airbag impact tests

Airbag impact tests were conducted to confirm the ability to supply sufficient gas pressure to the bags and the reaction force characteristics of the bags themselves. The two airbags and the gas supply mechanism were secured to a wall, and gas was supplied to the bags using the same system configuration as that installed in a vehicle. The bags were struck with an impactor when they were fully deployed. The impact test results confirmed that the necessary airbag internal pressure could be secured and that the bags did not tear or suffer any other damage. (Figures 6)

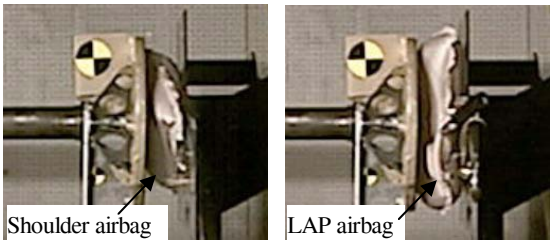

Figure 6. Airbag impact tests.

Static deployment tests

Static airbag deployment tests were conducted using belted Hybrid-III AF05 and 6YO crash test dummies seated in the rear seats. The purpose of these tests was to investigate the influence of airbag deployment under a condition with belted rear-seat occupants. The test setup in Figure 7 left and center shows the dummies leaning against the door and window with the shoulder belt resting on their neck.

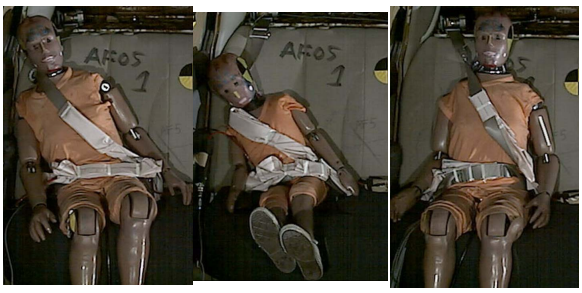

AF05 dummy 6YO dummy belts semi-twisted

Figure 7. Static deployment tests conditions.

This situation represents the slumping posture of rear-seat occupants. The setup in Figure 8 right simulates a situation where the belts are worn incorrectly in a semi-twisted condition, with the result that the bags are deployed between the dummy and the belts. The results of both of these static deployment tests showed injury levels that would not be any problem from the standpoint of occupant protection.

SIMULATION STUDY OF AIRBAG DEPLOYMENT BEHAVIOR

Confirmation of bag behavior for head support

As described in the preceding section, this airbag system is designed to restrain a rear-seat occupant in a frontal collision by deploying two airbags from the lap and shoulder belts in the area between the head and thighs. With this mechanism, it is important for the two airbags to come together without missing one another in the deployment process, so as to provide stable support for an occupant's head.

In order to verify that deployment behavior, simulations were conducted with the MADYMO (Mathematical Dynamic Models) to confirm airbag behavior and the effect of the system on reducing occupant injury levels. The simulations were performed by varying the inflator output, deployment timing and other parameters. The MADYMO simulation model is shown in Figure 8 at different elapsed times.

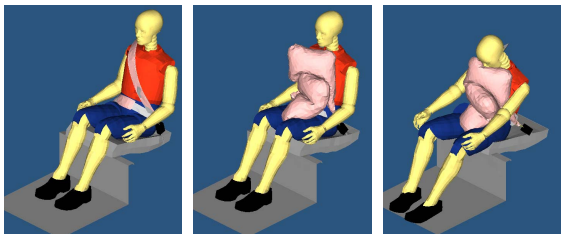

0 msec 35 msec 75 msec

Figure 8. Sled test simulation model (MADYMO)

A simulation conducted using the final test specifications showed that an occupant's head would be supported by the two bags and that the airbag internal pressure was higher than the level in the bag deployment tests. Figures 9 and 10 compare the internal pressure of the shoulder belt airbag and lap belt airbag, respectively, when the pressure was normalized to the level in the bag deployment tests.

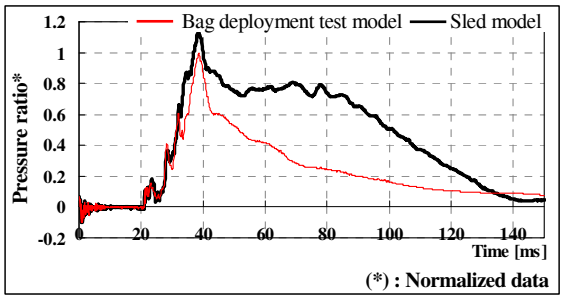

Figure 9. Comparison of the shoulder airbag internal pressure, bag deployment test model and sled model.

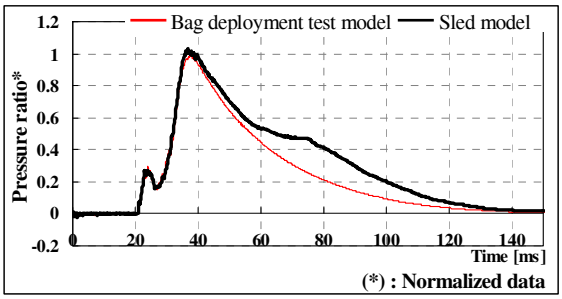

Figure 10. Comparison of the lap airbag internal pressure, bag deployment test model and sled model.

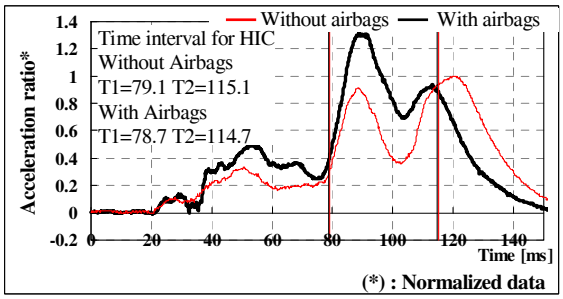

Figure 11. Comparison of the head G in x-axis direction, with and without airbags.

SLED TESTS

Sled test method

Sled tests were conducted to confirm the effect of the specifications obtained in the MADYMO simulations on improving rear-seat occupant protection. Hybrid-III AM50 crash test dummies were seated in the right and left rear seats of the sled with and without the new rear-seat airbag system, with the same type seatbelt with a pretensioner and a loadlimitter, and tests were conducted under conditions corresponding to a full-overlap frontal collision at a speed of 56 km/h. The results were then compared to confirm the effect of the system on reducing occupant injury levels.

Sled test results

Head injury level - Head acceleration (G) values in the x- and z-axis directions and the 3-axis resultant values obtained in the sled tests with and without the new airbag system are compared in Figures 11, 12 and 13, respectively. The head acceleration values were normalized to the peak values recorded without the airbag system.

In Figure 11, it is seen that head acceleration in the x-axis direction in the interval from 40 ms to 110 ms was higher with the airbag system than without it, owing to the reaction force generated by contact between the head and the shoulder belt airbag. The peak value with the airbag system was 31% higher than that without the system.

Similarly, in Figure 12, head acceleration in the z-axis direction was higher with the airbag system than without it in the 40-70 ms interval. During that initial period when the dummy leaned forward, the head was supported at the front from below by the airbags. However, in the latter period from 80 ms to 130 ms when the shoulder belt airbag suppressed the turning motion of the head, acceleration induced by centrifugal force decreased(Figure 13). The peak value with the airbag system was 23% lower than that without it.

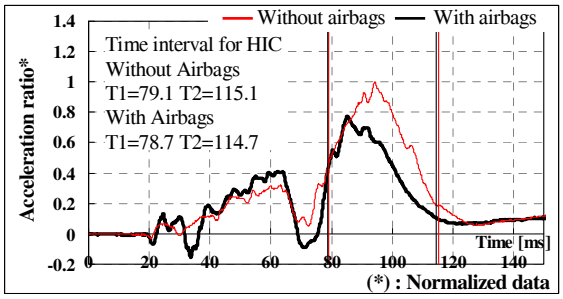

Figure 12. Comparison of the head G in z-axis direction, with and without airbags.

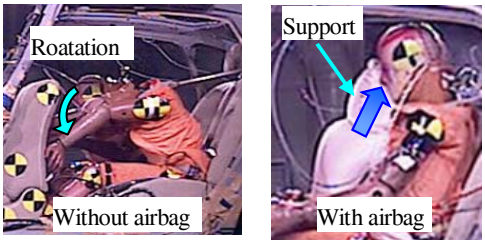

Figure 13. Comparison of the turning motion of the head.

As a result, after 80 ms the 3-axis resultant acceleration was lower with the airbag system than without it, although the former value was higher than the latter one in the initial impact interval from 40 ms to 70 ms

(Figure 14). The peak value with the airbag system was 10% lower in the latter period, and the system had the effect of reducing the head injury criterion HIC36 value by 26% .

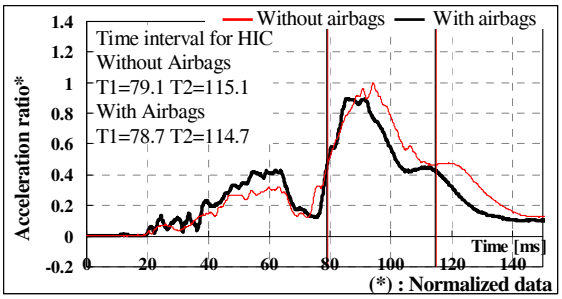

Figure 14. Comparison of the head resultant G, with and without airbags.

The dummy's behavior without and with the airbag system at three elapsed times is compared in Figure 15, respectively.

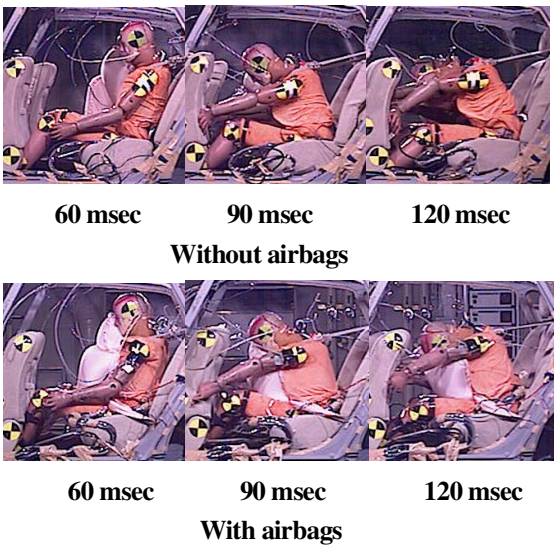

Figure 15. Comparison of the dummy's behavior, with and without airbags.

Neck injury level - The shear load Fx, tensile load Fz and bending moment My of the neck recorded with and without the airbag system are compared in Figures 16, 17, and 18, respectively. The injury levels have been normalized to the peak values without the airbag system.

Without the airbag system the neck shear load Fx was caused by shearing action between the dummy's upper body and the head and neck. The forward motion of the former was stopped by the shoulder belt while the latter tried to continue to move forward due to the inertial mass. In contrast, the results with the airbag system show a large reduction in Fx after 60 msec because the forward movement of the head was restrained by the airbags. The peak value of Fz was 30% lower than the value recorded without the airbag system(Figure 16).

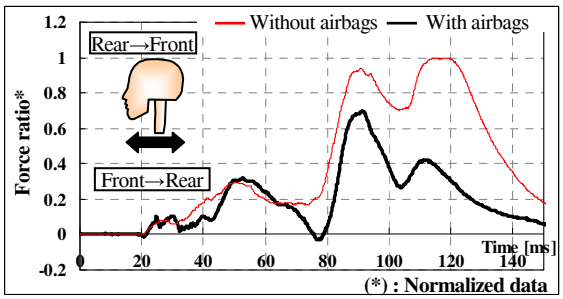

Figure 16. Comparison of the neck UPR shear force (N), with and without airbags.

The neck tensile load Fz was higher with the airbag system than without it in the 40-70 msec intervals because the head was supported at the front from below by the airbags in this initial period when the dummy leaned forward. This result is similar to that mentioned above regarding the acceleration of the head in the z-axis direction. However, Fz was lower with the airbag system than without it after 70 ms because the airbags worked to suppress the turning motion of the head, which reduced the tensile load due to centrifugal force. The system reduced the peak value of Fz by 7% compared with the result without the airbag system(Figure 17).

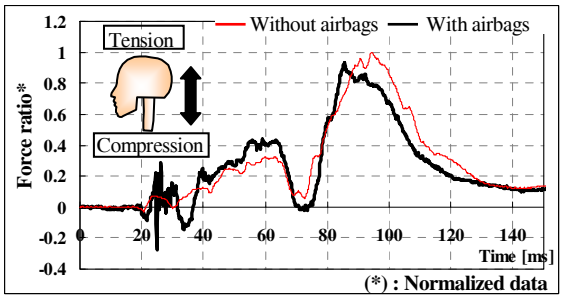

Figure 17. Comparison of the neck UPR tensile force (N), with and without airbags.

The neck bending moment My without the airbag system showed a larger peak on the negative side owing to a moment in the extension direction that

occurred when the lower neck was lifted upward by the upthrust load induced by the bottoming out of the pelvis. The forward movement of the dummy's upper body was stopped by the shoulder belt while the head was bent downward. In contrast, with the airbag system, the airbags supported the head at the front from below, which reduced the forward flexion of the head in the 60-75 ms interval. The upthrust load became a compressive load component in the z-axis direction of the neck, thereby suppressing the increase in the moment in the extension direction, and the peak value of My was reduced by 49%. In addition, following the peak on the flexion side around 100 ms, the airbags supported the head, which suppressed the amount of flexion and the peak value was reduced by 17% compared with the result recorded without the airbag system(Figure 18).

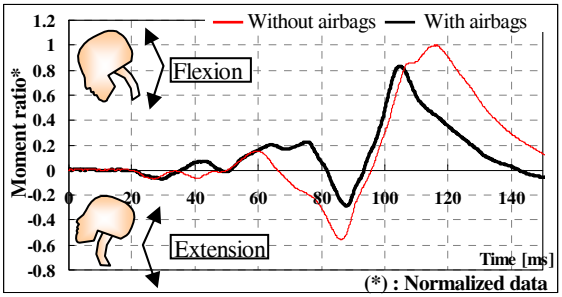

Figure 18. Comparison of the neck UPR bending moment in y-axis direction (Nm), with and without airbags.

CONCLUSION

This paper has described a newly developed rear-seat airbag system that is designed to provide improved protection performance for the head and neck, which together account for approximately 30% of the fatal injuries incurred by rear-seat occupants in frontal collisions. This system does not require any airbag mounting part or reaction force support structure in front of the rear-seat occupants, making it possible to install the system even under the traditional constraints present in the rear seats.

Sled tests conducted with a prototype model of the new airbag system confirmed that it is effective in reducing occupant injury levels. The following results were obtained in the tests.

- The new airbag system restrains an occupant's head and absorbs its kinetic energy, thereby suppressing the centrifugal force resulting from the turning motion of the head and reducing head injury levels.
- By suppressing the turning motion of the head, the new airbag system is also effective in reducing neck injury levels in terms of the shear load, tensile load and bending moment.

The present prototype system houses the airbags inside the covers of the shoulder and lap belts, making the belts stiffer and heavier and thus detracting from their ease and comfort of use. These are aspects that must be examined in future work. It will be necessary to examine ways of weight reduction of the airbags and making them thinner when folded up inside the belt covers, without sacrificing their deployment performance.

ACKNOWLEDGMENTS

The authors would like to thank everyone in Takata Corporation's Research and Development Division for their cooperation with the engineering of the airbags for the bag impact tests and the prototype system for the sled tests.

REFERENCES

[1] Institute for Traffic Accident Research and Data Analysis (ITARDA), ITARDA Information, No. 74 (2008).

[2] Institute for Traffic Accident Research and Data Analysis (ITARDA), Traffic Accident Survey and Analysis Report for FY 2007, III-3 Analysis of Vehicle Structures and Safety Equipment, 3-1 Analysis of Rear-seat Occupants (2008).

[3] Richard Kent et al., Rear seat occupant protection in frontal crashes and its feasibility, Paper 2007-0386, 20th ESV (2007).

PROTECTION SYSTEM FOR FAR-SIDE OCCUPANTS IN LATERAL CRASHES

Benedikt Heudorfer
Michael Kraft
Takata-Petri AG
Germany
Paper Number 09-0295

ABSTRACT

Although modern vehicles are equipped with multiple restraint systems such as airbags and seatbelts, there would be a further possibility to reduce occupant injury in even the best-pick category vehicles. The protection systems are mainly designed for occupants that are positioned closest to the intrusion. However, side-impact field data show approximately one-quarter to one-third of severely injured occupants sit on the far-side of the vehicle, furthest from the intrusion.

This study presents a novel protection system which is placed between the two front passengers to protect them from injuries caused by far-side impacts. The fixation of the performance-added-airbag to the seat is designed in a pivot-like method to ensure a laterally stiff protection element, minimizing the excursion of the occupant's torso and head. The concept is designed to incorporate only minimal changes to existing seat and seatbelt designs. With reference to field data accidents, different impact angles have been sled tested under LINCAP conditions.

Results show a high benefit of the proposed Mid-Mount Bag. Keeping the occupants on their own side of the vehicle as much as possible can mitigate many injuries caused by the vis-à-vis interior or by other occupants. The total torso excursion could be reduced by 45% compared to scenarios without adequate far-side protection.

With regard to the field data, approx. 70% of MAIS3+ far-side injuries can be avoided by the Mid-Mount Bag. Although installing additional airbag systems will have a cost impact, this impact is balanced by potentially saving numerous lives. The Mid-Mount Bag brings us closer to our dream of having zero victims due to traffic accidents.

INTRODUCTION

Throughout the past decades, major advances in automotive safety have been achieved. Today, the human toll due to road accidents is decreasing in nearly all developed countries [7]. Active safety which seems nowadays to take most of the attention is making good progress by putting new safety systems on the road in order prevent an immanent crash or support and guide the driver. Nevertheless, there are still further advances needed in passive safety. Looking at various safety rating schemes you will find listings which show the safest cars available. However, it is to be remembered that those ratings are focusing on standardized testing protocols. In the real world there are frequent accident scenarios which are only partially or not at all addressed by those rating schemes. In this paper, we consider lateral crashes in which an occupant is seated at the far side of the impact, i.e. the occupant is located at the non-stuck side of the vehicle.

MOTIVATION

An objective of this study was to examine injury patterns for belted far-side front seated occupants in lateral collisions. Concluding the results, various crash tests were conducted to better understand the occupant kinematics that cause the most frequent injuries as well as developing countermeasures in terms of a protection system to significantly reduce these injuries.

Roughly half of all car accident casualties are involved in side collisions. Throughout the literature, it is a well-know fact that this accident type causes severe injuries to the passengers. Especially those occupants who are seated on the non-struck or far side of the collision experience injuries that account for about one-third of all side collision caused injuries [1],[4]. Further field data activities dealt with a closer analysis on the causation of far-side injuries and occupant kinematics. This was done in order to identify the method to protect far-side occupants by means of a protection system.

ANALYSES OF FAR-SIDE INJURIES BASED ON NASS/CDS

In a NASS/CDS query from 1998-2005, far-side occupants were defined as front left passenger with right side damage and principle direction of force (PDOF) 90° ±50° or front right passenger with left side damage and PDOF 270° ±50°.

The following boundary conditions were set: only the MAIS 3+ respectively AIS 3+ filter was applied; unbelted occupants as well as rollover were excluded from the analysis. The resulting data contained a total number of 216 cases, whereby 163 cases were the front left passenger and 53 were the front right passenger.

On the injury level, it resulted in a total of 245 injuries to the front left passenger and 75 injuries to the front right passenger. Table 1 shows the

distribution of body regions by passenger seating position.

Table 1
MAIS 3+ injury distribution for belted occupants in far-side crashes by body region only one injury counted per body part

Front Left Passenger AIS 3+

Body Region	No.	Percentage
Chest	85	35%
Head/Neck	77	31%
Abdomen	26	11%
Pelvis	21	9%
Upper X	18	7%
Lower X	12	5%
Other	6	2%
Total	245	100%

Front Right Passenger AIS 3+

Body Region	No.	Percentage
Chest	26	35%
Head/Neck/Face	28	37%
Abdomen	6	8%
Pelvis	4	5%
Upper X	4	5%
Lower X	4	5%
Other	3	4%
Total	75	100%

Digges et al. also investigated injuries to restrained occupants in far-side crashes [2] in NASS/CDS data set. Herein it was concluded that the most frequent injuries in the case of a far-side accidents are head and torso injuries.

The injury mechanisms and kinematics of chest and abdominal injuries in far-side crashes have been researched in detail by Fildes et al. [5]. As a result from this paper, the head, chest and abdominal injuries are also the top three injuries associated with far-side crashes. Charles [6] highlights the head and thorax injuries as the top injuries as well.

Diagram 1 shows the distribution of AIS 3+ injuries by the injuring contacts. The blue bars are related to the front left passenger contacts. The green bars are related to the front right passenger contacts. The categories 'Seat/Back', 'Belt/Webb', 'Front Interior', 'Other/Misc' are somehow distributed equally between front left and right side passengers. At least there are no significant recognizable discrepancies.

The unequally distributed category 'Other Occupant' roots back to the fact that a front left side passenger is always seated in the vehicle, whereas not always is a passenger seated in the right front seat of the vehicle. It is a trivial fact that the category Right Interior addresses the front left passenger in a far-side crash, whereas the category Left Interior addresses the front right passenger in a far-side crash.

Diagram 1
Distribution of injuring contacts for AIS3+ injuries of front left and front right passengers

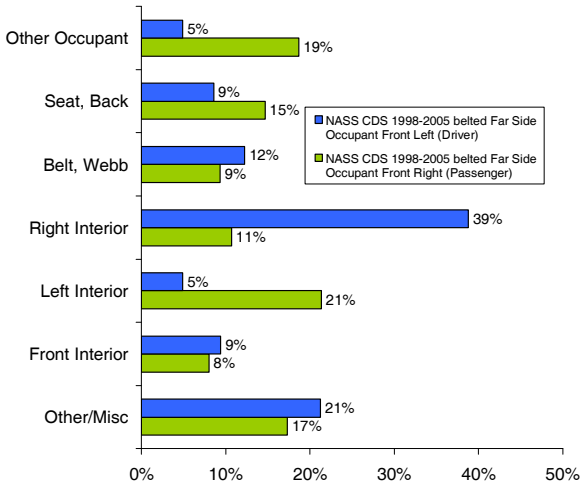

Charles [6] did a comparison of mortality, injury severity and injury patterns between near and far-side occupants in side collisions. He also showed two single cases where large deformations of the side structure of the vehicle are visible. Thereby injury sources such as vis-à-vis side interiors become evident.

All these field data define the requirements and boundary conditions for a restraint system. From the analyzed body regions it is obvious that an optimally designed restraint system needs to have both a protection zone for the head as well as for the thorax, respectively the chest. The results from the analysis of the injuring contacts concluded that a protection system, too, needs to protect against perpendicular contacts as well as oblique contacts from a view of a far-side seated occupant.

CONCEPTUAL CONSIDERATIONS

Altogether, the field data and injury pattern show that the following categories need to be addressed for maximum protection:

- Protect the far-side occupant not only for perpendicular impact but also for oblique impact.
- Limit the potential interaction with the vehicle interior as much as possible.
- Develop a protection system not only beneficial for dummies but also for humans.

Figure 1
Far-side dummy kinematics in a far-side lateral impact

Figure 1 shows the dummy excursion in a possible far-side condition. It is to be considered that current dummies have a fairly stiff spine (no bending, no stretching). Digges [3] shows the fundamental differences between a dummy and a human in a far-side condition. In a real crash the far-side occupant is well supported at the pelvis by means of the middle console and the lap belt. However, the shoulder belt typically slips off and hence the upper torso and head will rotate about the pelvis towards the intruding side wall. Significant bending and stretching of the spine of the far-side occupant is seen. The result is a much larger excursion of the head and upper torso when comparing those two measures with a dummy. As shown in Diagram 1, there are not only injuries from contact to interior parts but also from the belt and webbing. In consequence, the likelihood of severe injuries becomes much higher for humans than for dummies. But it is only true if the occupant is actually allowed the higher excursion. If we can avoid the occupant excursion we may also avoid the injuries.

Assuming the dummy/occupant is actually kept well within its seat (by a to-be-installed protection system); we can expect their lateral motion pattern of both the dummy and the occupant to be the same. This is a fair assumption because the difference in spine bending and stretching will not occur.

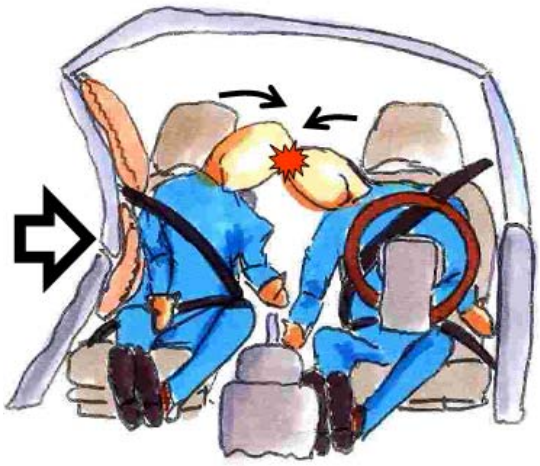

Figure 2
Both dummies are at risk for interaction

In case of two occupants in one seating row (driver and passenger next to each other) there is the further injury risk of interaction. This is shown in Figure 2. Calculations from t_1 (t_1 = triggering of restraint devices) show we want to focus on 50ms at which point the two occupants have the following status:

- Near-side occupant: Intrusion of the side structure is in full progress; the Head-Side Airbag and Thorax Airbag are fully engaged; the occupant is under its highest loading and the rebound is about to start.
- Far-side occupant: The propagation of the crash pulse throughout the vehicle structure is somewhat delayed and has just arrived at the far-side seat. Hence, the far-side occupant starts to move towards the middle of the vehicle and beyond.

As a result, the two occupants now move towards each other and there is a significant injury risk from potential occupant interaction. To prevent injuries in such a scenario a protection system is needed to keep the two occupants apart from each other.

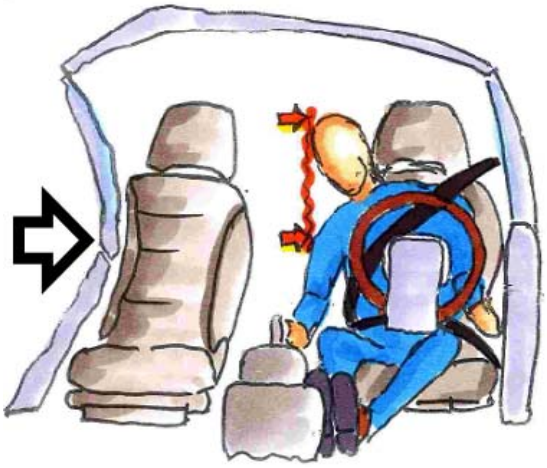

Figure 3
The far-side dummy/occupant needs to be kept as much as possible in its seat (smallest possible excursion)

Figure 3 illustrates the specification of the far-side protection device in terms of limiting the occupant excursion towards the middle of the vehicle. In summary, the following specification is postulated:

- Limit the occupant excursion towards the middle of the vehicle as much as possible, i.e. the CoG of the far-side occupant/dummy head should not cross the geometrical middle line of the vehicle.
- Cover various impact angles, e.g. 60° and 90° lateral impact (60° = 2 o'clock; 90° = 3 o'clock).
- The crash pulse should be equivalent to a standard side impact pulse e.g. LINCAP (max. acceleration at far-side seat: 20g).
- The integration of such new protection device should require minimum modifications to an existing vehicle design.
- Cost, package and weight need to be as low as possible.
- The comfort of the occupant should not be reduced by an additional protection device for the far-side condition.

Note: Throughout the development of the far-side protection system, it is assumed that the occupant is secured by a standard 3-point seatbelt including a pyrotechnic pretensioner.

Several concepts were considered as possible technical solutions:

- Extended seat side wings at shoulder and/or thorax (Feist [4])
- Improved seatbelt (e.g. X-type or H-type)
- Deployable middle console (e.g. airbag deploys upwards)
- Deployable head-shoulder-thorax support (airbag) in seat side wing

These concepts were compared with the provided specifications shown above. The preferred protection concept is an airbag mounted at the seat side wing. It is deployed by a hybrid or stored gas inflator and designed to be airtight for an extended time to provide protection not only during the first impact but also during a multiple crash scenario or a rollover. Further on this concept shall be called MID-MOUNT BAG.

MID-MOUNT BAG CONCEPT

With a novel protection system which is mounted to the seat frame in a specific way, it is possible to reduce injuries and fatalities in the case of far-side crashes significantly. The cushion is designed to keep the occupant restrained as shown in Figure 3. The specific cushion design and a special way of attachment of the protection system to the seat frame are two of three key factors for the restraint effect.

Figure 4 shows the principle function of the Mid-Mount Bag in a top view. In contrast to ordinary Side-Thorax Airbags, the Mid-Mount Bag is designed to limit the excursion of the occupant by keeping the person in its position as much as possible i.e. it is rather a supporting device than an energy absorbing one. The cushion has no means for venting.

The Mid-Mount Bag is attached and mounted to the seat frame on a lateral portion. The distal ends of the airbag can freely rotate around a lateral connection.

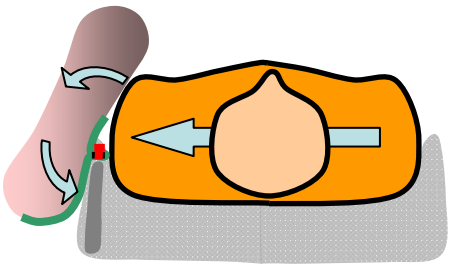

Figure 4
Principle mode of function of the Mid-Mount Bag.

Combining the advantages of the high internal pressure of the Mid-Mount Bag (approx. 200kPa) with a pyrotechnically pretensioned seatbelt, the excursion of the occupant/dummy is reduced significantly. The high pressure is the third key factor of the Mid-Mount Bag. The occupant applies a force on a lateral side of the Mid-Mount Bag, the bag then rotates around its rotational point and distributing the force to the side of the seat frame. This requires a stiff transfer of the force which is established by the internal pressure.

The design of the cushion contains some novel features. Figure 5 shows a side view of the Mid-Mount Bag.

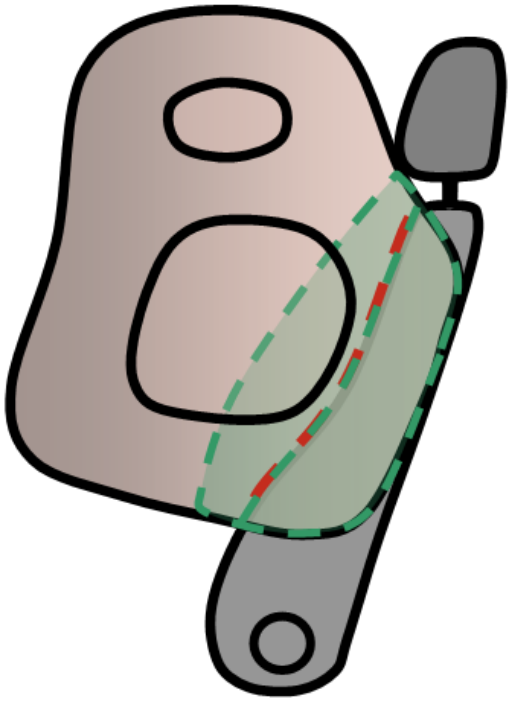

Figure 5
Side view of the Mid-Mount Bag

The cushion has been designed to meet not only perpendicular but also oblique crash types. The two big zero tethers' function is to reduce volume, allowing for a smaller inflator. Combining all those different properties of the Mid-Mount Bag, it was possible to create a protection system that achieves high benefit and improvement in the case of a far-side side collision.

RESTRAINT PERFORMANCE

Compared to ordinary side airbag applications, the Mid-Mount Bag has a slower deployment. This is due to a longer period of time for the crash pulse to reach the far-side seat/occupant. The deployment criterion was to achieve the pressure level of 200kPa within 40ms.

In Figure 6, the deployment sequence is shown. The deployment pattern must be as close as possible to the occupant in order to avoid the potential for the airbag to be hindered by the neighboring seat or occupant or any other interior part. The two high pressured areas atop and below the shoulder, including the special cushion attachment design to the seat frame, gives enough side support to adequately restrain the occupant.

This can be observed in the dynamic tests which were conducted with two different impact angles, 90deg and 60deg, and a crash pulse similar to the LINCAP test configuration.

Figure 7 shows the maximum excursion of the dummy at different impact angles. It is obvious from the pictures that the Mid-Mount Bag limits the excursion much more effectively.

Figure 6
Sequence of a deployment test

Impact angle: 90deg

Impact angle: 60deg

Figure 7
Maximum torso excursion at two different impact angles

The results of a more objective measurement are shown in Diagram 2. The excursion of the head CoG was measured in both cases with and without the Mid-Mount Bag at the 90deg and 60deg impact angle.

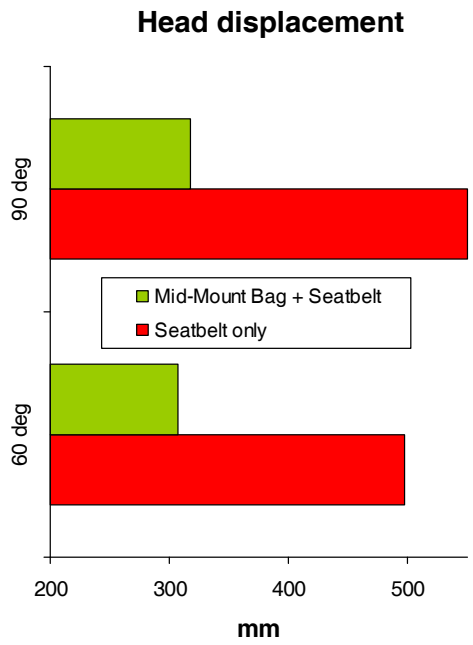

Diagram 2
Maximum head displacement at 60 deg and 90 deg impact angle

In these cases, the Mid-Mount Bag reduces the excursion by 45% in the 90deg impact angle and by 40% in the 60deg impact angle. In both cases, the head CoG did not cross the vehicle center thus fulfilling the previously set target specification.

In summary, the occupant was kept on its own vehicle seat and therefore avoided many of the typical injuries that are likely in today's vehicles without an appropriate far side protection device.

The force retaining the shoulder, which is applied by the seatbelt, is the most important for the restraining benefit. The smaller the impact angle becomes, the higher the effect of the safety belt becomes. Figure 8 shows the difference in the 60deg case with and without pretensioning.

Belt pre-tensioning

ON **OFF**

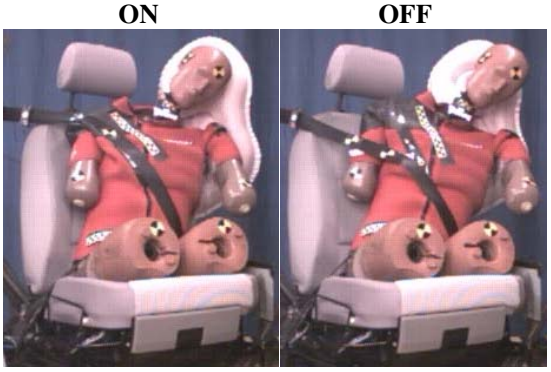

Figure 8
Comparison of torso excursion with and w/out belt pre-tensioning

OUT-OF-POSITION

Tests have been conducted to evaluate the system in OOP tests. In the absence of a defined position for a far-side device, a position according to the TWG was chosen. The most critical one was found to be a rearward facing position. The dummy was placed on the inboard side of the seat kneeling partially on the middle console. Figure 9 illustrates the dummy position. Here, the 3-year-old dummy is leaning with its torso and head directly towards the front of the tear seam through which the Mid-Mount Bag inflates.

The tests produced good results. None of the dummy values were higher than 60% of the allowed limits.

Other positions have not yet been tested due to the lack of any defined requirements for this specific application. But as soon as there are any direction-giving proposals exist, these positions will be further evaluated.

Figure 9
Dummy position in out-of-position testing

Concluding on the restraint performance the Mid-Mount Bag improves the situation for a far-side occupant in lateral collisions much by establishing an effective support between the both occupants. The Mid-Mount Bag supports the occupant that well that the occupant stays on its own vehicle side and does not cross the vehicle center line which was defined as the limit.

DISCUSSION

Considering the amount of work and resources put into the protection for near-side occupants in a side crash, it can be assumed that industry, regulatory bodies and consumer information institutes are deeply concerned about life endangered by a vehicular side-impact. But side-impact protection is not only near-side occupant protection. As shown in the chapter MOTIVATION, about a third of all side-impact injuries (MAIS 3+) are associated to far-side. However, there is no clearly determined group within the safety community to reduce these risks in daily traffic. Up until now, there have been many research papers explaining the need for a far-side protection system. A few in the industry have chosen to work towards an improvement but no determined actions were taken. This is an unfortunate situation were we clearly have an opportunity to reduce traffic fatalities.

The proposed Mid-Mount Bag concept has demonstrated its effectiveness under various requirements. Without any doubt, this concept can be further improved to produce an even better protection performance. However, there is the saying, ‘A bird in the hand is worth two in the bush’ meaning we need to take small steps in the right direction first instead of bigger steps in possibly the wrong direction.

CONCLUSIONS

The project set out to tackle the issue of occupants which are seated on the non-struck side of the vehicle in a lateral crash. By employing the Mid-Mount Bag, a clear advance in restraint performance is shown. However, no sacrifice was made towards passenger comfort. The concept is a straight forward combination of existing and new technology, offering a solution to a well known issue.

REFERENCES

[1] J. Augenstein, E. Perdeck, P. Martin, J. McKinnon, L. Labiste, J. Stratton, T. Horton, M. Singer (The William Lehmann Injury Research Center), K. Digges and J. Steps (G.W. University). 2000. “Chest/Abdominal Injuries in Side Crashes“. CIREN November 30, 2000

[2] K. Digges, (The Automotive Safety Research Institute), D. Dalmotas (Transport Canada). 2001. “Injuries to Restrained Occupants in Far-Side Crashes”. Paper Number 351. ESV Paper 2001

[3] K. Digges, P. Mohan, B. Alonso (Georg Washington University), H. Gabler (Virginia Polytechnic Institute and State University) 2005. “Characteristics of the Injury Environment in Far-Side Crashes”. AAAM Paper 2005

[4] F. Feist and J. Gugler. 2007. “APROSYS SP11 – Methodology to Address Non Struck Side Injuries”

[5] B. Fildes, M. Fitzharris (Monash University Accident Research Centre, Melbourne Australia), H. C. Gabler (Virginia Tech, Blacksburg, VA), K. Digges (Georg Washington University, VA), S. Smith (GM Holden Innovation). 2007. “Chest and Abdominal Injuries to Occupants in Far-Side Crashes”. ESV Paper 2007

[6] Charles McC. Mathias Jr. 2007. “Comparison of Mortality, Injury Severity and Injury Patterns Between Near Versus Far Occupants of Lateral Crashes”. University of Maryland, Baltimore. CIREN Quarterly Meeting March 2007

[7] OECD, International Transport Forum. “TOWARDS ZERO – Ambitious Road Safety Targets and the Safe System Approach”. 2008.
www.oecd.org/publishing
ISBN 978-92-821-0195-7

DYNAMIC SIDE IMPACT TESTING WITH THE 50TH PERCENTILE MALE WORLDSID COMPARED TO THE ES-2RE

Allison E. Louden
National Highway Traffic Safety Administration
United States
Paper Number: 09-0296

ABSTRACT

The agency released the final rule for Federal Motor Vehicle Safety Standard (FMVSS) No. 214 "Side Impact Protection" in September 2007, which put in place upgrades that involve moving deformable barrier (MDB)-to-vehicle and vehicle-to-pole crash tests with a 50th percentile adult male, the EuroSID 2re (ES-2re) and a 5th percentile adult female, the SID-IIs dummy. Recently, the National Highway Traffic Safety Administration (NHTSA) began evaluating the 50th percentile male WorldSID in these types of crashes using the same fleet vehicles. This paper includes an evaluation of the dummy's durability in crash testing and gives a comparison of the test results with those of the ES-2re dummy. The two dummies have different anthropometries and seating procedures which affect the final results. In general, the WorldSID produced more elevated responses than the ES-2re dummy for both test modes.

INTRODUCTION

The FMVSS No. 214 final rule upgraded the 50th percentile male dummy from the US SID to the ES-2re dummy. This dummy was a European enhanced side impact dummy which was used in the Economic Commission for Europe Standard, R95 (ECE R95). It was developed originally as the ES-1, which was later modified to ES-2. The ES-2 is the current dummy used in European standards. The ES-2 was modified with rib extensions, thus the name ES-2re and is the current dummy being used in the new FMVSS No. 214 test requirements. [1]

At the same time the EuroSID dummy was evolving, a second dummy was also being developed as a collaborative project to develop a world harmonized side impact dummy. The dummy's anthropometry was based on a NHTSA study done by the University of Michigan Transportation Research Institute (UMTRI) that looked at the anthropometry of actual humans in actual vehicle seats. [2][3] After extensive evaluations, the NHTSA concluded that the WorldSID was not ready for use in Federal regulations and its potential use had not been fully assessed by the agency for inclusion in the 2007 FMVSS No. 214 Final Rule. The agency further stated that, upon completion of its evaluation of the WorldSID, it would consider possible incorporation of the device in FMVSS No. 214. [4]

DUMMIES

ES-2re

The ES-2re sits in an upright position, with a seating height of 660mm (see Figure 1 for more details). It is instrumented with the following: an upper neck load cell, a shoulder load cell, three rib potentiometers that measure lateral deflection, three abdominal load cells that measure the lateral loads, a pubic load cell, and accelerometers at numerous locations to measure the "g" levels that are applied to the dummy during a side impact.

WorldSID

The WorldSID sits in a more slouched position and is slightly shorter than the ES-2re dummy (see Table 1 for more details). It was instrumented with the following: upper and lower neck load cells; IR-TRACCs in the shoulder, thoracic ribs, and abdomen ribs; a shoulder load cell; a pubic load cell; iliac and sacrum load cells; and accelerometers at numerous locations to measure the "g" levels that are applied to the dummy during a side impact. The WorldSID also has the option of having its data acquisition system onboard. All of the tests conducted with the WorldSID dummies utilized the onboard data acquisition system.

Table 1.
Dummy Anthropometry Measurements

	WorldSID	ES-2re
Shoulder width	480	485
Thorax width (nipple)	371	337
Pelvis width	410	355
Seating height (neck/torso interface)	600	660
Seating height (erect)	870	920
Leg Length	555	452

All measurements are in millimeters.

Both dummies are designed to study occupant response to potential injury in side impact crash tests. In Figure 1, the ES-2re is in the red suit (left) and the WorldSID is in the purple suit (right). As you can see, the ES-2re sits slightly higher than the WorldSID, which puts the head and ribs in different vertical locations.

Figure 1. ES-2re and WorldSID Dummies.

Anthropometry Analysis

Anthropometry had a large effect in the crash tests. The two dummies sat differently in the vehicle seats, which in turn allowed different body areas to be loaded, which caused differences in the final responses of the dummies.

Figure 2 shows the UMTRI manikin. [2] This manikin represents a series of real adult people and how they sit in vehicles. Figure 3 shows the ES-2re superimposed on the UMTRI manikin. The ES-2re sits taller and more upright in the vehicle seat. Notice the placement of the head and shoulder. The ES-2re head and shoulder are more vertical and rearward than those of the UMTRI manikin. The ribs of the ES-2re are approximately 20-25 degrees from horizontal, even though the dummy is sitting straight up.

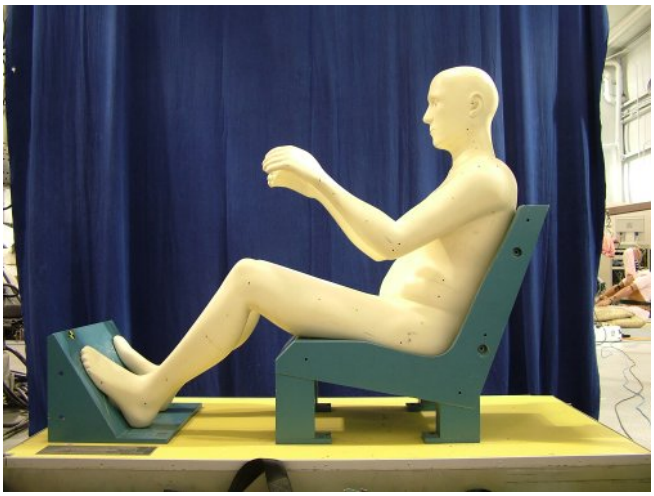

Figure 2. UMTRI Adult Male Manikin.

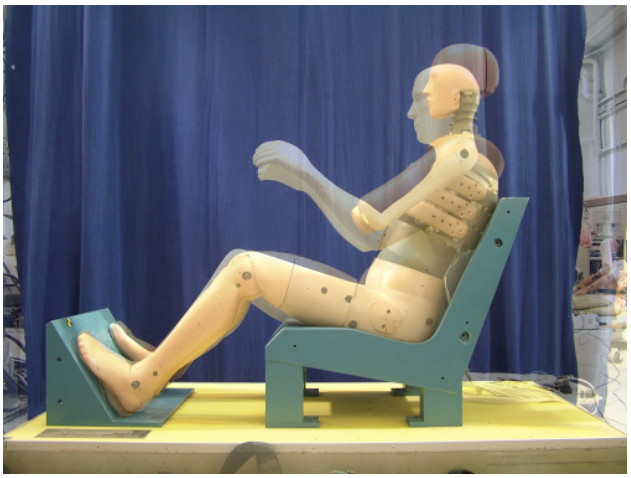

Figure 3. ES-2re Superimposed with the UMTRI Manikin.

Figure 4 shows the WorldSID dummy compared with the UMTRI manikin. The heads and shoulders are almost aligned with each other. The ribs of the WorldSID are in a horizontal plane. Figure 5 shows the ES-2re and WorldSID dummies superimposed on each other. The differences described earlier are more visible when the two dummies are superimposed. The ES-2re head and shoulders are above that of the WorldSID, and its ribs are angled compared to the WorldSID. Also note that the ES-2re dummy's abdomen vertically overlaps the WorldSID's lowest thoracic and top abdominal ribs.

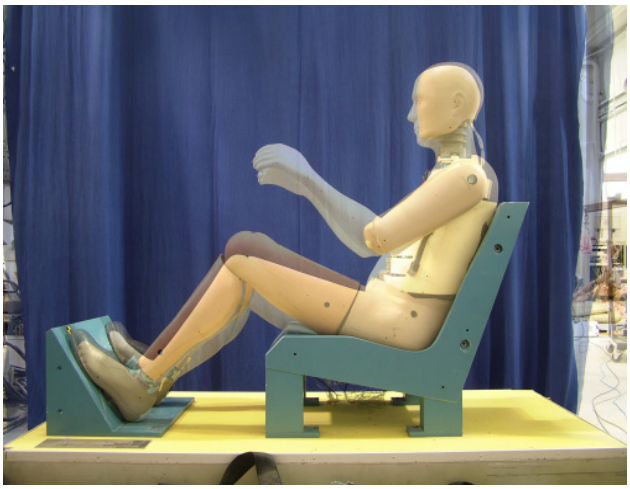

Figure 4. WorldSID Superimposed with UMTRI Manikin.

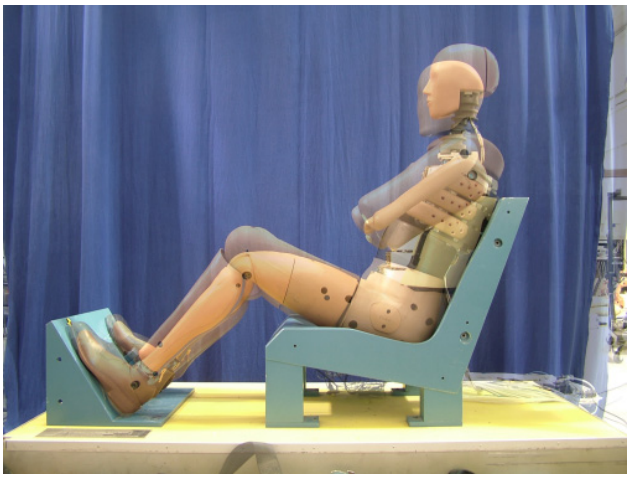

Figure 5. WorldSID and ES-2re Superimposed.

Figure 6 shows a side by side comparison of the two dummies without their jackets. The thoracic ribs do not align directly with each other as previously noted. This is especially important when analyzing the data. According to the pictures an assumption can be made about the approximate alignments of the ribs. The WorldSID shoulder rib aligns with the ES-2re's 2nd thoracic rib, and the WorldSID's 1st thoracic rib aligns with the ES-2re's 3rd thoracic rib. The ES-2re's abdomen aligns with the WorldSID's thoracic rib #3 and abdomen rib #1; the WorldSID's abdomen rib #2 is aligned with the ES-2re's pelvis.

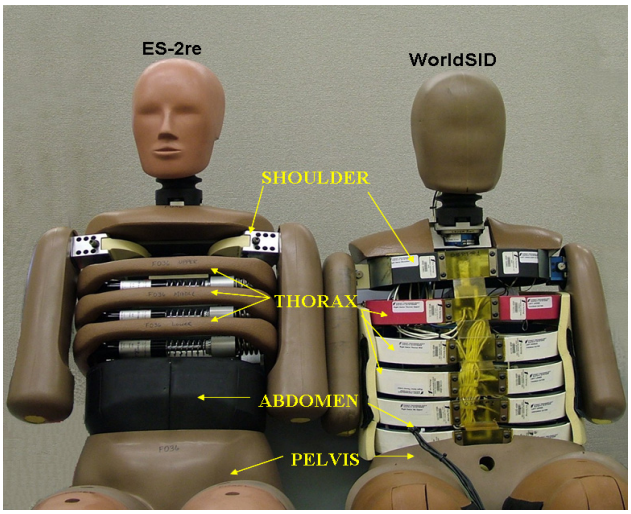

Figure 6. ES-2re and WorldSID Comparison View.

The anthropometry of the two dummies is very important in how the two dummies respond in the crash, especially in the pole test where the head CG determines the impact point on the vehicle.

TEST MATRIX and PROCEDURES

The NHTSA tested eight model year (MY) 2005 vehicles in the oblique pole test and five MY 2005 vehicles in the MDB test. The vehicles chosen to be tested with the WorldSID had been previously tested with the ES-2re dummy (Table 2). All of the vehicles had some form of head protection. The 2005 Subaru Forester and Volkswagen Beetle convertible had seat-mounted head and thorax air bags. The 2005 Saturn Ion had a head curtain but no thoracic air bag, whereas the other six vehicles had thoracic and head curtain air bags.

Table 2.
Test Matrix

Vehicles	MDB	Oblique Pole
2004 Honda Accord		√
2005 Subaru Forester	√	√
2006 Toyota Sienna		√
2005 Ford 500	√	√
2006 VW Jetta	√	√
2005 Saturn Ion	√	√
2005 Ford Expedition		√
2005 VW Beetle (Convertible)		√
2005 Honda CRV	√	

Test Setup

The tests were conducted per the FMVSS No. 214 2007 final rule test procedures. The dummies were instrumented with additional instrumentation than required by the rule. The MDB tests were conducted with two ES-2re or two WorldSID dummies seated in the left front and left rear seating positions. The oblique pole tests were conducted with one ES-2re or WorldSID dummy in the left front seating position.

The ES-2re dummies were seated in accordance with the final rule seating procedures; seat in midtrack, seat full down, and seat back angle determined by the OSCAR procedures (~25 degrees). The WorldSID was seated using the same initial conditions for the seat and adjusted per the seating procedures for the WorldSID dummy drafted by the WorldSID Task Group (version 1.0).[3] This seating procedure allowed for the seat back to be moved in both fore and aft directions in order to level the thorax and the head. In some of the vehicles, the seat back was moved one or two notches forward or rearward from the initial position.

The final seating position of the dummies plays a vital role in determining the vehicle-to-pole impact location in the oblique pole test. The final impact point is based on the head center of gravity (CG). In some instances, there was a difference in the final head position between the ES-2re and the WorldSID dummy.

Injury Criteria

The injury criteria used for the ES-2re were those specified in FMVSS No. 214. Some of the injury responses represent a 50% risk of AIS 3+ injury where others represent a 25% risk of AIS 3+ injury. [4] The WorldSID's injury criteria used for this testing were formulated by the WorldSID task group. Table 3 shows the corresponding injury assessment reference values (IARVs) used for both dummies. The WorldSID proposed values represent a 50% risk of AIS 3+ injury. [3]

Table 3.
Injury Assessment Reference Values (IARVs)

	WorldSID*	ES-2re
HIC36	1000	1000
Thorax Deflection (mm)	56	44
Abdomen Deflection (mm)	53	n/a
Lower Spine Resultant (g's)	78	82**
Abdomen Force (N)	n/a	2500
Pubic Force (N)	1790	6000
Pelvis Resultant (g's)	77	n/a

*WorldSID values are proposed IARV's by working group.
**Not in used in final rule, but used to monitor the lower spine results.

TEST RESULTS

The vehicles chosen for this testing were not designed to meet the requirements of the oblique pole test; however the purpose was to compare the different dummy responses. The dummy responses for each test are shown in the Appendix.

The MDB tests produced similar responses between the two dummies, although the WordSID had more elevated responses (i.e. 80-99% of the proposed IARV) for both occupants than the ES-2re dummy. The pole tests resulted in some vehicles exceeding the IARVs for both dummies. The WorldSID produced more elevated injury responses in both of the test modes.

MOVING DEFORMABLE BARRIER

The MDB tests resulted in all vehicles meeting IARVs for their corresponding dummy. For the WorldSID tests, the 2005 Saturn Ion met the IARV for maximum rib deflection by a very narrow margin (55.98 mm). It also had elevated responses for the abdomen deflection, pubic force, and pelvis acceleration (Figure 7). In the ES-2re tests, the 2005 Honda CRV had an elevated thorax deflection response in the left front seat. These minor differences may be attributed to the differences in dummy positioning in the vehicle and seat. The rib responses may also differ due to how the ribs react with the deformable barrier and door intrusion. Unlike the ES-2re's rib modules, which are constrained to deflect only in the pure lateral direction, the IR-TRACCs in the WorldSID's ribs may deflect obliquely, and the IR-TRACCs are

designed to measure displacement in the direction of the rib loading.

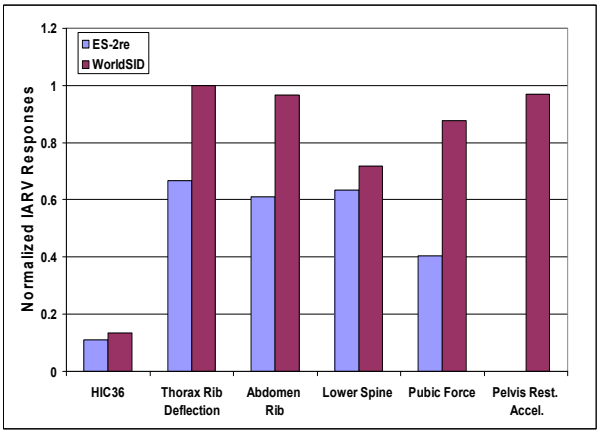

Figure 7. 2005 Saturn Ion Normalized IARV Responses.

OBLIQUE POLE

The test results for the oblique pole varied for each dummy, and the injury responses can be found in the Appendix. The tests with the ES-2re dummy resulted in five of the eight vehicles exceeding at least one IARV. The VW Jetta, Honda Accord and VW Beetle Convertible met all IARVs. The tests with the WorldSID dummy also had five of the eight vehicles exceeding at least one of the proposed IARV responses. As with the ES-2re, the Jetta and Accord met all the IARVs with the WorldSID, but the third vehicle was the Toyota Sienna rather than the VW Beetle.

Head Positioning and Responses

The impact point of the oblique pole test is determined by the final location of the head CG. Comparing the same vehicles with the two different dummies, a general trend was noticed. For the vehicles tested, the two dummies sat differently in the same vehicle seat. This was due to the differences in the dummies' anthropometries and to the WorldSID's seating procedure which allows the seat back to be moved to level the thorax and pelvis. These differences changed the impact point on the vehicles depending on which dummy was used. On certain vehicles, this difference affected the deployment time and path of the air bag, and also the structural deformation of the door during impact. This resulted in some significant differences in the HIC36 responses (Figure 8).

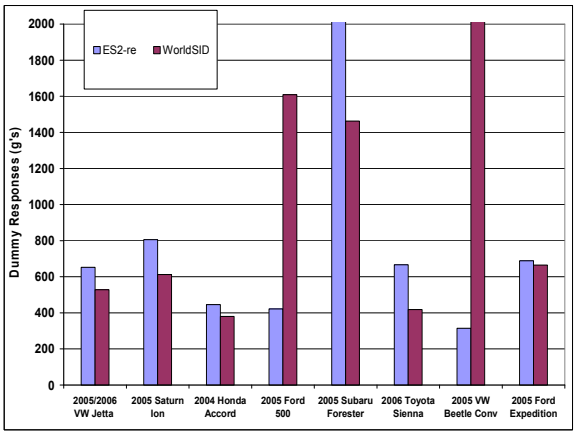

Figure 8. HIC 36 Responses for ES-2re and WorldSID.

Three vehicles, 2005 Ford Five Hundred, 2005 Subaru Forester, and 2005 Volkswagen (VW) Beetle, had very different HIC36 responses when comparing the two dummies. The Ford Five Hundred and the VW Beetle resulted in high HIC responses when tested with the WorldSID and low responses when tested with the ES-2re. The Subaru Forester resulted in high HIC responses for both dummies, but they were higher for the ES-2re.

In the 2005 Ford Five Hundred, the WorldSID's head CG was lower and 3½ inches more forward than the ES-2re in the same vehicle model (Figures 9 and 10). Therefore, the pole struck the vehicle more forward, and the air curtain deployed approximately 15 ms later than in the ES-2re test. This resulted in the WorldSID head striking the pole, which resulted in a HIC36 of 1609 compared to the ES-2re HIC36 of 422.

Figure 9. ES-2re Head Position in 2005 Ford Five Hundred.

Figure 10. WorldSID Head Position in 2005 Ford Five Hundred.

The 2005 VW Beetle also showed a large difference in the HIC36 response between the ES-2re and WorldSID. The HIC36 for ES-2re was 315 compared to 3630 for the WorldSID. As shown in Figure 11, the final placement of the WorldSID in the seat resulted in the seat back being more reclined and the dummy's head CG 1½ inches more rearward than the ES-2re. This affected the impact point of the pole and most likely, the deployment path of the seat mounted combination air bag. In the WorldSID test, the air bag inflated rearward from the side of the seat and didn't get in between the dummy's head and the pole in the correct time, thus resulting in a high HIC response.

Figure 11. ES-2re and WorldSID at 55ms in 2005 VW Beetle.

Thorax and Abdomen Responses

The WorldSID measures the deflection of three thoracic ribs and two abdominal ribs, whereas the ES-2re measures the deflection of three thoracic ribs and the force applied to the abdomen (Figure 6).

The thorax and abdomen directly interact with the door liner, arm rest, and/or thoracic air bag. When comparing the two dummies, the WorldSID gave higher thoracic responses than the ES-2re in four of the eight vehicles tested (Figure 12). The differences in the responses between the two dummies were minimal (within 10%) for four of the vehicles, while they were larger for the other four. The WorldSID had higher abdominal responses than the ES-2re in seven of the eight vehicles, and the responses from the eighth vehicle were nearly identical (Figure 13). The differences in the responses between the two dummies were minimal for three of the vehicles, while they were larger for the other five.

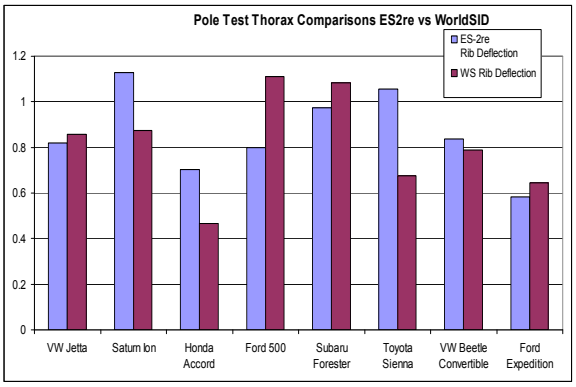

Figure 12. ES-2re and WorldSID Normalized Thorax Responses for Oblique Pole.

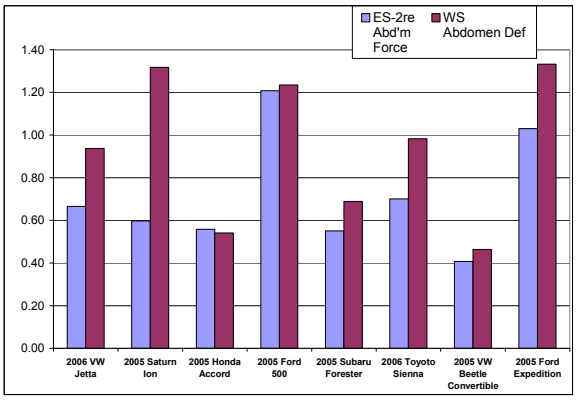

Figure 13. ES-2re and WorldSID Normalized Abdomen Responses for the Oblique Pole.

It is believed that the differences in the thoracic and abdominal responses between the two dummies can be attributed to the differences in their seating postures and positions. Even though the seat back positions were only different by a notch or two, the dummies responded differently. The WorldSID had higher rib responses in Rib 1, whereas the ES-2re had similar responses for all three ribs, and it usually was lower than the deflection that occurred in the WorldSID.

For example, the normalized abdominal responses for the 2005 Saturn Ion went from 0.60 with the ES-2re to 1.32 with the WorldSID. This could be due to the interaction of the armrest, which directly loaded the WorldSID's abdominal ribs, while it loaded the lower half of the abdomen and the upper edge of the pelvis in the ES-2re.

The posture differences in the dummies can possibly create different impact locations, structural deformation, and air bag deployments. These differences can also create different alignment of body regions and interior door surfaces.

Pelvis Responses

The WorldSID and ES-2re pubic load cell are located in very similar areas, but the pelvic areas surrounding the pubic load cell are made of different materials. Also, as discussed previously, the dummies have different abdomen designs. The WorldSID has two abdominal ribs whereas the ES-2re has three abdominal load cells, and the pelvic skin of the ES-2re extends higher than that of the WorldSID (Figure 6).

The WorldSID produced similar responses in all of the vehicles, while the ES-2re responses were more varied (Figure 14). Although low, the WorldSID produced higher responses than the ES-2re in five of the eight vehicles, and they were nearly identical in two of the others.

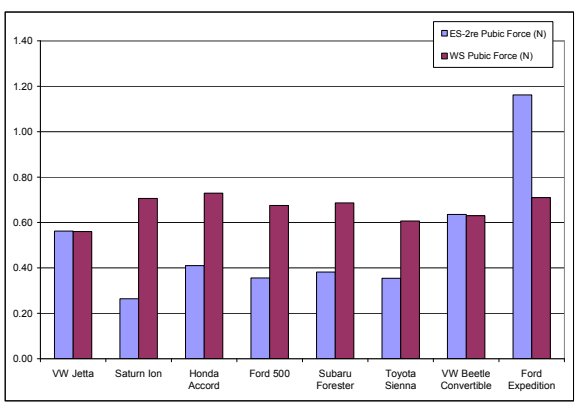

Figure 14. Normalized Pubic Load Cell Responses for ES-2re and WorldSID.

DUMMY DURABILITY

The WorldSID dummies were examined after each test, and pre and post test calibrated after the 3rd use. The dummies only had minor damages; the damage that did occur was a result of the oblique pole testing.

The maximum shoulder deflection was reached during four of the eight oblique pole tests. The shoulder IR-TRACC was damaged during one of these tests. Both ends were bent and one end was damaged (Figure 15). Also, over the testing period, the rib damping material de-bonded from the metal ribs.

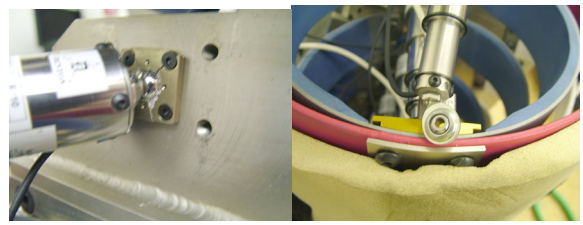

Figure15. WorldSID IR-TRACC Damage.

CONCLUSIONS

- Regardless of which dummy was used, the following were determined:
  - In the MDB tests, all dummy responses were below their corresponding IARVs for all five of the vehicles tested, although several had elevated responses. The driver WorldSID in the Saturn Ion had a maximum thoracic rib deflection of 55.98 mm, which was below the proposed IARV by a very narrow margin (56 mm).
  - In the oblique pole tests, at least one IARV was exceeded for the Saturn Ion, Ford Five Hundred, Subaru Forester, and Ford Expedition.
  - In the oblique pole test, all dummy responses were below their IARV for the Volkswagen Jetta and the Honda Accord.
  - In the oblique pole test, the 'meet/exceed' performance of the Volkswagen Beetle and the Toyota Sienna depended on which dummy was used. The VW Beetle exceeded the HIC criterion with the WorldSID and the ES-2re exceeded the HIC criterion in the Toyota Sienna.
  - In both the MDB and oblique pole tests, the WorldSID dummy produced more elevated (80-99% of proposed IARV) and high (exceeded IARV) responses than the ES-2re.
- The 50th Male WorldSID and ES-2re have different dummy anthropometries.
- The WorldSID is based on the UMTRI anthropometry study, which is based on actual humans sitting in vehicle seats.
- WorldSID sits in a more slouched position and sits lower in the seat than the ES-2re. This places the body regions of the WorldSID and ES-2re in different locations.

- Different head positions produce different impact locations in the oblique pole tests. This may affect the head impact location on the air curtain, sensor responses, and structural deformation.
- The WorldSID and ES-2re thorax and abdomen are aligned differently with the vehicle interior. This can produce different loading on the dummies (e.g. armrest to abdomen), possibly resulting in different responses.
- The overall WorldSID dummy durability is good.

REFERENCES

[1] "Specification of the EEVC Side Impact Dummy Eurosid 1", European Experimental Vehicles Committee, April 1990

[2] "Development of Anthropometrically Based Specifications for an Advanced Adult Anthropomorphic Dummy Family"; Volume 1-2, University of Michigan, December 1983.

[3]http://www.worldsid.org/Work_Items/Worldsid_Official_Documents.cfm

[4] "FMVSS No. 214 Final Rule", Federal Register, 72 FR 51907, September 11, 2007.

APPENDIX: DUMMY RESPONSES

Table 1.
MDB Driver WorldSID Responses

Vehicles	HIC36	Thorax Deflection (mm)	Abdomen Deflection (mm)	Lower Spine (G's)	Pubic Force (N)	Pelvis Resultant (g's)
Proposed Injury Criteria	1000	56	53	78	1790	77
VW Jetta (C+T)	131	37	26	48	1355	44
Saturn Ion (C)	136	56	51	56	1571	75
Ford Five Hundred (C+T)	42	17	22	47	778	38
Subaru Forester(Combo)	33	19	9	35	849	55
Honda CRV (C+T)	47	17	8	31	746	40

Table 2.
MDB Passenger: WorldSID Responses

Vehicles	HIC36	Rib Deflection (mm)	Abdomen Deflection (mm)	Lower Spine (G's)	Pubic Force (N)	Pelvis Resultant (G's)
Proposed Injury Criteria	1000	56	53	78	1790	77
VW Jetta (C+T)	131	18	23	38	871	47
Saturn Ion (C)	260	39	41	55	1192	54
Ford Five Hundred (C+T)	242	36	32	46	1068	68
Subaru Forester(Combo)	122	21	30	36	n/a	43
Honda CRV (C+T)	89	21	32	39	1052	74

Table 3.
MDB Driver: ES-2re Responses

Vehicles	HIC36	Rib Deflection (mm)	Lower Spine (G's)	Pubic Force (N)	Abdomen Force (N)
IARVs	1000	44	82	6000	2500
VW Jetta (C+T)	101	26	28	1969	733
Saturn Ion (C)	110	29	52	2431	1524
Ford Five Hundred (C+T)	66	25	35	1176	1006
Subaru Forester(Combo)	44	21	33	1694	598
Honda CRV (C+T)	100	35	31	1137	524

Table 4.
MDB Passenger: ES-2re Responses

Vehicles	HIC36	Rib Deflection (mm)	Lower Spine (G's)	Pubic Force (N)	Abdomen Force (N)
IARVs	1000	44	82	6000	2500
VW Jetta (C+T)	211	29	53	2542	1378
Saturn Ion (C)	168	27	47	2275	1511
Ford Five Hundred (C+T)	213	25	44	1407	1649
Subaru Forester(Combo)	226	23	35	1948	967
Honda CRV (C+T)	126	5	33	1847	1192

Table 5.
Oblique Pole Driver: WorldSID Responses

Vehicles	HIC36	Thorax Def. (mm)	Abdomen Def. (mm)	Lower Spine Result. (g's)	Pubic Force (N)	Pelvis Result. Accel. (g's)
Proposed Injury Criteria	1000	56	53	78	1790	77
2006 VW Jetta (C+T)	528	48	50	63	1002	57
2005 Saturn Ion (C)	612	49	70	80	1264	68
2005 Honda Accord (C+T)	380	26	29	52	1305	53
2005 Ford 500(C+T)	1609	62	66	82	1209	66
2005 Subaru Forester (Combo)	1463	60	37	79	1227	77
2006 Toyota Sienna (C+T)	418	38	52	68	1085	62
2005 VW Beetle Convertible(Combo)	3680	44	25	69	1127	81
2005 Ford Expedition (C)	665	36	71	77	1270	86

Table 6.
Oblique Pole Driver: ES-2re Responses

Vehicles	HIC36	Rib Deflection (mm)	Lower Spine (G's) (monitored)	Pubic Force (N)	Abd'm Force (N)
IARVs	1000	44	82	6000	2500
2006 VW Jetta (C+T)	652	36	60	3372	1663
2005 Saturn Ion (C)	806	50	76	1585	1494
2005 Honda Accord (C+T)	446	31	52	2463	1397
2005 Ford 500 (C+T)	422	35	68	2133	3020
2005 Subaru Forester (Combo)	2054	43	46	2291	1377
2006 Toyota Sienna (C+T)	667	47	60	2127	1751
2005 VW Beetle Convertible (Combo)	315	37	69	3815	1018
2005 Ford Expedition (C)	689	26	75	6973	2575

Legend:
Lower than 80% of IARV 80%-99% of IARV Exceeding IARV
C=Curtain only; C+T=Curtain and thorax; Combo=Head thorax combination

NEW PROGRAMM FOR THE ASSESSMENT OF CHILD-RESTRAINT SYSTEMS (NPACS) – DEVELOPMENT/RESEARCH/RESULTS – FIRST STEP FOR FUTURE ACTIVITIES?

Volker Sandner
Andreas Ratzek
Dr. Reinhard Kolke
Allgemeiner Deutscher Automobil Club (ADAC)
Germany
Werner Kraus (Chairman of NPACS)
Dr. Maximilian Lang
Österreichischer Automobil Club (ÖAMTC)
Austria
Paper Number 09-0298

ABSTRACT

The protection of children in traffic, especially in cars, is one of the most important tasks facing our society. Children in cars are dependent on the assistance of their parents to provide them with adequate protection through the use of child restraint systems (CRS). Good advice to parents on how to use and fit CRS properly and which CRS offers the best protection are essential.

In Europe, due to the use of differing assessment criteria and rating schemes, the information provided to parents has been very confusing to date. Since there are still major differences in CRS use within EU member states, increased consumer information is a predominant European task.

The largest single advantage gained from this EU project "New Program for the Assessment of Child Restraint Systems" is that all members of the NPACS Project, representing the Governments of four European countries, research institutes, ICRT European consumer organizations and FIA automobile clubs, have cooperated to develop a scientifically based EU-wide harmonised test program and rating procedure. This program covers advanced test criteria in frontal and side impact, as well as comprehensive usability tests to reduce the potential for CRS misuse; misuse has been the predominant problem with CRS use for years. In addition, the NPACS procedure has not only been developed as to help parents and other purchasers of CRS, but also to encourage child seat manufacturers with their current and future designs, encourage new technologies to be brought to the market and to reduce the potential for misuse of their products.

INTRODUCTION

The NPACS consortium was funded in 2005 by governments of four nations, United Kindom, the Netherlands, Catalunia and Germany and five non governmental organisations, ADAC, ÖAMTC, AIT&FIA, ICRT and GDV and had the objectives to provide scientifically based EU wide harmonised test and rating protocols to offer consumers clear and understandable information about dynamic performance and usability of child restraint systems. The group worked on reliable methods of dynamic testing, the assessment of their ease of use, and periodically evaluation of the performance of test products.

The first phase was to develop test protocols and conduct accordingly the new test procedures in a second phase. For the first time a new generation of child dummies, FTSS Q-series, was used and new injury criteria were developed. The side impact, today this is not tested for child safety at mandatory tests, was developed to reflect real accident data in laboratory tests. Another focus of the project was handling and misuse, which are not covered by ECE R-44 as well. Therefore handling tests with inexperienced subjects under different test conditions were made to develop a protocol for CRS ratings. Special handling dummies were developed to allow consistent results for testing and rating. Despite challenges in the validation process of the NPACS program, NPACS developed test procedures. Some of them are applied by the European Test Consortium (ETC) for Child Restrain Seats in 19 European Nations since May 2007.

REVIEW OF TEST METHODES

In a first step all potentially CRS test methods over the world were studied and the information collected. So a wide range of information had to be compared, differences listed and potential advantages and disadvantages worked out. The sources which delivered possible information could

be found in the ISO Draft N589/N653, ICRT CRS-Testing, NHTSA 2004, Euro NCAP CRS protocol and JNCAP protocol.
For frontal side and rear impact scenarios the data of all relevant crash test configurations of national standard and consumer tests, such as Euro NCAP, JNACP, ANCP, ECE-R44, CREP, FMVSS 213, were collected to get a objective view of the boundary conditions for a dynamic child seat test.

DEVELOPMENT OF TEST METHODS

Frontal impact

To start at a basic level, analyse of existing in-depth accident databases should be done to establish characteristics of accidents involving serious and/or fatal injured children. In a second step a proposal of test speed, impact angles and velocity should be made. Also taking into account the big data base of EuroNCAP crashed frontal impact cars by their mass and pulse.
In an additional step a selection of 30 - 50 cars of EuroNCAP tests, ADAC-database and registration statistics delivered date for seat belt geometry, geometry of the seatback and seat base and the stiffness of the cushions.
This information lead to a range of seat back angles, showing a difference of 4° rearward, in comparison to the ECE test bench, but a good correlation of the seat base angle, which is close to 15° to the horizontal.

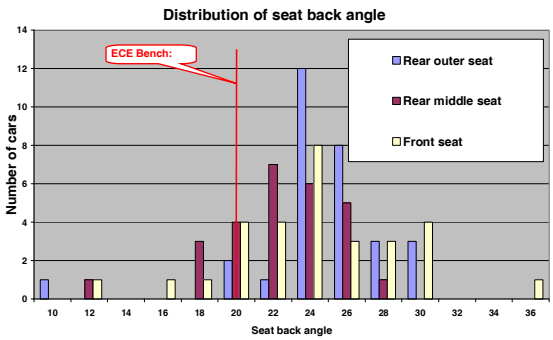

Figure 1. Distribution of seat back angle in comparison to the ECE R44 bench (1)

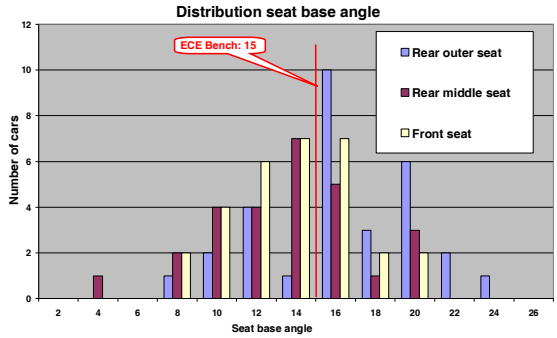

Figure 2. Distribution of seat base angle in comparison to the ECE R44 bench (1)

A quite huge variety of the upper and lower anchorage points could be measured while using different kind of vehicles. The biggest difference could be recognized in the horizontal distribution of the shoulder anchorage points, leading to the decision to test in most rearward, mid and most forward position of the d-ring loop and check out the influence of this anchorage point.

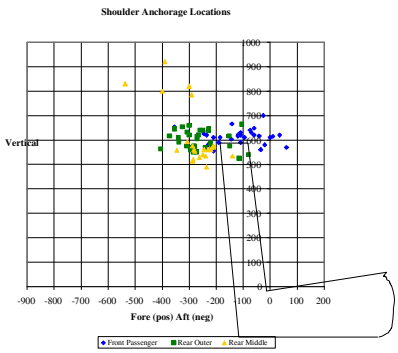

Figure 3. Distribution of upper anchorage point (2)

For the lower anchorage points inner and outer position of the seatbelt and locks a variation could be measured, but these points were allocated around the H-point area of the seat.

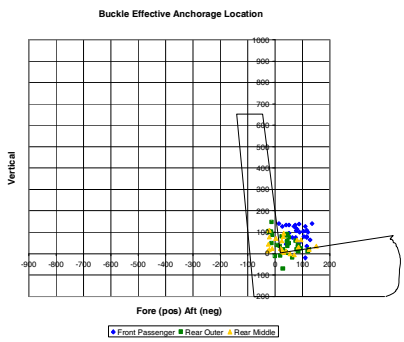

Figure 4. Distribution of lower anchorage points (2)

This evaluation lead to a specific seat bench with a certain seat belt geometry and a variation of the D-loop, the lock and lower anchorage point.

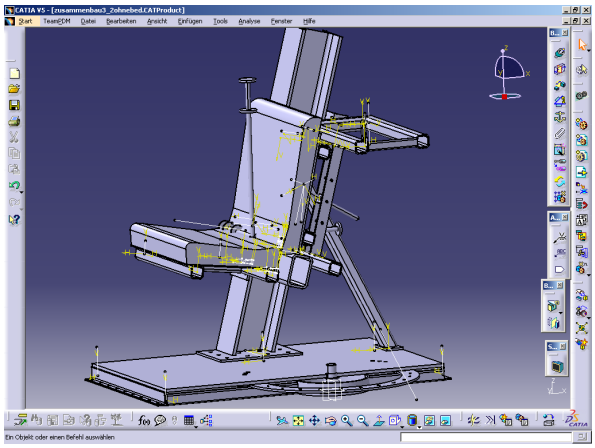

Figure 5. NPACS specific test bench (3)

To evaluate the frontal impact pulse NPACS has on one hand analyzed the B-pillar acceleration result of 23 vehicles tested by Euro NCAP. On the other hand the results of the EC CREST program, which examined accidents in Germany, France, Spain, UK and Italy, should be taken into account. Based on these results NPACS has defined an acceleration pulse for frontal tests.
The analyse of crash pulses of different vehicle sizes are shown in
Figure 6. There is a big variety in the length of the pulse, the frequency and the maximum acceleration. With the introduction of a 65kph pulse which is quite close in shape to the ECE-R44 pulse, but on a higher energy level, a lot of full scale pulses of several vehicle classes could be covered.
The developed NPACS frontal impact pulse is in between the borderlines of the CREST pulse requirement, so both terms were fulfilled.

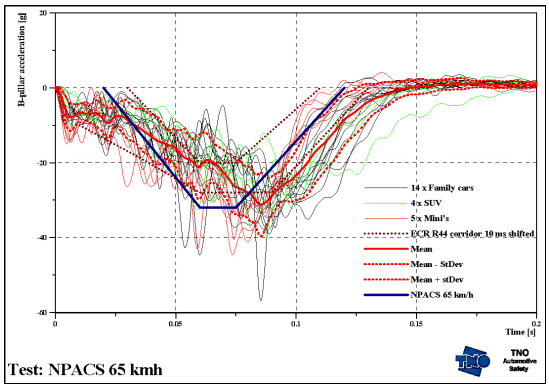

Figure 6. Deceleration pulses of Euro NCAP frontal offset tests and NPACS pulse (blue) (4)

In addition to the 0° frontal impact test a 30° test was considered as a relevant crash scenario, which lead to severe injuries. This type of test and in addition with the worst case belt geometry, which was the most forward one, the potential of CRS in a worst case scenario should be tested. But this chosen configuration led to extreme dummy loadings and even destroyed the dummies itself. Because of this the angular configuration was not taken into account for the rating in the near future.

Side impact

The work of EEVC WG18, show that side impacts cause the second highest number of fatal and serious injuries to restrained child car occupants. Therefore the introduction of a side impact test procedure is necessary, even there is no current dynamic side impact test in the European regulation.

In European consumer testing a side impact test is in use, with a fixed door system. A intruding door variant of ISO and some derivate are existing, too.

In order to get reliable data to compare full size and a sled test a number of 6 different CRS were tested in vehicles of 3 different classes, mini, small family and large family car. The test setup was done according the Euro NCAP/ECE R95 test procedure. On the struck side of the car 2 CRS and dummies were installed on the driver and passenger seat. The biggest intrusion, in this kind of side impact, is the B-pillar. To set up the worst case scenario the rearward facing CRS was placed on the rear bench of the struck side and the forward facing on the driver seat. In this case both kinds of CRS are charged with the maximum loading in the head form area, which is remembered as the most serious one.

The final decision which type of side impact should be introduced in the NPACS test procedure was taken in September 2005. It was possible with all three relevant test methods to differentiate CRS according their protection and to rate those seats. At the end he fixed door principle was dropped because an intruding door seems to be more realistic and could be seen in the full size crashes. The intruding door mechanism was pointed out to represent the side impact as its best. At the end the version of TUB was recognized as the most sufficient one, based on scientific research and introduced in the test procedure.

In Figure 7 the relation between the test results of the full size crashes and the different side impact test procedures could be seen. In this example the head acceleration of the forward facing CRS of Group 1 were used. The results of the sled tests are pointed out in the circle.

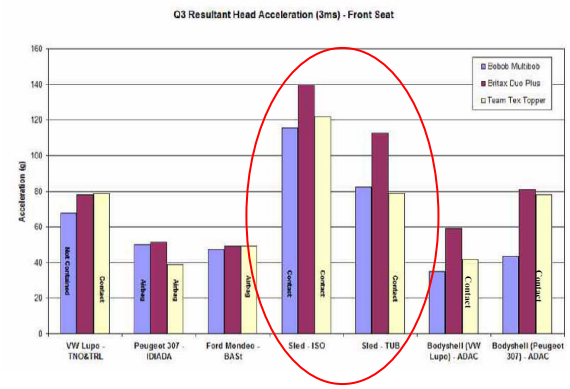

Figure 7. Comparison of side impact sled and vehicle tests (5)

It was considered that the most important body region in side impact, the head of the child, must be assessed according the head acceleration and the head containment.

Rear impact

One working package addressed the rear impact collision. In a scenario of purely rear impact and under 30° angular rear impact, rearward facing shells show pitching and in the angular situation possible contact to the outer surface. But a review of the accident data showed that rear impact accidents were a low priority for fatal and serious injuries to restrained children. This lead to the decision, not to introduce a rear impact dynamic test, right now.

Handling

Misuse data

The German GDV used their database to locate possible misuse during adjustment of the CRS, position in the car and belting of the child. These findings were separated in all single CRS weight classes and offered a good overview of potential risk while using a child seat.

Table 1.

misuse study of GDV (6)

4-point harness systems – Group I (Number of observed CRS = 12; misuse rate = 100%)		
Installation misuse	**Severity of misuse**	**No.**
loose seat attachment	medium (2) severe (3)	5
parents used their own mounting construction	medium	2
incorrect belt path	severe	1
incorrect use of the necessary, additional belts	severe	1
Securing misuse	**Severity of misuse**	**No.**
harness belt too loose	slight (1) medium (6)	7
belt buckle positioned too high	medium	5
weight/size of child above limit	severe	1
shoulder belt passing beneath the arm	severe	1

Handling Dummies

The GDV data showed a lot of problems which came up during the installation of a CRS and buckling up a child in a car. So the handling of a child seat is a very important issue to reduce severe injuries, because of misuse. To address this problem in the test procedure special dummies should be used to get information of the handling of the seat and the fixation of child in the seat. Additional information could be gathered out of the positioning of the dummy in the seat, possible adjustments, suitable belt routing or the fitment of the seat in the car. A special family of handling dummies, called "Kieler Kinder" should provide the information for the tester according the handling issue.

Figure 8 . Kieler Kinder, handling dummy and P-dummy

The positive effect of these handling dummies is a size which reflects the height, extremity length, weight, body sizes better than a 50%ile crash test dummy, e.g. the P- or Q-series.

For the final rating the seat has to be assessed according following criteria:

- Instructions
- Set up of cars/harness
- Installation
- Restraining child
- Ergonomics and comfort
- Cleaning and safety designs
- Removal of the occupant
- Removal of the ISOFIX seat

In a first consideration the use of a universal handling body in white was discussed, but due to a lot of problems caused by the enormous variety of vehicle geometry, differences in foams, seat belt anchorages the idea was cancelled. The handling test should now be carried out in a variation of different sized vehicles, 3 and 4 door cars, different seat belt geometry, but fulfilling the Gabarit specifications.

Dummy

For assessing the dynamic potential of CRS, child dummies have to be used according following boundary conditions:

- different size and weight, covering all ECE classes
- measurement capabilities according the need of NPACS
- the measurements need to be repeatable
- the dummies should be durable for the use in NPACS test scenarios
- the dummy family must be biofidelic

There are 4 different types of child dummies available on the market. In Europe the TNO P-series and Q-series, old and new version, are used for testing. In the USA the Hybrid III child dummies are used for CRS and out of position testing. Comparison testing was done by TRL in the same side impact situation with the 3 year old P,Q and HIII child dummies 3 times to show the repeatability. The best repeatability data for head and chest was delivered by the P3 dummy. But this dummy has one disadvantage due to the old construction the use of additional transducers in the dummy is restricted to head, chest and rudimentary neck measurement for frontal impact. The P-series is durable for the use in NPACS, also the Q.-series didn't show an damages in the different test hoses during their use in frontal and side impact. The big advantage of the Q-series is the more biofidelic behaviour and the possibility to measure not only head and chest acceleration. At the end the decision for the Q-series in it´s old version was driven by fulfilling most of the NPACS requirements. This dummy showed a good repeatability, good biofidelic response in the head and neck, the chest was estimated to be too stiff, it proved the durability in a lot of tests, covered nearly all required masses of the ECE R44 except the upper boundary of group III. For the Hybrid III only small data was available so this dummy was not taken into account.

Figure 9. Q-Series dummy family

Rating

For the overall rating, the results of the usability evaluation, the dummy reading of the frontal and side impact dynamic test and the observation of these tests are assessed. The individual results of these tests together are forming the overall rating of the CRS. Based on accident analyses, user and misuse surveys and on experience of studies and CRS tests the individual results of the test could be weighted against each other. The weighting proposed, on consultation with the NPACS Foundation Committee, is 50 percent for Usability, 25 percent for Frontal Impact and 25 percent for Side Impact. The reason for this weighting reflects the importance of a well installed CRS. Misuse of installation is the most common problem in the field, also pointed out in several studies. A well designed seat could show it's potential if the installation is not done correctly.

In general the rating is designed to work out differences between actual child restrains but still allow space for improvement.

It was considered that two effects, which are not measured will have a capping effect and reduce the score to 0 even when the seat scored points in the rated body regions. This effect will be caused in side impact by a failure to provide any head containment will lead to total score capping to the lowest band and in the frontal impact test, the total structural failure of the product will have the same effect. A third case, were capping could be applied is an abdominal loading of the dummy, caused by the lap belt. Because of insufficient assessing possibilities, only video data could be used, the abdominal rating is not used in the near future until a solution for a possible measurement is found.

VALIDATION

After the 1st phase of developing the test methods, pulses and the decision for the Q-dummy these methods should be validated according the repeatability and the reproducibility. This process included both the frontal and side impact test and in addition the usability test, too.

The result out of this huge test series should show a test procedure, producing reliable results of CRS even if this test were conducted in different test houses with different equipment and different dummies.

Frontal impact

Based on the data of the TWG the participating test labs built seat benches according the NPACS specification.

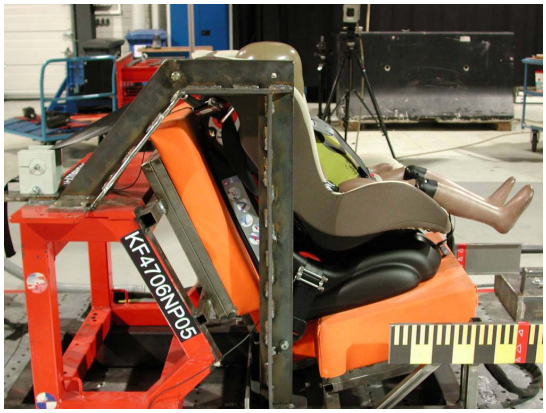

Figure 10. Frontal impact test design

In November 2006, frontal crash tests were conducted with the Chicco Key 1 (validation step 1A). The results were presented at the Validation Workgroup meeting in December 2006. The variations of the results of the test facilities are shown in Table 2.
Measurement variations between the test facilities for the frontal impact below.

Table 2.

Measurement variations between the test facilities for the frontal impact

	Basic tests				Additional tests	
	Q1, upright	Q1, reclined	Q3, upright	Q3, reclined	Q3, upright, 30°	Q3, upright, upper belt fore
Head a_{res}	20%	22%	6%	18%	6%	17%
Head excursion	23%	19%	13%	8%	16%	26%
Chest a_{res}	35%	40%	26%	25%	32%	27%
Chest compression	11%	14%	14%	14%	46%	18%
Neck M_{res}	57%	54%	55%	54%	11%	47%
Neck F_{res}	30%	25%	23%	15%	13%	18%
Pelvis a_{res}	22%	19%	18%	9%	8%	10%

Since the frontal impact test revealed major variations between the measurements, the analysing of the possible reasons was taken into account before continuing validation with other CRS.
Since different positioning of the seat belt retractor was identified as one potential cause for measurement variation, ADAC altered the retractor position for an additional test. Testing two extremely different retractor positions was aimed at demonstrating that different belt routing and belt webbing length may be the main cause for the measurement variations. The above tests show that the position of the belt retractor has little impact on the measurements, with a significant variation only for the neck moment:

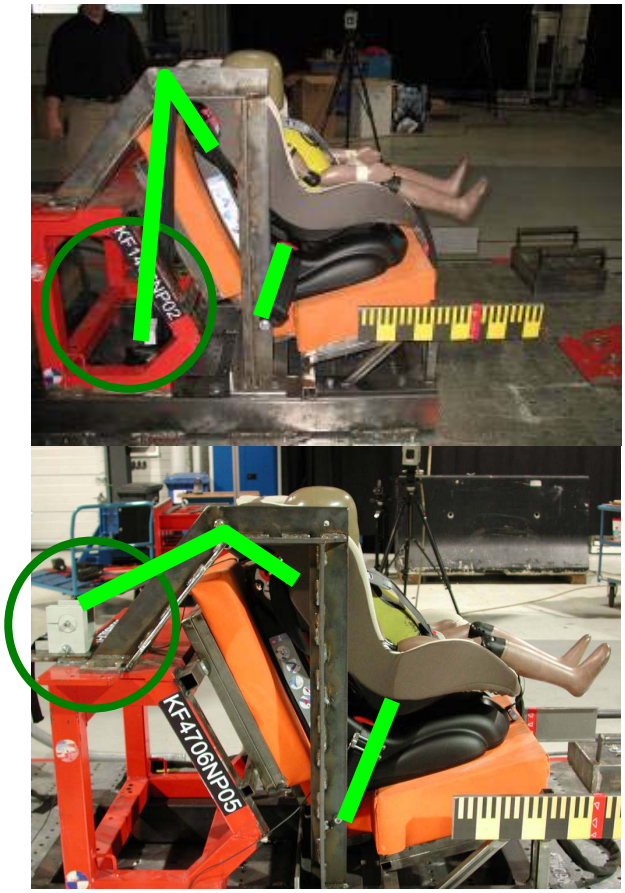

Figure 11. Testing different belt retractor positions (green circle

Table 3.

Influence of retractor position on the measurements and measurement variation in percent

	Retractor 1	Retractor 2	Deviation
Head a_{res} [g]	92	89	4%
Head excursion [mm]	490	500	2%
Chest a_{res} [g]	58	59	3%
Chest compression [mm]	36	n. a.	
Neck M_{res} [Nm]	34	29	17%
Neck F_{res} [N]	3506	3293	6%
Pelvis a_{res}	74	71	4%

Another reason why the test facilities obtain varying measurements might be attributable to inconsistent seat bench rigidity and belt attachment points. Also, the influence of different Q-dummy versions cannot be ruled out.
Excursion was measured using different methods. Since parallax-based errors may be the cause for the

measurement variation, it was agreed to use the ECE-R44 measuring method.
To improve the test procedure additional comparative testing will be needed for the frontal impact in order to identify the causes for major variations.
To discover differences in the rigidity of the test configurations, the belt forces and acceleration of the belt attachment points should be monitored.
In addition, all test facilities should use the same version of Q-dummy or even 1 dummy, which is circulated, to reduce the error potential.

Side impact

The first test on a new built test bench, according the specifications showed difficulties to remain within the corridors required in the protocol and that both the CRS mass and its attachment mechanism have an impact on the movement pattern of the intruding door. In addition, angular velocity was difficult to reproduce, which increased the problems to remain within the required corridor.

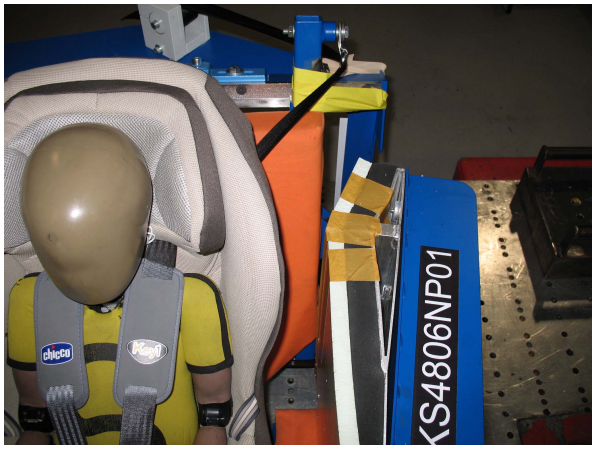

Figure 12. Side impact test setup with hinged door and belt routing

The Validation Workgroup verified the measurements (validation step 1A) at their meeting in December 2006. Three labs did tests with CRS and 2 different dummy sizes on their side impact test rig. Table 1 shows the variations between the measurements of these test facilities:

Table 1.

Variations between side impact measurements of the various test facilities (TRL, TUB and ADAC)

Measurements	Dummy: Q1	Dummy: Q3
Head a_{res}	12%	19%
Chest a_{res}	21%	19%
Chest compr.	18%	46%
Neck M_{res}	181%	58%
Neck F_{res}	46%	51%
Pelvis a_{res}	38%	26%

At subsequent meetings of the Validation Workgroup, some members pointed out that they faced major problems with the test setup and their measurements considerably differed from those of the other test facilities.
Since measurement results varied considerably it is useful to first identify the reasons for the variations before continuing the validation tests with other CRS.

In November 2007, the two remaining test labs, performing side impact validation tests, met for joint testing and an exchange of experiences for side impact tests. Overall, the following issues were identified for the need of optimisation:

- The corridor for the angular velocity of the door is not sufficient to deliver a reasonably exact description of the door movement. As a corrective, the inclusion of an angle over time requirement is needed
- Since different sensors and measuring methods deliver different angular velocity data, a uniform sensor should be specified and used by all test facilities.
- The initial distance between the centre of the tested CRS and the door panel should be specified.
- Dummy arm positioning is not sufficiently specified in the test protocol. This may influence the load transfer between the seat and the dummy thorax, and impact measurements. An additional description of the dummy installation procedure should help reduce the resulting measurement variations.
- To prevent that test setup alignment for every new CRS (and further CRS are needed for such additional test) a calibration routine should be implemented. This involves testing a calibration block (or a standard CRS initially) meeting all test protocol parameters. For subsequent CRS testing, the parameters remain

unchanged – corridors are no longer an issue.

To establish whether the above improvements reduce the test result variations, it was suggested to compare the measurements again at the Validation Workgroup meeting in January 2008. To exclude variations based on the dummy used (relatively frequent and unverifiable changes in the dummy versions), all test facilities should use the same dummy. This idea was not accepted by all parties and the next round robin test was conducted between only two test houses. Several problems seem to be solved an further improvement were made to achieve the corridors in different labs with different test rigs. But the results of this last round robin test, conducted under the NPACS Validation group, again showed deviation of the two participant labs in spite of new corridors, only one dummy used for the test. and the use of the calibration rig. Not only the reproducibility was checked, the repeatability was also an issue to have a focus on.

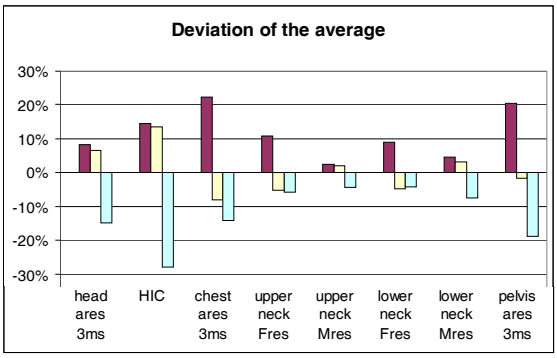

Figure 13. Deviation of the dummy readings (white and dark repeatability of same lab) (7)

RESULTS

One of the most challenging tasks is the protection of children in the traffic especially in cars. Adult occupants have the protection of frontal, side and curtain airbags, seatbelts with pretensioner and load limiter, retracting pedals, reinforced side structures and seats. The only possible protection of a child a a child seat. But a child seat which offers good protection must be installed in the right way otherwise it cannot provide the protection it could do. The target was and will be in future to push forward the development of child seats so that they can offer to bet possible protection and to minimize the handling mistakes and misuse possibilities.

A lot of different organisations in Europe are conducting CRS tests with different results. The NPACS-project, representing the Governments of four European countries, research institutes, ICRT European consumer organizations and FIA automobile clubs tried to bring all this knowledge together and used the latest test equipment on the market to form a new test and rating procedure for the European market.

A lot of research work was done to identify the worst case situations for dynamic and static tests to reflect the real world accidents and rate the seats for consumer information.

The following findings of the research in the NPACS program is proved and could be used for future activities:

- Test bench for frontal impact, reflecting modern car environment and geometry
- Frontal impact test pulse as a simplified frontal offset crash pulse
- The Q-series dummy were introduced and showed good performance in repeatability and durability combined with a good biofidelic relationship
- Handling dummies were developed and could be used for handling and usability tests
- A rating scheme based on accident data, which is taking into account the problem of misuse Usability and misuse tests

But there are still open issues which need further investigations:

- Influence of seat belt geometry on the test results
- The side impact is not validated right know, in spite of a lot investigation of corridors, calibration issues etc.
- Review of the injury criteria is needed
- The durability of the handling dummies must be improved

To come back to the question in the header: NPACS, First step for future activities? The answer of this question is yes. Some of the research results could be used for future activities, but the validation process showed the problems in the reproducibility especially in the side impact.

ACKNOWLEDGEMENTS

Members of the NPACS Foundation Committee

W. Kraus (President ÖAMTC)	Chairman
Prof. K. Langwieder	Chairman
F. van West (FIA Foundation)	Secretary
Dr. B. Moran	(UK DfT)

B. Lorenz (BASt)	(German Gov.)
Mrs. B. Schnottale (BASt)	(German Gov.)
I. Ferrer (IDIADA)	(Catalon. Gov.)
R. Wegman	(NL. Gov.)
Prof. R. Lowne	(Chair TWG)
A. van der Kolk	(ICRT)
R. Vroman	(ICRT)
Dr. M. Lang	(ÖAMTC)
C.Gauss	(ADAC)
W.Klanner	(ADAC)
T.Hummel	(GDV)
Mrs.E.Kerschl	(ÖAMTC)

Past Members

P. O´Reilly	(UK DfT)
A. Eaton	(UK DfT)

REFERECES

[1] NPACS Project C4, Static measurements,2004, TRL

[2] Presentation NPACS Task C4, Cologne 2004, Mr. G. Cheung, TRL

[3] ADAC Test bench, construction work

[4] Presentation NPACS frontal impact task force C6-C9,Mrs. K. de Jager/Mr. T. Versmissen Nov. 2005

[5]Presentation TWG September 2005, Mr. B.Moran, DfT

[6] Presentation NPACS TWG, A2a, T. Hummel, GDV

[7]Presentation NPACS VWG, Januar 2007, A. Ratzek, ADAC

CRASH ADAPTIVE VEHICLE STRUCTURES AND COMPONENTS

Dr. Matthias Nohr,
Karl-Heinz Blume,
DAIMLER, Sindelfingen
GERMANY
Paper Number: 09-0304

INTRODUCTION

Daimler firstly introduced PRE-SAFE® applications in the S-Class, 2002. Up to now sensor information is used to bring front seats in a crash optimized position, to close windows and sunroofs, to eliminate the risk of penetrating objects, to pre-stress restraint systems and to activate braking systems in advance of a physical impact.

Future PRE-SAFE® applications are under investigation at the Research and Development Lab of Daimler. In cooperation with suppliers and Research Institutes crash structures have been developed which can be adapted to the individual impact scenario.
In general the strengthening of vehicle BIW-structures can be introduced for frontal impact scenarios as well as for side impact scenarios.

The benefits of pressurized front and side members and door components have been evaluated. In general pressurizing is done by gas generators. These components are comparable to state of the art gas generators which are used for airbag applications. Within a few milliseconds the pressure increases up to 20bar. Depending on the initial shape of the structure, pressurizing can force an increase of the cross section and moment of inertia.

Various door beam designs have been investigated. Pressure increased the initial cross section by about 200%. Component and vehicle tests were conducted to assess the repeatability of beam deformation, to emphasis benefits and to set up validated simulation tools.

Using simulation tools active BIW-structures have been assessed for frontal and side impact scenarios.

Having pre-crash triggered crash structures available, an impact on vehicle crash performance, passenger protection and weight reduction is expected.

STATE-OF-THE-ART

Individual mobility and road transports have a fundamental impact on the economical situation and development of the country community. With a vehicle density of about 550 vehicles/1000 inhabitants, Germany is of a comparable order as the US with 470 passenger cars/1000 inhabitants. For China there is a rate published of about 15, for India of 7-8 vehicles/persons; - knowing that traffic distribution can vary quite drastically within the different areas within the countries.
For the year 2008 there was an overall market of about 55Mio vehicles at Germany, 240Mio passenger cars at US and about 27.3 Mio (non military used vehicles) at China (2004) and about 6-7 Mio vehicles at India. In total there is an estimated worldwide market of about 942Mio vehicles (passenger cars, commercial vehicles). Compared to the 942Mios vehicles the number of worldwide newly manufactured vehicles (passenger cars, trucks, busses) is less than 10% and was 73,1Mio vehicles (2007), with a German achievement (6.2Mio) of less than 10%.

The vehicles move on an established road infrastructure of about 32 Mio km (2007) worldwide. 32Mio km runs in the magnitude of 800 times the circumferences of the earth or more than 80 times the distance between moon and earth.

Within Europe there is a number of about 226Mio vehicles in the road with a total amount of 9800km/person/year and about 4444Billion Pkm.

With about 1.25Mio accidents and 41000 fatalities (EU25, 2005) the European Community has to deal with two main aspects:

- environmental impacts and
- safety issues.

ENVIRONMENTAL ASPECTS

The actual discussions are mainly focused on the reduction of fine dust pollution and greenhouse gas concentration (carbon dioxide, methane, nitrous oxide, sulfur hexafluoride). The European Commission ratified the United Nations Kyoto Protocol, which was initially presented 1997 in Kyoto and entered 2005 in force. The industrialized countries agreed a greenhouse gas reduction of 5.2% (8% for the European Union). For Germany the agreed overall greenhouse gas reduction is about 21% compared to the 1990's level, achievable until 2012.

Germany started in 1990 with an amount of 1014to Co2-äquivalents/year. Until 2002 a reduction of 15.4% was achieved. With a worldwide Co2-equivalent of about 30892Mio to/year the German

share is about 2.78% (Co2 Germany 2007: 861to), which amounts to about 10to/person/year.
For Germany it is established that less than 20% of the Co2-emission is related to transportation (s. Fig. 1).

Fig. 1: Co2 share representing German market.

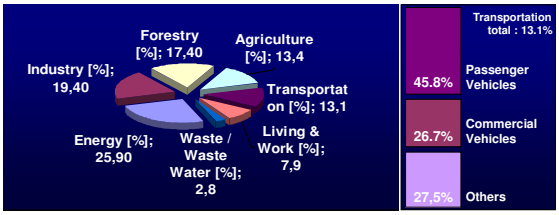

On a more detailed look, only about 50% of the transportation share is related to passenger cars.

To force the reduction of the passenger cars Co2-emission, the European Commission agreed on a directive, targeting maximum Co2-limits to 130g/km as an average-equivalent for new vehicles, sold in the European community starting 2012, with a minimum percentage of 65% volume and climbs up to 100% latest 2015. Penalties for non-compliance will follow.
It is expected that the new US-government might set up comparable targets in the next future.

Figure 2: CO2-levels and European market share [3].

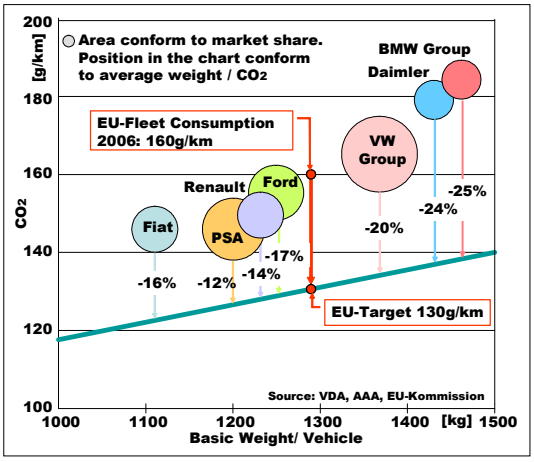

Comparing various car manufacturers, fuel consumption is obviously widely spread and so are market shares for the individual car makers (s. Fig. 2). The average Co2-equivalent for all new cars, sold in Germany in 2007 was about 170g/km (Europe (2007: 158g/km)). Daimler's 2007 Co2-average was 176g/km.

To achieve the EU-committed fuel efficiency there is a strong need to strengthen all main impact aspects which provide a higher level of fuel efficiency. Next to premium, luxury and super sports cars with a higher level of fuel consumption, Daimler offers with the SMART CDI a vehicle, which fulfills already today future requests (fuel consumption 3.3l, 88gr Co2/km). The new E-Class introduced 2009 cuts fuel consumption by 13% to 24%.

For our today's vehicles various counter measures are actually introduced or will be introduced in the next future. Under discussion are optimized and new propulsion systems and gear boxes, energy management countermeasures, rolling resistance tires, aerodynamic counter measures as well as adapted vehicle designs. Lightweight is another major key function for all vehicle components due to the fact that various counter measures will initially add weight (s. Fig. 3).

Fig. 3: Weight balancing aspects.

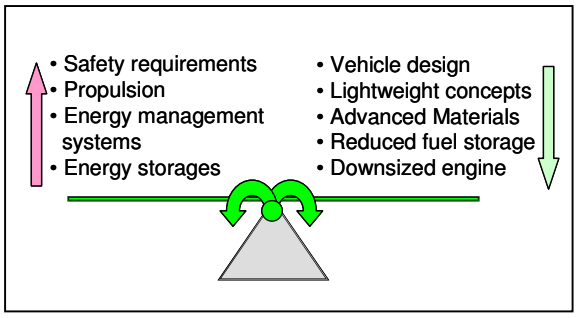

From theoretical investigations it is known that a weight reduction of 100kg can reduce fuel consumption by 0.2-0.5l for standard propulsion systems, depending on the utilization scenario.
To reach a minimum vehicle weight, advanced vehicle-, material-, joining- and manufacturing concepts are an absolute necessity.

Daimler has presented at Detroit 2009 a visionary contribution to sustainable mobility. 3 propulsion lines are presented: Blue ZERO E-Cell, Blue ZERO F-Cell, and Blue ZERO E-Cell Plus (s. Fig. 4).

Fig. 4: Blue ZERO vehicle lines.

The indicated traveling ranges ran from 200 (Blue ZERO E-Cell) to 600km (Blue ZERO E-Cell plus). To store energy, lithium-ion batteries with a weight of about 200-250kg are needed. 700bar hydrogen storages (Blue ZERO F-Cell) add additional masses of approximately 100-150kg. The entire propulsion systems could increase vehicles weight in order of about 150kg to 300kg compared to standard powered vehicles. To reduce vehicle weight, for all kinds of propulsions, intensive weight saving counter measures has to be applied.
There is a fundamental premise at Mercedes-Benz that there is no compromise or back stepping regarding safety, comfort or handling attitudes - standards for all Mercedes-Benz cars.

SAFETY CHALLENGE

It seems that road safety will be one major challenge for the future. Looking at German traffic fatalities one can see a reduction in total numbers from 21332 (1970) to today's level of 4467 (2008).

Nevertheless starting 2001 with about 40000 fatalities within EU 15 the WHO predicted that about 1.2 Mio people are fatally injured each year, worldwide. The number of severely injured people will run between 20 and 50Mio persons/year.

The European Community enforced the goal to reduce the European fatalities from 40000 (EU 15) in the year 2001 to 25000 (EU 25) in 2010, which is equivalent to a 50% reduction in fatality. The fatality rate for Germany came down from 6977 (2001) by almost 30% (2007). Up to now it is not obvious, if the 2010's safety-goal can be reached for Europe in time.

Taking a look into the future the grade of mobility could increase from today's 9600km/person to about 10300km/person (Europe, 2020). In addition it has to be expected that the vehicle/1000 persons-quote will increase quite quickly in countries like India and China.
Minor increases are expected for Western Europe, USA and Japan (less 10%).
Nevertheless we have to face ourselves with the expectation that with the increasing markets the number of fatalities could raise up to 2,1Mio/year between 2030/2050.

Sensors and software tools which are able to detect, predict and announce critical driving situations can help to break out of this vicious circle.
Using pre-crash sensors it is possible to establish PRE-SAFE® applications like introduced in Mercedes-Benz S-Class, 2002, and established at the 2009's E-Class (s. Fig. 5).

Fig. 5: Sensors incorporated at the new E-Class.

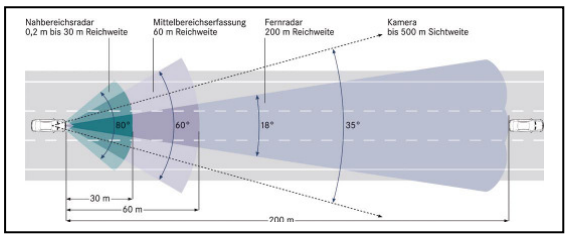

Pre-crash applications are triggered using 3 radar sensors (2 short range 24 GHz radar, 1 long range 77 GHz radar) installed in the bumper area. Various standard acceleration sensors are used for trigger confirmation.

Overall, for typical frontal impact scenarios, such as cross-over collision or running up to preceding trucks, it can be assumed that sensor information can indicate critical situations up to 100-200m in advance of an impact. Side /lateral sensing is still under development, but sensing will be limited to a few 100 millimeters.

For Germany/Europe studies have been shown that about 49% of severe accidents are frontal impacts and about 35% are side impacts (s. Fig. 6a, 6b).

Fig. 6a: Real world passenger car impact distribution.

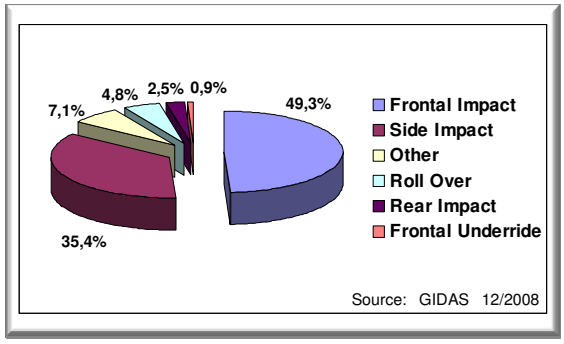

Fig. 6b: Fatality rate (cars involved, Europe) [4].

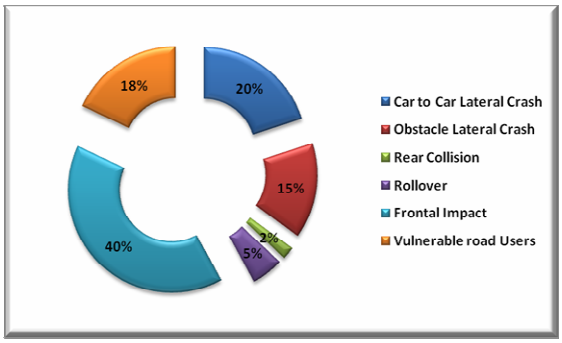

Using pre-crash information it is possible to adapt vehicle structures as well as restraint systems. Using a 77GHz radar sensor, obstacle detection can be done in a rage of about 200m with two 24GHz sensors up to 30m. Therefore there are about 3s available for triggering an action (closing velocity 200km/h). For side impact applications reaction time comes down to 0,14s (50km/h, 2m). Time which can be used to reduced the speed of the vehicle, change seating from a comfort optimized position to the safest position and to strengthen BIW-components and restraint systems.

Crash adaptive safety applications are introduced at passenger cars up to now mainly for interior, restraint and seat applications.
The optimization and pre-activation of the restraint systems in advance of a physical impact leads to various benefits such as lower speed deployment of the driver and passenger airbags as well as improved belt action do to pre-strengthening. Having sensor information available one has the ability to reduce the vehicle's velocity before crash. By reducing the impact speed passenger loadings are reduced in general.

Preparing vehicle structures in advance of an impact there is the possibility to

- increase deformation length/deformation space
  - (active motor hood (pedestrian protection s. Fig. 7)),
  - movable front-end (improved frontal impact, s. Fig. 8, Fig. 9))
- increase/decrease crash load levels (s. Fig. 10).

Fig. 7: Crash active motor hood (E-class).

Fig. 8: Movable front-end with improved crash length (research study).

Fig. 9: Pressurized crash box with improved crash length (research study).

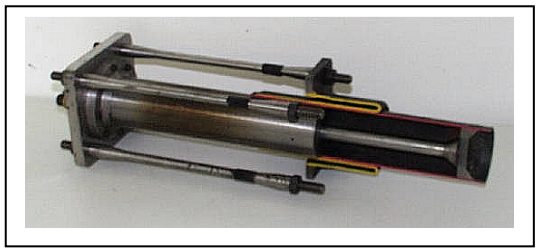

Fig. 10: Crash active crashbox.

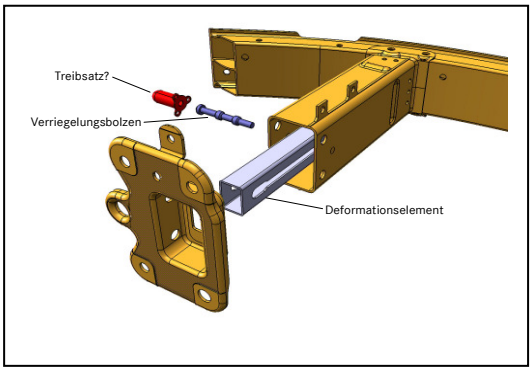

All solutions shown in Fig. 7 to 10 were investigated at the Daimler Research and Development Lab, in a strong cooperation with the Safety-Department. Safety benefits were confirmed for standard test procedures. Real life safety benefits can be expected.
Nevertheless all of these technical solutions have in common that the vehicle weight increases and the technology is proven up to now to a feasibility level.

Only the crash active motor hood, was introduced to fulfill pedestrian protection requirements.

Having crash performance, weight restrictions and packaging aspects and multi propulsion vehicle solutions in mind, one technical solution seem to be a very attractive approach to create overall benefits: ”Pressurized structures”.

PRESSURIZED VEHICLE COMPONENTS (P-VCs)

Together with the company AUTOLIV GmbH basic research and development has been conducted. Autoliv is technology experienced as a main supplier of standard airbags and “metallic airbags”, as are used in the LEXUS LS600H and Renault Laguna, acting as seat anti sub-marining devices (front and rear seat applications). Basic investigations for structural applications have been announced [1], [2]. For passenger cars BIW-applications are not established up to now.

The research project, which runs at Mercedes-Benz over 2 years, incorporating various departments, was directed mainly to BIW- and door components.

Investigations were performed to apply the technology to structural components which are especially loaded during front and side impacts.

During the design process various simulation tools, finite element codes like ABACUS and LSDYNA, have been used to analyze moments of inertia and to assess crash performance under quasi-static and dynamic load conditions.

In general two principals have been investigated:

- For the first principal the initial structural shape of the components stay in the same way they were before being pressurized (s. Fig. 11a). Therefore pressure has to be adjusted carefully.

- The second principal is described in a way that the structure expands from a small cross-section to a bigger one when being pressurized. This effect can provide great benefits, such as packaging benefits (s. Fig. 11b) or extending the crash length.

Fig. 11a: Pressure loaded front member. No significant geometry change.

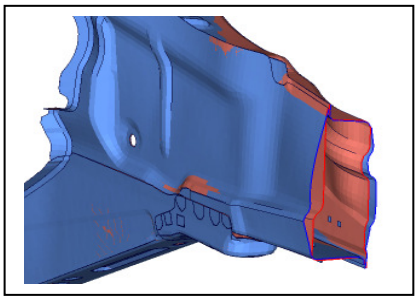

Fig. 11b: Pressure loaded side impact protection beam. Significant geometry increase.

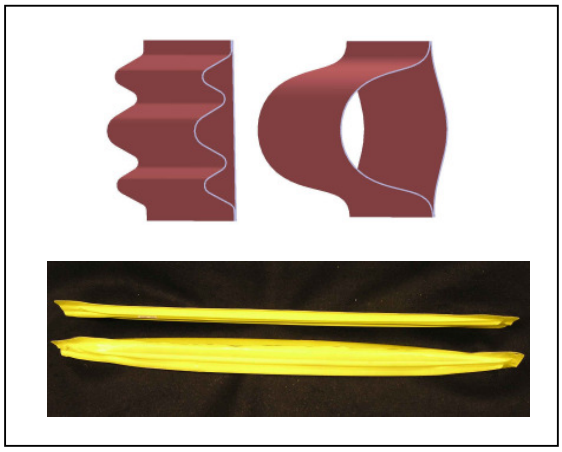

In addition two ways of action can generally be applied:

- Adding a gas generator which keeps a defined, almost constant pressure level over a period of time. This firing time should fit with the ongoing deformation of the involved structures and run for the various applications between 10ms and 20ms.

- Having a gas generator which is able to deform a component from an initial structural shape to a final one, without generating pressure longer than needed for deployment.

Modified standard gas-generators, like used for airbag applications, are suitable to fulfill the tasks. Other applications like explosive cords are a cost-effective and lightweight options. Up to now there are various technical and handling questions open, which contradict a short range product application.

In general there is an almost sealed component design necessary to work without an additional sealing bag. If that is not possible, due to cataphoretic treatment or other aspects, an additional bag has to be applied to the structure.

Various components such as front members (P-FMC), side members (P-SMC), e. g. door beams, rockers and seat lower cross members have been assessed theoretically.

In addition, there seems to be a good change to achieve safety and/or packaging benefits for non-structural applications (s. Fig. 12), such as mounting and assembly frames for hydrogen storages.

Fig. 12: Sub-frame for gas storages.

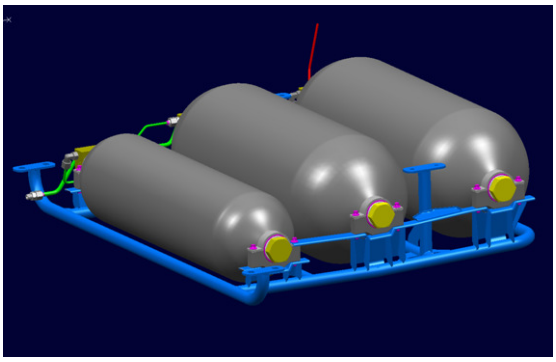

Detailed investigations have been conducted for front side members and door side impact members, knowing that lateral pre-crash sensing is not solved finally yet.

FRONT MEMBER APPLICATION (P-FMC)

Basic investigation, using the explicit finite element code LS-DYNA, proved the possibility to increase crash load levels and energy absorption for regular front members.

For assessment purposes a S-Class structure has been chosen. The side member is made from steel (ZstE 340), with about 110mm*75mm (heights/ width) and 1,75mm in thickness. Two facial sheets are glued and spot-welded together. The members are structurally quite inhomogeneous due to local reinforcements and weaknesses (holes) and mountings such as a highly stiff sub-frame (s. Fig. 13).

Fig. 13: Front structure of the Mercedes-Benz S-Class.

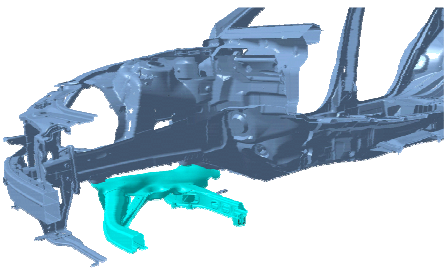

Simulations have been performed with a modified front structure (no engine, with and without sub-frame). For pressure levels of up to 15bar the mean crash load increased by more than 20% (s. Fig. 14).

Fig. 14: Mean crash-load versus pressure level (reduced front structure incorporating sub-frame).

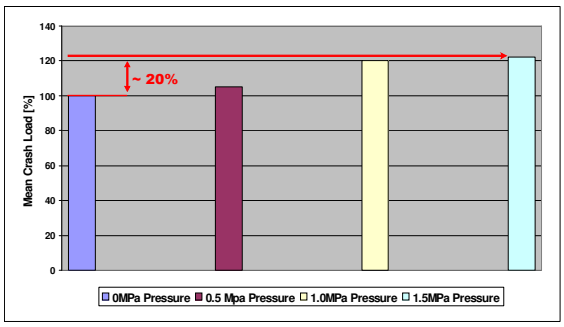

For the simulation model it was assumed that there is a constant pressure level over the whole deformation process. In total the mean crash load increased by about 30kN, deformation was reduced by 100mm. These results open crash-wise the opportunity to reduce the wall thickness in theory by 20 to 30% or to shorten the required crash-length.

In general there is an overall assessment required. A higher load level has to consider also front bulkhead intrusions, thickness reductions NVH-constrains and shortening the member length will have an impact on crash pulse, packaging and design.

The crash model of the pressurized structure was set up using fully integrated shell elements (type 16). A distributed load was applied representing the internal pressure. The pressure load is adapted over time, corresponding to pressure measurements from tests.

In particular, the interaction of pressure and structure has been considered, which only works in one direction, i.e. the pressure load causes deformation of the structure, but the deformation of the structure doesn't cause a change of the pressure load. Jointing was considered in a non-failure model (spot-welds, adhesive) during the pre-assessment stage. With the ongoing project the impact of the joints was getting obvious and therefore failure criteria were considered.

Further investigations have been directed towards the consideration of P-FMC for different car specifications, such as

- the size of the car (large vs. small),
- mass of car (heavy vs. light) and
- the propulsion (large versus small engine and multi propulsion BIW approaches).

In addition P-FMCs seems to be suitable to combine national specific crash rating requirements with reduced weight.

For the initial development step the crash boxes were kept non-pressurized. Pressure was added to one or to both front members. That allows to fulfill low impact crash and easy to repair requirements. Nevertheless the system could be optimized, by pressurizing the side member as well as crash boxes for high speed crashes.
If the crash boxes are not pressurized the system can be triggered by contact sensors. With an overall time request of about 20ms, frontal impacts can be addressed up to 50km/h with a S-Class vehicle concept. For higher impact speeds, or more sophisticated actor responses, pre-crash sensors, which provide 12ms to 16ms (100km/h, 200km/h closing velocity) additional time, are requested.
Two frontal impact scenarios (Euro-NCAP, US-NCAP) have been investigated (s. Fig. 15).

Fig. 15: Crash simulation Euro-NCAP, full frontal US-NCAP.

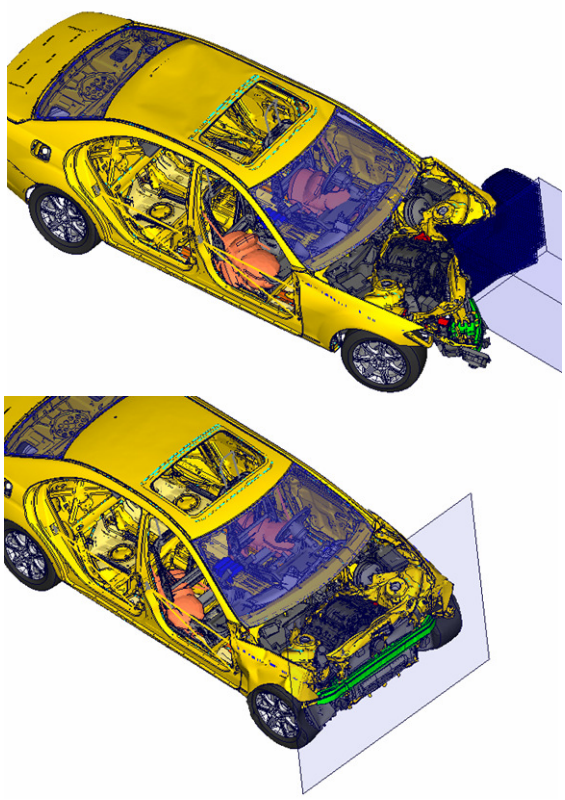

Simulations provided benefits regarding the mean crash loads between 29 to 39kN (s. Tab. 1) and energy absorption (unmodified reference structure).

For Euro-NCAP the deformation seems to be reduced by more than 100mm. For the full frontal US-NCAP set-up the improvement came down to 10mm.

Tab. 1: Simulation results for Euro- and US-NCAP.

	Intrusion (abs.), [mm]	Intrusion (delta), [mm]	Mean Crash Load (abs.), [kN]	Mean Crash Load (delta), [kN]
Test Set-Up (reference)	540		129	
Test Set-Up (pressure)	440	100	158	29
EURO-NCAP (reference)	1241		278	
EURO-NCAP (pressure/one side)	1127	114	309	31
EURO-NCAP (pressure/both sides)	1135	106	317	39
US-NCAP (reference)	624		455	
US-NCAP (pressure)	614	10	487	32

All simulations have been conducted with a simulation model comparable to the standard test configuration.

Further simulations and tests have to prove, if front structures might be shortened (EURO-NCAP) by using pressurized members, fulfilling all other requirements.

For validation tests have been conducted with a special test set-up. To correlate the structural deformation with US-NCAP, test mass and test velocity have been adjusted and set to v: 40km/h, impactor mass: 1190kg, equal 70kJ, pressure: 15bar (s. Fig. 16).

Fig. 16: Test set-up for dynamic component testing.

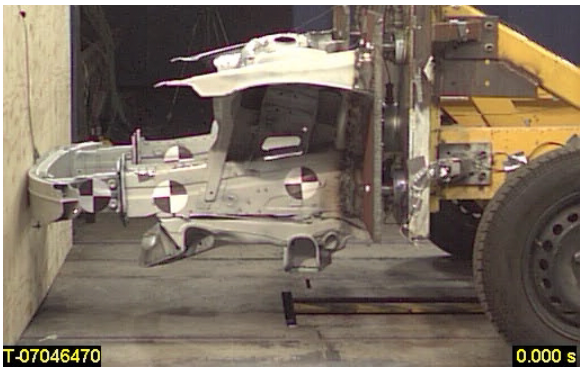

Results showed a good correlation between tests and simulations. Nevertheless it was getting obvious that jointing should be redesigned to achieve more repeatable results. In addition high speed videos proved a need to come up with a modified test set-up (mounting rupture).

With increased mean crash loads, P-FMCs could be introduced to cover small and large sized engines

without BIW- modifications. In addition it seems to be possible to introduce new propulsion concepts, which can incorporate higher component weights (batteries, hydrogen storages), without major structural modifications.
With a weight optimized design of P-FMCs it seems to be possible to safe 1.5 to 3kg/vehicle in weight.

Next to a crash assessment all technical functions have to be addressed.

SIDE MEMBER APPLICATION (P-SMA)
There are various load carrying components involved during a side impact (s. Fig. 17).

Fig. 17: Load carrying structures for side impact.

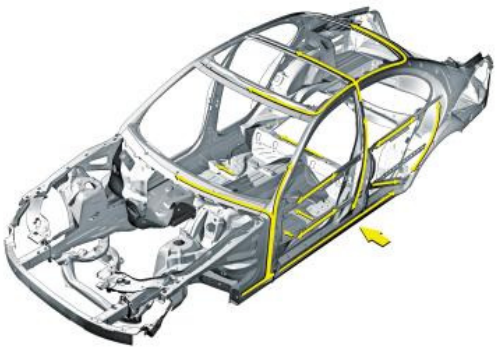

To assess achievable benefits pressurized rockers, seat lower cross beams and other components were assessed.

In the first step a side impact intrusion bar was investigated in detail.

Standard side protection door beams are made from steel or aluminum. The door/door beam-stiffness performance has to be assessed quasistatically (FMVSS214, door component test) and dynamically (IIHS and others, full vehicle side impact test).

Various beams have been designed and analyzed via simulation to fulfill FMVSS214 without gas generator ignition.

The main design parameters were:

- sealed double sheet design
- material: steel, aluminum, FRP or hybrid material
- ability to increase the cross-section more than 100%
- comparable moments of inertia without being pressurized

- weight reduction compared to serial product
- improvements for dynamic impact performance with and without pre-crash sensing
- jointing technology
- component/door assembly

The door beam of the actual C-Class is made from steel, grade: MSW 1200. It has a length of about 1030mm, a maximum depth of 26mm, which results in 1900gr weight. With an additional weight of 200gr to 400gr for the gas generator there was a real challenge to establish a design which provides weight reduction as well as safety performance benefits.

Instead of having an open shaped profile various crash active designs have been investigated (s. Fig. 18):

Fig. 18: Cross-section door beam study.

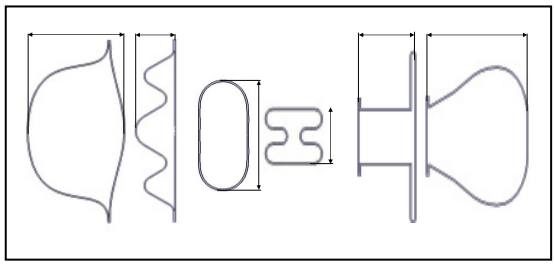

Design 1: Main deployment direction: ⇦ **Design 2:** Main deployment direction: ⇧ **Design 3:** Main deployment direction: ⇨

The extension rate, which describes the rate between deformed and undeformed cross-section shape came out to approximately 250%, 100%, 300%.

With materials of 1.0 mm for the front sheet and about 0.5mm for the rear sheet (design 3) weight was reduced to 1,2kg, without recognizing the gas generator's weight.

The SPS itself was seamwelded and almost sealed. The front door beam was directed within the door frame, comparable to the C-Class side protection beam. This fact allowed, for assessment purposes, to use the original door structure and mountings. Nevertheless simulations showed an important impact of the jointing area design. For the initial assessment the gas generator was mounted at the left end of the P-SMA.

In addition to the prototype set up other component designs have been established and assessed. Weight came down below 1kg (without considering gas generator weight) incorporating aluminum and aluminum/FRP designs. Especially CFRP, with a very high stiffness directed along the fiber direction and a quite low strength perpendicular to the fibers, constrains almost the application of an aluminum/ unidirectional CFRP reinforced P-SMA.

Depending on the initial design the main deployment direction is directed outward the car, to the driver/passenger, or up-/downward within the door.
From safety aspects there was a strong demand to have the main deployment directed outwards or within the door. During the assessment process up-/ downward directed deployments do not prove major benefits. Therefore there was a development focus on design 1.

All designs fulfilled undeployed FMVSS214 static requirements (s. Fig. 19).

Fig. 19: FMVSS214 static pole test.

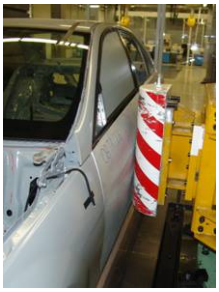

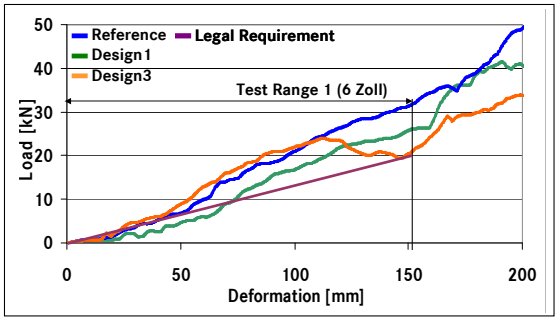

In the first design step the door beam has been designed, along with stiffness requirements, to fulfill FMVSS214 standard without being pressurized.

Analyzing the failure mode it was obvious that failure occurred mainly in the mid range of the beam. Therefore the position of the gas generator has been changed from one end of the SPS to the middle. Having the gas generator tube as a load carrying component introduced, the load level increased by 4.5kN

Additional benefits could be achieved by adding a flexible bridge, which could be realized by a

modified gas generator. This structure should be able to bridge the gab between the front and rear sheet of the SPS after deployment.
Having in addition a pre-crash trigger (20ms before impact) of the P-SMC, which seems to be not excluded by the static standard test procedure, the mean crash load would increase in addition.

Fig. 20: Performance various impact scenarios (design 1; sub-component test, sensing, pressure).

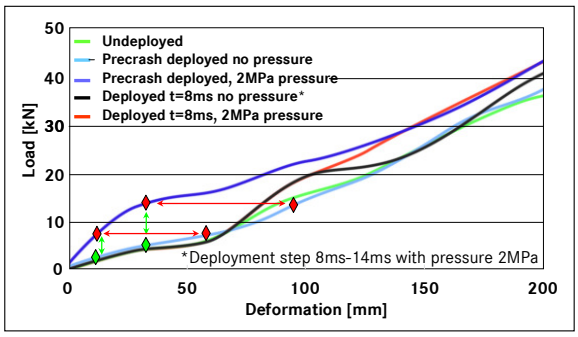

For pre-triggered, pressurized beams it was shown in door sub-component tests that the crash load stays on a high level right from the beginning. For in-crash deployed and pressurized beams, it took about 8ms, after applying pressure, to achieve the load level of the pre-triggered component.

Various door sub-component tests proved a load increase by deployment and applying pressure. Pre-triggering can course a change of the shape of the load-deflection-curve.

To deform the beam in the described manner an interior pressure of about 2 to 3MPa has to be applied. Pressurizing and deploying the beam takes about 20-27ms in total. With a seal component

pressure was kept nearly constant over 100 to 120ms, which corresponds with the ongoing deformation (s. Fig. 21).

Fig. 21: Pressure line versus time.

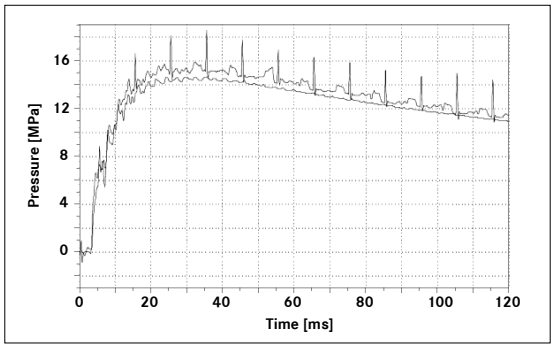

For IIHS configuration (s. Fig. 22), it was proven via crash simulation that deployment can be initiated during impact and will provide component strength.

Fig. 22: Test set-up for IIHS validation.

Tests and simulations proved comparable maximum intrusions for the design 1 and 3 to the reference car, with lower component weight (s. Fig. 23).

Reviewing the results, it has to be remembered, that the door was not specially designed and adapted to incorporate inflatable beams.

In a second assessment step the focus of the investigation was directed towards door trim behavior and occupant protection.
It was very exciting to see that the predicted intrusion velocity came down by more than 15% for the design 1 (pelvis area). Design 3 velocities were comparable to the reference.

Fig. 23: Assessment for 2 door-beam designs.

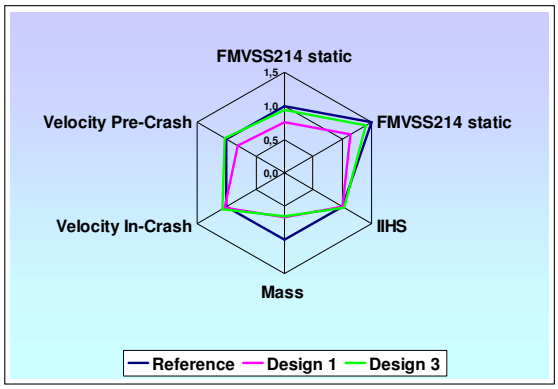

FMVSS 214 pole tests have been assessed for design 3 via simulation for the 5% and 50% pole position.
For both test configurations the maximum intrusions have been quite similar to the reference values.

CONCLUSION

As a long-term goal, emphasized safety assistance systems, as well as internet and car-to-car communication will lead to accident free driving. Nevertheless it is expected that infrastructural countermeasures have to be introduced to support the safety goals.
It is expected that the world automotive market could rise from about 800Mio vehicles today to 2Mrd vehicles before 2050.
Having no significant safety innovations, which can be applied worldwide, especially to the rapidly growing markets, we have to realize that road driving fatalities will exceed the 2Mio limit between 2020 and 2030. In addition we find a multiplier of about 80 between fatal and injured road users (Germany, 2007).

New propulsion and modified vehicle concepts are necessary to achieve confirmed fine dust pollution and greenhouse gas concentration levels.
For all vehicle concepts and propulsion systems there is a strong demand to optimize and reduce weight, not only for the BIW, but also for all other disciplines like power train, chassis, and interior.

Pressurized structural components seem to be a technology which can help to apply safety improvements and establish packaging and design freedoms without adding weight.

To transfer the technology to commercial applications a few challenges have to be solved. Knowing, that the maximum benefits will be achieved for pre-crash applications, front and lateral sensing has to be established, which allows to introduce pre-triggered, pyrotechnical based safety devices, without additional in-crash signal confirmation.

In addition optimized jointing, handling and assembly concepts have to be developed and established.

From the suppliers there is a strong need to come up with cost and weight reductions for gas generators or other deployment devices.

LITERATURE

[1]: B. Pipkorn, Y.Haland: Proposed Variable Stiffness of Vehicle longitudinal frontal members. International Journal of Crashworthiness (IJOC, 2005, Vol. 10, No. 6).
[2]: Patentschrift, Porsche: Einrichtung für bei Aufprallunfällen energieumwandelnd-verformbare Karosseriebereiche von Kraftfahrzeugen (DE19963068B4).
[3]: Auto Motor Sport, Eco Drive. 1/2009
[4]: A. Deb, E. C. Chirwa: An offset rigid barrier-based test: equivalence to the Insurance Institute for Highway Safety frontal offset impact safety test. IJOC 2006, Vol. 11, No 4.

ACKNOWLEDGEMENT

The project support by Mercedes-Benz Research, Development and Safety departments and various Autoliv experts is gratefully acknowledged.

EVALUATION OF ADVANCED COMPATIBILITY FRONTAL STRUCTURES USING THE PROGRESSIVE DEFORMABLE BARRIER (PDB)

Susan Meyerson, Christopher Wiacek
National Highway Traffic Safety Administration
United States of America
Pascal Delannoy
Teuchos, SAFRAN Group - UTAC Passive Safety Dpt
Guillaume Robert
UTAC SAS
France

Paper number: 09-0329

ABSTRACT

Vehicle compatibility combines aspects of both self and partner protection. Self protection involves a vehicle's compartment strength and occupant protection systems. Partner protection involves vehicle design attributes that work towards providing occupant crash protection of a vehicle's collision partner. Research has suggested that good engagement of the front structures and high compartment strength could be effective components for improving compatibility between passenger cars and other vehicles [1]. Studies have shown, however, that incompatible force distributions and greater relative front end stiffness are prevalent in the fleet. To research this issue, the Progressive Deformable Barrier (PDB) was evaluated for its ability to assess the compatibility between the front end force of vehicles equipped with and without compatibility countermeasures.

The paper investigates self protection and partner protection in the offset frontal crash test configuration using the data produced by a joint research program carried out at the Union Technique de l'Automobile du Motocycle et du Cycle (UTAC) in conjunction with the Directorate for Road Traffic and Safety (DSCR) in France and the National Highway Traffic Safety Administration (NHTSA) of the United States (U.S.). The program was initiated to investigate whether barrier deformation using the PDB, intrusion, and dummy injury measures could differentiate compatibility performances between vehicles with and without advanced frontal structures designed specifically to address vehicle compatibility.

INTRODUCTION

Safety researchers around the world, including the U.S. and France, have been concerned with vehicle compatibility in crashes for many years. NHTSA has conducted studies on vehicle aggressiveness (the injury risk vehicles pose to drivers of other vehicles in a collision) and methods for measuring it for over 25 years [2]. Examination of U.S. crash statistics shows a disparity in fatality risk for passenger car occupants in vehicle-to-vehicle collisions with light trucks and vans (LTVs). Past studies have shown that LTVs, as a class, were twice as aggressive toward their collision partners as passenger cars [2]. This mismatch in crash performance has considerable consequences for the traffic safety environment, as approximately half of all passenger vehicles sold in the U.S. are LTVs.

While LTVs are not nearly as widespread in Europe, vehicle compatibility has been a growing concern for its countries as well. Researchers have observed that European vehicles have generally been produced with greater mass, stiffer front ends, and higher compartment strengths to provide occupant crash protection in fixed offset barrier crash tests [1]. As vehicles get heavier and stiffer, however, the deformable barriers used for the evaluation of frontal offset crash protection begin bottoming out. As a consequence, the test becomes more severe for the stiffer, heavier vehicles, and they become more incompatible with smaller collision partners.

In 1996, European Enhanced Vehicle-Safety Committee Working Group 15 on vehicle compatibility was established in order to explore methodologies to assess vehicle compatibility, and develop test procedures to address it. In March 2002, vehicle compatibility was included as an area of focus for the exchange of information in the program of work adopted under the World Forum for the Harmonization of Vehicle Regulations (WP.29) 1998 Global Agreement. Both the U.S. and France are signatories to that agreement, and have concurrently undertaken international research collaborations.

DSCR has been researching the PDB test procedure approach for over 10 years as a means to address vehicle compatibility and recently proposed an

upgrade to United Nations Economic Commission for Europe (UNECE) Vehicle Safety Regulation 94 to incorporate the barrier [1][3]. The PDB progressively increases in stiffness horizontally at both the upper and lower load levels, thus earning its name, PDB, or Progressive Deformable Barrier. Its characteristics were designed to represent an actual vehicle structure with sufficient force level and energy absorption capacity to mitigate any occurrences of bottoming out. In doing so, the PDB may be better able to harmonize test severity among vehicles of different masses. The PDB test procedure aims to encourage lighter vehicles to be stronger without increasing the force levels of large vehicles [1]. By design, the PDB is also able to detect all frontal structures involved in a crash (i.e. cross members, subframes, blocker beams, and longitudinal frame rails). By detecting the impact deformations, the test procedure can encourage vehicle designs that incorporate structures to distribute homogeneous force levels over large surfaces.

In 2004, NHTSA and DSCR signed a bilateral agreement to enhance cooperation and increase the efficient use of resources. As a result, the two agencies elected to conduct joint analyses to promote the development of improved vehicle safety programs and related regulations. Vehicle compatibility was chosen as one focus area. The agencies initiated a joint research program to investigate the potential utility of the PDB in discerning levels of partner and self protection in full width and offset test configurations using heavy vehicles[4]. This research demonstrated that the PDB-XT was able to differentiate between vehicle frontal designs, such as unibody and body-on-frame construction. (*The PDB+ was renamed the PDB-XT and is the most recent configuration of the PDB.*) Based on these results, further research was initiated to determine if the PDB could identify structures designed for vehicle compatibility, such as Honda's Advanced Engineering Compatibility (ACE) body structure [5].

The paper investigates whether barrier deformation using the PDB, intrusion, and dummy injury measures could differentiate compatibility performances between vehicles without advanced frontal structures and those equipped with these structures designed specifically to address compatibility. It evaluates criteria of self protection and partner protection in the offset frontal crash test configuration. It also compares the results to car-to-car crash tests and real world crash analysis.

METHOD OF TEST EVALUATION

Test Severity

One approach toward evaluating both self protection and partner protection is to normalize the test severity for all vehicles—large and small—by using the PDB. Test velocity alone is not a good indication of the severity of the event because, unlike a rigid barrier test, a portion of the test energy is absorbed by the deformable element of the barrier. The energy absorbed by the barrier is a factor of the vehicle's mass, structural design, and stiffness. Therefore, the parameter used to equate the test severity for different vehicles at a common speed using the PDB is the Energy Equivalent Speed (EES) as defined in (Equation 1).

$$EES(km/h) = 3.6 \times \sqrt{\frac{2 \times Eabs}{M}} \qquad \text{(1a).}$$

Eabs = energy absorbed by the vehicle (J)
Eabs = Kinetic energy – Energy in the barrier
M = mass of the vehicle (kg)

$$Ebarrier = \int_{x_{min}}^{x_{max}} F dx \qquad F = P * S \qquad \text{(1b).}$$

P = barrier stiffness (MPa)
S = crushed surface (m^2)

Self protection

Self protection is conceptualized as the ability of a vehicle to protect its own occupants in a vehicle-to-vehicle crash. Many of the crashworthiness regulations around the world are directed toward evaluating a vehicle's "self protection," or how the vehicle protects its own occupants. To achieve good self protection, front end design must limit intrusion and acceleration levels in the passenger compartment as well as limit occupant injury criteria. The following parameters were measured to evaluate the level of self protection the vehicles offered:

- Compartment intrusion
- Dummy injury criteria
- Vehicle acceleration

Partner protection

The concept of partner protection involves vehicle design attributes that function to maximize protection of the occupants within the collision partner. In order to take advantage of the potential energy absorption of a vehicle front end in a vehicle-to-vehicle crash, good engagement of the vehicle's energy absorbing structures must occur. To achieve this result, the deformation of the front

end must be distributed over a large surface. In this study, post-crash test barrier digitization is used to examine the different barrier engagement patterns. The study also compares the following barrier-based parameters that have been identified in previous research as influential in the evaluation of partner protection [4]:

- Average Height of Deformation (AHOD): height at which the median deformation occurs, (evaluates the frontal geometry of a vehicle)
- Average Depth of Deformation (ADOD): average deformation over the barrier, (evaluates the frontal stiffness of a vehicle)
- Maximum Deformation (Dmax): the maximum depth of deformation to the barrier, (evaluates the localized stiffness of a vehicle)

Calculation method

- Average Height of Deformation (AHOD) (Equation 2):

For a given rectangular investigation region, the "depth profile" is computed as a function of height:

$$\rho(z) = k \int_{y_{\min}}^{y_{\max}} X(y,z)dy \qquad (2a).$$

Where k is a normalization constant ensuring that:

$$\int \rho(z)dz = 1 \qquad (2b).$$

The AHOD is then obtained as a mean value:

$$AHOD = \int z\rho(z)dz \qquad (2c).$$

- Average Depth of Deformation (ADOD) (Equation 3):

For a given investigation region with an area S:

$$ADOD = \frac{1}{S}\int X(y,z)dydz \qquad (3).$$

In addition to these PDB barrier-based parameters, the vehicles were also compared based on parameters developed in prior full width rigid barrier testing of these vehicles: KW400 and AHOF [6].

- KW400:

The stiffness-related crush energy absorbed by a vehicle in the first 400 mm of crush (also called the work stiffness).

- Average Height of Force (AHOF):

The average height of force delivered by a vehicle in the first 400 mm of crush.

TEST CONFIGURATION

This test procedure is based on the current PDB test protocol (Figure 1 and Figure 2) [3]. The barrier used is the barrier defined in the current test protocol version "XT".

PDB-XT 50% Offset	
Barrier	PDB-XT
Speed	60km/h
Overlap	50%
Dummies	H3 50% male H3 50% male + Leg Lx

Figure 1: Vehicle in front of the offset PDB.

In these tests, a Hybrid III 50th percentile male dummy fitted with Thor-Lx legs was seated in the driver's seat and a Hybrid III 50th percentile male dummy was seated in the passenger position. The dummies were positioned using a seating procedure that mimics the procedures used by humans to position themselves in the vehicle [7].

This procedure ensured the feet were in neutral position. In the case of the driver position dummy, the right foot was placed on the accelerator pedal, which provided proper dummy interaction with the vehicle interior to predict lower leg injuries. This procedure was developed to achieve repeatable positioning of the Thor-Lx feet with respect to the pedals in some vehicles. The data from the driver dummy's ankle measurements were inconclusive because of data acquisition problems.

VEHICLE SELECTION

In a previous cooperative research effort between DSCR and NHTSA [4], it was shown the PDB test

configuration was able to discriminate between a body-on-frame vehicle structure in a Chevrolet Silverado pickup truck and the unibody construction of a Chrysler Town & Country minivan. At the time it was stated future research could include evaluating the PDB's ability to identify secondary energy absorbing structures or other novel designs and assess their partner protection performance for crash compatibility. Research could also be expanded to appraise how the PDB performs with vehicles that have similar frontal stiffness and force matching to identify additional design factors that may play a roll in crash compatibility.

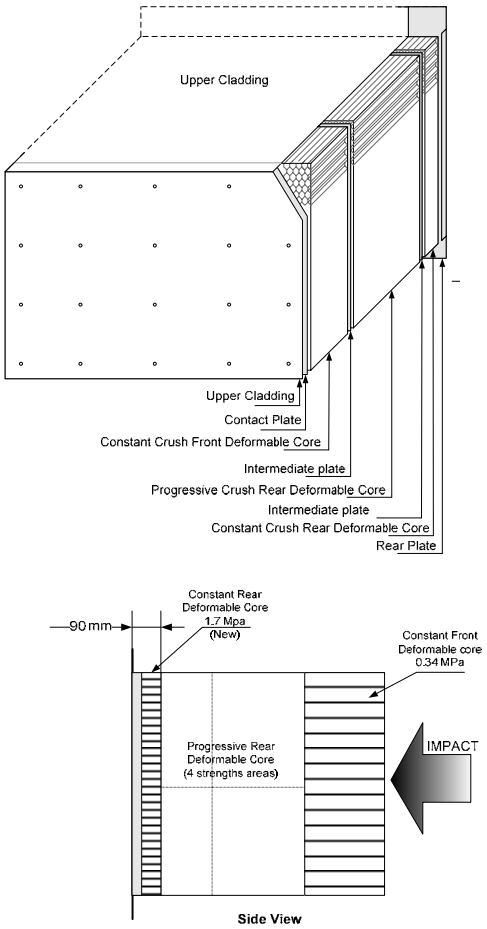

Figure 2 : PDB-XT barrier specification.

This series of tests evaluated the PDB's ability to differentiate the performance of vehicles with and without advanced frontal structures designed to improve self and partner protection when involved in a frontal crash with an incompatible vehicle. The 2005 Honda Odyssey minivan and 2006 Honda Civic compact car were selected because they were designed with Honda's Advanced Compatibility Engineering (ACE) body structure.

According to Honda marketing literature [5], the ACE body design helps spread out the forces of a frontal collision to help avoid concentrated impact forces that cause injuries. The ACE body structure is further reported to be highly effective at absorbing the energy of a frontal crash. It is also reported to help minimize the potential for under-ride or over-ride during head-on or offset frontal collisions with a larger or smaller vehicle.

According to Honda, the ACE body structure also creates a network of fully integrated load-bearing elements that helps attenuate peak impact forces by more evenly distributing them across a relatively large area in the front of the vehicle.

Honda further stated that unlike most conventional designs that direct frontal crash energy only to the lower load-bearing structures in the front end, the ACE body structure actively channels frontal crash energy to both upper and lower structural elements, including the floor frame rails, side sills, and A-pillars. Honda suggested that by engineering specific pathways that help distribute these frontal impact forces throughout a greater percentage of the vehicle's overall structure, the ACE body structure can more effectively route them around and away from the passenger compartment to help limit cabin deformation and further improve occupant protection. Honda reported that its unique front main structure composed of polygonal frame members is integral to the ACE body structure concept.

In addition to the two vehicles with ACE the previous generation 2004 Honda Odyssey—without the ACE body structure—was selected as a baseline vehicle.

Load cell data collected to compute frontal stiffness and force matching height, drawn from the U.S. New Car Assessment Program (USNCAP), was available for the two Honda Odyssey vehicles. In this test program, vehicles equipped with belted 50th percentile male Hybrid III dummies are impacted into a full width rigid barrier at 56 km/h, and load cell data is collected from the test. Additionally, the selected vehicles were part of a series of vehicle-to-vehicle tests in which the bullet vehicles were crashed into a Ford Focus in a full frontal crash configuration. For the recent PDB-XT offset tests, the Honda Odysseys were ballasted to approximately the same weight as in the vehicle-to-vehicle test series to allow for a direct comparison of the results.

Figure 3: 2005 Honda Odyssey

2005 Honda Odyssey	
Test Mass	2,245 kg
Width	1,920 mm
Structure	ACE

Figure 4: 2005 Honda Odyssey Specifications

Figure 5: 2004 Honda Odyssey

2004 Honda Odyssey	
Test Mass	2,245 kg
Width	1,920 mm
Structure	Without ACE

Figure 6: 2004 Honda Odyssey Specifications

TEST RESULTS

The following sections describe the test results based on test severity, self protection, and PDB-XT partner protection. Three PDB-XT tests were performed, but this discussion is focused on the performance of the two Odyssey vehicles. The results from the 2006 Honda Civic with ACE test yielded consistent findings and are presented in Appendix A for information only.

2005 Honda Odyssey with ACE

Test severity - The amount of energy absorbed in the offset PDB-XT was 104 kJ for the 2005 Honda Odyssey test with ACE. The calculated EES for this test was 49.6 km/h, which is 10 km/h less than the test speed.

Self protection - In terms of self protection, the 2005 Honda Odyssey maintained its occupant compartment integrity (Figure 7). The front end crushed the barrier uniformly without any undeformed load paths. The subframe appeared strong and transferred loads in the test. Additionally, the left rear subframe attachment bolt broke off. It should be noted that the upper turret above the wheel that connects to the crossbar deformed down in front of the tire. After the test, the front left door was not able to close properly after it was opened.

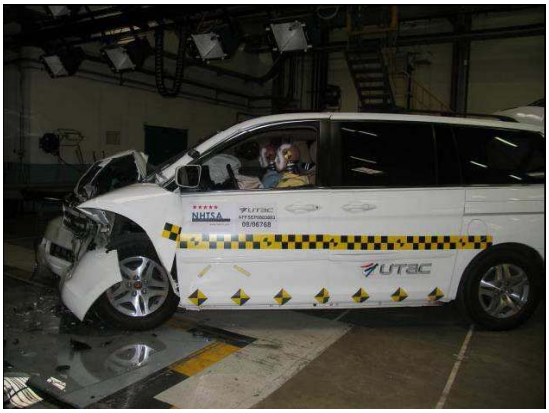

Figure 7: 2005 Honda Odyssey with ACE PDB-XT Offset.

The injury measures for the 50th percentile male driver and passenger dummies are reported in Figure 8.

	IARV*	Driver	Pass.
HIC36	1,000	290	284
Chest Def (mm)	50	26.6	26.5
Chest Gs	60	39.2	27.4
Left Femur (kN)	8	4.76	2.03
Right Femur (kN)	8	1.21	0.97
UL Tibia Index	1.3	0.46	0.76
UR Tibia Index	1.3	0.51	0.43
LL Tibia Index	1.3	0.39	0.34
LR Tibia Index	1.3	0.57	0.21

* As defined in UNECE R.94, except for Chest G's which is defined in U.S. FMVSS No. 208.

Figure 8: 2005 Honda Odyssey with ACE PDB-XT offset – Dummy Injury Measures

None of the occupant injury measures were elevated in this test. The calculated mean intrusion on the driver's side upper region (dashboard and A-pillar) was 30 mm and 87 mm in the lower region (pedal axle and footwell). Although the intrusion (Figure 9) was localized in the footwell area on the driver's side, the driver's side dummy lower leg injury measures were not significantly affected.

The maximum acceleration measured was 29 g at 86 ms, corresponding to 1.059 m of displacement (Figure 10). The average acceleration was 15.8 g.

Partner protection - A large deformation of the longitudinal and lower load path was observed in the PDB-XT offset test of the 2005 Honda Odyssey with the ACE body structure. Two levels of the load paths and the connection between them created a large reaction surface for engagement with a partner vehicle (Figure 11 and Figure 12). The vertical structural element protecting the left wheel was also imprinted on the barrier. There was no bottoming out of the barrier.

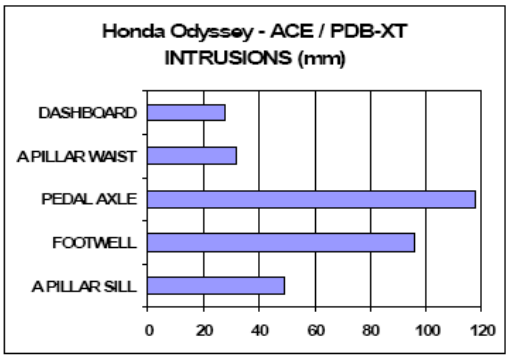

Figure 9: 2005 Honda Odyssey with ACE PDB-XT Offset – Driver Side Intrusions.

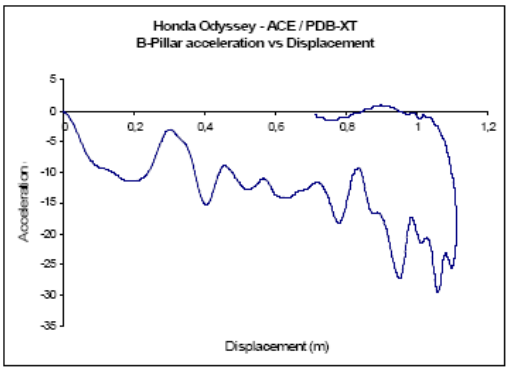

Figure 10: 2005 Honda Odyssey with ACE PDB-XT offset – Acceleration Pulse.

Figure 11: 2005 Honda Odyssey with ACE PDB-XT offset – front end deformation.

Figure 12: 2005 Honda Odyssey with ACE PDB-XT offset – barrier deformation.

In Figure 13, the barrier was able to detect the homogeneous frontal structure of the vehicle. The barrier did identify the deformation due to the crossbeam and the subframe in addition to the strong vertical connections between the load paths. The calculated partner protection parameters based on barrier digitization analysis are presented in Figure 14. The energy absorbed in the barrier was 104 kJ which represented 33 percent of the total kinetic energy.

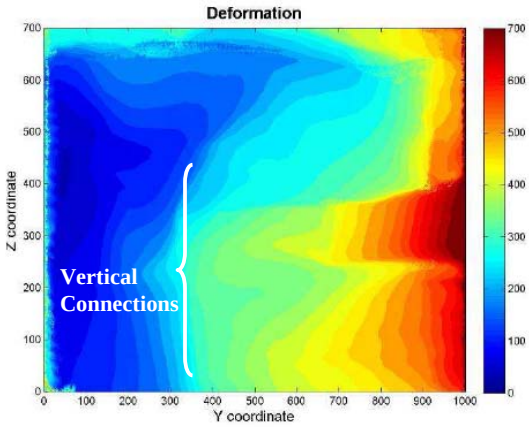

Figure 13: 2005 Honda Odyssey with ACE PDB-XT offset – barrier digitization.

Partner protection	
ADOD (X)	321 mm
AHOD (Z)	397 mm
Dmax	619 mm

Figure 14: Partner Protection Parameters for the 2005 Honda Odyssey with ACE PDB-XT offset test.

2004 Honda Odyssey without ACE

Test severity - The amount of energy absorbed in the offset PDB-XT test was 97 kJ for the 2004 Honda Odyssey without ACE. The calculated EES for this test was 50.6 km/h, which is approximately 9 km/h less than the test speed.

Self protection - In terms of self protection, the 2004 Honda Odyssey without ACE performed well. It resulted in good occupant compartment integrity, including the front left door maintaining its ability to open and close (Figure 15). The left longitudinal frame rail did not compress. Also the subframe detached at it rear attachment point to the floor pan.

Figure 15: 2004 Honda Odyssey without ACE PDB-XT offset.

The injury measures for the 50th percentile male driver and passenger dummies are reported in Figure 16. The head, chest and leg injury measurements of the dummies were low.

	IARV*	Driver	Pass.
HIC36	1,000	283	273
Chest Def (mm)	50	28.7	33.4
Chest Gs (3ms)	60	37.1	28.7
Left Femur (kN)	8	1.61	2.78
Right Femur (kN)	8	0.75	1.36
UL Tibia Index	1.3	0.28	0.45
UR Tibia Index	1.3	0.29	0.16
LL Tibia Index	1.3	0.22	0.27
LR Tibia Index	1.3	0.32	0.11

* As defined in UNECE R.94, except for Chest G's which is defined in U.S. FMVSS No. 208.

Figure 16: 2004 Honda Odyssey without ACE PDB-XT offset Dummy Injury Measures.

The calculated mean intrusion on the driver's side upper region (dashboard and A-pillar) was 59 mm and 155 mm for the lower region (pedal axle and footwell). The intrusion was highly localized in the footwell area (Figure 17). However, the driver's side lower leg injury measurements were not significantly affected.

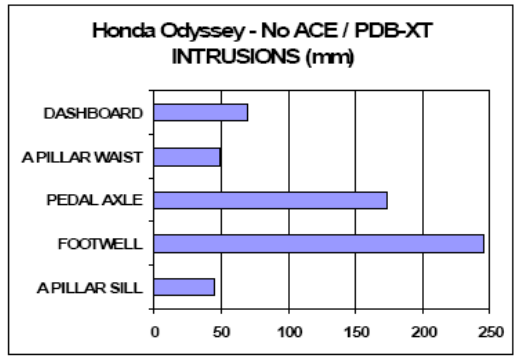

Figure 17: 2004 Honda Odyssey without ACE PDB-XT Offset – Driver side intrusions.

The maximum acceleration measured was 32 g at 93 ms, corresponding to 1.164 m of displacement (Figure 18). The average acceleration was 15.4 g.

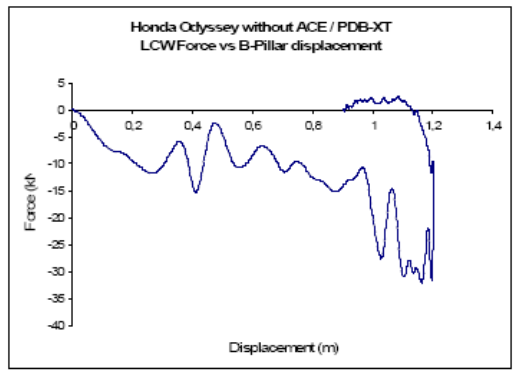

Figure 18: 2004 Honda Odyssey without ACE PDB-XT offset – Acceleration

Partner protection - There was good integrity and no bottoming out of the PDB-XT after the 2004 Honda Odyssey without ACE test. The deformation was not, however, homogeneous. The barrier detected the non-deforming left longitudinal frame rail and the horizontal crossbeam and lower subframe (Figure 19) in the test. The left wheel also engaged and deformed the barrier. The PDB-XT was able to detect the unique load paths of this vehicle (Figure 20).

The calculated partner protection parameters based on barrier digitization analysis (Figure 21) are presented below (Figure 22). The energy absorbed in the barrier was 97 kJ which represented 30 percent of the total kinetic energy.

Figure 19: 2004 Honda Odyssey without ACE PDB-XT - front end deformation.

Figure 20: 2004 Honda Odyssey without ACE PDB-XT – barrier deformation.

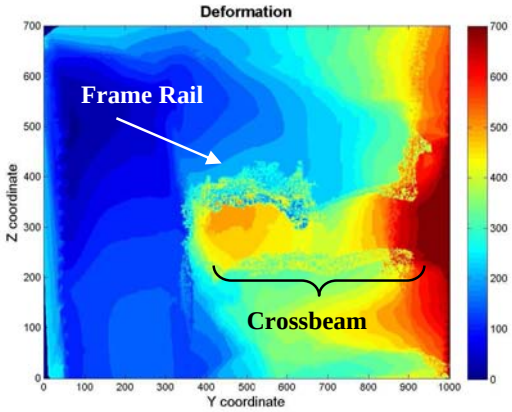

Figure 21: 2004 Honda Odyssey w/o ACE PDB-XT – barrier digitization.

Partner protection	
ADOD (X)	287 mm
AHOD (Z)	401 mm
Dmax	676 mm

Figure 22: Partner Protection Parameters for the 2004 Honda Odyssey without ACE PDB-XT offset test.

DISCUSSION

Self protection

The 2005 Honda Odyssey with ACE and 2004 Honda Odyssey without ACE had similar injury numbers for both the driver and passenger dummies. The vehicles demonstrated good performance in protecting the head, chest, and legs of the dummies in the PDB-XT offset test condition.

The Honda Odyssey with ACE had lower intrusion numbers than the Odyssey without ACE. The pedal axle intrusion values in the Odyssey without ACE were more than double that of the Odyssey with ACE. It is unknown why there was not an appreciable difference in the lower leg injury measurements.

Partner protection

The test results showed that structural differences between the two vehicles are detected by the PDB-XT in the offset test configuration (Figure 23). The 2004 Honda Odyssey without ACE barrier deformation was more localized and the left longitudinal frame rail (round yellow-orange coloration) and the vehicle's crossbeam are detected. In contrast, the deformation of the 2005 Honda Odyssey with ACE barrier was large and homogenous as identified by the graduated color change across its surface. The deformation was also wider and taller, protecting more of the front of the vehicle, and provided a broader reaction surface. The 2006 Honda Civic with ACE barrier deformation was consistent with the 2005 Honda Odyssey with ACE (Appendix A).

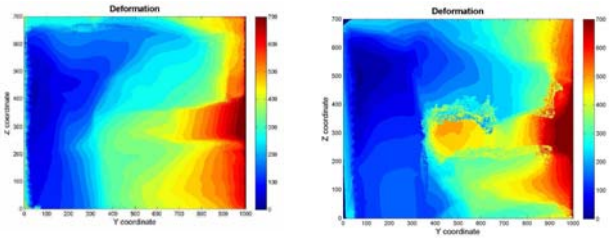

with ACE without ACE

Figure 23: Honda Odyssey Comparison of barrier deformation – Offset.

Figure 24 summarizes the partner protection parameters calculated for this test configuration. The AHOD values for the Honda Odyssey with and without ACE were within 1 percent of each other. This is consistent with USNCAP tests that similarly found the average height of force (AHOF400) values to be 450 mm, and 443 mm for the Odyssey with and without ACE, respectively [6]. The

ADOD for the Odyssey with ACE was slightly higher but the Dmax was less. This is an indication the deformation was more uniform with the ACE structure.

Figure 24 also includes the results of earlier PDB offset tests with a 2005 Chrysler Town & Country unibody minivan and a 2003 Chevrolet Silverado body-on-frame pickup truck. For all four tests the AHOD values are similar. Of interest, Dmax was greatest in the 2004 Honda Odyssey without ACE and even greater than the Chevrolet Silverado. The Chevrolet Silverado was the stiffest vehicle in this series of tests as measured by KW400. It should be noted, the test weight for the Chevrolet Silverado and the two Honda Odyssey minivans were within about 50 kg. The Chysler Town & Country was almost 300 kg less than the Honda minivans.

	T&C	Silverado	Odyssey w/ACE	Odyssey w/o ACE
ADOD (X) (mm)	275	289	321	287
AHOD (Z) (mm)	404	414	397	401
Dmax (mm)	570	654	619	676

Figure 24: Comparison of Partner protection Parameters in the Offset Tests.

The barrier digitization showed the 2005 Honda Odyssey with ACE and the 2005 Chrysler Town & Country (Figure 25) produced a homogenous deformation in the barrier as indicated by the graduated color change across its surface and absence of abrupt color changes indicating increased penetration. The 2003 Chevrolet Silverado and 2004 Honda Odyssey without ACE produced more localized deformation at the location of the longitudinal frame rails. In prior series of tests, the 2003 Chevrolet Silverado and the 2003 Chrysler Town & Country were also crashed into a full width PDB-XT. The patterns of deformation between the full-width test and the offset test were also similar.

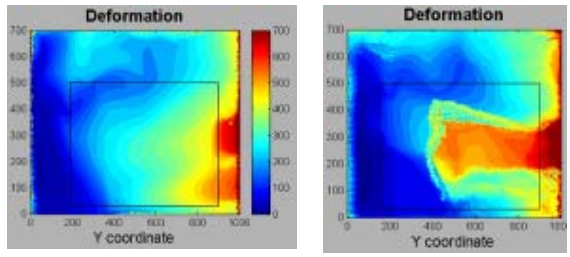

Town & Country Silverado

Figure 25: Comparison of barrier deformation – Offset.

NHTSA had also been evaluating the merits of a stiffness metric, KW400, in its compatibility research program [6]. As part of this research, NHTSA conducted four full frontal vehicle-to-vehicle crash tests using a 2005 Chrysler Town & Country, a 2003 Chevrolet Silverado, a 2003 Honda Odyssey without ACE and a 2005 Honda Odyssey with ACE. Each vehicle impacted a standard collision partner, the 2002 Ford Focus. In this series of tests all the striking vehicle's were ballasted to a test weight of 2,273 kg and struck the target vehicle with an impact speed of 71.8 km/h. A review of the KW400 metric obtained from full frontal USNCAP barrier tests for these vehicles would suggest that the Chevrolet Silverado is the stiffest vehicle, the two Odysseys are less stiff, and the Chrysler Town & Country is the least stiff vehicle. When looking at the acceleration at the center of gravity (CG) from the vehicle-to-vehicle crash test with the Ford Focus, however, the data suggests that the 2005 Honda Odyssey with ACE is the stiffest vehicle and the Chevrolet Silverado is the least stiff of the bullet vehicles (Figure 26).

	KW400 N/mm	Accel. At CG in Focus (m^2/s)	Accel. At CG in Striking Vehicle (m^2/s)
2002 Ford Focus	934		
Bullet Vehicles			
2005 Chrysler Town & Country	1,137	90.5	47.6
2003 Honda Odyssey w/o ACE	1,448	108	32.1
2005 Honda Odyssey w/ACE	1,456	113.5	40.3
2003 Chevrolet Silverado	1,619	86.2	32.9

Figure 26: Vehicle-to Vehicle Full Frontal Test Results Including USNCAP Computed Stiffness [8].

An examination of the post crash photos for these tests shows that the Chevrolet Silverado did not fully engage the frame rails of the Focus and actually pushed the frame rails outward (Figure 27). Photos from the Chrysler Town & Country test exemplified homogeneous loading on the Focus (Figure 28). In the photos of the Ford Focus crashed by the Honda Odyssey without ACE, it is evident that the Honda Odyssey overrode the Ford Focus frame rails (Figure 29) but the Honda Odyssey with ACE, provided homogeneous loading (Figure 30). A review of the barrier digitization of the four vehicles shows similar deformation patterns as the Focus.

Figure 27: 2002 Ford Focus Post Crash with 2003 Chevrolet Silverado.

Figure 28: 2002 Ford Focus Post Crash with 2005 Chrysler Town & Country.

Figure 29: 2002 Ford Focus Post Crash with 2003 Honda Odyssey without ACE.

Figure 30: 2002 Ford Focus Post Crash with 2005 Honda Odyssey with ACE.

The frontal crush profile of the Focus measured after the vehicle-to-vehicle tests is an indicator of the level of structural engagement between the vehicles (Figure 31). The 2005 Chrysler Town & Country test resulted in uniform deformation of the bumper on the 2002 Ford Focus. This was consistent with the results of the offset and full width barrier digitization analysis showing homogenous deformation in the barrier. The 2003 Honda Odyssey without ACE did not fully engage the 2002 Ford Focus and produced non-uniform crush. The 2005 Honda Odyssey with ACE produced more crush and uniform deformation when compared to the non-ACE test. This was also consistent with the offset barrier analysis. The crush profile of the 2002 Ford Focus after the 2003 Chevrolet Silverado test could not be measured.

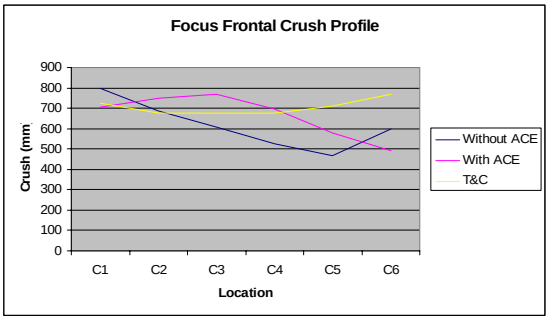

Figure 31: Focus Frontal Crush Profile at Bumper.

The higher stiffness of the Honda Odyssey and a more robust engagement with the 2002 Ford Focus appears to explain the higher acceleration at the CG in the 2002 Ford Focus when compared with the 2005 Chrysler Town & Country (the test weights for the striking vehicles were the same). In this same series of tests the 2005 Chrysler Town & Country experienced a higher acceleration at its CG compared to the stiffer 2005 Honda Odyssey with ACE. It also should be noted that 2003 Chevrolet Silverado and 2003 Honda Odyssey without ACE, which did not have good engagement with the 2002 Ford Focus, experienced the lowest acceleration at

the CG compared to the vehicles that showed good engagement. For all tests, the injury measurements were low for the striking vehicle. Furthermore, the accelerations at the CG provided a better indication of the interaction between the vehicles than relying on the dummy injury measures because it decoupled the occupant performance, which is subject to tuning of the restraint system from the forces the vehicle experienced.

Real-World Performance of ACE

The 2005 Honda Odyssey was the first vehicle released in the U.S. with ACE. Since that time Honda has been incorporating the ACE attributes into its vehicles as they undergo major designs. As of the 2009 model year, almost all Honda vehicles sold in the U.S. incorporate this new body structure philosophy.

A query of the 2005 through 2008 National Automotive Sampling System - Crashworthiness Data System (NASS-CDS) identified approximately 70 frontal crashes involving Honda vehicles with ACE. Almost all of the frontal cases identified were minor low delta-v crashes and did not significantly engage and crush the ACE structure. Also, at the time of the review, pictures for many of the 2008 cases were not published and the performance of the vehicle's structure could not be assessed. However a few cases shed some light on the real-world performance of the ACE design in the field.

For example, NASS-CDS Case No. 2007-04-0137 involved a 2006 Ford Escape and a 2005 Honda Odyssey with ACE. This was a relatively minor severity crash between two vehicles with a weight disparity. The 2006 Ford Escape weighted 1,545 kg compared to the 2,102 kg 2005 Honda Odyssey.

According to the case summary, the 2006 Ford Escape was traveling eastbound negotiating a left curve. The 2005 Honda Odyssey was traveling westbound negotiating a right curve. The front of the 2006 Ford Escape impacted the front of the 2005 Honda Odyssey with a CDC code of 01FYEW02. The principle direction of force with respect to the 2005 Honda Odyssey was 20 degrees. In this frontal oblique impact the total delta-v for the 2005 Honda Odyssey was estimated to be 15 kp/h. The frontal air bag in the 2006 Ford Escape did not deploy but deployed in the 2005 Honda Odyssey.

The 43 year old female drive of the 2006 Ford Escape and the 68 year old driver of the 2005 Honda Odyssey sustained minor injuries from the event. It was not known if the drivers were restrained.

Based upon the photos, the ACE structure appeared to have engaged the 2006 Ford Escape in a consistent pattern to what was observed in the PDB-XT tests (Figure 32). The upper corner ACE structural element that connects to the crossbeam crushed downward at the left tire and absorbed the energy of the Escape. This is similar to what was observed in Figure 16.

Given the weight difference between the two vehicles, the lighter 2006 Ford Escape did not experience significant damage (Figure 33). For this case the intrusion values were not measured by the NASS-CDS researchers, however, based upon an examination of the interior photos, any intrusion was likely insignificant.

Figure 32: NASS-CDS No. 2007-04-0137 – 2005 Honda Odyssey.

Figure 33: NASS-CDS No. 2007-04-0137 – 2006 Ford Escape.

Future considerations

The DSCR is developing a parameter to assess the homogeneity of the vehicle crush pattern using the barrier digitization analysis. It will be based on the shape of the deformation, discriminating between localized deformation and homogeneous deformation. This parameter has the potential to be

very useful in differentiating the crash characteristics between two vehicles.

In this testing, a load cell wall was installed behind the PDB-XT to measure the global front end force. The PDB-XT procedure is able to measure this force with a high level of accuracy. With further research, it could be used for evaluating self and partner protection. (See test results in Appendix B).

With regard to the real world analysis, due to the limited data available at the time, there were an insufficient number of NASS-CDS cases to fully explore the performance of the ACE structure in vehicle-to-vehicle crashes. NHTSA will continue to monitor NASS-CDS for new cases.

CONCLUSIONS

This paper is an extension of PDB research that was presented at the 2007 Enhanced Safety of Vehicles Conference held in Lyon, France [4]. It investigated whether barrier deformation using the PDB, intrusion, and dummy injury measures could differentiate compatibility performances between vehicles equipped with and without advanced frontal structures, designed specifically to address compatibility. It also evaluated criteria of self protection and partner protection in the offset frontal crash test configurations and then compared these results to those of vehicle-to-vehicle crash tests and real world crash analysis.

The barriers performed as expected and no bottoming out with these vehicles occurred. With respect to self protection, both Honda Odysseys had similar dummy injury numbers, but the 2004 Honda Odyssey without ACE produced higher intrusion results. The testing also demonstrated the ability to assess partner protection. The PDB-XT digitization analysis was able to differentiate between the homogeneous crush of the 2005 Honda Odyssey with ACE and the localized crush of the 2004 Honda Odyssey without ACE.

The ACE produced a homogeneous deformation to the PDB-XT barrier suggesting it would provide good horizontal and vertical engagement with a partner vehicle throughout the crash event. This was verified through the analysis of vehicle-to-vehicle crash tests and preliminary real-world crash investigations. An analysis of various compatibility metrics indicated that stiffness alone may not indicate aggressivity. Similarly, AHOD and/or AHOF values among vehicles may not insure a proper engagement of the front structure over the full course of the crash. This was particularly apparent in the 2003 Chevrolet Silverado and 2002 Ford Focus tests.

In this test series, broader and less localized PDB-XT barrier deformation indicated better structural engagement with a partner vehicle. It was found, however, that when a stiffness disparity occurs with better engagement, it can result in the partner vehicle unequally sharing the crash energy. The homogeneity of the barrier deformations also provides an indicator of the degree of uniformity of the vehicle's frontal stiffness. The analysis in this paper suggests that further evaluation is needed to address both the stiffness of a vehicle as well as the homogeneity of that stiffness.

ACKNOWLEGDEMENTS

Under the bilateral agreement between NHTSA and DSCR, resources were leveraged to carry out a joint research program on vehicle compatibility. Results and knowledge gained from this test procedure evaluation proved to be useful to both countries.

REFERENCES

1. Delannoy, P., Martin, T., Castaing, P., "Comparative Evaluation of Frontal Offset Tests to Control Self and Partner Protection," 19th International Technical Conference on the Enhanced Safety of Vehicles, Paper No. 05-0010, June 2005.

2. National Highway Traffic Safety Administration, "Initiatives to Address Vehicle Compatibility," June 2003, NHTSA Docket No. NHTSA-2003-14623-1.

3. Proposal for draft amendments to Regulation No. 94 (Frontal collision), ECE/TRANS/WP.29/ GRSP/2007/17, http://www.unece.org/trans/main/ wp29/wp29wgs/wp29grsp/grsp2007.html, September 28, 2007.

4. Delannoy, P., Martin, T., Meyerson, S., Summers, L., Wiacek, C., " PDB Barrier Face Evaluation By DSCR And NHTSA's Joint Research Program," 20th International Technical Conference on the Enhanced Safety of Vehicles, Paper No. 07-0303, June 2007.

5. www.hondanews.com/categories/872/ releases/4696

6. Patel, S., Smith, D., Prasad, A. and Mohan P., "NHTSA's Recent Vehicle Crash Test Program on Compatibility in Front-To-Front Impacts," 20th International Technical Conference on the Enhanced Safety of Vehicles, Paper No. 07-0231, June 2007.

7. Saunders, J., Louden, A., Prassad, A., "Offset Test Design and Preliminary Results," 20th International Technical Conference on the Enhanced Safety of Vehicles, Paper No. 07-0240, June 2007.

8. Ford Focus crash tests with the 2003 Chevrolet Silverado, 2003 Honda Odyssey, 2005 Chrysler Town & Country and 2005 Honda Odyssey, NHTSA database test numbers are 5473, 5684, 5542 and 5685, respectively. See www.nhtsa.dot.gov

APPENDIX A

2006 Honda Civic with ACE

Figure 34: 2006 Honda Civic.

2006 Honda Civic	
Test Mass	1,487 kg
Width	1,572 mm
Structure	With ACE

Figure 35: 2006 Honda Civic Specifications

Test severity - The amount of energy absorbed in the offset PDB-XT test was 59.3 kJ for the 2006 Honda Civic with ACE. The calculated EES for this test was 51.3 km/h, which is 9 km/h less than the test speed.

Self protection - In terms of self protection, the 2006 Honda Civic maintained good integrity of the occupant compartment space (Figure 36). There was a large amount of deformation of the longitudinal and lower load paths. Overall the front end crushed uniformly without any undeformed load paths. It should also be noted that the upper turret above the wheel that connects to the crossbar deformed down in front of the tire.

Figure 36: 2006 Honda Civic with ACE PDB-XT offset.

The injury measures for the 50th percentile male driver and passenger dummies are reported in Figure 37. The occupant injury measures were low.

	IARV*	Driver	Pass.
HIC36	1,000	428	263
Chest Def (mm)	50	30.8	36.4
Chest Gs	60	34.6	31.5
Left Femur (kN)	8	1.46	2.8
Right Femur (kN)	8	1.26	0.74
UL Tibia Index	1.3	0.31	0.43
UR Tibia Index	1.3	0.68	0.34
LL Tibia Index	1.3	0.30	0.30
LR Tibia Index	1.3	0.63	0.23

* As defined in UNECE R.94, except for Chest G's which is defined in U.S. FMVSS No. 208.

Figure 37: 2006 Honda Civic with ACE PDB-XT offset – Dummy Injury Measures

The calculated mean intrusion on the driver's side upper region (dashboard and A-pillar) was 27 mm and 57 mm for the lower region (pedal axle and footwell). The intrusion was localized in the footwell area (Figure 38). However, the driver's side dummy lower leg injury measures were not significantly affected.

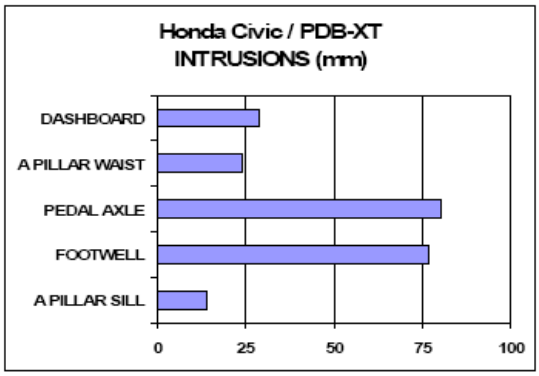

Figure 38: 2006 Honda Civic with ACE PDB-XT Offset – Driver Side Intrusions.

The maximum acceleration measured was 44 g at 77 ms, corresponding to 0.978 m of displacement (Figure 39). The average acceleration was 18.4 g.

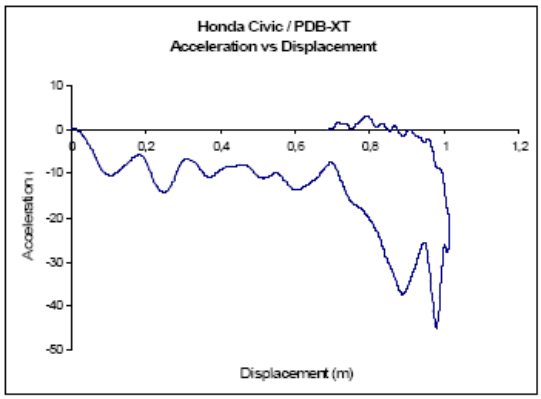

Figure 39: 2006 Honda Civic with ACE PDB-XT offset – Acceleration Pulse.

Partner protection - In the PDB-XT offset test, the forces generated by the longitudinal and lower load paths of the 2006 Honda Civic with ACE were distributed and crushed uniformly, resulting in homogeneous deformation of the barrier (Figure 40 and Figure 41). The two levels of load paths and connections between them created a large reaction surface for engagement with a partner vehicle. There was good engagement between the front of the vehicle and the barrier. No bottoming out of the barrier was observed.

Figure 40: 2006 Honda Civic with ACE PDB-XT offset – front end deformation.

Figure 41: 2006 Honda Civic with ACE PDB-XT offset – barrier deformation.

In Figure 42, the barrier was able to detect the lower load path of the vehicle. The calculated partner protection parameters based on barrier digitization analysis are presented in Figure 43. The energy absorbed in the barrier is 59 kJ that represented 28 percent of the total kinetic energy.

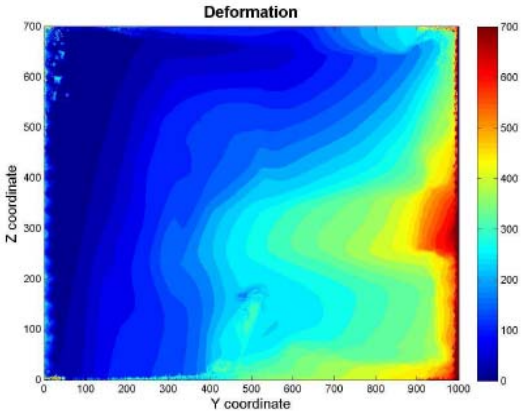

Figure 42: 2006 Honda Civic with ACE PDB-XT offset – barrier digitization.

Partner protection	
ADOD (X)	262 mm
AHOD (Z)	402 mm
Dmax	488 mm

Figure 43: Partner Protection Parameters for the Civic with ACE PDB-XT offset test.

APPENDIX B

Global force

PDB-XT Offset test (2005 Honda Odyssey with ACE) - The maximum global force was 463 kN at 1.078 meter displacement of the B-Pillar (Figure 44).

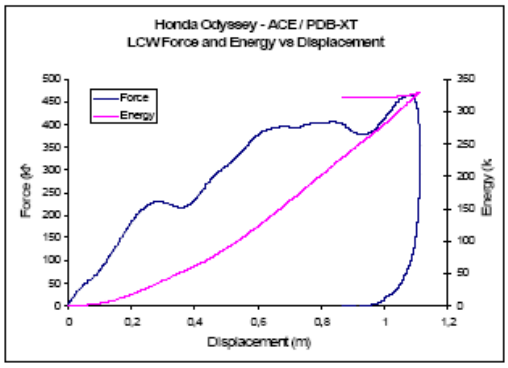

Figure 44: 2005 Honda Odyssey with ACE PDB-XT offset – Global force.

PDB-XT Offset test (2004 Honda Odyssey without ACE) - The maximum force was 476 kN at 1.183 m displacement of B-Pillar (Figure 45).

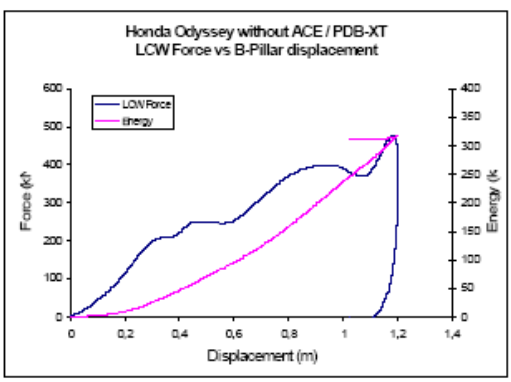

Figure 45: 2004 Honda Odyssey without ACE PDB-XT offset – Global force.

PDB-XT Offset test (2006 Honda Civic with ACE) - The maximum force was 363 kN at 1.002 m displacement of B-Pillar (Figure 46)

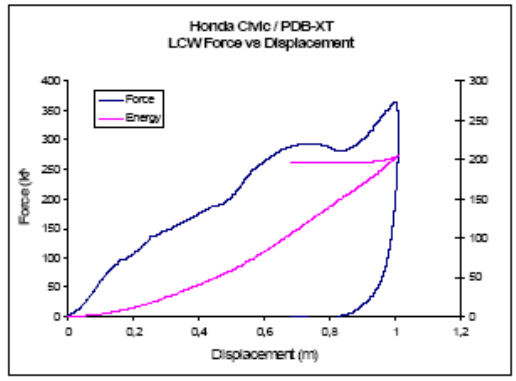

Figure 46: 2006 Honda Civic with ACE PDB-XT offset – Global force.

VALIDATION METHODOLOGY ON AIRBAG DEPLOYMENT PROCESS OF DRIVER SIDE AIRBAG

Jeong Keun, Lee
Won Pil, Ha
Jae Hyun, Lee
HYUNDAI MOBIS
Korea
Duk Byung,Chae
KOSTECH
Korea
Jae Hyung, Kim
KOLON
Korea
Paper Number 09-0363

ABSTRACT

Recent years the numerical method of the simulation for the airbag deployment process has been improved with new material model and thermodynamic model, and has become a standard application of finite element codes. With such simulation tools, it is possible to attempt supporting the airbag module design and evaluating the injuries of dummy in airbag hazard area or out-of-position. Although the simulation model for the airbag's deployment process is usually correlated with the static airbag deployments and reaction force results, up-to-date the numerical approach to represent the fluid flow within the airbag is both costly and time consuming. This paper will provide an overview of the correlation process for reducing the resource to be invested. The following two tests are conducted for acquiring the reference data.
1. Static deployment test for acquiring the airbag internal pressure during the deployment process and
2. Drop tower test for acquiring the fully deployed airbag's reaction force.
The drop tower test is simulated to determine the parameter related to the leakage of fabric and vent holes with the airbag model using the uniform pressure method offering the relatively short solving time. And then Static deployment test is simulated for determining the parameter related to the unfolding phase with the airbag model using the corpuscular (particle) method. These two simulations are compared to the test results and satisfactory correlation is found in both the cases.
The drop tower simulation using the uniform pressure method leads to reduce the total correlation time and to easily extend the application for protection of the driver occupant while in-position. This airbag model can be used in parametric studies to investigate the effects of airbag module design changes and to study the out-of-position (OOP) load case.

INTRODUCTION

The safety system integration for in-position situation has held a main portion of the safety related simulation which usually uses the uniform pressure method for inflating the airbag. The airbag model adopted the uniform pressure distribution within the airbag volume provides adequate results for the in-position situation because the occupant and the airbag does not have a reciprocal action until the airbag is fully deployed. It is the basic assumption for the uniform pressure method that the gas inside the airbag is an ideal gas and assuming that the pressure and temperature are uniform everywhere inside the airbag. These assumptions are acceptable in the occupant analysis for the in-position situation.
Recent years the need of simulation beyond the uniform pressure method is increased in airbag module design and the OOP situation. In terms of the OOP situation or the airbag module design, the effect of gas flow plays a very important role at the early stage of airbag deployment. In order to simulate the deployment process of folded airbag with various folding pattern and the vent hole design, the meaningful safety simulation tools that allow the integration of the computational fluid dynamics analysis into the finite element airbag model are developed. These sophisticated simulation tools allow to handle the interaction between the gas and the airbag fabric, but the calculation is very expensive in CPU time [1], [2], [3].
Several validation tests and corresponding simulations are usually conducted to get the reliable airbag model on the deployment kinematics and these successive correlating processes are very time consuming job that have to be reduced.
In this study, the effective validation methodology that alternately adopts the uniform pressure method and the recently developed corpuscular method in the LS-DYNA 971 is described. And the model setup for the driver side airbag module is described.

Driver Side Airbag Model Setup

A typical 60 liter driver side airbag used in a mid-size car is selected in this study. Flat airbag cushion is folded with ∑-Roll folding and then the finite element model of the folded airbag cushion is placed in the canister with Y-tear pattern cover is built. The dynamic relaxation is performed until the internal energy of the folded airbag cushion in the canister become stable. The steering wheel is modeled, as it is an important part for the airbag support. The inflator characteristics and the mechanical properties of airbag cushion fabric are considered to achieve the accurate airbag model.
Figure 1 shows the modeling process for the finite element airbag module.

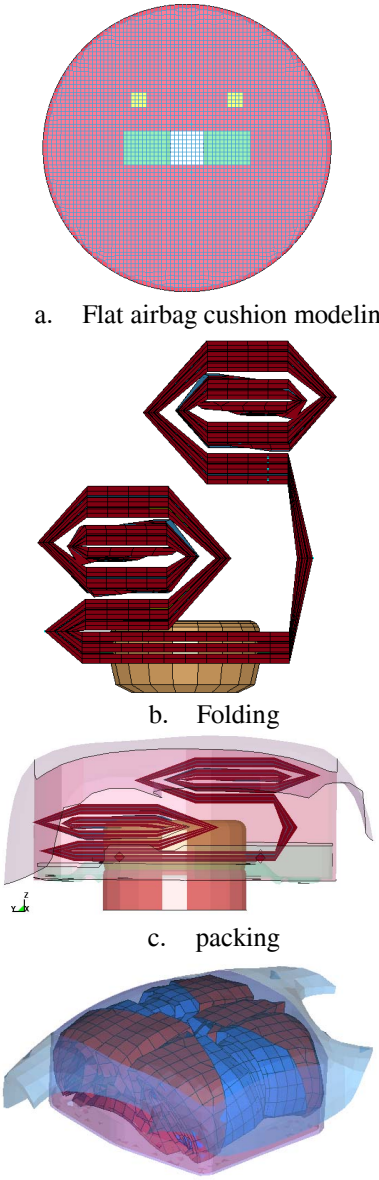

a. Flat airbag cushion modeling

b. Folding

c. packing

d. Relaxation

Figure 1. The modeling process for the finite element airbag module

<u>Fabric Material Property</u> - Both 'tightly' and 'loosely' woven fabrics can show differences on mechanical properties, because woven fabrics can resist in-plane shear loads once the yarn lock-up angle has been reached and the lock-up angle is much lower for tightly woven than loosely woven fabrics [4]. The differences of material property on material direction can affect the shape of fully deployed bag.
Recently developed tools for safety analysis provide a material model that incorporates an in-plane shear stiffness property into warp and weft properties. This shear material model is appropriate for a typical airbag fabric in opposition to the ISOLINEAR and OTHOLINEAR material model which are both linear and cannot rotate relative to each yarn. To gain the in-plane shear stiffness of tightly woven airbag fabrics, the picture frame test can be conducted. The picture frame test device that is made for this study is shown in Figure 2. The corners of the test frame have revolute joint to transform an applied axial loading into the shear deformation of specimen.

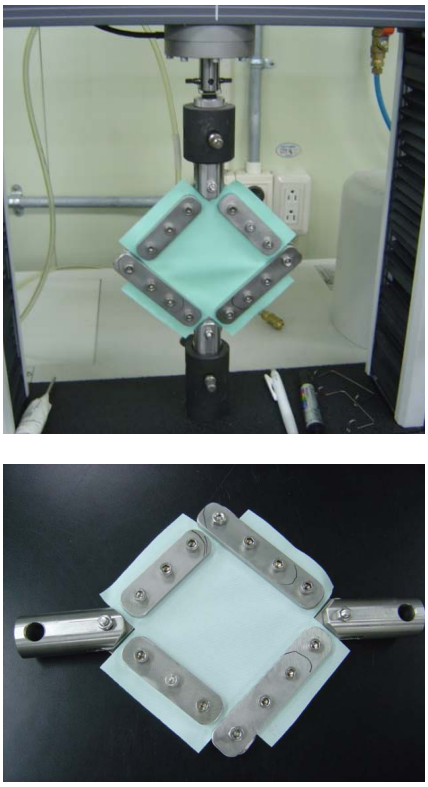

Figure 2. The picture frame test device and fabric specimen

The axial force and axial displacement acquired during a test are converted the true shear stress and the true shear strain in order to be used for the fabric material model. The converted non-linear stress-strain curve is used for representing the initial soft response of the fabric due to the crimp effect [5]. The picture frame tests are conducted with the various

loading velocity, and Figure 3 shows the force-strain curve with 1.0x and 1.6x loading velocity. The result shows the inclination of the force-strain curve increases in proportion to the loading velocity. The picture frame simulation is conducted with the fabric test result and the validation procedure that is based on the test setup. The use of LS-DYNA's MAT_FABRIC material and recent parameter helps enhancement of prediction of the picture frame test data.

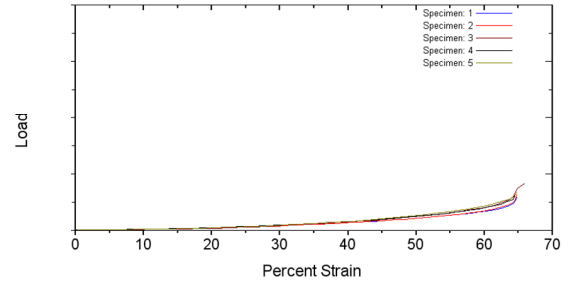

a. 1x

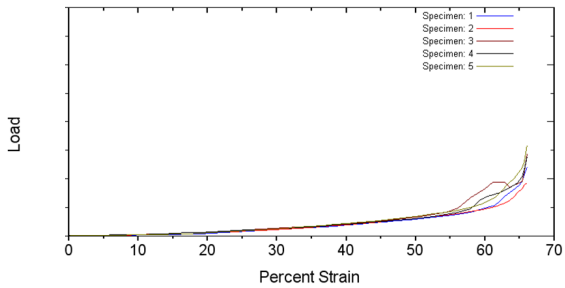

b. 1.6x

Figure 3. The picture frame test result with different loading velocity

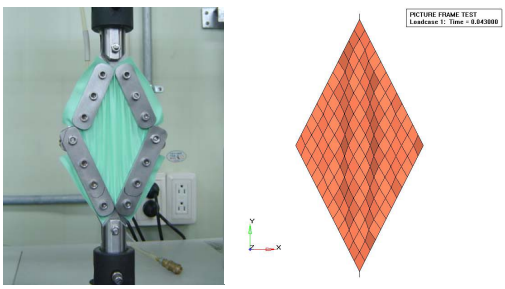

a. Deformed shape

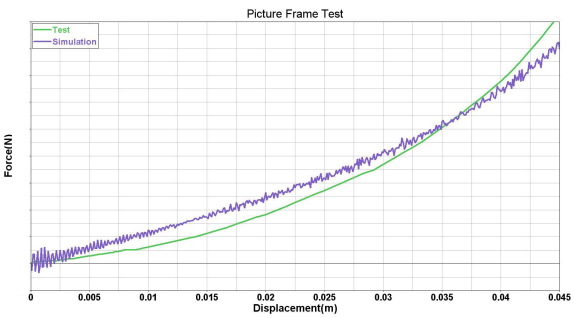

b. Force-displacement

Figure 4. Comparison between the picture frame test result and simulation result

In Figure 4 the deformed shape with wrinkle on fabric and the force-displacement results are depicted. The figure shows the simulation result is coincident with the test result. The validated material model based on the sufficient tests is the basis for the reliable airbag model.

Inflator Definition – Two types of inflator are modeled according to the validation phase: AIRBAG_HYBRID_JETTING and AIRBAG_PARTICLE.
AIRBAG_HYBRID_JETTING is used for the conventional uniform pressure method that gives relatively short CPU elapsed time.
AIRBAG_PARTICLE corresponding to the corpuscular method is newly developed for airbag deployment simulation in LS-DYNA. In this method, the gas is modeled as a set of individual particles. The corpuscular method shows the accuracy and agreement with experimental results in [1].
The multiple radial jets at gas discharge orifice are modeled in AIRBAG_PARTICLE option, the vertical jetting vector is employed for comparable result in AIRBAG_HYBRID_JETTING option. Due to these two options have similar parameters, they can be easily switched each other for airbag deployment simulation.

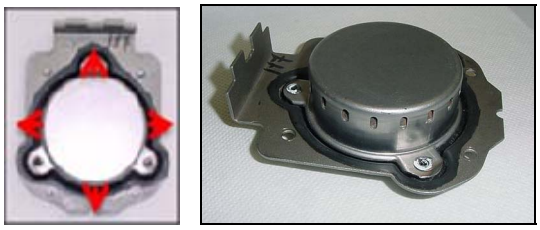

Figure 5. Radial jets and gas discharge orifices

Experimental pressure data of tank test is converted to mass flow rate and temperature input using the MADYMO Tank test Analysis (MTA) program. The inflator gas exit temperature and mass flow rate that are validated through a tank test simulation in LS-DYNA are used for defining inflator.

Drop Tower Test and validation

The two phase validation process for reducing the resources is employed in this study. The following two tests are conducted for acquiring the reference data; a) Drop tower test for acquiring the fully deployed airbag's reaction force, b) Static deployment test for acquiring the airbag internal pressure during the deployment process. The drop tower test is simulated to determine parameters related to the leakage of fabric and vent holes with the airbag model using the uniform pressure method offering the relatively short solving time. And then Static deployment test is simulated for determining the parameter related to the unfolding phase with the

airbag model using the corpuscular (particle) method.

Flat Driver Side Airbag – Drop tower test and simulation with flat driver side airbag are conducted to determine parameters related to the leakage of fabric and vent holes. The main events during drop tower test are depicted in Figure 6.

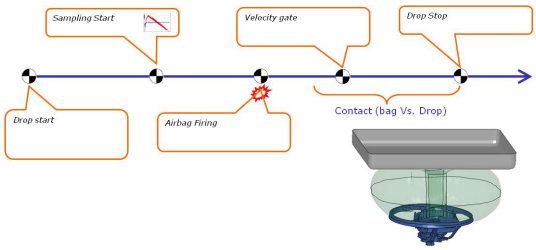

Figure 6. Scheme of Drop Tower Test

To represent the flat airbag cushion on the steering wheel, the pre-position simulation is conducted as a type of pre-simulation as shown in Figure 7.

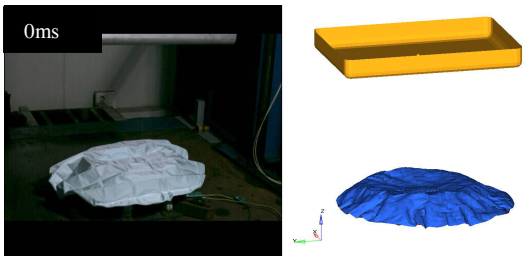

Figure 7. Initial stage of Drop Tower Test with flat bag

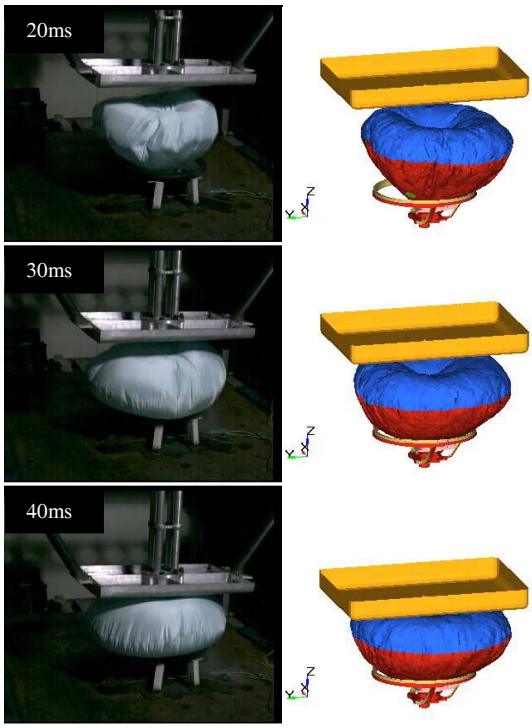

a. Comparison of kinematics

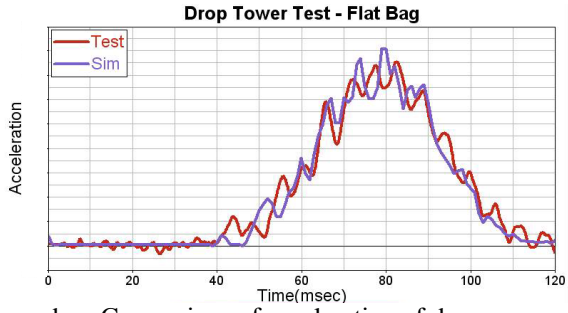

b. Comparison of acceleration of drop mass

Figure 8. Comparison between the drop tower test result and simulation result with flat bag

Drop tower test and simulation results for the flat airbag are depicted in Figure 7 and the simulation time history of acceleration data is closely correlated to the test result. Several parameters related to the leakage need to be tuned, because typical leakage model may not be able to cover the leakage characteristics of the specific airbag module.

Folded Driver Side Airbag – Drop tower test with folded airbag is conducted to validate the folded DAB model. In this phase parameters related to the contact definition of airbag fabric itself and the control of the strain that is caused element distortion during folding process are tuned. Increasing the scale factor on slave penalty stiffness, the contact parameter, leads to higher contact forces. The higher contact forces accelerates the airbag deployment and leads to lower pressure peak during unfolding due to faster volume increase. LS-DYNA provides a numerical option to assure that airbags that have reference geometry is able to open to the correct geometry [6, 7]. During airbag folding, some elements are stretched and distorted compare to the reference geometry and these elements result in tensile strains. The airbag that is initially stretched result in the incorrect geometry. So this numerical option can be used to control the transition from initial mesh to reference mesh. But inadequate value for this factor can cause a lower pressure that result from larger element size in vent orifice area or a pressure peak change that result from different contact forces of airbag self contact.

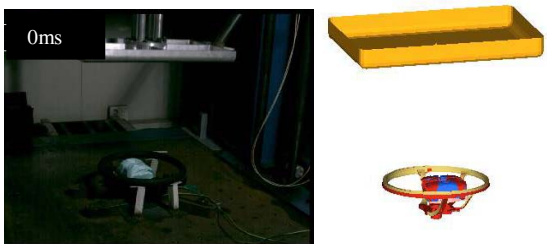

Figure 9. Initial stage of Drop Tower Test with folded bag

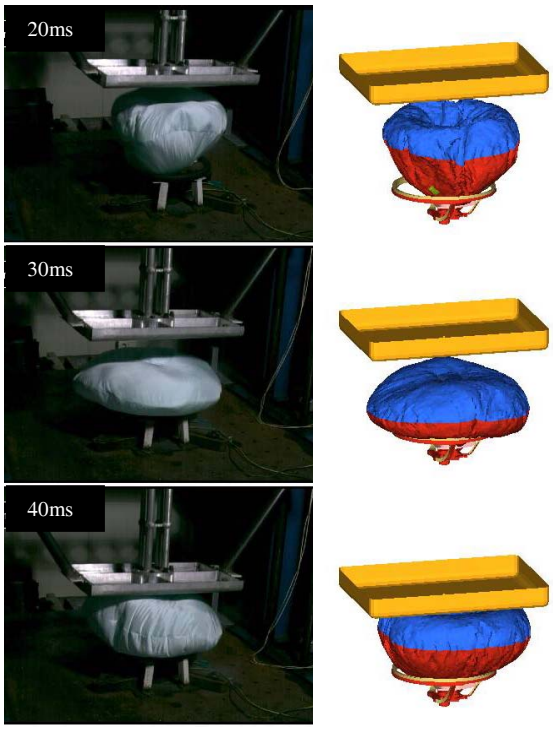

a. Comparison of kinematics

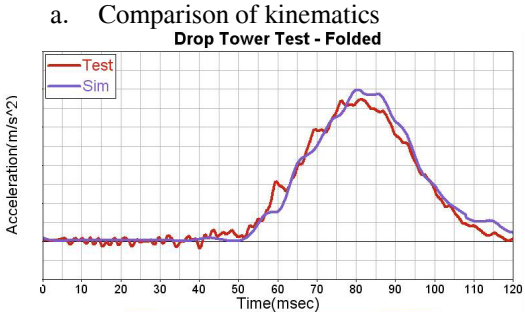

b. Comparison of acceleration of drop mass

Figure 10. Comparison between the drop tower test result and simulation result with folded bag

<u>Driver Side Airbag Module</u> – The folded airbag cushion is placed in the canister with Y-tear pattern cover. Tear seam mechanism that uses material failure of element requires smaller time step than the constraint failure mechanism and it can help to reduce the elapsed CPU time. The tear seams are defined as taking advantage of the constraint with failure.

The dynamic relaxation is conducted as a type of pre-simulation until the internal energy of the folded airbag cushion in the canister reaches sufficiently stable state as shown in Figure 12.

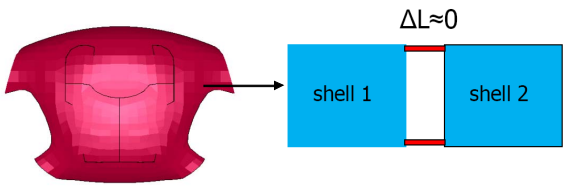

Figure 11. Tear Seam Mechanism

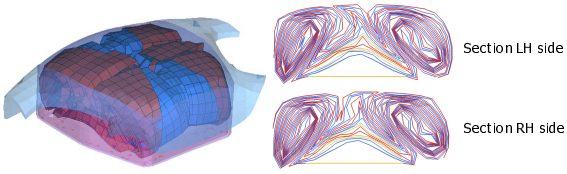

Figure 12. Dynamic relaxation of folded airbag within canister

Drop tower test with airbag module is conducted to validate the DAB module model. In this phase parameters related to the contact definition between the DAB cover and the airbag fabric is tuned. These three drop tower tests and simulations with the uniform pressure method contribute to fast confirmation of the parameters related the gas leakage, contact, stress and strain.

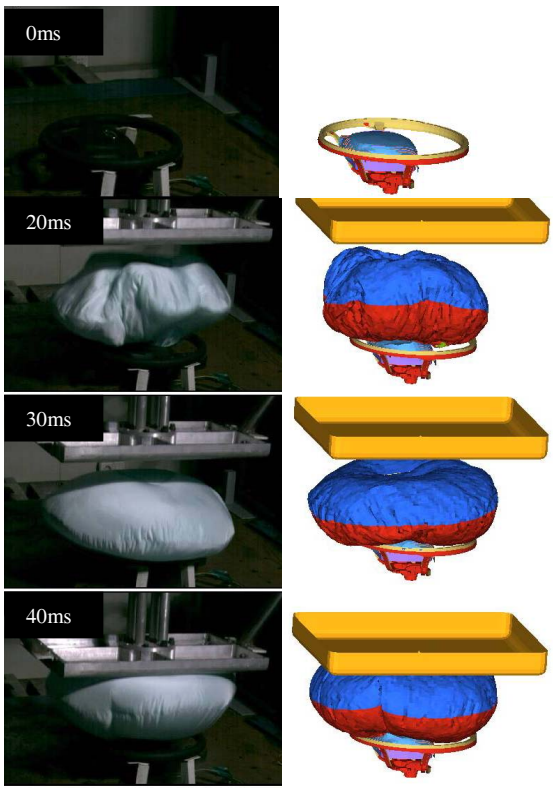

a. Comparison of kinematics

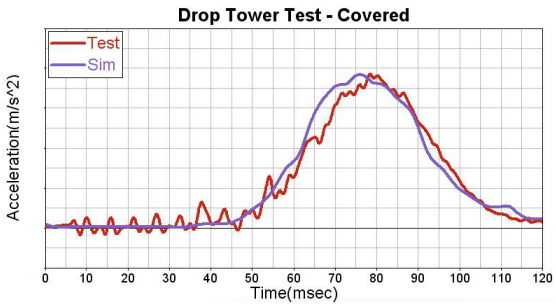

b. Comparison of acceleration of drop mass

Figure 13. Comparison between the drop tower test result and simulation result with airbag module

Static Deployment Test and validation

The drop tower test is a widely used tool for the validation of the airbag characteristic. Good correlation between the tests and simulation models in of the measured acceleration has been achieved with the conventional FE airbag models based on uniform pressure method. Although the reliable and predictable airbag model for fully deployed status provides a confidential result in interaction between the airbag and the in-position occupant, in case of evaluating the injuries of occupant in airbag hazard area or out-of-position and the airbag module design such as the effect of different airbag folding patterns on the OOP occupant or the DAB cover, the drop tower test is not a suitable validation tool.
In OOP situation, the airbag shape and reaction force on each region in time history are important factors for the occupant injuries. Various dynamic test methods with the head form, pendulum or the matrix of load cells have been developed to provide a better evaluation data for airbag deployment simulation model. The distribution of the pressure inside airbag provides an insight into the airbag module and a direct comparison between a test and a flowing gas integrated simulation, whereas the simulation that uses impactor has additional interaction between airbag and impactor. To this purpose, airbag static deployment tests were conducted to acquire the pressure distribution inside a folded airbag and covered airbag.
The folded and covered airbag are modeled with a corpuscular method using 200,000 particles in LS-DYNA for the gas flow, based on the previously validated model with the uniform pressure method and the drop tower tests.

<u>Folded Driver Side Airbag</u> – Airbag static deployment test and simulation with folded driver side airbag is conducted. The transmission hose is fixed onto the retainer ring of airbag and the pressure transducer is connected with the transmission hose. Even though the transmission hose is fixed onto the airbag fabric for flat airbag, the mounting of transmission hors for folded or covered airbag is subjected to restriction on position. The folded airbag is mounted on the steering wheel and inflated with primary output because the primary output of advanced airbag is adopted for static OOP tests scenario of FMVSS 208 issued by NHTSA.
The pressure peak level at the early moment of the deployment, punch-out phase, of the simulation is substantially coincident with the test data. The decrease in pressure during opening the airbag is also observed, and similar pressure level can be seen in the fully deploying stage. The kinematics during airbag opening of the simulation is coincident with the test data before 15ms. The central area of simulation result expands more toward the perimeter of the bag. But a subjective evaluation provides little information such as the above mentioned, so quantitative assessment method is adopted to evaluate the accuracy of the simulation model in kinematics.

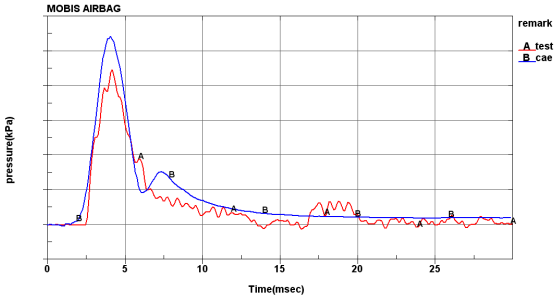

Figure 14. Comparison between the test pressure result and simulation result with folded bag and primary inflator output

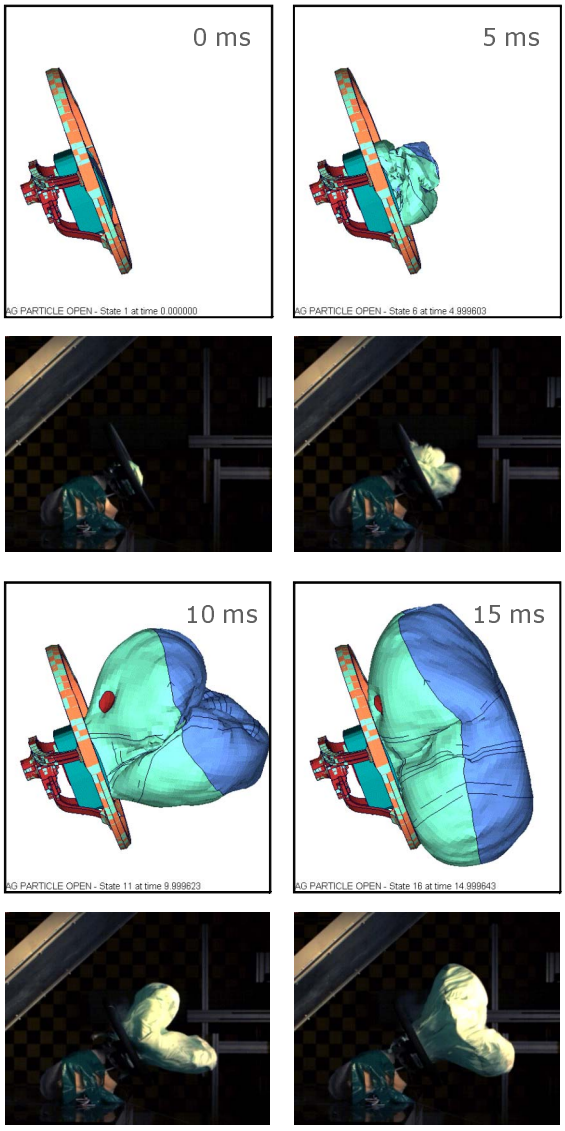

Figure 15. Airbag deployment kinematics with folded bag and primary inflator output

Radial lines with origin in steering wheel are used for estimation of the deployment shape error between test and simulation. 19 lines are used for side view and 36 lines are used for front view as depicted in figure 16. The test and simulation result are scaled in the same size and then positioned at same origin. The distance between the origin of radiated line and intersection on airbag outline is measured. Total error is calculated with equation below.

$$error = \frac{L_{test} - L_{cae}}{L_{test}} \times 100$$

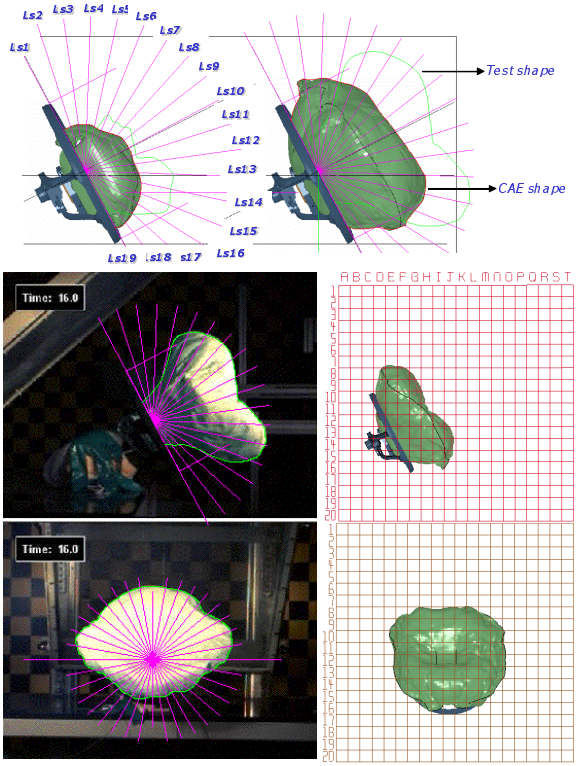

Figure 16. Radiated lines for quantitative error assessment

	side t=6.0				side t=16.0			
	L_test	L_cae	error	error sum	L_test	L_cae	error	error sum
1	72.16	120.69	-67.5	67.53	72.20	123.76	-71.4	71.41
2	75.23	120.48	-60.1	60.15	77.20	163.44	-111.7	111.71
3	82.16	119.51	-45.5	45.46	85.67	217.46	-153.8	153.83
4	90.92	115.22	-26.7	26.73	100.88	147.90	-46.6	46.61
5	104.17	112.08	-7.6	7.59	145.42	250.88	-72.5	72.52
6	147.24	111.97	24.0	23.95	314.62	269.36	14.4	14.39
7	140.77	113.29	19.5	19.52	335.00	264.95	20.9	20.91
8	144.89	113.33	21.8	21.78	344.19	244.00	29.1	29.11
9	144.65	111.00	23.3	23.26	331.86	231.96	30.1	30.10
10	135.38	119.70	11.6	11.58	307.92	236.50	23.2	23.19
11	131.03	124.11	5.3	5.28	292.62	251.53	14.0	14.04
12	184.04	137.02	25.5	25.55	317.04	274.15	13.5	13.53
13	214.64	143.13	33.3	33.32	363.40	292.38	19.5	19.54
14	214.04	147.63	31.0	31.03	377.48	281.13	25.5	25.52
15	222.87	156.41	29.8	29.82	341.34	272.81	20.1	20.08
16	195.26	166.82	14.6	14.57	173.22	220.24	-27.1	27.14
17	158.87	173.95	-9.5	9.49	114.60	181.79	-58.6	58.63
18	125.90	179.40	-42.5	42.49	98.67	153.15	-55.2	55.21
19	101.55	173.31	-70.7	70.66	85.27	135.99	-59.5	59.48
	error ave(%)			30	error ave(%)			46

Table 1.
Results of quantitative error assessment in side view for folded airbag

a. Side view@6ms

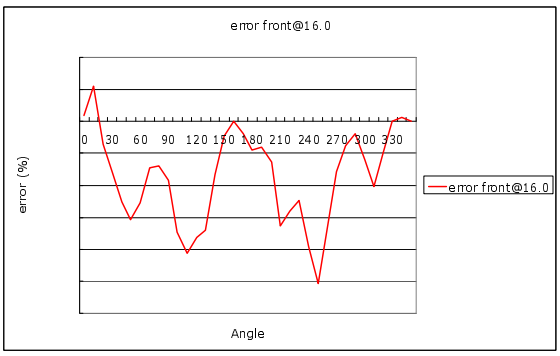

b. Front view@16ms

Figure 17. Deployment shape error for folded airbag

The measured distances and errors in side view at 6ms and 16ms are summarized in Table 1. The diagram of error in terms of angle provides insight into the tendency of shape difference. The average error for folded airbag's kinematics is 29% and a point of reference has to be determined through statistical research.

<u>Driver Side Airbag Module</u> – Airbag static deployment test and simulation with covered driver side airbag (DAB Module) is conducted. The covered airbag are modeled with a corpuscular method in LS-DYNA for the gas flow, and the model is based on the previously validated model with the uniform pressure method and the drop tower tests. The distances and errors are also measured for covered airbag in side view and front view.

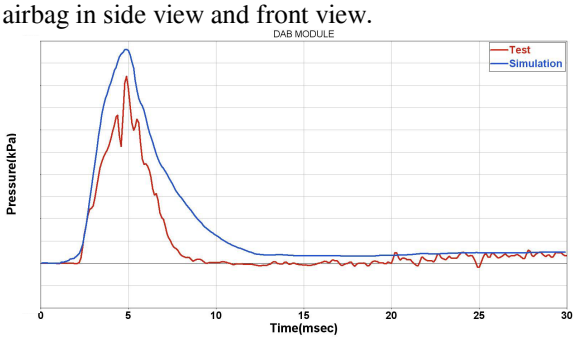

Figure 18. Comparison between the test pressure result and simulation result with covered airbag and primary inflator output

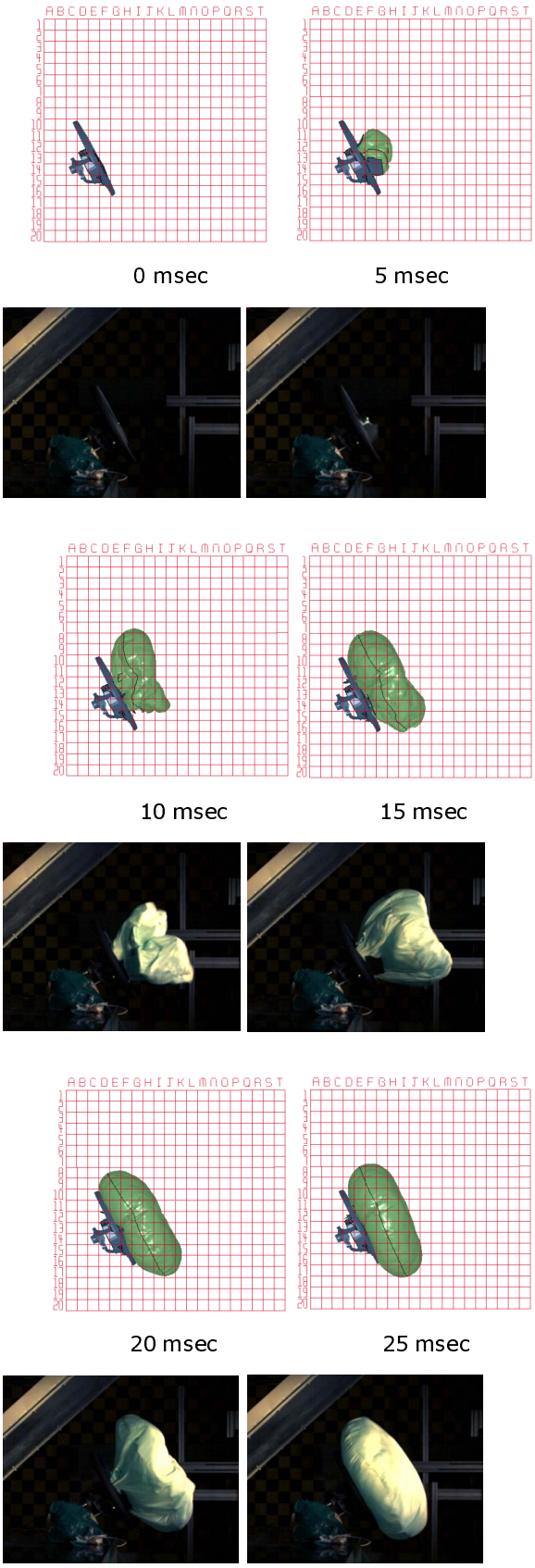

Figure 19. Airbag deployment kinematics with covered bag and primary inflator output

Good correlation of the pressure peak level was observed at the early stage of deployment (about 5ms) and the pressure level at the fully deployed stage (about 25~30ms) of the simulation is coincident with the test data on the whole. The kinematics during airbag opening of the simulation is coincident with the test data before 15ms similar to the folded airbag simulation result.

CONCLUSIONS

The validation process to reduce the total simulation time has been developed. This validation process using the uniform pressure method and the corpuscular method alternatively can decouple the parameters into several problems; gas leakage, contact and cover tearing, the target parameter of validation can be easily determined through correlation to corresponding test data. The uniform pressure method (AIRBAG_HYBRID_JETTING) and the drop tower tests are employed to decide the gas leakage and the contacts. The corpuscular method (AIRBAG_PARTICLE) and small modifications for the contacts and cover tearing are appended to the model based on the validated uniform pressure method. Each validation stage corresponding to the drop tower tests and the static deployment tests shows the good agreement with experimental results in time history.
Switching the simulation method, from the uniform pressure method to the corpuscular method, is quite easy and has no discontinuity because the AIRBAG_HYBRID and AIRBAG_PARTICLE in LS_DYNA have similar parameters for airbag definition. As shown in Figure 20, proposed validation process, switching the simulation method alternatively, can shorten the total simulation time against the case using the corpuscular method only. Therefore the predictable and reliable simulation model is able to get easily, more accurate investigation into the airbag cushion and module design can be made to improve the occupant injuries.

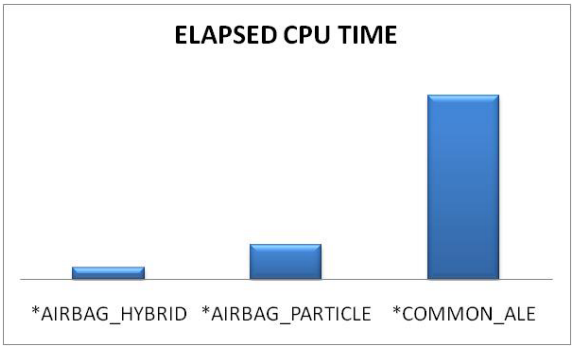

Figure 20. Comparison of computing time between the different simulation model on 4 CPU

REFERENCES

[1] A. Hirth, A. Houfe and L. Olovsson, "Airbag Simulation with LS-DYNA Past-Present-Future", 6th European LS-DYNA Conference, 2007.

[2] Zhang H., Raman S., Gopal M. Han T., 2004, "Evaluation and Comparison of CFD Integrated Airbag Models in LS-DYNA, MADYMO and PAM-CRASH", SAE Paper 2004-01-1627.

[3] Jörg Hoffmann, Michael Freisinger, Mike Blundell, Peter Ritmeijer, 2007, "Investigation into The Effectiveness of Advanced Driver Airbag Modules Designed for OOP Injury Mitigation", ESV2007 Paper Number 07-0319.

[4] Madymo 6.4 Theory Manual. TNO Madymo BV. Delft, The Netherlands.2007, pp108~117.

[5] Ulrich Stein, Gerd Weissenbach, Manfred Schlenger, Mark Tyler-Street and Peter Ritmeijer, "The Development and Validation of the Material Model Fabric_Shear for Modelling Advanced Woven Fabrics", 10th International MADYMO Users Meeting, 2004.

[6] LS-DYNA Keyword User's Manual, version 971, LSTC, 2007.

[7] LS-DYNA Theory Manual, version 960, LSTC, 1999.

THE INFLUENCE OF SUB-FRAME GEOMETRY ON A VEHICLE'S FRONTAL CRASH RESPONSE

Chung-Kyu Park*, Robert Thomson**, Aleksandra Krusper***, Cing-Dao (Steve) Kan*
*National Crash Analysis Center, The George Washington University, Washington, DC, USA
**VTI-Swedish National Road and Transport Research Institute, Gothenburg, Sweden
***SAFER-Vehicle and Traffic Centre, Chalmers University of Technology, Gothenburg, Sweden
Paper 09-0403

ABSTRACT

The importance of a vehicle sub-frame is often discussed in vehicle compatibility. To observe how the sub-frame geometry influences the vehicle response, three different sub-frame configurations were modeled and simulated in US NCAP crash test configurations as well as car-car simulations. The former simulations were used to observe how the design changes would influence self protection in a crash test influencing the original design of the vehicle. The latter simulations were to observe how the modification would influence vehicle compatibility under "real world" conditions.

The rigid barrier impacts could detect the changes in the design. The most forward placement of the sub-frame had a stiffer response than the other configurations as observed in acceleration pulse and barrier wall loads. Self protection also tended to be improved over the baseline configuration. In car-car testing, it was difficult to identify a clear subframe configuration that provided improved compatibility. Both the standard and forward placed subframe had better performance than the most rearward configuration. Neither the baseline nor extended sub-frame versions were clearly better for all car-car impact configurations but an extended sub-frame exhibited better self protection, especially when the vehicle was lower than its collision partner.

INTRODUCTION

The main problem in frontal collisions between two vehicles with similar - or even identical - structures and mass are the geometrical mismatches that can occur. The geometric incompatibility has two main origins, the pre-impact alignment of the vehicles and the structural layout. The horizontal misalignment is often called the fork effect and a vertical misalignment is referred to as under/overriding. Horizontal overlap of the vehicles is highly unpredictable and can vary more than 1.5m for different crash scenarios. Vertical misalignment is not influenced as much by vehicle alignment as the vertical positions of structures seldom varies more than a few centimeters from a reference condition. Thus variations within the vehicle structures are the main source of vertical misalignment.

The challenge to design vehicles for compatibility is to achieve good vehicle crash performance that can accommodate the foreseeable impact orientations for lateral overlap and interact with the vertical structural variations within the vehicle fleet. Because of the large range of geometric possibilities, many researchers promote the concept of structures with many vertical load paths with strong lateral connections [1,2]. The idea is that the distribution of load carrying elements across the vehicle front can interact with a wide variation of vehicle designs and impact configurations. One proposal for vehicle designs to improve compatibility is the inclusion of a lower load path and many vehicles already have a sub-frame that can provide this function.

The structural layout of different vehicles was investigated in a recent European Community funded projects VC-Compat [3]. The database developed in VC-Compat is the most relevant information as it contains relatively modern vehicles. To demonstrate the role of a sub-frame in frontal crashes, the alignment between vehicle structures was analysed [4] and

Figure 1 shows the results for longitudinals and subframes.

Crash testing of vehicles with and without sub-frames has been conducted in various research activities[2,3,5]. However controlled changes in overlap height and horizontal offset has not been possible due to the costs. As a first step to understand how the front structures perform due to different vertical and horizontal alignments, a simulation study of the NCAC Ford Taurus model was conducted [6]. This study provided important information describing how the loads in the front structures changed due to vehicle alignment. One interesting performance feature was that the vehicle response (measured by vehicle accelerations and intrusions) did not vary monotonically with changes

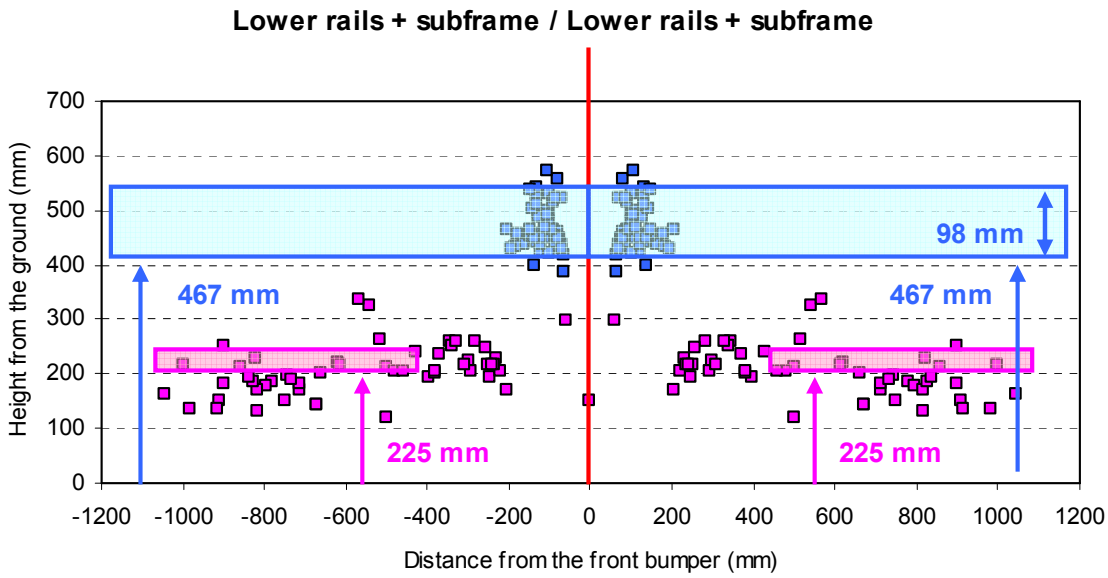

Figure 1: Vertical and Longitudinal Positioning of Vehicle Structures [4]

in the vertical overlap. To further understand how specific vehicle structures altered the vehicle crash performance, a study of the influence of the subframe geometry was conducted using the same numerical vehicle models.

METHODOLOGY

In order to study the performance of the vehicle structures, it was important to control as many confounding variables as possible. The same basic vehicle model was used as a basis for the study to avoid any influence of different mass and/or global frontal stiffness.

The FE vehicle of study was the 2001 model year Ford Taurus available from the FE model achieve of National Crash Analysis Center (NCAC) [7]. This model was chosen because it was the closest representation of a European mid-sized vehicle that was publicly available. The Taurus was developed for the US market where the FMVSS 208 full frontal crash test defines the primary performance criteria. As a result, the vehicle design exhibits a deformation response for the longitudinals and occupant compartment which were not completely representative of a similar European vehicle designed for an offset deformable barrier test. Some modifications of the vehicle model were made to provide a more "European" performance. The main change to the model was the introduction of a beam, shown in Figure 2, to restrict the upward rotation of the longitudinals.

To shorten the simulation time, a simplified version of the model was used. Parts with a low priority for frontal structural interaction were taken out and the rear components of the vehicle were made rigid. Essentially all components forward of the B-Pillars were deformable to allow intrusion to be included in the analyses [6]. This simplified Finite Element (FE) Taurus model is referred to as the Basic model and is the basis for subsequent modifications.

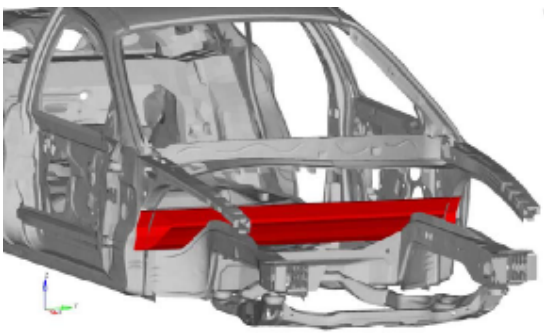

Figure 2: Simplified FE vehicle model of Taurus

The weight of vehicle is about 1.39 ton. Failure of the mounts between the sub-frame and floor of vehicle are defined in the FE model when the load reaches the (50 kN).

It is assumed that the outputs of the simplified model in crash simulations are not directly comparable with the real crash test data

quantitatively. The results are considered comparable with simulation results under different crash conditions with the same simplified model.

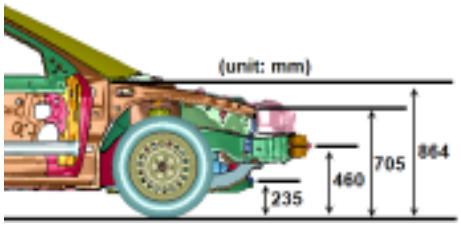

(a) Height

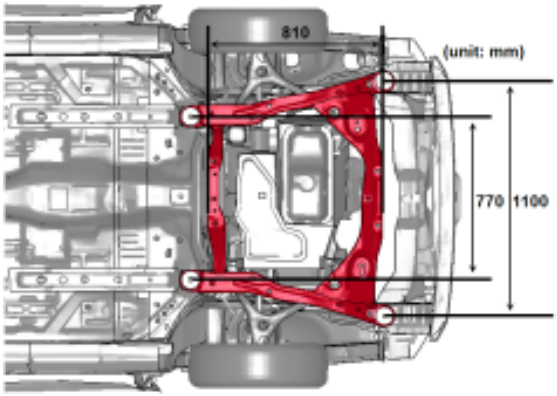

(b) Sub-frame

Figure 3: Dimension of frontal structure of Taurus

The simulations of frontal Full Width Rigid Barrier (FWRB) and Car-to-Car (C2C) tests were performed by LS-DYNA [8]. The Basic mode was used for both reference and partner vehicles. In future discussions, the reference vehicle is called Vehicle 1 (V1) and the partner vehicle is Vehicle 2 (V2). The reference vehicle was then modified to investigate the influence of different sub-frame geometries. The original sub-frame geometries are shown in Figure 3. The three configurations investigated were the original, a 100 mm forward extension (ExSub) and a 100 mm shortened sub-frame (ShSub) shown in Figure 4. The speed of each vehicle in a FWRB or C2C tests is 56 km/h. The partner vehicle is horizontally and vertically offset from the reference vehicle. In the horizontal offset, there are three cases, full, 60% and 40% overlap of vehicle. In the vertical offset, there are 2 cases, full and 25% overlap of vehicle. The partner vehicle in 60% and 40% horizontal overlap is translated 742mm and 1080mm in lateral direction respectively. The partner vehicle in 25% vertical overlap is moved 105mm up. Table 1 summarizes simulation cases. There are many cases so

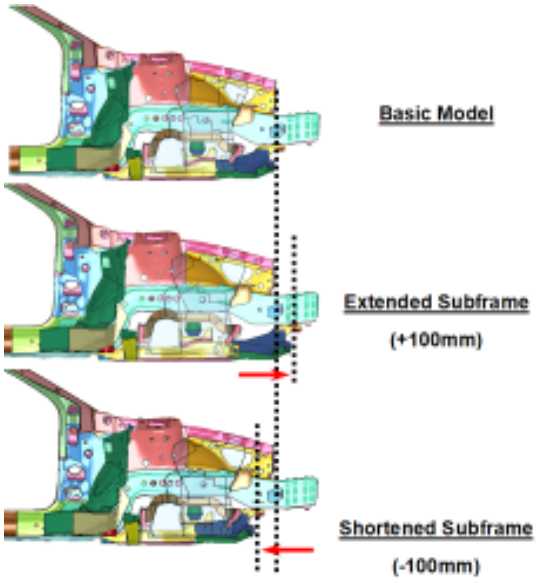

Figure 4: Description of modification of the length of sub-frame of vehicle

abbreviations for the simulation cases are used. For example, B2E_H60V25 means that the reference vehicle (the first letter, B) is the Basic model and the partner vehicle (the next letter, E) is the ExSub model in C2C test. H60 means 60% horizontal overlap and V25 is a 25% vertical overlap.

In any vehicle crash test, there are many measurable outputs. Among those outputs, however, some specific ones are essential measurements to evaluate safety and crashworthiness performance. In a compatibility test, it's not yet been clearly agreed what measurements are objective and relevant to evaluate the self and partner protection of vehicles. In this study, the intrusion profiles of vehicles are mainly considered. The measurement locations of the intrusion of vehicle are described in Figure 5

Table 1: List of simulation case

	Vehicle 1 (under-ridden)	Vehicle 2 (over-riding)	Horizontal Overlap	Vertical Overlap	Cases (Abbreviation)
FWRB	Basic	-	-	-	Basic or B
	ExSub				ExSub or E
	ShSub				ShSub or S
C2C	Basic	Basic	Full	Full	B2B_H100V100
	Basic	ExSub			B2E_H100V100
	Basic	ShSub			B2S_H100V100
	Basic	Basic		25%	B2B_H100V25
	Basic	ExSub			B2E_H100V25
	ExSub	Basic			E2B_H100V25
	Basic	ShSub			B2S_H100V25
	ShSub	Basic			S2B_H100V25
	Basic	Basic	60%	Full	B2B_H60V100
	Basic	ExSub			B2E_H60V100
	Basic	ShSub			B2S_H60V100
	Basic	Basic		25%	B2B_H60V25
	Basic	ExSub			B2E_H60V25
	ExSub	Basic			E2B_H60V25
	Basic	ShSub			B2S_H60V25
	ShSub	Basic			S2B_H60V25
	Basic	Basic	40%	Full	B2B_H40V100
	Basic	ExSub			B2E_H40V100
	Basic	ShSub			B2S_H40V100
	Basic	Basic		25%	B2B_H40V25
	Basic	ExSub			B2E_H40V25
	ExSub	Basic			E2B_H40V25
	Basic	ShSub			B2S_H40V25
	ShSub	Basic			S2B_H40V25

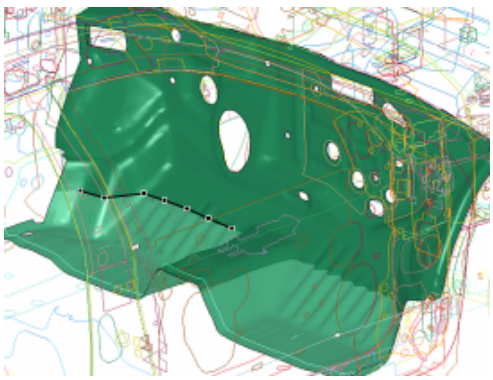

(a) Horizontal intrusion

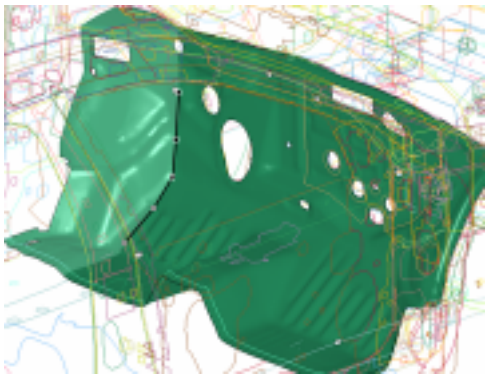

(b) Vertical Intrusion

Figure 5: Description of measurement locations

FRONTAL FULL WIDTH RIGID BARRIER (FWRB) TEST

The simulations of the FWRB test with three vehicle models were performed to check how the crash performance (self-protection) of vehicles is changed when the sub-frame of the vehicle is extended or shortened. The impact speed of the vehicle was 56km/h (35mph).

Figure 6 shows the deformation of the vehicles in FWRB test when the speed of vehicle reaches zero (maximum dynamic crush). In the ExSub model, the sub-frame is quite bent which absorbs a lot of crash energy. The sub-frame in not as bent as much in the ShSub model, instead the whole frontal unit of the vehicle is bending upwards.

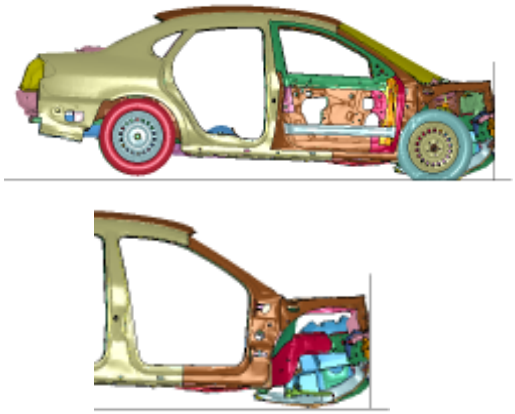

a) Basic model

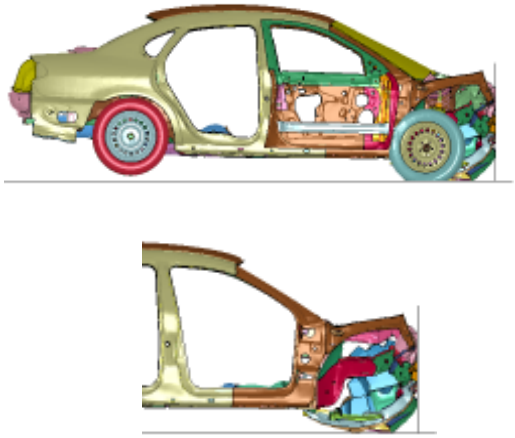

(a) ExSub model

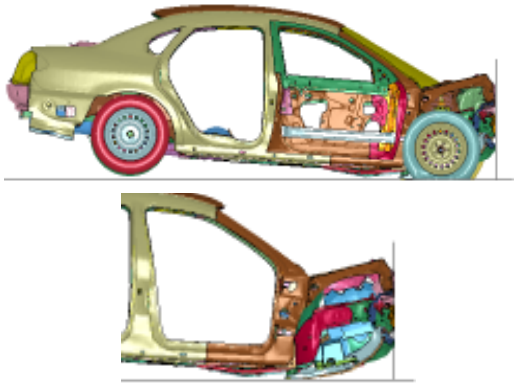

(c) ShSub model

Figure 6: Deformation of vehicle in FWRB test

Figure 7 shows the acceleration and velocity profiles of vehicles in FWRB test. There are four peaks in the acceleration profile of the Basic model. The first peak occurs when the rails of the vehicle impact the rigid wall, the second peak happens when the front cross-member of the sub-frame impacts the rigid wall, the third peak comes when the engine of vehicle impacts the firewall of the vehicle, and the fourth peak appears before the vehicle rebounds. The acceleration profile of the ExSub model is similar to the Basic model, but peak times occur earlier in the crash event. In the ShSub model, the engine of vehicle hits the rigid wall at the second peak and the cross-member of sub-frame of vehicle impacts the rigid wall at the third peak.

The dots in the acceleration profiles indicate the impact time of the sub-frame cross-member against the rigid wall. In the Basic model, it occurred near the highest acceleration level and at 80% of vehicle crush. In the ExSub model, it occurred earlier when accelerations are still climbing and at 50% of vehicle crush and, in the ShSub model, the sub-frame cross-member contact with the wall occurred at the time of peak acceleration and at 90% of vehicle crush.

The wall forces in FWRB tests are shown in Figure 8. Dots indicate the time (or crush) when the cross-member of the sub-frame of the vehicle impacts the rigid wall. The initial stiffness (Ks), which is the slope of the curve from 0 to 200mm of vehicle crush [9,10,11], are similar in all three models. After 0.015sec (or 150mm of vehicle crush), however, the ExSub model becomes stiffer but the ShSub model becomes softer than the Basic model.

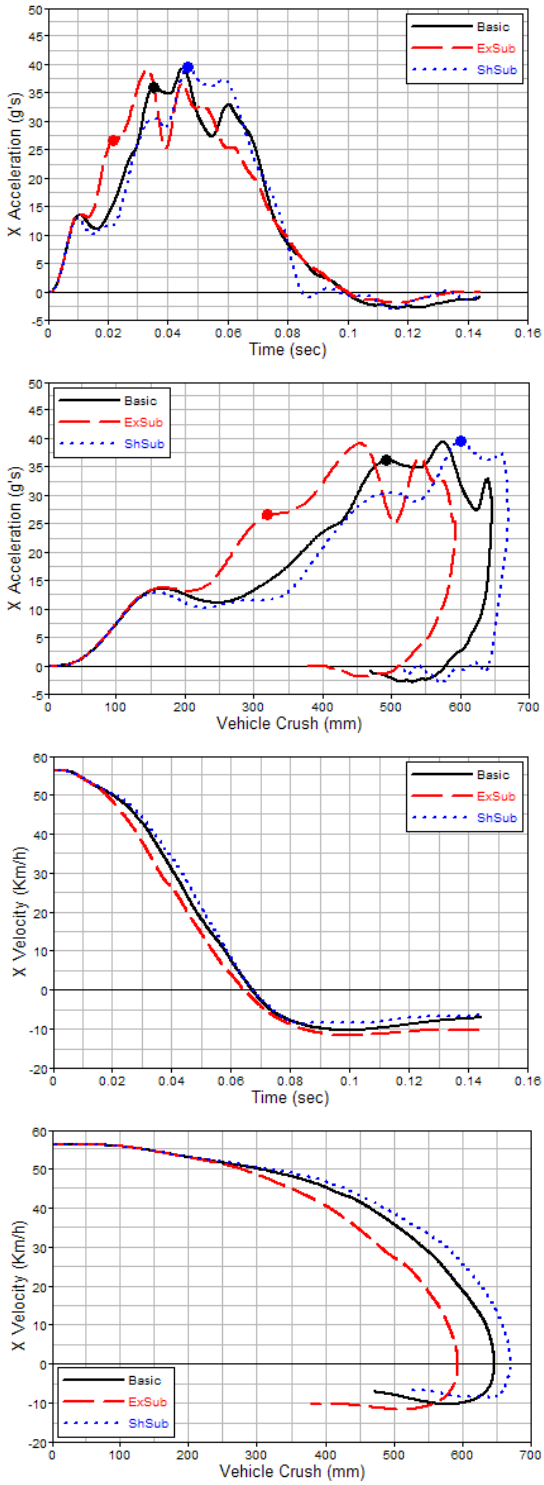

Figure 7: Acceleration, velocity, and deflection histories of vehicle in FWRB test

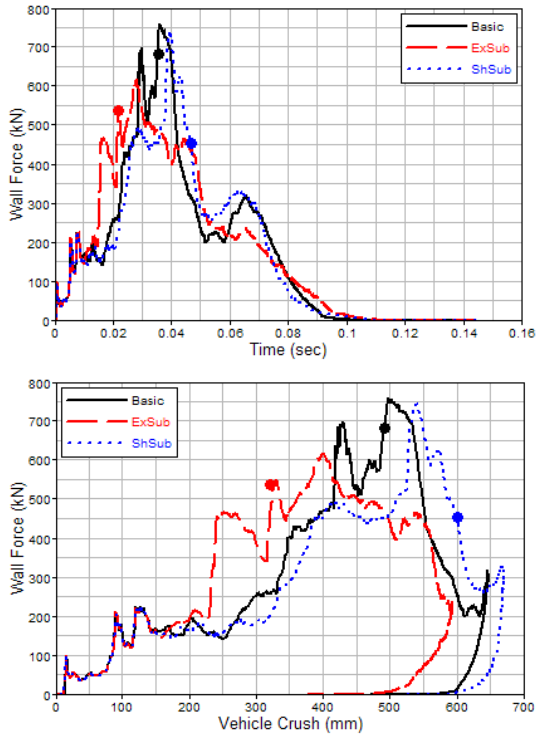

Figure 8: Wall force histories of load cells in FWRB test

The work stiffness (Kw400) [10,11], which is the area of the curve from 25mm to 400mm of vehicle crush, AHOF [12,13] and AHOF400 [10,11,14] are summarized in Table 2. It shows that the work stiffness of ExSub model is stiffer but the ShSub model is softer than the Basic model. The AHOF and AHOF400 of the ExSub model is lower than one of the Basic model but the ShSub model is higher. The intrusion profiles of the three models are shown in Figure 9. The ExSub model has less intrusion at right toepan but the ShSub model has more intrusion at the right toepan and dashboard than the Basic model.

According to the results, the modification of the sub-frame of the vehicle in terms of length makes the effective stiffness of vehicle change. The extended or shortened sub-frame of vehicle makes the vehicle stiffer or softer respectively. This change of the stiffness of vehicle affects the crash performance (self-protection) of the vehicle structure. The stiffer vehicle shows less intrusion in the vehicle (better crash performance) and is exhibited in the longer sub-frame case.

Table 2: Summary of work stiffness, AHOF and AHOF400 of vehicles in FWRB test

	Basic model	ExSub model	ShSub model
Work stiffness (Kw400)	950 N/mm	1,521 N/mm	763 N/mm
AHOF (Difference from Basic model)	363 mm	346 mm (-17mm)	419 mm (+56mm)
AHOF400 (Difference from Basic model)	450 mm	386 mm (-64mm)	475 mm (+25mm)

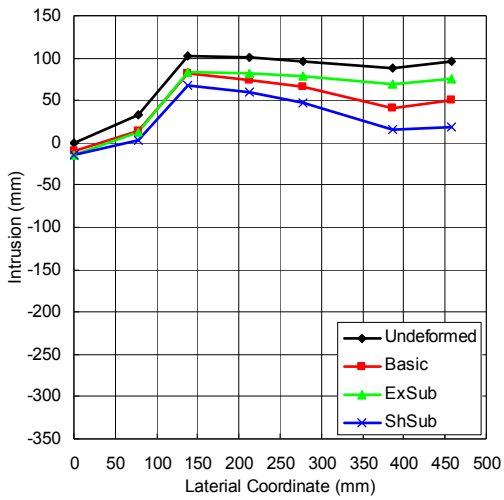

(a) Horizontal intrusion profile

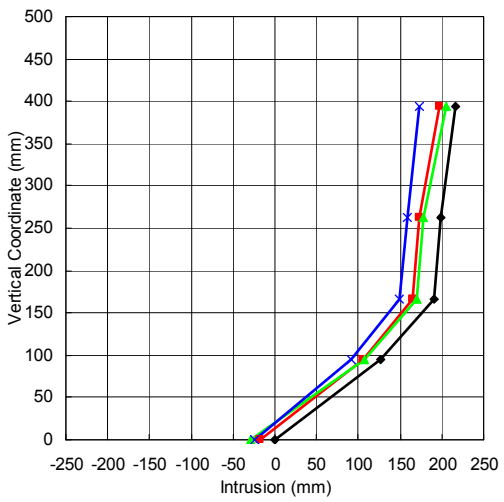

(b) Vertical intrusion profile

Figure 9: Intrusion profiles of vehicles in FWRB test

FRONTAL CAR-TO-CAR (C2C) TEST

The simulations of frontal C2C test with three vehicle models were performed to check how the compatibility performance (self and partner protection) of vehicles is changed when the sub-frame of the vehicle is extended or shortened. The impact speed of both vehicles was 56km/h. The intrusion profiles of vehicles in the C2C tests with modified vehicles are compared with baseline conditions in B2B cases to evaluate the compatibility performance of the modified vehicles.

Horizontal offset

Figure 10 shows the most extreme case for intrusion profiles of both vehicles for a 40% horizontal and full vertical overlap. The results from C2C tests with all three sub-frame models are displayed. The range of intrusions values is much greater than in the FWRB tests. This is not unexpected as the FWRB provides the best structural interaction possibilities.

In B2E cases, the intrusions in the ExSub model are smaller, but for one of the partner vehicles (Basic model) the intrusions are larger than those in the B2B cases. In B2S cases, the intrusions of both the ShSub and the partner vehicle (Basic model) are larger than one in B2B cases. The results show that the vehicles which have a longer sub-frame in C2C tests have the best self protection since the vehicle with the longer sub-frame is stiffer. However, the longer sub-frame gives worse partner protection. One exceptional case is B2S_H60V100 in which the ShSub model has less intrusion than the Basic model even though the Basic model has a longer sub-frame than the ShSub model. This difference was explained by the deformation mode of the vehicle. In the horizontal offset C2C test, the vehicles are rotated and a large moment is applied on the vehicle body. There is a particularly large moment on the body of the Basic model in B2S_H60V100 and this caused the buckling deformation on the floor near left B-pillar of the Basic model which is shown in Figure 11. Therefore, the larger intrusions of the Basic model in B2S_H60V100 are reported than for the ShSub model. This phenomenon underlines the need for a strong occupant compartment for self protection.

Mixed offset

Figure 12: Intrusion profile of vehicle in 60% horizontal and 25% vertical overlap test (V1)Figure 12 and Figure 13 show the intrusion profiles of both vehicles in a frontal crash with 60% horizontal and

25% vertical overlap. Figure 12 shows the cases with the Basic model as the reference and in Figure 13 all three sub-frame configurations are the reference vehicle with the Basic model acting as the partner. The partner vehicle is positioned relative to the reference vehicle. The first feature to notice is that more intrusion occurs in the mixed offset conditions

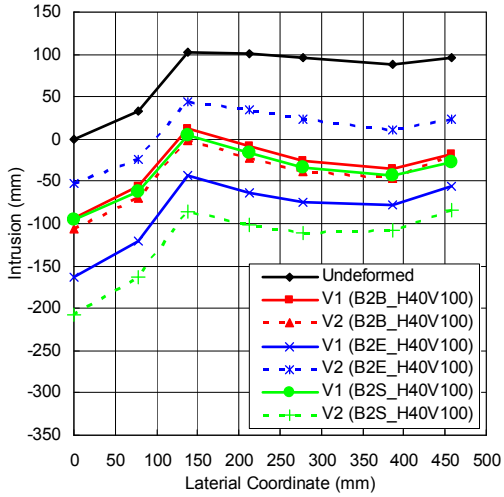

(a) Horizontal intrusion profile

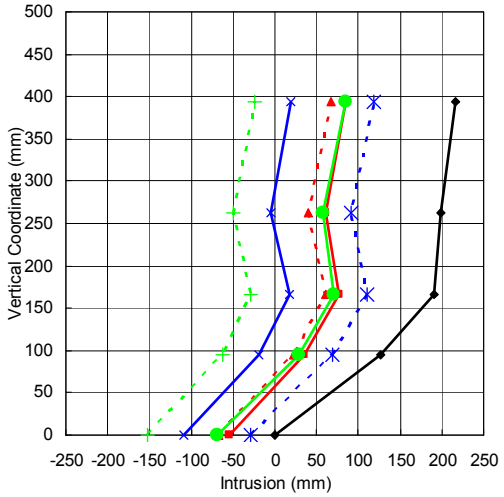

(b) Vertical intrusion profile

Figure 10: Intrusion profile of vehicle in 40% case

Changes in the Y-velocity of vehicles in C2C tests could be used to identify sudden changes in the behaviour of the Basic model in B2E_H60V25 and B2S_H60V25. This means that the buckling deformation, as previously shown in Figure 11 occurred. This resulted in intrusions of the Basic model in B2S_H60V25 which were larger than those in ShSub model even though the sub-frame of Basic model is longer.

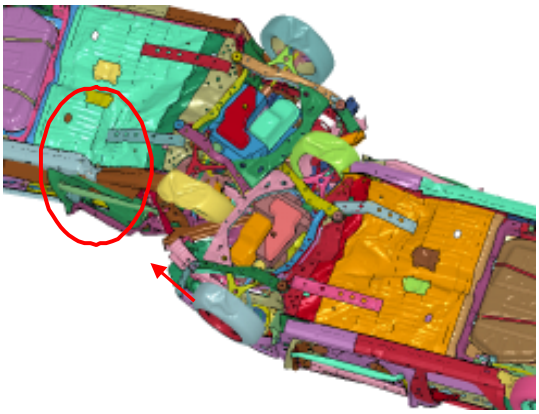

Figure 11: Buckling deformation of vehicle induced by moment force in B2S_H60V100

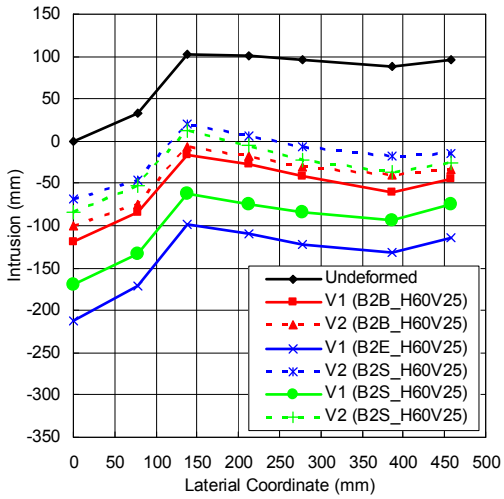

(a) Horizontal intrusion profile

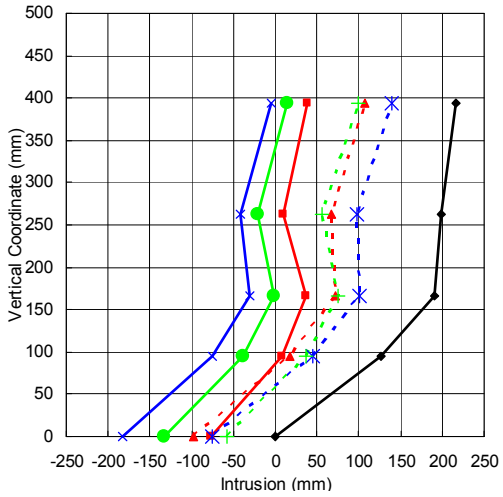

(b) Vertical intrusion profile

Figure 12: Intrusion profile of vehicle in 60% horizontal and 25% vertical overlap test (V1)

The results in Figure 12 and Figure 13 show that the relative positioning of the vehicles is important. The longer subframe had a different outcome if it was in the underriding (V1) or overriding vehicle (V2).

In Figure 13 the modified vehicles become the reference vehicle and the partner vehicle, Basic model, is offset, which means that the modified vehicles are under-riding the Basic model. In both cases, the ExSub model and its partner vehicle have less intrusion, which means that the ExSub model gives good self and partner protection when it underriding. The extended sub-frame vehicle model was stiffer than the Basic and ShSub models. This shows that the under-ridden vehicle in frontal C2C

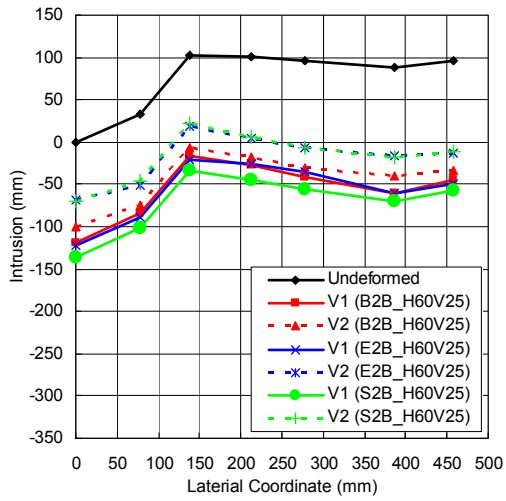

(a) Horizontal intrusion profile

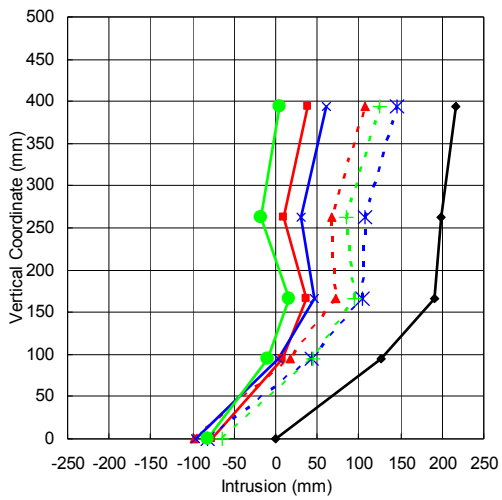

(b) Vertical intrusion profile

Figure 13: Intrusion profile of vehicle in 60% horizontal and 25% vertical overlap C2C test (2)

crash should be stiffer to have good compatibility performance.

DISCUSSION

According to the result for each C2C test listed in Table 1, the safety performance of the vehicles was evaluated and summarized in Table 3. The compatibility performance was evaluated by two parameters, self and partner protection. These factors were evaluated by comparing the intrusions of the reference and its partner vehicles in C2C tests to the modified vehicle to the intrusion in B2B cases. Table 3 shows that the ExSub model gives good compatibility performance when it is under-riding its crash partner. The case of E2B_H100V25 is exceptional and indicates the importance of sufficient compartment strength.

The intrusions of the partner vehicle (Basic model) were large and the sub-frame mounts in the Basic model were not failed during the E2B_H100V25 crash simulation. However, it can not be said that the compatibility performance is really bad. Actually, the intrusions of the vehicles in the cases of full horizontal and full or 25% vertical overlap C2C tests were not much different with each other. In other words, it can not be clearly said that the compatibility performance is really bad in those cases.

The differences of AHOF and AHOF400 for the two vehicles in C2C tests are also summarized in Table 3. In the case of E2B with 25% vertical overlap test, the differences of AHOF and AHOF400 are large and the compatibility performance is good. In this study, the differences of AHOF and AHOF400 between two vehicles in C2C tests are not consistent, which means that geometric and structural interactions are more important to evaluate and need to be studied further to understand compatibility performance in frontal C2C test.

CONCLUSIONS

The study of sub-frame geometries in this study resulted should be carefully investigated. The structural changes conducted can be considered outside the basic design criteria of the original vehicle. However these changes are interesting to investigate to understand how structural changes to the subframe influence vehicle compatibility performance.

Table 3:Summary of results of C2C tests with three vehicle models (O: Good, △: No better, and X: Poor)

Cases			Difference[1] (mm) in		Vehicle [12]		Compatibility Performance[3]
	Horizontal Overlap	Vertical Overlap	AHOF	AHOF400	Self Protection	Partner Protection	
B2E	100%	100%	-17	-64	△	O	O
	60%				X	O	X
	40%				X	O	X
	100%	25%	88	41	△	△	△
	60%				X	O	X
	40%				X	X	X
E2B	100%	25%	122	169	△	X	X
	60%				O	O	O
	40%				O	O	O
B2S	100%	100%	56	25	△	X	X
	60%				X	X	X
	40%				△	X	X
	100%	25%	161	130	O	X	X
	60%				X	△	X
	40%				O	X	X
S2B	100%	25%	49	80	△	O	O
	60%				X	O	X
	40%				△	△	△

1. Difference is given by subtracting AHOF or AHOF400 of vehicle 1 from one of vehicle 2.
2. Self- and partner-protection of vehicle 2 is opposite of vehicle 1.
3. The results are compared with B2B under same C2C test condition.

The longer sub-frame provided better self protection in most cases. In particular it provided better self protection when the vehicle was underriding its collision partner. In most cases it even provided an improvement in partner protection. Shorter sub-frames had more intrusions in general and did not exhibit any significant safety benefits in this study.

Acknowledgements
The authors thank the Program för fordonsforskning (Vehicle Research Program) for supporting the research activities. The assistance from the industrial partners: Volvo Car Corporation, Volvo 3P, Saab Automobile, Scania, and Autoliv Development is also appreciated.

References

1 Edwards, M., Davies, H., Hobbs, A., Development Of Test Procedures and Performance Criteria To Improve Compatibility In Car Frontal Collisions, Paper Number 86, Experimental Vehicle Safety Conference, 2003

2 Delannoy, P., "Compatibility assessment proposal close to real life accidents" - ESV NAGOYA 2003 Paper n° 94, 2003

3 Improvement of Vehicle Crash Compatibility through the Developmentof Crash Test procedures (VC-COMPAT), European Community 'Competitive and Sustainable Growth' program Contract GRD2-2001-50083, VC-Compat webpage: www http://vc-compat.rtdproject.net/.

4 Martin, T., "Deliverable D9. Car geometrical/structural database and analysis of

car to car geometric compatibility, Improvement of Vehicle Crash Compatibility through the Development of Crash Test procedures (VC-COMPAT), European Community 'Competitiveand Sustainable Growth' program Contract GRD2-2001-50083, 2005

5 Mizuno, K., Arai, Y., Kubota, H., Yonezawa, H., Hosokawa, N., Effectiveness and Evaluation of SEAS of SUVin Frontal Impacts, Proceedings of the International Crashwortiness Conference, 2006

6 Thomson, R., Krusper, A., Avramova, N., Rachid, K., The Role Of Vehicle Design On Structural Interaction, Proceedings International Crashworthiness Conference, 2008.

7 National Crash Analysis Center, http://www.ncac.gwu.edu/vml/models.html

8 Livermore Software Technology Corp., 'LS-DYNA keyword user's manual – version 971', 2007

9 Kahane, C., " Vehicle Weight, Fatality Risk and Crash Compatibility of Model Year 1991-99 Passenger Cars and Light Trucks", DOT HS 809 662, NHTSA Technical Report, October 2003

10 Smith, D., "Compatibility Research Plan", HONDA/NHTSA Research Staff Meeting, December 5, 2005

11 Smith, D., " NHTSA compatibility research update", SAE 2006 Government/Industry Meeting , May 10, 2006

12 Summers, S., Hollowell, W., and Prasad, A., "Design considerations for a compatibility test procedure", SAE Technical Paper No. 2002-01-1002

13 Jerinsky, M., and Hollowell, W., "NHTSA's Review of vehicle compatibility performance metric through computer simulation," ASME International Mechanical Engineering Congress and Exposition, Paper Number IMECE2003-44045, Washington, D.C., 2003

14 Mohan, P., Marzougui, D., Kan, C-D, "Modified approach to accurately measure height of force (HOF)," SAE Technical Paper No. 2007-01-1182

DEVELOPMENT OF A COMPUTATIONAL MODEL OF THE WORLDSID 50TH MALE

Christian Gehre
PDB – Partnership for Dummy Technology and Biomechanics
Germany

Ebru Taylak
Victor Oancea
Dassault Systèmes Simulia Corp.
United States

Sebastian Stahlschmidt
Alexander Gromer
DYNAmore GmbH
Germany

André Berger
Charles Thibaud
ESI Group
Germany

Paper Number 09-0411

ABSTRACT

Today the numerical simulation is an inherent process of the development of the passive safety of vehicles. So it is understood that every state of the art dummy has a virtual counterpart. Based on the positive experiences of the development of high quality dummy models within FAT working groups, German automobile manufacturers, represented by PDB, and the software vendors Dassault Systèmes SIMULIA, DYNAmore and ESI Group decided to develop a high quality WorldSID 50th FE model. It will be available for Abaqus, LS-DYNA and PAM-CRASH.

The WorldSID programme was initiated to develop an advanced worldwide accepted dummy of improved biofidelity to access the injury risk to occupants in side impacts.

The finite element model of the WorldSID is based on the latest production version of the physical dummy. Its FE mesh was developed by using the technical drawings of the dummy and additional scans of dummy parts.

At first, it was necessary to identify the material properties of the dummy parts. An extensive test programme was started to obtain the required data. All materials were tested quasi-statically and dynamically. The material samples were taken from dummy parts and custom-built material plates.

The first release of the model includes the geometry and the material properties. It is used to design set-up and boundary conditions of component and sled tests to validate the components as well as the complete model. A large number of tests of different types of loading for neck, thorax, lumbar spine, pelvis and arm were conducted to obtain data for the validation process. The overall response and kinematics of the dummy is validated by using sled tests with different rigid barriers.

The final release of the model will be published in 2010. Pre-releases of the model will be available till then.

INTRODUCTION

In November 1997 the WorldSID Task Group was formed under the led management of the ISO (International Organization for Standardization). The Task Group's aim was to develop a harmonised, technologically advanced side impact dummy with improved biofidelity to replace the variety of side impact dummies used in regulation and in consumer testing. The development of the WorldSID 50th under direction of ISO/TC22/SC12/WG5 was completed in March 2004 when the first production version was released [1].

After the completion of the WorldSID and due to the activities of the WorldSID Task Group to introduce the dummy in legislation, it is clear that there will be a need of a high quality finite element model of the WorldSID 50th in the future. Therefore, PDB, an association of five German car manufacturers, and the software vendors Dassault Systèmes SIMULIA, DYNAmore and ESI Group started the development of this model in autumn 2006. The methodology of the project is very similar to that of the German FAT dummy projects. FAT working groups developed the US-SID, EuroSID 1, ES-2/ES-2re and BioRID II dummy models. These models are

frequently used worldwide and proved their suitability in enhancing vehicle safety since many years.

APPROACH

The development of the WorldSID FE model is primarily based on the requirements of future customers, represented by PDB.

All validation tests cover a wide range of expected loading conditions in vehicle environments. The validation based on the certification tests is only a very small part of the validation programme.

Development plan

A four step development plan was introduced to the project. The dummy release 0 is the first result of the project. This model contains the FE mesh, correct masses and inertia, all joints and sensors. The materials are generic or derived from other dummy models. Release 0 is used for pre-studies to define component tests for the validation work.

The second step, dummy release 1, comprises all data of the material tests as well as roughly validated components.

The development of the model is almost completed after the third step, the release of version 2. All parts are validated on component and sled test level.

Finally, Version 3 is released after a period of 12 months of use and user feedback of version 2.

Interim versions of the model are also released. So a pre-version 1 was mainly used to define the validation tests of the components. This preliminary version used almost all results of the material tests and was roughly validated by using the certification tests.

Release 1 of the dummy model was completed in the 1st quarter of 2009 and the release of version 2 is expected by end of 2009.

Definition of validation tests

The validation of the model by using tests with loading conditions close to vehicle environments requires a new approach of defining these tests. The idea is to identify the loading type of a component in vehicle environment, to isolate this loading and finally, to transfer it into a simple test set-up.

Figure 1 shows this process in principle. At first, the estimated load to a component in a vehicle crash and its load path is identified. Different set-ups of component tests that cover these loading conditions are discussed. The focus is not only on these needs, the simplicity of the set-up is also an important requirement. The repeatability of simple tests is typically higher than of more complex configurations. Simple and highly repeatable tests are usually more helpful to validate a component because the uncertainties in the tests are clearly limited.

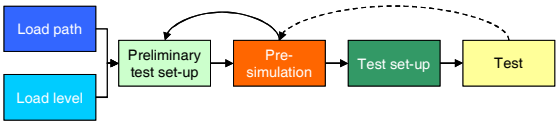

Figure 1. Definition of component tests.

Different proposals of set-ups are verified by using pre-simulations. Finally, the results of the first tests are compared with pre-simulation and estimations regarding load level and load path. The configuration and the boundary conditions are modified, if there is any problem or uncertainty.

This method is also applicable for material investigations and sled tests with the whole dummy.

In general, it is difficult to use a model that is under development to run pre-simulations to design validation tests for the same model. However, the requirements to the predictability of such models can be less restricting because simplifications and restrictions of the pre-simulation are considered. Iteration loops as shown in Figure 1 are common. Additionally, pre-simulations can also be conducted with other dummy models of a similar design.

STRUCTURE OF THE MODEL

In a first step the mesh was generated based on CAD data, generated from the technical drawings of the WorldSID [2] and 3D scans of several parts.

Figure 2. WorldSID FE model (LS-DYNA).

The rubber and foam parts are mainly made of hexahedron elements. Solely the pelvic flesh is made of tetrahedron elements because of the very complex geometry. The WorldSID finite element model is shown in Figure 2.

The size of the finite elements of the dummy is set to ensure a time step of one microsecond. The current models are made of approximately 135,000 nodes and 200,000 elements. They are equipped with the same measurement devices as the physical dummy.

VALIDATION TESTS

A significant effort was made to generate a comprehensive database on the static and dynamic material behaviour, and the dummy performance in component and whole dummy tests.

The validation starts on the material level with detailed analysis of the material properties. Component tests of the most important body segments are improving the level of validation. Finally, sled tests with the complete dummy are used to investigate the interactions of the components and to improve the quality of the model globally.

Material Data

In total 26 materials were tested to obtain the required data to define the materials. The material samples (Figure 3) were directly cut from dummy parts, if possible. All rubber- and vinyl-like samples were taken from custom-built plates. Their characteristic was verified with samples taken from dummy parts.

Figure 3. Material samples of the WorldSID.

Depending on the type of material and the load they experience in a crash, static and dynamic tension and compression tests were conducted. The measured response curves can be directly implemented into typical foam and rubber material models.

Compression tests with constrained lateral expansion and free expansion were performed for the rubber-like materials. Lateral strains were not constrained and not considered.

All tests were conducted quasi-statically and dynamically. The strain rates range from 20/s up to 400/s. Cyclic compression and tension tests were additionally performed for rubber-like materials.

Component Level

The implementation of valid material models ensures a certain level of validation. However, it is necessary to assure the validation with additional component tests of the most important dummy parts.

Head – The skin of the head was validated by using data of the head drop tests that are required for the certification of the WorldSID. The set-up of the frontal and lateral test is shown in Figure 4.

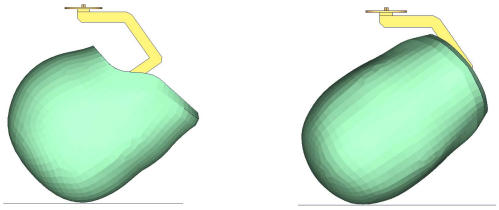

Figure 4. Set-up of the frontal and lateral head drop test.

Neck – At first, the neck was roughly validated by using results of the certification tests. As shown in Figure 5 the head has been replaced by a substitute. The pendulum is decelerated by a piece of honeycomb. As this test has to be conducted with every WorldSID periodically, the available data represents different specimen. So the scatter due to variances of the hardware is covered.

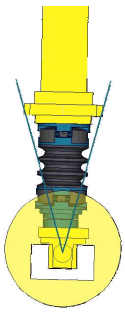

Figure 5. Neck pendulum tests.

The certification test does not cover the expected loading conditions of the neck in a vehicle environment. Therefore, a second test set-up was chosen to obtain data of lateral and oblique neck

bending modes. Two different necks were tested to consider the variance of the hardware.

As shown in Figure 6 head and neck were mounted on an accelerated sled. Two different crash pulses were used. The head hit the contact plate in the severe pulse only. A load cell measured head impact force.

The head was equipped with triaxial angular rate sensors.

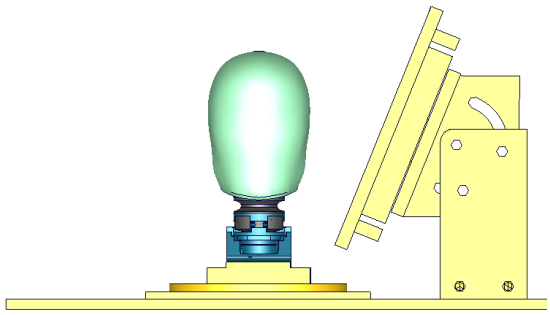

Figure 6. Set-up of the neck sled tests.

Thorax – The thorax is one of the most important body segments of a side impact dummy. Therefore, a special the focus of the validation was on the ribcage of the WorldSID. More than 400 pendulum tests at different impact velocities, impact angles and with different pendulum masses were conducted. Figure 7 shows the set-up of the test of the third inner thorax rib exemplarily.

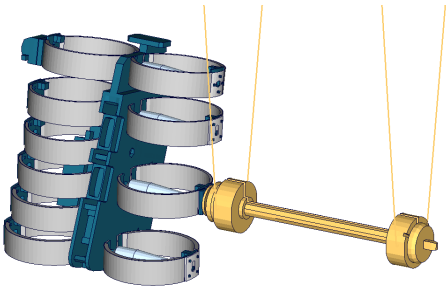

Figure 7. Set-up of the pendulum test with the 3rd inner thorax rib.

At first, the inner ribs were tested to get data for the validation of the rib steel (Nitinol). The blue damping material was scraped from the ribs to obtain the pure response of the steel.

Afterwards, the inner ribs were tested with damping material. The properties of the damping material were adjusted to get the right rib responses. The properties of Nitinol remained unchanged because the material was already adjusted in the first step of the validation.

After the validation of the inner ribs, the ribcage had to be validated for both, inner and outer rib. Pendulum tests (Figure 8) with different boundary conditions were used to obtain the required data. As all material parameters of the ribs are defined and validated in the tests with the inner ribs, the parameters to tune the model to these tests are limited. However, if the material models of Nitinol and blue rib damping material are defined correctly, the responses of the simulations with the whole ribs should correlate well with the tests.

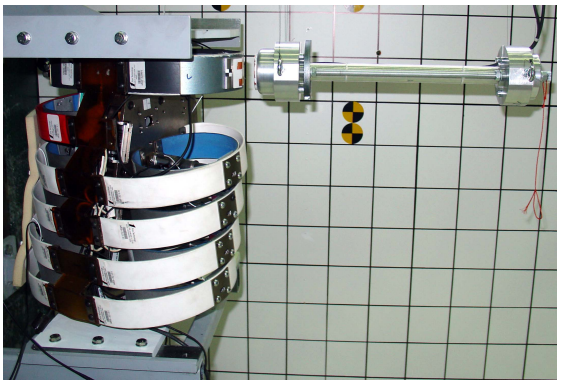

Figure 8. Set-up of pendulum tests with the complete shoulder rib.

The variance of the ribs was not analysed explicitly because most of the ribs had to be replaced during the extensive tests. Hence, the scatter of the hardware is included indirectly in the data set.

The data of the certification tests with the assembled dummy were also used to support the validation process. However, there was no focus on these kinds of data.

Lumbar Spine – The set-up of the lumbar spine tests is very similar to that of the neck sled tests. Two lumbar spines were mounted on an accelerated sled. The crash pulse as well as the mounting angle of the dummy parts was varied.

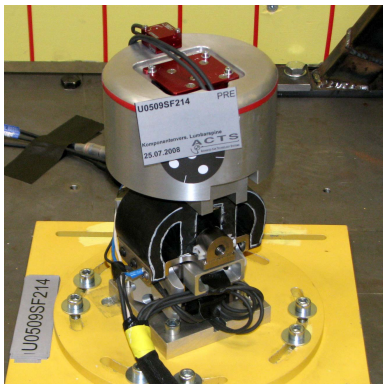

Figure 9. Set-up of the lumbar spine tests.

A replacement of the upper torso is mounted on top of the lumbar spine rubber. Accelerometers and angular rate sensors are directly embedded into this part. The geometry of the mass replacement was defined by using pre-simulations.

The focus was on realistic kinematics and on the right ratio of bending and shear of the spine rubber. High-speed videos of WorldSID crashes were taken as benchmark.

After the run of the pre-tests, the test set-up had to be modified. Mass and centre of gravity of the thorax replacement was tuned to improve the test results.

The lumbar spine is indirectly tested in the certification tests. Figure 10 show exemplarily one of the pendulum tests with the dummy. Due to the long load path and the large number of involved dummy parts, the relevance of these certification tests on the validation of the lumbar spine rubber is limited. However, some of the certification tests were also used to improve the performance of the lumbar spine.

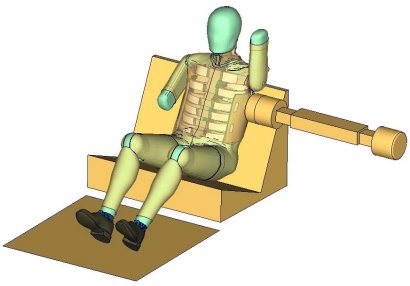

Figure 10. Certification test of the WorldSID.

Iliac Wings – Pendulum tests were used to obtain data for the validation of the bony pelvis. Main design parameter of the tests was the pubic force. It should be very close to the expectations in vehicle crashes. Two different set-ups with different impact locations and velocities were defined.

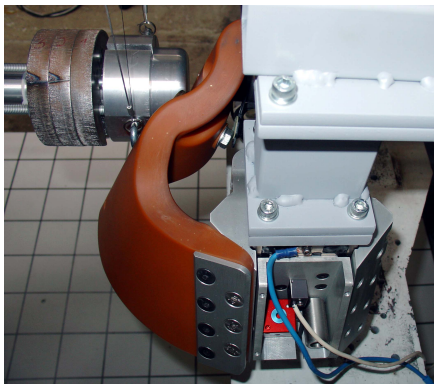

Figure 11. Set-up of the iliac wing pendulum tests.

At first, the half pelvis was tested. This set-up helped to validate the pubic buffer and the iliac wing. The complete pelvis was tested afterwards. These tests were conducted to investigate the interaction between left and right iliac wing and the influence of the soft pubic buffer on the pelvis kinematics.

All test configurations and its boundary conditions were defined by using pre-simulations.

Arm – Pendulum tests were used to validate the stiffness of the arm joint and to improve the material models of the foam and the plastic bone of the arm. Impact location and impact velocity were varied in the tests. Figure 12 shows one of the test configurations exemplarily.

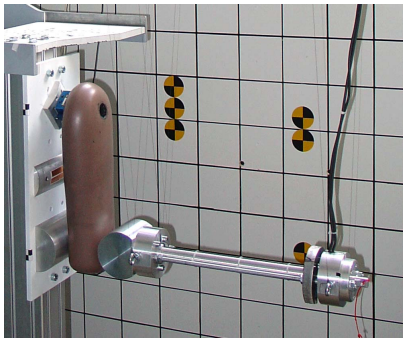

Figure 12. Set-up of the arm pendulum tests.

Sled Tests

The defined sled tests imparts loads on the dummy, which are similar to loads in the vehicle. The boundary conditions of these tests are well known and precisely described. That ensures a clearly higher level of repeatability of test results than tests with vehicles.

In general, sled tests are very important for the validation of a dummy model. Firstly, they are required to check the interactions of the validated sub-components and secondly, they cover typical loading conditions including similar kinematics of the dummy in vehicle tests.

Two different kinds of sled tests are defined. The first series with flat barrier faces can be compared to the barrier tests conducted within the EuroSID 1 and ES-2/ES-2re test programme [3].

The second test programme uses more sophisticated barriers. The curved front is derived from typical deformation patterns of vehicles in oblique pole tests.

The posture of the dummy was measured with a 3D measurement system prior every tests. So it is possible to reproduce it in the simulations exactly.

Flat Barrier – The test with the flat barriers were conducted at two different impact velocities. They represent severe and mid severe loading conditions. Target parameter for the definition of the velocity was the maximum deflection of the ribs and pubic force.

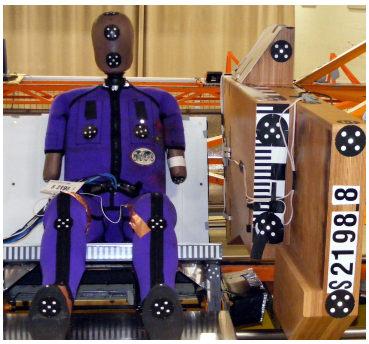

Figure 13. Set-up of the sled test with flat barrier.

Figure 13 shows the set-up of the test with the flat barrier. The main load is applied to the dummy through the shoulder. The lateral head excursion is limited by a contact plate to avoid damages of the neck or the sensors mounted in the head.

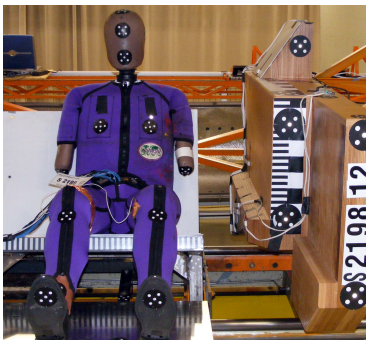

Figure 14. Set-up of the sled test with pelvis pusher.

The second set-up with the flat barrier is shown in Figure 14. Compared to the first configuration, the load is mainly applied through pelvis and shoulder to the dummy.

Curved Barrier – The tests with the flat barriers represents purely lateral crashes. There is almost no rotation of the upper torso. So it was decided to create a new kind of rigid barrier that induces upper torso rotation. The 75° degree pole test was taken as starting point of the development of this barrier face.

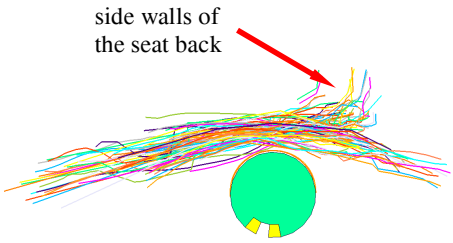

Figure 15. Intrusion profiles of different cars.

At first, the intrusion of several cars was analysed. Figure 15 shows feature lines of the door trim and the back of the seat at a certain time of a pole crash. Based on this information a new barrier face was defined. Pre-simulations were run with the ES-2 dummy model finalise the geometry. A draft of the new barrier is shown in Figure 16. The final version will be equipped with an arm rest. The impact velocities are not defined yet but will be similar to those of the tests with the flat barriers.

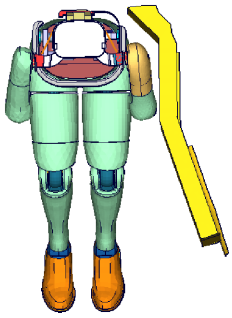

Figure 16. Draft of the curved barrier face.

RESULTS

The validation of the dummy is not completed. Results of validation tests of some materials and body segments are shown exemplarily.

Material Level

For some of the materials, the experimental data could be incorporated directly as input into the material models, for some others the data needed further calibration.

First step in the calibration process was to evaluate various material models to fit the quasi-static compression, tension and volumetric test data. Second step was to run material tests and come up with material parameters to predict the strain rate sensitive material behaviour. Figure 17 shows a simulation of a compression test exemplarily.

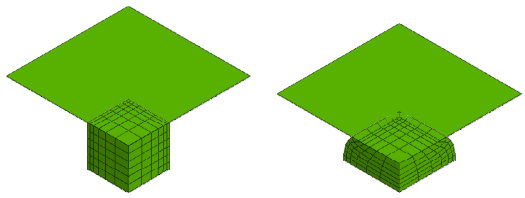

Figure 17. Abaqus component model for compression testing.

Rubber Materials – The results of the definition and validation of the WorldSID materials are exemplarily described for rubber materials of PAM-CRASH.

Rubber is usually modelled as incompressible visco-elastic material with viscous response. Material models of the Ogden family [4] do have these characteristics and are used for the World-SID model. All Ogden parameters are derived from the measured material properties such as uniaxial tension, compression and shear.

The accuracy of the generated material parameter was validated by simulating the material tests.

As mentioned above the material tests were conducted at different velocities. Parameters of the so-called Prony series have to be defined to cover viscous strain rate effects of the rubber.

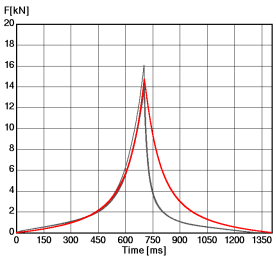

Figure 18. Quasi-static loading of rubber in test (black) and simulation (red).

Figure 18 shows a comparison of the test and simulation results of quasi-static compression. The deviances between both curves during the unloading phase have to be improved in a next step, if this behaviour is considered essential for the accuracy of the results of the global dummy model. Compared to that, the correlation of the signals in a dynamical load case is clearly better (Figure 19).

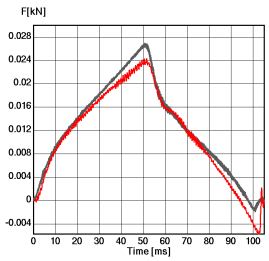

Figure 19. Dynamical loading of rubber in test (black) and simulation (red).

Component Level

The shown results of the validation are preliminary because the model is not completed yet. Beside the tuning of the material parameters the validation of the components includes also improvements of the modelling.

Neck – The neck component consists of moulded rubber neck, head, lower and upper neck brackets, neck buffers and neck interface plates. As shown in the previous section the neck assembly is attached on a sled and accelerated. The focus of the validation was on the right kinematics of head and neck and on the good correlation of lateral neck shear force F_y and neck bending moment M_x.

The behaviour of the moulded rubber neck relative to the head on the top and the neck brackets at the bottom is determined by the half spherical screws and the neck buffers. The moulded neck and the buffer material models have been calibrated based on the quasi-static and dynamic material tests. The behaviour of the half spherical screws has been validated using the neck certification tests. Similarly, the head skin material was validated using the material tests and the head drop certification tests.

Comparisons between the experimental results (black) and the preliminary results from Abaqus simulations (red) of the oblique tests using the low severity pulse are shown below.

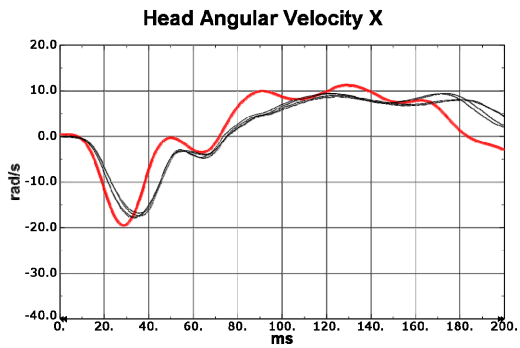

Figure 20. Angular velocity of the head.

The angular velocity of the head is a good indicator to evaluate the kinematics of the head by using responses curves. As the curves of Figure 20 indicate, the head of the model starts lightly earlier to rotate than the physical head. The upper neck torque confirms (Figure 21) these findings. However, the correlation between model and hardware is already acceptable.

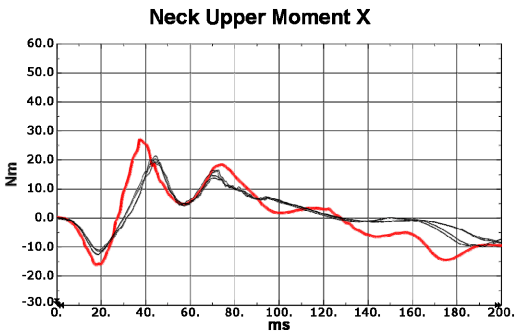

Figure 21. Upper neck bending moment M_x.

The performance of the neck is very similar in the other load cases. Nevertheless, the neck component validation is not completed yet. Studies to improve the neck kinematics are still ongoing.

Thorax –The WorldSID has one shoulder rib, three thorax ribs and two abdomen ribs which are designed in a similar way. The ribs consist of an inner and outer band made of Nitinol. This material is a memory shape alloy which undergoes a crystal transformation during deformation including high influence on the material stiffness. On the inner band of the ribs a damping material is used. The damping properties are similar to the rib damping material of the SID-IIs.

All curves shown in this section are taken from the LS-DYNA model.

In the first step, material tests are used to generate baseline material parameter sets for ribs and damping material. The responses curves of the tests with the material sample were directly implemented in the material models.

All ribs are modelled in the same way and use the same material models. The mesh fineness permits the modelling of different connection methods.

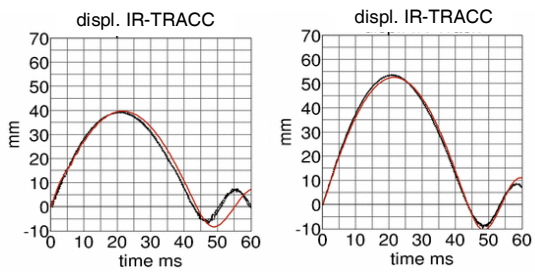

Figure 22. Displacement of the 3rd thorax rib w/o damping material (different impact velocities).

The Nitinol material was calibrated by using pendulum tests of the inner ribs without damping material. The connectors of rib and rib clamping bracket were validated in these tests too. Figure 22 shows the deflection of the 3rd thorax rib under different loading conditions. The responses of the LS-DYNA model (red) are shown exemplarily.

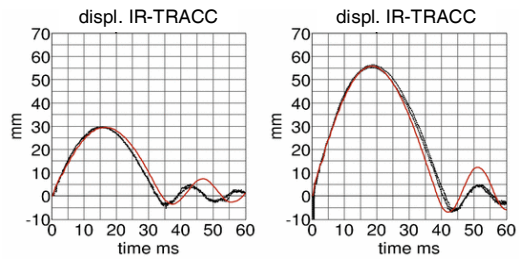

Figure 23. Displacement of the 3rd thorax rib w/ damping material (different impact velocities).

Afterwards, the blue damping material was validated by using pendulum tests of the complete inner ribs. Results of the third thorax rib with damping material at two different load levels are shown in Figure 23.

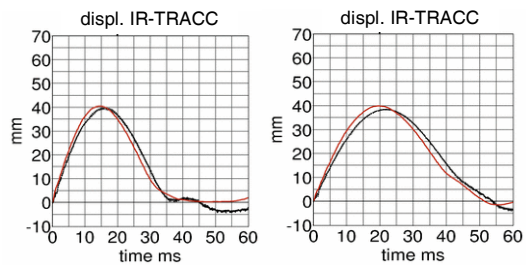

Figure 24. Displacement of the complete 3rd thorax rib (different pendulum masses).

Finally, the assembly of inner and outer ribs is validated by using pendulum tests of the almost fully assembled thorax. Solely the rib above and below the tested rib was disassembled to avoid contacts of the pendulum with those ribs. These tests are used to validate the whole rib assembly, including the sternum material and the connection method of the outer rib clamps. The tests are carried out using different velocities and different pendulum masses. Some results are shown in Figure 24.

The simulation results show good correlation to the test data. The level of validation, exemplarily shown for some responses of the 3rd thorax rib, is similar for all the other rib tests. Thus, the thorax validation is completed for the first releases of the WorldSID. The performance of the ribs might be improved after the simulation of the sled tests.

Lumbar Spine – The lumbar spine is a very important part of the WorldSID. Only its right implementation in the model ensures correct kinematics of the upper torso. Therefore, the lumbar spine sled tests have to cover a wide range of loading conditions.

The sled tests are mainly used to improve the Ogden and Prony parameters of the lumbar spine rubber. Especially the parameters for triaxial loading can only be defined with these tests because material tests with triaxial loading were not conducted. The interactions between the different parts involved in those tests needs to be considered in the validation process too.

Figure 25 shows the lateral shear force F_y and the torque M_x about the longitudinal axis of the dummy. Two different lumbar spines were tested (black curves) at the same time and their performance is clearly different. The PAM-CRASH model (red) correlates fairly well with one the specimen. The rubber of the other specimen seems to be different to that used in the material tests. However, in a next step the computational model will be tuned to correlate to the second lumbar spine. The final model will either match the first or the second lumbar spine. Averaging of the responses of the two specimens does not make sense in this special application.

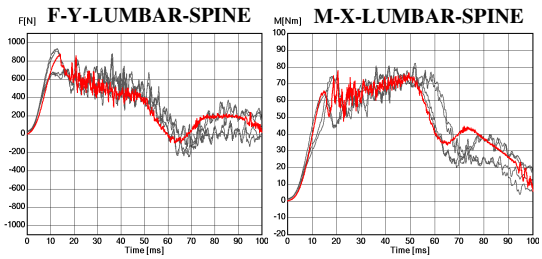

Figure 25. Shear force and bending moment measured in the sacro-iliac load cell.

Detailed analysis of tests and simulation indicates that pre-stress, which results from gravity loading, has to be considered in the model.

Pelvis – In order to validate the behaviour of the pelvic bones and the pubic buffer, tests were performed on the half pelvis and the full pelvis.

Two configurations were used to test the half pelvis. In the first configuration, the iliac wing was hit at a position in alignment with the pubic load cell. The accelerations measured on the impactor and the pubic load cell forces are used to calibrate the pubic buffer material. In the latter configuration, the iliac wing was hit at its outmost position. This test is used to validate the pelvic bone material. The iliac wing material will influence forces and moments measured at the sacro-iliac load cell, which is the interface between pelvis bone and the sacrum block.

The full pelvis was impacted only at its outmost position on one side. This is an ideal case to validate the interaction and the load path between the left and right iliac wing, as well as the influence of the pubic buffers on the overall pelvis kinematics.

Each component test was repeated for two different velocities, to help calibrate the rate sensitive behaviour of the iliac wing and the pubic buffer materials.

Preliminary results from the Abaqus simulations are shown in the plots below.

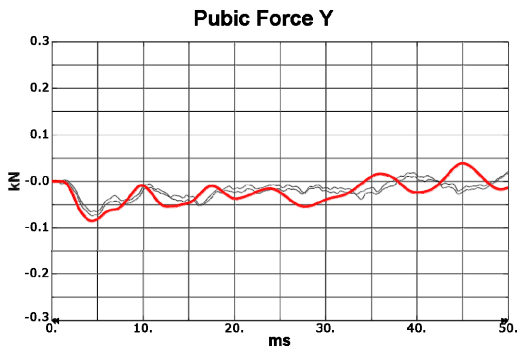

Figure 26. Pubic force in the full pelvis test.

The correlation of the pubic force F_y in one of the tests using the full pelvis set-up is shown in Figure 26. The achieved level of correlation is acceptable.

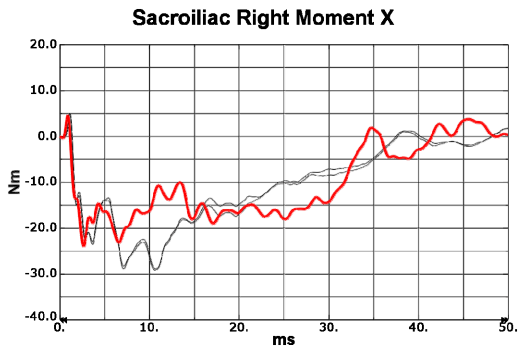

Figure 27. Iliac wing torque at the sacro-iliac load cell (full pelvis test).

Compared to that, the torque M_x at the sacro-iliac load cell does not correlate well with the experiment in the same test (Figure 27). Peak and unloading phase of the signal deviate too much from the tests. More investigation is needed to identify the problem.

Sled Tests

The validation of the model using the barrier tests is not completed yet. However, the first simulation runs with the flat barriers are very promising. So the amount of work to improve the level of validation of the sub-components is acceptable. New components tests are obviously not needed.

Figure 28 shows exemplarily one of the models used to define the boundary conditions of the sled tests. Initially, the arm position was defined as shown in Figure 28 (2nd notch). After the first pre-test the position was changed (Figure 14, 1st notch) because of the unrealistic rib deflection. While the shoulder rib was deformed up to the design maximum, there was almost no deflection at the thorax and abdomen ribs. This deformation pattern is not helpful for the validation of the model and does not correlate with the experiences with the WorldSID in vehicle environments. The arm covers the rib cage in the revised set-up. So the deformation of the ribs is more balanced now.

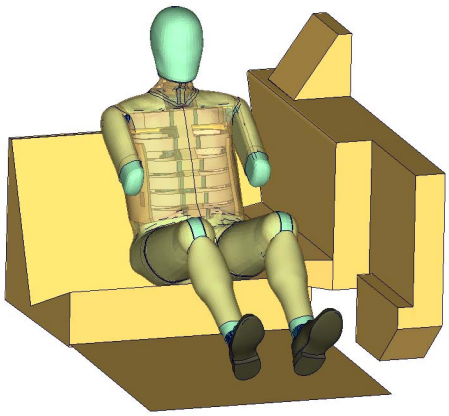

Figure 28. Computational model of a sled test with the WorldSID.

LIMITATIONS

The current releases of the WorldSID are only validated by using material, component and dummy certification tests. So the individual components have a very good validation level for all codes. The validation of the interactions of all of these components is still in progress. It will be done by using the sled tests with the dummy as well as with dummy without jacket. So the performance of the model will be increased after completion of the validation using sled test data.

In general, the WorldSID is an unique and very new dummy. The experiences with this dummy is much lower than for others like ES-2 or ES-2re. Thus, it is possible that some behaviour appears in the future, that is not covered by the extensive validation databases of the WorldSID model.

FURTHER DEVELOPMENT

The validation of the model will be completed by integration of the results of the sled tests with the flat barriers. Afterwards, the design of the curved barriers will be discussed and modified, if necessary. These tests should help to improve the models again.

CONCLUSION

A group of car makers and software vendors developed high quality FE models of the WorldSID 50th dummy for the crash solvers Abaqus, LS-DYNA and PAM-CRASH. The models are based on the requirements of the automotive industry. All validation tests on material, component and sled test level are consequently based on experiences with the WorldSID and other side impact dummies in vehicle crashes.

The current models are validated on material and component level. The achieved quality is remarkable, especially as the results of the sled are not implemented yet.

The models of all three crash codes are at a very similar level. First releases are ready to use after implementation of the component and certification test data.

REFERENCES

[1] Internet www.worldsid.org/news_and_releases_home_page.htm, WorldSID Production Design Completed, 2008-03-13.

[2] International Organization for Standardization; International Standard 15830; Road Vehicles; Design and performance specifications for the WorldSID 50th percentile male side-impact dummy; Geneva; 2005.

[3] Franz U., Schuster P., Schmid W.; FAT Side Impact Dummy models – Remarks on Usage and potential Pitfalls; 4th European LS-DYNA User Conference; Ulm; Germany; 2003.

[4] Virtual Performance Solution 2008; Explicit Solver Notes Manual; 2008.

NHTSA's Recent Test Program on Vehicle Compatibility

Sanjay Patel, Aloke Prasad
National Highway Traffic Safety Administration (NHTSA)
United States

Pradeep Mohan
The George Washington University
United States
Paper Number: 09-0416

ABSTRACT

The objective of this study was to understand the structural interaction in frontal collisions between a compact passenger car and different Option 2 light truck based vehicles (LTVs).

Vehicle-to-vehicle (VTV) crash tests were conducted to understand how these new concepts perform. Full frontal VTV crash tests into Model Year(MY) 2002 Ford Focus were conducted with the MY2006 Ford F-250 secondary energy absorbing structure (SEAS) attached and with the SEAS removed. Full frontal VTV crash tests into Focus were also conducted with the MY2006 Honda Ridgeline and MY2007 Chevrolet Silverado with the SEAS attached only. Ridgeline and Silverado SEAS are fixed below the rails and can not be removed like F-250. The results of these tests are presented and discussed in this paper. The largest LTVs are being equipped with new frontal structures to prevent override with passenger cars and it cannot be properly evaluated with the current full frontal barrier test. A new instrumented rigid override barrier (ORB) concept has been developed to evaluate the strength of SEAS and tested for this purpose. This paper summarizes and discusses the design and testing of the ORB.

Furthermore, Finite Element (FE) models of MY2006 Ford F-250 and MY2007 Chevrolet Silverado were developed by the National Crash Analysis Center at the George Washington University under a contract with National Highway Traffic Safety Administration (NHTSA) and Federal Highway Administration (FHWA). The structural interaction in frontal collisions between a compact passenger car and the two LTVs was investigated using computer simulations.

INTRODUCTION

In December 2003, a voluntary commitment was signed by 15 major members[1] of the Alliance in the USA to begin designing LTVs up to 10,000 pounds Gross Vehicle Weight Rating (GVWR) in accordance with one of the following two geometric alignment options no later than September 1st, 2009 [Alliance 2003, 2005, and 2006].

Alliance submitted an amendment to the agreement to the NHTSA on May 10th, 2006, which added a strength requirement for the SEAS. Alliance's research plan for further improving front-to-front compatibility also was refined to contemporaneously investigate potential dynamic geometric, stiffness, and other relevant front-end performance characteristics that would enhance partner protection without sacrificing self-protection in front crashes. This quasi-static test requirement states that the SEAS shall withstand a load of at least 100 kN exerted by a loading device, before this loading device travels 400 mm from the forward-most point of the significant vehicle structure.

Option 1: The light truck's primary frontal energy absorbing structure (PEAS) shall overlap at least 50% of the Part 581 zone (as defined in 49 CFR 571.3) AND at least 50% of the light truck's PEAS shall overlap the Part 581 zone (if the PEAS of the light truck is greater than 8 inches tall, then overlap of the entire Part 581 zone is required).

Option 2: If a light truck does not meet the criteria of Option 1, there must be a SEAS, connected to the primary structure whose lower

[1] BMW, DaimlerChrysler, Ford, GM, Honda, Hyundai, Isuzu, Kia, Mazda, Mitsubishi, Nissan, Subaru, Suzuki, Toyota, Volkswagen.

edge shall be no higher than the bottom of the Part 581 bumper zone.

The voluntary agreement was implemented in 2004 and, as of August 2008, 81% of MY2007 applicable vehicles were designed in accordance with the front-front criteria. With this voluntary agreement underway, it is useful to examine the light vehicle compatibility problem to see what vehicle structural changes have been made over years.

The emergence of SEAS in 2004 on large LTVs led to lack of consensus in developing a vehicle dynamic test, largely because the various fleet examples of SEAS were so different. One thing was clear however, to evaluate the performance of all the different types of SEAS frontal structures a new test was needed. The most promising evaluation concepts were either a deformable barrier test of some kind, or a low rigid ORB designed to engage and deform the SEAS to measure its strength in a dynamic test. While other organizations evaluated deformable barrier concepts, NHTSA focused on the ORB.

The objective of this study was to understand the structural interaction in frontal collisions between a compact passenger car and various Option 2 LTVs. The goal was to understand how these new concepts perform in ORB impacts and in VTV tests.

VTV crash tests were conducted to characterize the structural interaction between compact passenger cars and Option 2 LTVs. The results of these tests are presented and discussed in this paper. A new ORB concept was developed and tested for this purpose. This paper also summarizes and discusses the design and testing of the ORB.

In addition, Finite Element (FE) models of the 2006 Ford F250 and 2007 Chevrolet Silverado were developed by the National Crash Analysis Center at the George Washington University under a contract with NHTSA and the FHWA. The Ford F-250 has a cross member type SEAS while the Chevrolet Silverado had a non-cross member type SEAS. The structural interaction in frontal collisions between a compact passenger car and the two LTVs was investigated using computer simulations.

The FE models were validated against full frontal rigid barrier laboratory crash tests [http://www.ncac.gwu.edu/vml/models.html]. Full frontal impacts with a compact passenger car were performed with and without the SEAS to evaluate the change in structural interaction.

The ORB test procedure was expected to evaluate the strength and energy absorption characteristics of SEAS. The performance of SEAS in VTV tests was expected to show a benefit from using SEAS.

Updated ORB design

The initial full frontal tests and ORB design as shown in Figure 1 were described but the results were not included in ESV paper 07-0231 because the results were not completely analyzed at the time of writing that paper. As shown in Figure 1, lower one raw is ORB and upper four rows are not part of the ORB. During Honda Ridgeline SEAS test, its forces on ORB exceeded the Load Cell (LC) capacity (load cells were saturated). So after the initial test series, a redesigned ORB as shown in Figure 2, similar to first generation design except higher capacity LCs was designed and tested.

Figure 1. The initial ORB design.

Each load cell on the initial ORB was 250 x 250 mm in size; 222400 N (50,000 lbf) capacity (single axis). The ORB was 500 mm from the instrumented back-wall. The ORB is modular in design, with the width adjustable by adding or removing individual load cells and the supporting structure. The top of the ORB was infinitely adjustable to 16”–20” height (Part 581 zone) and was adjusted to be below the PEAS of the vehicle being tested.

Figure 2. The redesigned ORB

The redesigned ORB as shown in Figure 2 is similar to the first generation ORB except that each 250 x 250 mm load cell is now replaced by four 125 x 125 mm; 300,000 N (67,440 lbf) capacity single axis load cells.

VEHICLE CRASH TEST RESULTS

NHTSA conducted three ORB crash tests to evaluate the performance of vehicles with SEAS:

2006 Ford F-250 (Blocker Beam SEAS)
2006 Honda Ridgeline (PEAS Extension)
2007 Chevrolet Silverado (PEAS Extension)

These PEAS Extensions are basically SEAS with added structure at the bottom of the rails (PEAS) to bend rails downward.

The tests were subjected at vehicle speeds of 25 mph (40 kph), based on an estimate of the speeds required to generate a significant loading on the SEAS. The tests with the F-250 and Ridgeline were conducted with the 1st generation (initial) ORB, while the test with the Silverado was conducted with the redesigned ORB.

2006 Ford F-250 Results

The F-250 used a blocker-beam as SEAS. The SEAS can be easily removed for comparison tests without the SEAS.

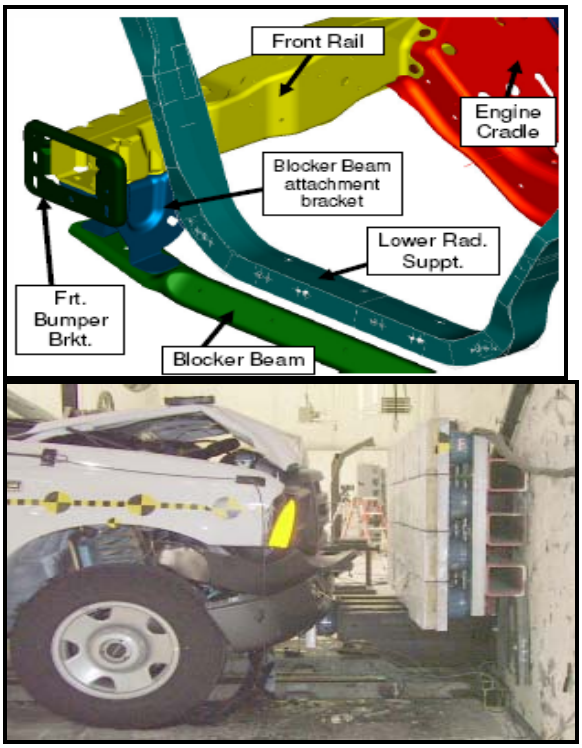

Figure 3. Ford F-250 SEAS design and test

Figure 3 shows the location of the PEAS and SEAS of the F-250.

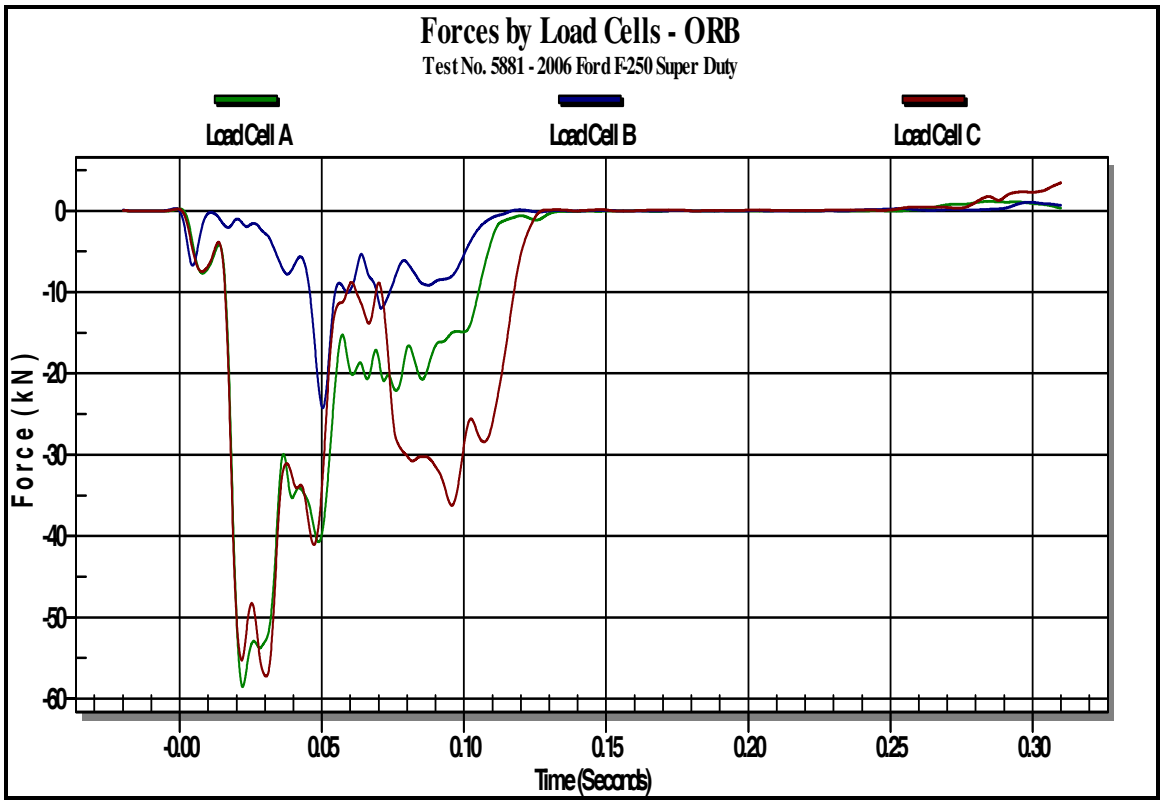

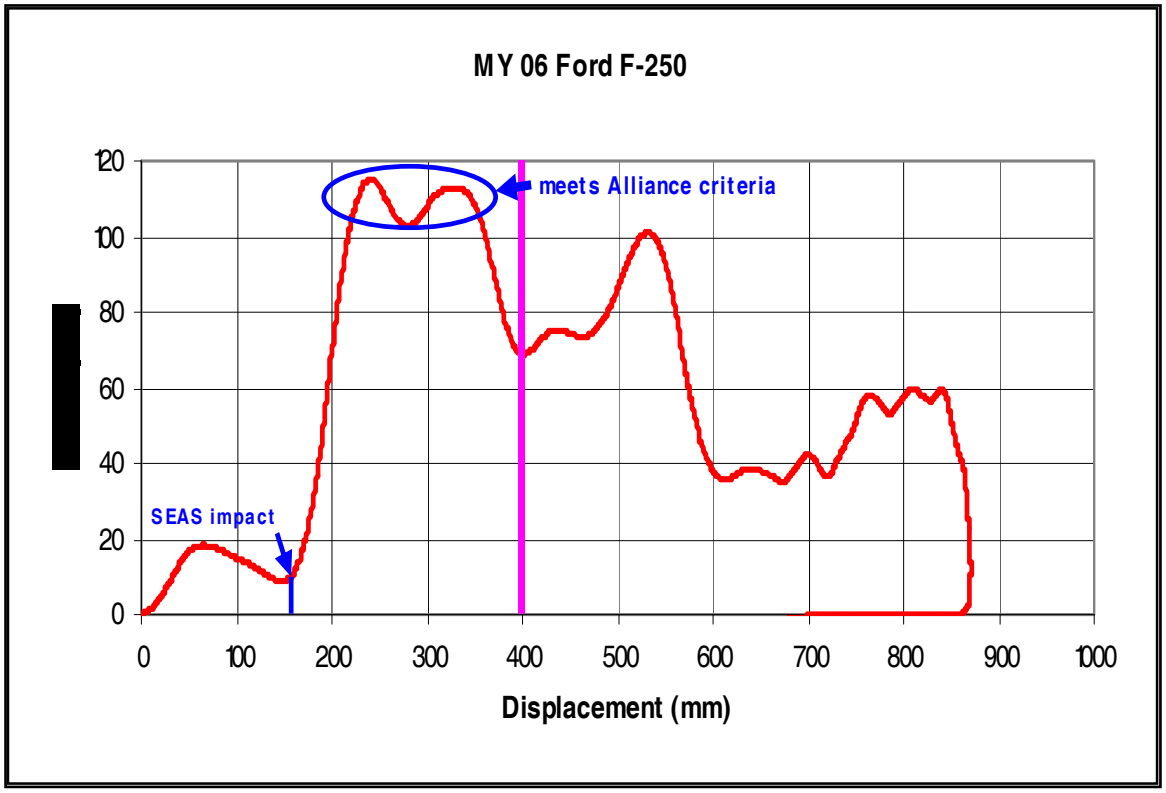

Figure 4. Ford F-250 forces recorded by the ORB load cells and Force-Deformation plot

Figure 4 shows that the vehicle met the Technical Working Group's (TWG) criteria of the SEAS withstanding a force of 100 kN within displacement of 400 mm from the forward-most point of the vehicle structure. It was noted that no load cells were overloaded as shown in the plot above but the vehicle's end brackets which are used to attach the SEAS to the rails generated higher forces.

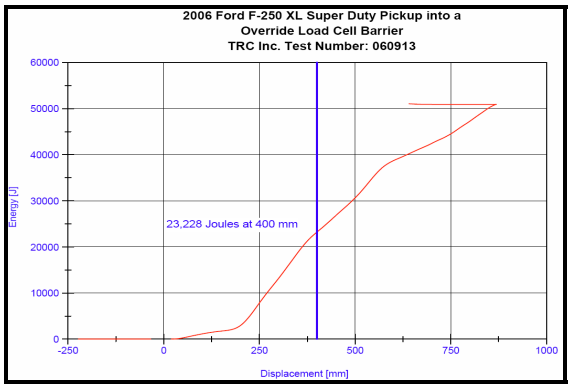

Figure 5. The energy absorbed by the SEAS

Total crash Energy = 181,237 J
% absorbed by SEAS in 400 mm = 12.8 %

VTV crash tests into the 2002 Ford Focus were conducted with the F-250 SEAS attached and with the SEAS removed. The crash pulses and dummy injury assessment values from the two tests are shown in Figure 6.

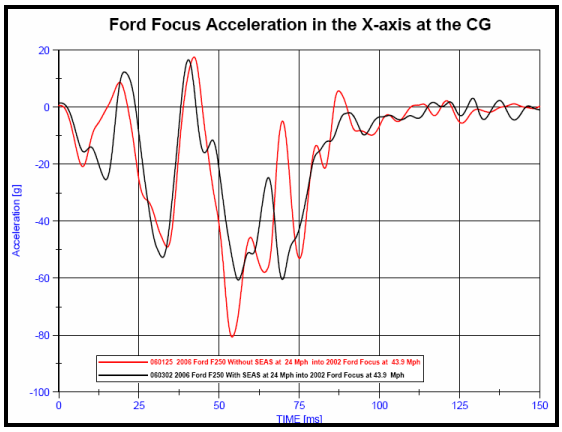

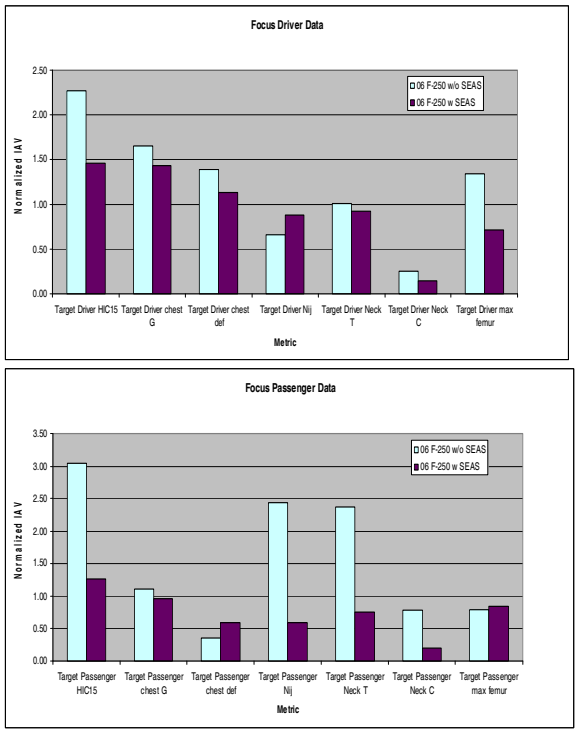

Figure 6. Ford Focus deceleration and dummy injury assessment values

In the comparison VTV test with Ford Focus, the SEAS on the F-250 appears to have improved compatibility by lowering the dummy assessment values and the peak g in the partner vehicle. Post test pictures show reduced crush (and more occupant compartment space) in the Focus in the impact with the F-250 with the SEAS attached.

2006 Honda Ridgeline Results

The location of the PEAS (red color) and SEAS (yellow color) in the Ridgeline is shown in Figure 7. The PEAS extended into the Part 581 zone. This overlap of the PEAS into the Part 581 Zone resulted in high loads on the ORB in this test.

Figure 8 shows the pre-test and post-test pictures of the ORB and SEAS alignment and the deformed PEAS and SEAS respectively.

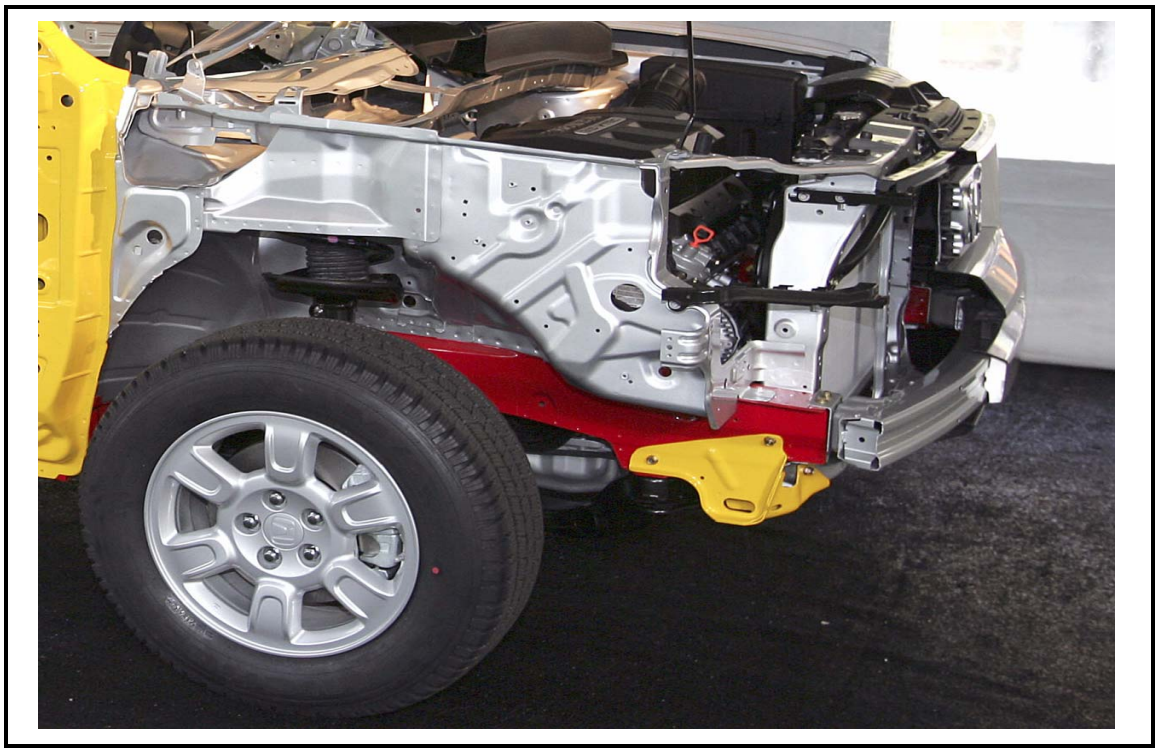

Figures 7. Honda Ridgeline SEAS design (PEAS in red and SEAS in yellow color)

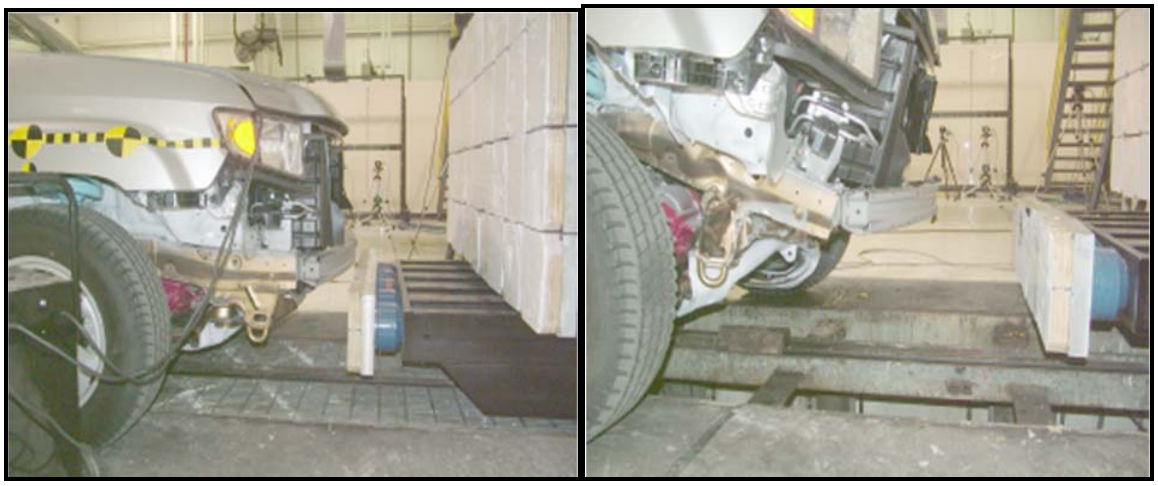

Figure 8. The pre and post-test pictures of the ORB with the align PEAS and deformed PEAS- SEAS respectively.

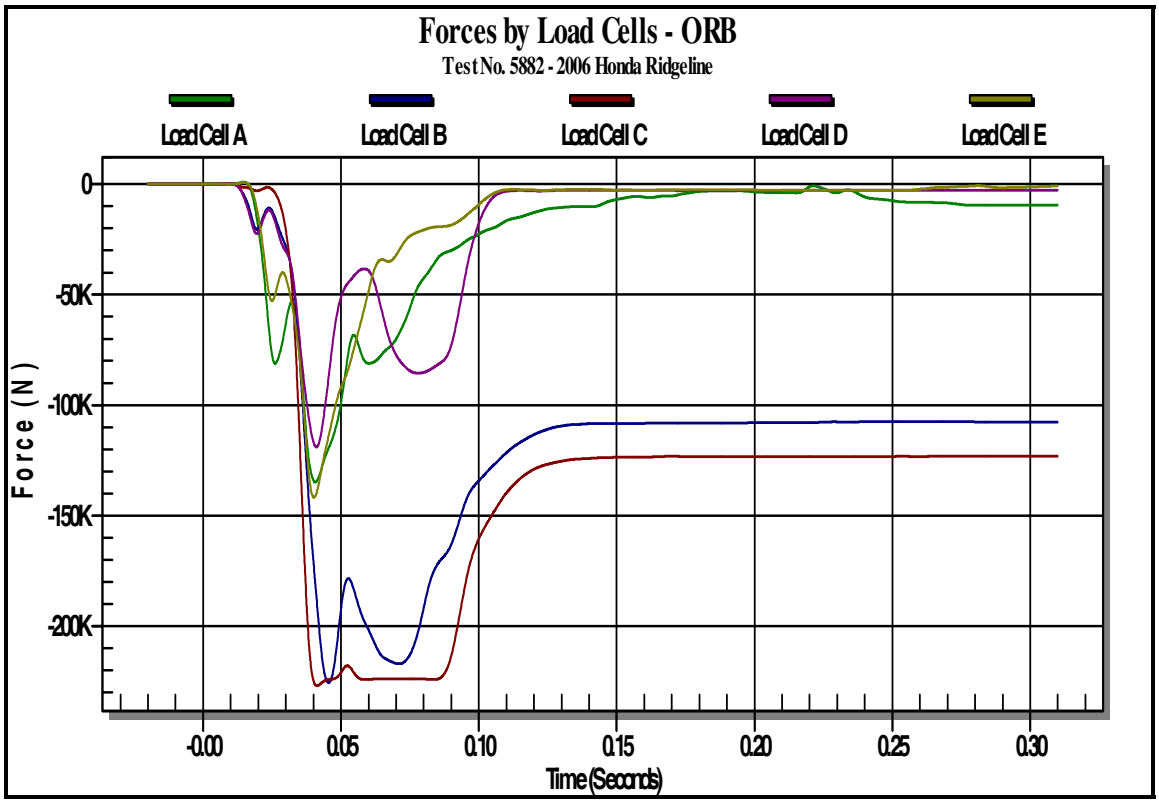

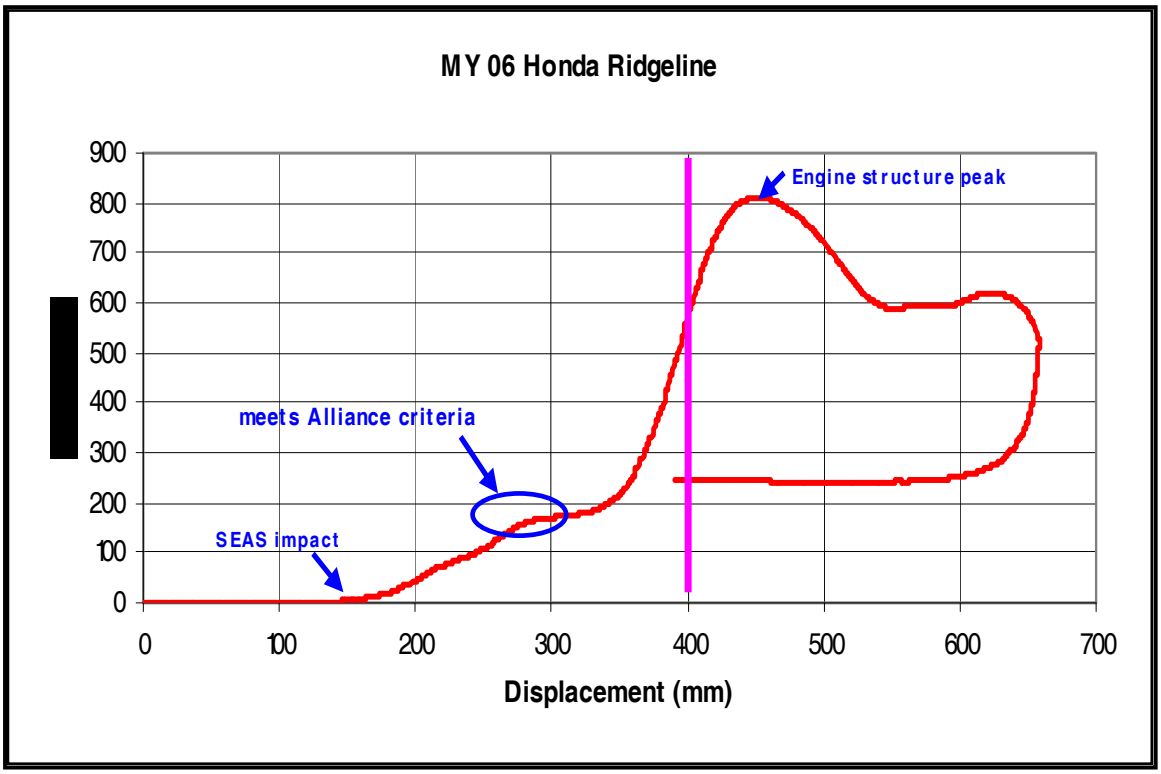

Figures 9. Honda Ridgeline forces recorded by the ORB load cells and Force-Deformation plot

The forces on the ORB easily exceeded 100 kN in 400 mm displacement. However, forces in two of the five ORB exceeded the load cells capacity as shown in Figure 9 plot of individual ORB load cells. The results of this test beyond 400 mm displacement are of questionable quality.

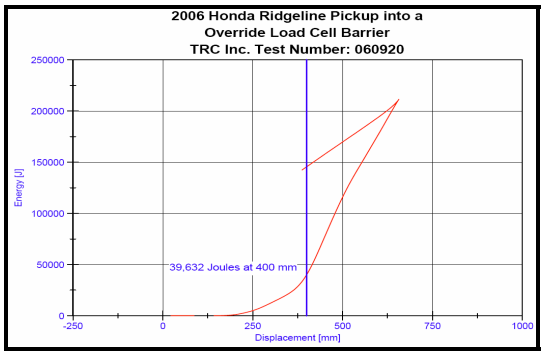

Figure 10. The energy absorbed by SEAS

Total crash Energy = 143,838 J
% absorbed by SEAS in 400 mm = 27.5 %

VTV crash test into the 2002 Ford Focus was conducted with the Ridgeline SEAS only, since SEAS can not be removed for this vehicle. The injury measures in this test were much higher. These high injury values suggest that the Ridgeline SEAS structure was stiff. This result calls for further research to evaluate SEAS structure and especially redesign the ORB to measure its strength.

2007 Chevrolet Silverado Results

The Silverado has brackets attached to PEAS as shown in Figure 11-12. These brackets are intended to bend the PEAS downwards in a frontal crash.

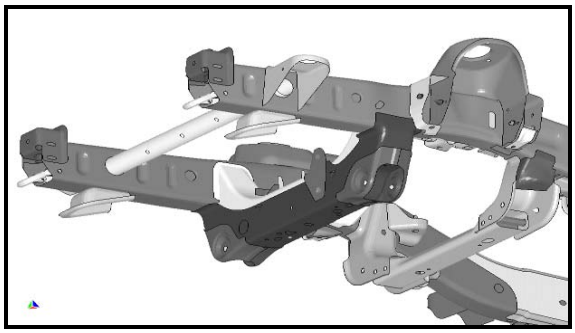

Figure 11. Silverado SEAS design

Figure 12. The pre-test picture of the alignment of the ORB and the SEAS

Figure 13. The post-test picture showing the deformed PEAS and SEAS

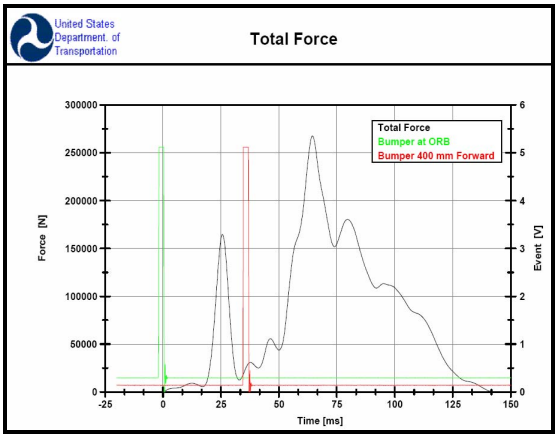

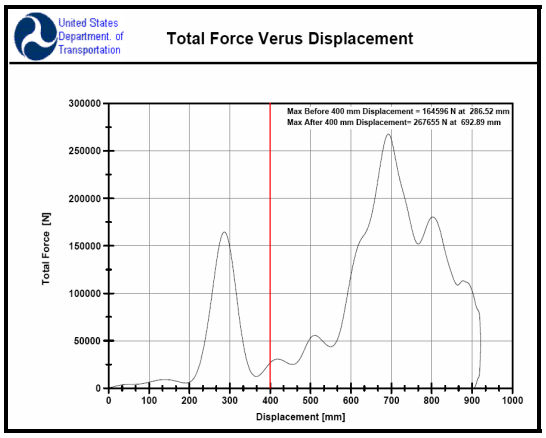

Figure 14. Chevrolet Silverado forces recorded by the ORB load cells (Force-Deformation plot)

The SEAS for this vehicle met the TWG criteria of 100 kN in 400 mm displacement and observed that forces were not exceeded the load cells capacity.

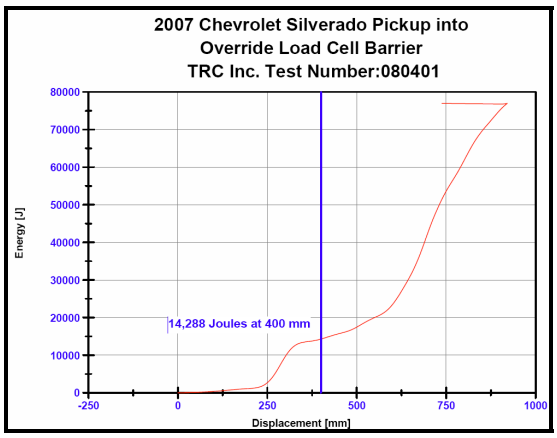

Figure 15. The energy absorbed by SEAS

Total crash Energy = 160,276 J
% absorbed by SEAS in 400 mm = 8.9 %

VTV crash test into the 2002 Ford Focus was conducted with the Silverado SEAS only. SEAS for this vehicle can not be removed. VTV test could be conducted with the SEAS brackets removed by cutting off the brackets at the attachment point with the PEAS. However, such a test has not been conducted. The results from the VTV test (with SEAS) with the Ford Focus had high injury assessment values for the Focus occupants.

COMPUTER SIMULATION RESULTS

The structural interaction between passenger cars and Option 2 LTVs in frontal crashes was investigated using computer simulations. The NCAC/GWU has developed a fleet of virtual vehicles which were used to evaluate the effectiveness of static geometric alignment on structural interaction. The vehicle models chosen for this study as shown in Figure 16, were based on the 1996 Dodge Neon, 2006 Ford F-250 and the 2007 Chevrolet Silverado. All of these FE models were validated to full frontal rigid barrier impact tests [http://www.ncac.gwu.edu/vml/models.html].

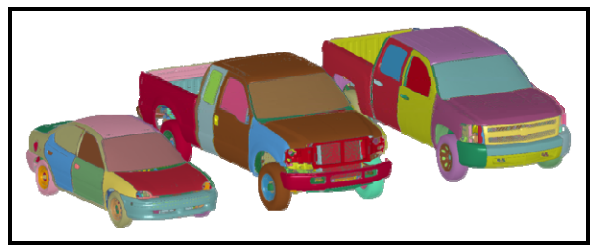

Figure 16. Finite Element Models of Neon, F-250 and Silverado

Frontal impacts between the following vehicle's pairs were analyzed in this study:

1996 Dodge Neon–2006 Ford F-250 (Option 2 LTV, cross-member type SEAS)
1996 Dodge Neon–2007 Chevy Silverado (Option 2 LTV, PEAS Extension)

The Force-Deformation (F-D) characteristic for the Neon, F-250 and Silverado in a full frontal fixed barrier impact is shown in Figure 17. From the F-D curves, it is evident that the frontal structure of the F-250 and the Silverado are much stronger than that of the Neon. True AHOF400 (average height of force delivered by a vehicle in the first 400 mm of crush), and the Kw400 (measure of stiffness based on crush energy absorbed by a vehicle in the first 400 mm of crush) [Mohan, 2008] were calculated for each of the vehicles. Table 1 summarizes the difference in mass, geometry and stiffness between the target vehicle (Neon) and the two bullet vehicles (F-250 and Silverado). The simulations were conducted such that the target vehicle (neon) experienced an impact severity similar to that of the frontal NCAP test condition.

Consequently, the energy required to crush 400 mm of the front end of the F-250 and the Silverado is much higher than the Neon, as reflected by their respective Kw400 measures. VTV full frontal simulations were conducted between Neon-F-250 and Neon-Silverado. The closing speed was chosen to match the impact severity of an NCAP test for the Neon.

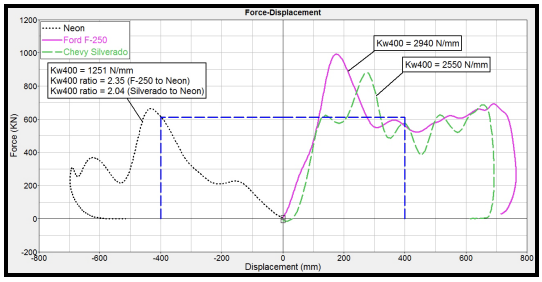

Figure 17. Force Deformation Comparison of Neon, F-250 and Silverado

Table 1. Mass, AHOF400 and Kw400 for Neon, F-250 and Silverado

		Target Veh.	Bullet 1	Bullet 2
		Neon	F-250	Silverado
Mass	kg	1335	2998	2622
Mass Ratio			2.25	1.96
True AHOF400	mm	448	704	584
AHOF Ratio			1.57	1.30
Kw400	N/mm	1251	2940	2550
Kw400 Ratio			2.35	2.04
Approach Veloci	mph	35	15.59	17.8
Closing Speed	mph		50.59	52.80

The front-end structural alignment between the Neon-F-250 and the Neon-Silverado is shown in Figure 18 and Figure 19. There is a significant vertical geometric mismatch between the PEAS of the Neon and F-250. The SEAS positioned below the PEAS of the F-250 overlaps 50% of the Neon PEAS as required by the Alliance voluntary commitment to improve compatibility in frontal impacts for Option 2 LTVs. Due to the presence of SEAS, the Silverado is classified as an Option 2 LTV in this study. Geometrically, the vertical mismatch of the PEAS is much lower between Neon-Silverado when compared to Neon-F-250.

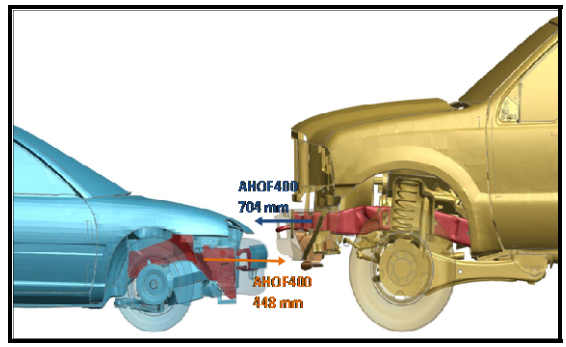

Figure 18. Geometric Alignment, Neon-F250

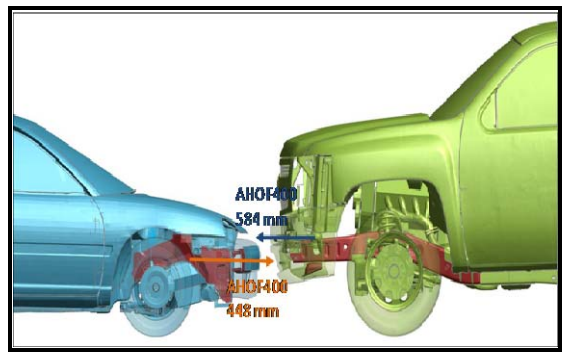

Figure 19. Geometric Alignment, Neon-Silverado

F-250-Neon Simulation Results

Full frontal simulations between the Neon and F-250 were conducted with and without the F-250 SEAS to evaluate the influence of SEAS on structural interaction between the two vehicles. The interaction between the PEAS of the Neon and the F-250 is illustrated in Figure 20 (with SEAS) and Figure 21 (without SEAS). The SEAS on the F-250 prevents the Neon from completely under riding the F-250. The front of the Neon PEAS interacts with the F-250 SEAS and crushes axially in the beginning, but as the SEAS starts to fail the Neon PEAS starts to bend towards the ground. Without the SEAS on the F-250, the structural interaction between the frontal structures is significantly reduced resulting in notable underriding of the Neon front end.

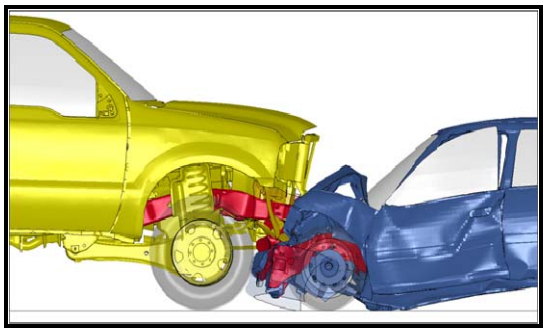

Figure 20. Structural Interaction between Neon and F-250 (with SEAS)

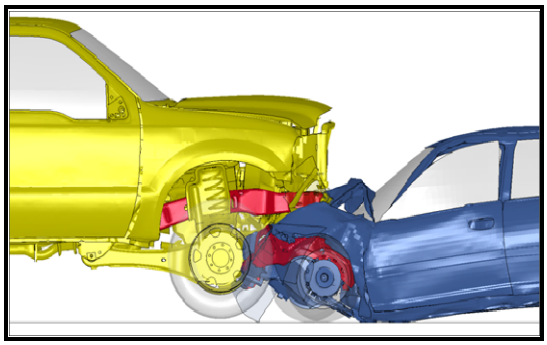

Figure 21. Structural Interaction between Neon and F-250 (without SEAS)

The change in structural interaction was primarily investigated based on the amount of crash energy absorbed by the vehicles involved in the crash. The amount of structural intrusion into the occupant compartment of the vulnerable vehicle was also compared.

The crash energy absorbed by the vulnerable vehicle (compact car, Neon in this study) is further divided into two groups:

- Front engine compartment energy
- Occupant compartment energy

The front engine compartment energy is the energy absorbed by the components that are designed to absorb the crash energy. The occupant compartment energy is the energy absorbed by the occupant compartment, which is primarily designed to prevent any structural collapse into the occupant compartment.

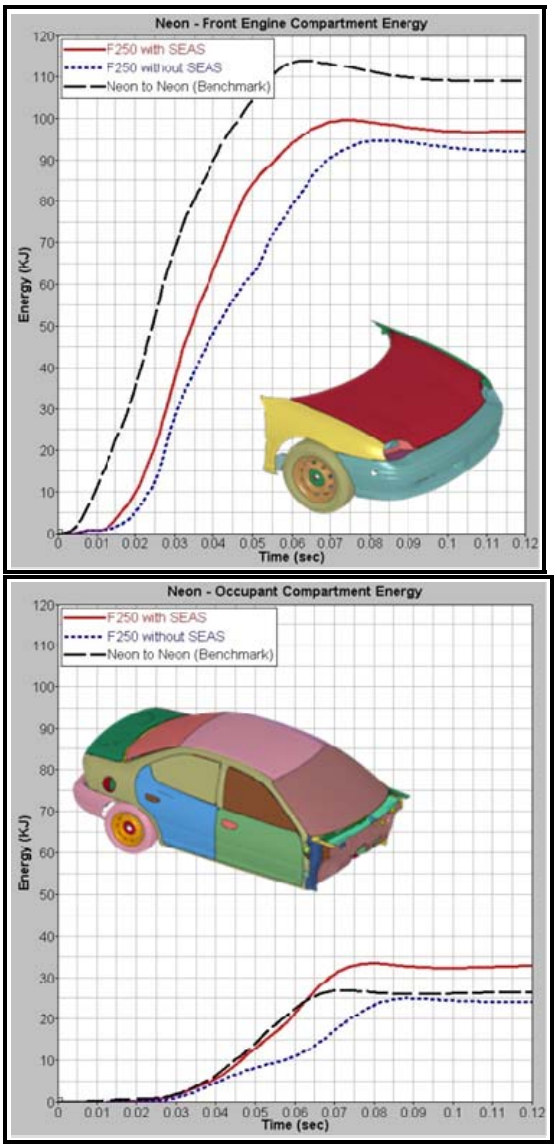

Figure 22. Energy Distribution (Neon-F-250)

The benchmark for energy comparison is a full frontal simulation between identical Neon's at the same impact severity. The mass, the AHOF400 and the Kw400 are all equal. The energy distribution for the Neon front engine compartment and occupant compartment for full frontal impact between Neon-F-250 (with SEAS), Neon-F-250 (without SEAS) and Neon-Neon is shown in Figure 22. Due to significant mismatch between the Neon PEAS and the F-250 PEAS, the Neon frontal structures do not deform ideally (as design optimized for frontal impact into fixed barrier). Consequently, the energy absorbed by the Neon front engine compartment is lower compared to the benchmark simulation between identical Neon's.

The presence of SEAS shows that the occupant compartment energy initially follows the benchmark simulation, but due to the taller, stiffer and heavier F-250, the Neon occupant compartment continues to crush and absorb more energy to satisfy the conservation of energy principle. On the other hand, without the SEAS, there is significant underride of the Neon frontal structures and the energy absorbed by the Neon occupant compartment converges to the benchmark simulation. Based on past crash testing, NHTSA has found that structural mismatch may reduce compartment acceleration on the partner vehicle; however, it is never desired.

The energy comparison would not be conclusive without evaluating the resulting intrusions into the occupant compartment of the vulnerable vehicle. The intrusion into the Neon occupant compartment in full frontal impact with F-250 (with and without SEAS) and Neon is shown in Figure 23. The structural underride between the Neon and F-250 without SEAS resulted in lower toe pan intrusions compared to the impact between Neon and F-250 with SEAS. This is expected as the lower load path is not utilized due to the geometrical mismatch of the structures without the SEAS on the F-250. The toe pan intrusions in the case of the Neon to F-250 with SEAS are very similar to the benchmark impact between identical Neons. However, in both cases (Neon to F-250 with SEAS and without SEAS) the driver side A-pillar intrusions are nearly twice (160mm) that of the benchmark impact between identical Neons. This intrusion is highly undesirable as the dash, steering column and the air bag modules are moving rearward and are compromising the survival space of the occupant. This may also result in lowering the effectiveness of the driver air bag in reducing risk of serious injuries.

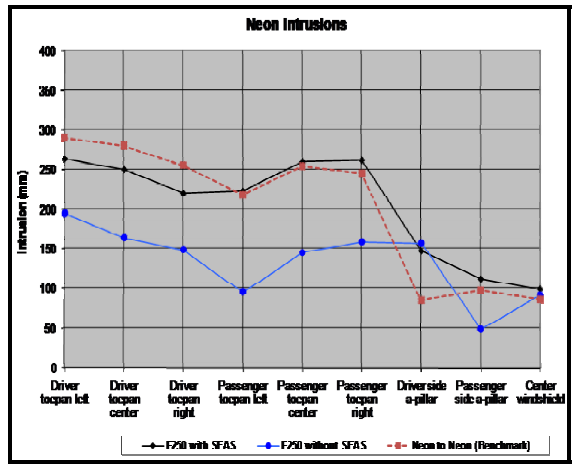

Figure 23. Neon Intrusions (Neon-F-250)

Silverado-Neon Simulation Results

The structural interaction between the PEAS of the Neon and the Silverado is illustrated in Figure 24 (with SEAS) and Figure 25 (without SEAS). The presence or absence of SEAS on the Silverado has negligible effect in the overall crush kinematics of the Neon frontal structures.

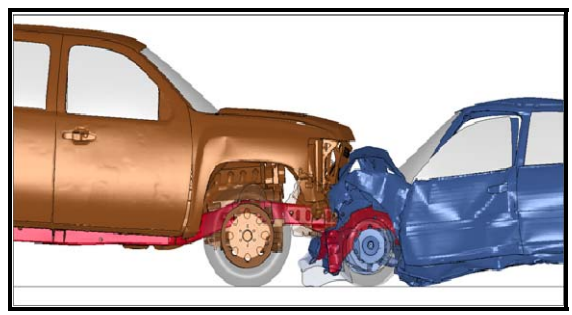

Figure 24. Structural Interaction between Neon and Silverado (with SEAS)

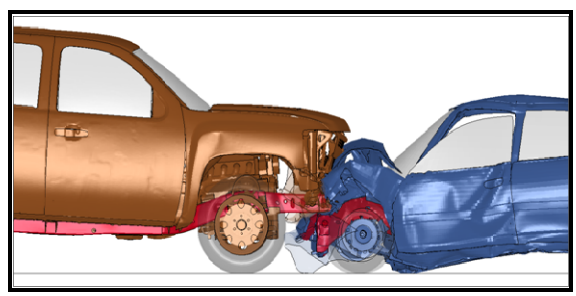

Figure 25. Structural Interaction between Neon and Silverado (without SEAS)

The energy distribution between the front engine compartment and occupant compartment of the

Neon for full frontal impact between Neon-Silverado (with SEAS), Neon-Silverado (without SEAS) and Neon-Neon is shown in Figure 26. The energy absorbed by the Neon frontal structures in a frontal impact between Neon-Silverado is similar to the benchmark simulation between identical Neons. The Neon frontal structures deform ideally (as design optimized for frontal impact into fixed barrier) absorbing the crash energy. However, the energy absorbed by the occupant compartment is significantly higher when compared to the benchmark simulation. Since, the Silverado is much heavier and stiffer than the Neon; the Neon structure has to absorb the remainder of the crash energy to satisfy the conservation of energy principle.

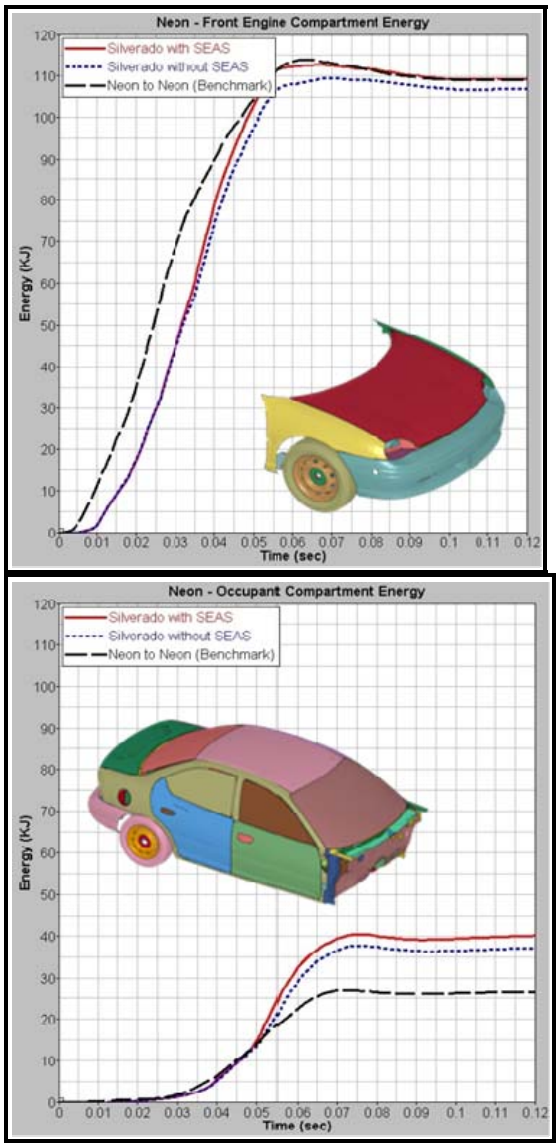

Figure 26. Energy Distribution (Neon-Silverado)

One interesting observation is that both the front engine compartment and occupant compartment energies of the Neon are marginally lower when impacted by the Silverado without the SEAS. The design and placement of the SEAS makes the Silverado PEAS stiffer and reduces its contribution to energy absorption in a frontal impact with the Neon. When the SEAS is removed, there is slightly higher energy absorption by the Silverado PEAS which lowers the amount of energy to be absorbed by the Neon frontal structure.

The resulting Neon compartment intrusions complement the observation above on energy distribution. The resulting toe pan and A-pillar intrusions are notably higher for the Neon-Silverado (with and without SEAS) simulation compared to the benchmark simulation Figure 27. Without the SEAS, the intrusions at the toe pan are slightly lower as some of the crash energy is absorbed by the Silverado PEAS.

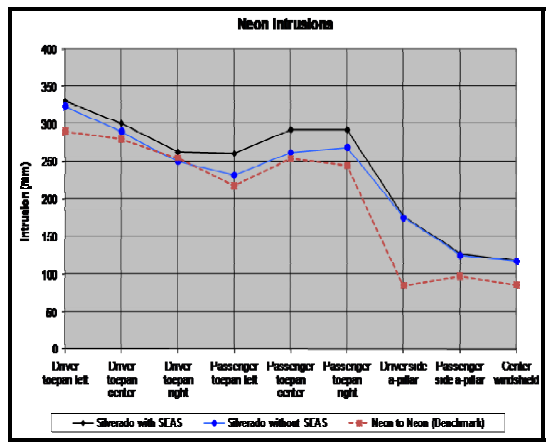

Figure 27. Neon Intrusions (Neon-Silverado)

SUMMARY OF COMPUTER SIMULATIONS

The observations from the Neon-F-250 simulations demonstrate that the cross-member type SEAS design helps prevent underriding of the Neon frontal structures. However, the SEAS in the Silverado was a non-contributing factor in the overall crush kinematics of the Neon frontal structures, mainly because of the vertical overlap of the PEAS structures of the Neon and Silverado. In fact, the Silverado without SEAS showed slight improvement in both intrusions and energy absorption of the Neon. Improvement in geometric compatibility is essentially a step in the right direction. Further

improvement in structural interaction is possible by lowering the aggressiveness of the LTV's.

This preliminary analysis was limited to understanding the structural interaction in full frontal impacts. Other frontal and oblique impact conditions and impact locations and their effect on structural interaction were not considered in this preliminary analysis.

CONCLUSIONS

The industry voluntary test for the SEAS is a quasi-static push test that requires the SEAS structure to withstand a minimum of 100 kN of force before 400 mm deflection from the front of the primary structure (e.g., the rails on which it is mounted). Such a test may guarantee a minimum strength, but it does not prohibit the structure from being designed too strong for good car compatibility. An energy absorption evaluation could optimize the SEAS for compatibility.

The ORB dynamic tests showed that the vehicles tested meet the proposed SEAS performance criteria suggested by the Alliance's TWG.

The full frontal simulations between a compact passenger car (Neon) and the Ford F-250 without the SEAS showed reduced intrusions in the Neon toepan area. However, there was significant underride of the Neon which resulted in increased intrusions near the driver side A-pillar. In the case of F-250 with SEAS, there was increased structural interaction between the SEAS and the Neon PEAS which prevents frontal structures from underriding each other. As a consequence there is more intrusion into the occupant compartment when compared to the frontal impact without the SEAS. This observation was based on the simulation results with FE model of the 1996 model year Neon. In recent years, the structural design and self-protection levels of compact passenger cars have significantly improved (based on frontal NCAP and IIHS front offset test results) and the observation may be different in frontal impacts between these newer compact cars and the Ford F-250 with and without the SEAS. The presence or absence of SEAS on the Chevrolt Silverado had negligible effect in the overall crush kinematics of the Neon frontal structures. This is primarily attributed to the SEAS design and its location.

Further study is needed to determine the effective performance requirements for SEAS. This study was limited to the three SEAS designs that were available in production vehicles at the time of testing. Other SEAS designs and their performance may need to be considered before an appropriate ORB test procedure is identified. The difference in the design of the PEAS confounds the study of the effects of SEAS in VTV tests. In the case of the Ford F-250, where the SEAS could be removed, the VTV tests show a benefit from SEAS. However, the SEAS on the F-250 had the lowest strength. Additional criteria for the SEAS, like energy absorbed, may be considered in the future.

Like most programs using crash tests, this study is subject to limitations in the number of vehicles studied. Additional SEAS designs will need to be studied, along with their effect in mitigating injuries in the partner vehicle, before any conclusions can be made about the effectiveness of the proposed TWG performance criteria.

Option 2 LTV's reward the added SEAS to reduce override of passenger cars. These structures will require a new test procedure for evaluation. This paper shares the designs of the ORB, and results from tests of Option 2 vehicles equipped with and without SEAS.

Reference

Barbat S. (2005). "Status of Enhanced Vehicle-to-Vehicle Crash compatibility Technical working Group Research and Commitments; 19th ESV Conference, Washington, D.C., Paper No. 05-463.Alliance of Automotive Manufacturers, letter to Acting Administrator, NHTSA, May 10, 2006, (Docket # NHTSA-2003-14623-24).

Patel S., Smith D., Prasad A., (NHTSA) & Mohan P. (The George Washington University), "NHTSA's recent vehicle crash test program on compatibility in front-to-front impacts", 20th ESV Conference, Paper No. 07-0231.

Baker, B., Nolan, J., O'Neill, B., Genotes, A., (2007). "Crash Compatibility between Cars and Light Trucks: Benefits of Lowering Front-End Energy-Absorbing Structure in SUVs and Pickups", Insurance Institute for Highway Safety, Arlington, VA, 2007.
Alliance of Automotive Manufacturers, letter to Ronald C. Medford, NHTSA, July 30, 2007, (Docket # NHTSA-2003-14623-63).

http://www.autoalliance.org/archives/archive.php?id=134&cat=Fact%20Sheets "Alliance of Automobile Manufacturers, "Voluntary commitment to enhance vehicle to vehicle crash compatibility", December 2003.

http://www.access.gpo.gov/nara/cfr/waisidx_99/49cfr581_99.html

Mohan, P., "Development of Objective Metrics to Improve Compatibility in Frontal Collisions", Doctoral Dissertation, The National Crash Analysis Center, The George Washington University, Washington DC, August 2008.

DESIGN AND OPTIMIZATION APPROACHES TO PROVIDE A FRAME FOR DESIGNER IN THE VEHICLE DEVELOPMENT PHASE WITH THE FOCUS ON ENHANCED SAFETY

Ferruh Özturk, Nursel Özturk, Necmettin Kaya, İdris Karen
Uludağ University, Engineering and Architecture Department
Görükle Campus, 16059 Bursa
Türkiye
Page Number: 09-0422

ABSTRACT

The safety of a vehicle is today of great importance for the automotive industry. The light weight vehicle designs are to increase in worldwide over the next years with respect to environmental and road safety regulations to make surface transport safer and more effective. The vehicle design models are usually complex in nature and nonlinear in terms of computational issues. The design and optimization in the area of transport are usually challenging tasks due to the highly nonlinear behaviour of structural parts with respect to durability, crashworthiness and vehicle dynamics issues. The design optimization process is usually limited by the excessive costly computational requirements in case of nonlinear model simulations and with respect to the difficulties for efficient exploration of multi-objective design space in the area of vehicle safety research such as crashworthiness. Although some studies which are given in literature have been carried out to solve the safety problems such as crashworthiness, they have not been efficiently solved yet. Recently, significant research in the area of vehicle safety and light weight vehicles through simulation based optimization undertaken, and it is expected to continue further resulting in reductions in cost and time for new vehicle development process. The purpose of this paper is to explore design optimization approaches for development of light weight cars to satisfy safety needs for automotive structure and its components. In this paper, the shortcomings of traditional approaches, new design optimization approaches, stochastic and intelligent approaches that can be implemented to handle complex and nonlinear models are presented to provide a frame for designer in the vehicle development phase with the focus on enhanced safety for lightweight vehicles in the automotive industry.

INTRODUCTION

The number of safety and light weight vehicle regulations has been presented to improve safety and quality of road transport. The regulations will continue to increase in over the next years. This will have increase environmental and road safety issues worldwide with respect to making surface transport safer, more effective, and more competitive. The automotive industry must present new approaches especially in the automotive design process to produce new products, which are least sensitive to disturbing factors of manufacturing and environment issues with the focus to safety and lightweight.

Road transport safety has improved significantly over the last decades as indicated by a 50% reduction of the total number of fatalities in the EU. This decrease is with respect to continue as new safety regulations and technologies and through improved passive and active safety systems, but with increased mobility the current situation with 43,000 deaths and 1.9 million injured on European roads requires further efforts. A target of halving the number of fatalities on European roads by 2010 has been set (as compared to 2001), and further reduction is reported for 75% by 2020. Therefore, further research on enhanced safety concepts should be carried out in order to achieve these targets [1-6].

It is obvious that a significant improvement in vehicle safety will depend upon the presentation of innovation and advanced design optimization techniques. In addition, a substantial reduction of accident fatalities can be achieved through an integrated system design and optimization

approaches considering both vehicle technology and infrastructure.
The purpose of this paper is to explore design optimization approaches for development of vehicles to satisfy enhanced safety needs for automotive structure and its components. The design optimization approaches with less computational efforts, stochastic optimization and intelligent approaches are presented with the focus on enhanced safety applications especially with respect to crashworthiness and optimum design of vehicle systems and components.
This paper is organized as follows: vehicle safety R&D aspects are taken into account in "Vehicle Safety R&D" Section. It is based on current situation, roadmaps and future research directions referencing automotive related organizations and papers published in literature by academis and industry. The optimization techniques with reference to vehicle safety are outlined through stochastic techniques and simulation approaches in "Optimization Techniques in Vehicle Safety R&D" Section. Finally, "Conclusions" Section is included to summarize vehicle safety R&D and design optimization issues to design safer vehicles in the automotive industry.

VEHICLE SAFETY R&D

Safety aspects and mobility are growing concerns in both developed and developing countries. The safety of a vehicle and road transport is today of great importance and a high priority research area for the automotive industry.
The reduction in road accident fatalities and injuries can only be achieved by introduction of improved technologies for newer vehicles and road transport systems regarding vehicle safety standards. Therefore, further research on enhanced safety concepts must be carried out in order to reduce the accident fatalities and to achieve better occupant protection on road transport. In addition, the cost reduction to present safer vehicle designs through shorter lead times must be satisfied by introducing new optimization approaches.
Although significant improvements have been achieved to meet the safety needs of society and industry, there is an increasing demand to further increase passive and active safety systems.
There is a need to define the road maps and strategies for future research areas to achieve given targets and overcome the limitations of existing systems. This will help to reach the social and industrial needs in more effective and cost efficient way and it will prevent independent works with the lack of common position on the issues of vehicle safety and road transport. In this section, vehicle safety R&D is investigated regarding papers published by academia and industry in literatre and also from the side of automotive related organizations.
The automotive related organizations are established to bring together independent companies and R&D providers belonging to industry, private and public research institutes and universities to enhance vehicle safety and other automotive related issues in the automotive sector throughout Europe [1-6]. For example, EARPA is the association of automotive R&D organizations. EARPA-AVDT presents the safety aspects to introduce the future safer vehicles and to introduce new technologies for safe and secure road transport systems. ERTRAC is a technology platform. ERTRAC's goal is to provide a framework to focus co-ordination efforts of public and private resources on the necessary research activities in the vehicle development area. Safety issues are also covered by APROSYS, APSN, FURORE organizations. APROSYS Integrated Project (IP) deals with the development and introduction of critical technologies that improve vehicle safety for all European road users in all relevant accident types. Another organization regarding safety issues is APSN (Advanced Passive Safety Network). It is established to promote passive safety research and to help in the dissemination of information and results, all with a view to reducing the number of casualties on European roads. The APSN is aimed at providing prioritised future vehicle safety research needs and actions. FURORE is a thematic network platform to discuss breakthrough technologies and the corresponding research demand for the future vehicles. EUCAR developed an Automotive R&TD Master Plan in order to define a European approach to technologies for automotive development and to present the major R&D challenges the automotive industry is facing. The CARS 21 final report reflects the deliberations, opinions and agreements within the CARS 21 High

Level Group, which was set up to chart the way towards sustainable development of a competitive European automotive industry. In CARS21 final report, it is stated that a holistic, integrated approach involving vehicle technology, infrastructure and the road user is the best means for increasing road safety and a crucial point is due to R&D investments to improve the current levels on road transport with particular relevance to safety and security [2].

Research field descriptions and road maps regarding vehicle safety and road transport are defined by these organizations in details bringing together Universities, R&D organizations and automotive sector representatives.

Vehicle safety R&D is becoming one of the important research area through the design of enhanced safety components using new optimization techniques and intelligent systems. Research targets and road maps show that the significant enhancement in vehicle technologies and safety is crucial for future vehicle design concepts to satisfy social and industrial needs. It can be concluded that the reduction in accident fatalities and injuries can be achieved through introduction of new design optimization approaches, intelligent systems and innovation to produce safer vehicles with new structures and safety aspects.

Recently, several papers have been published in literature with respect to vehicle safety especially about crashworthiness and structures [7-18]. The most common point is that the implementation of multi-objective optimization methods through stochastic techniques are required to design enhanced safety vehicle structures and systems to handle with uncertainty and variability and able to explore pareto optimal design space for global optimization. Multidisciplinary simulation and multi objective optimization methodologies, techniques for handling uncertainty and variability to design are reported to support the design and optimize the vehicle components of future advanced safer vehicles, for example, the development of new methods, that will guide protective safety design for the improvement of safety in case of crashworthiness of cars in frontal and side impacts through global optimization approaches.

OPTIMIZATION TECHNIQUES IN VEHICLE SAFETY R&D

The automotive industry must present new approaches especially in the automotive design process to produce newer models with the focus to enhanced vehicle safety issues through lightweight products, which are least sensitive to disturbing factors of manufacturing and environment to make surface transport safer, more effective and competitive. In this section, the optimization techniques which are implemented in vehicle development process are introduced referencing to vehicle safety aspects, especially crashworthiness and vehicle structures.

The design and optimization in the vehicle development process regarding safety aspects such as crashworthiness are usually challenging tasks due to complex models and highly nonlinear behaviour of vehicle structure with respect to durability, fatigue and vehicle dynamics. The design optimization process is usually limited by the excessive costly computational requirements in case of nonlinear model simulations and with respect to the difficulties for efficient exploration of multi-objective design space. For vehicle safety problems, such as crashworthiness, the responses are often includes uncertainties and it has several drawbacks that can cause numerical difficulties to find search direction through time consuming approaches and in some applications, it may not even be possible to compute the derivatives Although some studies which are given in literature have been carried out to solve the crashworthiness problem, the problem has not been efficiently solved yet [7-18].The crashworthiness design and optimization are challenging tasks due to the highly nonlinear behaviour of a structure. Therefore gradient based approaches such as steepest descent, conjugate gradient, Newton methods are hard and expensive to find the search directions and also explore design space. In these techniques, the search direction is computed at an initial estimate for the minimum design. The initial point definition for estimation of a starting design may cause drawbacks with respect to convergence rate and even to stick in infeasible solution areas [19-21].

In traditional approach, complexity of design models can cause limitations due to analysis,

optimization and simulation process requirements of vehicle structures.

The structural layout, which is defined by initial design concept, and shape optimization have significant effect on product performance and manufacturing cost. Therefore, how to achieve optimal initial design concept and how to achieve efficient shape optimization process are important issues which took significant attention by researchers in recent years. Initial design concept is often based on experience of designers and it includes uncertainties which may cause unexpected shortcomings during the development phase and the life of the product. These shortcomings of traditional design approaches can be handled by defining stochastic optimization techniques with topology design approach [22]. Topology design approach is widely used to define initial conceptual structural layout of products. It provides an initial design concept for downstream applications following design. In traditional approach the starting design outlines are not optimal therefore further optimization works on the structure will not be the right solutions. Topology optimization searches for the best conceptual structural layout on a predefined design domain with specific boundary and loading conditions to achieve optimal initial design structure.

Another problem in automotive industry is how to achieve Safer vehicle design concepts by considering structure performance and manufacturing cost in the early stages of product development. The optimisation methods are used to design products, which are light-weight to improve the cost and fuel efficiency, without sacrificing strength and performance due to safety requirements. During the optimisation, the shape and size of structure can be changed, but the topology of the structure is not changed. Therefore, optimisation techniques have to be considered in the conceptual design phase to create an optimal initial design layout.

Recently, topology design, artificial intelligence and stochastic optimization techniques are widely implemented to design optimization problems in vehicle safety and road transport areas. The shortcomings of traditional approaches in vehicle design can be handled by defining the optimal topology as initial design concept and by using artificial intelligence techniques and stochastic optimization approaches such that uncertainties can be prevented with less computational efforts.

Most real world engineering problems involve at least an element of uncertainty in loading conditions, in material characteristics, in analysis process, in manufacturing, etc. Many optimization approaches do not consider this uncertainty for the design optimization process. In recent years there is a growing interest in the automotive industry, especially in the design process due to the effectiveness of the stochastic optimization and artificial intelligence techniques for improving the quality characteristics of the products and to overcome the above mentioned shortcomings [19-21].

Stochastic optimization does not have above mentioned drawbacks with respect to search direction and exploration of design space which are important aspects in case of multi-objective vehicle safety cases. Widely used stochastic design optimization techniques are Genetic Algorithms (GA), Particle Swarm Optimization (PSO), Simulated Annealing (SA). In stochastic optimization different background variables can vary stochastically during the optimization procedure. A major difference between stochastic optimization and traditional optimization methods is that stochastic optimization is rather a reproduction of the real model considering uncertainties.

Modelling and simulation techniques are also implemented in optimization algorithms to enhance the presentation of solution space, to reduce the number of experiments and to analyse sensitivity of design parameters such as Response Surface Method (RSM), Design of Experiments (DO), Taguchi Method (TM) [17-19]. For crash simulation problems with a highly non-linear behaviour of the objective function, the use of local gradient based optimization algorithms is not suitable. volutionary algorithms are more efficient for these problems.

Artificial intelligence techniques are also used to define design optimization models in case of uncertainties. Neural network, also called artificial neural system, is an information processing technique which is developed to simulate the functions of a human brain. Neural network is composed of elementary processing units which are called as neurons. Neurons are interconnected

by weighted connections. Among various neural network architectures, back propagation (BP) is a widely used technique for training of multi layer perceptrons (MLP). An identical process is repeated for each weight of the hidden layer connections if there is more than one hidden layer. Several repeated solutions with different initial weights and network parameters are used to converge to the optimal solution [20].

The real world design and manufacturing problems are usually multi-objective, often conflicting, and they have uncontrollable variations in their design parameters with complex nature. The objectives must be satisfied simultaneously in order to obtain an optimal robust solution. The whole problem must be taken as multi-objective with the Pareto optimal set instead of single objective optimization. Traditional optimization methods are not only time consuming in solving complex nature problems that include multivariable and multi-objective but also they may not be used efficiently in finding global or near global optimum solutions. In addition, they can stick to the local optimum values such as in case of crashworthiness problems.

Traditional design procedure is an iterative process. It starts with an initial concept design that is based on the experience, knowledge and intuition of the designer. Analysis and redesign steps are carried out to evaluate and modify the product layout. This is time consuming and inefficient procedure that can create sub-optimal structure layouts since starting topology is not optimal. The designer may consider many alternative topologies and one of them is chosen as being final component layout. This procedure may result with final component layout, which is often non-optimal. However, in topology optimisation approach, designer does not have to choose optimal topology among alternatives and no priori knowledge about topology is required. The goal of topology optimisation is to find the best use of material for a component [23].

CONCLUSIONS

In this paper, design optimization techniques are outlined with reference to enhanced vehicle safety research to support more sustainable transport development. It is shown that stochastic optimization and intelligent approaches can be implemented to handle complex and nonlinear design models to provide a frame for designer in the vehicle development phase with the focus on enhanced safety in the automotive industry. In general, conclusions can be given as follows:

- There is a need to develop computationally efficient techniques to design competitive products for safer vehicle structures by increasing transport safety in line with the objectives for European transport policy in order to reduce the annual road victims.
- There is a need to consider uncertainties in crashworthiness using stochastic optimization techniques to achieve efficient designs, for dynamic problems, without considering uncertainties may cause infeasible solutions.
- There is a need to develop design frames to be employed at early design stages since the problem is due to initial design, which highly depends on experience and skill of designer, this can cause inefficient design alternatives which are not optimal.

Although some studies which are given in literature have been carried out to solve the safety problems such as crashworthiness problem, the problem has not been efficiently solved yet. Further research is essential to improve the vehicle safety and road transport systems through the use of advanced optimization techniques and innovation. This will help to reduce the casualties on road transport to the lowest limits and to achieve the targets set related to road transport safety.

ACKNOWLEDGEMENT

The authors acknowledge the supports of this research by the Scientific and Technological Research Council of Turkey (TÜBİTAK) research Project No. 104M240 and by the Uludag Universtity Commission of Scientific Research Projects under Contract No. M-2008-64.

REFERENCES

[1] ERTRAC, European Road Transport Research Advisory Council, Research Framework, *http://www.ertrac.org.*

[2] CARS 21, A Competitive Automotive

Regulatory System for the 21st century, Final Report, http://europa.eu.int/comm/enterprise/automotive

[3] APROSYS, Sustainable Surface Transport, Integrated Project on Advanced Protection Systems, *http://www.aprosys.com*

[4] APSN, Advance Passive Safety Network, *http://www.passivesafety.com*

[5] EARPA, European Automotive Research partners Association, *http://www.earpa.org*

[6] EUCAR - The European Council for Automotive R & D, *http://www.eucar.com*

[7] Forsberg, J. and L. Nilsson. 2006. "Evaluation of response surface methodologies used in crashworthiness optimization." International Journal of Impact Engineering, 32, 759–777.

[8] Kim, C.H. and J.S. Arora. 2003 "Nonlinear dynamic system identification for automotive crash using optimization: A review." Struct Multidisc Optim, 25, 2–18.

[9] Hoppe, A., Kaufmann, M. and B. Lauber. 2005. "Multidisciplinary Optimization considering Crash and NVH Loadcases." Lecture at ATZ/MTZ Virtual Product Creation, D-Stuttgart.

[10] Forsberg, J. and L. Nilsson. 2007. "Topology optimization in crashworthiness design." Struct Multidisc Optim, 33: 1–12.

[11] Redhe, M., Giger, M. and L. Nilsson. 2004. "An investigation of structural optimization in crashworthiness design using a stochastic approach." Struct Multidisc Optim, 27, 446–459.

[12] Choa, Y.-B., Baeb, C.-H., Suhb,_M.-W. and H.-C. Sin. 2006. "A vehicle front frame crash design optimization using hole-type and dent-type crush initiator." Thin-Walled Structures, 44, 415–428.

[13] Qi, W., Jin, X.L. and Zhang, X.Y. 2006. "Improvement of energy-absorbing structures of a commercial vehicle for crashworthiness using finite element method." Int J Adv Manuf Technol, 30: 1001–1009.

[14] Redhe, M. and L. Nilsson. 2006. "A multipoint version of space mapping optimization applied to vehicle crashworthiness design." Struct Multidisc Optim, 31: 134–146.

[15] Youn, B.D., Choi, K.K., Yang, R.-J. And L. Gu. 2004. "Reliability-based design optimization for crashworthiness of vehicle side impact." Struct Multidisc Optim, 26, 272–283.

[16] Duddeck, F. 2008. "Multidisciplinary optimization of car bodies." Struct Multidisc Optim, 35, 375–389.

[17] Tzannetakis, N., Vooren, P. and B. Lauber. 2005. "The Use of OPTIMUS for Advanced Multi-Disciplinary Structural Optimization in Automotive Applications" NAFEMS Seminar: Optimization in Structural Mechanics"2005 Wiesbaden, Germany.

[18] Tzannetakis, N., Peer, J.V., Donders, S. and Y. Tsuchida, 2003. "A system approach to design for Six Sigma through best in class simulation" Process Integration & Design Optimization. LMS International, 2003.

[19] Yıldız, A.R., Öztürk, N., Kaya, N. and F. Öztürk. 2007. "Hybrid multi-objective shape design optimization using Taguchi's method and genetic algorithm" Journal of Computers and Structures – Structural and Multidisciplinary Optimization, 34, 317-332.

[20] Öztürk, N. and F. Öztürk. 2004. "Hybrid Neural Network and Genetic Algorithm Based Machining Feature Recognition." Journal of Intelligent Manufacturing, Vol. 15. No. 3, 287-298.

[21] Karen, I., Kaya, N., Öztürk, N., Alankuş, O. and F. Öztürk. 2008. "Hybrid Artificial Intelligence and Structural Design Optimization Approach in the Automotive Industry." FISITA 2008 - World Automotive Congress, 14-19 September 2008, Munich, Germany.

[22] Yıldız, A.R., Kaya, N., Alankuş, O. and F. Öztürk. 2004. “Optimal design of vehicle components using topology design and optimization.” International Journal of Vehicle Design, Vol. 34, No. 4, 387-398.

CHARACTERISTICS OF SMALL OVERLAP CRASHES

Christopher P. Sherwood
Joseph M. Nolan
David S. Zuby
Insurance Institute for Highway Safety
United States
Paper No. 09-0423

ABSTRACT

Small overlap frontal crashes occur when vehicles are loaded outboard of their longitudinal structural members. Studies from the 1990s as well as current research have found that these crashes continue to account for a significant percentage of all serious frontal crashes. The National Automotive Sampling System/Crashworthiness Data System database was used to study the characteristics of these crashes in current model vehicles for drivers with injuries (excluding extremity injuries) rated 3 or greater on the abbreviated injury scale. Cases were individually analyzed to only include vehicles in which the majority of the loading was located outboard of the left longitudinal member. Occupant compartment intrusion was the primary factor in the resulting injuries, showing a strong correlation between the magnitude of intrusion and injury severity. Results suggest that vehicle designs must improve their ability to prevent occupant compartment intrusion when a vehicle is loaded at the outboard edges of its front end.

INTRODUCTION

Vehicle crashworthiness has improved greatly during the past 30 years, as indicated by the reduction in the occupant death rate per million vehicle registrations of 1-3 year old cars from 265 in 1979 to 98 in 2007 [1]. Despite these improvements, 28,869 vehicle occupants were killed in crashes in the United States in 2007. Frontal crashes accounted for half of these deaths even though new cars almost universally pass frontal crash tests with flying colors and have for several years. Ninety-five percent of 2008 model year vehicles earned 4 or 5 stars out of 5 for frontal crash protection in the National Highway Traffic Safety Administration's New Car Assessment Program [2] and 91% earned the Insurance Institute for Highway Safety's (IIHS) highest rating of good for frontal crashworthiness. Although these two consumer information programs can be credited for some of this progress, neither currently provides incentives to further improve frontal crashworthiness.

In an attempt to identify opportunities to advance crashworthiness beyond the current state of the art, researchers at IIHS recently studied frontal crashes of good-rated vehicles that resulted in serious injuries or deaths [3]. Crashes were sorted by type of front damage, and three major crash types were identified: narrow center damage (from crashes with trees and poles), moderate overlap damage (like that from the IIHS 64.4 km/h (40 mi/h) 40% offset test), and small overlap crashes (with the majority of loading outboard of the longitudinal member). Small overlap crashes tended to exhibit high levels of intrusion, similar to that observed in the early days of the IIHS frontal offset test program, suggesting that structural design improvements do not extend to crashes with small amounts of vehicle overlap.

Identification of small overlap crashes as a significant contributor to frontal crash injuries and fatalities is not new. In a study of fatal frontal crashes in the United Kingdom, Hobbs [4] found that 27% of the crashes had deformation in which neither longitudinal member was involved. O'Neill et al. [5] analyzed frontal crashes in the United States and determined that frontal crashes with less than 33% overlap accounted for 22% of fatal crashes. Scheunert et al. [6] examined real-world crash data in Germany to study the distribution of frontal crash types and determined that 26% of the crashes were equivalent to a 30% overlap crash test. In a more recent study of fatal frontal crashes in Sweden, Lindquist et al. [7] found that 34% of the deaths occurred in crashes in which there was no deformation of the outboard longitudinal members. The methodologies and terminologies varied among these studies, but results consistently indicated that about one-quarter of all serious frontal crashes involved loading substantially less than 40% of the vehicle's front end. The focus of the present study was to conduct an in-depth analysis of the characteristics of small overlap frontal crashes that resulted in serious injuries or deaths with the idea of understanding how vehicles can be improved to better protect people in this important frontal crash mode.

METHODS

Cases were obtained from the National Automotive Sampling System/Crashworthiness Data System (NASS/CDS) database. Small overlap crashes were defined as frontal crashes in which the majority of loading to the vehicle was outboard of the longitudinal member. The majority of these crashes should be captured by FLxx and FRxx SAE J224 Collision Deformation Classification (CDC) codes (Figure 1). There are instances, however, in which a small overlap crash may have been given a code suggesting a different type of crash. To capture all small overlap crashes, the initial inclusion criteria captured a much wider range of crash types, and then all cases were inspected in detail.

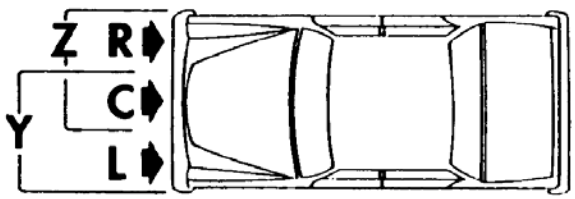

Figure 1. SAE J224 CDC horizontal damage codes for frontal crashes.

The SAE J224 code combinations were limited to those shown in Figure 2. The crash principal direction of force (PDOF) was between -30° and 0°, resulting in crash clock directions of 11 or 12 o'clock. All crashes had primary damage to the frontal plane (plane of damage = F) on either the left or left/center zones (horizontal damage = L or Y). Vehicles also had damage to (at a minimum) the bumper and other structures up to the level of the hood (vertical damage = E or A). Finally, the general damage code for the type of crash was either E (corner), W (wide), N (narrow), or S (sideswipe). There was no requirement on the deformation extent. Vehicles involved in a rollover or fire were excluded. All vehicles were model year 2000-08 passenger vehicles (body type = 1-49). Occupants were nonejected drivers ages 16 and older who were using lap/shoulder belts and who were fatally injured or had a maximum abbreviated injury score (MAIS) between 3 and 6. Because the point of this study was to understand how deaths and life-threatening injuries might be prevented in small overlap crashes, drivers were excluded if the only MAIS 3-6 injury was to the lower or upper extremities.

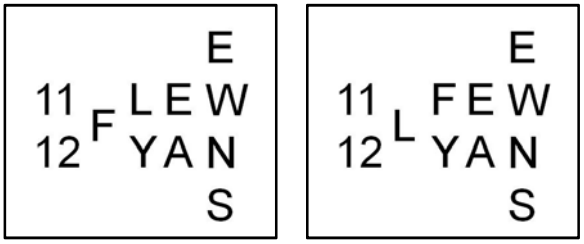

Figure 2. Possible CDC codes for inclusion criteria

In some small overlap frontal crashes there is almost no longitudinal deformation of the bumper or longitudinal members, and for this reason occasionally these cases are misinterpreted as lateral impacts. To capture all potential small overlap frontal crashes, some lateral impacts also were included for visual inspection. These crashes had the same search criteria as the frontal impacts with the following exceptions: plane of damage (left), horizontal damage (F or Y), and PDOF (-30° to 0°).

It is common for NASS/CDS cases to have fatalities with limited injury information, resulting in injury severity score (ISS) values of zero. Two of the fatalities in this study had these misleading ISS values. To better represent the severity of these injuries, they were given adjusted ISS values of 50. This estimate was based on the approximate average of the remaining six fatalities in the study. All ISS values included in the results are the adjusted ISS values.

The purpose of the present study was to analyze the injury mechanisms and crash characteristics in small overlap crashes that have some relevance to potential crash test scenarios. Cases with complicating factors such as multiple impacts, incorrect belt use, injuries caused by events unrelated to the primary impact, or injuries primarily due to pre-existing medical conditions were excluded.

RESULTS

A total of 21 cases met all inclusion criteria. The majority of the vehicles (17 of 21) had CDC codes with left horizontal damage (FLEE-10, FLAE-5, FLAW-2) denoting damage to the left third of the vehicle. Two of the vehicles had a left/center horizontal damage code (FYEW), and the remaining two vehicles were coded by NASS/CDS as having primary damage to the left plane (LYAW, LYES). The authors believe that the latter two vehicles actually were involved in small overlap frontal crashes. Both vehicles had initial contact on the bumper, had the wheels torn off the vehicle (rather than driven into the axle), and had longitudinal, as well as lateral, intrusion.

Fifteen of the case vehicles were cars and six were light trucks (pickups, SUVs, or vans). No case vehicles were minivans. Crash partners, in order of frequency, were light trucks (8), trees/posts/poles (TPP) (6), cars (3), minivans (2), and heavy vehicles (HV) (2). Heavy vehicles included a school bus and the rear

trailer tires on a tractor trailer. The combinations of case vehicles and crash partners are listed in Table 1, with TPP-HV denoting trees, posts, and poles combined with heavy vehicles. In 76% of the cases, the crash partner was a light truck or TPP-HV.

Table 1.
Case vehicle and crash partner combinations

Case vehicle	Crash partner	Number
Car	Car	3
Car	Minivan	2
Car	Light truck	5
Car	TPP-HV	5
Light truck	Light truck	3
Light truck	TPP-HV	3

All case vehicles had occupant compartment intrusion. Because the focus of this study was on life-threatening injuries to the driver, all intrusion values discussed in the paper are for the driver seating area (instrument panel, A-pillar, steering wheel, roof rail, door, etc.) and exclude measurements in the toepan region. Some vehicles had both longitudinal and lateral intrusion, although longitudinal intrusion generally was larger and occurred in more vehicles. Of the 21 vehicles, 16 had a maximum intrusion value that was longitudinal in direction, whereas 5 vehicles had a maximum lateral intrusion value. For the 18 vehicles with specific measurement values, the average maximum intrusion value was 32 cm. Vehicles with a maximum longitudinal intrusion had an average value of 34 cm, whereas vehicles with lateral intrusion had an average value of 25 cm.

To provide a comparison for the magnitude of intrusion in these vehicles, they were compared with those measured in the IIHS frontal offset crash test. Longitudinal intrusion at the left instrument panel is a common NASS/CDS measurement, and also is recorded by IIHS. There were 17 cases with measured longitudinal left instrument panel intrusion in which the same vehicle also had been tested by IIHS. The average IIHS intrusion value was 8 cm, whereas case vehicles had an average intrusion of 23 cm. When only the vehicles with maximum longitudinal intrusion (12) were included, the average IIHS intrusion value remained 8 cm, whereas the average vehicle intrusion increased to 29 cm. This comparison of instrument panel intrusion likely underestimates the difference in intrusion extent between these small overlap crashes and their frontal offset test counterparts because many of these vehicles had components with even higher intrusion values. These other components (A-pillar, steering wheel, roof rail) often were those contacted by the occupant resulting in injuries.

Eight of the 21 case vehicles did not have delta V values reconstructed, or the values were coded by investigators as “results appear low.” The remaining 13 vehicles had a mean value of 32 km/h (range 18-54 km/h). The method for determining delta V is based on stiffness estimates of a vehicle’s front structure, which are based on crash tests involving the longitudinal structural members. In small overlap crashes, these structures are not loaded, and in many cases the actual damage locations are not measured. For this reason, there is little confidence in the accuracy of the delta V estimates.

Case occupants had an average age of 44 years (range 19-69), with 15 males and 6 females. There were eight fatalities. Injury data for the drivers is shown in Figure 3. For two of the fatalities, there was limited injury information. For one driver, the only information was a statement by the investigator that the driver died of fatal head/neck injuries. This driver was assigned an AIS 6 head injury. For the second fatality, there was no injury information, and thus all data shown in Figure 3 is based on 20 occupants.

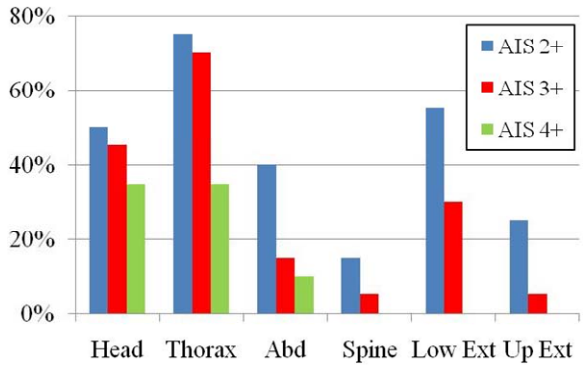

Figure 3. Percentage of drivers with injuries to each body region by AIS level.

For AIS 2+ injuries, the most commonly injured body regions were the thorax (75%), head/face (50%), lower extremities (55%), and abdomen (40%). For AIS 3+ injuries, the most commonly injured body regions were the thorax (70%), head/face (45%), and lower extremities (30%). These trends were slightly different for AIS 4+ injuries, for which injuries to the head/face and thorax were equal (35%). It should be noted that the percentage of lower extremity injuries was directly influenced by the study’s inclusion criteria, which excluded drivers whose only AIS 3+ injury was to lower (or upper) extremities.

There was a strong relationship between intrusion and injury severity. Figure 4 shows ISS values as a function of maximum occupant compartment intrusion.

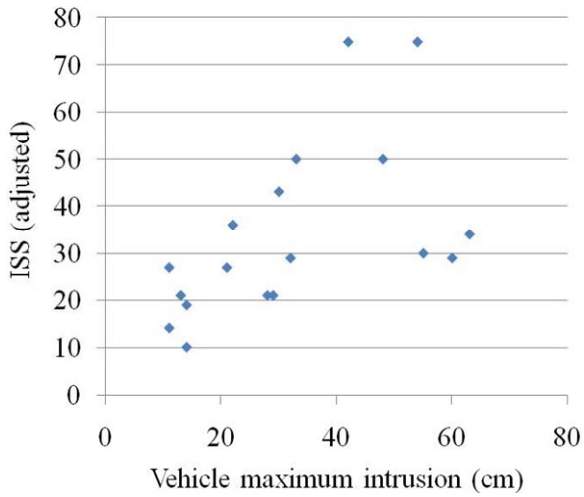

Figure 4. ISS as a function of vehicle intrusion.

For each driver's most severe injuries, a proposed injury mechanism was determined. This determination was based on vehicle intrusion patterns, injury information, occupant contact points, etc. For the majority of crashes, there was sufficient intrusion that injuries clearly were due to contact with interior structures, and even an optimal restraint system could not have prevented them. Three distinct patterns of intrusion were associated with these injuries (Table 2). Both lateral and longitudinal intrusions were observed. Injuries associated with longitudinal intrusion tended to be more severe than those associated with lateral intrusion. There were four cases, however, in which the proposed injury mechanism was due to a combination of loads produced by the restraint system and longitudinal intrusion. Although these cases were characterized by lower levels of intrusion (11-14 cm), contact with intruding structures could not be ruled out as a possible injury source.

Table 2.
Injury mechanisms, intrusion amounts, and injury severity scores

Injury mechanism	Cases	Intrusion	ISS
Longitudinal intrusion	7	54 cm (long)	49
Lateral intrusion	5	25 cm (lat)	23
Longitudinal and lateral intrusion	5	27 cm (long)	31
Longitudinal intrusion and restraint system	4	12 cm (long)	18

Although small overlap crashes are a relatively specific crash type, there still were several crash scenarios and damage patterns among the case vehicles. Crashes were further organized to capture these different crash scenarios based on several factors: crash partner, crash angle, and vehicle damage location.

Crash partners were divided into two categories: passenger vehicles and TPP-HV. Crash angles were classified as being either collinear or oblique. When a case vehicle and partner vehicle had similar damage patterns, crash angle was classified as collinear. However, if the partner vehicle's front damage was more horizontally distributed than that of the case vehicle, such that the partner vehicle's damage looked more like that associated with moderate overlap crashes, then the crash angle was classified as oblique. All of the crashes with different damage patterns for case and partner vehicles were described by NASS/CDS investigators as involving the partner vehicle crossing the roadway centerline and into the path of the case vehicle (Figure 5). The oblique nature of the crash could be caused either by the angle of the partner vehicle as it crossed the centerline or by the case vehicle steering away in a defensive maneuver. No attempt was made to further specify the oblique angle. All vehicles that struck TPP-HV were classified as collinear.

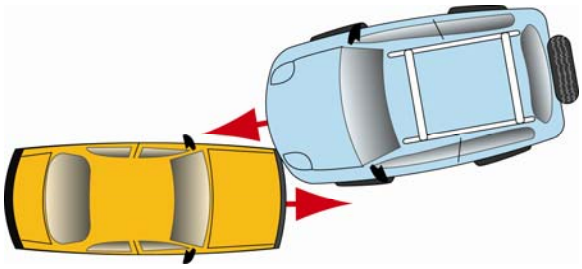

Figure 5. Diagram of vehicle-to-vehicle oblique small overlap crash (10° shown); case vehicle shown in yellow, partner vehicle in blue.

Vehicle damage location was divided into three possible groups: sideswipe, no sideswipe, and severe override. Sideswipe was defined as direct damage to the case vehicle by the partner vehicle rearward of the A-pillar. An example of sideswipe is shown in Figure 6. Induced damage to the occupant compartment — for example, rearward motion of the A-pillar resulting

Figure 6. Example of vehicle with sideswipe.

in driver door deformation — was not considered as sideswipe. There also were two cases with a distinctly different damage pattern in which there was severe override of the case vehicle and direct loading of the upper portion of the occupant compartment (Figure 7). In each case, the case vehicle was a car struck by an SUV. The distribution of the seven crash types and average ISS values is shown in Table 3.

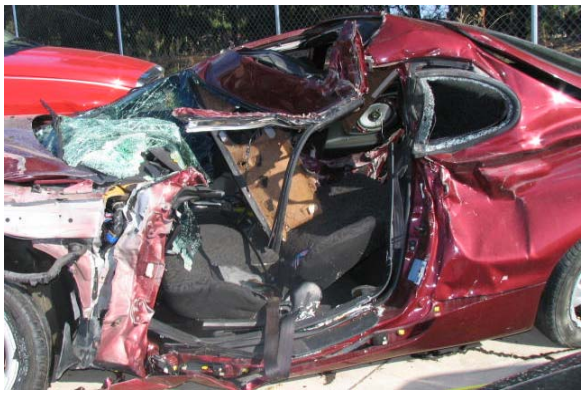

Figure 7. Example of vehicle with severe override.

Table 3.
Distribution of crash types
(number of cases) and ISS values

Small overlap crashes (21)						
		Passenger vehicle (13)				
TPP-HV (8)		Oblique (9)		Collinear (4)		
No side	Side	No side	Side	No side	Side	Over
(5)	(3)	(4)	(5)	(1)	(1)	(2)
ISS-25	ISS-35	ISS-57	ISS-27	ISS-19	ISS-10	ISS-31

Eighty-one percent of the cases (17 of 21) were either oblique crashes with passenger vehicles or crashes into TPP-HV. These two crash types also had the highest average ISS values, with the exception of the two severe override crashes. The remaining crashes were either vehicle-to-vehicle collinear crashes (two crashes with the lowest ISS values) or the two unusual severe override crashes.

Differences between sideswipe and no sideswipe crashes were caused by the initial impact location. In crashes with sideswipe damage, the partner vehicle struck the case vehicle farther outboard, engaging less of the vehicle front end than crashes without this damage. Sideswipe crashes also were more likely to result in injuries caused by lateral intrusion, with all but one sideswipe crash having lateral intrusion as a contributing factor.

DISCUSSION

The CDC designation often used to represent small overlap crashes, FLxx, accounted for only 81% of the cases identified in this study. Studies that limit their analyses to these CDC codes likely are missing a significant number of small overlap crashes. In fact, the definition of small overlap crashes in this study was relatively conservative, and it is likely there are additional cases with more damage to the longitudinal members that share many of the same factors.

The amount of occupant compartment intrusion was strongly related to injury severity. Previous attempts to correlate injury severity with other surrogates of crash severity (delta V, maximum vehicle crush, CDC extent zone) were not successful [8]. This likely was due to the fact that NASS/CDC measurement techniques and delta V reconstruction software are not particularly suited to small overlap crashes. The lack of confidence in the delta V estimates prevents determining whether differences in intrusion values were due to differences in crash severity or vehicle structural designs. The present study, however, shows a strong relationship between occupant compartment intrusion and injury severity.

Crashes into narrow objects and oblique crashes with other passenger vehicles accounted for the majority of cases in this study and resulted in some of the highest ISS values. It is not clear why collinear vehicle-to-vehicle crashes accounted for such a small number of cases. The study sample may not have been large enough to capture more cases. Another possibility is that these crashes result primarily in lower extremity injuries and not the severe injuries to the head, thorax, and abdomen that were required for inclusion in this study. One of the characteristics of many vehicle-to-vehicle small overlap crashes is the “rim-locking effect” resulting in significant deformation into the footwell area [9]. Studies of small overlap crashes including occupants with only serious lower extremity injuries likely will find crash populations with different characteristics.

Although there were few vehicle-to-vehicle collinear crashes, there were several vehicle-to-vehicle oblique crashes. In oblique crashes, the partner vehicle consistently had damage to a large proportion of the front end, including significant loading of the left longitudinal member. The oblique nature of these crashes likely allowed the partner vehicle to more fully engage the case vehicle, preventing a “sliding collision” or glance-off crash. Thus a greater proportion of the kinetic energy went into deformation of the occupant compartment of the case vehicle. Continued research

will focus on the importance of this oblique angle in vehicle-to-vehicle crashes.

The presence of sideswipe damage to a case vehicle was primarily a factor of the outboard location of the crash partner. These crashes were more likely to result in lateral intrusion and had lower ISS values than no sideswipe crashes (28 vs. 37 cm). Study vehicles all exhibited loading to the entire vertical profile of the front end because all had crashed into either a vehicle with an equal or taller profile or a TPP. None of the case vehicles had damage suggesting they had struck a vehicle with a shorter profile.

Crash tests devised to evaluate countermeasures for small overlap crashes should incorporate several factors. The test should fully engage the vehicle and occupant compartment in a longitudinal direction, rather than loading the vehicle far enough outboard to cause a sideswipe crash. The test barrier should be at least as high as current LTVs, if not higher. Shorter barriers will not engage the full vertical profile of the vehicle front end. The importance of the type of barrier (pole or simulated vehicle) or angle of impact (collinear or oblique) is not currently known. It should be noted, however, that these two different crash scenarios resulted in very similar damage patterns to the case vehicles in this study.

Small overlap crashes are defined as those in which the longitudinal members and other front structures typically designed to absorb crash energy are missed. Failure to engage this structure may account for the subsequent significant deformation of the occupant compartment that is the primary factor in the driver's injuries. Two countermeasures for this crash type are suggested in the literature. The first is a design that deflects the vehicles away from full engagement and result in "sliding collisions" [10]. Results suggest the potential for significant reductions in occupant compartment intrusions. The consequence, however, are vehicles that continue on the roadway in an uncontrolled manner. The possibility of secondary crashes should be considered. The second countermeasure involves modifications to the primary structural members of the vehicle front end, including increases to the width of these structures. Honda has redesigned many of its vehicle models to include this Advanced Compatibility Engineering™ (ACE™) structure [11]. Computer simulations show that the ACE™ structure, when compared with previous structural designs, reduces the amount of occupant compartment intrusion in small overlap vehicle-to-vehicle collinear crashes. The effect of these countermeasures in narrow object impacts or oblique vehicle crashes is not known.

CONCLUSIONS

Drivers in small overlap crashes are most likely to be seriously injured due to occupant compartment intrusion. There was a strong relationship between the magnitude of intrusion and injury severity. Among small overlap crashes with serious injuries, collinear crashes into narrow fixed objects and vehicle-to-vehicle crashes in which the partner vehicle strikes the case vehicle obliquely were the most common. Despite structural improvements prompted by frontal offset crash tests, this study suggests that vehicle structures must improve if they are to prevent occupant compartment intrusion when a vehicle is loaded outboard of the longitudinal members.

ACKNOWLEDGMENT

This work was supported by the Insurance Institute for Highway Safety.

REFERENCES

[1] Insurance Institute for Highway Safety. 2007. Fatality facts. Arlington, VA. Available: http://www.iihs.org/research/fatality_facts_2007/default.html

[2] Office of the Federal Register. 2008. Federal Register, vol. 73, no. 134, pp. 40016-40049. National Highway Traffic Safety Administration – Final decision notice. Docket no. NHTSA-2006-26555; Consumer Information; New Car Assessment Program. Washington, DC: National Archives and Records Administration.

[3] Brumbelow, M.L. and Zuby, D.S. 2009. Impact and injury patterns in frontal crashes of vehicles with good ratings for frontal crash protection. Paper no. 09-0257. *Proceedings of the 21st International Technical Conference on the Enhanced Safety of Vehicles*. Washington, DC: National Highway Traffic Safety Administration.

[4] Hobbs, C. 1991. The need for improved structural integrity in frontal car impacts. *Proceedings of the 13th International Conference on Experimental Safety Vehicles*. Paper no. S9-O-12. Washington, DC: National Highway Traffic Safety Administration.

[5] O'Neill, B.; Lund, A.K.; Zuby, D.S.; Preuss, C.A. 1994. Offset frontal impacts – a comparison of real-world crashes with laboratory tests. *Proceedings of the 14th International Technical Conference on the Enhanced Safety of Vehicles*. Paper no. 94-S4-O-19. Washington, DC: National Highway Traffic Safety Administration.

[6] Scheunert, D.; Justen, R.; Herrmann, R.; Zeidler, F.; Decker, J.; and Kallina, I. 1992. What is a realistic frontal offset test procedure? *Proceedings of the 1992 International IRCOBI Conference on the Biomechanics of Impacts*. Bron, France: International Research Council on the Biomechanics of Impacts.

[7] Lindquist, M.; Hall, A.; and Bjornstig, U. 2004. Car structural characteristics of fatal frontal crashes in Sweden. *International Journal of Crashworthiness* 9:587-97.

[8] Pintar, F.; Yoganandan, N.; and Maiman, D. 2008. Injury mechanisms and severity in narrow offset frontal impacts. *Proceedings of the 53rd Annual Conference of the Association for the Advancement of Automotive Medicine*. Des Plaines, IL: Association for the Advancement of Automotive Medicine.

[9] Eichberger, A.; Schimpl, W.; and Fellner, B. 2008. Development of a crash test configuration for car-to-car frontal collisions with small lateral overlap. *Conference Proceedings of the 17th Annual EVU Congress*. Graz, Austria: European Association for Accident Research and Analysis (EVU).

[10] Stephan, W.; Bernd, F.; Wilhelm, B.; and Hermann, S. 2001. Sliding collisions in case of frontal crash with small lateral offset. Graz, Austria: Steyr-Daimler-Puch Fahrzeugtechnik. Available: http://www.tuev-sued.de/uploads/images/1134986822332304384899/Winkler.pdf.

[11] Saito, M.; Gomi, T.; Taguchi, Y.; Yoshimoto, T.; and Sugimoto, T. 2003. Innovative body structure for the self-protection of a small car in a frontal vehicle-to-vehicle crash. Paper no. 239. *Proceedings of the 18th International Technical Conference on the Enhanced Safety of Vehicles* (CD-ROM) Washington, DC: National Highway Traffic Safety Administration.

A VALIDATED OBLIQUE POLE SIDE IMPACT SLED TEST METHOD FOR ANALYZING OCCUPANT RESPONSE

Jeff Dix
Hoon Lee
Nissan Technical Center North America Inc.
United States of America
Doug Stein
Autoliv North America
United States of America
Paper Number 09-0466

ABSTRACT

This paper describes a new test methodology for evaluating occupant injury response in a near side oblique pole impact per FMVSS 214. Given the complexity, time, and cost of using full vehicle pole impact crash tests to develop occupant restraint systems, it is desirable to have a simple test method that allows engineers to develop an optimized restraint system in a timely and cost effective manner. The authors will present a new sled test method that accurately simulates a full vehicle oblique pole side impact test using only minimal vehicle components. This test method was validated using both the ES2-RE representing an AM50 occupant and a SID IIs representing an AF05 occupant. The authors will provide data showing correlation with full scale oblique pole impact vehicle tests. Furthermore, to demonstrate the effectiveness of this test methodology a case study will be presented showing a restraint system that has been optimized for both AM50 and AF05 occupants in an oblique pole impact.

INTRODUCTION

In the mid 1990's, restraint system suppliers and vehicle manufacturers began implementing side impact restraint systems for head protection in side impact crashes involving narrow objects such as utility poles and trees. Starting with MY1999 passenger vehicles, the NHTSA made accommodations for this technology in the FMVSS 201 "Occupant Protection in Interior Impact" with the inclusion of an optional 24 km/h vehicle side impact (90 degrees) into a 254mm diameter rigid pole for vehicles equipped with a "dynamically deployed upper interior head protection system" [1]. On September 11, 2007 the NHTSA published a Final Rule incorporating a 32 km/h oblique (75 degree) lateral pole impact crash test into the FMVSS 214 "Side Impact Protection". In addition to head protection, this new regulation requires thorax, abdomen, and pelvis protection in lateral impacts for both 50th percentile male and 5th percentile small female drivers beginning with some MY2011 passenger vehicles [2]. Most recently (July 8th, 2008) the NHTSA issued a Final Notice of enhancements made to the USNCAP (New Car Assessment Program) to include the oblique pole impact crash test results with the 5th percentile small female in its 5-Star vehicle safety rating – beginning with MY2011 passenger cars [3].

Since the initial pole impact test requirement in FMVSS 201P evaluated only head injury potential; development of countermeasures for head protection could be accomplished through the use of linear impact tests with a full scale crash test used for final validation. As such, full scale sled testing was not required. A majority of side impact sled tests during this time were performed for the purpose of developing and evaluating side impact restraint systems for thorax, abdomen, and pelvic injury protection in a vehicle to vehicle crash. One such method, developed in 1994-95 [4] utilized an acceleration type sled with a sliding dolly affixed to simulate the rapid door intrusion into the passenger compartment; while also simulating the important characteristics of dummy-to-door trim geometry, gap closure timing, and door stiffness.

With the additional requirements of the oblique pole side impact test outlined in the upgraded FMVSS 214 regulation to include thorax, abdomen, and pelvis injury, a new pole side impact sled test method was developed. This sled test method can provide engineers a tool to develop optimized side impact countermeasures, such as side airbags, prior to conducting a full scale vehicle test. This new test method is, to a large degree, based on this earlier test device and the experience gained in more than 13 years of use, as well as those experiences from many full scale side impact crash tests and the development

of side impact restraints for both the moving barrier and pole impact test conditions.

TEST METHOD

This section describes the sled test method and apparatus in general terms only. It does not include significant detail on mounting the test specimen hardware or tuning the system to achieve the desired level of correlation. As is typical for side impact sled testing, these details are, to a large degree, dependant on the subject vehicle geometry and crush characteristics. The following section titled "Test Setup" will describe the process used to understand these variables and account for them in the test configuration.

Before discussing the sled test method, it is important for the reader to first consider certain characteristics of the full scale crash test (FMVSS 214 Oblique Pole Impact):

At the time of impact (T=0):

- the vehicle is traveling at a 15 degree crabbed angle (front angled toward pole) at a constant velocity of 32 km/h,
- the test dummy is traveling at a constant velocity of 32 km/h (same as vehicle) with it's head (center of gravity) aligned, in the direction of travel, with the centerline of the pole.
- the pole is fixed rigidly to earth. We could say that the pole is traveling at a constant velocity of zero.

After initial contact:

- The entire vehicle undergoes a change in velocity, with certain subcomponents (door, door trim, seat, roof rail, etc…) changing more quickly than others (accelerating toward the non-struck side of the vehicle).
- The test dummy also experiences a change in velocity, but not until it is acted on by certain other components (door trim, seat, roof rail, side airbag, curtain airbag, and pole).
- The pole does not change velocity. It maintains the constant speed of zero km/h throughout the duration of the test and beyond.

The device described here is designed for use with an acceleration type sled, but can be easily adapted for use with a deceleration sled application – the basic test method remains the same with respect to the configuration of the door, trim, seat, and test dummy. When used with an acceleration sled, the sled must be capable of achieving the impact test speed (32 km/h) then maintaining that speed for the duration of the test (up to 100 msec). The device used by the authors is an acceleration sled retrofitted with a servo-controlled carriage braking system.

As illustrated in Figure 1, the device consists of the main sled carriage with a rigid pole attached to it (a); a sliding dolly to which the door element, seat, and dummy are mounted (b); a seat slider for attaching the seat to the dolly (c); various crush elements (d), (e), and (f), and a position switch (g).

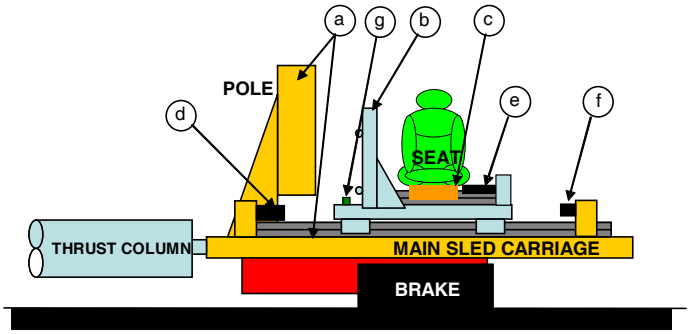

Figure 1. Schematic of test device

The test method proceeds as follows:

The main sled carriage and pole are accelerated to 32 km/h over a stroke of about 200mm, and then maintained at that speed under velocity based servo-control braking to counteract the thrust column forces still trying to accelerate the sled. The resulting velocity profile is shown in Figure 2.

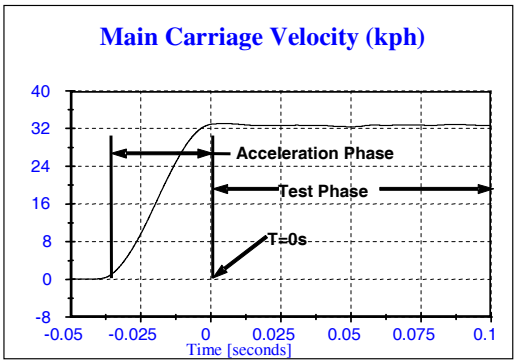

Figure 2. Sled carriage and pole velocity profile

The sliding dolly, in addition to the seat slider and seat, is built with two vertical pillars used to support the struck door components. The door components are supported by two (or more as needed) horizontal bars (1 inch electrical conduit) that are attached at each end to the vertical pillars using a sliding swivel arrangement, which allows the bars to deform toward the seat and occupant when struck by the pole. Once the door components are mounted to this structure, the seat is positioned on the slider such that its orientation with the door trim simulates the target vehicle geometry. A crush element (e) is then added to ensure the seat remains in contact with the door once it is struck, while still allowing the seat to travel with the door relative to the dolly to which they are both mounted (Figure 3).

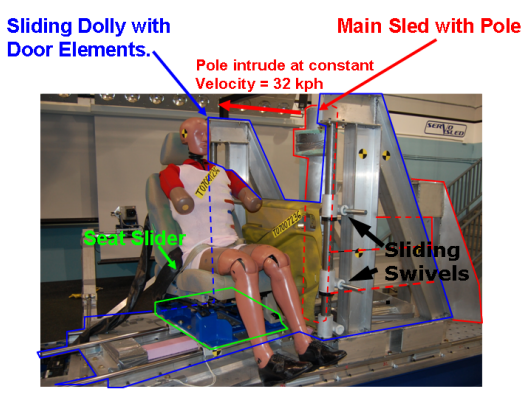

Figure 3. Test setup showing sliding swivel arrangement for mounting door components

This dolly assembly remains essentially motionless during the acceleration of the main sled due to its inertia and the low friction linear bearings used to attach it to the main sled.

When the pole (a) has achieved the impact speed and is at the initial vehicle contact position (measures the same distance from dummy head to pole as in full scale crash at T=0) a position switch (g) triggers T=0 for the data acquisition system and the airbag deployment timer. At this position (or slightly later – depending on the target vehicle characteristics) the sled/pole engage a crush element (d) sized to accelerate the dolly to simulate the motion of the target vehicle's center of gravity during the crash, thus simulating the body-side and floor structure stiffness. During this time the pole surface will also engage the door components and begin to deform them toward the test dummy. As the door components and conduit supports used in this method are not structurally significant the force required to deform them has very little influence on the acceleration of the dolly.

From there, the pole surface, and deformed door components continue at constant velocity (32 km/h) as the vehicle's dummy-to-door "gap closure" is reproduced, and finally – the seat and test dummy are impacted. When the relevant portion of the test is complete, the on-board brakes for the carriage safely stop the entire assembly, with the crush element (f) allowing the dolly to gently couple with the sled carriage during this deceleration phase.

TEST SETUP

A primary goal of this activity was to develop a test method that was reasonably simple and economical to setup and use with a minimum of vehicle components required. In order to achieve this goal the following assumptions were made.

1. As noted in the introduction, the purpose for the development of this test method was to provide a way to evaluate restraint systems to reduce thorax, abdomen, and pelvis injury. Because head injury performance can be more easily evaluated using linear impact component testing, this sled test method is not recommended for developing the curtain airbag. As such, the curtain airbag was included in the sled test only to provide the correct occupant kinematics, and was simplified as follows:

    a. The curtain airbag was modeled as a bladder that was constructed from the front row chambers of the inflatable curtain airbag for each of the tested vehicles.

    b. The bladder was unrolled in the pre-test condition, and pressurized to the correct pressure using shop air before the test.

c. The bladder was tethered to the front and rear uprights on the sliding dolly in the correct location relative to the vehicle in the fore and aft position.

2. The coupling between the occupant and the vehicle through the seatbelt was assumed to be negligible. Therefore, the seatbelt was omitted in order to simplify the test fixturing and setup. As a result the occupant kinematics during rebound is not valid.

3. In a full vehicle test the door structure is crushed and stopped by the pole before significant loading of the restraint system by the occupant occurs. Therefore, it is assumed that door structure can be simplified as follows

   a. Provide the door trim and its mounting structure only.

   b. Include any hard components that the dummy may interact with (i.e., window regulator motor, …)

4. In order to reproduce the side airbag deployment path in the vehicle; a piece of foam was used to represent the surface of the B-Pillar trim (ES2-RE).

Reference Table 1, for a summary of the components used for this correlation activity.

Table 1.
Components included in testing.

	Curtain Airbag	Seat	Seat-belt	Side Airbag	B-Pillar	Door Trim	Door
Vehicle Test	O	O	O	O	O	O	O
Sled Test	Δ	O	X	O	Δ*	O	Δ

* For ES2-RE setup only.
O Included
Δ Simplified Structure
X Not included

Figure 4 shows the test setup used for this testing for each of the test configurations considered; ES2-RE and SID IIs dummies as well as SUV and Sedan vehicles.

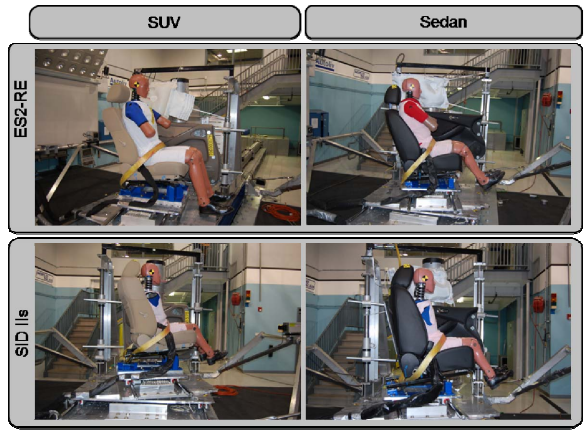

Figure 4. Test setup

In order to achieve the correct gap closure between the door trim and the seat for the side airbag deployment the stiffness of crush element (d) (reference Figure 1) was tuned such that the velocity of the sliding dolly (to which the door components and the seat are mounted) matched the test vehicle's velocity measured at the center of gravity. Injury for the vehicle tests being correlated to occurred at ~50 ms; therefore, the sliding dolly velocity was correlated to the vehicle test through 60 ms to ensure correlation during dummy loading.

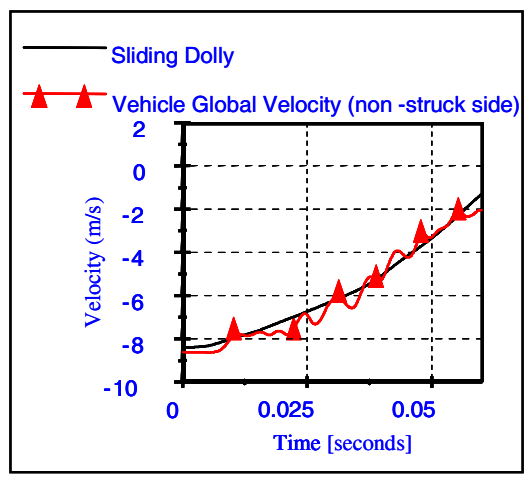

Figure 5. Sliding dolly velocity

CORRELATION

Correlation was achieved using both SID IIs and ES2-RE dummies for both an SUV and a sedan vehicle. The two vehicles were confirmed in order to verify that this test method can be applied to a wide range of vehicle architectures.

Agreement between the sled and vehicle tests was confirmed by normalizing the sled test result with respect to the vehicle test with 1.0 being a perfect agreement between the two tests. For the purposes of this paper a normalized injury of between 0.8 and 1.2 (+/- 20 percent) was judged to be an acceptable agreement. Overall both the SUV and sedan vehicles' normalized injury for the SID IIs dummy was within the acceptable range (Figure 6). The only exception was the iliac force in the SUV environment; which was significantly more than the vehicle test (2.35 normalized injury). The acetablum matched the vehicle test very well for both peak values as well as the shape of the curve. Furthermore, the pelvis acceleration for both the sled and vehicle tests also matched very well indicating that the total loading on the pelvis was very similar in the sled and vehicle tests. The SID IIs dummy used in the SUV vehicle test was instrumented with a build level 'C' iliac wing and did not have the enhancements, which correct the potential of the load cell under reporting the force level [5]. The dummy used in the sled testing was instrumented with a build level 'D' iliac wing. It is believed that the reason for the differences in the iliac load between the sled and SUV vehicle test is due to the load cell under reporting the force level in the vehicle test. This is further supported by the fact that the pelvis loading in the sedan environment agreed very well with the vehicle test as can be seen in Figure 7. In the case of the sedan vehicle, both the vehicle and sled tests were conducted with a dummy instrumented with the level 'D' iliac load cell.

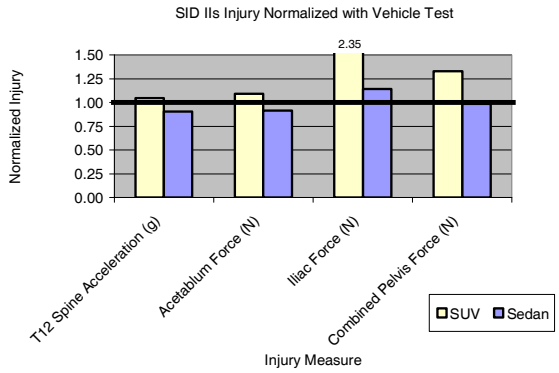

Figure 6. SID IIs injury agreement

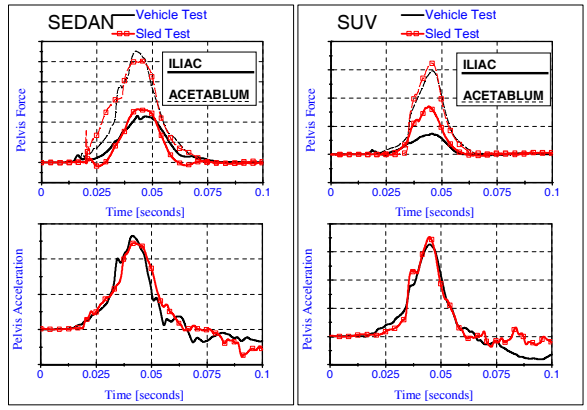

Figure 7. SID IIs pelvis loading time history

Figure 8 summarizes the results of the ES2-RE testing. The abdominal force for both vehicle environments as well as the pubic force for the sedan environment achieved the acceptable normalized injury range of 0.8 to 1.2. However, the rib deflection for both vehicle environments as well as the pubic force for the SUV environment was not within the acceptable range.

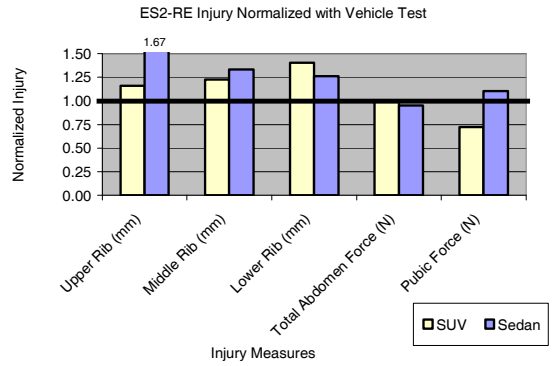

Figure 8. ES2-RE injury agreement

Sled testing of both the SUV and the sedan environments consistently showed higher rib deflections for the ES2-RE Dummy. Analysis of the dummy kinematics for the vehicle and sled testing indicated that the seatbelt affected the kinematics of the thorax. In the sled test the dummy torso rotates counterclockwise in the plan-view towards the pole as the dummy is impacted. However, in the vehicle test the seatbelt tended to restrict this motion. Based on these findings the test fixture for the SUV was modified to include the seatbelt. With the addition of the seatbelt the dummy kinematics matched the vehicle test much better, reducing the amount of torso rotation in the plan-view (Figure 9). Furthermore the rib deflections matched the vehicle test well (Figure

10 & 11). As a result it was concluded that the seatbelt must be included in the sled test in order to achieve acceptable agreement of the rib deflection.

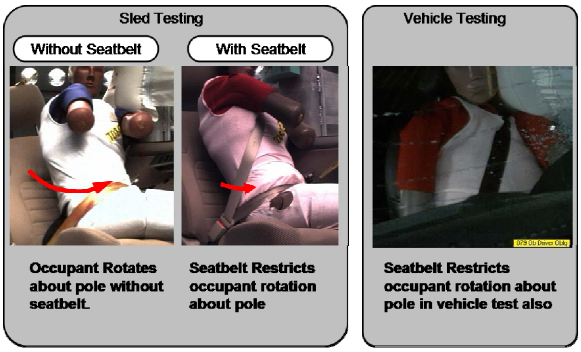

Figure 9. Seatbelt influence on ES2-RE dummy kinematics

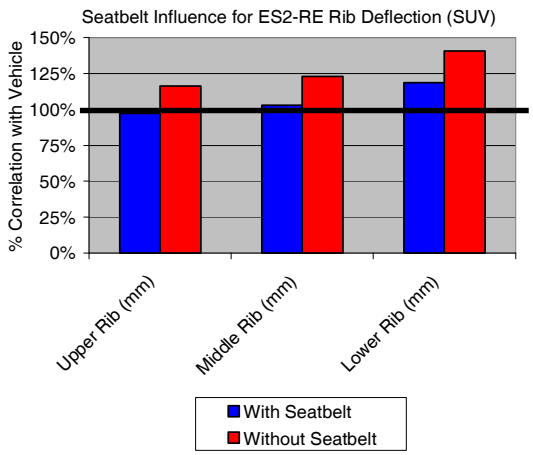

Figure 10. Seatbelt influence on ES2-RE rib deflections (SUV)

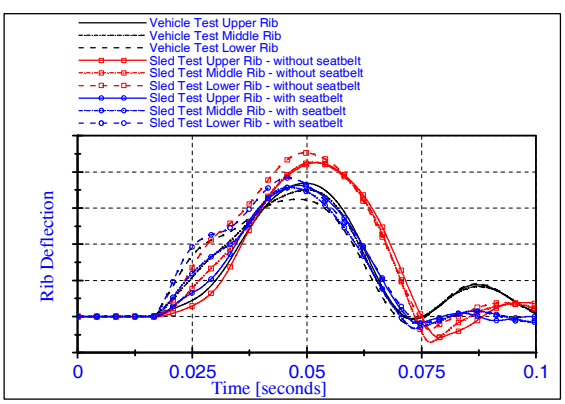

Figure 11. Seatbelt influence on ES2-RE rib deflections time history (SUV).

The pubic force for the SUV environment was slightly below the acceptable range with a normalized injury of 0.73, 27 percent lower than the vehicle test. It is believed that the reduced pubic force level observed in the sled test is due to the lack of the interior components and floor structure included in the sled test. In the vehicle test there are two forces applied on the dummy pelvis. The first being (F_1) the external force applied on the dummy pelvis by the pole impact. The second force (F_2) is the reaction force resulting from the inboard side of the dummy interacting with the vehicle interior components such as the center console. In the vehicle test the net force measured by the ES2-RE pubic load cell is the summation of these two forces ($F_{Total} = F_1 + F_2$). In the sled test the reaction force F_2 is not accounted for because the vehicle's interior components and floor are not included resulting in a lower pubic force (Figure 12).

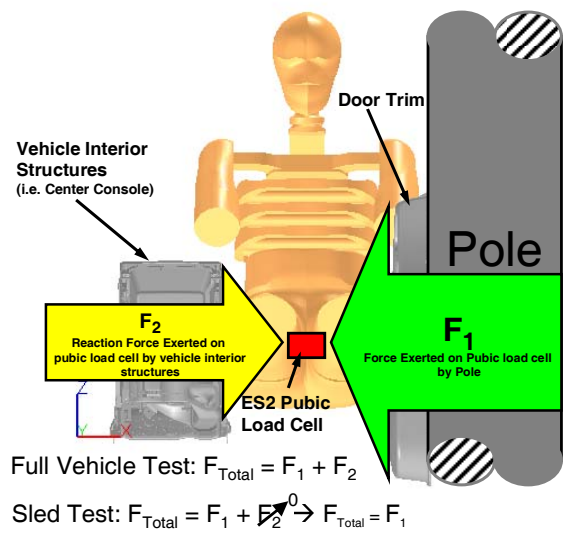

Figure 12. ES2-RE pelvis loading

Further testing is required in order to verify if this theory is correct. It may be possible to improve the agreement of the pubic force by including the center console structure in the sled testing. However, given the desire to maintain the simplicity of the test setup the authors feel the current level of correlation is acceptable especially given the agreement level of the pelvis acceleration (Figure 13) which can be used to predict the pubic force in the vehicle test. However, care should be taken to understand the relationship between the pubic force and the pelvis acceleration for the subject vehicle, as it may vary from vehicle to vehicle depending on the vehicle layout.

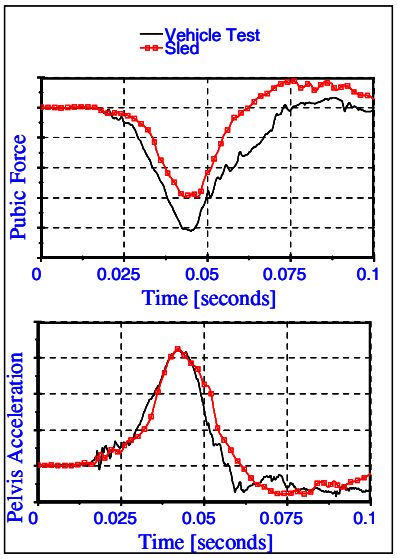

Figure 13. ES2-RE pubic force (SUV)

SIDE AIRBAG OPTIMIZATION CASE STUDY

In order to demonstrate the effectiveness of this test methodology, a case study using the SUV environment was conducted. The goal of this study was to optimize the side airbag to reduce the ES2-RE average rib deflections by 20% while reducing the injury levels for the other ES2-RE body regions as well as for the SID IIs by as much as possible. A design of experiments approach was used for this testing with the following variable being considered:

1. Three inflators were considered for this study which will be referred to as inflators: A, B, and C (inflator 'A' is the baseline inflator)

2. Two side airbag cushion types were considered for this study. The first being a single chamber cushion that provides coverage to the thorax and pelvis (baseline). The second type of cushion considered was a dual chamber pelvis – thorax cushion. The two chambers were created by the addition of internal baffle in the single chamber cushion that was positioned between the thorax and pelvis portions of the airbag. The intent is to maintain a higher pressure in the pelvis chamber to increase the energy absorption of the pelvis. Figure 14 shows the two cushion shapes evaluated.

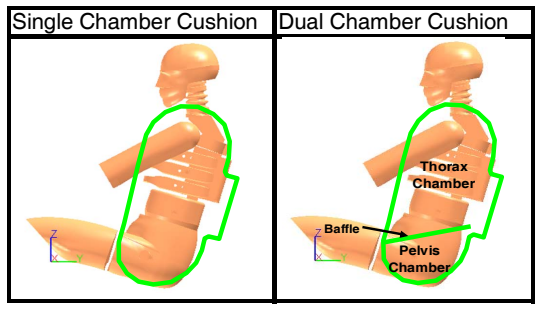

Figure 14. Side airbag cushion configurations evaluated

3. The third variable considered was the vent size to determine the optimal stiffness considering both the AM50 and AF05 occupants.

The test matrix for the ES2-RE dummy was conducted first to determine the optimal bag configuration to reduce the rib deflections (inflator, cushion type, and vent size). Once this was completed a small test series was completed for the SID IIs varying the vent size to determine the optimal bag stiffness for the ES2 and SID IIs dummies. Table 2 outlines the approach used for the sled testing.

Table 2.
Testing approach.

Occupant			Series 1 AM50 (ES2-RE)	Series 2 AF05 (SID IIs)
Side Airbag Parameters	Inflator	'A' (Baseline)	O	
		'B'	O	
		'C'	O	
	Cushion Type	Single Chamber *(without baffle)*	O	
		Pelvis / Thorax Dual chamber *(with baffle)*	O	
	Vent Diameter		20 mm 25 mm 30 mm 35 mm 40 mm	20 mm 30 mm 40 mm

For the purpose of this study all injuries were normalized with respect to the baseline test results to allow for easy comparison. The baseline side airbag specification is as follows:

- Inflator ‘A’
- Single chamber cushion
- Vent = 32mm Diameter

Inflator ‘B’ showed better performance for all body regions with the largest improvement in the average rib deflection (Figure 15). Therefore, Inflator ‘B’ was chosen as the optimal inflator. The Dual chamber cushion showed a slight improvement for the pelvis injury (4%). However, both average rib deflection and abdominal force were worse with the dual chamber cushion (8%, and 11% respectively). Since average rib deflection was the primary criteria being optimized the single chamber cushion was selected as the optimal cushion type (Figure 16). From the sensitivity analysis it was found that vent sizes ranging from 27mm to 37mm diameter achieved the target of 0.8 normalized injury for the ES2-RE average rib deflection (Figure 17). Furthermore the abdomen and pelvis injury was better for the ES2-RE with the smaller vent sizes. Therefore the optimal vent sized for the ES2-RE was determined to be a 27mm diameter based on achieving the 0.8 normalized injury for the ES2-RE average rib deflection and minimizing the injuries to the other body regions.

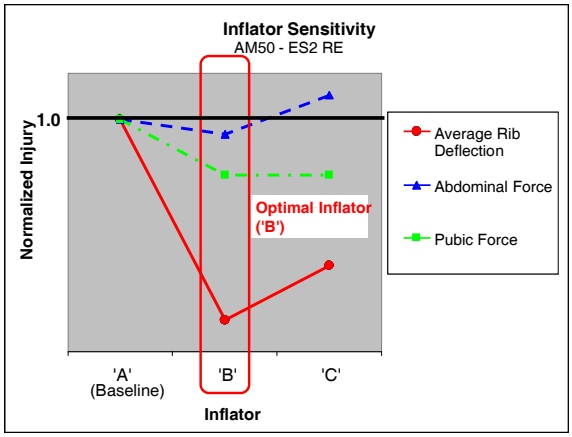

Figure 15. Inflator sensitivity for the ES2-RE injury measures.

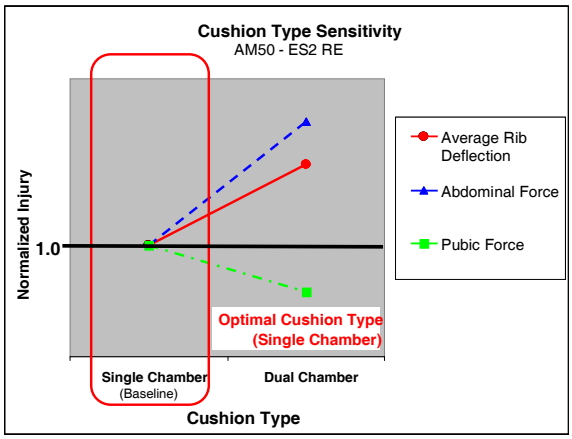

Figure 16. Cushion type sensitivity for the ES2-RE injury measures.

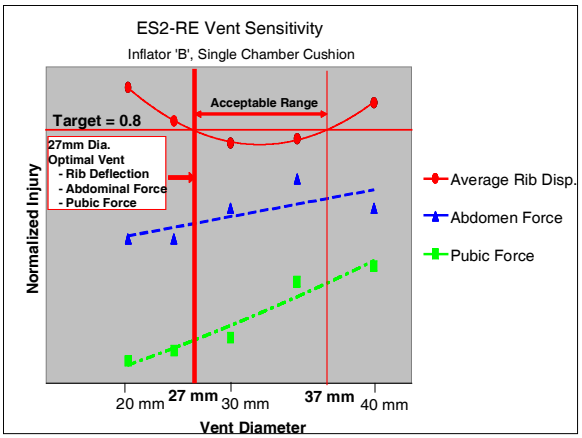

Figure 17. Airbag vent size sensitivity for the ES2-RE injury measures (inflator ‘B’, single chamber cushion data shown)

Once the optimal side airbag specification for the ES2-RE was determined a second test series was conducted for the SID IIs dummy. For this series the vent size was varied using Inflator ‘B’ with the single chamber cushion in order to determine the optimal vent size to minimize the injury for the SID IIs while achieving the target performance for the ES2-RE average rib deflection. Figure 18 shows the vent sensitivity for the SID IIs with the acceptable range for the ES2-RE average rib deflection (Inflator ‘B’, single chamber cushion). As with the ES2-RE dummy the injury results for the SID IIs were also found to improve with a smaller vent size. As a result the optimal vent size for the SID IIs was judged to be a diameter of 27mm (same as the ES2-RE). Therefore, the optimal side airbag specification considering both ES2-RE and SID IIs dummies was determined to be:

- Inflator: 'B'
- Cushion Type: Single chamber
- Vent size: 27 mm Diameter

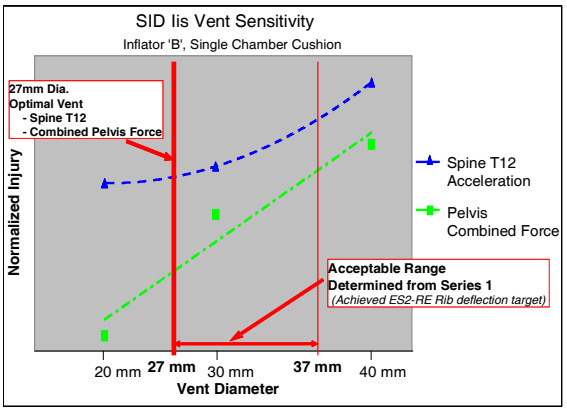

Figure 18. Airbag vent size sensitivity for the SID IIs injury measures (inflator 'B', single chamber cushion)

Through the use of this test method the target of reducing the ES2-RE average rib deflection by 20% while improving all other injury measures for both ES2-RE and SID IIs dummies was achieved with a minimum number to test components. Figure 19 summarizes the injury results of the optimized side airbag for both the ES2-RE and SID IIs dummies.

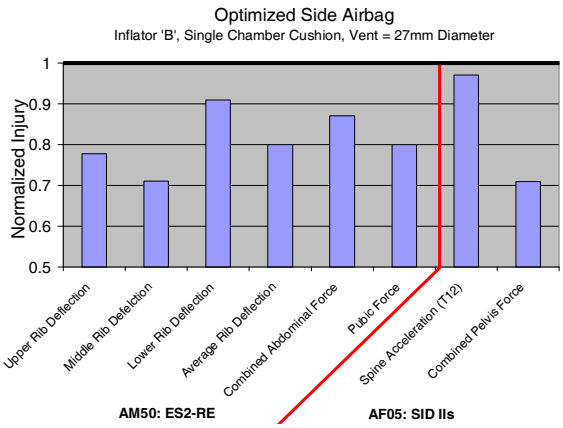

Figure 19. Optimized Side Airbag Normalized Injury for the ES2-RE and SID IIs dummies.

CONCLUSION

- This test method provides good correlation to vehicle testing while using a minimum number of components. Correlation was shown for a wide range of occupant sizes and seating positions as well as vehicle architectures.
- Through the case study presented the authors showed this test method to be an effective tool for developing optimized side impact restraint systems.

ACKNOWLEDGMENTS

The authors would like to thank our colleagues for their technical and analytical support. We would like to thank the following people in particular for their support on this project: Koichi Sagawa, Erik Robins, Dan Steimke, Lois Mueller, Christina Morris, Jennifer Pranke, and Analia Jarvis, Ron Parrott, Andy Young, Nate Schlis, Jim King, Mike Manicai, David Crumb, Kevin Stephen, and Chuck Sherwin.

REFERENCES

1. Department of Transportation, Standard No. 201 Occupant Protection in Interior Impact, Part 571.201
2. Department of Transportation, FMVSS 214 Final Rule, Docket No. NHTSA-2007-2934
3. Department of Transportation, New Car Assessment Program, Final Decision Notice, Docket No. NHTSA- 2006-26555
4. D. Stein, Apparatus and Method for Side Impact Testing, SAE Paper No. 970572
5. First Technology Safety Systems, SID IIs SBL D service bulletin

DEVELOPMENT OF A COUNTERMEASURE AIRBAG TO MINIMISE THE RISK OF SERIOUS INJURY FROM INTERACTION WITH AN ADJACENT OCCUPANT OR FAR-SIDE INTERIOR IN SIDE IMPACT CRASHES

Joon-Geun Cha, Il-Sang Kim

Hyundai Motor Company

Republic of Korea

Thomas Belcher, Suzanne Tylko, Ola Bostrom, Hee Loong Wong

Australian Government, Transport Canada, Autoliv Research, HMCA

Paper Number 09-0467

ABSTRACT

In current production vehicles, passive safety systems for the protection of vehicle occupants exposed to side impact crashes have primarily been designed to reduce the risk of injury to the occupant seated on the struck side of the vehicle from interaction with the intruding structure and/or external objects. However, occupants involved in side impact crashes may also be injured due to interaction with an adjacent occupant, and a single occupant seated on the non-struck side of a vehicle may be injured due to interaction with the vehicle far-side interior.

This paper reports on the results of a 32 km/h full scale vehicle-to-pole side impact crash test conducted using a small hatchback vehicle mounted on a carrier sled at 75 degrees to the direction of travel. A single WorldSID dummy was positioned on the non-struck side of the vehicle and a countermeasure airbag was deployed on the inboard side of each front row seat. The countermeasure airbags used in this test are designed to provide side support to vehicle occupants involved in side impact crashes to limit lateral excursion and reduce the likelihood of serious injury due to interaction with an adjacent occupant or vehicle far-side interior.

The results of this single occupant test are compared to results obtained from an earlier investigation of occupant-to-occupant interaction, in which the countermeasure airbags were observed to reduce the risk of head injury from occupant interaction. In the single dummy occupant test reported in this paper, the countermeasure airbags successfully prevented the dummy from interacting with the pole and intruding far-side interior of the vehicle.

INTRODUCTION

According to the results of analysis of NASS/CDS from 1993 to 2006 by Gabler et al in 2008, the relative risk of non-struck side driver is increased to 3.2 times when driver is with an unbelted right front passenger as compared to the belted driver [2][3].

Figure 1. Relative risk of driver in side impact crash from 1993 to 2006 NASS/CDS

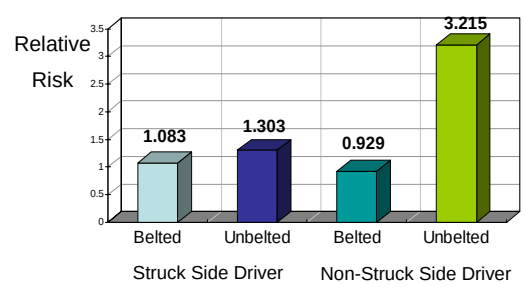

$$\text{Risk} = \frac{\text{Number of MAIS 3+ Drivers Exposed to Side Crash}}{\text{Number of Drivers Exposed to Side Crash}}$$

$$\text{Relative Risk} = \frac{\text{Risk of MAIS3+ with Right Front Passenger}}{\text{Risk of MAIS3+ without Right Front Passenger}}$$

Current Seat Belt Systems for Side Impact

In 1991 Mackay et al found the conventional seat belt system was not designed for protection in far side crashes [1]. The observations from real world crashes indicate that the occupants slipped out of the shoulder belt approximately 35% of the time. The belt system could therefore be improved to enhance the restraint performance for occupants on both the struck side and non-struck side.

Figure 2. Seat belt system without the pretension function.

Side support airbag and belt pretensioner as Countermeasures

The countermeasure airbags used in this test are designed to provide side support to vehicle occupants involved in side impact crashes to limit lateral excursion and reduce the likelihood of serious injury due to interaction with an adjacent occupant or vehicle far-side interior.

The side support airbag was designed by Autoliv, Sweden. The size of container is 90 x 120 x 200 (Depth x Width x Height). The volume of side support airbag (SS Bag) is about 3 liters. The pressure of proto stage SS bag is 2 bars.

And the seat belt pretensioner is activated in 9 msec from start the crash. The designated stroke of the pretensioner is 100 mm.

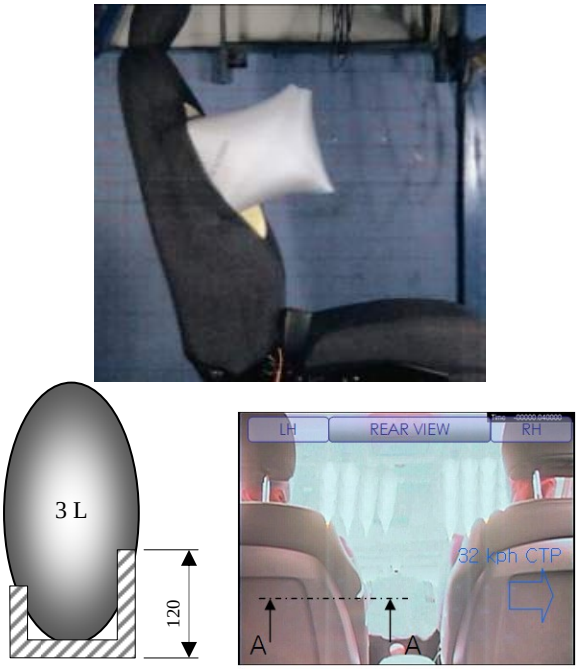

Figure 3. Side support airbag manufactured by Autoliv.

Table 1. Dimension of side support airbag

Items	Description
Container Size	90 x 120 (H 200)
Bag Volume	3 Liters
Bag Pressure	2 Bars
Time to deploy	10 msec
Vent	Non

Figure 4. Seat belt system with the pretension function.

CRASH TESTS, Test 1 and Test 2

Newland et al studied the impact injury risk from the occupant-to-occupant interaction in side impact crashes in 2008 [2]. They found that the occupant interaction indicating risk of serious head injury to both the driver and front seat passenger was observed in vehicle to pole side impact. The results show that despite the introduction of countermeasures to protect struck side occupants from contact to intruding structure or external objects, these occupants may be severely injured by impacting adjacent occupants. The feasibility of a potential countermeasure, developed to offer protection for two adjacent occupants as well as a single occupant seated on the non-struck side, was investigated through analysis of the dummy injury responses produced in pole side impact tests, with and without the countermeasure installed. The countermeasure was observed to reduce the risk of head injury from occupant interaction.

Table 2. Configuration of side impact crash tests for Test 1 and Test 2

Items	Description
Vehicle Impact Speed	32 kph
Pole diameter	254 mm
Impact angle	75 degrees
Test Dummies	Two WorldSIDs
Impact Type	Car-to-Pole

Table 3. Restraint system conditions

Items	Test 1	Test 2
Side airbag for thorax and pelvis	X	X
Curtain airbag for head	X	X
Pyrotechnic seat belt pretensioner		X
Side Support airbag		X

Figure 5. shows the movement of dummies in different configurations. In Test 1 without countermeasure, driver was impacted by the intruding vehicle interior first. The driver was rebounded to passenger side. And then HIC was recorded over 8,000 on both dummies in second impact. But in Test 2 with countermeasure, driver and passenger were well protected by side support airbag and seat belt pretensioner.

Figure 5. Worldsid trajectory, Test 1 (left) and Test 2 (Right).

Figure 6. 32 kph car-to-pole side impact crash.

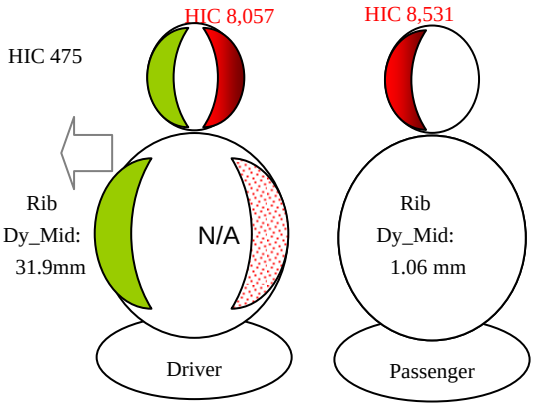

Figure 7. Dummy Injuries, Test 1

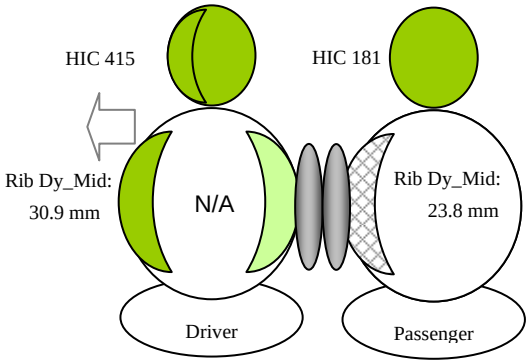

Figure 8. Dummy Injuries, Test 2

CRASH TESTS – Occupant to Far-side interior

Following the study reported by Newland et al [2], another 32 km/h full scale vehicle-to-pole side impact crash tests has been conducted using the same small hatchback vehicle mounted on a carrier sled at 75 degrees to the direction of travel. A single WorldSID dummy was positioned on the non-struck side of the vehicle and a countermeasure airbag was deployed on the inboard side of each front row seat. The countermeasure airbags used in this test are designed to provide side support to vehicle occupants involved in side impact crashes to limit lateral excursion and reduce the likelihood of serious injury due to interaction with an adjacent occupant or vehicle far-side interior.

Figure 9. 32 kph car-to-pole side impact crash.

Figure 10. WorldSID trajectory, Occupant to Far-side interior.

Figure 10. shows the movement of dummy in almost same configuration with Test 2. In this occupant to far-side interior, driver was resisted by the side support airbag. HIC was recorded just 48.9 and rib displacement was just 4.3 mm.

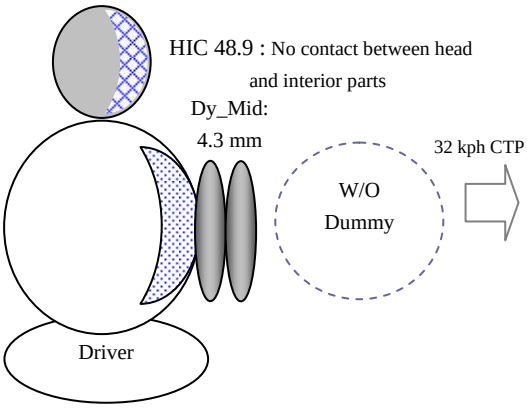

Figure 11. Dummy injuries, Occupant to far-side interior.

ANALYSIS OF CRASH TEST

The main focus of this test was to confirm the avoidance of severe contact between the head and interior parts. To develop the side support airbag, we considered the severe condition of no occupant on the struck side and there is an occupant on the non-struck side.

In this test there are no contact between head and vehicle interior parts. And the injuries of dummy were very low.

CONCLUSIONS

The results of this single occupant test are compared to results obtained from an earlier investigation of occupant-to-occupant interaction, in which the countermeasure airbags were observed to reduce the risk of head injury from occupant interaction. In the single dummy occupant test reported in this paper, the countermeasure airbags successfully prevented the dummy from interacting with the pole and intruding far-side interior of the vehicle.

To develop the side support airbag for production, we have to consider many possible scenarios. In addition, the kinematic of the WorldSID was further analyzed for its biofidelity in this single occupant crash simulation which could lead to further verification by utilizing cadaver testing.

REFERENCES

[1] G. M. Mackay, J Hill, S. Pakin, J. A. R. Munns, 'Restrained Occupants on the Non-struck side in Lateral Collisions', Proceedings of 13th ESV Conference, Paris, France, 1991.

[2] Craig Newland, Thomas Belcher, Ola Bostrom, Hampton C. Gabler, Joon-Geun Cha, Hee Long Woong, Suzanne Tylko, Ross Dal Nevo, 'Occupant-to-Occupant Interaction and Impact Injury Risk in Side Impact Crashes', Stapp Car Crash Journal, Vol. 52, San Antonio, U.S.A., 2008.

[3] H. C. Gabler, M. Fitzharris, J. Scully, B. N. Fildes, K.Digges, L. Sparke, 'Far Side Impact Injury Risk for Belted Occupants in Australia and the United States', Proceedings of 19th ESV Conference, U.S.A, Washington D.C., 2005.

REAR SEAT OCCUPANT PROTECTION IN FAR SIDE CRASHES

Jörg Hoffmann
Toyoda Gosei Europe N.V.
Germany
Kenji Hayakawa
Takaki Fukuyama
TOYODA GOSEI CO., LTD.
Japan
Paper Number 09-0475

ABSTRACT

The risk of being injured in side impact crashes is very high. Accident statistics show that numbers of vehicle occupants severely injured or killed of non-struck side occupants is approximately 30 percent. Based on accident data from the National Automotive Sampling System/Crash Data Study (NASS/CDS) an investigation concerning injuries and their levels of non-struck side occupants in side impact crashes was carried out. From the accident data, covering the years from 1998 to 2007, the injured body parts, their injury levels and the vehicle parts causing these injuries were analysed. The study showed that hard contacts between the occupants and the rigid vehicle parts cause most severe injuries. As a result of the accident analysis an occupant protection concept for non-struck side occupants on vehicle rear seat was designed. A numerical simulation model representing a non-struck side occupant, its vehicle environment and the airbag based protection system was set up to investigate different parameters, such as airbag shape and position, different dummy types and seating positions. Prototypes of the airbag concept were built and validated in sled tests. The study showed that this occupant protection concept is able to reduce the severity of head and chest injuries of non-struck side occupants in side impact accidents. Furthermore, a positive effect on the interaction between rear seated occupants in side impact crashes was observed.

Keywords: Side crash, airbag, rear seated passengers

INTRODUCTION

Today, research in side impact, side impact regulations and safety systems is mainly carried out in order to protect vehicle occupants seated on struck side of the car. However, far-side occupants, those located on the side opposite the lateral impact are also of risk of injuries during a side impact crash (Digges and Dalmotars, 2001). The protection of occupants seated on non-struck side of the passenger vehicle is not considered yet.

The objective of this study was to examine injury patterns of non-struck side passengers seated on the rear row of the car during collision. From accident analysis, a crash test scenario was derived and extensive numerical simulations were conducted to better understand the occupant kinematics that causes the most frequent injuries. Based on this work a protection system was proposed and its performance to protect the occupants was investigated.

ACCIDENT INVESTIGATION

The United States National Highway Traffic Safety Administration (NHTSA) investigates 4,000 to 5,000 crashes each year and provides the data in the National Automotive Sampling System / Crashworthiness Data System (NASS/CDS) database. The accident analysis presented in this paper was based on the examination of NASS/CDS data extracted from the files of the years 1998 to 2007.

The analysis which follows focuses on occupants of passenger vehicles subjected to far side impact. The investigation was limited to passenger cars as well as light and heavy trucks. Only occupants that were restraint by a three-point safety belt were included in the study. Children younger than six years and smaller than 120 cm were excluded from the study.

When reviewing NASS/CDS data according to the selected parameters, 2264 cases of belted passengers seated in the front row, and 190 cases of belted passengers seated on rear row injured according to MAIS1+ were found. Of these 517 front passengers and only a small number of rear passengers, 28 cases, were injured according to MAIS3+. In the following Figure 1 the ratio of serious injured occupants to all injured occupants (MAIS3+/MAIS1+) in far side crashes is shown for front and rear passengers.

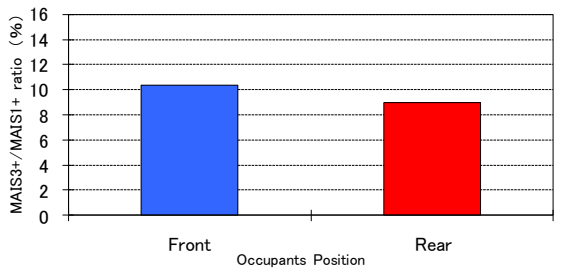

Figure 1: Accident ratio of far side impact accident seated in front and rear row

Far side struck occupants have a significant risk of injury. The fraction of all occupants who experienced serious injuries in a far side impact account for 11.7% on front row and 9.0% on rear row.

Based on the data obtained from the NASS/CDS database the sources causing MAIS3+ injuries were also derived. Figure 2 depicts the distribution of far side injuries, sorted by region, that were found for 517 cases of front seated passengers.

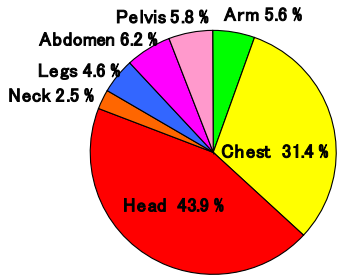

Figure 2: Injured body regions of front seated passengers suffered in far side impact

Head injuries account for more than forty percent of all MAIS3+ injuries, the largest fraction of all. The chest incurred about one-third of all injuries. Abdomen and pelvis are less injured body regions during the vehicle accident.

In the database 28 cases were recorded for rear seated passengers injured on MAIS3+ level. Here, head injuries account for more than one-third of injuries caused by a far side impact, which is shown in Figure 3. The risk of being injured in the chest area is about one-third and abdomen 10% of all.

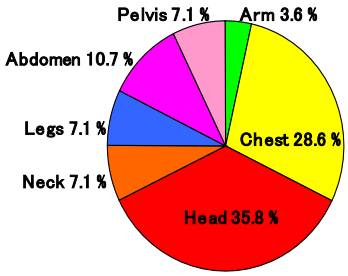

Figure 3: Injured body regions of rear seated passengers suffered from in side impact

As it was shown in Figure 2 and Figure 3, the distribution of far side impact by body region is very similar for both front and the rear seated occupants. Head and chest are most at risk followed by abdominal injuries. Overall, these injuries account for approximately three-third of all injuries reported in the NASS/CDS database.

Sources causing MAIS3+ injuries were analysed next and subdivided into near side interior, belt & buckle, other occupant, seat back and floor & console or roof. It appears that a hard contact of the human body part with the near side interior, the vehicle side facing the impact, is the main source of injuries front seated passengers suffer from (Figure 4). This was found for one-third of the injuries.

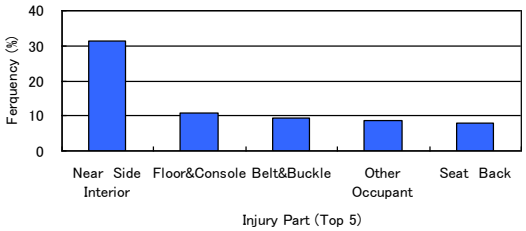

Figure 4: Vehicle parts causing far side impact injuries of front seated passengers

When evaluating the accident data for front seated passenger it can be stated that beside of a hard contact with the near side interior (one-quarter of all), the contact between the occupant and the belt & buckle as well as the contact with the seat back plays a major roll in suffering injuries at MAIS3+ level. Injuries caused by a hard contact with the vehicle

roof or caused by the interaction between the occupants are less frequent as shown in Figure 5.

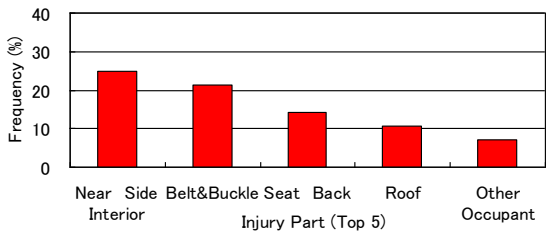

Figure 5: Vehicle parts causing far side impact injuries of rear seated passengers

The analysis presented in Figure 6 depicts the distribution of far side injuries as a function of the striking vehicle. The evaluation of the data shows that passengers seated in the front row of the car are mostly injured when the striking vehicle is a mid size or compact/mini car. This account for about one-quarter each. The striking vehicle for over more than 45% of the side struck occupants seated in the rear row was a mid size car. The vehicle group of van and light tucks accounts for one-third of all MAIS3+ injuries of rear occupants.

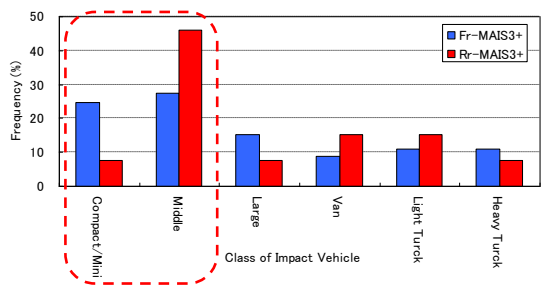

Figure 6: Frequency of injured passengers at MAIS3+ level related to vehicle class

NASS/CDS data base also provides information about the principal direction of force (PDOF). Zero degree is the front, 90 degree is normal to the side and 180 degree is the rear of the struck car. When evaluating the data related to MAIS3+ injuries, the most likely principle direction of force in far side accidents was 60 degrees which account for about 70% of serious injured passengers. Less injury was observed for a principle direction of force at 90 degrees or at 120 degrees as depict in Figure 7.

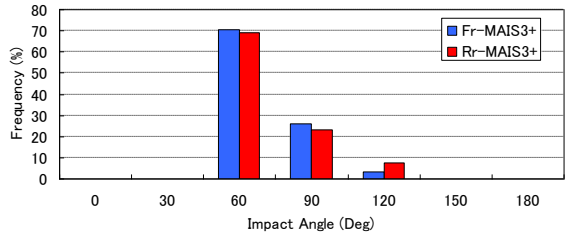

Figure 7: Distribution of far side impact injuries at MAIS3+ level by impact direction

A further evaluation was made according to the impact region of the stuck car. The impact to the occupant compartment is categorized by the NASS as follow: The Y (front 2/3 of the car side), P (centre 1/3 of the car side), Z (rear 2/3 of the car side) and D (distributed) and depict in Figure 8. (The University of Michigan, 2007)

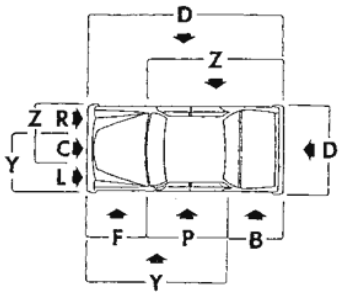

Figure 8: Definition of the vehicle impact area by The University of Michigan (2007)

The impact at front 2/3 of the vehicle was the most likely damage location for the vehicles investigated as shown in Figure 9. Impacts to this region also accounted for about 40% impacts in the region of rear 2/3 account for 18% of serious injured front seated passengers. The impact at 2/3 rear and centre 1/3 (each 30%) followed by impact on front 2/3 (23%) caused serious injuries for rear passengers.

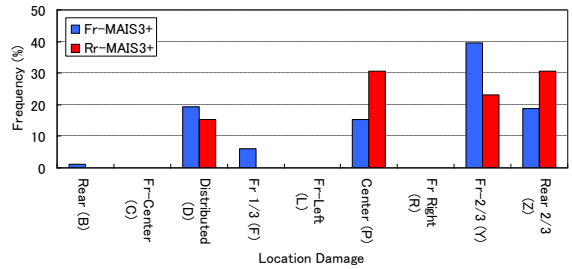

Figure 9: Distribution of far side impact injuries at MAIS3+ level by impact direction

Figure 10 presents the distribution of far side injuries by rigid barrier conversion velocity. The calculation was made according to Sukegawa et al (2007) by applying the energy absorption distribution map for the lateral stuck vehicle. As depict, the median barrier conversion velocity for all far side struck occupants with a MAIS3+ injury level was 31 to 40 km/h.

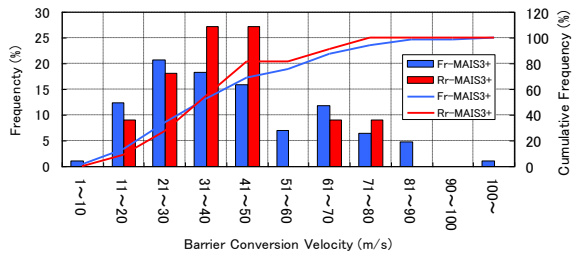

Figure 10: Distribution of far side injuries by barrier conversion velocity

The goal of this accident analysis was to establish priorities for injury countermeasure development for passengers seated in fare side struck vehicles. Two trends can be found.

The injury pattern. – The database exposed that the injury ratio of MAIS3+ to MAIS1+ is nearly the same for vehicle passenger seated on front or rear row during a far side impact. It can be stated that the occupants head and chest account for more than 2/3 of all injuries evoked by fare side impacts. The vehicle's side interior of the impact adverted vehicle side, the belt and the buckle as well as the seat back are the major injury sources. The interaction between the occupants plays a minor roll.

The accident scenario. – The occupants seated in the car classified as compact/mid size vehicles are mainly involved in far side impact crashes. The principle direction of force is at 60 degree and with a converted barrier velocity of 31 to 40 km/h fifty percent of the accidents are covered.

Protection of the head, chest and abdomen have priorities for countermeasure development. These three body regions accounted for approximately three-quarter attributed to far side impact of front and rear passengers.

PROTECTION CONCEPT

A new protection device was considered to enhance the protection of passengers seated on non-struck rear row position. An airbag was proposed to support the occupant kinematics during the event of crash and absorb impact energy and thus, mitigate the injury level. This airbag was installed in the centre console between the two passengers on the rear seat of an upper class car and it is supposed to enhance the protection capabilities in combination with a seatbelt system. The protection device also was designed to meet specific demands concerning side effects such as out-of-position scenarios.

The occupant protection device is integrated into the rear centre consol and shown in a full deployed position in Figure 11.

Figure 11: Rear centre console airbag front view left and side view right

The main design parameters of the rear centre console airbag are described in the following Table 1.

Table 1: Design parameter of the rear centre console airbag

Parameter	Value
Protection area	Thorax and head as depict in Figure 12
Airbag width	330 mm at head area and 230 mm at shoulder area
Airbag type	2D type with 100 mm tether
Airbag volume	66 litre
Inflator output	190 kPa in 60 litre tank (pyro inflator)
Vent hole size	2 holes with a diameter of 20 mm each
Cushion	Silicon coated
Time to fire	t = 9 ms

The airbag module with the cushion and the inflator is located in the upper part of the rear centre console. Once it is deployed it covers the whole thorax and head area of the seated occupants in the most forward and most rearward seating position. In order to position the airbag stable the airbag height was selected for a tight contact to the roof and the arm rest of the rear centre console. Two tethers form the width of the bag to 330 mm in the head area and to 230 mm in the shoulder area. In the following Figure 12, the geometry of the airbag and its location related to the side impact dummy ES2 is depict.

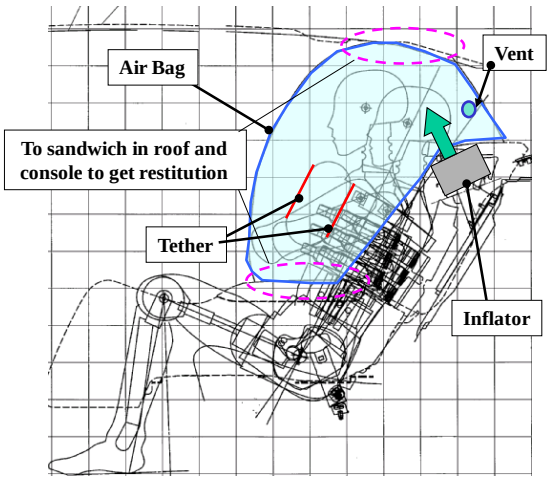

Figure 12: Protection area of the rear centre console airbag

As derived from NASS/CDS data investigations the rigid barrier conversion velocity in far side impacts is 31 to 40 km/h. Intensive numerical simulations were carried out to define a equivalent crash test setup using a AE-MDB (Advanced European Movable Deformation Barrier).

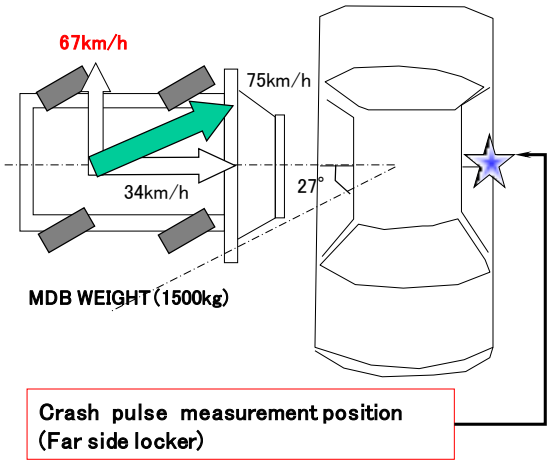

Figure 13: Crash test set up of far side impact

The Figure 13 depicts the crash test set up. The total delta-v of 75 km/h is the resultant change in velocity and includes both the lateral, of 34 km/h, and longitudinal, of 67 km/h, components. The AE-MDB with its mass of 1,500 kg hits the upper class car between the front and rear wheel with an impact angle of 27°. The car was equipped with two ES2 dummies on front row and one ES2 dummy on struck side on the rear seat. The crash pulse was measured on the B-pillar/rocker and the acceleration and velocity history are shown in the following Figure 14.

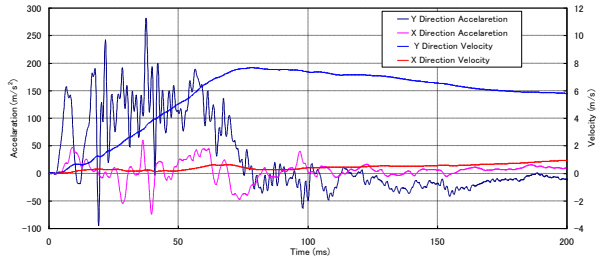

Figure 14: Acceleration and velocity history of the far side impact crash test

The acceleration signal was filtered with CFC180 and achieved a maximal value of 28 g during the intrusion of the movable barrier. Here, the struck vehicle was moved in y-direction up to a velocity of 7.6 m/s.

CONCEPT EVALUATION

Three steps were considered to evaluate the protection concept. As a start the injury severity as base line conditions was studied. Numerical simulations with the multi body software Madymo (Madymo, 2006) were performed placing one and two ES2 dummies on the rear row. As a second step the occupant protection concepts should be installed and the protection performance should be investigated under the same conditions as baseline. The derived output of the numerical simulations should be confirmed with a fare side impact sled test. This represents the third step of the concept evaluation.

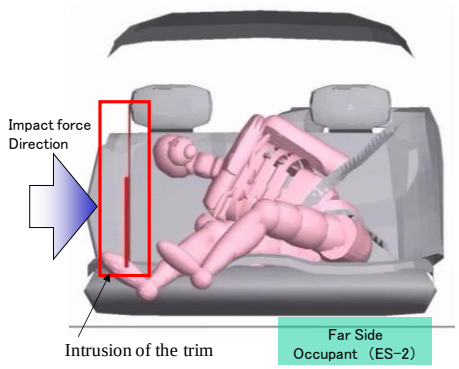

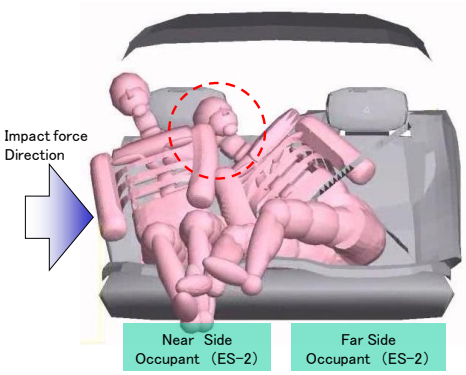

Figure 15: Numerical simulation sled model with far side dummy only (top) and with far side and near side dummy (bottom)

The results of the numerical simulation are presented in the following Figure 16.

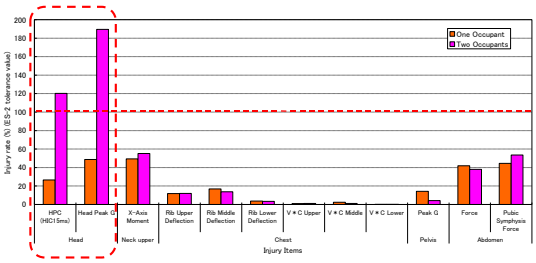

Figure 16: Injury results of the base line simulation with one and two occupants

It can be stated that the head performance criteria (HPC) is 20% higher as the maximal biomechanics limit of HPC 1,000. The head acceleration even exceeds the limit by more then 90%. The high head loads can be attributed to the hard contact between the far side seated dummy head and the near side seated dummy shoulder as can be seen in the bottom figure of Figure 15.

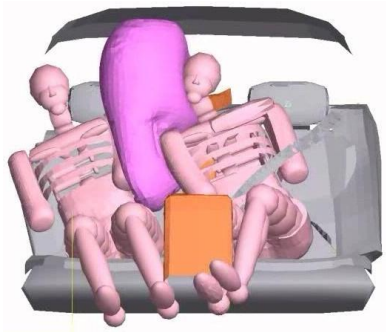

Figure 17: Numerical simulation sled model with rear centre console (top) and with rear centre console and rear centre airbag (bottom)

The Figure 17 above show the dummy kinematics at 110 ms during the far side impact with the Madymo simulations. The rear centre console prevents the dummy seated at the far side from intense lateral movement of the pelvis. The support of the dummy in pelvis area results in reduced head loads. Although there is no contact between the two dummies, the head acceleration can be lowered to just below the load limit and the HPC can be reduced to an acceptable load level of less then 20% of the respective load limit.

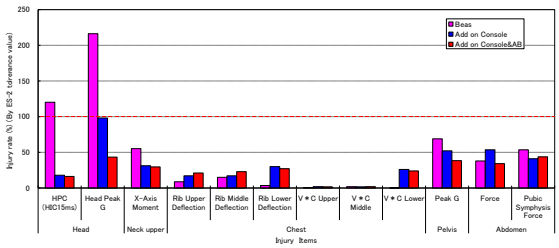

Figure 18: Injury results of simulation with far sine impact protection concept for rear seated passengers

As by the simulation results in Figure 18 shown, there is an increased protection performance when applying the rear centre airbag. An interaction between the two dummies is prevented. The head acceleration can be further mitigated to a level of 40% of the load limit. By introducing this protection concept for rear seated passengers, a slight increase of the chest deformation has to be taken into account, but the loads are still on a low level.

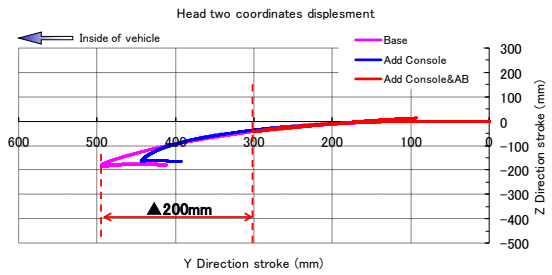

Figure 19: Head trajectory

The dummy kinematic were analysed for different body parts. In Figure 19 the trajectory of the head during the far side impact is plotted. The application of the rear centre console significantly reduces the head movement in y-direction by 50 mm. The combination of rear centre console and rear centre airbag is able to limit the head displacement in y-direction to 300 mm.

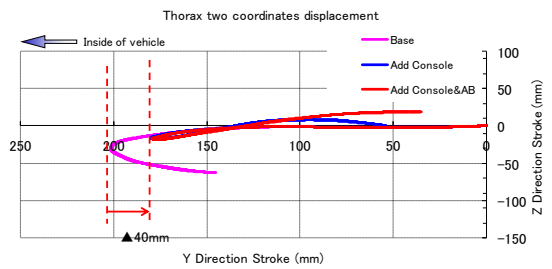

Figure 20: Thorax trajectory

A change of the thorax kinematic was also observed. The main effect was evoked by the application of the rear centre console. A reduction of 40 mm was observed. The rear centre airbag has only a minor effect of chest displacement as can be seen in the above Figure 20.

Based on the multi body simulations with the protection concept two sled test were performed to confirm the simulation results (Figure 21). A rear centre airbag prototype was built to equip a test set-up with rear centre console and two belted ES2 dummies. The vehicle side intrusion derived from the base line crash test was pre-set.

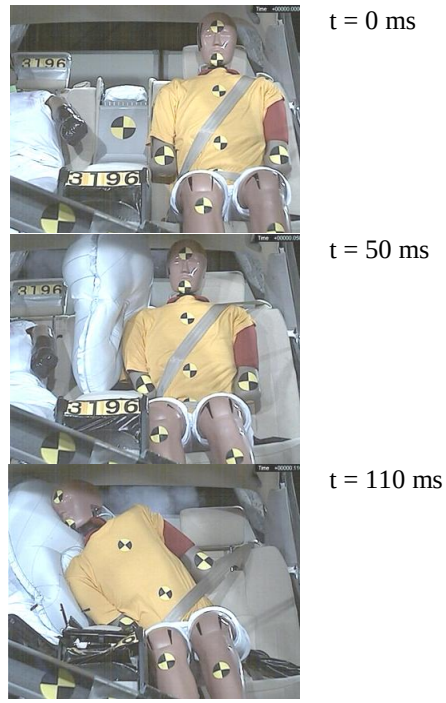

Figure 21: High speed video frames of sled test with rear centre console and rear centre airbag

In Figure 22 the results of numerical simulation and sled tests are compared. There is the same trend of the injury level of the different injury values. The average of the injury values obtained from two sled tests are below the injury values derived form the numerical simulation with Modymo.

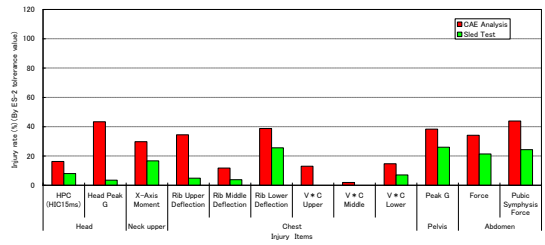

Figure 22: Comparison of numerical simulation and sled test results with the protection concept

When designing a new airbag system its side effects have to be considered too. Different dummy sizes are available to investigate a variety of different out-of-position scenarios. In order to confirm the potential side effects of a rear centre airbag the following scenarios, presented in Table 2, were investigated in deployment tests. The test results are shown in Appendix 1.

Table 2: Overview of the different out-of-position scenarios investigated

Dummy	Dummy position	
3YO	Turn backwards and half overlap of the airbag module	
3YO	Turn backwards and full overlap of the airbag module	
3YO	Face front	
3YO	Turn sideways	
6YO	Face front	
6YO	Turn sideways	
SID2-S	Position 1	
SID2-S	Position 2	

Three year old dummy (3YO), six year old dummy (6YO) and SID2-S dummy were used for out-of-position testing. It can be stated for all tested scenarios that the loads of the dummy were well below its regulated limits.

CONCLUSION

Within this study an accident investigation based on NASS/CDS data was carried out to analyse the accident characteristics and injury pattern in far side accidents. It can be stated that far side struck occupants are at significant risk of serious injury.

The median lateral barrier conversion velocity for occupants exposed to far side impact was 31 to 40 km/h. A test procedure applying a AE-MDB was developed to investigate future countermeasures.

A new protection concept was introduced for passenger seated on the rear row of the vehicle. An airbag deploys between the rear centre console and the vehicle roof in order to prevent the far side seated passenger form hard contact with the passenger seated on the impact side of the car. Intensive numerical simulations were carried out to optimise the rear centre airbag design parameters. It could be demonstrated that the protection concept with rear centre console and rear centre airbag is able to support the lateral dummy movement and thus to mitigate the occupant loads in the case of a far side impact significantly.

Side impact sled tests with prototypes of the new airbag concept were performed in order to confirm the multi body simulation results. It was shown that all injury criteria were far below its regulated limits and the trend which was observed in the simulation could be confirmed.

In addition to sled tests, deployment tests were performed to evaluate the injury risk of the protection device in out-of-position scenarios. It could be demonstrated in all test conditions with different dummy sizes in different positions to the rear centre airbag module, that the risk of suffering injuries is low.

The performed study was limited to the protection of belted rear seated passengers. Further work should continue the investigation of the protection principle for unbelted occupants in this position. The proposal and the investigation of a protection concept aiming to restraint passengers seated in the front row of the car during far side impact is additional future work. The experiences gained during this study will help to create a protection concept. Furthermore, the

application of human body model simulations in order to analyse the local loads of the occupant during far side impact and the protection effect of the restraint system proposed in this study will be future work. By this means the protection pattern can be understood in a wider sense.

REFERENCES

[1] Digges, K., Gabler, H., Mohan, P., Alonso, B., "Characteristics of The Injury Environment in Far-Side Crashes", 49th Annual Proceedings Association for The Advancement of Automotive Medicine, September 12-14, (2005)

[2] Gabler, H., C., Fitzharris, M., Scully, J., Fildes, B., N., Digges, K., Sparke, L., "Far Side Impact Injury Risk For Belted Occupants in Australia and United", ESV2005 Oral Presentations, Paper No.05-0420, USA (2005)

[3] Hideki, Y., Tomohiro, Y., Hiroko, T., Kouji M., "Research on side collision test method that considers the recent realities of accident", National Traffic Safety and Environment Laboratory, Meeting for reading research papers, Japan (2008)

[4] Madymo 6.2.2 Reference / Theory Manual, TNO Madymo BV. Delft, The Netherlands (2006)

[5] Sukegawa, Y., Kubota, M., Yamazaki, S., Yamada, K., "Energy absorption characteristics of passenger car side", JARI Research Journal, Vol. 29, No. 9, Japan (2007)

[6] The University of Michigan Transportation Research Institute, Transportation Data Center Data Set Codebook, No.2007-18, NASS CDS 1998-2007 Version 20-Jul-07, USA (2007)

[7] Ueno, M., Hatano, K., Fukushima, N., "Accidnt Analysis of Lateral Collisions in Japan", JARI Research Journal, Vol. 30, No. 9, Japan (2008)

APPENDIX 1

Table 3: Results of out-of-position tests

3YO – Turn backwards and half overlap of the airbag module

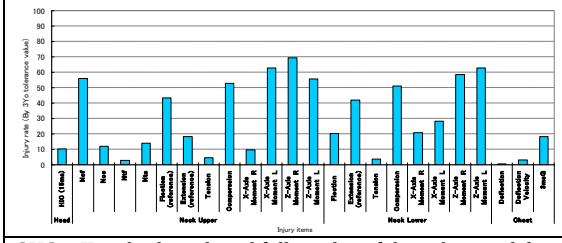

3YO – Turn backwards and full overlap of the airbag module

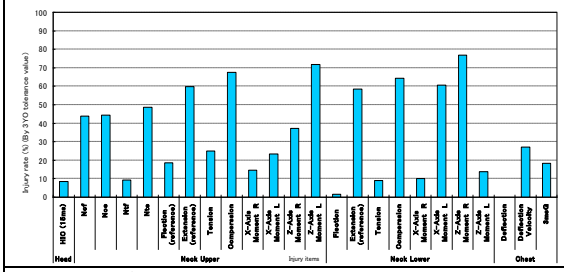

3YO – Face front

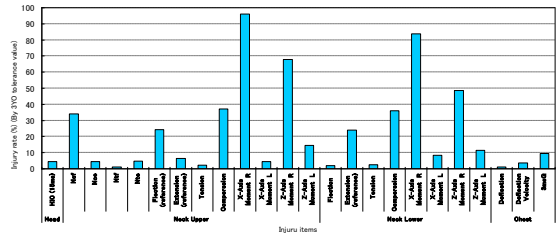

3YO – Turn sideways

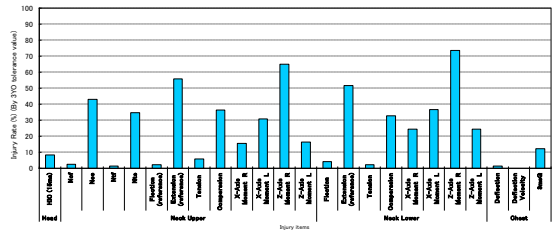

6YO – Face front

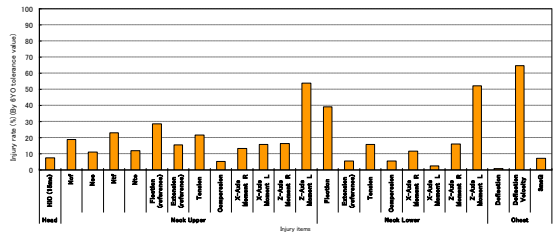

6YO – Turn sideways

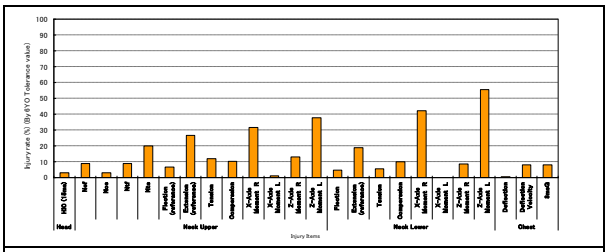

SID2-S – Position 1

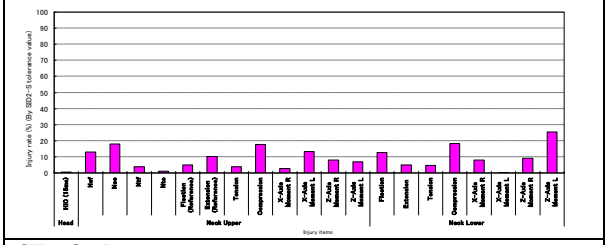

SID2-S – Position 2

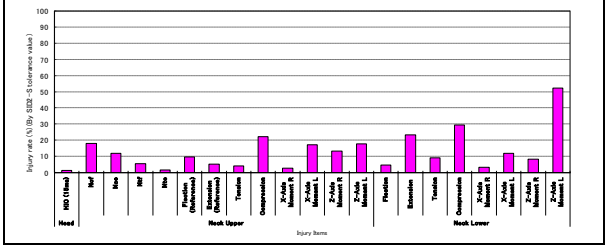

THE MINICARS RSV – STILL A CAR FOR THE FUTURE

Donald Friedman
Center for Injury Research
United States
Paper Number 09-0480

ABSTRACT

Nearly a half century ago, the General Motors Research Laboratories, developed the high performance Electrovair, with an induction motor drive and solid state controller; the Lunar Rover, GM's Mark on the Moon; passive occupant protection; separation cruise control; optical lane following; and an electrochemical rechargeable Lithium Iodine engine.

In 1968, a new company called Minicars grew out of this earlier work. This group developed prototype electric, gas and hybrid electric powered versions of a small car for the U.S. government. In 1970, Minicars was a subcontractor to AMF for the development of its Experimental Safety Vehicle.

The Minicars' Research Safety Vehicle (RSV) was conceived in 1975 as a 1985 prototype. It was to be an S3E vehicle: Safe, Environmental, Efficient and Economical. It was built with foam filled, thin wall sheet metal sections and a polyurethane skin. This car passively protected occupants in 80 kph (50 mph) full frontal, 129 kph (80 mph) half car offset frontal, 64 kph (40 mph) angled side, rear and 48 kph (30 mph) rollover dynamic tests. An electronic version incorporated antilock brakes, radar separation cruise control, and emergency braking when a crash was unavoidable. A production version was to weigh 2,200 pounds, carry four people, and get 32 mpg. It also had 16 kph (10 mph) frontal and rear no damage bumpers and 80 km (50 mile) run flat tires.

Only years later have advanced air bags – as featured in the RSV – become standard in all light vehicles. In the decades since the ESV program and dynamic regulatory testing began, National Highway Traffic Safety Administration (NHTSA) now estimates that airbags save 2,500 lives annually, but we still lose about 12,000 people in frontal, 9,000 in side and over 10,000 in rollover crashes. We can do better by simply looking back to what the RSV program achieved.

INTRODUCTION

The basic technology began sixty years ago when the transistor was newly invented. Cutting edge production technology was employed by the Navy to develop missile and fire control systems using subminiature vacuum tubes. Infrared optical systems were unknown except for secret military purposes like the Sidewinder missile. Navigation was by dead reckoning. Computers used punch card input and storage.

Nearly half a century ago, the General Motors research laboratories developed the high-performance electric vehicle called the Electrovair, shown in Figure 1, with an induction motor drive and solid state controller; the lunar rover shown in Figure 2, GM's mark on the moon; passive occupant protection; separation cruise control; optical lane following; and an electrochemical rechargeable lithium iodine engine.

Figure 1. GM Electrovair.

Figure 2. Lunar Rover.

METHOD

This paper uses the history of automobile safety technology as developed in the late 60's and 70's as a basis for discussion and conclusions.

40 years ago the American Machine and Foundry (AMF) contracted with Minicars, Inc. to develop one of the Experimental Safety Vehicle (ESV) in competition with GM, Ford and Fairchild Hiller. The specifications were for kph 80 kph (50 mph) frontal impact protection to unrestrained occupants, 64 kph (40 mph) side impact protection and 48 kph (30 mph) rollover protection. All the specifications were met and AMF won the competition. All of the ESVs were heavy and ugly as illustrated by the AMF version in Figure 3.

Figure 3. AMF Version of ESV.

37 years ago, Minicars received a contract from NHTSA for the "Crashworthiness of a Subcompact Car". It was to develop structural modifications to a Ford Pinto such that it could provide 80 kph (50 mph) frontal impact protection and 48 kph (30 mph) side and rear protection. A companion program involved developing frontal airbags to work with the structure for unrestrained occupants. [1][2] The structural modifications were to create closed section boxes of thin sheet metal in the vehicle's structural voids to absorb energy. These sections were retrofitted then with the first dual chamber designed airbags. The resulting vehicle shown in Figure 4, a station wagon version, met all the specifications. A remarkable result because the Pinto was a flimsy vehicle in a US fleet of heavy, monstrous vehicles.

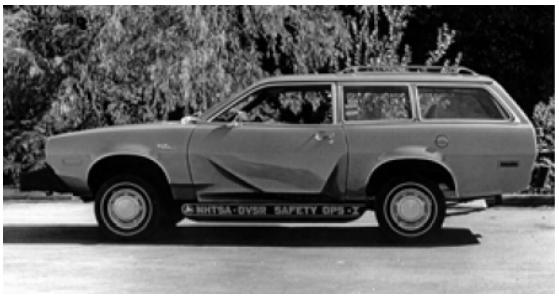

Figure 4. NHTSA Subcompact Car Wagon.

35 years ago Minicars received a contract for the phase 1 development of a Research Safety Vehicle (RSV) in competition with Ford, VW, Calspan/Chrysler and AMF. The RSV was to be characterized and specifications prepared for a 4 passenger vehicle, protecting unrestrained occupants in 80 kph (50 mph) frontal, 64 kph (40 mph) side and rear impacts and in a 48 kph (30 mph) rollover. The program began with an accident analysis considering the societal cost by vehicle class, clock position and Delta V range as shown in Figure 5 & 6.

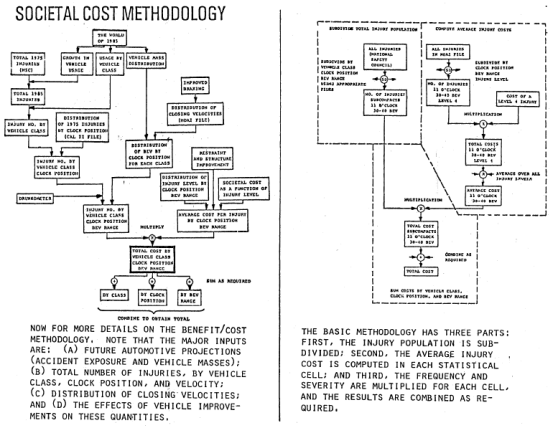

Figure 5. Societal Cost Methodology.

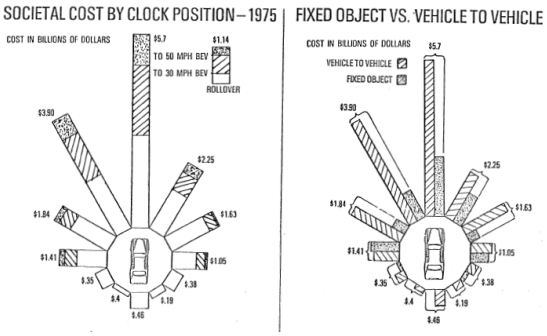

Figure 6. Clock Position and Delta V Range.

At the time the best data was from interpreting the Multi-disciplinary Accident Investigation (MDAI) files. That data by AIS level and impact clock position was as shown in Figure 7. It identified the angled offset frontal as the major source of frontal injury, although it is still ignored today. Since the current systems are designed for ± 9° frontal barrier tests, is there any wonder why we are saving 2500 lives and losing 12,000?

The structural design concept was carried over from the Subcompact Car Crashworthiness program. It was to be foam filled, thin wall, sheet metal structure. A "safety payoff analysis" was conducted to assess and order the benefits (payoff) from each additional safety design feature. The conceptual design is shown in Figure 8.

The detailed areas of different density foam filling are shown in the body and doors in Figure 9. The styling buck which defined the concept is shown in Figure 10.

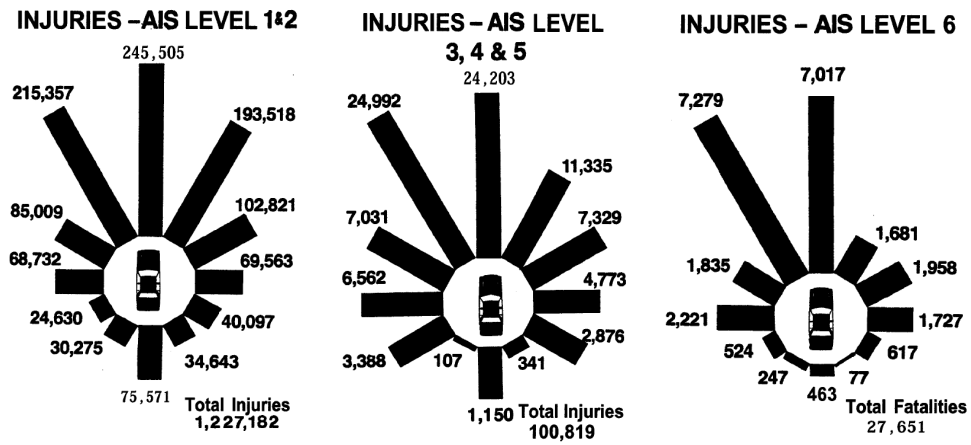

Figure 7. 1970 Accident data by clock position and AIS level from MDAI files.

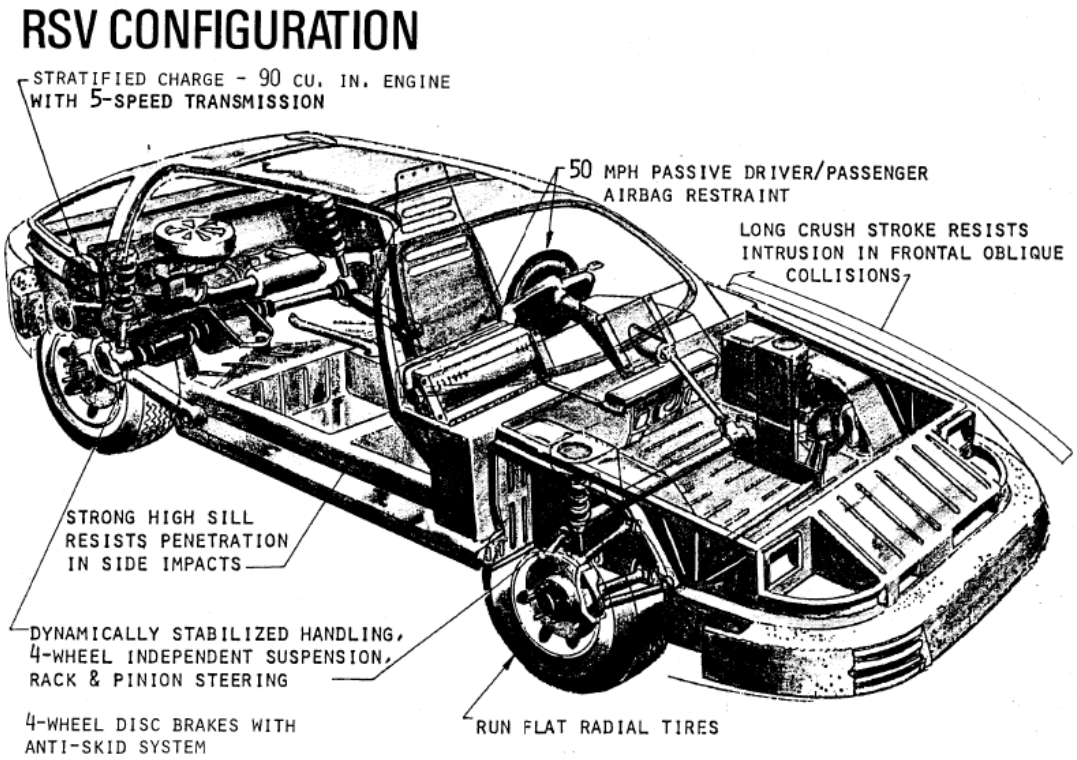

Figure 8. RSV Conceptual Design

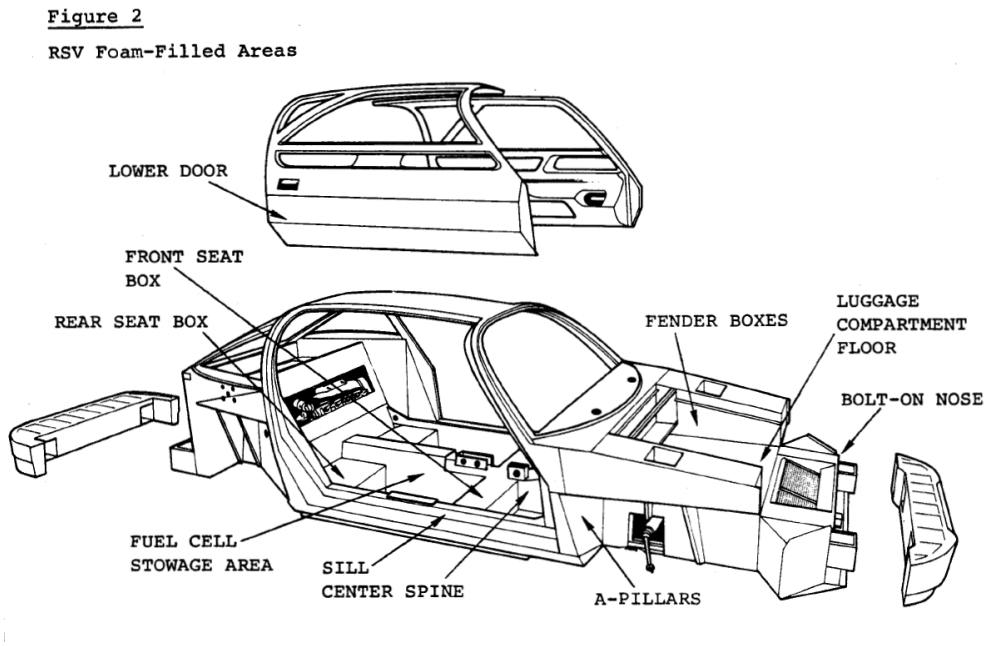

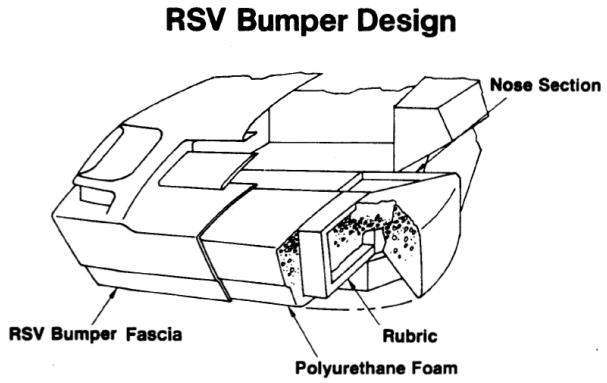

Figure 9. Detailed areas of foam filling.

Figure 10. Side view of RSV.

30 years ago the first prototype Minicars Research Safety Vehicle and the Large Research Safety Vehicle toured the United States in conjunction with a Department of Transportation, Public Service Announcement on television, narrated by Loren Green (of Bonanza). That Public Service announcement and the NHTSA commissioned film; "The RSV Answer" is available on request. [3] See Figure 11 and 12

Figure 11. Minicars Safety Research Vehicle.

Figure 12. Minicars Large Safety Research Vehicle.

The LRSV, like the Subcompact Car Crashworthiness Pinto was modified by stripping some 900 pounds from a 1978 Chevrolet Impala and substituting foam filled sheet metal box sections and installing a transverse mounted Volvo dual turbo charged engine matched to a four speed transmissions and front wheel drive. Three were built; one was frontal crashed at 64 kph (40mph) and a second at 48 kph (30 mph) in the side. The third was kept in Washington until destroyed. The administrator of NHTSA had it driven to Detroit and drove the president and executive VP's of GM, Ford and Chrysler around town. A drawing of the LRSV showing the foam filling is in Figure 13.

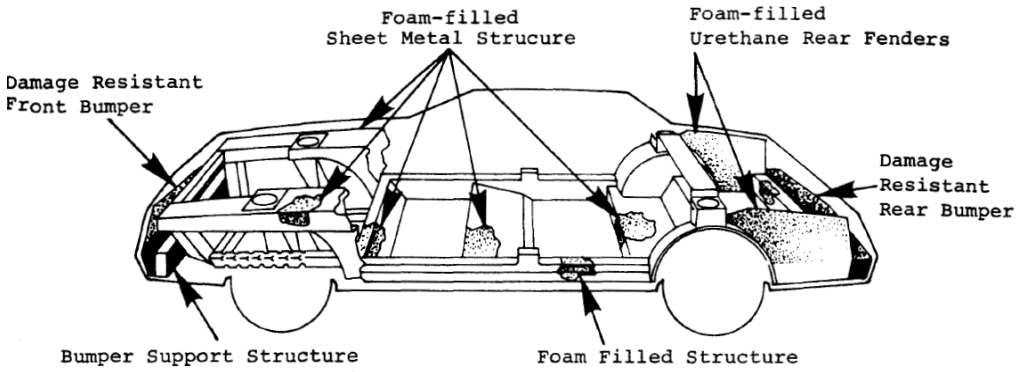

Figure 13. Foam filled areas on the LRSV.

29 years ago at the 1980 ESV conference in Wolfsburg, Germany, reports on the performance of 10 prototype vehicles independently tested in England, France, Germany and Japan were submitted. Except for handling deficiencies (panned by Porche and Mercedes) and normal prototype glitches, the vehicles did very well.

28 years ago in 1981 the final reports on the program were published. [4], [5], [6] The summary page describing the program is Figure 14.

Technical Report Documentation Page

1. Report No.	2. Government Accession No.	3. Recipient's Catalog No.

4. Title and Subtitle	5. Report Date
The Minicars Research Safety Vehicle Program Phase III - Volume I, Technical Final Report	September 1981
	6. Performing Organization Code
7. Author(s) D.E. Struble, V.K. Ausherman, C.E. Strother, A.V. Khadilkar, S.R. Syson	8. Performing Organization Report No. FR-2100-09-81
9. Performing Organization Name and Address Minicars, Inc. 55 Depot Road Goleta, California 93117	10. Work Unit No. (TRAIS)
	11. Contract or Grant No. DOT-HS-7-01552
12. Sponsoring Agency Name and Address U.S. Department of Transportation National Highway Traffic Safety Administration 400 Seventh Street, S.W. Washington, DC 20590	13. Type of Report and Period Covered Final Report Jan 1977 to Sep 1981
	14. Sponsoring Agency Code

15. Supplementary Notes

16. Abstract

The objective of the RSV Program was to provide research and test data applicable to the automobile safety performance requirements for the mid-1980s, and to evaluate the compatibility of these requirements with environmental policies, efficient energy utilization, and consumer economic considerations. The program was designed to answer the question, "Can small fuel-efficient cars be made safe?," and to address such topics as: How safe should cars in general, and small cars in particular, be? What technologies will be required to make them this safe? Are these technologies feasible? Can they be, or have they been, sufficiently developed to justify the promulgation of more stringent safety standards?

The RSV Program has demonstrated that it is possible to make cars much safer than they are presently. It has produced automobile designs that are consistent, at affordable cost, with the national objectives for fuel economy and environmental protection. It has indicated, at least to a limited degree, that the technological findings are applicable, at varying levels, to a variety of car designs. And it has provided evidence that these findings can be wrapped in a package of considerable appeal to the public.

This Final Report is a comprehensive compilation of the findings of the Phase III efforts of Minicars, Inc. It describes the design and testing of the RSV systems, and the performance levels achieved. Specific topics include a vehicle description and performance specification, the structure, occupant restraints, braking and handling, propulsion, the vehicle exterior, driver controls, the radar and electronics, the Large Research Safety Vehicle, and the accident environment analysis.

17. Key Words	18. Distribution Statement
RSV, Safety, Crashworthiness, Airbags, Radar, Large RSV, Foam-filling, High Technology RSV, Occupant Protection, Anti-skid Braking, Minicars, Automotive Electronics	Document is available to the U.S. public through the National Technical Information Service, Springfield, Virginia 22161

19. Security Classif. (of this report)	20. Security Classif. (of this page)	21. No. of Pages	22. Price
Unclassified	Unclassified		

Form DOT F 1700.7 (8-72)

Figure 14. Minicars RSV Program Final Report Cover.

The overall dimensions and shape of the RSV are shown in Figure 15. Notice that the roof is rounded without corners to allow the vehicle to roll like a cylinder. It was a concept then and a proven geometric way to improve occupant injury potential today. See the companion papers in this conference "Vehicle Roof Geometry and its Effect on Rollover Roof Performance" and "A Proposed Rollover and Comprehensive Rating System". [7][8]

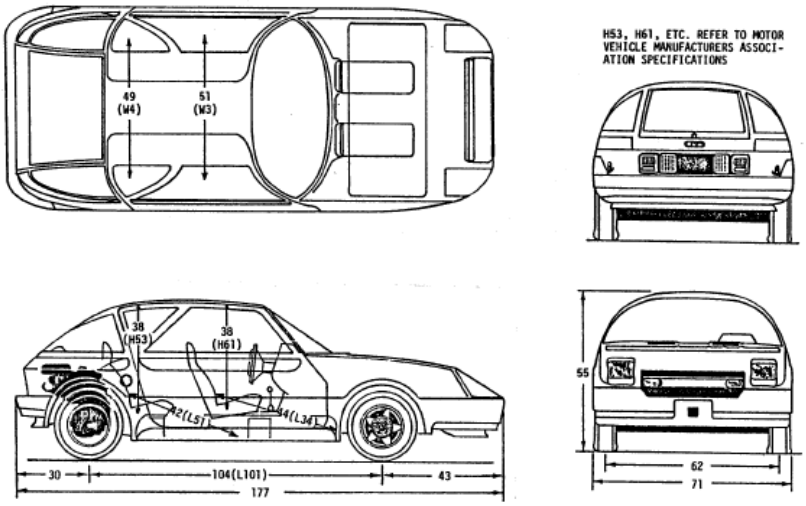

Figure 13. Foam filled areas on the LRSV.

SAFETY CONCEPTS INHERENT IN THE RSV

The research safety vehicle included and demonstrated the following innovative and unique features in the base design:

- 50 mph frontal impact protection airbags for unrestrained occupants of the front seat [4] (see Figure 16)
- 40 mile an hour side impact protection with adding and come posit glazed windows [9] (see Figure 17)
- 40 mph rear impact protection with seatbacks suspended from the roof with a clear plastic headrest [10] (see Figure 18)
- 10 mile an hour front and rear restorable bumpers [4] (see Figure 9)
- A 25 mph energy absorber that was replaceable behind the bumper [4] (see Figure 9)
- A rigid structure from the firewall in the rear to the foot well in the front [11] (see Figure 8)
- A Honda CVCC four-cylinder transverse engine in the rear with four speed manual transmission
- Doors that integrated with the structure providing longitudinal strength and side impact padding [10] (see Figure 19)
- An 84 mile per hour frontal offset impact capability
- A pedestrian friendly front end design.
- Gull wing doors (16" clearance to adjacent vehicles) which closed over structure for easy entry and exit to the front and rear seats (see Figure 20)

The passenger airbag system is shown in Figure 16. It is a large bag system, in which the torso portion is inflated first and then that bag is vented to the head bag. At that time less than 15% of vehicles had belts and wore them. The key issue for the industry as expressed by Dr. David Potter, executive VP of Environmental staff at GM, was product liability. Although not implemented in the base vehicle, the electronic version with proximity radar for emergency braking could pre-impact deploy the bags relatively slowly avoiding out of position and onset bag slap injuries to the chest. Although Nissan built their ESV around this deployment concept it is still

not in use today. Another innovation was the solution to rear impact head rests. As shown in Figure 17, a transparent plastic head rest was connected between the roof and the top of the seat back. This assured that in a rear impact the neck would go into flexion while allowing a lightweight seat back.

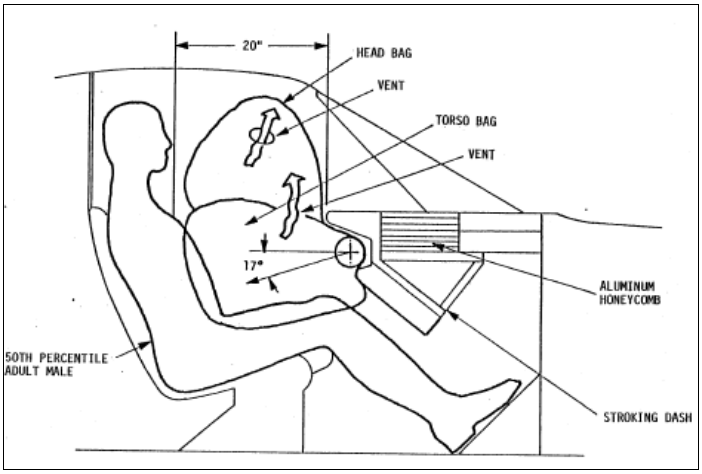

Figure 16. Airbags for unrestrained occupants of the front seat.

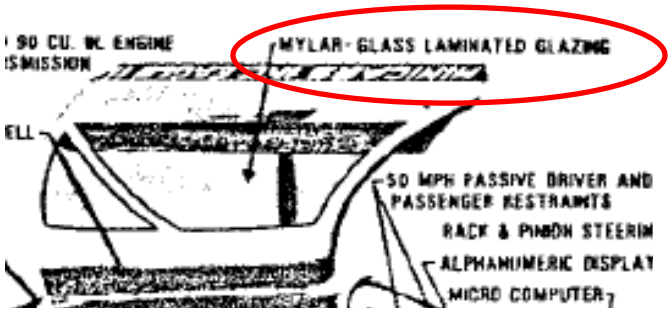

Figure 17. Side impact protection with adding and composite glazed windows.

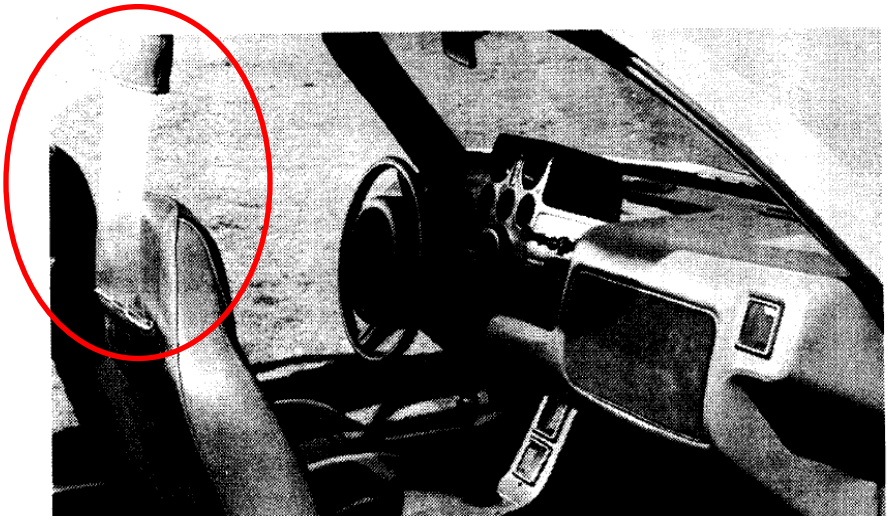

Figure 18. Seatbacks suspended from the roof with a clear plastic headrest.

The vehicle was designed with deeply padded gull wing doors for side impact protection. The windows were made of a glass plastic laminate which was integrated to the doors to avoid rollover ejections for the largely unbelted occupants of the time.

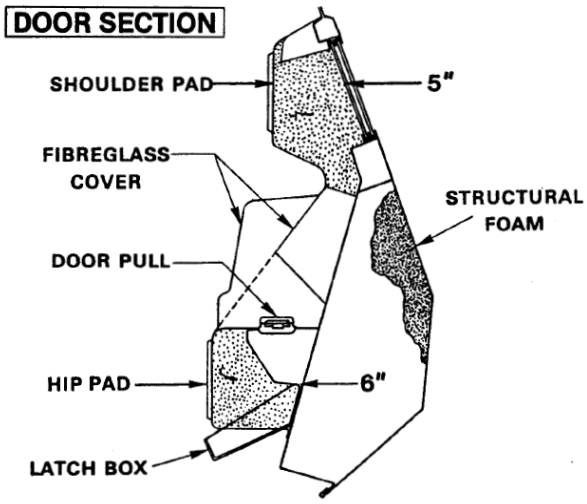

Figure 19. Door with side impact padding.

Figure 20. Gull Wing Doors.

The front end of the vehicle was designed for pedestrian and larger vehicle compatibility. It was designed in three sections. The bumper was of restorable plastic good to 16 kph (10 mph) but also to contact a pedestrian at up to 40 kph (25 mph) and capture him on the hood and luggage compartment. There was a bolt-on energy absorber of medium density foam which would collapse and absorb energy of another 24 kph (15 mph), before the third and main structural section was to deform. This provided a mild low G crash pulse as shown in Figure 21and 22.

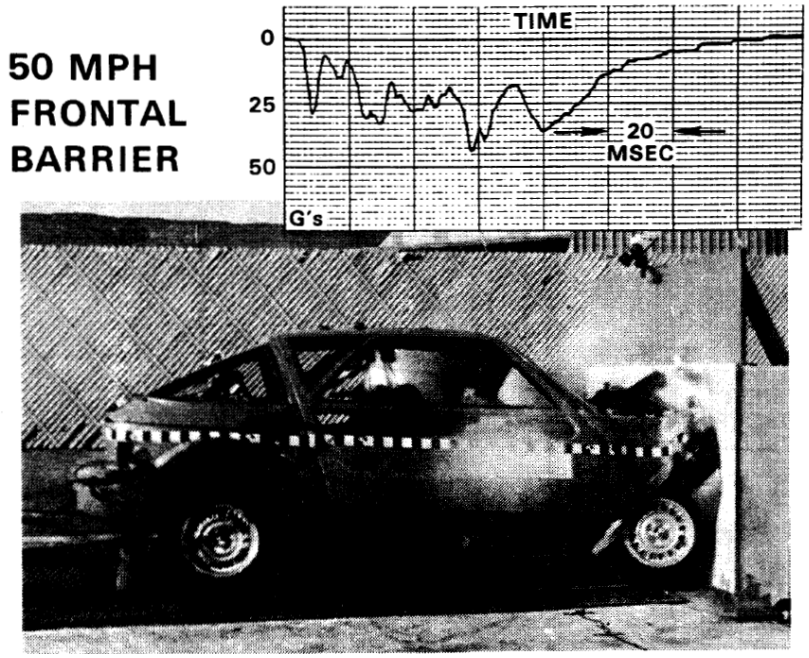

Figure 21. 50 mph Front Barrier Test with the RSV.

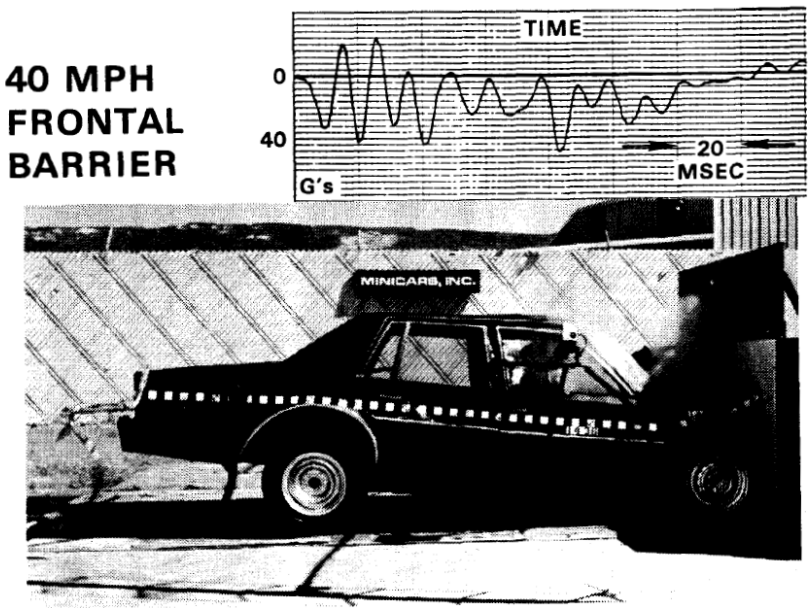

Figure 22. 40mph Frontal Barrier Test with the LRSV.

THE ELECTRONIC RSV

Although the basic RSV was targeted as a production vehicle for 1985 a number of features were anticipated to be available a few years later. Those features were incorporated into an Electronic RSV [9], [12], which was identical to the regular models, as follows:

- A 4 speed electronically shifted automatic transmission
- A radar cruise control system
- Four wheel anti-lock brakes
- Radar activated emergency braking (Collision Mitigation System)
- Radar activated proximity warning
- airbag pre-impact firing sensors

DISCUSSION

The Minicars RSV was such a departure from the U.S. industry position on what could be done in the way of safety improvements and occupant protection that NHTSA destroyed all vehicles, lost 22 boxes of test films and data and did not publicize the final report. But that is not the point. The point is that here we are 30 years later and though we are beginning to see some voluntary implementation of some features, it is because it may help to sell cars not necessarily because it will improve safety.

In the US, there are more than 10,000 fatalities each year in rollovers. Almost half of the fatalities are from ejections, which wouldn't happen with the RSV's pitch balance, composite windows, rounded roof and strong roof structure. [7]

Consumers review an occupant protection rating system which gives four or five stars to vehicles which don't protect 12,000 fatalities in frontal impacts and 9,000 in side impacts

At the time the RSV came into being the societal cost of crashes in the US was about $30 billion, today it is about $300 billion. In the current reassessment of economic priorities, there ought to be some consideration for implementing improved safety features in small economical cars. The myth that small cars cannot be made as safe as large cars must be dispelled. It is only a correct statement if the caveat "all other things being kept equal" is added.

The airbags in the RSV were designed with dual chambers, shown in Figure 23 whose walls limited the extent to which the bag protruded towards the occupant and it distributed the gas through a central chamber venting the gas to peripheral chambers. The driver bag was wheel mounted shown in Figure 24 and 25 on a collapsible column which provided 5 inches of additional decelerating stroke. The size of the bags captured the occupant such that he was protected in 30° principle direction of impact force circumstances. Current bag systems provide 9° of principle impact force protection to 35 mph.

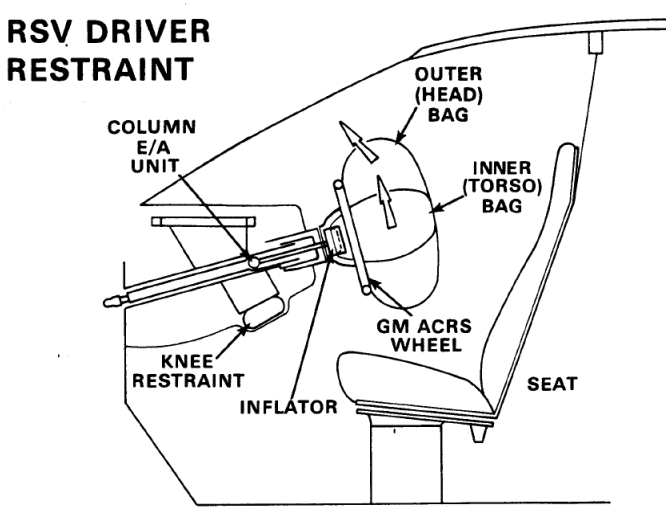

Figure 23. Driver restraint side view.

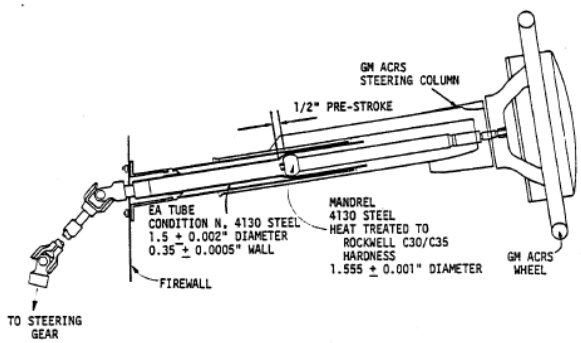

Figure 24. Driver steering column.

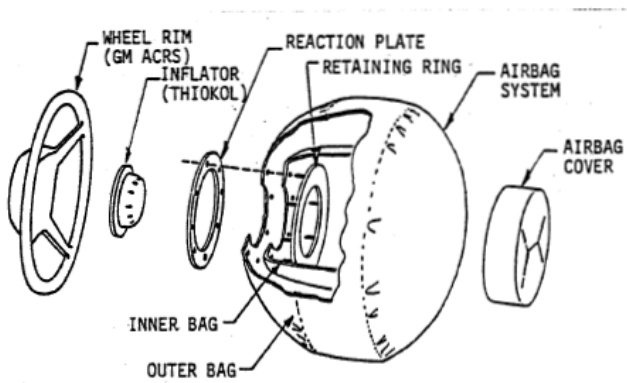

Figure 25. RSV collapsible column and driver bag.

When airbags were finally implemented as a supplemental safety system it was projected that they would be 9% better than the three-point belts. That projection seems to have come true since NHTSA estimates that airbags save 2,500 lives annually. Today's airbags are small, non-chambered and only cover 9 degrees of impact. We still lose 12,000 people in frontal collisions every year. If the type of airbag built into the RSV were in use today, at least 6000 more lives would be saved. [7]

The RSV wasn't a dream and its performance can be a reality today.

CONCLUSIONS

Although designed 35 years ago the RSV is still a prototype for improved occupant protection safety. Two of the features of the RSV, highlighted here are:

- the roof structure, geometry and composite glazing
- the pre-impact sensed deployment of chambered airbags

The combination of just these two features alone has the potential to save thousands of lives.

The author is highly concerned that in the U.S. we are complacent and satisfied with the results of the limited safety features the manufacturers have implemented and the Department of Transportation has done nothing about it for years. Still we loose thousands of Americans in Frontal and Side Impact Crashes and it is completely unnecessary. The RSV features would have saved many lives that have been lost, but for the governments indulgence of the manufacturers reluctance to put safety ahead of profits. And the worst thought is that it continues today, where manufacturers seem to say they have done all they can with safety for Frontal and Side impacts, yet the RSV shows definitively that they have not.

REFERENCES

[1] "Improving the Crashworthiness of Subcompact Cars," 1973, DOT-HS-1 12-3-746.

[2] "Advanced Air Bag Restraints for Subcompact Car Drivers", 1973, DOT- HS-1 13-3-742 5.

[3] "RSV - The Answer", Video

[4] Struble, D.E., V. Ausherman, C. Strother, A. Khadilkar and S. Syson. 1981. "The Minicars Research Safety Vehicle Program Phase III." Vol. I. Technical Final Report.

[5] Ausherman, V., A. Kadikar, S. Syson, C. Strother, and D. Struble. 1981. "The Mincars Research Safety Vehicle Program Phase III."

[6] Friedman, D. 1981. "The Minicars Research Safety Vehicle." Minicars, Inc.

[7] Friedman, D., G. Mattos and R. Grzebieta. 2009. "Vehicle Roof Geometry and Its Effect on Rollover Roof Performance." ESV 2009.

[8] Friedman, D., G. Mattos and R. Grzebieta. 2009. "A Proposed Rollover and Comprehensive Rating System" ESV 2009.

[9] Friedman, D. and E. Belohoubeck "The Near-Term Prospect for Automotive Electronics Minicars Research Safety Vehicle," RCA Laboratories, SAE 780858, September, 1978.

[10] Struble, D.E. 1979. "Highlights of the Minicars' RSV Program." Engineering & Research, Inc.

[11] Minicars, Inc. "RSV Phase I.". brochure

[12] Kossar, J. "The High Technology Research Safety Vehicle," Experimental Conference. Germany. 1980.

Uniform Application of NASS CDS Child Safety Data Definitions and Data Extraction

Ana Maria Eigen
JoAnn L. Murianka
National Highway Traffic Safety Administration
United States of America

Paper 09-0550

ABSTRACT

The authors hope to provide an intermediate method of data extraction, taking advantage of the improvements in child passenger data collection and recording. The authors also wish to highlight the importance of appropriate usage of the data. As suggested in the Eigen 2007, the enhanced data set SAS files, also known as the 30-file data set, will be contrasted with the 11-file data set format, the traditionally available NASS CDS SAS files, and analysts will be referred to the NHTSA web site for supplementary information. Further, frequently asked questions will be addressed to provide uniform information dissemination to all users. The primary data source will be the National Automotive Sampling System (NASS) Crashworthiness Data System (CDS). As conclusion, the authors propose a three-step extraction methodology to be used until the enhanced data files can be released. This includes traditional data extraction to retain weighting factors, extraction of the enhanced variables, attributes, and associated graphics, and manually integrating the two data sources.

INTRODUCTION

Available Data Evolution

NASS started recording crash data in 1979. From that moment, paper forms recorded crash environment, vehicle damage, occupant demography, and injury. As technology advanced, NASS CDS kept pace with the electronic data reporting. Beginning with 1997 qualified crashes, the data forms were uploaded from pen computers used by the researchers and after careful review by Zone Center staff, the electronic data became part of the web site query data. With the enhancements offered in the enhanced 30-file SAS data set, the 11-file SAS format was not able to be adapted to the greater formatting needs and new variables and attributes. The two SAS data sets will be described in the Definitions section. For this reason, data analysts have been obligated to adapt existing data for suitable analysis. The delayed release of the data has been attributed to the stringent quality control practices that have characterized the data system.

Since 2000, with variable and attribute development for the 2002 child safety data enhancements, variables and attributes were designed taking into account state-of-the-art child restraint technologies and state-of-the-practice educational and installation guidelines. This expertise was inherent in the continual contact with child restraint manufacturers, child safety education networks, and hands-on-familiarity with technologies pursuant to a long trajectory of experience in the child occupant safety field. This high degree of scrutiny was present in the interactions, especially with the Zone Centers, owing to the complexity inherent in accurately coding a highly detailed data set. Discussion of the annotation fields and their use will further elucidate this point. It is also noted that this degree of oversight was present through crash year 2007 with data released in 2008.

It is envisioned that the enhancements and practices put into place will guide subsequent years of data collection and codification. These enhancements are contemplated in the enhanced 30-file data set. Stringent quality control practices have allowed for the release of two years of enhanced data. In the absence of the enhanced data, this work discusses strategies to bridge its absence by using the traditional 11-file SAS format supplemented by NHTSA case viewer query.

Research Questions

1. How can one use the enhanced 30-file NASS CDS data set for meaningful data extraction?
2. How to bridge the current absence of this enhanced data set?

DEFINITIONS

During the course of this paper, two data repositories for the NASS CDS data will be discussed and noted in the References. These are a NHTSA file transfer protocol (ftp) site and NHTSA web site case viewer. Interwoven in this discussion will be the 11-file data set available since crash year 1988 and the expanded, 30-file data set, available since 2002 but to date available only for data years 2002 and 2003. Both the 11-file and 30-file data sets are compiled in SAS format. The 11-file set is the original means of translating and condensing the vast amount of data stored in an Oracle system. With improvements in data collection and increased storage needs, the 30-file set is the Oracle-look-alike file compiled in SAS and allowing the end user the advantage of most

researcher-collected information. The 30-file data set will be referenced throughout the paper as the ***enhanced data set***. The data provided since 1988 in the format known by all CDS data users will be referenced as the ***11-file data set***.

The National Center for Statistics and Analysis (NCSA) has been the purveyor of crash data since its inception to support rulemaking and research within NHTSA and provide researchers with internationally recognized tow away crash data. NCSA continually seeks to improve their data collection practices by keeping pace with technology and addressing user data needs. Since 1988, NASS CDS has been made available to researchers. Originally the data was made available by compact disk disseminated by The Volpe Center to requestors. Most recently, NCSA has worked to make its data universally accessible by way of the World Wide Web ftp site and two state-of-the-art case viewers.

In 1995, the data files were supplemented by an accident summary, accident type, vehicle type, and person description text files, forming the current ***11-file data set***. For convenience, data compiled from 1988 through 1994 and available via ftp site also will be referenced as ***11-file***, yet, this was a 7-file format without the text files, later added in 1995. Although many modifications have occurred in terms of data collection, the ***11-file data set*** is constrained by an inflexible database structure, which was cutting edge at its moment of inception. Advancements in vehicle and child safety restraint technologies, and rollover data collection, have gone unnoticed owing to the inability to adapt the older data set structure to the exigencies of more robust attributes for existing variables and newer variables.

With this in mind, provision of the ***enhanced data set*** structure was initiated for crash year 2002. Although the data sets are still published in SAS format, this new structure allows for an Oracle look-a-like data set, which more closely resembles the complete data set collected by the crash investigators. To date, crash years 2002 and 2003 have been published. Delays in publication of the subsequent data years have been attributed to funding issues. It is important to note that NASS CDS data undergoes a thorough review process before publication. At the writing of this paper, crash data through calendar year 2007 has been available under the older, ***11-file data set*** structure. This paper is intended to aid researchers in working around the issues inherent to the delays, as no firm commitment exists for the completion of quality control and subsequent release of the ***enhanced data set*** for data year 2004 and beyond.

In 1997, NASS CDS transitioned from paper form data collection to electronic data collection. This information could be uploaded easily to a central quality control repository. The on-line case viewer became a reality which not only allowed data found in the SAS format to be viewed but also made available the photographs, scene diagrams, and mannequin injury sketches. This provided the final phase in complete reporting so necessary in clinical analysis. In 2004, an enhancement was made to the case viewer. This allowed for cases, with all associated graphics, to be downloaded in an Extended Markup Language (XML) file facilitating aggregation of data for analysis of a body of crashes. This format was also made available for crash year 2005. In tandem, though, the traditional case viewer was released for those years. In an effort to provide the greatest amount of data in the most accurate fashion, a number of 2008 cases have been reviewed and placed on a preliminary case viewer.

These database formats and additional data will be referenced throughout the paper. Relating these sources and data types is envisioned to allow researchers to undertake analysis using a variety of sources to reap the maximum benefit from the exceptional data collection and coding efforts of the NASS CDS field researchers.

BACKGROUND

Data Collection History

Before 2002, the codification efforts of NASS CDS found their strength in crashworthiness of the vehicle. The scene geometry, inclusive of road side furniture and forensic review of the roadway segment, were well-reported. Disaggregation of crash data to the vehicle level has always been of paramount importance to the accurate reporting. Equally important but lacking real-time information was the human element. Basic demography was generally well collected and recorded and when appropriate complete medical information was included. This data, however, was collected at the crash level, rather than attributed to a given event. Further NASS CDS, has kept pace with vehicle modification, with respect to model year changes and hardware. Most child safety seats are not factory-installed, and might be best described as retro-fit items. For this reason, their continued study and success must be accurately tracked and reported.

As understanding of the technologies increased and the number of child safety restraints increased, NASS CDS continued their commitment to data collection and recording excellence. During 2001, an in-depth

inventory of available technologies was undertaken. The NASS CDS field researchers were polled with respect to their understanding of these technologies. It was found that a vast gap in knowledge existed with the state-of-the-art practice in child safety restraint technologies.

Since then, an intensive modification of the reporting has been designed, supported by a complete overhaul of the data collection instruments. To support the enhanced data collection, intensive training has been provided to field researchers, resulting in one researcher being dedicated to coding child seat cases from each primary sampling unit.

DISCUSSION

Changes in Child Restraint Variables and Attributes

Prior to 2002, there were only a limited number of variables regarding child restraint type, use, and installation recorded in CDS, several of which were outdated and no longer reflective of current child restraint types and installation usage techniques.

The predominant child restraint data collection tool used by field researchers was a one page interview consisting of eight questions which was part of the main NASS interview. Normally, the interview was conducted over the telephone and in the majority of cases the child restraint was no longer available, which resulted in much of the child restraint data coded as "Unknown". Nonetheless, there were rare occurrences when the child restraint remained in the vehicle and/or with the crash occupants which allowed for identification and coding of the attributes available at that time. In those instances when the child restraint was available and permission was granted for doing so, photographs of the child restraint were taken and combined with the interview information.

From 1988 through 2001, the majority of child restraint types were coded as "Unknown/Other", due in part to the lack of information in the field, for example, the child restraint was no longer available coupled with the fact that the crash occupants were unfamiliar with the seat and were unable to recall identifying details.

Seat Belt Installation Considerations

The Proper Use/Misuse information regarding a child restraint was captured in the seat belt variables. There has never been a single variable or attribute which provides the overall proper/improper use of a child restraint, yet this attribute was at times relied upon to do just that.

The Proper Use/Misuse variables were defined as: Proper Use of Manual Belt (used properly with child safety seat – indicated when the manual belt was installed so as to comply with the manufacturer's directions); and Proper Use of Automatic Belt (used properly with child safety seats – indicated when the automatic belt was installed so as to comply with the manufacturer's directions). Proper/improper child seat installation is difficult to determine even when the child seat is available and remains installed in the vehicle as it was prior to the crash, because the pre-crash environment itself had changed. In addition proper/improper information was not coded regarding the child seat's type and use for the respective child occupant, which again lead to misinterpretation, so the attribute was removed beginning with the 2003 CDS file.

Rationale for Enhancement with Retrospective of Nine Years of Crash Data

Prior to 2002, the child restraint list/"pick list" used by field researchers to identify child restraints was populated with approximately 30 different makes of child restraints covering approximately 120 different child seat models belonging to five child seat types. The pick list was outdated, no longer reflective of current child restraint types and designs. The original attributes for Seat Type were Infant, Toddler, Convertible, Booster, Integral, Other and Unknown.

The original child restraint interview asked limited questions about the child restraint itself, one question about how the restraint was used and two questions pertaining to the child restraint's securement to the vehicle.

Some of the child restraint attributes coded harness design but not how the harness was used. Photographic guidelines did not focus on obtaining a picture of the child restraint's make, model and date of manufacture label, so often this information was not obtained during inspection of the child restraint.

Prior to 2002, the field researchers coding child restraint information received very basic child restraint and seat belt education during normal entry level training.

Steps Taken to Reach the Current Levels of Enhancement

In 2002, the child restraint attributes were changed to reflect current child restraint use/marketing terms:

The onus is upon each SAS analyst to determine a system to reap maximum benefit from the enhancements, while performing statistical analysis using the weighting factors. The subsequent section provides the location of currently available data, which in some cases supersedes the data in the ***11-file data set***. This is evident in Table 1, where the older formatting continues to report two booster seat categories available as attributes, one of which no longer exists, as discussed in Murianka 2005. Also, relevant restraint data developed for the 2002 data onward that could not be accommodated in the ***11-file data set*** is also highlighted in Table 1 and discussed in subsequent sections. Focus will be given to the Child Safety Seat, Manual Restraint Use, Component associated with Manual Restraint Use tabs found on the NHTSA web site NASS CDS case viewer.

Table 1.

SAS child seat types, by data definition years

Pre-2002, ***11-file data set***		**2002 to Present,** ***Enhanced data set***	
SAS Format Code	**Type Definitions**	**SAS Format Code**	**Type Definitions**
1	Infant	1	Infant
2	Toddler	2	Convertible
3	Convertible	2	Convertible
4	Booster with Shield	3	Forward Facing Only
5	Booster w/o Shield	4	Booster Seat
5	Booster w/o Shield, 2 Toddler	5	Booster Seat/Forward Facing Only
5	Booster w/o Shield, 3 Convertible	6	Booster/ Convertible
7	Other Type	7	Integrated Seat
7	Other Type	8	Harness
7	Other Type	9	Vest
7	Other Type	10	Special Needs
7	Other Type	98	Other
8	Unknown Type	99	Unknown

For illustration, the internal data viewer, known as NASS MAIN, is used to show the extent of the ***enhanced data set***. The public case viewer, found on the NHTSA web site, is generally similar to the NASS Main but contains less information. Some of the additional information presented in the next section will not be made available until the ***enhanced data set*** is released for 2007.

Figure 1 highlights the location of the child restraint information within the context of the NASS CDS viewer, available on the NHTSA web site, and its correspondence with child seat information found in the ***11-file data set***. The Occupant Form, shown in Figure 1 and analogous to information found in the Occupant Assessment File of the ***11-file data set***, outlines demographic, restraint system, and crash outcome information, by occupied seating location. This tab places the occupant within the vehicle and describes the safety devices available to him. Further, crash outcomes such as vehicle entrapment or occupant ejection from the vehicle are described. From this information, it is also possible to ascertain whether the occupant departed the vehicle under his own power or was aided. In the case of occupant ejection, the degree of occupant expulsion is considered. Occupant injury outcome, analogous to information found in the Occupant Injury file of the ***11-file data set***, is discussed with respect to crash survival and the injuries are detailed with respect to their nature and severity. Figure 2 places the restraint technology in a seating position and identifies the factory-installed restraint usage and its interaction with the child safety technology. Figure 3 focuses on the components of the factory-installed restraint technology. Belt retractor and pretensioner technologies are among those reported for the safety belts and related back to the secured child safety seat.

Figures 1 through 3, with their insets, are meant to show the presence of the ***enhanced data set*** variables and their interrelationship with highlighted tabs and families of tabs. Further, this is also a means by which the counts provided in the ***11-file data set*** might be integrated with the complete case viewer data. The case viewer does not provide weighting factors, for this reason the ***11-file data set*** must still be queried to obtain estimates based upon the year, primary sampling unit, case identification number, and occupant number. The concatenation of these values represents the unique identifier subject to the crashes weighting factor. This can be merged with data extracted from the case viewer. For the data years 2004 and 2005, an XML file can be saved for easier transfer of the data elements. Finally, the correspondence of the ***11-file data set***, variables and attributes, and their placement within the case viewer, with the ***enhanced data set*** allows for the analyst to optimize NASS CDS information usage.

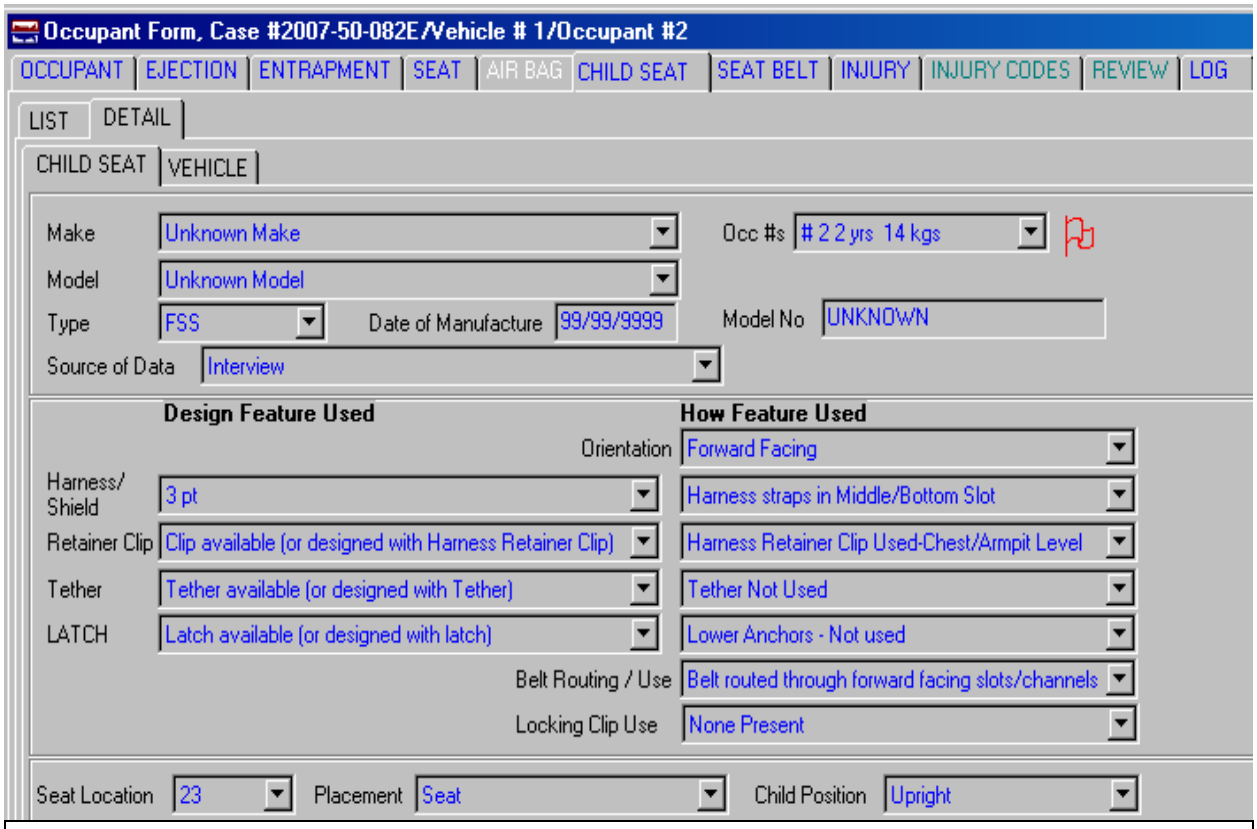

Inset 1: Child Seat Tab Contents

In contrast to the pre-2002 child safety seat types, the current child seat tab allows the data analyst to ascertain the precise type of seat, with current terminology, accurately identified by the NASS CDS field researcher. The child seat tab summarizes the enhanced child restraint variables collected currently.

In this case, a forward facing safety seat (FSS) was reported. Constrained by older formatting, the ***11-file data set*** identified a toddler child seat type but confirms the unknown make. A carefully researched listing of the newest child seat makes and models was compiled through 2007. On this occasion the technology might have reached market before it could be included in the listing or the seat was unavailable at the time of the vehicle inspection, as the source of data for this tab was the interview. Since the NASS Researcher is constrained to specifically identify known elements, the make and model were identified as "Unknown" in this case. When the seat is present, information on date of manufacture and model number might also be collected. The manufacture data is particularly important when attempting to identify a specific child restraint make, model and type in addition to its date of manufacture. With age, prolonged exposure to extreme temperature, plastic deformation or debilitation possible from a previous crash or forces imparted by the belt over the fastening surfaces might be identified as producing decrements in seat performance. An exhaustive inspection of the vehicle and child restraint coupled with the data gathered from each component specific interview will yield the design feature used and the manner in which it was used. This is another point where the expertise of those imparting quality control is crucial, as subtleties exist in the design of given types of child safety restraints.

As a reference back to the injury data and safety systems data, the occupant number, age, and weight are provided as a quick demographic summary when analyzing the child seat tab. Finally, many data analysts wish to establish the occupant kinematics throughout the crash. The child position provides a baseline for those recreating the crash.

Figure 1. Sample Occupant Form, Child Seat Tab

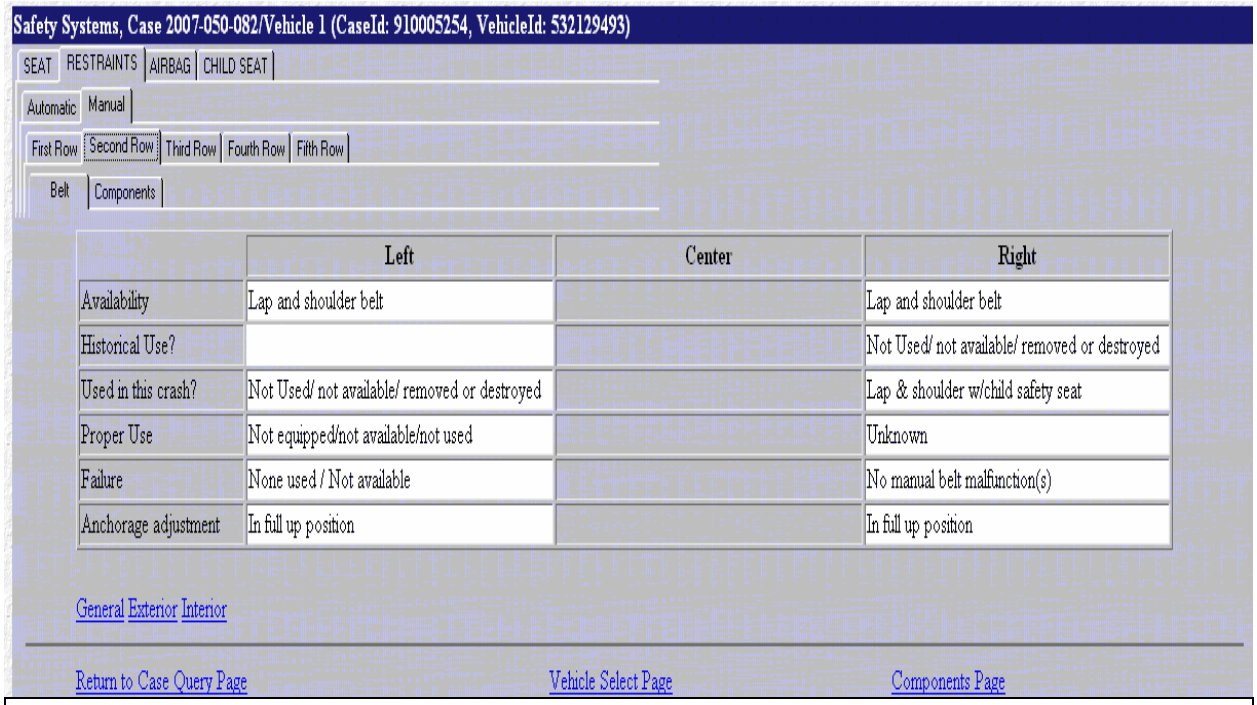

	Left	Center	Right
Availability	Lap and shoulder belt		Lap and shoulder belt
Historical Use?			Not Used/ not available/ removed or destroyed
Used in this crash?	Not Used/ not available/ removed or destroyed		Lap & shoulder w/child safety seat
Proper Use	Not equipped/not available/not used		Unknown
Failure	None used / Not available		No manual belt malfunction(s)
Anchorage adjustment	In full up position		In full up position

Inset 2: Manual Restraint Use Tab, Interaction with Child Safety Technology

The child restraint does not act independently within the vehicle. Instead, it is dependent upon factory-equipped, vehicle restraint technologies. These technologies are rarely designed in consideration of interaction with a retrofit device, including the child safety seat, and its integration into a safety technology suite. Correct installation is subject to the degree of knowledge that the installer has regarding the vehicle's restraint system and the respective installation techniques required for various types of child restraint systems.

The NASS CDS field researcher must be equally knowledgeable of various vehicle restraint systems so that the method used to install the child restraint is accurately captured and coded within the case. This is achieved by in-depth specialized training in the families of child restraint devices, their installation in a variety of vehicles, and their subsequent identification. With the training and the enhancement of the variables and attributes, the most complete, nationally representative child safety data set may be published.

For the right occupant, the type of manual restraint can be identified, as can its interaction with the child safety seat. This is particularly important for determining that in the right second seat position the vehicle installed technology was fastened, that the child restraint was secured with the lap and shoulder belt, and that the position of the anchorage adjustment was in the full up position. This level of detail is absent in the ***11-file data set*** but populates the ***enhanced data set***.

Figure 2. Manual Restraint Tab for Child Safety Seat Position, with Right Seat Position Example, Full Tab shown.

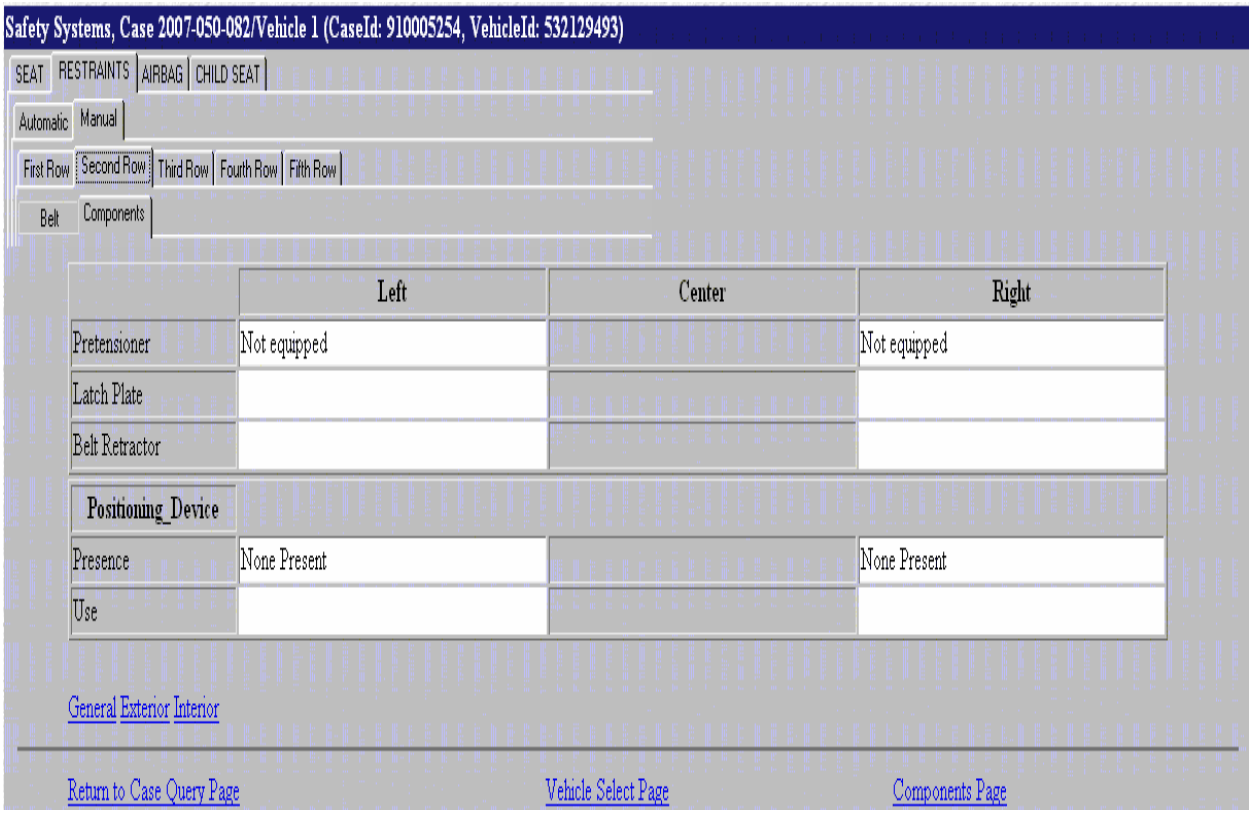

Inset 3: Components Tab, associated with Manual Restraint, Safety Belt

More new technologies associated with the factory-equipped vehicle safety belts are found in this tab. Presence of pretensioners, types of latch plate, and belt retractors can be noted, if present. Finally, any belt positioning technology, present in the vehicle and its status at the time of the crash might also be noted in this tab.

Please note that in the newest vehicles, especially those that have been inspected, the data provides the analyst with a clear picture of the child safety seat and factory-installed restraint equipment. Again, keeping pace with the newest technologies has given rise to these new variables and attributes but uniformity of database structure applied to the older cases might give the impression of incomplete information. This is not the case; instead, it is an indication of the completeness of the newest cases. This information is absent in the ***11-file data set*** but populates the ***enhanced data set***.

Figure 3. Manual Restraint Components Tab for Child Safety Seat Position

A search of the NASS CDS case viewer may be made selecting from the parameters set forth on the query page, as seen in Figure 4. The sample query might be framed seeking fatally injured children from birth to four years old restrained by a child safety seat. An excerpt of the sample query results are seen in Figure 5, in a format similar to that found in the ***11-file data set***. Upon saving the Hypertext Markup Language (HTML) information in an EXCEL spreadsheet or text document, or ACCESS database file, this information can be imported into SAS. This file will form the basis of the search of the ***11-file data set*** to obtain the requisite weighting factors for the analysis. The strength of this exercise is yielded upon manually reviewing elements such as those found in Figure 6, replicating the ***enhanced data set***, but absent in the ***11-file data set***.

As mentioned previously, Figure 6 is a screen shot of NASS Main, which, in some cases, has more detail than the public viewer, and forms part of the sample query framed above. It is the anticipation that this information will be contained in the ***enhanced data set*** to be released to the public. When consulting the "Source of Data" tab in Figure 6, the information regarding the child seat came from an interview with the occupant's Mother. The interviewee indicated that the Child Seat Type was a FF, forward facing only seat, and that it had a 3-point harness. If the seat was indeed a forward facing only seat then it likely had a 5-point harness or a shield. The case must be coded according to what was identified and/or what was actually seen/found by the field researcher, not what should be. In other words attributes are coded as described in the interview process or when the child seat itself is available, as found by the field researcher. When something unusual is coded, there is normally an annotation made to the case for explanation. The annotation field is available to the NASS researcher to provide comments outside the scope of the coded elements. An annotation was made in this case referencing the source of the child restraint information and the choice of Seat Type. For this reason, there may be instances when some of the attributes coded for design features or how feature used in a case do not make sense to an analyst.

Anomalies Explained

There are occasions when data do not seem to make sense. It should be noted that it is by design owing to the rigorous edit checks in place, through the 2007 crash year. The subsequent example provides some insight regarding one such example. The screen shots found in Figures 1, 2, and 3 were taken from the sample case, with Figure 6 containing excerpts of that case.

The annotation field is an esoteric, many times chaldaic device, whose understanding is confined to the Zone Center governing the usage of this field. It has been reported that the annotation has been used as an elucidating vehicle for unique elements defying the rigidity of the coding structures. Further, the annotation has also been used by Zone Centers to impart instructions or direct corrections to the researchers. Owing to the disparate motivations for including the annotations, the framers of NASS CDS have opted to exclude this information. The exclusion is based upon both consistency and cost-saving. Consistency is important to the system, as the two Zones Centers must work seamlessly to sample and report crashes. The cost-savings enters owing to the sanitization to which this field might be subjected. Unlike the crash summary, which is not subjected to edit check but has general guidelines governing the type of information to be included, this field has no proper rules to govern its preparation or the elements deemed appropriate for inclusion.

There have been instances where organizations have approached NCSA for clarification of seemingly incompatible entries as described above, these could form the basis for a published compilation of explained anomalies. Currently, the explanation is only beneficial for the individual or organization that has received the clarification, nevertheless, the case information remains confusing for others who might lose confidence in the data set owing to questionable query results but who have not known to seek help in interpreting the data. Data analysts have suggested that queries of this sort be published in a frequently asked questions section of the NCSA web site or in supplements akin to an Analytical Users Guide.

It should be noted that edit checks are in place for the wide variety of incompatibilities known to exist. This ongoing identification of new technologies and their interactions with the various restraint and vehicle technologies underscores the strength of NASS CDS data and its value to the child safety community. The preceding section, however, deals with ever-developing situations subject to identification by headquarters and Zone Center staff. The annotation field has served to bridge what might have been told to the researcher, which must be coded, and what might reasonably have been. To reinforce, the NASS CDS researcher may only code based upon their sources, ranging from a full-vehicle inspection with child safety seat resident in vehicle

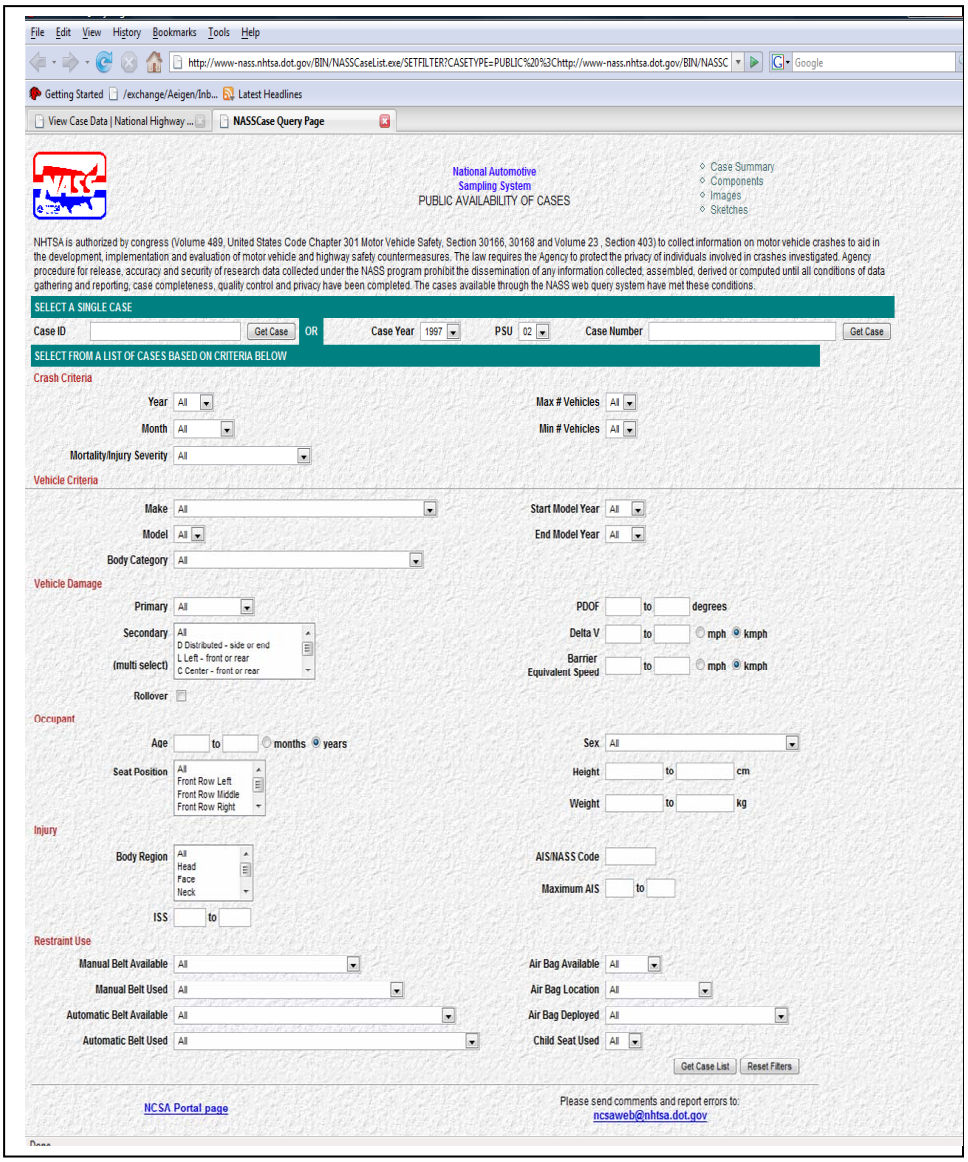

Figure 4: NASS CDS case viewer query screen

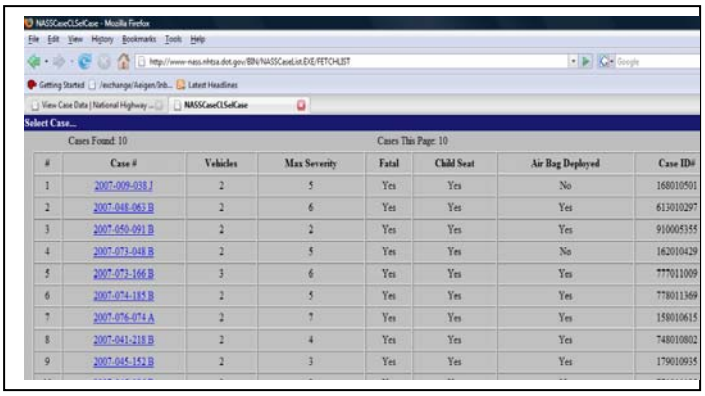

#	Case #	Vehicles	Max Severity	Fatal	Child Seat	Air Bag Deployed	Case ID#
1	2007-009-038 J	2	5	Yes	Yes	No	168010501
2	2007-048-063 B	2	6	Yes	Yes	Yes	613010297
3	2007-050-091 B	2	2	Yes	Yes	Yes	910005355
4	2007-073-048 B	2	5	Yes	Yes	No	162010429
5	2007-073-166 B	3	6	Yes	Yes	Yes	777011009
6	2007-074-185 B	2	5	Yes	Yes	Yes	778011369
7	2007-076-074 A	2	7	Yes	Yes	Yes	158010615
8	2007-041-218 B	2	4	Yes	Yes	Yes	748010802
9	2007-045-152 B	2	3	Yes	Yes	Yes	179010935

Figure 5: Partial Result of Query Page Search on fatally injured children 0 to 4 years old, restrained by a child safety seat.

with an interview as background information to merely a telephone interview with someone familiar with the crash, generally a related or unrelated caregiver.

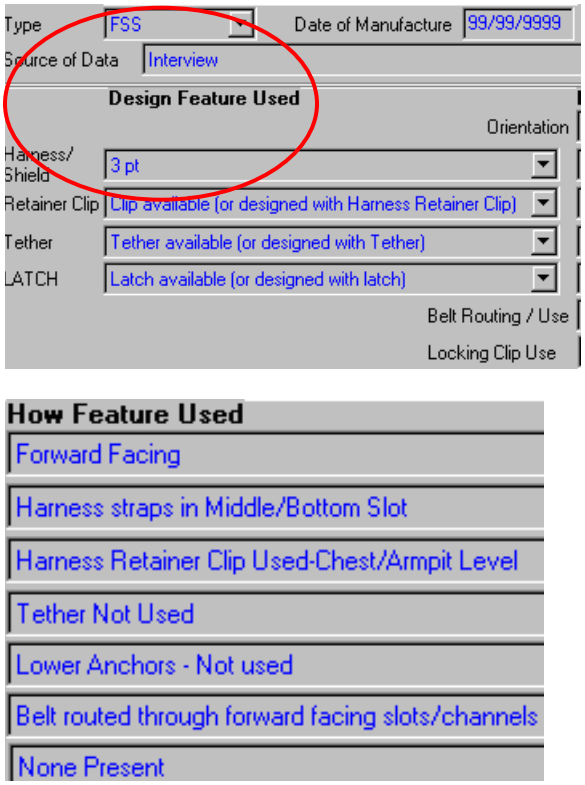

Figure 6: Excerpts from Figure 1.

Data Set Size versus Relevance

Suggestions for meaningful usage of pre-2002 and 2002 data onward

Although some problems exist with the pre-2002 data, this should not deter use on an aggregate level. The aggregation allows for an accurate, nationally representative estimate of child seat usage, in all forms. Finer disaggregation before 2002 might include some form of age or weight distinctions to clarify the limited attributes. Unfortunately, the advent of the enhanced seat data cast doubt on the validity of the previous years. The indication should be that greater detail, based upon informed child safety parameters, was included after 2002. The prior years might be better considered a counting of overall child safety incidence but not of less value and another example of perennial adjustments made to keep apace with technology and data recording advances.

Deciphering the Hidden Mysteries of the Coded Information

Child Seat Tab, Added Attribute - Source of Data

A uniform means of accessing and interpreting the data is provided. By omitting the annotations made by NASS researchers, possible inconsistencies are introduced. Coded elements are actually accurate but may only make sense after consulting published data elements, such as accident summaries, and unpublished data elements, such as annotation fields. A NASS-wide standardization of the annotation field usage must be instituted to guarantee a feasible means of complete information provision. This is the final installment in the series of the ***enhanced data set*** introductory papers prepared by the authors, as an interim approach is available to query the child safety data. This is, nonetheless, an inadequate means of query and only with the release of the ***enhanced data set***, at pace with the ***11-file data set***, can meaningful and efficient analysis be performed. As of the paper submission deadline for the 21st International Technical Conference on the Enhanced Safety of Vehicles Conference (ESV), only two years of data will have been made publicly available though the ***enhanced data set*** collection took effect for crash year 2002. To date, the enhanced variables must be sought out case-by-case through the NASS CDS case viewer.

Reprise of Archaic Formatting after 2002

It was evident that the formatting was an issue of archaic database structures rather than errors in data collection and codification, per Murianka 2005. NASS CDS continues to keep pace with evolving technologies and providing state-of-the art training from subject matter experts and industry representatives. The enhanced data collection is well documented in the enhanced data sets and on the NHTSA web site. The ***11-file data set***, however, is unable to support this new data and has suffered from lagging data provision not only in the area of child safety but also in the areas of rollover and vehicle-installed restraint systems.

To date, the general public has been granted access to the ***enhanced data set*** for crash years 2002 and 2003. The data were released after exhaustive quality control. Data for 2004 through 2007 are pending and the motivation for this document is to provide supplementary means for data extraction in the absence of the expanded files for these years.

CONCLUSION

The child safety data analyst will benefit from the newest data collection by performing an integrated data search. For years 2004 onward, the stringent quality control procedures are ongoing.

In the absence of the ***enhanced data set***, an interim methodology for data extraction was proposed. This included the following steps.

1. ***11-file data set*** SAS query – The traditional case identification ensures the retention of weighting factors necessary in any NASS CDS analysis.
2. NHTSA web site NASS CDS query – With the cases identified in Step 1, an analyst will be able to pull up a case file containing enhanced variables, attributes, and associated graphics. The case viewer is available from 1997 through 2007. An XML case viewer, with cases from 2004 and 2005, is also available facilitating data extraction.
3. Upon identifying relevant case information, this will either be manually entered from the case viewer or automated using XML output.

The three-step extraction process is cumbersome, although, it is a remedial activity until the ***enhanced data set*** can be released. Also, as shown in the sample query output for Figure 5, the cases might be identified via case viewer query, on the NHTSA web site and merged with the ***11-file data*** set to obtain available vehicle and occupant parameters, with case weighting factors.

It should be noted that sophisticated case extraction tools have been written but in their absence the three-step approach is the one used by the authors. It is also reinforced that without the publication of the annotation fields seemingly incompatible results might appear; nevertheless, these are the result of coding what is known by the researcher not what should be.

At the suggestion of the NHTSA Rulemaking, this document will be made available to the National Center for Statistics and Analysis for supplemental publication, at their option, as a transitional data usage manual until the ***enhanced data set*** is released in its entirety.

REFERENCES

Eigen, A., Murianka, J., Four Years of Enhanced Child Restraint Data Collection in NASS CDS, ESV 07-0235, Lyon, 2007.

Murianka, J., Eigen, A., Enhanced Child Restraint Data Collection in NASS CDS, ESV 05-0216, Washington, DC, 2005.

Association for Advancement of Automotive Medicine, Abbreviated Injury Scale (AIS) 1990 - Update 98, Barrington, 1998.

National Automotive Sampling System Crashworthiness Data System 1997 – 2007 case viewer, http://www-nass.nhtsa.dot.gov/BIN/NASSCaseList.exe/SETFILTER?CASETYPE=PUBLIC%20%3Chttp://www-nass.nhtsa.dot.gov/BIN/NASSCaseList.exe/SETFILTER?CASETYPE=PUBLIC%3E

National Automotive Sampling System Crashworthiness Data System 2004 – 2005 case XML viewer, http://www-nass.nhtsa.dot.gov/BIN/NASSCaseList.exe/SETXMLFILTER

National Automotive Sampling System Crashworthiness Data System 1988 – 2007 file transfer protocol web site, ftp://ftp.nhtsa.dot.gov/NASS/,

National Automotive Sampling System Crashworthiness Data System 2002 – 2003 file transfer protocol web site, ftp://ftp.nhtsa.dot.gov/NASS/,

United States Department of Transportation, National Highway Traffic Safety Administration, National Automotive Sampling System, Crashworthiness Data System, 2002-2005, NHTSA, Washington, D.C.

United States Department of Transportation, National Highway Traffic Safety Administration, "National Automotive Sampling System, Crashworthiness Data System, 2000 Coding and Editing Manual", NHTSA, Washington, D.C.

UPDATED ANALYSIS OF LOWER EXTREMITY INJURY RISK IN FRONTAL CRASHES IN THE UNITED STATES

Rodney W. Rudd
National Highway Traffic Safety Administration
United States
Paper Number 09-0556

ABSTRACT

Injuries to the lower extremities continue to occur in frontal crashes despite increased attention on vehicle structure and restraint design. Since lower extremity injuries can lead to costly rehabilitation and long-term disability, it is important to understand their causation and how well modern design practices are affecting their incidence and severity. This study investigates lower limb injury risk and causation in a U.S. crash database, and compares the risk and severity based on the nature of the crash and vehicle specifications. This study uses weighted NASS-CDS data to give an overall view of lower limb injury risk over a period from 1994 until 2007. Crashes will be categorized by intrusion level, delta-V, and vehicle model year. Particular interest will be paid to leg, foot and ankle injuries as well as occupant factors and intrusion levels.

A review of the representative data suggests that foot and ankle injury prevalence has not decreased in newer model-year vehicles, and that injury risk to the foot and ankle has actually increased despite structural improvements aimed at reducing footwell deformation. When broken down by delta-V, the trends vary, but the majority of the injuries occur at lower crash severities. Although vehicle structures and restraints have been optimized for improved performance in consumer information and regulatory tests, the risk of sustaining lower extremity injuries, especially to the foot and ankle, remains an issue that deserves further attention.

INTRODUCTION

Improvements to restraint system performance in the 1980s and 1990s precipitated an increase in attention paid to lower extremity injuries sustained in frontal crashes. A number of publications highlighted the importance of the lower extremities in terms of the overall injury distribution – with the lower extremities accounting for a large portion of the frontal crash injuries sustained [States, 1986; Pattimore *et al.*, 1991; Morgan *et al.*, 1991; Dischinger *et al.*, 1994, Pilkey *et al.*, 1994]. Though rarely life-threatening, lower extremity injuries can lead to long-lasting disability with physical and psychosocial effects [Read *et al.*, 2004]. Despite extensive study, the factors related to foot and ankle injury causation remain unclear, though some studies have postulated that toepan intrusion and pedal interaction were responsible for many of the injuries.

An in-depth analysis of crashes from the U.K. indicated that the majority of the ankle injuries were caused by intrusion of the toepan [Manning *et al.*, 1998]. Thomas *et al.* [1995] also concluded that toepan intrusion increased the risk of sustaining lower limb injuries. Conversely, an investigation of field crashes spanning the period from 1988 to 1995 in the U.S. suggested that almost all lower limb injuries occurred in frontal crashes with delta-V below 50 km/h and with toepan intrusion levels below 3 cm [Crandall *et al.* 1995; Crandall *et al.*, 1998]. Crandall *et al.* [1998] cautioned that the effects of footwell intrusion may not be fully captured by a static post-crash measurement.

Occupant anthropometry has also been shown to affect lower extremity injury risk. Crandall *et al.* [1996] concluded that foot and ankle injury risk decreased with increasing driver height. That same study also indicated a higher risk for females than for males. Differences in seating positions associated with different heights, in addition to greater injury tolerance for larger occupants, likely play a role in this outcome. Differences in seating positions associated with different vehicle types are also likely to affect lower extremity injury distribution and risk [Rudd *et al.* 2006].

The objective of this study was to take an updated look at the nature of lower extremity injuries in frontal crashes. The Insurance Institute for Highway Safety (IIHS) included measurements of toepan intrusion in its frontal offset rating program, and the result was that many newer vehicle designs experience less toepan deformation in offset frontal crashes than earlier models. One of the primary interests was how modern vehicle designs have affected the lower extremity outcome in frontal crashes. Other issues of interest included vehicle type, occupant height, and crash severity.

METHODS

Case data were selected from the National Automotive Sampling System/Crashworthiness Data System (NASS/CDS) for analysis in this study (case years 1994 through 2007). Model year 1995 and newer light vehicles involved in tow-away frontal crashes without rollover were included. Adult occupants (thirteen years of age or older) seated in an outboard first row position (seatpos 11 or 13) with an available frontal air bag were applicable for analysis if they were properly belted and not ejected from the vehicle. Since knowledge of injuries was critical to this analysis, only those cases with known injury information were included.

The crashes were classified as full frontal, left offset, or right offset based on the criteria specified by Stucki *et al.* [1998]. The vehicle's general area of damage (GAD1), principal direction of force (DOF1), object contacted and damage location were used to determine the crash mode. Vehicles involved in rollover crashes were not considered. All data presented have been weighted according to NASS/CDS recommendations except where noted.

The representative CDS data were analyzed using SAS 9.1 software (SAS Institute Inc., Cary, NC) and standard errors from the sampling procedures were accounted for using the PROC SURVEY functions with the stratification information. Risks were calculated by dividing weighted incidence by weighted exposure. Odds ratios and confidence intervals were calculated using SURVEYLOGISTIC.

This study focused on injuries to the lower extremities, which were broken down into the following sub-regions: pelvis, hip, thigh, knee, leg, and foot/ankle. The injuries were divided into the specific sub-regions based on their AIS code, and the breakdown follows clinical definitions for the lower extremity regions [Kuppa *et al.*, 2003]. Knee sprains were not considered to be AIS 2 injuries for this analysis. In the second half of the analysis, special emphasis was placed on the leg, foot and ankle, where ankle injuries include malleolar fractures.

RESULTS

There were 15,364 occupants in the selection of CDS cases meeting the frontal crash and occupant criteria, which represented 6,423,619 total occupants after weighting. Of the frontal crash occupants selected, 1,370 sustained at least one AIS 2+ lower extremity injury, which became 151,362 occupants after weighting. Summary statistics for the occupants and crashes are shown in Table 1. The age distribution for the occupants is shown in Figure 1 and the height breakdown by gender is shown in Figure 2. A distribution of total delta-V is provided in Figure 3 sorted by the crash type. A large majority of the crashes had a delta-V of less than 30 km/h.

Table 1.
Summary statistics for CDS dataset

	Group	Mean	Percentage
Age		36.3 years	
	Male	37.5 years	49.4%
	Female	38.2 years	50.6%
Height		171.0 cm	
	Male	178.0 cm	
	Female	164.1 cm	
Delta-V		20.0 km/h	
Crash Type			
	Full Frontal		20.9%
	Left Offset		41.2%
	Right Offset		37.7%
Seating Position			
	Driver		82.5%
	Right Front Passenger		17.5%

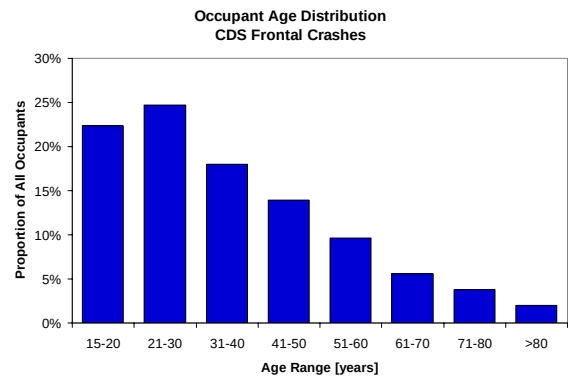

Figure 1. Occupant age distribution (weighted) in CDS frontal cases, all occupants.

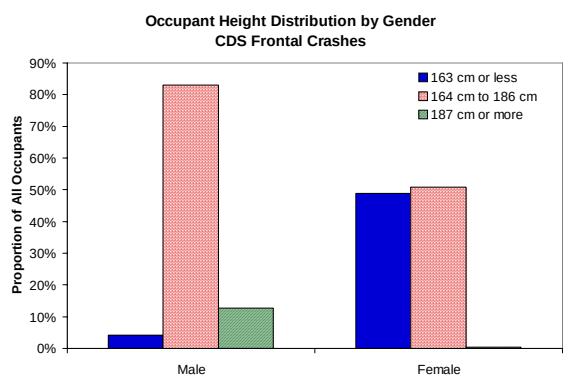

Figure 2. Occupant height distribution by gender (weighted) in CDS frontal cases, all occupants.

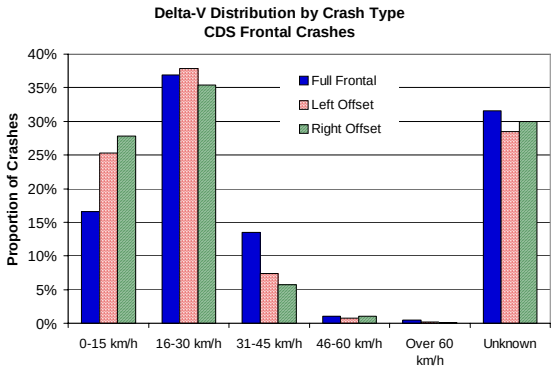

Figure 3. Crash delta-V distribution (weighted) in CDS frontal cases by crash type.

The distribution of all AIS 2+ lower extremity injuries by sub-region was determined as a function of some vehicle and occupant factors. A comparison by vehicle model year, where 1995-2000 model years were considered the older group and 2001+ were considered the newer group, is shown in Figure 4. The proportion of knee and foot/ankle injuries is higher in the newer group, while the other sub-regions constituted fewer of the lower extremity injuries. Hip injuries made up a similar proportion for both groups.

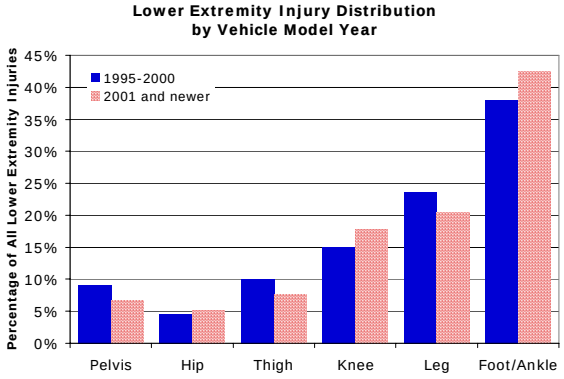

Figure 4. Distribution of body regions sustaining at least AIS 2+ injury in CDS frontal crashes by vehicle model year.

Vehicles were also classified by type, where pickups, sport utility vehicles, and vans were lumped together in the LTV group. The injury distribution comparison for passenger cars compared to LTVs is shown in Figure 5. The proportion of below-knee injuries is somewhat lower for LTV occupants, but LTV occupants tended to have more above-knee injuries overall compared to car occupants.

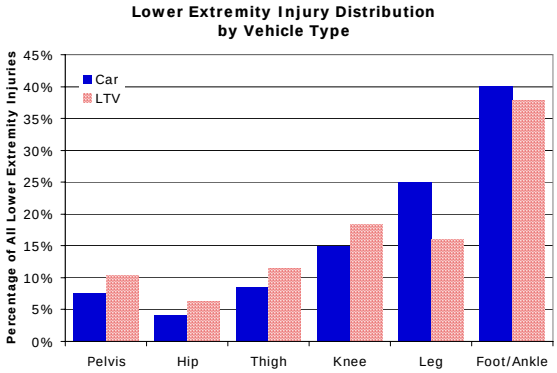

Figure 5. Distribution of body regions sustaining at least AIS 2+ injury in CDS frontal crashes by vehicle type.

Prior studies have indicated a gender bias with respect to lower extremity injuries, so the distribution among males and females was calculated and is shown in Figure 6. Men suffered a greater proportion of pelvis and thigh injuries, but the female group sustained a larger number of foot and ankle injuries.

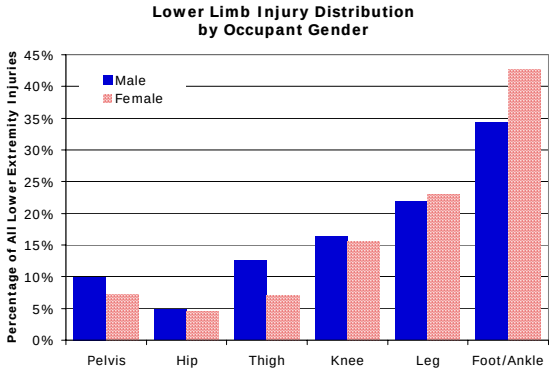

Figure 6. Distribution of body regions sustaining at least AIS 2+ injury in CDS frontal crashes by occupant gender.

Prior studies have also indicated differences in lower extremity injuries based on occupant anthropometry. The injured occupants were segregated by height into three groups, one for those 163 cm (5'4") or shorter, one for those between 164 cm and 186 cm (5'5" to 6'1"), and a third for those taller than 187 cm (6'2"). The distribution based on height is shown in Figure 7. The most prevalent trends are for an increase in above-knee injuries and a decrease in foot/ankle injuries with increased occupant height.

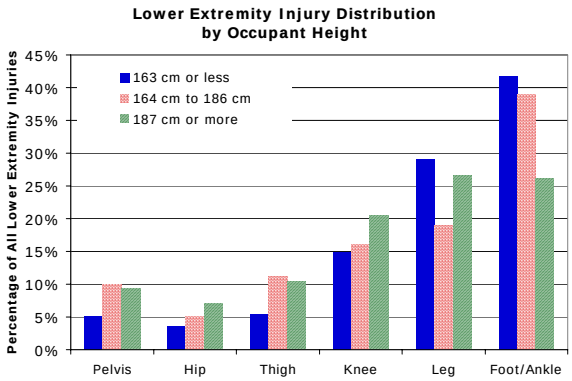

Figure 7. Distribution of body regions sustaining at least AIS 2+ injury in CDS frontal crashes by occupant height.

AIS 2+ injury risk was calculated for the lower extremity sub-regions based on the vehicle and occupant factors compared in Figures 4 through 7. Odds ratios were calculated between groups, and are shown below the risk values in Table 2. Statistical significance of each comparison, based on α=0.05, is indicated by an asterisk next to the odds ratio. A comparison of risk values for drivers based on the crash type has also been included.

Further analysis was conducted looking only at injuries to the leg and foot/ankle complex. Injury incidence and risk were calculated based on the effects of toepan intrusion, delta-V, gender/height and vehicle type/height. Each of the accompanying charts shows the distribution of frontal crashes for three sets of conditions: the left column (dark blue) shows the distribution for all frontal crashes, the middle column (speckled red) shows the distribution among crashes in which an AIS 2+ leg injury was sustained, and the right column (green stripes) shows the distribution among crashes in which an AIS 2+ foot or ankle injury was sustained. All columns of each color add up to 100 percent. Following each chart, a table lists the calculated leg and foot/ankle AIS 2+ injury risk values for the various levels of vehicle and occupant effects.

Figure 8 shows the effects of toepan intrusion. Most frontal crashes (96%) occur with little or no toepan intrusion, and nearly 70% of the leg and foot/ankle injury crashes also occur with little or no toepan intrusion. Injury risk generally increases with higher levels of toepan intrusion (Table 3). The foot/ankle complex is generally at a higher risk than the leg, regardless of intrusion level.

Table 2
Injury risk (AIS 2+) and odds ratios for lower extremity sub-regions based for various vehicle and occupant factors

	Pelvis	Hip	Thigh	Knee	Leg	Foot/Ankle
Model Year						
Old (1995-2000)	0.27%	0.14%	0.30%	0.45%	0.71%	1.15%
New (2001+)	0.23%	0.17%	0.26%	0.60%	0.69%	1.44%
New vs. Old	*0.83*	*1.26*	*0.86*	*1.33*	*0.97*	*1.26*
Vehicle						
Car	0.25%	0.14%	0.28%	0.50%	0.84%	1.34%
LTV	0.27%	0.17%	0.30%	0.49%	0.42%	1.00%
LTV vs. Car	*1.08*	*1.19*	*1.06*	*0.98*	*0.50*	*0.74*
Gender						
Male	0.25%	0.12%	0.32%	0.41%	0.55%	0.86%
Female	0.27%	0.17%	0.26%	0.58%	0.86%	1.59%
Female vs. Male	*1.08*	*1.38*	*0.83*	*1.41*	*1.57**	*1.86*
Height						
Short (≤163 cm)	0.19%	0.14%	0.20%	0.56%	1.10%	1.58%
Average (164 -186 cm)	0.29%	0.15%	0.33%	0.48%	0.57%	1.16%
Tall (≥187 cm)	0.18%	0.14%	0.21%	0.40%	0.53%	0.52%
Short vs. Average	*0.65**	*0.91*	*0.62*	*1.17*	*1.96**	*1.36*
Tall vs. Average	*0.62*	*0.91*	*0.62*	*0.84*	*0.93*	*0.44**
Crash Type (Drivers only)						
Full Frontal	0.50%	0.14%	0.37%	0.63%	0.65%	2.12%
Left Offset	0.28%	0.19%	0.29%	0.48%	0.78%	1.26%
Right Offset	0.20%	0.14%	0.27%	0.52%	0.42%	1.06%
Left vs. Full	*0.56**	*1.39*	*0.79*	*0.77*	*1.19*	*0.59*
Right vs. Full	*0.40**	*1.07*	*0.74*	*0.83*	*0.64*	*0.50*

Note: Comparisons between groups (odds ratios) are shown in *italicized text*. An asterisk (*) indicates statistical significance for the differences in injury risk for the comparison groups.

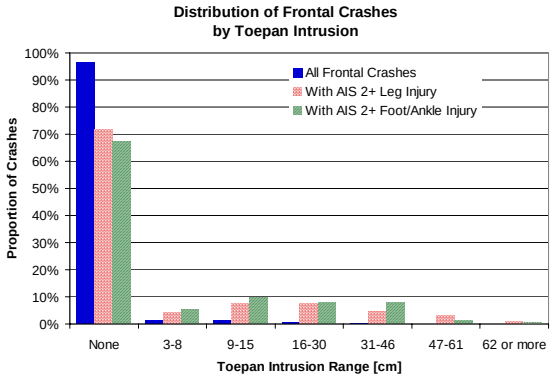

Figure 8. Distribution of crashes by toepan intrusion level for all frontal crashes, those in which the occupant sustained at least one AIS 2+ leg injury, and AIS 2+ foot/ankle injury.

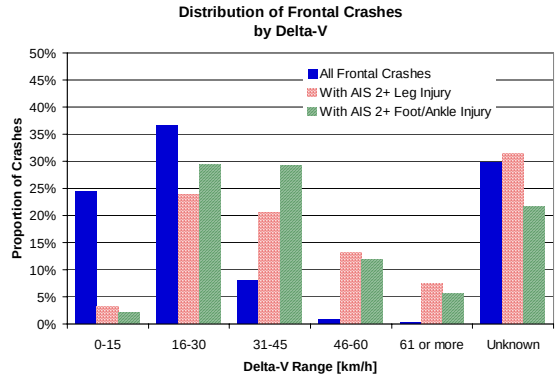

Figure 9. Distribution of crashes by delta-V for all frontal crashes, those in which the occupant sustained at least one AIS 2+ leg injury, and AIS 2+ foot/ankle injury.

Table 3.
AIS 2+ injury risk based on recorded toepan intrusion level

Toepan Intrusion Level	Leg Injury Risk	Foot/Ankle Injury Risk
None	0.52%	0.86%
3-8 cm	2.25%	4.59%
9-15 cm	4.56%	10.3%
16-30 cm	8.99%	16.0%
31-46 cm	14.6%	42.9%
47-61 cm	56.4%	39.9%
62+ cm	44.8%	50.8%

The majority of all frontal crashes occur with a delta-V of less than 30 km/h (Figure 9). When considering those with leg or foot/ankle injuries, the largest subset is the 16-30 km/h group and almost none occur in the lowest severity group. Similar to the trend seen for toepan intrusion, greater severity as indicated by a higher delta-V generally results in a higher injury risk (Table 4). One important consideration to make here is the inherent limitations in the calculation of delta-V. Crashes with other than full overlap may result in an underestimated delta-V.

Occupants were broken down by their gender and height, and the distribution of crashes is shown in Figure 10. The blue columns give an indication of the overall gender and height breakdown for frontal crash exposure. Of the occupants 163 cm or shorter, females dominated the overall number exposed, but had a disproportionately high number of leg and foot/ankle injuries. In the middle height range, females tended to have more foot/ankle injuries than

Table 4.
AIS 2+ injury risk based on delta-V

Delta-V Range	Leg Injury Risk	Foot/Ankle Injury Risk
0-15 km/h	0.10%	0.10%
16-30 km/h	0.46%	0.99%
31-45 km/h	1.80%	4.51%
46-60 km/h	10.5%	16.5%
61+ km/h	23.2%	29.9%
Unknown	0.75%	0.90%

males. The risk values for the various height and gender groups are shown in Table 5. Odds ratios for females compared to males have also been included in this table for the three height groups. Statistical significance at the α=0.05 level was denoted by an asterisk next to the odds ratio. Women have a significantly higher risk of foot/ankle injuries compared to men for the short and middle height groups. Leg injury risk is significantly higher for women compared to men 163 cm or less.

Occupants were also broken down by height based on the type of vehicle. Figure 11 shows the distribution for cars and LTVs and risk values are tabulated in Table 6. Short car occupants sustain a disproportionately high number of leg and foot/ankle fractures, and their risk is higher than in LTVs though only significant at the 0.05 level for the leg. Car occupants below 186 cm in height generally had a higher risk of leg and foot/ankle injury, but the tallest occupant group showed higher risk in LTVs. Tall occupants were nearly twice as likely to sustain a foot/ankle injury in an LTV compared to a car.

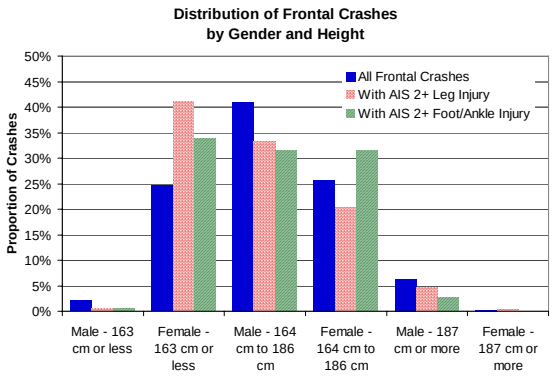

Figure 10. Distribution of crashes by occupant gender and height for all frontal crashes, those in which the occupant sustained at least one AIS 2+ leg injury, and AIS 2+ foot/ankle injury.

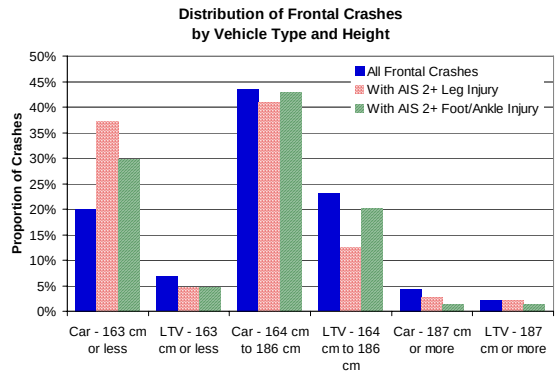

Figure 11. Distribution of crashes by vehicle type and occupant height for all frontal crashes, those in which the occupant sustained at least one AIS 2+ leg injury, and AIS 2+ foot/ankle injury.

Table 5.
AIS 2+ injury risk and odds ratios based on occupant gender and height

Gender	Height	Leg Injury Risk	Foot/Ankle Injury Risk
Male	≤163 cm	0.22%	0.27%
	164-186 cm	0.57%	0.95%
	≥187 cm	0.51%	0.53%
Female	≤163 cm	1.18%	1.69%
	164-186 cm	0.56%	1.51%
	≥187 cm	1.14%	0.17%
Female vs. Male	*≤163 cm*	*5.39**	*6.38**
	164-186 cm	*0.97*	*1.60*
	≥187 cm	*2.27*	*0.33*

Note: Comparisons between genders (odds ratios) are shown in *italicized text*. An asterisk (*) indicates statistical significance for the differences in injury risk for the comparison groups.

Table 6.
AIS 2+ injury risk and odds ratios based on vehicle type and occupant height

Vehicle	Height	Leg Injury Risk	Foot/Ankle Injury Risk
Car	≤163 cm	1.31%	1.83%
	164-186 cm	0.66%	1.21%
	≥187 cm	0.45%	0.40%
LTV	≤163 cm	0.48%	0.83%
	164-186 cm	0.38%	1.08%
	≥187 cm	0.68%	0.74%
LTV vs. Car	*≤163 cm*	*0.36**	*0.45*
	164-186 cm	*0.58*	*0.89*
	≥187 cm	*1.51*	*1.86*

Note: Comparisons between vehicle types (odds ratios) are shown in *italicized text*. An asterisk (*) indicates statistical significance for the differences in injury risk for the comparison groups.

DISCUSSION

The CDS dataset contained mostly drivers, and the distribution by gender was close to even. About two-thirds of the occupants were 40 years of age or younger. Most of the males were in the middle height group (164 cm to 186 cm), and the females were fairly evenly divided between the lowest and middle height group. Of the crashes with a known delta-V, over 85% were at a delta-V of 30 km/h or less. Based on this distribution, even with a higher injury risk in higher severity crashes, it makes sense that a large portion of the lower extremity injuries will occur with a delta-V below 50 km/h as claimed by Crandall et al. [1998]. The greatest potential for exposure, even though injury risk is lower, is generally in crashes less severe than the NCAP and IIHS tests.

One of the primary objectives of this study was to compare lower extremity injury prevalence in frontal crashes of newer vehicles to that in older vehicles. The distribution of injuries to the lower extremities was found to be slightly different for the newer group compared to the older group. There was a tendency for occupants of newer vehicles to suffer more foot/ankle and knee injuries and less pelvis, thigh and leg injuries. Foot/ankle injury risk was higher for the newer vehicles as indicated by the odds ratio of 1.26, though this was not significant at the 0.05 level (confidence interval 0.65, 2.42). One key factor related to the model year analysis was the cutoff year for the newer versus older vehicles. An analysis of IIHS results indicated that more than two-thirds of

the 2001 model year vehicles received Good or Acceptable scores in the frontal offset crashworthiness evaluation. The proportion of Good or Acceptable vehicles continued to increase thereafter, so this was chosen as a cutoff based on the assumption that a sizeable number of the vehicles would have better structural frontal crash performance. With this breakdown, approximately 29% of the total number of weighted cases was in newer vehicles. It was felt that this cutoff ensured the new group contained enough crashes for a comparison yet reflected more modern vehicle designs. One limitation in this approach comes from the staggering of vehicle redesign cycles, which means that some 2001 and newer vehicles are older designs that may not reflect newer design practices.

The overall distribution of injuries did not vary much in passenger cars compared to LTVs, though LTVs did seem to have a larger proportion of above-knee injuries. To offset this difference, LTV occupants appeared to have a smaller proportion of leg injuries compared to car occupants. In terms of AIS 2+ injury risk, there were no significant differences between the two vehicle types, but below-knee risk was generally lower in the LTVs. With vehicle interior geometry varying so widely among LTVs, and even among passenger cars, any effects of differences in seating position on injury risk are probably not evident with such an analysis. A more appropriate, and telling, characterization would have to take actual geometry into account.

The role of gender on injury distribution and risk was similar to that found in previous studies. Males tended to sustain a greater relative number of pelvis and thigh injuries while women suffered a notably greater proportion of foot/ankle injuries. Females were 1.86 times more likely to sustain an AIS 2+ foot/ankle injury than men, a difference that was nearly significant if α=0.10. Women were found to be 1.57 times more likely to sustain leg injuries. Prior studies have postulated that both geometric and footwear differences may explain the higher risk for women [Crandall et al., 1996]. An analysis of footwear was not performed in this study, but the height analysis offers some additional insight.

Shorter occupants sustained more foot/ankle injuries than their taller counterparts, based on the overall injury distribution. The shortest occupants tended to sustain fewer above-knee injuries relative to taller occupants, but the middle and tall height groups were more similar to one another. Looking at the calculated risk values suggests that shorter occupants tend to fare worse for injuries to the lower regions (knee, leg, foot/ankle). Those 163 cm in height or less are nearly twice as likely as middle-height occupants to sustain an AIS 2+ leg injury. The shortest occupants were significantly less likely to sustain a pelvic fracture. Crandall et al. [1996] suggested that the smaller drivers' higher injury risk may be associated with differences in the gap between the heel and the floor during pedal application. It is likely that the gap arises from both shorter foot length and overall geometry factors that result from shorter leg and thigh length within a vehicle geometry that is not as accommodating for shorter occupants. Pedals that adjust in both longitudinal and vertical directions may help to eliminate the heel gap among shorter drivers during braking maneuvers.

The crash type analysis in Table 2 shows that full frontal-type crashes generally resulted in a higher lower extremity injury risk compared to left- or right-offset crashes. The highest risk value was for foot/ankle injuries in full frontal crashes, which was close to being significantly higher than that in both the left- and right-offset modes. Injuries to the leg were more likely to occur in left-offset crashes compared to full frontals, but the difference was not significant. Since greater toepan intrusion is typically expected in an offset crash compared to a frontal, this result suggests that toepan intrusion may not be driving factor for foot/ankle injuries since the full-frontal mode had the highest risk.

Additional analysis was conducted with a special emphasis on below-knee injuries. Since toepan intrusion has been debated as a cause of increased lower extremity injury risk, the distribution of crashes was calculated based on the level of toepan intrusion for all crashes and for those with below-knee injuries. Overall, as shown in Figure 8, most crashes occur with little or no toepan intrusion – even those with AIS 2+ injuries to the leg, foot and ankle. As expected, injury risk increases with greater toepan intrusion, but with about 70% of the tibia and foot/ankle injuries occurring with less than 3 cm of intrusion, it appears that despite a higher risk, intrusion is not necessary to produce AIS 2+ injuries. Based on the exposure numbers alone, it is evident that efforts to reduce toepan intrusion may not completely address the problem.

Almost no leg or foot/ankle injuries occur in the crashes with delta-V below 15 km/h, though the majority occur in crashes with a delta-V below 45 km/h, considering only those crashes with known delta-V. As with toepan intrusion, injury risk does consistently increase with higher crash severity as

measured by delta-V. Even though the calculated foot/ankle injury risk is below 5 percent for crashes with delta-V 45 km/h or less, sizeable reductions in injury prevalence could be achieved by addressing moderate severity crashes based simply on exposure. Findings related to the delta-V must be viewed as generalizations due to the inherent limitations in the calculation of delta-V in anything other than a full frontal crash.

Taking another, more detailed, look at the effects of occupant height and gender in Figure 10 and Table 5, it becomes evident that the effect of gender may be related to more than just typical height differences between men and women. Relatively few males were in the shortest height group, but they demonstrated about one-sixth the foot/ankle injury risk of the female occupants of similar height – and the result was significant. In the middle height group, the female occupants had a higher risk of foot/ankle injury compared to the males. Females in the shortest subset were five times more likely than males to sustain an AIS 2+ leg injury. While the proportion of males in the shortest subset was small compared to the females (about 7% of total weighted cases), the differences in foot/ankle injury risk for all occupants shorter than 186 cm does suggest that height alone does not explain the difference between genders. The difference could be due to a lower injury tolerance among the female population or because of differences in foot size despite equivalent height. If women generally have smaller feet, the heel gap issue proposed by Crandall et al. [1996] may affect women more so than men.

The vehicle type analysis was conducted again, but with further breakdown of the cases by occupant height as shown in Figure 11 and Table 6. In this dataset, car occupants outnumbered LTV occupants by a factor of about 2 based on weighted counts. Among the shortest occupants, those occupying cars were injured more frequently than those in LTVs. While not statistically significant at the α=0.05 level, the foot/ankle risk in LTVs was 0.45 of that in cars for this group (confidence interval 0.2, 1.01). The leg injury risk for LTV occupants compared to car occupants for this height group was significant at 0.36. It is possible that the generally higher seating position in LTVs compared to cars offers some benefit to occupants 163 cm or shorter in height, though a more detailed geometric analysis would need to be performed given the vast range of seating positions available in both vehicle classes. Among middle height occupants, the foot/ankle risk in cars and LTVs was similar. Tall occupants in LTVs were more likely to suffer a foot/ankle or leg injury than those riding in cars. While it is unlikely that the tallest occupants develop a gap between their heel and the floor, overall lower limb positioning associated with the higher seating position may predispose their lower extremity, especially the foot and ankle, to more injurious loading conditions. This finding does not follow the general trend for taller occupants to have lower injury risk, so further investigation of the seating position and vehicle interior geometry effects should be conducted.

CONCLUSION

This study presented updated lower extremity injury trends based on vehicle and occupant factors in order to show where improvements can be made in frontal crash safety given that the prevalence of lower limb injuries has remained high. Since the IIHS frontal offset test has placed an emphasis on reduced toepan intrusion, it was desired to evaluate any lower limb injury trends in newer model vehicles. The analyses conducted yielded the following conclusions about lower extremity injuries in frontal crashes:

- The risk of AIS 2+ foot/ankle injury is slightly higher for occupants of MY 2001 and newer vehicles
- Females are more likely to sustain leg and foot/ankle injuries than males
- Occupants less than 164 cm in height are twice as likely to sustain leg injuries than those 164 cm to 186 cm in height
- Although the injury risk is about 1%, most foot/ankle injuries occur with less than 3 cm of toepan intrusion
- Female occupants less than 164 cm in height are at significantly higher risk of foot/ankle and leg injuries than males in the same height range
- Tall occupants of LTVs show higher risk of below-knee injury compared to those in cars
- Full frontal crashes have a higher risk of foot/ankle injuries compared to offset frontal crashes

Understanding the kinematics and dynamics of the lower extremities under different loading conditions and with different occupant configurations is not possible based on field data alone. Further explanation of these findings may be possible with computational modeling or with physical tests. Such an effort is critical for minimizing real-world foot/ankle injury risk, as the general trend with newer vehicles has not shown a reduction from the efforts to reduce toepan intrusion.

REFERENCES

Crandall, J.R., Martin, P.G., Sieveka, E.M., Klopp, G.S., Kuhlmann, T.P., Pilkey, W.D., Dischinger, P.C., Burgess, A.R., O'Quinn, T.D. and Schmidhauser, C.B. (1995) "The Influence of Footwell Intrusion on Lower Extremity Response and Injury in Frontal Crashes." 39th Annual Proceedings of the Association for the Advancement of Automotive Medicine, pp. 269-286.

Crandall, J.R., Martin, P.G., Bass, C.R., Pilkey, W.D., Dischinger, P.C., Burgess, A.R., O'Quinn, T.D. and Schmidhauser, C.B. (1996) "Foot and Ankle Injury: The Roles of Driver Anthropometry, Footwear, and Pedal Controls." 40th Annual Proceedings of the Association for the Advancement of Automotive Medicine, pp. 1-18.

Crandall, J.R., Martin, P.G., Sieveka, E.M., Pilkey, W.D., Dischinger, P.C., Burgess, A.R., O'Quinn, T.D. and Schmidhauser, C.B. (1998) "Lower Limb Response and Injury in Frontal Crashes." Accident Analysis and Prevention, vol. 30, no. 5, pp. 667-677.

Dischinger, P.C., Burgess, A.R., Cushing, B.M., Pilkey, W.D., Crandall, J.R., Sieveka, E.M. and Klopp, G.S. (1994) "Lower Extremity Trauma in Vehicular Front-Seat Occupants." SAE World Congress and Exposition, paper number 940710.

Manning, P., Wallace, A., Owen, C., Roberts, A., Oakley, C. and Lowne, R. (1998) "Dynamic Response and Injury Mechanism in the Human Foot and Ankle and an Analysis of Dummy Biofidelity." Proceedings of the 16th International Technical Conference on the Enhanced Safety of Vehicles, pp. 1960-1998.

Morgan, R. and Eppinger, R. (1991) "Ankle joint injury mechanism for adults in frontal automotive impact." Proceedings of the 35th Stapp Car Crash Conference, paper number 912902.

Pattimore, D., Ward, E., Thomas, P. and Bradford, M. (1991) "The nature and cause of lower limb injuries in car crashes." Proceedings of the 35th Stapp Car Crash Conference, paper number 912901.

Pilkey, W.D., Sieveka, E.M., Crandall, J.R. and Klopp, G. (1994) "The Influence of Foot Placement and Vehicular Intrusion on Occupant Lower Limb Injury in Full-Frontal and Frontal-Offset Crashes." Proceedings of the 14th International Technical Conference on the Enhanced Safety of Vehicles, pp. 734-741.

Rudd, R.W., Hanna, R., Sherwood, C., Burke, C. and Fakhry, S.M. (2006) "Non-Ankle Lower Extremity Injury Distribution in NASS and CIREN Frontal Crashes." Journal of Biomechanics, vol. 39, p. S144.

States, J.D. (1986) "Adult Occupant Injuries to the Lower Limb." In Biomechanics and Medical Aspects of Lower Limb Injuries. Society of Automotive Engineers, Warrendale, PA.

Stucki, S.L., Hollowell, W.T. and Fessahaie, O. (1998) "Determination of Frontal Offset Test Conditions Based on Crash Data." Proceedings of the 16th International Technical Conference on the Enhanced Safety of Vehicles, pp. 164-184.

Thomas, P. (1995) "Lower Limb Injuries – The Effect of Intrusion, Crash Severity and the Pedals on Injury Risk and Injury Type in Frontal Collisions." SAE World Congress and Exposition, paper number 952728.

BENEFIT OF ADAPTIVE OCCUPANT RESTRAINT SYSTEMS WITH FOCUS ON THE NEW US-NCAP RATING REQUIREMENTS

Steffen Sohr
Axel Heym
TAKATA-PETRI
Germany
Paper Number 09-0322

ABSTRACT

Against the background of an always growing traffic volume on the roads and the thereby resulting aim to reduce the number of traffic fatalities continuously, the recent years saw a number of research projects and field studies.
As a result of this, legal tests and consumer requirements have been significantly tightened. Consequently, car manufacturers and suppliers are faced with completely new challenges as to the adaptation of occupant restraint systems. Here, so-called "smart" restraint systems gained more and more importance.

The US-NCAP requirements for the MY 2010, adopted by NHTSA in 2008, are a new milestone for the improvement of occupant protection. For the minimization of the total injury risk in frontal impacts, the protection criteria for head (HIC), neck (Nij), and thorax (chest deflection) are under special consideration.

With regard to the new requirements, it seems to be quite challenging to achieve a very good rating in frontal crash tests by standard restraint systems, especially when different dummy sizes and the legal requirements according to FMVSS 208 have to be considered.

The present study shall demonstrate which potential adaptive airbag and seat belt technologies can possess. Thus, the performance of different concepts of adaptive airbag techniques, knee bags, double pretensioning systems and adaptive force limiter are compared. Following, an evaluation of the different concepts as to their efficiency and benefits in terms of critical injury criteria will be made. Finally, a survey is given on how the consequent use of adaptive restraint systems can address the future requirements (law, ratings).

CHALLENGES OF THE NEW US-NCAP RATING

Based on the significant improvement of passive safety level in recent years, NHTSA has decided to change the existing front and side crash rating programs. These changes are effective for the 2011 model year. NHTSA will maintain the 35 mph (56 kph) full frontal barrier test for the frontal crash test program, but the 50%ile dummy on passenger side will be replaced by the 5%ile dummy. The assessment of the frontal impact star rating is extended by additional injury criteria for neck (N_{ij}, compression/tension force), chest deflection and femur forces. [1]

The current moving deformable barrier test at 38.5mph (63kph) is still used for the side impact crash configuration. In future this test includes new side impact test dummies (SID-2s and ES-2 dummy) and new assessment criteria (HIC36, rib deflection, abdomen and pelvic force). Additionally, a 20mph (32kph) oblique pole test with a 5% female ES-2 dummy will be applied for the assessment of new vehicles.

For rollover, NHTSA will continue to use the static stability factor (SSF) and the manoeuvrability assessment (tip-up or no tip) to rate the risk of vehicles to rollover. It is expected that the agency will update this rollover risk assessment, as soon as more real-world crash data of vehicles equipped with electronic stability control are available.

With the new US-NCAP rating, NHTSA will establish a new overall Vehicle Safety Score (VSS) that combines the front, side, and rollover star rating.

Furthermore, vehicles equipped with selected advanced technologies (crash avoidance technologies) will be noted: A text display will be used to inform about a standard vehicle (without advanced technologies) or an optional presence.

- Electronic Stability Control (ESC)
- Lane Departure Warning (LDW)
- Forward Collision Warning (FCW)

This article is focussed on the challenges resulting from the new requirements for the frontal crash test.

The assessment of the occupant protection in the frontal impact bases on injury probabilities of the considered body regions (head, neck, chest, and thigh) which correlate with a defined injury severity. For detecting the single probabilities selected injury / protection criteria on the basis of risk injury curves (generally AIS 3+, except femur axial forces: AIS 2+) are used. Here, the AIS3+ injury risk curves correspond to those taken for FMVSS 208. Figure 1 illustrates this exemplarily for the driver side (50%-ile dummy).

Injury Criteria	Risk Curve
Head (HIC_{15})	$P_{head}(AIS\,3+) = \Phi\left(\frac{\ln(HIC15) - 7.45231}{0.73998}\right)$ where Φ = cumulative normal distribution
Chest (deflection in mm)	$P_{chest_defl}(AIS\,3+) = \frac{1}{1+e^{10.5456-1.568*(ChestDefl)^{0.4612}}}$
Femur (force in kN)	$P(AIS\ 2+) = \frac{1}{1+e^{5.795-0.5196\,Femur_Force}}$
Neck (Nij and tension/compression in kN)	$P_{neck_Nij}(AIS\,3+) = \frac{1}{1+e^{3.2269-1.9688Nij}}$ $P_{neck_Tens}(AIS3+) = \frac{1}{1+e^{10.9745-2.375Neck_Tension}}$ $P_{neck_Comp}(AIS3+) = \frac{1}{1+e^{10.9745-2.375Neck_Compression}}$ $P_{neck} = \max imum(P_{neck_Nij}, P_{neck_Tens}, P_{neck_Comp})$

Figure 1. Injury criteria and probabilities for driver side (AM 50). [1]

From the product of the single probabilities the so-called combined injury probability P_{comb} is calculated for each the driver and passenger side.

$P_{comb\ [Driv./Pass.]}=1-(1-P_{head})(1-P_{neck})(1-P_{chest})(1-P_{femure})$

For the actual assessment a "relative risk score" factor (RRS) is taken being a quotient from combined injury probability and a statistical quantifying parameter[1]:

$RRS_{[Driv./Pass.]} = P_{comb\ [Driv./Pass.]} / 0.15$

The probability and RRS values may then extract the "star rating" – separated into driver and passenger side - (See Figure 2).

	Frontal/ Side	
	probability	**RRS**
★★★★★	P < 0.10	RRS <0.667
★★★★	0.10 ≤ P 0.15	0.667 ≤ RRS <1.0
★★★	0.15 ≤ P < 0.20	1.0 ≤ RRS < 1.33
★★	0.20 ≤ P < 0.40	1.33 ≤ RRS < 2.667
★	P ≥ 0.40	RRS ≥ 2.667

Figure 2. Star rating based on combined probability and/or relative risk score (RRS). [7]

A total assessment is made by a so-called „Vehicle Safety Score" (VSS), uniting the weighted risk assessments from frontal crash test, side MDB pole test, as well as from the rollover assessment (See Appendix A).

The probability functions (See Figure 1) allow the conclusion that the following injury criteria for the rating according to US-NCAP New (frontal crash test) are to be considered especially critical:

Driver side:

- HIC 15
- chest deflection

Passenger side:

- HIC 15
- N_{ij}
- Chest deflection

For a conceivable scenario to achieve a „5 star rating" on the driver and passenger side (RRS < 0,667 the following target values should be reached:

Driver side:

- HIC 15 ≤ 200
- chest deflection ≤ 23 mm
- $N_{ij} \leq 0{,}3$[2]
- Femur Force ≤ 2,5 kN

[1] For the time being NHTSA has set this statistical quantifying parameter on 0.15, based on the statistical survey to assess the safety level of vehicles of MY 2008.

[2] Due to the stored probability functions for the calculation of the single probabilities P_{neck_Nij}, P_{neck_Comp} und P_{neck_Tens}, the N_{ij} is normally the most critical load criterion.

Passenger side:

- HIC 15 ≤ 250
- chest deflection ≤ 19 mm
- $N_{ij} \leq 0,3$
- Femur Force ≤ 1,5 kN

Considering these target values on the one hand and the legal load cases according to FMVSS 208 on the other, it can be safely assumed that only very few vehicles from latest model years would have been able to reach a "5 star" rating in the frontal impact according to US-NCAP NEW.

HOW ADAPTIVITY SHOULD WORK

Basically, the adaptation of components of an occupant restraint system can be divided into two groups: active and passive adaptation.
An outstanding feature of active adaptation is the integration of a control mechanism into the system component.

Passive adaptivity is a special feature already inherent in the component that has not been added afterwards. Due to its viscous characteristics even the gas vent from an airbag, e.g., has to be considered an adaptive adaptation [2].

Further considerations, however, will focus on active adaptation because the efficiency factor here can increase to a much higher degree than for passive adaptations.

It is the goal of adaptive protection components to adjust the force application at the occupant to the initial and boundary conditions of the accident. This mainly involves the accident severity, type and sort of accident, the occupants' mass, size, position, and, possibly, even their age.

In simple terms we can say that adaptivity means the ability of the protection system to adapt its stiffness to selected accident and occupant parameter in order to increase the biomechanical quality of the complete protection system. Pre-studies reveal which parameters are especially relevant for an adaptation in a frontal impact. [3]

It is without any doubt that the accident severity comes in the first place of factors followed by mass and size of the occupant. Adjusting the level of a belt force limiter, for instance, allows to adapt the protection performance of a system very well as shown in [4].

Furthermore, adaptation mechanisms may also result in an increase of efficiency. Here, especially the first phase of interaction between restraint element and occupant is put into the focus of attention. Pressure-controlled venting holes of an airbag, being under series production for many years now, are a classical example to illustrate this [5].

Reducing the gas mass during the filling phase of the airbag by using a dual-staged gas inflator or redirecting the gas flow does not lead to an increase of efficiency of the protection system due to functional reasons. [6]

But those measures can restrict the aggressiveness of the airbag system and thus contribute to reduce the danger of the occupant to get injured by the airbag deployment in out-of-position situations.

ADAPTIVITY COMBINED WITH STANDARD AND ADVANCED RESTRAINT SYSTEMS

In parallel to the introduction of adaptive solutions, an enlargement of the system components by design can increase the protection potential purposefully.

In contrast to a „Standard Restraint Systems", the „Advanced Restraint Systems", e.g., are characterized by a special airbag tailoring, knee airbags, digressive belt force limiters, and/or inflatable seat cushions (See Figure 3).

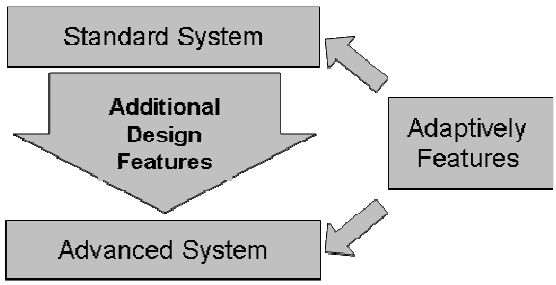

Figure 3. Adaptivity and its impact on standard and advanced restraint systems.

Depending on the restraint system performance and the boundary conditions (e.g. vehicle and module package, costs) it might be useful to prefer „advanced" components instead of adaptive solutions or respectively to combine both features.

For example, the use of a knee airbag can reduce the chest deflection but increase the head loadings. Adaptivity in the airbag makes it possible to neutralize this effect and, moreover, to reduce the head loadings clearly.

The following chapters will show concrete examples illustrating this.

EFFICIENCY AND BENEFIT OF DIFFERENT ADAPTIVE CONCEPTS FOR FRONTAL CRASH CONFIGURATIONS

On the basis of the design of today's restraint systems for the different frontal crash configurations, the target conflict is even getting sharper as to safe fulfillment of legal requirements (FMVSS 208) and new US-NCAP rating .

It is especially an airbag design (stiffness, shape) focussed on unbelted load cases according to FMVSS 208 (0° and 30° impact) and on the requirements of phase 2b (30mph, 5%- und 50%-dummy) that will lead to worse rating results in the future. In the case of demanding crash pulses (high motorization) this dilemma will even get worse.

The results of this study are based on valid occupant crash simulation of driver and passenger side. As to its interior geometry, the selected vehicle obviously corresponds to a European middle-class car. The dummy models used are the 50%-ile male and the 5% -ile female dummy (See Figure 4).

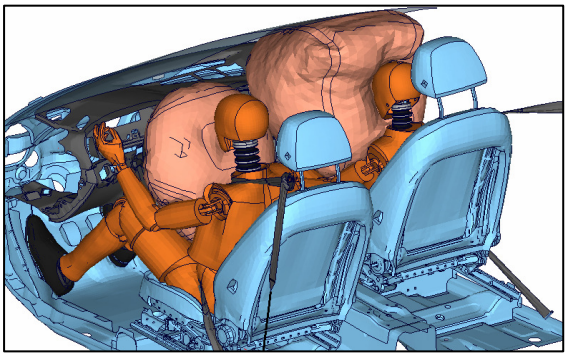

Figure 4. CAE model for driver and passenger side. [7]

The vehicle components and the dummies as well are exclusively modelled by the FE-method. In advance, the parameters of the airbag and seat belt model have been validated in their range of variations by component tests.

Basis for the choice of crash pulses for the simulation models were vehicles with extremely high front end stiffness (See Figure 5).

From previous studies we learned that especially these crash pulses require the highest performance from the protection system.

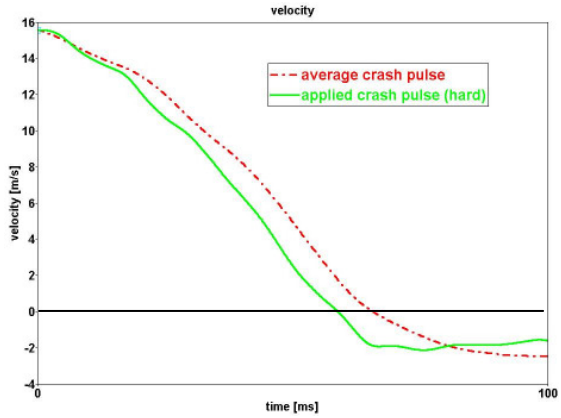

Figure 5. Comparison of US-NCAP crash pulses.

The evaluation of the simulation results does not only include the classical occupant load values (see above) but also the kinematics of the dummies themselves (e.g. the risk for „submarining") and the double forces/moments in the lumbar region. Only thus, a holistic analysis of the effects of single components in the occupant protection system can be made.

Furthermore, all changes and/or adaptive measures at the protection system are evaluated for several crash configurations. The influence on the configurations of FMVSS 208 is considered as well. The measure for the evaluation is a shortfall of 20% under the legally allowed limits for the dummy loads.

Thus, the statements or recommendations, that can be made, become broader, but the focus, however remains to be the new US-NCAP.

DRIVER SIDE

First step of the analysis is to study the single changes at the protection system separately. So it becomes possible to evaluate the respective potential apart from the others and to quantify its use for an advanced and/or adaptive protection system.

The use of an adaptive seat belt force limiter in the retractor, which is able to switch from a high level to a lower one at a defined moment, is analyzed first.

According to the US-NCAP NEW assessment the injury probability reduces by approximately 10% (see Figure 6).

Without this adaptive seat belt force limiter a safe fulfillment of FMVSS208 would not be possible in the vehicle under evaluation (load case: 5%-ile dummy). Thus, the adaptive belt becomes a confirmed part for all further variants.

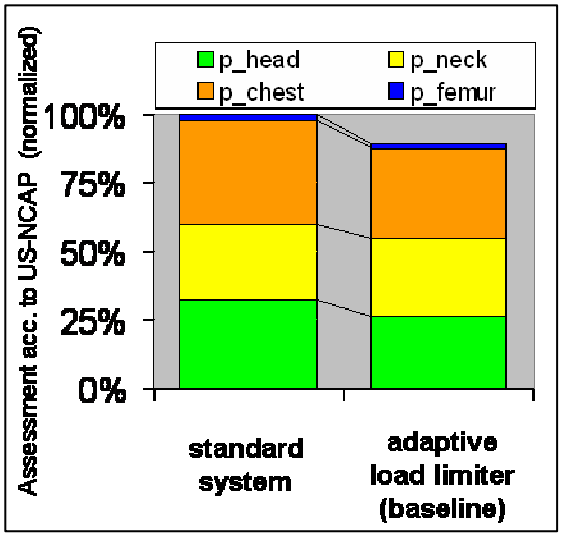

Figure 6. Adaptive belt load limiter compared to standard system.

The application of a knee bag reduces the injury risk by further 25% (see Figure 7).

The knee bag induces a reinforced support of the occupant in the pelvis area. This is accompanied by a reduction of the belt force in this area leading to positive effects on the chest deflection.

The modified kinematics of the occupant caused by the knee bag also results in reduced head loads of the dummy.

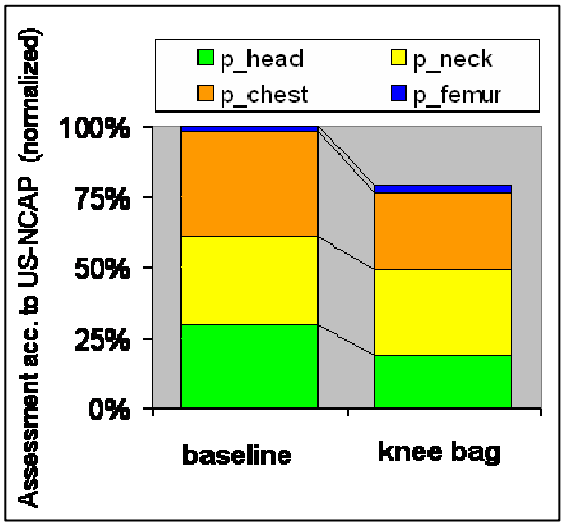

Figure 7. Kneebag compared to baseline.

Optimizing the airbag shape allows to evidently increase the protective effects in the US-NCAP NEW. The airbag tailoring is trimmed so that the head restraint becomes better and the force application on the thorax is restricted to bio-mechanically acceptable values (see Figure 8).

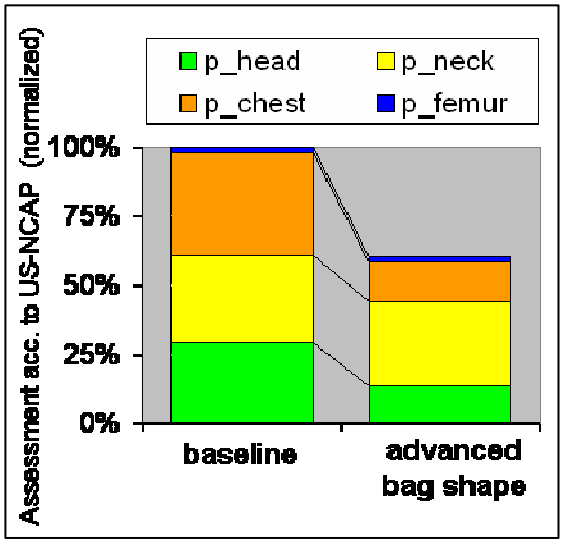

Figure 8. Advanced airbag shape compared to baseline.

The use of an adaptive airbag component, such as well as the adaptive seat belt, shows a high potential for an improvement of the protective effects in connection with the 5%-ile dummy.

Under the boundary conditions of the US-NCAP NEW, i.e. with the 50%-ile dummy, the efficiency of the analyzed airbag adaptivity is rather low.

A double belt pretensioning in the retractor and in the belt bracket or in the buckle results in a reduction of the total injury risk by approximately 10%.

As already mentioned in the beginning, the baseline crash pulse corresponds to an extremely stiff vehicle front end structure. Therefore the vehicle response was also used as a parameter within the CAE study to see which impact an average US-NCAP crash pulse has on the load values.

In comparison to the other selected modifications particularly head, neck and femur injury probabilities could be reduced significantly (See Figure 9, No. 6: average crash pulse).

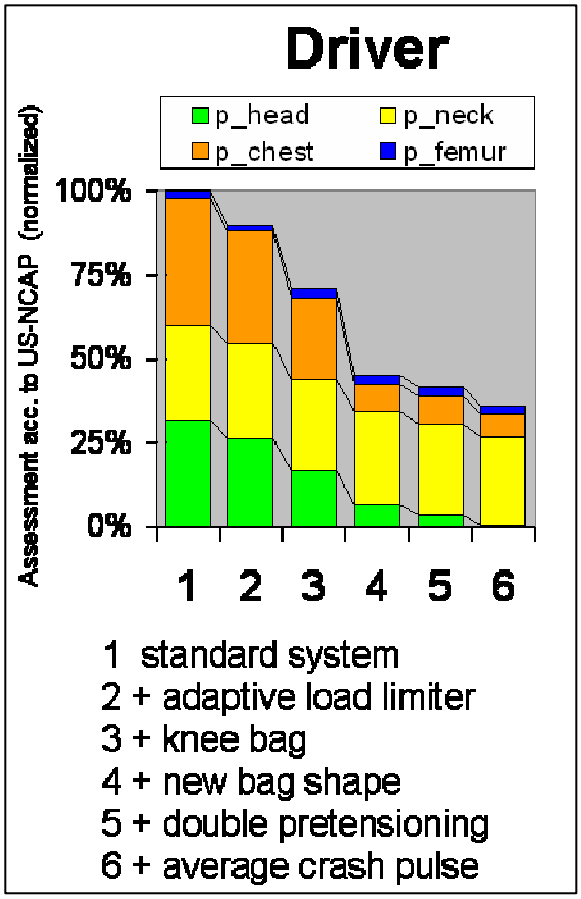

Figure 9. Overview: Benefit for driver side.

Figure 9 demonstrates clearly to which regions of the body the injury risk can be addressed by adaptive and advanced measures. The total of all measures leads to a reduction of more than 60%.

This outstanding result almost completely traces back to improvements in the head and chest area.

In contrast, the probability for injuries in the neck and lower leg regions is hardly addressed by the analyzed modifications under the given boundary conditions.

PASSENGER SIDE

The basic design for the passenger side was in that case a standard restraint system with 3D airbag shape and constant belt force limiting (without knee airbag).

As for the driver side, the influence of the restraint performance of the complete system is reported separately for each modification. This allows to derive the potential of an adaptive and advanced protection system for the passenger side.

In a first step, based on the standard system an adaptive airbag system reduces the head injury probability (HIC15) for the 5%-ile female dummy significantly. Hence, clear benefits for the total assessment according to US-NCAP can be achieved (See Figure 10).
The second modification in form of a dual-stage belt load limiters, which goes down to a lower force limit (e.g. to 2kN) at a very early stage, is made.

This modification leads also to a positive effect on the US-NCAP rating (particularly chest deflection), though the chest load values are mainly dominated by the airbag. As already described for the driver side, an adaptive belt load limiting is a basic prerequisite for the safe fulfillment of legal requirements with equally good results in the ratings. The biggest benefit here is drawn from the reduction of the chest acceleration.

The combination of adaptive belt force limiting and adaptive airbag system is therefore primarily necessary to address the target conflict between 208 load case (56kph, 50%AM belted) and US-NCAP requirements (5%AF).

The combined adaptivity in the belt and airbag system allows a reduction of the HIC15 by 30% and of chest deflection by approximately 10% in the present parameter variation compared to the standard system (See Figure 10).

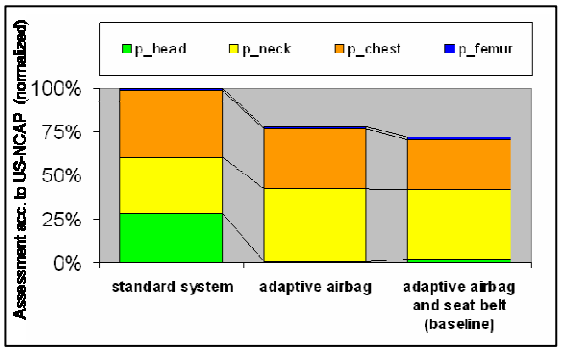

Figure 10. Adaptive airbag and belt load limiter compared to standard system.

The adaptive components as part of a new basic system are also used in all other parameter variations.

As already stated for the driver side, the use of a knee bag leads to an improved pelvis restraint. Thus, especially the chest deflection can be reduced by approximately 40%.

In combination with the adaptive belt load limitation and an adaptive airbag system, the reduction of the head loads turns out to be surprisingly high (HIC15 by about 70%). At the same time, it has to be accepted that the knee bag causes a significant increase of the axial femur force when the loads are on a low level.

As to the FMVSS 208 load cases, this modification also effects benefits for the chest acceleration (primarily 5%-ile dummy).

All in all, the injury probability can be reduced by approximately 12 % when a knee bag is used (See Figure 11).

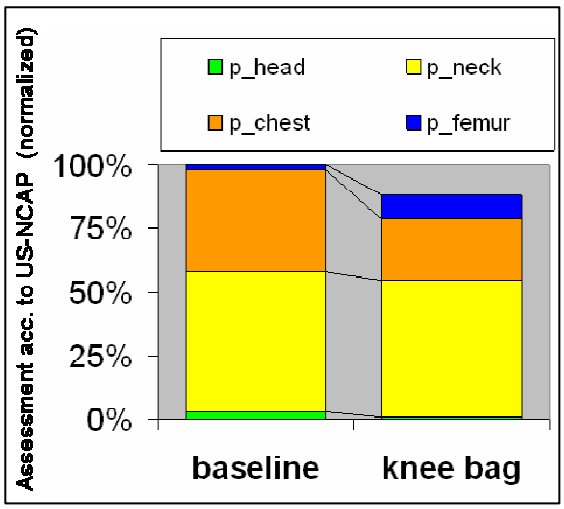

Figure 11. Knee bag compared to baseline.

The modifications studied by now showed clear reductions for the head and chest loads. Benefits for the neck loads (N_{ij}), however, could not been proved yet.

The next step will therefore be an optimization of the airbag shape as this seems to dominate the neck loadings of the 5%-ile dummy.

Due to the positive influence of the knee bag on the head and chest loads it will further be part of the considerations.

First a modification of the standard 3D shape is made for the region of the head and chest contact. This already allows a significant reduction of the neck injury risk. But at the same time head and chest loads change for the worse. Nevertheless, the total injury risk declines by 15% when all load criteria are considered. (See Figure 12, advanced airbag shape).

This is why the second step analyzes the Takata patented *Twinbag* [8]. Using a two-chamber airbag shape the „coupling“ of head and thorax and the resulting force application in this area can be improved systematically. This variant allows to reduce the chest deflection again by more than 50% compared to the basic variant (adaptivity in belt/airbag + knee airbag).

Furthermore, in comparison to the baseline the neck injury probability (N_{ij}) can be reduced by approximately 30%.

The use of the *Twinbag* results in a reduction of the combined injury risk by more than 30% (See Figure 12, *Twinbag*).

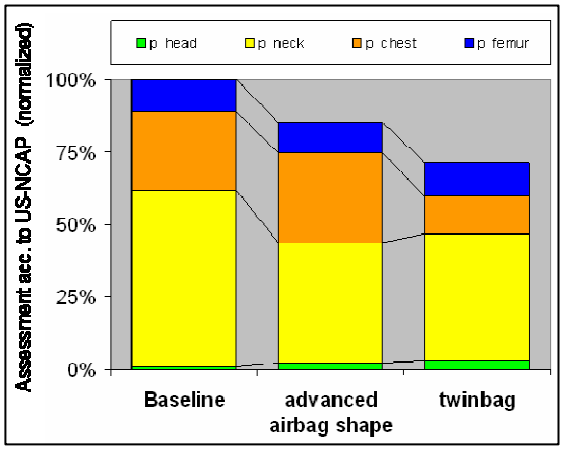

Figure 12. Advanced airbag shape and Twinbag compared to baseline (all modifications with knee bag).

The modification in the belt using double pretensioning (retractor and anchor or buckle), analyzed hereinafter, leads to a significant improvement of chest acceleration and chest deflection values, but it has a negative effect on head and neck loadings resulting in a clearly worse rating in the US-NCAP.

Analogous to the driver side, finally the influence of a (average) crash pulse on the evaluation according US-NCAP NEW is studied. On the passenger side, too, this variant results in an improvement of the head and chest loadings, those, however, not being that clear referring to the total rating of the 50%-ile dummy on the driver side (See Figure 13, No. 5: average crash pulse).

Finally, the study should find out whether disregarding an optimized airbag shape may allow for doing without an adaptive airbag system. Here, the *Twinbag* formidably shows its benefit on the combined injury probability using a hard crash pulse and the modifications explained above (adaptive belt limiter + knee airbag).

With reference to the combined injury probability this variant shows an improvement of approximately 55% even without the use of airbag adaptivity when directly compared to the standard system. This mainly traces back to considerable reductions in HIC15 and chest deflection (See Figure 13, No. 6: *Twinbag* w/o airbag adaptivity).

In contrast to the driver side, the injury risk for the neck (N_{ij}) also sinks by 15% to 20% when the system is supported by the analyzed modifications at the airbag shape (advanced airbag or *Twinbag*).

Figure 13 gives an overview on the studied modifications and their potential with reference to the injury risks according to US-NCAP NEW rating.

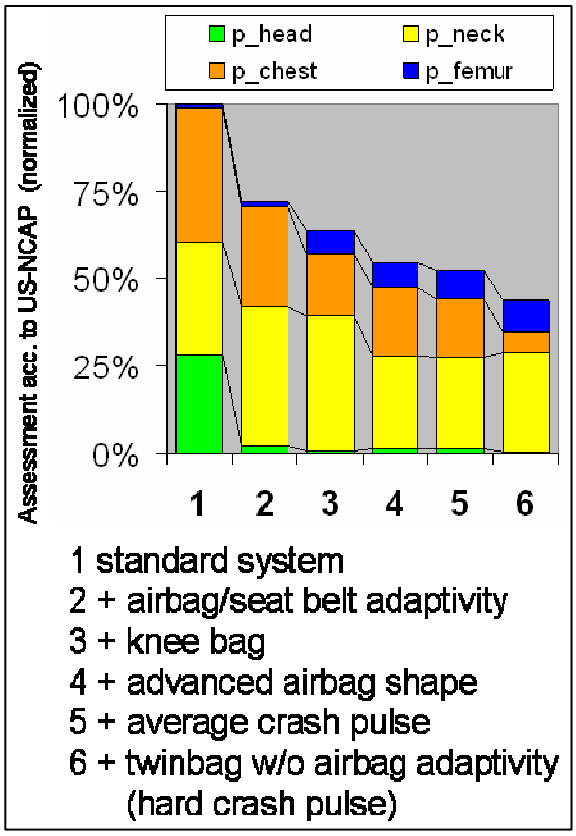

Figure 13. Overview: Benefit for passenger side.

CONCLUSIONS

According to the new US-NCAP requirements, the assessment of the frontal impact star rating is extended by additional injury criteria for neck (N_{ij}, compression/tension force), chest deflection and femur forces. With conventional airbag and seatbelt technologies, it seems to be very difficult to achieve a 5-star rating; on top of that if the tuning of the restraint system is based on a hard crash pulse.

Facing the legal requirements according to FMVSS 208 – unbelted and belted load cases (particularly Phase 2a and 2b) and the new US-NCAP rating scheme, HIC15, chest a3ms und chest deflection can be addressed sufficiently using an adaptive seat belt and airbag system on driver and passenger side.

On the driver side and on the passenger side as well a significant reduction of the injury risk could be evidenced for the 5%-ile and 50%i-le dummy load cases, particularly with regard to the head and thorax loadings. Combined with a knee bag and/or measures at the airbag shape the use of adaptivity for the restraint system can be obviously extended.

In principle, the airbag stiffness/damping is adapted to the unbelted load case with a 50%-ile dummy according to FMVSS 208. On the driver side an adaptive (airbag) system is primarily not needed to improve the rating according to US-NCAP. Provided an occupant classification system (OCS), here an adaptive parameter might be required to address the 5%-ile dummy load cases according to FMVSS 208. Due to the requirements for the 50%-ile dummy (unbelted) the usually applied extension of the venting area in the airbag is normally not to realize.

When the moments of activation of the adaptive airbag and belt system differ, the load cases for the 5%-ile and 50%-ile dummy can be addressed separately.

On the passenger side especially the injury probability for head and thorax is clearly reduced by the use of an adaptive airbag and airbag system. Here, benefits fort he neck loads can be proven having a positive effect on the total rating.

The combination of adaptive and advanced technologies (adaptive airbag / seat belt, knee bag, airbag shape) leads to a reduction of the combined probability of about 50%.
Using a knee bag or a double pretensioning belt system (retractor and buckle ore anchor), pelvis forward movement and dummy kinematics can be controlled sufficiently.

An optimized / advanced airbag shape can help to control load paths on head and thorax and to reduce chest deflection and neck loads (N_{ij}).

In the end, the analyzed parameter variations show that adaptivity with regard to legal and consumer requirements are an important part in the adaptation of the restraint system.

REFERENCES

[1] DEPARTMENT OF TRANSPORTATION National Highway Traffic Safety Administration [Docket No. NHTSA-2006-26555]: Consumer Information - New Car Assessment Program. 2008

[2] Heym, A.: Grundsatzuntersuchung zum Einsatz von adaptiven Insassenschutzsystemen beim Frontalaufprall von Pkw. In: diploma thesis, TU Berlin, 1996

[3] Adomeit, H., Wils, O. and Heym, A.: Adaptive Airbag-Belt-Restraints - An Analysis of Biomechanical Benefits. In: Proceedings of the 1997 International Congress & Exposition. Motor Vehicle Safety Design Innovations SAE special publication, 1226, February, pp. 163-177.

[4] Miller J., Patrishkoff D., Maripudi V.: Geringere Verletzungen durch intelligente Rückhaltesysteme. In: 4th International Akzo Symposium on Automotive Occupant Restraint Systems, Bonn, 2006

[5] Ruck H., Heym, A., Sachse U.: Pressure-Controlled Venting Holes in Airbags: Another Step on the Way Toward Increased System Adaptivity. In: Vehicle Safety 2000, London, 2000

[6] Schramm Ch., Fürst F. , Van den Hove M., Gonter M.: Adaptive Restraint Systems –The Restraint Systems of the Future. In: 8th International Symposium and Exhibition on Sophisticated Car Occupant Safety Systems – Airbag 2006, Karlsruhe, 2006

[7] Takata-Petri AG. Internal CAE study about the benefit of adaptivity with focus on new US-NCAP requirements. Berlin, 2009

[8] Patent US 7,360,790 B2

APPENDIX A

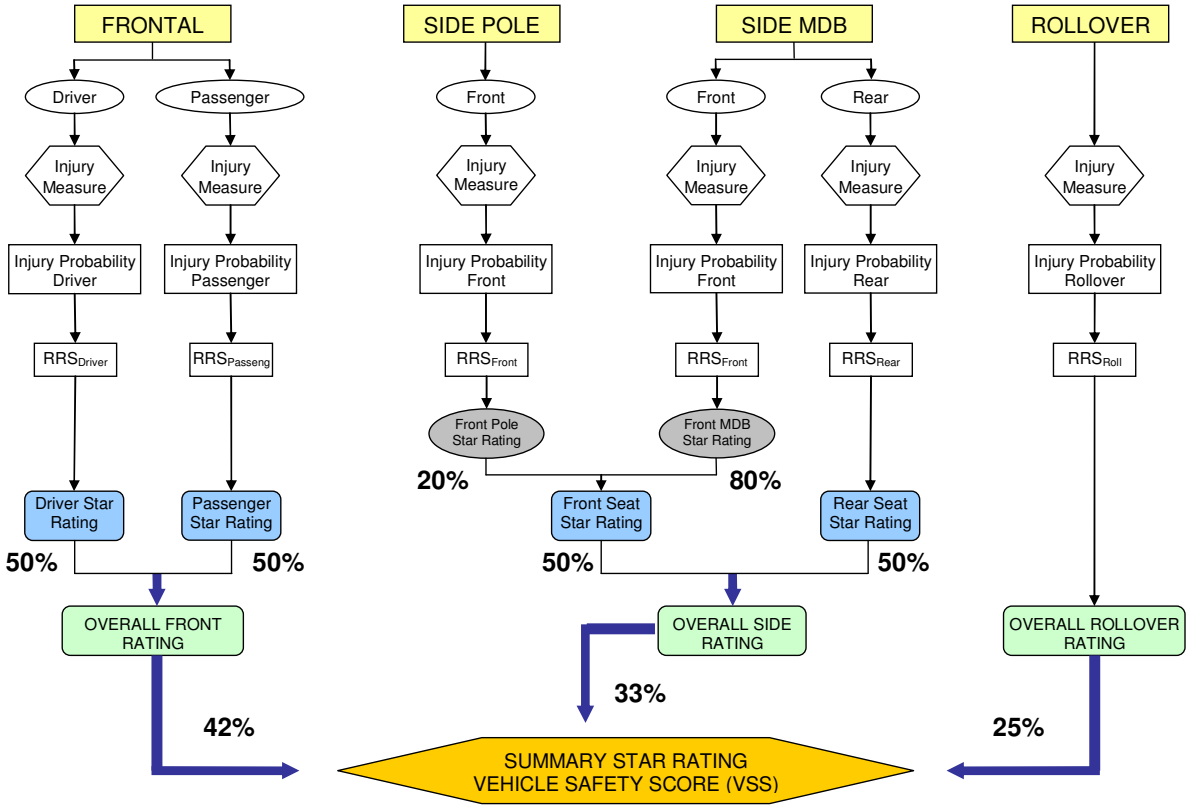

Figure A1. Overall vehicle rating acc. to US-NCAP New based on weighted Relative Risk Scores (RSS).